Novel and Selective Small Molecule Inhibitors and Activators For The Prolyl Hydroxylase Domain Enzymes

James P Holt-Martyn

Wolfson College, Michaelmas 2018



A thesis submitted to the Faculty of Physical Sciences at the University of Oxford in partial fulfilment of the requirements of the degree of Doctor of Philosophy.

Design and Synthesis of Potent and Selective Inhibitors For The HIF-α Prolyl Hydroxylases

James Preston Holt-Martyn, Wolfson College, University of Oxford.
Submitted for the degree of Doctor of Philosophy, Michaelmas 2018.

Hypoxia Inducible Factors (HIF) functions are master regulators of oxygen homeostasis and have a key role in the physiological responses to hypoxia including angiogenesis and erythropoiesis. Under hypoxia, levels of HIF-α subunits increase, they hetereodimerise with HIF-1β sub unit and promote the initiation of transcription of target genes. Under normoxia, oxygen dependent HIF-α degradation is promoted by hydroxylation of either of two proline residues (Pro402 and Pro564). The interaction of prolyl-hydroxylated HIF-α with the Von Hippel -Lindau protein (pVHL) promotes hydrolytic degradation of HIFα through an E3 ubiquitin ligase proteasomal pathway. HIF prolyl hydroxylation is catalysed by three 2-oxoglutarate (2OG)-dependent oxygenases known as prolyl hydroxylase domain (PHD 1-3) proteins, through an Fe(II) mediated catalytic process using 2OG, and oxygen. The PHDs are part of the family of Fe(II) bound 2OG dependent oxygenases. There are approximately 70 human 2OG oxygenases many of which have biologically important roles. Small-molecule inhibitors have reached advanced clinical trials; however, many clinical candidates inhibit other structurally similar 2OG oxygenases (OGFOD1 and vCPH) potentially altering the therapeutic effect. This thesis describes the design and synthesis of potent and 2OG oxygenase selective inhibitors for the PHDs.

The 1,3,8-triazaspiro[4.5]decane-2,4-dione and 4-hydroxy-2-(pyrazole)pyrimidine-5-amide series were chosen as initial 'hits' (reported in the patent literature). The main analogues of the series were characterised *in vitro* and in cells as potent and selective PHD inhibitors over structurally similar 2OG oxygenases (**Chapter 2**). Broad structure activity relationship (SAR) of both initial series demonstrated the sensitivity for PHD2 inhibition (**Chapter 3**). Combination of SAR work described in Chapters **2** and **3** lead to the development of the novel 4-hydroxy pyridine series. In-depth SAR resulted in optimised analogues including **1** (IC50 69 nM) and highly selective over structurally similar 2OG oxygenases including OGFOD1. The completed SAR work led to the development of two novel pharmacophores **2** and **3**. Both pharmacophores displayed potent PHD inhibition and selectivity over OGFOD1. Analogues including **1** and **3** displayed on target cellular activity stabilising HIF-1α at 20 μM (**Chapter 4**).

The 4-dimethylamine pyridine analogue displayed an increase in substrate hydroxylation on PHD2 in contrast to the DMSO control (**Chapter 3**). SAR and cellular characterisation indicated that the effect observed was not an assay artifact (**Chapter 5**).

Fenofibrate was used as a starting point for the development of novel inhibitors of the oxygen consumption rate (OCR) via mitochondrial inhibition (**Chapter 6**). Analogues were synthesised in order to conduct broad SAR and on-target cellular activity was observed in a Seahorse XF assay (50% reduction in the OCR at 1 μM). A selection of amino and amide analogues warrant further investigation.

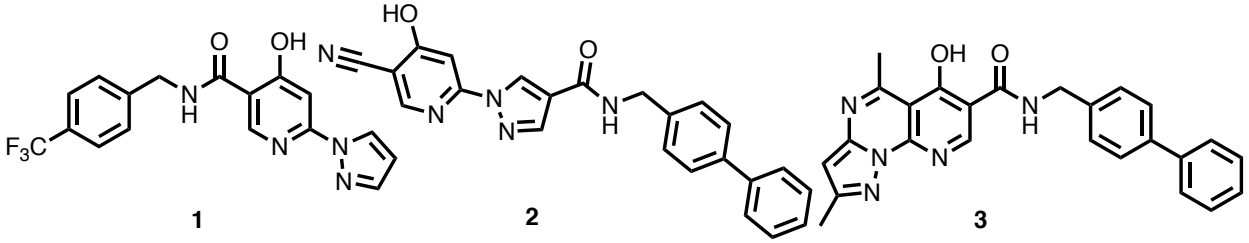

Figure A: Novel PHD inhibitors generated during the course of this thesis.

Acknowledgements

Thank you to Prof Chris Schofield for being my mentor rather than my supervisor. Thank you for guiding me but not commanding me and most importantly for allowing me to fail. I believe the positive outcomes of this DPhil project are because the confidence gained in my own ideas and the belief to execute them. A belief that now will never leave me.

Thank you to Prof Chris Pugh and Prof Sir Peter Ratcliffe for helping me understand the HIF biological pathway in a physiological perspective. The more different perspectives you can see the problem the better chance you have of developing a better product.

Massive shout out to the synthetic LG1 crew over the years. Rob, Roman (housekettle), Dong, Dave, KD, Marios, Hide, Cyrille, Gonzalo, Lennart, Jule and Shafali for all the synthetic help and the banter. LG1 will always be more fun than LG2.

Thank you to everyone in LG2 for helping me out in biochemistry. Special mention to Kerstin and Martine.

Thank you to Tony for the mentoring and guidance in biological assays. Your teaching and tolerance of many questions has allowed me to see medicinal chemistry in a completely different perspective and to be very selective on which assay to chose. “You can’t make a drug, when your primary assay is rubbish”

Thank you to Drs Mike McDonough and Rashed Chowdhury for their insight and perspective into X-ray crystallography and their in-depth knowledge of PHD2.

Thank you to Tzu-lan Yeh for all the cell work done on the HIF project.

Thank you to the British Heart Foundation for the funding, training especially the tutorials in my first year and my Dphil degree.

Thank you to all my Wolfson friends: Tom, Karwei, Ben, Pinar, Nushy, Oli, Nina, Joe, Gemma, Marc, Elias and Maria you've made the last four and a half years at Oxford have been an amazing experience, a chapter of my life that i will always cherish.

A special thank you to Mum. Who proof read the whole thesis and as a result made the thesis read a million times better!

Thank you to, Dad, Gran, Nan, Bumps and Lils for all the love and support.

Table of Contents

List of Experiments done by others i

Abbreviations ii

Chapter 1 : Introduction

1.1 The Hypoxia-Inducible Factor (HIF) Signalling Pathway 1

1.2 The Hypoxia-Inducible Factors (HIFs) 4

1.3 The HIF Hydroxylases 7

1.4 The PHD isoforms 10

1.5 HIF asparaginyl hydroxylase (FIH) 13

1.6 2OG Oxygenases that may affect the HIF System 14

1.7 Therapeutic Application of HIF PHD inhibitors 20

1.8 Clinically trailed inhibitors of the HIF hydroxylases 23

1.9 Thesis Outline 32

1.10 References 33

Chapter 2 : Identification and Validation of Selective PHD2 Inhibitors

2.1 Criteria For Selective PHD Inhibitors 48

2.2 Starting Points 52

2.3 *In-Vitro* Screening Methods 54

2.4 1,3,8-triazaspiro[4.5]decane-2,4-dione Series 55

2.5 4-hydroxy-2-(1*H*-pyrazol-1-yl)pyrimidine-5-carboxamide Series 59

2.6 Cellular Characterisation of Initial Hits 65

2.7 Crystal Structure of 1,3,8-triazaspiro[4.5]decane-2,4-dione Series 68

2.8 Crystal Structure Crystal Structure of 4-hydroxy-2-(1*H*-pyrazol-1-yl)pyrimidine-5-carboxamide Series 72

2.9 HIF-1α Substrate Displacement and Selectivity 74

2.10 2OG Oxygenase Selectivity 76

2.11 Summary 78

2.12 Compound Characterisation 81

2.13 References 101

Chapter 3 : Structure Activity Relationship of the 1,3,8-triazaspiro[4.5]decane-2,4-dione and 4-hydroxy-2-(1*H*-pyrazol-1-yl)pyrimidine-5-carboxamide series

3.1 Medicinal Chemistry Evaluation 105

3.2 1,3,8-triazaspiro[4.5]decane-2,4-dione Series : The Role of The Pyrimidine Ring 106

3.3 1,3,8-triazaspiro[4.5]decane-2,4-dione Series : The Role of The Core 109

3.4 4-hydroxy-2-(1H-pyrazole-1-yl)pyrimidine-5-carboxamide Series : The Role Of The Metal Chelating Groups 113

3.5 4-hydroxy-2-(1H-pyrazole-1-yl)pyrimidine-5-carboxamide Series : The Removal or Blocking The Hydroxyl Group 116

3.6 4-hydroxy-2-(1H-pyrazole-1-yl)pyrimidine-5-carboxamide Series : Transferring or Replacing The Hydroxyl Group 119

3.7 Summary 124

3.8 Compound Characterisation 126

3.9 References 170

Chapter 4 : Novel PHD Inhibitors

4.1 Synthetic Investigation of The 4-hydroxy Pyridine Series 171

4.2 In-depth Structure Activity Relationship of The Amide Substituent of the 4-hydroxy Pyridine Pharmacophore 179

4.3 3-hydroxypyridine Series 184

4.4 Additional Interactions Within The Active Site On The C-4 position of The Pyrazole Group 186

4.5 Cellular Characterisation of The 4-hydroxy Pyridine Pharmacophore 192

4.6 The Reverse 4-hydroxypyridine Pharmacophore 196

4.7 Cellular Characterisation of Reverse 4-hydroxy Pyridine Pharmacophore 206

4.8 Tricyclic Pharmacophore 207

4.9 Cellular Characterisation of Tricyclic Pharmacophore 212

4.10 2OG Oxygenases Selectivity 213
4.11 PHD Isoform and Substrate Selectivity 215
4.12 Summary and Future Work 218
4.13 Compound Characterisation 222
4.14 References 304

Chapter 5: Investigation of Small Molecules for Increased Substrate Hydroxylation on PHD2

5.1 Potential Activation 307
5.2 Investigation of the Amine Substituent 310
5.3 Investigation of The Role of The 4-Phenylbenzyl Substituent 313
5.4 Investigation of the Metal Chelating Substituent 317
5.5 Cellular Investigation of **84** 318
5.6 'Inverted' Medicinal Chemistry 325
5.7 Summary 331
5.8 Compound Characterisation 334
5.9 References 351

Chapter 6 : Novel Inhibitors To Reduce The Oxygen Consumption Rate (OCR) for Hypoxic Tumours in Radiotherapy

6.1 Introduction 354
6.2 Previous Work: High Throughput Screening To Assess Oxygen Consumption 356
6.3 Previous Work: Fenofibrate and its derivatives to reduce the OCR 358
6.4 Further Investigation of Fenofibric Esters and Amides 360
6.5 Investigation of The Quaternary Carbon 363
6.6 Investigation of The Role of The Chlorine Substituent 365
6.7 Summary & Future Work 369
6.8 Compound Characterisation 371
6.9 References 384

Chapter 7 : Conclusion

7.1 Novel PHD Inhibitors 387

7.2 Small Molecule PHD Activators 394
7.3 Novel Oxygen Consumption Rate Inhibitors 396
7.4 General Comments 397

Chapter 8 : Materials and Methods

8.1 Chemical Synthesis 399
8.2 PHD2/3 RapidFire Assay Protocol 400
8.3 PHD2 MALDI Assay Protocol 402
8.4 PHD2 NMR Displacement Protocol 402
8.5 PHD2 Crystallography Protocol 403
8.6 FIH RapidFire Protocol 404
8.7 OGFOD1 MALDI Protocol 405
8.8 vCPH MALDI Protocol 406
8.9 Cell Based Protocols 407
8.10 Oxygen Consumption Rate Cellular Protocol 409

List of Experiments Carried out by Others

- X-ray crystallography experiments were carried out by Dr Rasheduzzuman Chowdhury at the department of Chemistry, University of Oxford.
- MALDI experiments against PHD2 were carried out by Dr.Tzu-lan Yeh at the department of Chemistry, University of Oxford.
- MALDI experiments against vCPH were carried out by Mr Gareth Langley at the department of Chemistry, University of Oxford.
- MALDI experiments against OGFOD1 were carried out by Dr Christopher Lohans at the department of Chemistry, University of Oxford.
- Hep3B cell line experiments for PHD2 were carried out by Dr.Tzu-lan Yeh at the Welcome Trust for Structural Genomics at Oxford.
- Oxygen consumption rate (Seahorse) experiments were carried out by Mr James Coates at the Welcome Trust for Structural Genomics, University of Oxford..
- RapidFire™ experiments against PHD3 were carried out by Dr Anthony Tumber and Ms Kerstin Lippl at Target Drug Discovery Institute, University of Oxford.
- RapidFire™ experiments against PHD2 and the HIF-1α CODD & NODD substrates were carried out by Dr Anthony Tumber at Target Drug Discovery Institute, University of Oxford.
- RapidFire™ experiments against FIH and PHD2 with other HIF substrates were carried out by Dr Anthony Tumber at Target Drug Discovery Institute, University of Oxford.
- PHD2 NMR studies for substrate displacement were carried out by Dr Martine Abboud at the department of Chemistry, University of Oxford.

- Recombinant protein production and purification was carried out by Ms Kerstin Lippl (PHD2), Mr Gareth Langley (vCPH) and Dr Christopher Lohans at the department of Chemistry, University of Oxford.

Abbreviations

µl Microliters

µM Micromolar

2OG 2-Oxoglutarate

2,4-PDCA 2,4-pyridinecarboxylic acid

aa amino acids

ACN Acetonitrile

ARNT Aryl hydrocarbon receptor nuclear translocator

bHLH Basic helix-loop-helix

Brettphos Pd G3 [(2-Di-cyclohexylphosphino-3,6-dimethoxy-2′,4′,6′- triisopropyl-1,1′-biphenyl)-2-(2′-amino-1,1′ -biphenyl)]palladium(II) methanesulfonate methanesulfonate

Brine Saturated aqueous sodium chloride solution

Bn Benzyl

CAD *C*-Terminal transactivation domain

CBP CREB (cyclic adenosine monophosphate-response element binding protein) binding protein

CH_2Cl_2 Dichloromethane

clogP Calculated partition coefficient

Cs_2CO_3 Cesium Carbonate

CODD *C*-Terminal oxygen-dependent degradation domain

COMU (1-Cyano-2-ethoxy-2-oxoethylidenaminooxy)dimethylamino-morpholino-carbenium hexafluorophosphate

C-P4H Collagen prolyl-4-hydroxylase

CVs Column volumes

DABAL-Me_3 Bis(trimethylaluminum)–1,4-diazabicyclo[2.2.2]-octane

DMOG Dimethyloxalylglycine

DNA Deoxyribonucleic acid

DSBH Double-strand-β-helix

DMSO Dimethyl Sulfoxide

DMAc N,N-dimethylacetamide

DMF N,N-dimethylformadmide

ee enantiomeric excess

et al. et alia

EPO Erythropoeitin

EtOAc Ethyl Acetate

ESI-MS Electrospray ionisation mass spectrometry

FIH Factor inhibiting HIF

FLAG DYKDDDDK epitope

FGI functional group interconversion

FTO fat mass and obesity-associated protein

HATU 1-[Bis(dimethylamino)methylene]-1H-1,2,3-triazolo[4,5-b]pyridinium 3-oxid hexafluorophosphate

Hep3B Human hepatoma cell-line

HIF Hypoxia inducible factor

HPLC High Performance Liquid Chromatography

HRMS High Resolution Mass Spectrometry

hr Hour

HRE Hypoxia response element

HTS High-throughput screening

Hz Hertz

IC_{50} Half-maximal inhibitory concentration

JMJD Jumonji-C domain containing protein

KDM Lysyl demethylase

LiOH Lithium Hydroxide

LiCl Lithium Chloride

MALDI-TOF Mass assisted laser desorption ionisiation-time-of-flight

MeOH Methanol

MINA53 Myc-induced nuclear antigen

min Minutes

mRNA Messenger ribonucleic acid

mg Milligrams

mmol Millimole

ml Millilitres

m.p. Melting point

MW Microwave

m/z Mass/charge

NAD *N*-Terminal transactivation domain

Na_2SO_4 Sodium Sulphate

ND Not determined

nM Nanomolar

NMR Nuclear magnetic resonance

NODD *N*-Terminal oxygen-dependent degradation domain

NOG *N*-Oxalylglycine

Notch Neurogenic locus notch homolog protein

OGFOD1 2OG- and Fe(II)-dependent oxygenase domain-containing protein 1

PDB RCSB Protein Data Bank

Pd^{t}BuXPhos G3 [(2-Di-*tert*-butylphosphino-2′,4′,6′-triisopropyl-1,1′-biphenyl)-2-(2′-amino-1,1′-biphenyl)] palladium(II) methanesulfonate

PHD HIF prolyl hydroxylase or prolyl hydroxylase domain

RT or rt Room temperature

rRNA Ribosomal RNA

RockPhos Pd G3 [(2-Di-*tert*-butylphosphino-3-methoxy-6-methyl-2′,4′,6′-triisopropyl-1,1′-biphenyl)-2-(2-aminobiphenyl)]palladium(II) methanesulfonate

RuPhos Pd G3 (2-Dicyclohexylphosphino-2′,6′-diisopropoxy-1,1′-biphenyl)[2-(2′-amino-1,1′-biphenyl)]palladium(II) methanesulfonate, RuPhos-G3-Palladacycle

T3P Propylphosphonic anhydride solution ≥ 50 wt. % in DMF

^{t}BuOH Tert-butanol

THF Tetrahydrofuran

TET Ten–eleven translocation protein

TMS-I Trimethylsilyl - Iodide

Tpa1p Termination and polyadenylation 1 protein

pVHL Von Hippel-Lindau tumour suppressor protein

VEGF Vascular endothelial growth factor

VHL Von-Hippel-Lindau tumour suppressor

Standard abbreviations for nucleotides, standard amino acids, SI-units/prefixes and chemical elements are used throughout

CHAPTER 1 : Introduction

1.1 The Hypoxia-Inducible Factor (HIF) Signalling Pathway

The hypoxia inducible factors (HIF) are α/β heterodimeric transcription factors that bind to hypoxia response elements (HRE) within DNA, activating cellular responses to hypoxia in animals.[1-3] HIF is continuously synthesised in most human cells.[1-3] Its levels are regulated by the oxygen mediated post-translational hydroxylation of specific proline-residues in HIF-α subunits.[1-3] In mammalian cells, HIF-α prolyl hydroxylations occurs on the *C*- and *N*-terminal sites within the oxygen dependent degradation domains (CODD and NODD respectively). HIF-α hydroxylation is catalysed in humans by three related oxygen dependent dioxygenases, the prolyl hydroxylase domain (PHD) enzymes 1, 2 and 3.[4-8] The *trans*-4-Hydroxy-prolyl forms a recognition site for the interaction of HIF-α with the von Hippel-Lindau (pVHL) ubiquitin E3 ligase complex, resulting in polyubiquitination and degradation of HIF-α subunits via the 26S proteasomal pathway.[4-8] In hypoxic mammalian cells, PHD activity is reduced due to lowered oxygen availability, resulting in a reduction of HIF-α degradation and leading to stabilisation of HIFα. The stabilised HIF-α translocates to the nucleus to form an active transcriptional complex with HIF-β. The so formed dimer subsequently binds to HRE sequences leading to the activation of HIF-α target genes (**Figure 1**).[4-8] Additional transcriptional regulation of HIF-α occurs via asparaginyl hydroxylation within the HIF-α *C*-terminal transactivation domain (CTAD); this hydroxylation down-regulates transcriptional activity by preventing the binding of HIF-α to co-activator proteins CBP/p300.[9-13] Factor inhibiting HIF (FIH) catalyses an asparaginyl

hydroxylation in the *C*-terminal transcription activation domain of HIF-α subunits.[9-13] Collectively, FIH and the PHDs are known as the HIF hydroxylases. The PHDs are established as cellular oxygen sensors, with respect to their kinetic properties, with respect to binding/reaction with oxygen. The HIF hydroxylases thus connect the transcriptional response to hypoxia itself to oxygen availability.

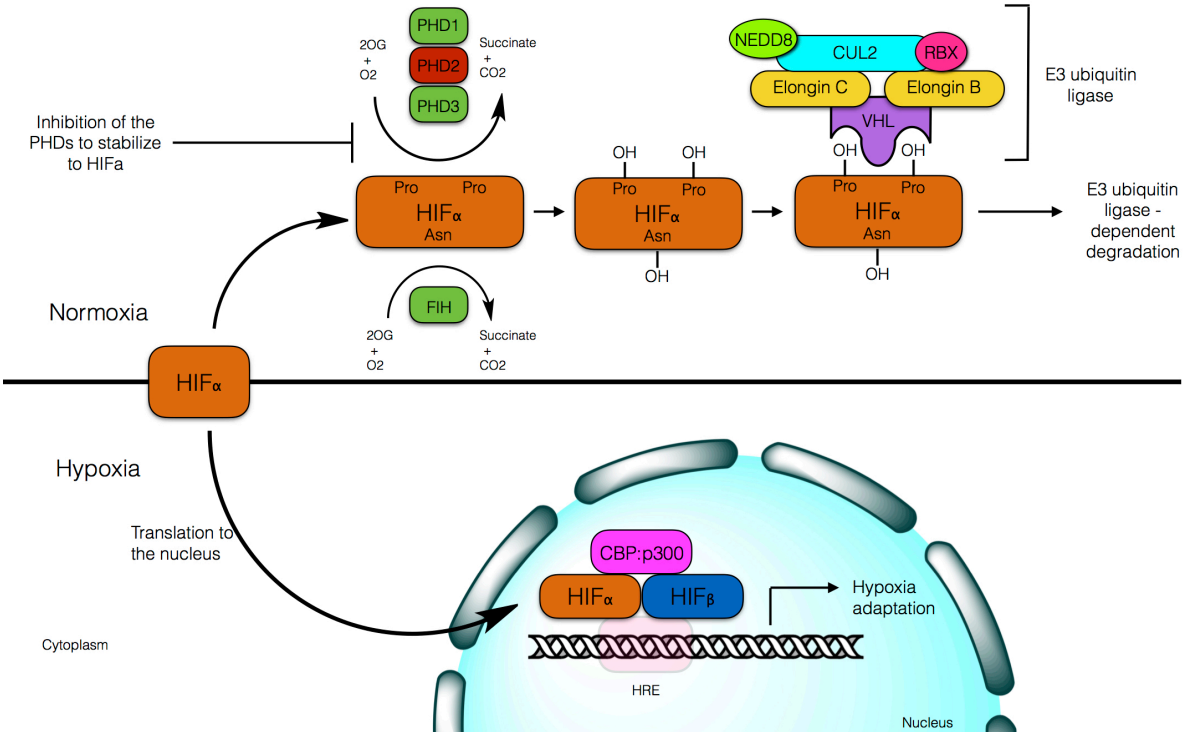

Figure 1 : Schematic diagram illustrating HIF-α regulation by the PHDs and FIH. In normoxia (non-limiting levels of O_2), HIF-α is efficiently hydroxylated at the conserved proline residues in the oxygen degradation domains (ODD) of HIF-α (Pro402 and Pro564), then targeted for pVHL E3 ubiquitin ligase proteasomal degradation. FIH hydroxylates the *C*-terminal residue Asn-803 blocking the binding of the CBP/p300 co-activators. In hypoxia (limited levels of O_2) the hydroxylation of HIF-α is suppressed, leading to stabilisation of HIF-α and its translocation to the nucleus. HIF-α and HI-Fβ hetereodimerise resulting in HIF promoted transcriptional activity.

Thousands of genes are negatively or positively regulated by HIF throughout the human genome.[14-16] **Figure 2** shows a selection of direct HIF transcriptional targets. HIF regulated pathways have multiple systemic and cellular actions supporting oxygen homeostasis,

either via a reduction in demand of oxygen (cell survival decisions, reprogramming energy metabolism or cytostasis) or enhancing the delivery of oxygen (vasomotor controls, erythropoiesis or angiogenesis).[17-19] The broad function of HIF targeted genes has led to the HIF oxygen sensing pathway being named as a master regulator of oxygen homeostasis.[1-3] Additional phenotypes obtained by genetic techniques suggest that HIF may have more extensive biological functions. For example, HIF has proposed roles in inflammatory and immune signalling.[20-22]

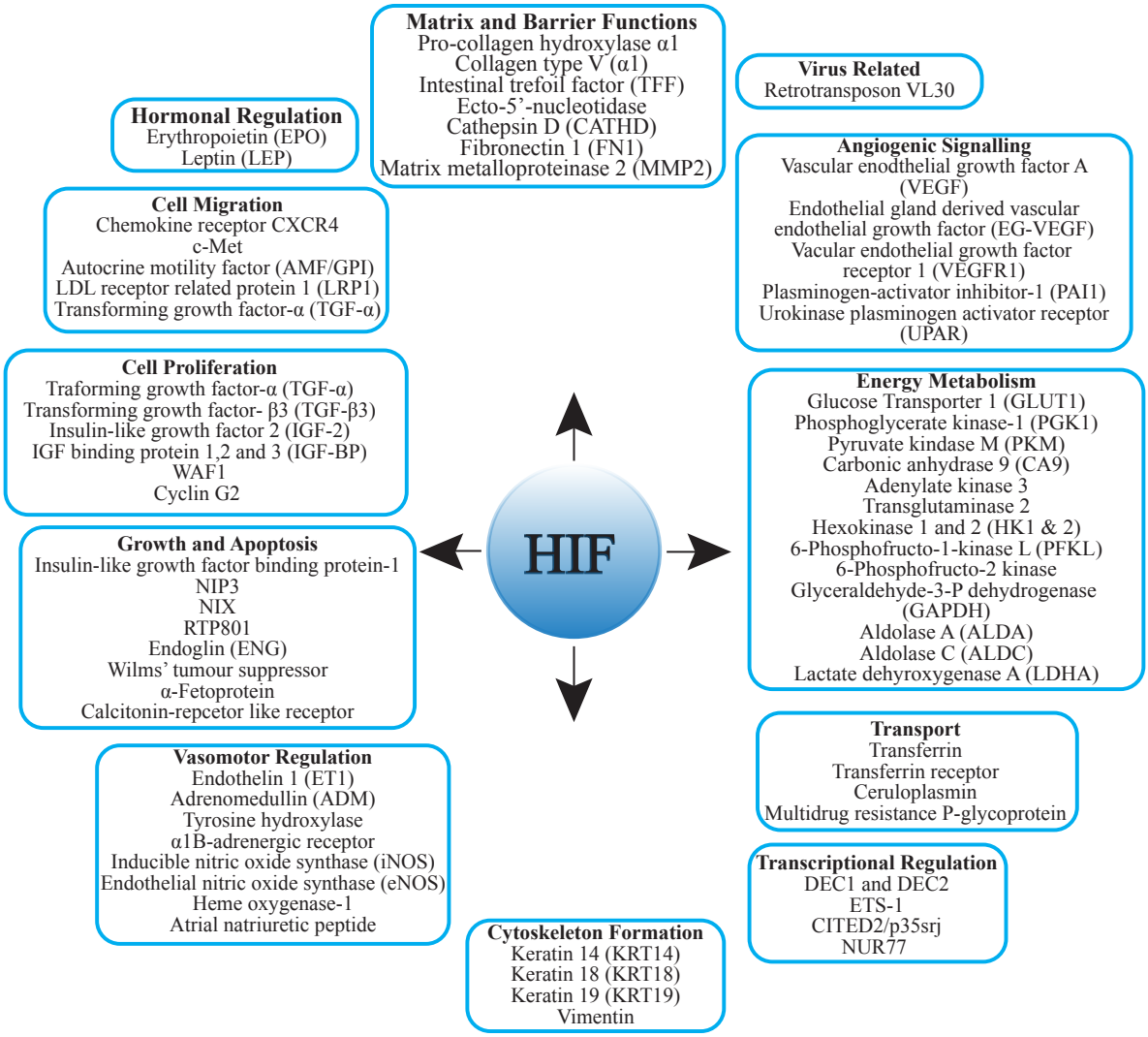

Figure 2 : HIF regulated transcriptional targets. Figure adapted from Chowdhury *et al.*[14]

1.2 The Hypoxia-Inducible Factors (HIFs)

Three HIF-α isoforms exist in mammalian cells.[1] HIF-1α, the first to be discovered, is widely expressed across different cells and tissues.[1] HIF-2α is expressed in the parenchyma, interstitial cells and endothelial cells of multiple organs.[23,24] HIF-3α is the least well studied of the HIFα isoforms; however, it is known that HIF-3α is expressed in lung epithelial and human kidney cells.[25] Northern blot analysis has revealed HIF-3α mRNA expression to be relatively high in skeletal muscle, the heart and the placenta but low in the kidney, liver and lungs.[26] HIF-1α and HIF-2α are structurally similar and are regulated in a similar ways, whereas HIF-3α differs structurally.[27] The HIF-1α and HIF-2α subunits both contain two PAS domains and a bHLH domain, which are important for dimerisation with HIF-1β and binding to the HRE within the DNA.[2,15] Both HIF-1α and HIF-2α subunits contain the CODD and NODD domains and the *C*- and *N*-terminal transactivation domains (TADs) respectively, that promote for activation of HIF target transcription (**Figure 3**).[2,15] HIF-3α also contains two PAS domains and a bHLH domain; however, HIF-3α only contains one ODD domain (*C*-terminal) and one TAD domain (*N*-terminal) (**Figure 3**).[25] The TAD of HIF-3α only shares 58% and 52% similarity with the N-terminal TADs of HIF-1α and HIF-2α respectively, suggesting a different physiological role for HIF-3α.[25] HIF-3α mRNA is involved in multiple splicing events and there are at least 6 human HIF-3α variants.[28,29] These variants differ in their transcriptional functions, sensitivity to oxygen and the ability to interact with HIF-1β.

As HIF-1α and HIF-2α are structurally similar, they are predicted to be able to bind to the same HREs (in correlation with HIF-β), however their target genes differ in a context-dependent manner and are driven by multiple cellular mechanisms.[27] Indeed, studies attempting to define specific isoform transcription have revealed the complexity of the hypoxic cellular response. Variables that have been reported to influence the transcriptional response include the duration of hypoxia, the cell type, severity of the hypoxia and the presence of functional VHL.[27] Studies have shown that HIF-1α and HIF-2α can (sometimes) bind to the same HREs and the bHLH domain is not involved in target gene selectivity. The *N*-TAD domains are involved in HIF-1α/HIF-2α target gene selectivity.[30,31] HIF-2α is more restricted in expression across cell and tissue types and studies have shown temporal organisation of HIF-2α responses following longer periods of hypoxia (i.e > 12 hours).[32,33] HIF-2α is not (normally) involved in glycolytic gene upregulation but up-regulates target genes that are involved in angiogenesis and stem cell maintenance.[34,35] HIF-1α responses occur in acute hypoxia (i.e < 24 hours stimulation) and up-regulates target genes involved in glycolysis thereby promoting cells to switch to anaerobic glycolysis.[32,33] Studies have shown that HIF-1α is involved in transcriptional regulation independently of HIF-1β, interacting with other DNA binding proteins such as the Notch protein which is reported to be regulated by FIH.[27,36]

HIF-3α's functions are still not fully understood. It has been proposed to have a two functions: 1) activation of specific target genes 2) negative regulation of HIF-1α and HIF-2α.[37] HIF-3α up-regulates genes that are up-regulated by HIF-1α and HIF-2α such as EPO and GLUT1 and in zebrafish it has been shown to upregulate genes unique to HIF-3α

such as sqrdl.[37,38] It has been suggested that HIF-3α negatively regulates HIF-1α and HIF-2α by competing for binding with HIF-1β.[39] HIF-3α lacks a TAD, when bound to the HREs HIF-3α suppresses expression of HIF (some) target genes.[39] Interestingly, HIF-3α is a target gene for HIF-2α, thereby acting as a negative loop for HIF-1α and HIF-2α genetic upregulation.[38,40]

HIF-1β is also known as the aryl hydrocarbon receptor nuclear translocator (ARNT).[1] Two human homologues of HIF-1β exist: ARNT2 and ARNT3.[41] Like HIF-1β, ARNT2 heterodimerises with the HIF-α isoforms.[42] HIF-1β and ARNT2 differ in tissue expression, ARNT2 is only expressed in the kidneys and CNS whilst HIF-1β is reported to be expressed universally in human cells.[43-45] HIF-α and HIF-1β are constitutively expressed;

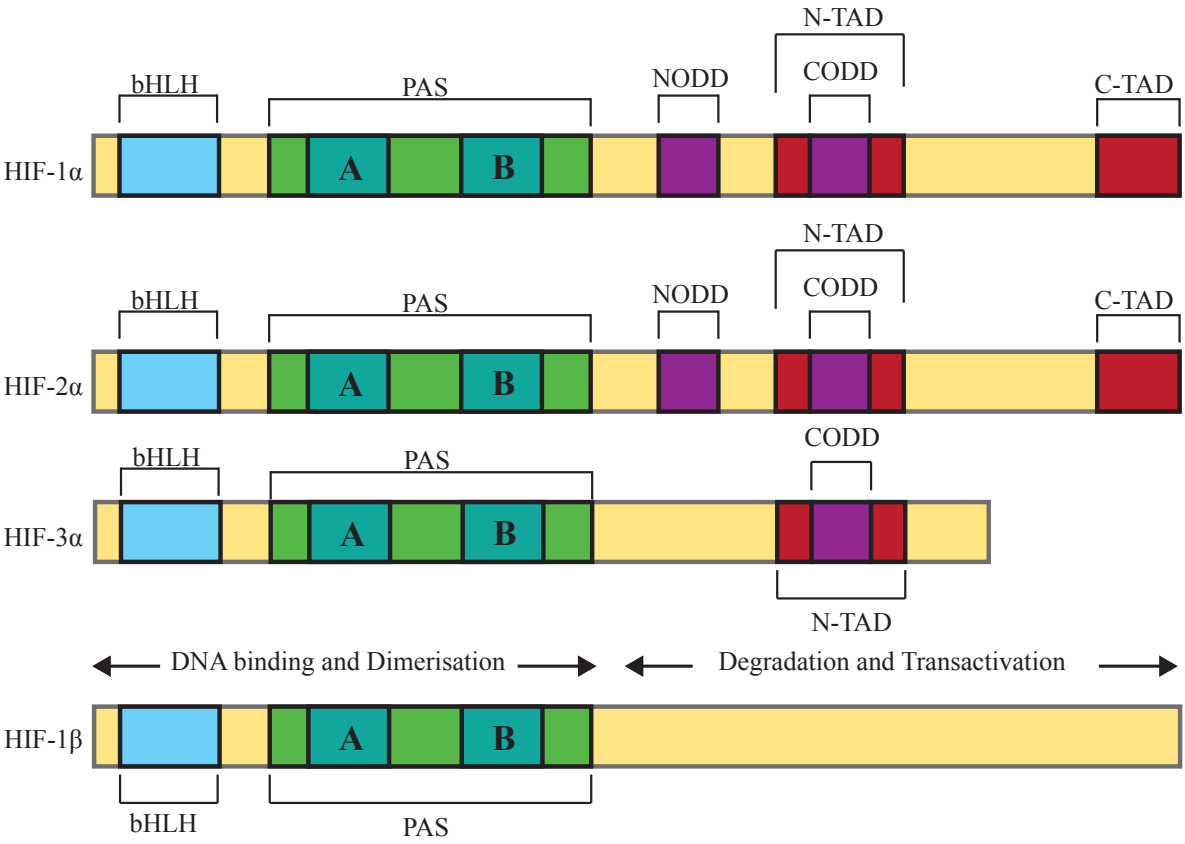

Figure 3 : The human HIF domain structure of all HIFα isoforms and HIF-1β. adapted from Chowdhury *et al*.[14]

however, the general view is that HIF-β is not regulated by the availability of cellular oxygen. Hypoxic regulation of HIF-1β has been observed in some cell lines such as Hep3B, but not others cell lines such as HepG2.[46,47] The precise nature of hypoxic regulation has been shown to depend on the severity of the hypoxic response and the length of the hypoxic event.[46,47]

1.3 The HIF Hydroxylases

The HIF hydroxylases are ferrous iron (Fe^{2+}) and 2-oxoglutarate (2OG) dependent dioxygenases, a superfamily of enzymes with more than 60 human examples.[48-50] The 2OG oxygenases are found throughout aerobes (except archaea) and catalyse a variety of oxidative reactions and are involved in a broad range of biological roles.[48,50,51] However, in humans, only *N*-methyl demethylations via hydroxylation of a methyl group and hydroxylation reactions have only been identified.[52,53] Human 2OG oxygenases catalyse a broad range of biological oxidations including histone demethylations and nucleic acid oxidation.[48,50,51] Some of their reactions have potential to modify gene expression. Therefore, some 2OG oxygenases have the potential to affect expression of HIF. Some 2OG oxygenases including some histone demethylases are HIF target genes.[50]

2OG oxygenases, including the PHDs and FIH, contain a double-stranded β-helix protein (DSBH) fold (also known as a JmjC motif or jelly-roll fold) (**Figure 4**).[50,54] The DSBH fold (normally) supports three conserved residues for Fe^{2+} binding which forms a HXD/E…H metal chelating triad and coordinating the Fe^{2+} atom in a octahedral manner.[50,54] The 2-oxoacid substituent of 2OG binds to the Fe^{2+} in a bi-dentate manner (**Figure 4A**).[48,50] The

C-5 carboxylate and methylene moieties of 2OG are diverted inwards towards the protein fold.[48,50] The *C*-5 carboxylate is positioned to interact with a basic residue - Arg-383 and Lys-214 in PHD2 and FIH respectively.[55,56] Almost all 2OG oxygenases, including the PHDs and FIH, use 2OG and oxygen as co-substrates. A consensus mechanism has been purposed, as supported by spectroscopic, crystallographic, modelling and kinetic analyses (**Figure 5**).[48,50] Firstly, 2OG binds to the active site Fe^{2+}, followed by binding of the substrate (e.g HIF-α). Substrate binding enables oxygen to bind by displacing a H_2O molecule from the metal.[48,57] Oxidative decarboxylation of 2OG produces a reactive Fe^{IV}-oxo intermediate, which hydroxylates the substrate, possibly via a radical rebound mechanism.[48,57] The hydroxylated substrate is then released, along with succinate before rehydration of the metal centre.[48,57]

The rates of the steps within the mechanism described above can vary. Indeed, for the PHDs, the available evidence indicates that the Fe^{IV}-oxo intermediate occurs too quickly to be observed spectroscopically, suggesting the hydroxylation reaction is not the rate-limiting step.[58,59] PHD2 is known to form an unusually stable complex with 2OG. PHD2 also catalyses the unusually slow turnover of 2OG in the absence of substrate.[60] Indeed, for PHD2, the available evidence suggests that a rate-limiting step in the catalytic mechanism is the binding of O_2 and displacement of the metal bound H_2O in the PHD2-substrate complex.[58,59,61] The K_M of O_2 ($K_M(O_2)$) for PHD2 is reported to be relatively high, ranging between 200-250 μM depending on which HIFα substrates are used.[62,63] The high $K_M(O_2)$ suggests that PHD2 will be sensitive to changes in O_2 concentrations. The $K_M(O_2)$ for FIH is significantly lower than for PHD2, and is reported to range from 90-150 μM, suggesting

FIH is less sensitive than the PHDs to reduced oxygen availability. FIH is more active in hypoxia than the PHDs in cells.[62,63]

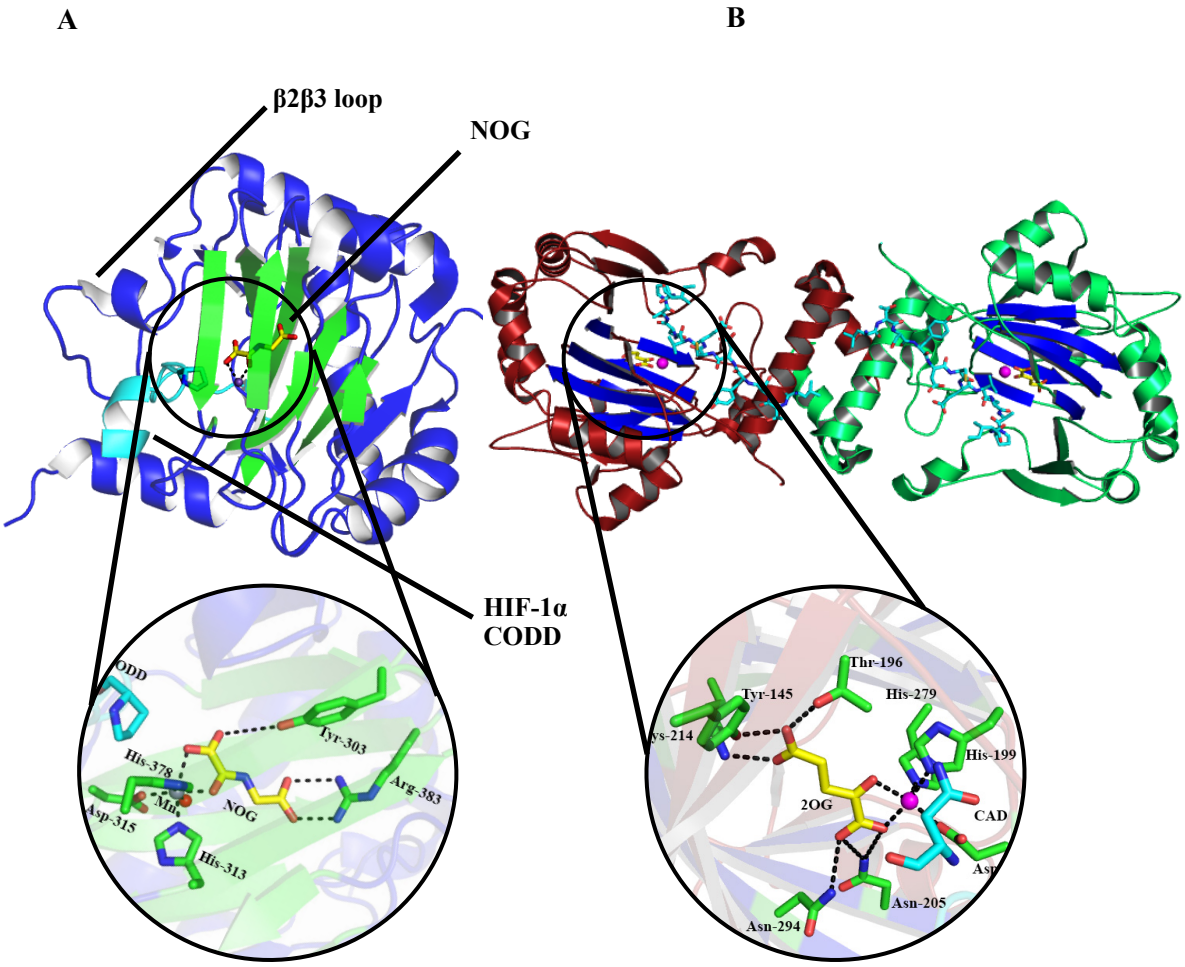

Figure 4: Views from crystal structures of the catalytic domains PHD2 (truncated(t) tPHD2) (PDB ID: 3HQR) and FIH (PDB ID: 1H2N).[56,67] **A**) Cartoon representation of tPHD2 in complex with NOG (yellow) HIF-1α CODD peptide (light blue), active site residues (green), H_2O (red) and Mn (purple) at active site of PHD2, highlighting the interactions between NOG, Mn(II) and the protein. **B**) Cartoon representation of FIH in complex with 2OG (yellow) and Fe(II) (purple), HIF-CAD (light blue) and active site (green) with the active site of FIH highlighting the residue interactions between 2OG, Fe(II) and the protein.

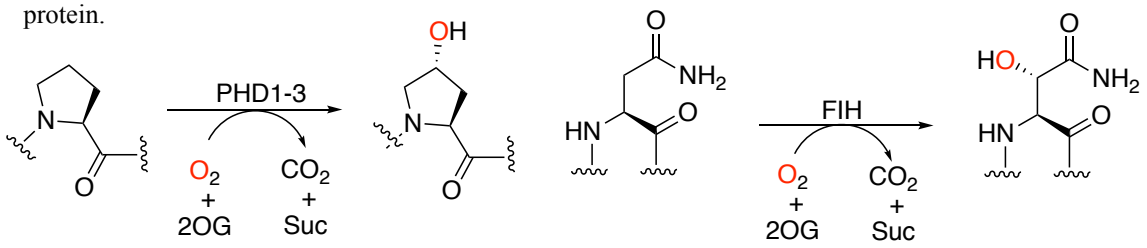

Scheme 1: **A**) Prolyl hydroxylation of HIFα CODD/NODD as catalysed by the PHDs. **B**) Asparaginyl hydroxylation of HIFα CAD as catalysed by FIH. Chan *et al.*[19]

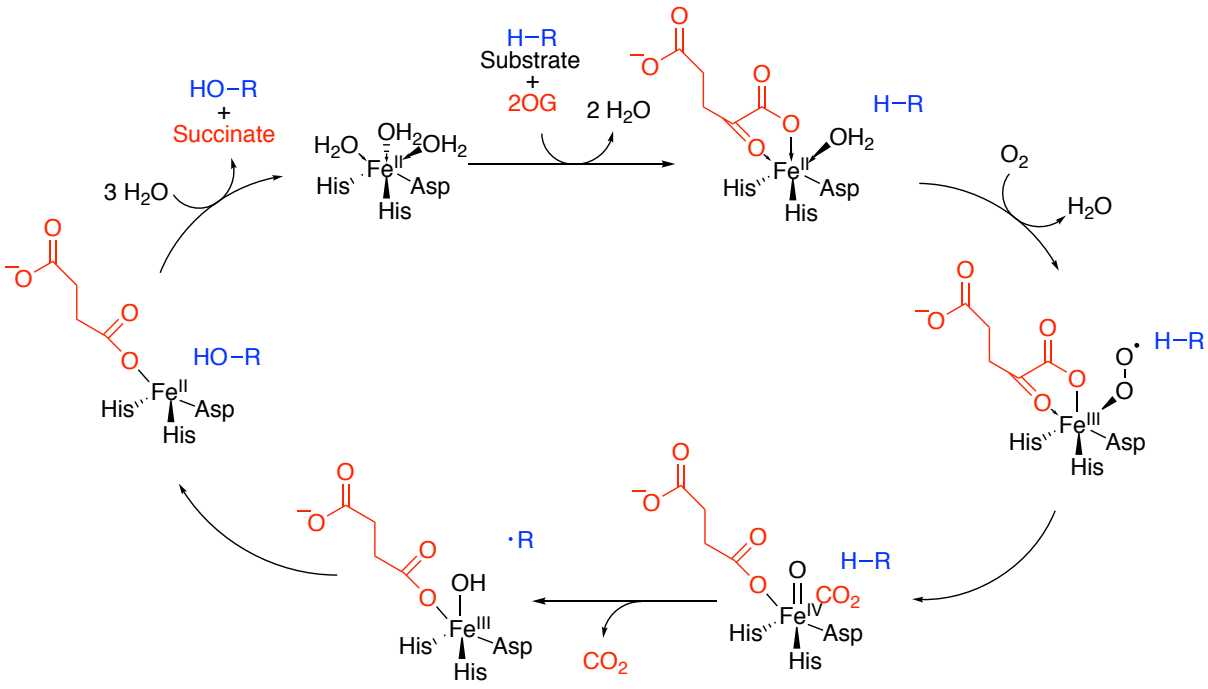

Figure 5: Outline catalytic mechanism for the 2OG Fe(II) dependent oxygenases. Refer to main text for details. Figure adapted from Chan *et al.*[19]

1.4 The PHD isoforms

PHD1, PHD2 and PHD3 are 407, 426 and 239 amino-acid residues in length respectively and are ~40 - 60% similar in sequence.[5,6] The PHDs *C*-terminal catalytic domains are highly conserved (~55%), yet they differ in substrate preference.[64] PHD1 and PHD2 have been shown to accept NODD and CODD, whilst PHD3 only efficiently hydroxylates the CODD substrate as observed with isolated protein and cells.[6,62,65] Indeed, for PHD2 the NODD substrate binds less tightly to PHD2 than the CODD substrate indicated by a higher dissociation constant (K_d).[66] Crystallographic structures of PHD2 with and without the

HIF-α substrates have revealed a flexible loop between the β2 and β3 strands (residues ~ Gln237 - Lys255), which is involved in substrate binding.[56,64,66,67] The flexible loop folds over the highly conserved LXXLAP motif of the HIF-α substrates.[56,64,66,67] Comparison of NODD and CODD complex structures and without the HIF-α substrates indicate clear differences in NODD/CODD binding interactions with the flexible β2/β3 loop and *C*-terminus.[66] Residues within the flexible loop (Val241, Ser242, Lys244 and Ile251) interact with the 'XX' residues, which differ between NODD and CODD of the LXXLAP motif.[66] Replacing the residues within the flexible loop with residues that are present in PHD3 (Ala, Gly, Arg and Leu) resulted in an increase in CODD substrate selectivity indicating the flexible loop plays a role in substrate selectivity.[66] In relation to *C*-terminal binding, the CODD substrate interacts with the *C*-terminus via a salt-bridge ($Asp571_{CODD}$-$Arg396_{PHD2}$). In contrast, the NODD substrate forms more hydrophobic interactions with the *C*-terminal region of PHD2 than CODD.[66]

It has been reported that PHD1 and 3 regulate HIF-2α more than HIF-1α, whilst PHD2 regulates HIF-1α more than HIF-2α.[68] The PHD isoforms differ substantially in these *N*-terminal domains and to date are not fully characterised. Only the PHD2 isoform contains a MYND type zinc finger, which is reported to increase the inhibition of HIF. The MYND subunit is highly conserved in PHD2 evolution.[6,69] PHD3 has a significantly shorter *N*-terminus in contrast to PHD1 and 2.[6,70,71] Differences in the *N*-terminal regions, such as polymorphisms of the PHD2 *N*-terminal region, have been linked adaptations to high altitude in the Tibetan population, indicating the importance of the *N*-terminus in the HIF pathway.[1]

PHD2 is more abundant and widespread compared to PHD1 and PHD3 as observed in multiple cell lines under normoxic conditions.[6] PHD1 and PHD3, have been shown to be more restricted in expression.[68] RNA analysis for all PHD isoforms indicates that PHD1 is highest in the testes[71]. PHD3 is highest in the heart.[71] Additionally, the PHD isoforms are localised in different sub-cellular compartments. PHD2 is found mainly in the cytoplasm, PHD1 exclusively in the nucleus and PHD3 in both the nucleus and cytoplasm.[72] On the basis of abundance, the widespread expression and the increased inhibition of HIF, PHD2 is regarded as the main oxygen sensor. Indeed, homozygous deletion of PHD2 results in death in mice embryos, due to severe heart and placental defects, whereas PHD1 and 3 knockdowns in mice were viable.[71,73] PHD1 and 3 double knockdowns resulted in erythrocytosis.[68]

Reports have suggested that PHD4 (also known as PH-4 or P4H-TM) exists. However, amino acid sequence analyses indicates that PH-4 is more similar to the collagen prolyl hydroxylases.[74,75] *In-vitro* experiments have reported that PHD4 hydroxylates both NODD and CODD substrates of HIF-α.[75] Additionally, unlike the other PHD isoforms, PHD4 possesses a transmembrane domain and is found in the endoplasmic reticulum.[74,75] *In vivo* studies have reported that overexpression of PHD4 resulted in a decrease in HIF-2α levels and reducing LM8 osteosarcoma growth in mice via upregulation of TGF-α which increased vessel density.[76] Upon this discovery, Breier *et al.* silenced HIF-2α expression in the LM8 cells, and observed tumour growth without changes in vessel density, suggesting the overexpression of PHD4 disrupts the angiogenic balance of LM8 cells through upregulation of TGF-α.[76]

Multiple substrates in addition to the HIF-αs have been reported for the PHDs, however to date, there is no structural or kinetic studies on the 'alternative' substrates.[19] Indeed, in unpublished work within the Schofield group, Lippl *et al.* have not found evidence for activity with the alternative substrates for recombinant PHD1-3 with *in vitro* hydroxylation assays.

1.5 HIF asparaginyl hydroxylase (FIH)

The HIF asparaginyl hydroxylase (FIH) is more closely related to the JmjC-domain sub family of the 2OG oxygenases than the PHDs.[49] FIH is expressed in multiple tissues and many cell lines. Like PHD2, FIH is mainly found in the cytoplasm.[55,77,78] Structurally FIH differs from the PHDs, which use their *C*-terminal region for substrate binding and are monomeric, whereas crystallographic studies reveal that FIH functions as a dimer and oligomerises via its *C*-terminal region.[55,77,78] FIH can also accept a range of substrates other than the HIF-α CAD domain, including a range of ankyrin-repeat domain proteins (ARD) (including from the Notch proteins described in **Chapter 1.2**) and can hydroxylate residues other than asparagine, including histidine residues.[79] Kinetic analyses indicate that FIH has a stronger affinity for the ARD of Notch1 than HIF-α CAD (K_M of 0.2 and 50 μM respectively).[80] Indeed, the discovery that HIF-1α interacts with the Notch proteins has led to the suggestion that the ARD proteins act in a synergistic manner to regulate the hydroxylation of HIF-α CAD through interacting with FIH.[80] Crystallographic analyses indicate that different FIH substrates bind in a similar fashion; however, the ARD proteins normally adapt a defined helical conformation and theoretically precise binding to FIH

must involve the unfolding of (some) ARD helices.[9,10] By contrast the HIFα-CAD does not have a secondary structure, at least in its uncomplexed form. Knowledge of how the ARD protein unfolded by FIH is unknown; knowledge of how FIH unfolds the ARD proteins may help enable substrate selective inhibition of FIH.[19]

1.6 2OG Oxygenases that may affect the HIF System

This section describes, studies on a selection of 2OG oxygenases that are involved in a broad range of biological processes that may affect components of the HIF system.

Collagen Hydroxylases

The collagens form a group of extracellular matrix proteins, which forms the majority of the extracellular matrix.[81] They are responsible for maintaining the structural integrity of the extracellular matrix.[49,82] Pathological fibrosis of organs such as the skin, liver and kidneys is characterised by excessive accumulation of the extracellular matrix.[49,82] Liver fibrosis is a response to chronic inflammation as a result of infection (such as by hepatitis C) or of alcohol abuse. Kidney fibrosis is associated with renal disease.[82] Medicinal intervention in the progression of fibrosis may be beneficial in the diseases defined above.

Fibrillar collagen is a major component of the extracellular matrix and is composed of a triple helix made up of three separate collagen strands.[83,84] The stability of the triple helix depends on the post-translational *C*-4-hydroxylation of the proline residues in a canonical X-Y-Gly-motif, where X is a proline residue and Y is either a lysine or proline residue.[83,84]

There are three types of 2OG oxygenases involved in collagen biosynthesis: *C*-4 prolyl hydroxylases (CP4Hs), the *C*-3 prolyl hydroxylases (C3PHs) and the *C*-5 lysine hydroxylases (PLODs) (**Scheme 2**).[50,85,86] *Trans* prolyl-4-hydroxylation of multiple residues of the Y-motifs in the triple helices is proposed to stabilise collagen via the stereoelectronic gauche effect.[87] The full roles of *C*-3 prolyl and *C*-5 lysine hydroxylases remain unclear; however, *C*-5 lysine hydroxylation can enable glycosylation which can enable cross-linking.[88] The *C*-3 prolyl hydroxylase is believed to cause local destabilisation of the triple helix leading to cross-linking at both X and Y positions of the X-Y-Gly-motif in collagen strands.[89]

Inhibition of the *C*-P4H leads to a reduction in the structural stability of collagen likely preventing interaction with other collagen strands in the extracellular matrix, suggesting potential therapeutic invention of *C*-P4H will be useful.[83,84] To date no drugs targeting *C*-P4H have completed clinical trials.

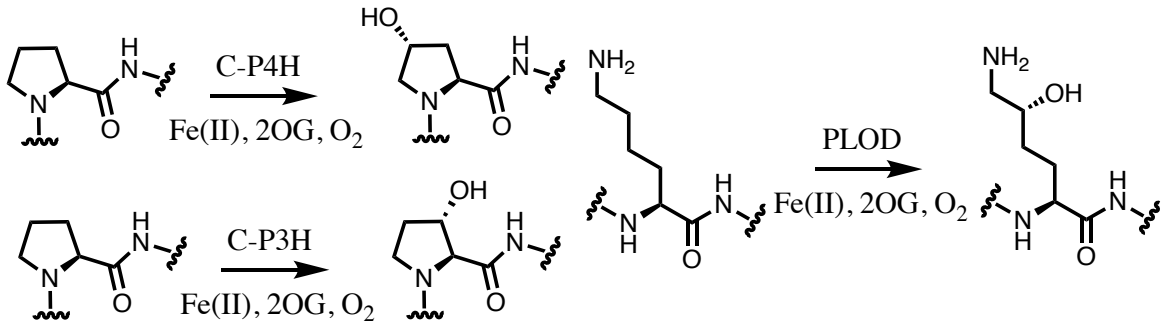

Scheme 2 : Post-translational hydroxylation of proline residues in collagen catalysed by collagen prolyl-4-hydroxylase (C-P4H) and collagen prolyl-3-hydroxylase (C-P3H). The lysine residues in collagen are hydroxylated by the collagen lysine hydroxylase (PLOD).[49]

Ribosome hydroxylases

Ribosomes are large proteins that synthesise proteins in all cells and consist of a large and small subunit using messenger RNA (mRNA) as the code and aminoacyl-transfer RNAs (tRNA) as substrates to form the desired protein. Three 2OG oxygenases: NO66, MINA53 and OGFOD1 are human ribosomal hydroxylases.[49,50] NO66 and human MINA53 hydroxylate at the *C*-3 position of histidinyl residues in Rp18 and Rpl27a, respectively.[90-92] These histidinyl residues extend into the core of the ribosome; however, it is unknown what the function of the post-translation modifications are. Studies suggest that NO66 and MINA53 regulate cell proliferation and growth.[90-92]

OGFOD1 hydroxylates at the *C*-3 position of a proline residue of the small ribosomal subunit RPS23 in humans, a post-translational modification that is conserved in all eukaryotes (**Scheme 3**).[93,94] This proline residue is the closest amino acid to the ribosomal decoding centre and in yeast has a major impact on recognizing the stop codon.[93] OGFOD1 knockouts resulted in translational arrest, growth defects and stress granule formation and it has been suggested that OGFOD1 has a role in cell growth.[93,94]

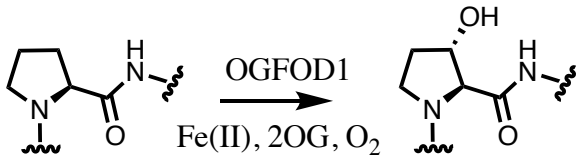

Scheme 3 : Post translational modification of ribosomal residue RPS23. *C*-3 prolyl hydroxylation catalysed by OGFOD1.[49]

Histone Demethylases

DNA is packaged into chromatin by histones, small (100 - 150 aa) basic globular proteins. In order to form nucleosomes, each nucleosome typically consists of eight histone proteins. The eight histones make up four pairs known as H2A, H2B, H3 and H4. Methylation of N^{ε}-methyl transcriptional lysines is a transcription regulatory mechanism that either represses or activates depending on the context.[49,50] N^{ε}-demethylation of lysines complements the methylation of the histone tails to establish a dynamic response in transcriptional regulation. Histones can additionally be post-translationally modified via ubiquitnation, acetylation and phosphorylation. Histone methylation is especially prevalent on the histone H3 *N*-terminal tail, modifications can lead to a high complexity of genetic regulation.[49,50] Post-translational modification of these histone tails plays a central role in epigenetic regulation of gene expression in part *via* regulation of the accessibility of DNA for transcription. Some histones modifying enzymes are regarded as drug targets.[95]

The histone lysine demethylases (KDMs) are split into two groups depending on the catalytic mechanism. The lysine-specific demethylases or KDM1 operate via a flavin dependent oxidase mechanism and are limited to only to di- and mono-methylated lysine residues as substrates.[53,96-98] The 2OG-dependent KDMs (KDM2-7 subfamilies) belong to the Jmjc subfamily; the Jmjc domain is required for their catalytic activity. There are ~15 human 2OG-dependent KDMs, which work via the consensus 2OG oxygenase mechanism producing an hemiaminal intermediate, this fragments into the demethylated product and formaldehyde, this mechanism allows for tri-, di- and mono lysine demethylation (**Scheme 4**).[49,50,52,98]

Over production of Jmjc KDMs has been linked to genetic diseases linked to neural function and development, such as autism and X-linked mental retardation.[99,100] Over-expressed JmjC KDMs has been observed in several cancers.[99,100] Due to the high level of complexity of KDM involved genetic regulation, the functions of individual KDMs are still to be fully elucidated and therefore drug discovery is at an early stage. Four clinically used inhibitors for chromatin-modifying enzymes are in use, the histone methyltransferase inhibitors (Decitabine and Azacitidine) and two histone deacetylase inhibitors (Romidepsin and Vorinostat).[101-103]

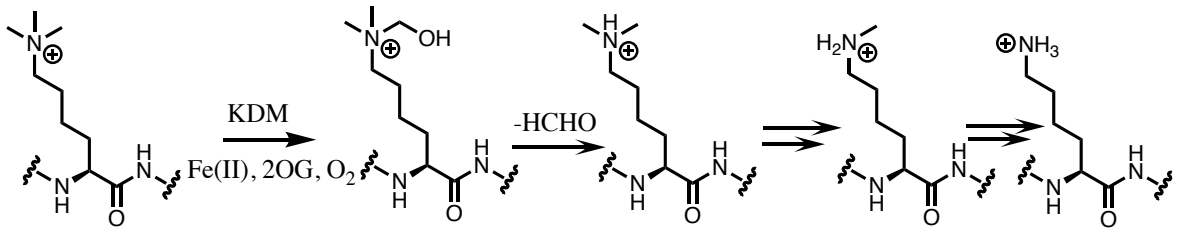

Scheme 4 : The 2OG dependent histone lysine demethylases (KDM) catalyse the N$^{\varepsilon}$-demethylation of all three methylated forms of *N*$^{\varepsilon}$-methylated of lysines.[49]

Nucleic Acid Modifications Catalysed by 2OG Oxygenases

Modifications to nucleic acids play key roles in gene expression regulation and over a 100 different types of post-translational modifications have been identified on RNA. Methylation of adenine to give *N*^{6}-methyladenine (m^{6}A) is the most frequent modification observed in eukaryotes for nucleic acids.[49,50,104] To date, the physiological roles of m^{6}A are still not fully understood. The methylation of adenine is common and has been suggested that this methylation plays a role in the regulation of gene expression in both diseased and healthy cells.[105] Two human 2OG oxygenases are reported, the fat and mass obesity-associated protein (FTO) which catalyses the demethylation of m^{6}A and AlkB homologue 5

(ALKBH5).[104,106,107] FTO is found in the brain and is regulated by fasting and feeding, therefore has been suggested as a targeted treatment of obesity.[108]

There are 8 human homologues of the E. coli enzyme AlkB that catalyse a wide range of demethylation and hydroxylation reactions; only AlkBH2 and 3 have been reported to catalyse DNA demethylation.[49] AlkBH2 demethylates *N*[1]-methyladenine (m[1]A) and *N*[3]-methylcytosine (m[3]C) of a double-stranded DNA, while AlkBH3 selectively catalyses demethylation of m1A and m3C in single stranded DNA.[104,108]

Other 2OG oxygenases using nucleic acids as substrates have been reported, including the ten-eleven translocation enzymes (TETs 1-3), which hydroxylate 5 methylcytosine (5mC) to form 5-hydroxymethylcytosine (5hmC) leading to 5-formylcytosine (5fC) and 5-carboxycytosine (5caC) are reported.[49,50,104,109]

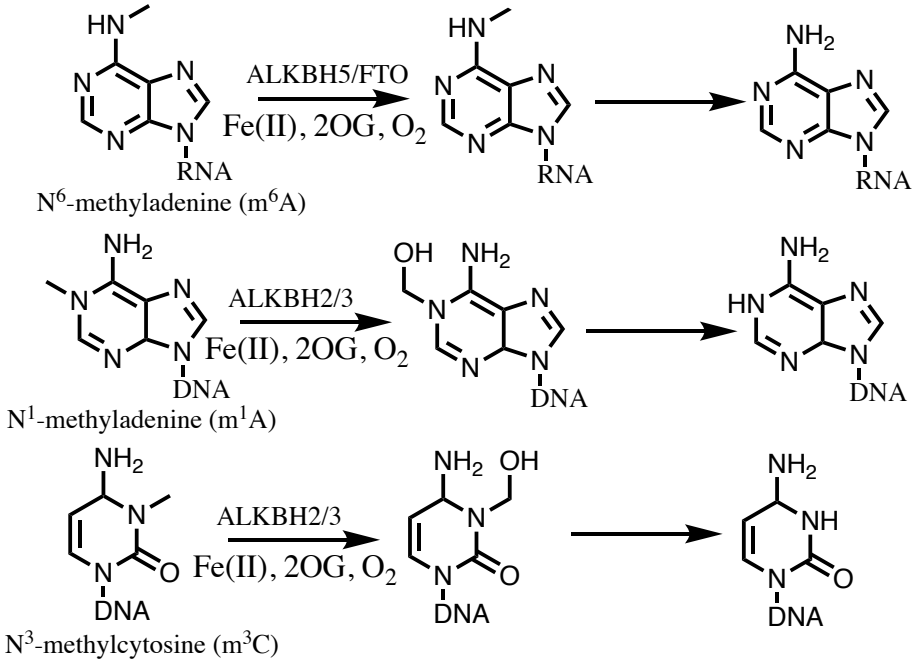

Scheme 5 : An overview of 2OG dependent nucleic acid demethylation reactions. ALKBH5 and FTO act principally on RNA and ALKBH2/3 on DNA.[49]

1.7 Therapeutic Application of HIF PHD inhibitors

Anaemia

A decrease in the amount of red blood cells (erythrocytes) in circulation (referred to as anaemia) is a major contributor to global mortality and morbidity.[110] A recent study suggested one third of the global population may be affected. Anaemia can occur in various ways, including infection, nutrition, chronic kidney disease and iron deficiency.[111] Deficiencies in Erythropoietin (EPO) are broadly linked to anaemia associated with multiple chronic diseases especially those linked to systemic inflammation.[19] EPO production mainly occurs in the liver and kidneys, although many other organs express EPO at relatively low levels. EPO production has been shown to be substantially sensitive to changes in oxygen concentrations in the blood (prompted the physiological investigation into hypoxic genetic regulation).[19]

Recombinant human EPO (rhEPO) is currently used to treat anaemia in patients, however HIF PHD inhibitors have potential advantages over current treatments.[19,112,113] Firstly unlike EPO, they can be delivered orally. Many clinical studies have indicated that higher doses of rhEPO correlate with an increase in cardiovascular events. This has been linked to the high doses of rhEPO rather than the increased levels of haemoglobin.[114] High plasma concentrations of EPO have been linked to vascular toxicity.[115] In contrast, clinical studies using PHD inhibitors have shown targeted levels of haemoglobin can be achieved with normal physiological plasma concentrations of EPO.[116-119] It is possible that activating the HIF pathway may improve effects of EPO *via* other synergistic HIF mediated pathways.[19]

HIF target genes are involved in iron metabolism, transport and absorption and thereby potentially enhancing iron availability for erythropoiesis.[15,120] However, the additional effects are difficult to predict due to the broad tissue distribution and the complexity of the HIF system.

Ischaemia

Poor blood flow (organ ischaemia) is one of the biggest clinical problems of the modern age, occurring in circulatory and cardiovascular diseases and potentially during surgical operations.[19] Poor organic flow commonly affects the kidneys, limbs, heart and the brain and can be either chronic or acute.[19] Hypoxia occurs in all ischaemic environments. The HIF system is induced to an extent, but it is complicated by metabolite clearance and delivery.[121-124] It has been envisaged that using PHD inhibitors will augment the HIF stabilisation and be protective and/or reparative will respond to ischaemic diseases.[19] A substantial amount of protective ischaemic protective pathways are linked to HIF. Longer term effects of stabilised HIF may include stem cell activation, angiogenesis and revascularisation.[125,126] Multiple studies have been aimed to answer whether the system of HIF activation can improve the effect of ischaemia in animal models. Most studies suggested a positive effect of PHD inhibitors in the short term; however, the long term effects are unknown.[19]

Inflammation

Inflammation occurs due to multiple factors, such as dysregulated immunity, tissue injury and responses to pathogens.[19] Inflammation is a common response in multiple diseases.[19] The HIF system is activated by hypoxically inflamed tissue and by non-hypoxic pathways.[21] The HIF system broad affects on inflammatory and immune cells, such as apoptosis, differentiation and cytokine production.[21] Various studies described conflicting responses in different cell lines. It has been suggested that these conflicting responses are due to opposing effects of the HIFα isoforms (HIF1α vs HIF2α).[19] For example, macrophage activation can be phenotypically modified to either the HIF1α mediated response M1 (pro-inflammatory) or the HIF-2α mediated response M2 (anti-inflammatory).[127] The role of HIF pathway in the inflammatory response is complex because of its widespread effects on inflammatory and non-inflammatory cells, such as destabilising cell entry.[128]

Mouse model studies using PHD inhibitors have shown HIF activation has a positive effect on inflammation.[129] Administration of FG-4497 in a colitis mouse model reduced inflammatory infiltrate and increased tissue architecture preservation.[129] HIF-1α mediated responses were proposed to account for the improved outcome.[129] Administration of PHD inhibitor FG-4497 in a sepsis-induced lung injury reduced lung injury and improved survival rate.[130] In contrast to the previous example, it was suggested that the protective response was via HIF-2α mediated response by maintaining lung vascular barriers via upregulation of vascular endothelial protein tyrosine phophatase (VE-PTP).[130]

1.8 Inhibitors of The PHDs in Clinical Trials

Small molecule inhibition of the 2OG oxygenases for human medicinal chemistry began from the pioneering work of the collagen prolyl hydroxylases (CPH).[19] However, CPH medicinal chemistry projects were halted due to unforeseen effects, possibly due to inhibition of then to be discovered PHDs.[19] The inhibitors developed in the early work for CPHs were non-selective inhibitors for the 2OG oxygenases such as pyridine-2,4-dicarboxylate, *N*-oxalylglycine (NOG) (**1**) and pro-drug versions of NOG such as dimethyl ester of *N*-oxalylglycine (DMOG) (**2**).[6,8,131] However, these inhibitors were useful to validate the PHDs as potential drug targets.[6,8,131] Structure activity relationship (SAR) of NOG analogues demonstrated that relative selectivity within the 2OG oxygenases could be achieved with NOG analogues.[132] To date, the majority of medicinal chemistry efforts on the PHDs have largely focused on the catalytic domain and using 2OG as a template (**Figure 6**). Most reported PHD inhibitors developed to date are likely to work by interacting with the active site of PHDs competing with 2OG (shown by work on PHD2), usually binding to the ferrous iron in a bidentate manner and not displacing HIF-α from the enzyme-substrate complex.[56,67,133,134]

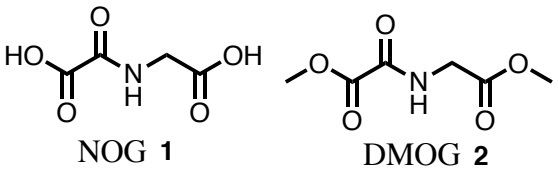

Figure 6 : Chemical structures of the early stage 2OG oxygenase inhibitors, DMOG is a prodrug form of NOG.[19]

PHD inhibitors have entered clinical trials for anaemia treatment, with the first PHD inhibitor tested clinically being FG-2216 (**3**) from Fibrogen. **3**, to date is one of the best studied PHD inhibitors. **3** is a bicyclic isoquinoline with a glycinamide side chain, identical to that in NOG and which is conversed in all but one clinically trialled PHD inhibitor.[67,133] Crystallographic analysis revealed the glycinamide side chain of **3** interacts with PHD2 (in an identical manner to NOG and 2OG) forming electrostatic interactions with Arg-383 and potentially Tyr-329 (**Figure 7A**).[67,133] **3** binds to the ferrous iron via the carbonyl oxygen of the glycinamide side chain and the isoquinolyl nitrogen. The *C*-3 hydroxyl group forms a hydrogen bond with residue Tyr-303, suggested by SAR as important for PHD2 inhibition.[67,133] The isoquinoline ring slots in the entrance of the active site between the hydrophobic aromatic amino acids (**Figure 7A**).[67,133] Clinical trials with **3** were suspended in 2007 by the FDA due to an adverse event. Although the FDA allowed trials of **3** to continue, Fibrogen replaced **3** with the structurally similar compound FG-4592 (**4**).[19] The main difference between the two clinically trialled PHD inhibitors from Fibrogen is the addition of a phenoxy-group on the isoquinolyl ring. It has been suggested that **4** displaces HIF-α substrates in comparison to **3** (**Figure 7C**).[19] Indeed, NMR-based competition binding assay indicates that **4** partially displaces the CODD substrate; whereas **3** did not displace the CODD substrate (**Figure 10A**).[135] However, cell-based results suggest no substrate selectivity for NODD and CODD.[135] Unfortunately, no reported co-crystal structures exist for FG-4592 (**4**) and other clinically trialled PHD inhibitors such as Daprodustat (**6**) (GSK1278863) and Molidustat (**8**) (BAY 85-3924) with the PHDs. It has been suggested that inhibitors induce conformational change when binding to PHD2, resulting in impeding

crystallographically productive packing. Vadadustat (**5**) is structurally similar to the Fibrogen clinical candidates **3** and **4**, sharing the glycinamide side chain and has a structurally similar 3-hydroxy-pyridine core, i.e. the aromatic moiety of the isoquinoline of FG-2216 replaced with a 5-(3-chlorophenyl)pyridin-3-ol group (**Figure 7B**).[135] **5** is only able to displace the NODD substrate on the NMR competition binding assay, indicating that the different aromatic substituents can impact substrate displacement.[135] A crystal structure of PHD2 complexed with **5** shows a similar binding mode to FG-2216. Indeed, these observed similarities indicate conservation of interactions between this type of inhibitor and therefore it can be proposed that **4** interacts in a similar manner.[135]

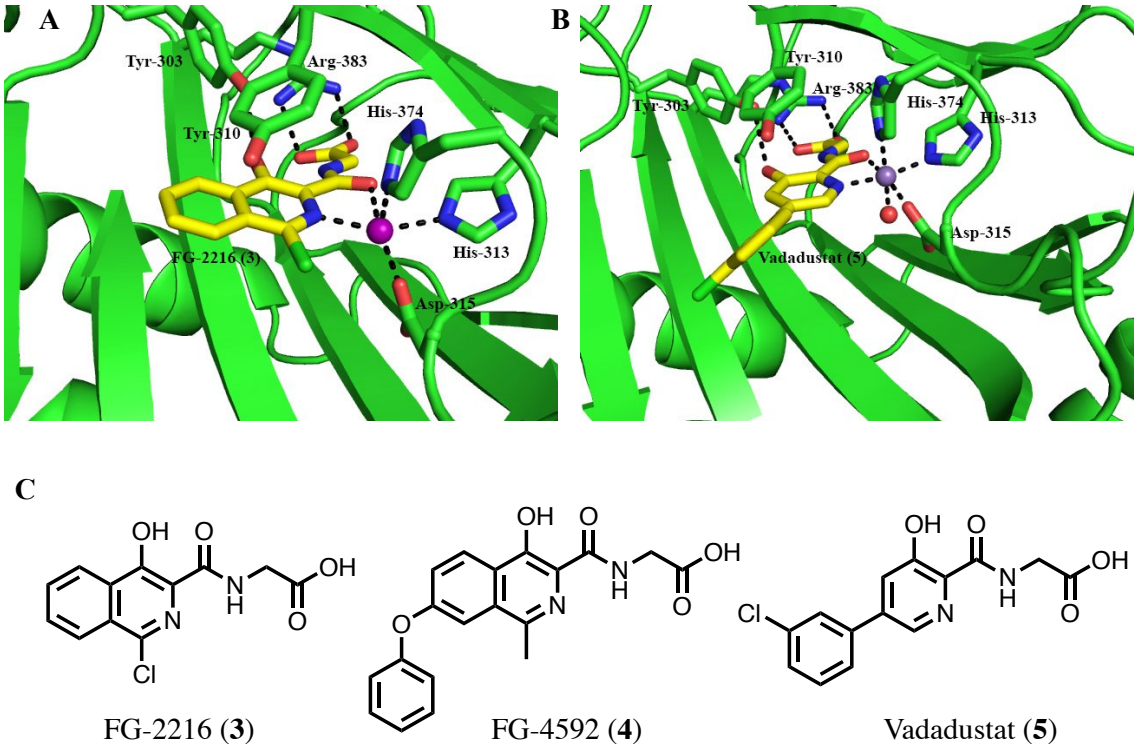

Figure 7 : Views of PHD inhibitor binding modes. **A**) FG-2216 (**3**) (PDB ID: 2y34) [67,133] **B**) Vadadustat (**5**) (PDB ID: 5OX6).[135] Chemical structure of clinical candidates FG-2216 (**3**), FG-4592 (**4**) & Vadadustat (**5**).

Daprodustat (GSK1278863) (**6**) is in clinical trials for anaemia. Like the other clinically trialled PHD inhibitors, **6** shares a 2OG/NOG glycinamide substituent.[19,135,136] However the glycinamide chain is connected to a pyrimidine-trione barbiturate ring in which the nitrogens are functionalised by two cyclohexyl rings.[19,135-137] Similar to **4**, there is no crystal structure to confirm the binding mode of **6**. CCT6 (**7**) is a structurally similar inhibitor to **6** and a crystal structure with PHD2 has been reported (**Figure 8**).[135] The only difference between **6** and **7** is the N substituent. **6** has cyclohexane rings, whilst **7** has the methyl substituent. A crystal structure of PHD2 complexed with **7** reveals identical interaction of the glycinamide motif to those observed with **3** and **5**. **7** binds to the ferrous iron by the carbonyl oxygens of the glycinamide and barbiturate ring.[135] It has been hypothesised that the functionalised cyclohexane rings that point into the HIF-α binding site may disturb HIF-α binding; however, **6** only displaced NODD, but not CODD, in the NMR competition binding assay.[135] The cyclohexane rings of **6** have been observed to undergo hydroxylation producing multiple metabolites via the P450 enzyme. Some reports have suggested that the hydroxylated metabolites may result in altering inhibition for PHD2 and other 2OG oxygenases.[136,137]

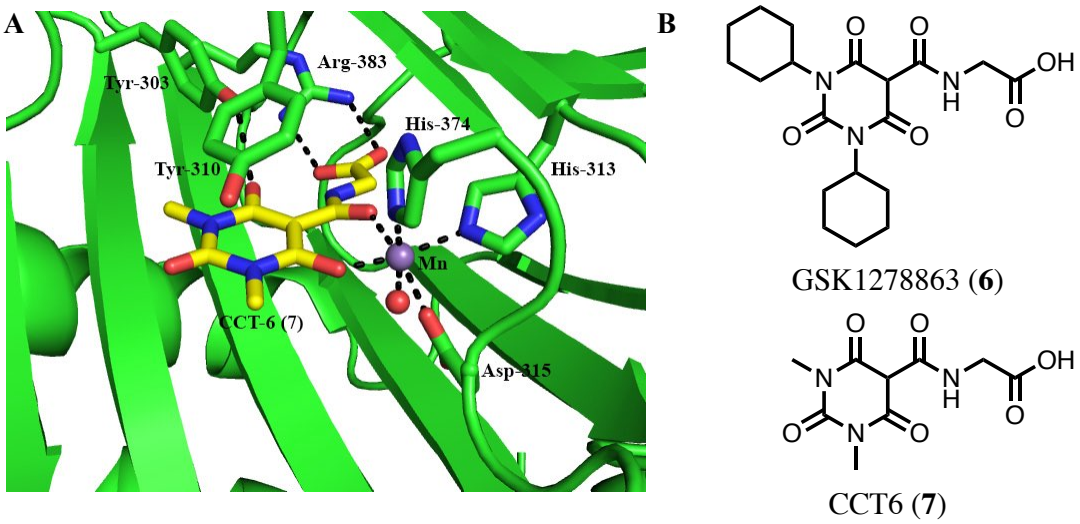

Figure 8 : **A**) View of CCT6 (**7**) binding mode to PHD2 (PDB ID: 5OX5).[135] **B**) Chemical structures of the barbiturate based PHD inhibitors **6** & **7**.

Molidustat (BAY 85-3924) (**8**) which has been developed by Bayer, is currently in clinical trials for anaemic diseases.[117] **8** structurally differs from the other clinically trialled PHD inhibitors. **8** has a 4-linked cyclic inhibitor, with a triazole linked to di-hydropyrazole to a pyrimidine ring (on the 4-position), which has a morpholine motif (on the 6-position) of the pyrimidine ring.[134] There is no binding information on **8** with the PHDs; however, recent work has provided structural information on the structurally related compound IOX4 (**9**).[134] This series of inhibitors bind similarly to PHD inhibitors described above. However, instead of the *C*-5 carboxylate replicating 2OG interactions, it is replaced by a triazole (**Figure 9**). NMR results indicate that **8** binds PHD2 competitively with 2OG and crystallographic analysis reveals **9** binds to the ferrous iron between the nitrogen atoms of the pyrimidine and pyrazolone rings.[134] The NMR displacement assays with both the NODD and CODD substrates indicated that Molidustat did not displace either substrate.[135]

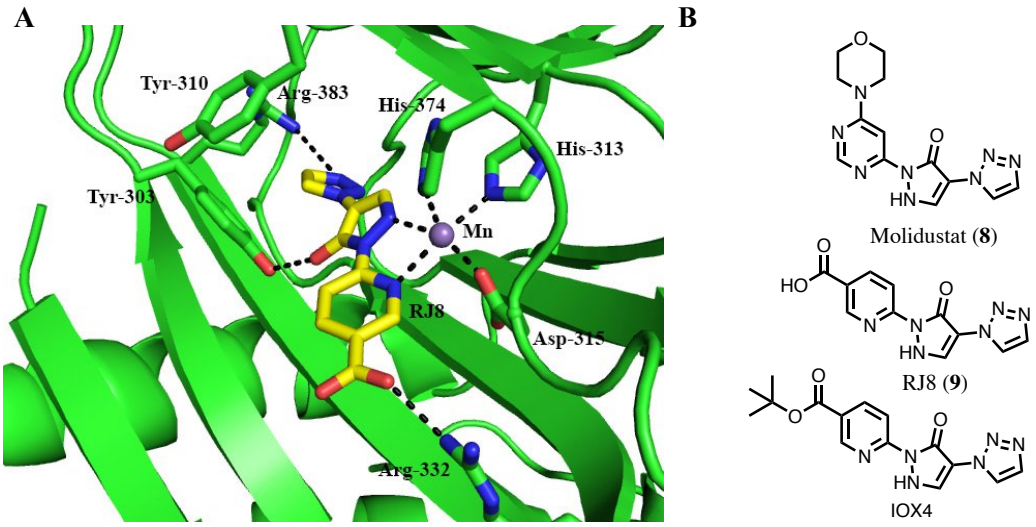

Figure 9: **A**) View of PHD2 inhibitor RJ8 binding mode of PHD2 (PDB ID: 5A3U).[19,134] **B**) Chemical structures of structurally similar PHD2 inhibitors RJ8, **8** and **9**.

Biophysical analyses have revealed that all clinical candidates displace 2OG by chelating to the ferrous iron in the active site.[135] Indeed, competition studies involving 2OG, HIF-1α substrates using 1D selective HSQC NMR suggested differences in the extent of substrate displacement, described above. However, the cellular results do not show NODD/CODD selectivity.[135] Displacement of HIF-1α substrates does not correlate with inhibition of 2OG binding; 2OG competition would prevent hydroxylation of substrate irrelevant of substrate displacement. Indeed, overlaying views from crystal structures of $PHD2_{181-426}$ complexed with structurally similar inhibitors to the clinical candidates and the CODD substrate suggests that some of the clinical candidates should displace the CODD substrate from the active site region (**Figure 10)**. According to **Figure 10B**, Vadadustat (**5**) may be predicted to displace the CODD substrate, yet no displacement was observed by using NMR. GSK1278863 (**6**) (**Figure 10C**) model suggests that the cyclohexane ring of **6** sterically clashes with the CODD substrate.

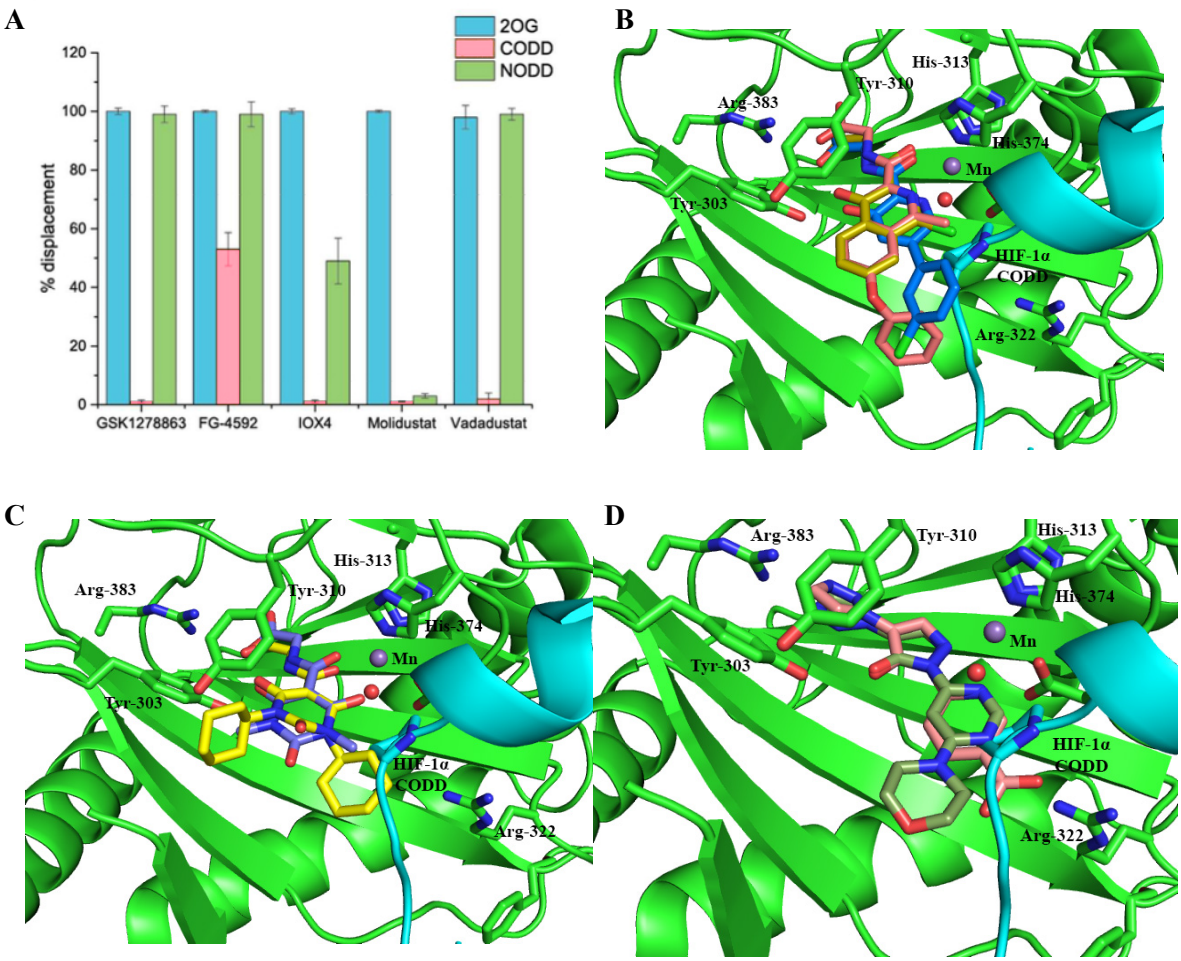

Figure 10 : **A**) Percentage of displacement observed of NODD/CODD substrates caused by the addition of PHD inhibitors to PHD2.Zn(II).2OG.^{13}NODD or ^{13}CODD adapted from Yeh *et al.*[135] **B**) Views from crystal structure of $PHD2_{181\text{-}426}$ complexed with FG-2216 (**3**) (PDB ID: 2y34), overlaid with crystal structure of $PHD2_{181\text{-}426}$ complexed Vadadustat (**5**) (PDB ID: 5OX6), an overlay of FG-4592 (model).[67,135] **C**) View from crystal structure of $PHD2_{181\text{-}426}$ complexed with CCT6 (**7**) (PDB ID: 5OX5) and an overlay of GSK1278863 (**6**) (model).[135] **D**) View from crystal structure of $PHD2_{181\text{-}426}$ complexed with **RJ8** (PDB ID: 5A3U), an overlay of Molidustat (**8**).[19]

The common use of 2OG, ferrous iron suggests that mimicking how 2OG interacts within the active site and chelating to the ferrous iron may result in inhibition of other 2OG oxygenases.[49,50,138] As stated previously, the human 2OG oxygenases (of which there are ~60) oxidise a diverse range of substrates and are involved in a broad range of biological functions (**Chapter 1.6**). **Figure 11** shows the possible therapeutic effects of inhibitors inhibiting the PHDs and other 2OG oxygenases. The role of many 2OG oxygenases are

involved in regulation of gene expression (e.g nucleic acid and histone demethylases) and therefore may alter the biological therapeutic effect of the PHD inhibitors if inhibited.[49,50,138]

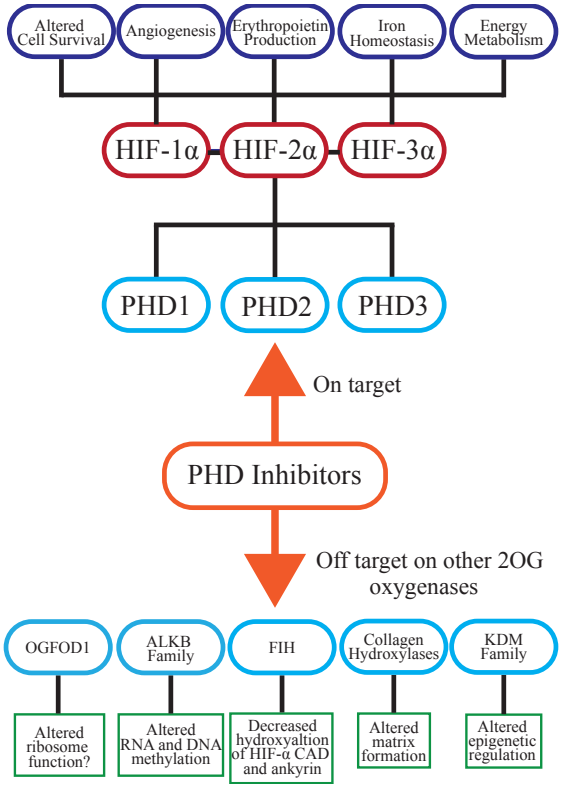

Figure 11: Selected potential on-target and off-target effects of PHD2 inhibitors and other 2OG oxygenases. Figure adapted from Maxwell *et al*. [138]

The selectivity of the PHD2 clinical candidates were tested (IC_{50}s) against a representative selection of 2OG oxygenases, all testing was performed by members of the Schofield group (**Table 1**).[135] FIH was screened because HIF target genes are regulated by FIH, which has additional non HIF-α substrates. OGFOD1, vCPH and Tpa1p were screened because they are all prolyl hydroxylases and their active sites are closely related to PHD2. JARID1A and JMJD3 were screened as representation of the JmjC histone Nε-methyl KDM family. Different levels of inhibition within the PHD isoforms (PHD 1-3), may reflect the overall

therapeutic effects of the PHD inhibitors.[135] **Table 1** shows the screening results of the clinical candidates against the selected panel of 2OG oxygenases. In general, the results indicated the clinical candidates inhibit other 2OG oxygenases less well than the PHDs. However, FG-4592 (**4**), GSK1278863 (**6**), Molidustat (**8**) and Vadadustat (**5**) showed similar or stronger levels of inhibition of OGFOD1 and vCPH in comparison to PHD inhibition. **4, 5, 6** and **8** showed similar levels of inhibition for the PHD isoforms. All of the clinical candidates showed strong selectivity for the PHDs over FIH and the JmjC histone N$^{\varepsilon}$-methyl lysine demethylases JARID1A and JMJD3. The high levels of inhibition of OGFOD1 and vCPH suggest that mimicking how 2OG interacts could lead to inhibition of structurally similar 2OG oxygenases. Overall, the therapeutic effect of these PHD inhibitors in a clinical setting, may differ due to off-target inhibition of other 2OG oxygenases, especially if the treatment is long term anaemia (**Figure 11**).

Table 1 : Selectivity of FG-4592 (**4**), GSK1278863 (**6**), Molidustat (**8**) and Vadadustat (**5**) against isolated recombinant human 2OG dependent oxygenases. Adapted from Yeh *et al*.[135] Assay conditions have been previously reported [135]. PHD1-3, FIH, vCPH: viral Collagen Prolyl Hydroxylase. OGFOD1: 2OG and iron-dependent oxygenase domain containing 1, Tpa1p: termination and polyadenylation protein 1, JARID1A (KDM5A); lysine-specific demethylase 5A, JMJD3 (KDM6B): lysine-specific demethylase 6B.

	IC_{50} [μM]									
CPD	PHD2 Rapid Fire™	PHD1 MALDI	PHD2 MALDI	PHD3 MALDI	FIH	vCPH	OGFOD 1	Tpa1p	JARID1 A(KDM 5A)	JMJD3 (KDM6 B)
4	**2.76**	**1.4**	**1.26**	**1.32**	**>100**	**5**	**<1**	**12.8**	**>100**	**>100**
6	**0.09**	**1.5**	**2.87**	**0.61**	**21**	**13**	**2.1**	**5.1**	**>100**	**>100**
8	**1.32**	**1.45**	**1.85**	**0.72**	**66**	**26.8**	**5.1**	**3.8**	**>100**	**35**
5	**1.33**	**0.84**	**2.30**	**0.26**	**29**	**1**	**1.4**	**ND**	**30**	**37**

1.9 Thesis Outline

The work in this thesis focused on the development of novel PHD inhibitors with strong selectivity over structurally similar 2OG oxygenases. The specific aims of the work are described:

- To discover and characterise initial hits that fit a required criteria for the development of selective PHD inhibitors (**Chapter 2**)
- Structure activity relationship of the initial hits (**Chapter 3**).
- The use of discovered and developed structural knowledge to develop novel PHD inhibitors (**Chapter 4**).
- Investigation of small molecules that increased the turnover of CODD substrate via PHD2 interaction (**Chapter 5**).

Chapter 6 describes related work outside of the primary aim of thesis.

- The development of novel mitochondrial complex 1 inhibitors to reduce the oxygen consumption rate (OCR) to reduce resistance to radiotherapy in cancer cells (**Chapter 6**).

1.10 References

1 Wang, G. L., Jiang, B., Rue, E. A. & Semenza, G. L. Hypoxia-Inducible Factor 1 is a Basic-Helix-Loop-Helix-PAS Heterodimer Regulated by Cellular O2 Tension. *Proceedings of the National Academy of Sciences* **92**, 5510-5514, doi:10.1073/pnas.92.12.5510 (1995).

2 Schofield, C. J. & Ratcliffe, P. J. Oxygen sensing by HIF hydroxylases. *Nat Rev Mol Cell Biol* **5**, 343-354, doi:10.1038/nrm1366 (2004).

3 Kaelin, W. G., Jr. & Ratcliffe, P. J. Oxygen sensing by metazoans: the central role of the HIF hydroxylase pathway. *Mol Cell* **30**, 393-402 (2008).

4 Maxwell, P. H., Wiesener, M. S., Chang, G. W., Clifford, S. C., Vaux, E. C., Cockman, M. E. *et al.* The tumour suppressor protein VHL targets hypoxia-inducible factors for oxygen-dependent proteolysis. *Nature* **399**, 271-275 (1999).

5 Bruick, R. K. & McKnight, S. L. A conserved family of prolyl-4-hydroxylases that modify HIF. *Science (Washington, DC, U. S.)* **294**, 1337-1340, doi:10.1126/science.1066373 (2001).

6 Epstein, A. C. R., Gleadle, J. M., McNeill, L. A., Hewitson, K. S., O'Rourke, J., Mole, D. R. *et al.* C. elegans EGL-9 and mammalian homologs define a family of dioxygenases that regulate HIF by prolyl hydroxylation. *Cell (Cambridge, MA, U. S.)* **107**, 43-54, doi:10.1016/S0092-8674(01)00507-4 (2001).

7 Ivan, M., Kondo, K., Yang, H., Kim, W., Valiando, J., Ohh, M. *et al.* HIFα targeted for VHL-mediated destruction by proline hydroxylation: Implications for O2 sensing. *Science (Washington, DC, U. S.)* **292**, 464-468, doi:10.1126/science.1059817 (2001).

8 Jaakkola, P., Mole, D. R., Tian, Y. M., Wilson, M. I., Gielbert, J., Gaskell, S. J. *et al.* Targeting of HIF-alpha to the von Hippel-Lindau ubiquitylation complex by O-2-regulated prolyl hydroxylation. *Science* **292**, 468-472 (2001).

9 Dames, S. A., Martinez-Yamout, M., De Guzman, R. N., Dyson, H. J. & Wright, P. E. Structural basis for HIF-1a/CBP recognition in the cellular hypoxic response. *Proceedings of the National Academy of Sciences of the United States of America* **99**, 5271-5276 (2002).

10 Freedman, S. J., Sun, Z.-Y. J., Poy, F., Kung, A. L., Livingston, D. M., Wagner, G. *et al.* Structural basis for recruitment of CBP/p300 by hypoxia inducible factor-1a. *Proceedings of the National Academy of Sciences of the United States of America* **99**, 5367-5372 (2002).

11 Hewitson, K. S., McNeill, L. A., Riordan, M. V., Tian, Y. M., Bullock, A. N., Welford, R. W. *et al.* Hypoxia-inducible factor (HIF) asparagine hydroxylase is identical to factor inhibiting HIF (FIH) and is related to the cupin structural family. *J Biol Chem* **277**, 26351-26355, doi:10.1074/jbc.C200273200 (2002).

12 Lando, D., Peet, D. J., Whelan, D. A., Gorman, J. J. & Whitelaw, M. L. Asparagine hydroxylation of the HIF transactivation domain: A hypoxic switch. *Science* **295**, 858-861 (2002).

13 McNeill, L. A., Hewitson, K. S., Claridge, T. D., Seibel, J. F., Horsfall, L. E. & Schofield, C. J. Hypoxia-inducible factor asparaginyl hydroxylase (FIH-1) catalyses hydroxylation at the beta-carbon of asparagine-803. *Biochem J* **367**, 571-575, doi:10.1042/BJ20021162 (2002).

14 Wenger, R. H., Stiehl, D. P. & Camenisch, G. Integration of oxygen signaling at the consensus HRE. *Sci STKE* **2005**, re12 (2005).

15 Chowdhury, R., Hardy, A. & Schofield, C. J. The human oxygen sensing machinery and its manipulation. *Chem Soc Rev* **37**, 1308-1319 (2008).

16 Semenza, G. L. Hypoxia-inducible factors in physiology and medicine. *Cell* **148**, 399-408, doi:10.1016/j.cell.2012.01.021 (2012).

17 Prabhakar, N. R. & Semenza, G. L. Adaptive and maladaptive cardiorespiratory responses to continuous and intermittent hypoxia mediated by hypoxia-inducible factors 1 and 2. *Physiol Rev* **92**, 967-1003, doi:10.1152/physrev.00030.2011 (2012).

18 Masson, N. & Ratcliffe, P. J. Hypoxia signaling pathways in cancer metabolism: the importance of co-selecting interconnected physiological pathways. *Cancer Metab* **2**, 3, doi:10.1186/2049-3002-2-3 (2014).

19 Chan, M. C., Holt-Martyn, J. P., Schofield, C. J. & Ratcliffe, P. J. Pharmacological targeting of the HIF hydroxylases - A new field in medicine development. *Molecular aspects of medicine* **47-48**, 54-75, doi:10.1016/j.mam.2016.01.001 (2016).

20 Nizet, V. & Johnson, R. S. Interdependence of hypoxic and innate immune responses. *Nat Rev Immunol* **9**, 609-617, doi:10.1038/nri2607 (2009).

21 Eltzschig, H. K. & Carmeliet, P. Hypoxia and inflammation. *N Engl J Med* **364**, 656-665, doi:10.1056/NEJMra0910283 (2011).

22 Eltzschig, H. K., Bratton, D. L. & Colgan, S. P. Targeting hypoxia signalling for the treatment of ischaemic and inflammatory diseases. *Nat Rev Drug Discov* **13**, 852-869, doi:10.1038/nrd4422 (2014).

23 Tian, H., McKnight, S. L. & Russell, D. W. Endothelial PAS domain protein 1 (EPAS1), a transcription factor selectively expressed in endothelial cells. *Genes Dev.* **11**, 72-82, doi:10.1101/gad.11.1.72 (1997).

24 Zhao, J., Du, F., Shen, G., Zheng, F. & Xu, B. The role of hypoxia-inducible factor-2 in digestive system cancers. *Cell Death Dis* **6**, e1600, doi:10.1038/cddis.2014.565 (2015).

25 Gu, Y. Z., Moran, S. M., Hogenesch, J. B., Wartman, L. & Bradfield, C. A. Molecular characterization and chromosomal localization of a third alpha-class hypoxia inducible factor subunit, HIF3alpha. *Gene Expr* **7**, 205-213 (1998).

26 Maynard, M. A., Qi, H., Chung, J., Lee, E. H. L., Kondo, Y., Hara, S. *et al.* Multiple Splice Variants of the Human HIF-3alpha Locus Are Targets of the von Hippel-Lindau E3 Ubiquitin Ligase Complex. *J. Biol. Chem.* **278**, 11032-11040, doi:10.1074/jbc.M208681200 (2003).

27 Dengler, V. L., Galbraith, M. D. & Espinosa, J. M. Transcriptional regulation by hypoxia inducible factors. *Crit Rev Biochem Mol Biol* **49**, 1-15, doi:10.3109/10409238.2013.838205 (2014).

28 Pasanen, A., Heikkila, M., Rautavuoma, K., Hirsila, M., Kivirikko, K. I. & Myllyharju, J. Hypoxia-inducible factor (HIF)-3alpha is subject to extensive alternative splicing in human tissues and cancer cells and is regulated by HIF-1 but not HIF-2. *Int J Biochem Cell Biol* **42**, 1189-1200, doi:10.1016/j.biocel.2010.04.008 (2010).

29 Heikkila, M., Pasanen, A., Kivirikko, K. I. & Myllyharju, J. Roles of the human hypoxia-inducible factor (HIF)-3alpha variants in the hypoxia response. *Cell Mol Life Sci* **68**, 3885-3901, doi:10.1007/s00018-011-0679-5 (2011).

30 Hu, C. J., Sataur, A., Wang, L., Chen, H. & Simon, M. C. The N-terminal transactivation domain confers target gene specificity of hypoxia-inducible factors HIF-1alpha and HIF-2alpha. *Mol Biol Cell* **18**, 4528-4542, doi:10.1091/mbc.E06-05-0419 (2007).

31 Lau, K. W., Tian, Y. M., Raval, R. R., Ratcliffe, P. J. & Pugh, C. W. Target gene selectivity of hypoxia-inducible factor-alpha in renal cancer cells is conveyed by post-DNA-binding mechanisms. *Br J Cancer* **96**, 1284-1292, doi:10.1038/sj.bjc.6603675 (2007).

32 Koh, M. Y., Lemos, R., Jr., Liu, X. & Powis, G. The hypoxia-associated factor switches cells from HIF-1alpha- to HIF-2alpha-dependent signaling promoting stem cell characteristics, aggressive tumor growth and invasion. *Cancer Res* **71**, 4015-4027, doi: 10.1158/0008-5472.CAN-10-4142 (2011).

33 Koh, M. Y. & Powis, G. Passing the baton: the HIF switch. *Trends Biochem Sci* **37**, 364-372, doi:10.1016/j.tibs.2012.06.004 (2012).

34 Hu, C.-J., Wang, L.-Y., Chodosh, L. A., Keith, B. & Simon, M. C. Differential roles of hypoxia-inducible factor 1alpha (HIF-1alpha) and HIF-2alpha in hypoxic gene regulation. *Mol Cell Biol* **23**, 9361-9374 (2003).

35 Takeda, N., Maemura, K., Imai, Y., Harada, T., Kawanami, D., Nojiri, T. *et al.* Endothelial PAS domain protein 1 gene promotes angiogenesis through the transactivation of both vascular endothelial growth factor and its receptor, Flt-1. *Circ Res* **95**, 146-153, doi:10.1161/01.RES. 0000134920.10128.b4 (2004).

36 Zheng, X., Linke, S., Dias, J. M., Zheng, X., Gradin, K., Wallis, T. P. *et al.* Interaction with factor inhibiting HIF-1 defines an additional mode of cross-coupling between the Notch and hypoxia signaling pathways. *Proc Natl Acad Sci U S A* **105**, 3368-3373, doi:10.1073/pnas. 0711591105 (2008).

37 Zhang, P., Yao, Q., Lu, L., Li, Y., Chen, P. J. & Duan, C. Hypoxia-inducible factor 3 is an oxygen-dependent transcription activator and regulates a distinct transcriptional response to hypoxia. *Cell Rep* **6**, 1110-1121, doi:10.1016/j.celrep.2014.02.011 (2014).

38 Yang, S. L., Wu, C., Xiong, Z. F. & Fang, X. Progress on hypoxia-inducible factor-3: Its structure, gene regulation and biological function (Review). *Mol Med Rep* **12**, 2411-2416, doi: 10.3892/mmr.2015.3689 (2015).

39 Hara, S., Hamada, J., Kobayashi, C., Kondo, Y. & Imura, N. Expression and characterization of hypoxia-inducible factor (HIF)-3 alpha in human kidney: Suppression of HIF-mediated gene expression by HIF-3 alpha. *Biochemical and Biophysical Research Communications* **287**, 808-813 (2001).

40 Hatanaka, M., Shimba, S., Sakaue, M., Kondo, Y., Kagechika, H., Kokame, K. *et al.* Hypoxia-inducible factor-3alpha functions as an accelerator of 3T3-L1 adipose differentiation. *Biol Pharm Bull* **32**, 1166-1172 (2009).

41 Hogenesch, J. B., Gu, Y. Z., Jain, S. & Bradfield, C. A. The basic-helix-loop-helix-PAS orphan MOP3 forms transcriptionally active complexes with circadian and hypoxia factors. *Proc Natl Acad Sci U S A* **95**, 5474-5479 (1998).

42 Sekine, H., Mimura, J., Yamamoto, M. & Fujii-Kuriyama, Y. Unique and overlapping transcriptional roles of arylhydrocarbon receptor nuclear translocator (Arnt) and Arnt2 in xenobiotic and hypoxic responses. *J Biol Chem* **281**, 37507-37516, doi:10.1074/jbc.M606910200 (2006).

43 Carver, L. A., Hogenesch, J. B. & Bradfield, C. A. Tissue specific expression of the rat Ah-receptor and ARNT mRNAs. *Nucleic Acids Res* **22**, 3038-3044 (1994).

44 Drutel, G., Kathmann, M., Heron, A., Schwartz, J. C. & Arrang, J. M. Cloning and selective expression in brain and kidney of ARNT2 homologous to the Ah receptor nuclear translocator (ARNT). *Biochem Biophys Res Commun* **225**, 333-339, doi:10.1006/bbrc.1996.1176 (1996).

45 Hirose, K., Morita, M., Ema, M., Mimura, J., Hamada, H., Fujii, H. *et al.* cDNA cloning and tissue-specific expression of a novel basic helix-loop- helix/PAS factor (Arnt2) with close sequence similarity to the aryl hydrocarbon receptor nuclear translocator (Arnt). *Mol. Cell. Biol.* **16**, 1706-1713 (1996).

46 Mandl, M., Kapeller, B., Lieber, R. & Macfelda, K. Hypoxia-inducible factor-1beta (HIF-1beta) is upregulated in a HIF-1alpha-dependent manner in 518A2 human melanoma cells

under hypoxic conditions. *Biochem Biophys Res Commun* **434**, 166-172, doi:10.1016/j.bbrc.2013.03.051 (2013).

47 Wolff, M., Jelkmann, W., Dunst, J. & Depping, R. The Aryl Hydrocarbon Receptor Nuclear Translocator (ARNT/HIF-1beta) is influenced by hypoxia and hypoxia-mimetics. *Cell Physiol Biochem* **32**, 849-858, doi:10.1159/000354487 (2013).

48 Hausinger, R. P. Fe(II)/a-ketoglutarate-dependent hydroxylases and related enzymes. *Crit. Rev. Biochem. Mol.* **39**, 21-68 (2004).

49 Rose, N. R., McDonough, M. A., King, O. N., Kawamura, A. & Schofield, C. J. Inhibition of 2-oxoglutarate dependent oxygenases. *Chem Soc Rev* **40**, 4364-4397, doi:10.1039/c0cs00203h (2011).

50 Aik, W. S., Chowdhury, R., Clifton, I. J., Hopkinson, R. J., Leissing, T., McDonough, M. A. *et al.* in *2-Oxoglutarate-Dependent Oxygenases* 59-94 (The Royal Society of Chemistry, 2015).

51 Loenarz, C. & Schofield, C. J. Physiological and biochemical aspects of hydroxylations and demethylations catalyzed by human 2-oxoglutarate oxygenases. *Trends Biochem Sci* **36**, 7-18, doi: 10.1016/j.tibs.2010.07.002 (2011).

52 Klose, R. J. & Zhang, Y. Regulation of histone methylation by demethylimination and demethylation. *Nat Rev Mol Cell Biol* **8**, 307-318 (2007).

53 Thinnes, C. C., England, K. S., Kawamura, A., Chowdhury, R., Schofield, C. J. & Hopkinson, R. J. Targeting histone lysine demethylases - progress, challenges, and the future. *Biochim Biophys Acta* **1839**, 1416-1432, doi:10.1016/j.bbagrm.2014.05.009 (2014).

54 Aik, W., McDonough, M. A., Thalhammer, A., Chowdhury, R. & Schofield, C. J. Role of the jelly-roll fold in substrate binding by 2-oxoglutarate oxygenases. *Curr Opin Struct Biol* **22**, 691-700, doi:10.1016/j.sbi.2012.10.001 (2012).

55 Dann III, C. E., Bruick, R. K. & Deisenhofer, J. Structure of factor-inhibiting hypoxia-inducible factor 1: an asparaginyl hydroxylase involved in the hypoxic response pathway. *Proceedings of the National Academy of Sciences of the United States of America* **99**, 15351-15356 (2002).

56 McDonough, M. A., Li, V., Flashman, E., Chowdhury, R., Mohr, C., Lienard, B. M. *et al.* Cellular oxygen sensing: Crystal structure of hypoxia-inducible factor prolyl hydroxylase (PHD2). *Proc Natl Acad Sci U S A* **103**, 9814-9819, doi:10.1073/pnas.0601283103 (2006).

57 Krebs, C., Galonic Fujimori, D., Walsh, C. T. & Bollinger, J. M., Jr. Non-heme Fe(IV)-oxo intermediates. *Acc Chem Res* **40**, 484-492 (2007).

58 Flashman, E., Hoffart, L. M., Hamed, R. B., Bollinger, J. M., Jr., Krebs, C. & Schofield, C. J. Evidence for the slow reaction of hypoxia-inducible factor prolyl hydroxylase 2 with oxygen. *Febs J* **277**, 4089-4099 (2010).

59 Tarhonskaya, H., Hardy, A. P., Howe, E. A., Loik, N. D., Kramer, H. B., McCullagh, J. S. *et al.* Kinetic Investigations of the Role of Factor Inhibiting Hypoxia-inducible Factor (FIH) as an Oxygen Sensor. *J Biol Chem* **290**, 19726-19742, doi:10.1074/jbc.M115.653014 (2015).

60 McNeill, L. A., Flashman, E., Buck, M. R., Hewitson, K. S., Clifton, I. J., Jeschke, G. *et al.* Hypoxia-inducible factor prolyl hydroxylase 2 has a high affinity for ferrous iron and 2-oxoglutarate. *Mol Biosyst* **1**, 321-324, doi:10.1039/b511249b (2005).

61 Tarhonskaya, H., Chowdhury, R., Leung, I. K., Loik, N. D., McCullagh, J. S., Claridge, T. D. *et al.* Investigating the contribution of the active site environment to the slow reaction of hypoxia-inducible factor prolyl hydroxylase domain 2 with oxygen. *Biochem J*, doi:10.1042/ BJ20140779 (2014).

62 Hirsila, M., Koivunen, P., Gunzler, V., Kivirikko, K. I. & Myllyharju, J. Characterization of the human prolyl 4-hydroxylases that modify the hypoxia-inducible factor. *J Biol Chem* **278**, 30772-30780, doi:10.1074/jbc.M304982200 (2003).

63 Koivunen, P., Hirsila, M., Kivirikko, K. I. & Myllyharju, J. The length of peptide substrates has a marked effect on hydroxylation by the hypoxia-inducible factor prolyl 4-hydroxylases. *J Biol Chem* **281**, 28712-28720, doi:10.1074/jbc.M604628200 (2006).

64 Flashman, E., Bagg, E. A., Chowdhury, R., Mecinovic, J., Loenarz, C., McDonough, M. A. *et al.* Kinetic rationale for selectivity toward N- and C-terminal oxygen-dependent degradation domain substrates mediated by a loop region of hypoxia-inducible factor prolyl hydroxylases. *J Biol Chem* **283**, 3808-3815, doi:10.1074/jbc.M707411200 (2008).

65 Landazuri, M. O., Vara-Vega, A., Viton, M., Cuevas, Y. & del Peso, L. Analysis of HIF-prolyl hydroxylases binding to substrates. *Biochem Biophys Res Commun* **351**, 313-320 (2006).

66 Chowdhury, R., Leung, I. K., Tian, Y. M., Abboud, M. I., Ge, W., Domene, C. *et al.* Structural basis for oxygen degradation domain selectivity of the HIF prolyl hydroxylases. *Nat Commun* **7**, 12673, doi:10.1038/ncomms12673 (2016).

67 Chowdhury, R., McDonough, M. A., Mecinovic, J., Loenarz, C., Flashman, E., Hewitson, K. S. *et al.* Structural basis for binding of hypoxia-inducible factor to the oxygen-sensing prolyl hydroxylases. *Structure* **17**, 981-989, doi:10.1016/j.str.2009.06.002 (2009).

68 Appelhoff, R. J., Tian, Y. M., Raval, R. R., Turley, H., Harris, A. L., Pugh, C. W. *et al.* Differential function of the prolyl hydroxylases, PHD1, 2 and 3 in the regulation of Hypoxia inducible factor (HIF). *J Biol Chem* (2004).

69 Loenarz, C., Coleman, M. L., Boleininger, A., Schierwater, B., Holland, P. W., Ratcliffe, P. J. *et al.* The hypoxia-inducible transcription factor pathway regulates oxygen sensing in the simplest animal, Trichoplax adhaerens. *EMBO Rep* **12**, 63-70, doi:10.1038/embor.2010.170 (2011).

70 Schofield, C. J. & Ratcliffe, P. J. Signalling hypoxia by HIF hydroxylases. *Biochemical and Biophysical Research Communications* **338**, 617-626 (2005).

71 Fong, G. H. & Takeda, K. Role and regulation of prolyl hydroxylase domain proteins. *Cell Death Differ* **15**, 635-641 (2008).

72 Metzen, E., Berchner-Pfannschmidt, U., Stengel, P., Marxsen, J. H., Stolze, I., Klinger, M. *et al.* Intracellular localisation of human HIF-1 alpha hydroxylases: implications for oxygen sensing. *J Cell Sci* **116**, 1319-1326 (2003).

73 Takeda, K., Ho, V. C., Takeda, H., Duan, L. J., Nagy, A. & Fong, G. H. Placental but not heart defects are associated with elevated hypoxia-inducible factor alpha levels in mice lacking prolyl hydroxylase domain protein 2. *Mol Cell Biol* **26**, 8336-8346, doi:10.1128/MCB.00425-06 (2006).

74 Oehme, F., Ellinghaus, P., Kolkhof, P., Smith, T. J., Ramakrishnan, S., Hütter, J. *et al.* Overexpression of PH-4, a novel putative proline 4-hydroxylase, modulates activity of hypoxia-

inducible transcription factors. *Biochemical and Biophysical Research Communications* **296**, 343-349 (2002).

75 Koivunen, P., Tiainen, P., Hyvarinen, J., Williams, K. E., Sormunen, R., Klaus, S. J. *et al.* An endoplasmic reticulum transmembrane prolyl 4-hydroxylase is induced by hypoxia and acts on hypoxia-inducible factor alpha. *J Biol Chem* **282**, 30544-30552, doi:10.1074/jbc.M704988200 (2007).

76 Klotzsche-von Ameln, A., Prade, I., Grosser, M., Kettelhake, A., Rezaei, M., Chavakis, T. *et al.* PHD4 stimulates tumor angiogenesis in osteosarcoma cells via TGF-alpha. *Mol Cancer Res* **11**, 1337-1348, doi:10.1158/1541-7786.MCR-13-0201 (2013).

77 Elkins, J. M., Hewitson, K. S., McNeill, L. A., Seibel, J. F., Schlemminger, I., Pugh, C. W. *et al.* Structure of factor-inhibiting hypoxia-inducible factor (HIF) reveals mechanism of oxidative modification of HIF-1 alpha. *J Biol Chem* **278**, 1802-1806, doi:10.1074/jbc.C200644200 (2003).

78 Lancaster, D. E., McNeill, L. A., McDonough, M. A., Aplin, R. T., Hewitson, K. S., Pugh, C. W. *et al.* Disruption of dimerization and substrate phosphorylation inhibit factor inhibiting hypoxia-inducible factor (FIH) activity. *Biochem J* **383**, 429-437 (2004).

79 Cockman, M. E., Webb, J. D. & Ratcliffe, P. J. FIH-dependent asparaginyl hydroxylation of ankyrin repeat domain-containing proteins. *Ann N Y Acad Sci* **1177**, 9-18, doi:10.1111/j.1749-6632.2009.05042.x (2009).

80 Wilkins, S. E., Karttunen, S., Hampton-Smith, R. J., Murchland, I., Chapman-Smith, A. & Peet, D. J. Factor inhibiting HIF (FIH) recognizes distinct molecular features within hypoxia-inducible factor-alpha (HIF-alpha) versus ankyrin repeat substrates. *J Biol Chem* **287**, 8769-8781, doi:10.1074/jbc.M111.294678 (2012).

81 Myllyharju, J. & Kivirikko, K. I. Collagens and collagen-related diseases. *Ann Med* **33**, 7-21 (2001).

82 Franklin, T. J. Therapeutic approaches to organ fibrosis. *Int J Biochem Cell Biol* **29**, 79-89 (1997).

83 Brodsky, B. & Shah, N. K. Protein motifs. 8. The triple-helix motif in proteins. *FASEB J* **9**, 1537-1546 (1995).

84 Myllyharju, J. & Kivirikko, K. I. Collagens and collagen-related diseases. *Ann. Med.* **33**, 7-21 (2001).

85 Heikkinen, J., Risteli, M., Wang, C., Latvala, J., Rossi, M., Valtavaara, M. *et al.* Lysyl hydroxylase 3 is a multifunctional protein possessing collagen glucosyltransferase activity. *J Biol Chem* **275**, 36158-36163, doi:10.1074/jbc.M006203200 (2000).

86 Krane, S. M. The importance of proline residues in the structure, stability and susceptibility to proteolytic degradation of collagens. *Amino Acids* **35**, 703-710, doi:10.1007/s00726-008-0073-2 (2008).

87 Jenkins, C. L. & Raines, R. T. Insights on the conformational stability of collagen. *Nat Prod Rep* **19**, 49-59 (2002).

88 Myllyharju, J. & Kivirikko, K. I. Collagens, modifying enzymes and their mutations in humans, flies and worms. *Trends Genet* **20**, 33-43, doi:10.1016/j.tig.2003.11.004 (2004).

89 Vranka, J. A., Sakai, L. Y. & Bachinger, H. P. Prolyl 3-hydroxylase 1, enzyme characterization and identification of a novel family of enzymes. *J Biol Chem* **279**, 23615-23621, doi:10.1074/jbc.M312807200 (2004).

90 Tsuneoka, M., Koda, Y., Soejima, M., Teye, K. & Kimura, H. A novel myc target gene, mina53, that is involved in cell proliferation. *J Biol Chem* **277**, 35450-35459, doi:10.1074/jbc.M204458200 (2002).

91 Teye, K., Tsuneoka, M., Arima, N., Koda, Y., Nakamura, Y., Ueta, Y. *et al.* Increased expression of a Myc target gene Mina53 in human colon cancer. *Am J Pathol* **164**, 205-216, doi:10.1016/S0002-9440(10)63111-2 (2004).

92 Suzuki, C., Takahashi, K., Hayama, S., Ishikawa, N., Kato, T., Ito, T. *et al.* Identification of Myc-associated protein with JmjC domain as a novel therapeutic target oncogene for lung cancer. *Molecular cancer therapeutics* **6**, 542-551, doi:10.1158/1535-7163.MCT-06-0659 (2007).

93 Singleton, R. S., Liu-Yi, P., Formenti, F., Ge, W., Sekirnik, R., Fischer, R. *et al.* OGFOD1 catalyzes prolyl hydroxylation of RPS23 and is involved in translation control and stress granule formation. *Proc Natl Acad Sci U S A* **111**, 4031-4036, doi:10.1073/pnas.1314482111 (2014).

94 Horita, S., Scotti, J. S., Thinnes, C., Mottaghi-Taromsari, Y. S., Thalhammer, A., Ge, W. *et al.* Structure of the Ribosomal Oxygenase OGFOD1 Provides Insights into the Regio-and Stereoselectivity of Prolyl Hydroxylases. *Structure* **23**, 639-652, doi:DOI 10.1016/j.str.2015.01.014 (2015).

95 Hojfeldt, J. W., Agger, K. & Helin, K. Histone lysine demethylases as targets for anticancer therapy. *Nat Rev Drug Discov* **12**, 917-930, doi:10.1038/nrd4154 (2013).

96 Anand, R. & Marmorstein, R. Structure and mechanism of lysine-specific demethylase enzymes. *J Biol Chem* **282**, 35425-35429, doi:10.1074/jbc.R700027200 (2007).

97 Kooistra, S. M. & Helin, K. Molecular mechanisms and potential functions of histone demethylases. *Nat Rev Mol Cell Biol* **13**, 297-311, doi:10.1038/nrm3327 (2012).

98 Walport, L. J., Hopkinson, R. J. & Schofield, C. J. Mechanisms of human histone and nucleic acid demethylases. *Curr Opin Chem Biol* **16**, 525-534, doi:10.1016/j.cbpa.2012.09.015 (2012).

99 Laumonnier, F., Holbert, S., Ronce, N., Faravelli, F., Lenzner, S., Schwartz, C. E. *et al.* Mutations in PHF8 are associated with X linked mental retardation and cleft lip/cleft palate. *J Med Genet* **42**, 780-786, doi:10.1136/jmg.2004.029439 (2005).

100 Tahiliani, M., Mei, P., Fang, R., Leonor, T., Rutenberg, M., Shimizu, F. *et al.* The histone H3K4 demethylase SMCX links REST target genes to X-linked mental retardation. *Nature* **447**, 601-605, doi:10.1038/nature05823 (2007).

101 Xu, W. S., Parmigiani, R. B. & Marks, P. A. Histone deacetylase inhibitors: molecular mechanisms of action. *Oncogene* **26**, 5541-5552, doi:10.1038/sj.onc.1210620 (2007).

102 Gravina, G. L., Festuccia, C., Marampon, F., Popov, V. M., Pestell, R. G., Zani, B. M. *et al.* Biological rationale for the use of DNA methyltransferase inhibitors as new strategy for modulation of tumor response to chemotherapy and radiation. *Molecular cancer* **9**, 305, doi: 10.1186/1476-4598-9-305 (2010).

103 Rotili, D., Altun, M., Hamed, R. B., Loenarz, C., Thalhammer, A., Hopkinson, R. J. *et al.* Photoactivable peptides for identifying enzyme-substrate and protein-protein interactions. *Chem Commun (Camb)* **47**, 1488-1490, doi:10.1039/c0cc04457a (2011).

104 Aik, W., Scotti, J. S., Choi, H., Gong, L., Demetriades, M., Schofield, C. J. *et al.* Structure of human RNA N(6)-methyladenine demethylase ALKBH5 provides insights into its mechanisms of nucleic acid recognition and demethylation. *Nucleic Acids Res* **42**, 4741-4754, doi:10.1093/nar/gku085 (2014).

105 Luo, G. Z. & He, C. DNA N(6)-methyladenine in metazoans: functional epigenetic mark or bystander? *Nat Struct Mol Biol* **24**, 503-506, doi:10.1038/nsmb.3412 (2017).

106 Jia, G., Fu, Y., Zhao, X., Dai, Q., Zheng, G., Yang, Y. *et al.* N6-methyladenosine in nuclear RNA is a major substrate of the obesity-associated FTO. *Nat Chem Biol* **7**, 885-887, doi:10.1038/nchembio.687 (2011).

107 Zheng, G., Dahl, J. A., Niu, Y., Fedorcsak, P., Huang, C. M., Li, C. J. *et al.* ALKBH5 is a mammalian RNA demethylase that impacts RNA metabolism and mouse fertility. *Mol Cell* **49**, 18-29, doi:10.1016/j.molcel.2012.10.015 (2013).

108 Gerken, T., Girard, C. A., Tung, Y. C., Webby, C. J., Saudek, V., Hewitson, K. S. *et al.* The Obesity-Associated FTO Gene Encodes a 2-Oxoglutarate Dependent Nucleic Acid Demethylase. *Science* **318**, 1469-1472 (2007).

109 Ito, S., Shen, L., Dai, Q., Wu, S. C., Collins, L. B., Swenberg, J. A. *et al.* Tet proteins can convert 5-methylcytosine to 5-formylcytosine and 5-carboxylcytosine. *Science* **333**, 1300-1303, doi:10.1126/science.1210597 (2011).

110 Sankaran, V. G. & Weiss, M. J. Anemia: progress in molecular mechanisms and therapies. *Nat Med* **21**, 221-230, doi:10.1038/nm.3814 (2015).

111 Kassebaum, N. J., Jasrasaria, R., Naghavi, M., Wulf, S. K., Johns, N., Lozano, R. *et al.* A systematic analysis of global anemia burden from 1990 to 2010. *Blood* **123**, 615-624, doi:10.1182/blood-2013-06-508325 (2014).

112 Besarab, A., Bolton, W. K., Browne, J. K., Egrie, J. C., Nissenson, A. R., Okamoto, D. M. *et al.* The effects of normal as compared with low hematocrit values in patients with cardiac disease who are receiving hemodialysis and epoetin. *N Engl J Med* **339**, 584-590, doi:10.1056/NEJM199808273390903 (1998).

113 Unger, E. F., Thompson, A. M., Blank, M. J. & Temple, R. Erythropoiesis-stimulating agents--time for a reevaluation. *N Engl J Med* **362**, 189-192, doi:10.1056/NEJMp0912328 (2010).

114 Szczech, L. A., Barnhart, H. X., Inrig, J. K., Reddan, D. N., Sapp, S., Califf, R. M. *et al.* Secondary analysis of the CHOIR trial epoetin-alpha dose and achieved hemoglobin outcomes. *Kidney international* **74**, 791-798, doi:10.1038/ki.2008.295 (2008).

115 McCullough, P. A., Barnhart, H. X., Inrig, J. K., Reddan, D., Sapp, S., Patel, U. D. *et al.* Cardiovascular toxicity of epoetin-alfa in patients with chronic kidney disease. *Am J Nephrol* **37**, 549-558, doi:10.1159/000351175 (2013).

116 Barrett, T. D., Palomino, H. L., Brondstetter, T. I., Kanelakis, K. C., Wu, X., Haug, P. V. *et al.* Pharmacological characterization of 1-(5-chloro-6-(trifluoromethoxy)-1H-benzoimidazol-2-yl)-1H-pyrazole-4-carboxylic acid (JNJ-42041935), a potent and selective hypoxia-inducible factor prolyl hydroxylase inhibitor. *Mol Pharmacol* **79**, 910-920, doi:10.1124/mol.110.070508 (2011).

117 Flamme, I., Oehme, F., Ellinghaus, P., Jeske, M., Keldenich, J. & Thuss, U. Mimicking hypoxia to treat anemia: HIF-stabilizer BAY 85-3934 (Molidustat) stimulates erythropoietin production without hypertensive effects. *PLoS One* **9**, e111838, doi:10.1371/journal.pone.0111838 (2014).

118 Besarab, A., Provenzano, R., Hertel, J., Zabaneh, R., Klaus, S. J., Lee, T. *et al.* Randomized placebo-controlled dose-ranging and pharmacodynamics study of roxadustat (FG-4592) to treat anemia in nondialysis-dependent chronic kidney disease (NDD-CKD) patients. *Nephrol Dial Transplant* **30**, 1665-1673, doi:10.1093/ndt/gfv302 (2015).

119 Holdstock, L., Meadowcroft, A. M., Maier, R., Johnson, B. M., Jones, D., Rastogi, A. *et al.* Four-Week Studies of Oral Hypoxia-Inducible Factor-Prolyl Hydroxylase Inhibitor GSK1278863 for Treatment of Anemia. *J Am Soc Nephrol* **27**, 1234-1244, doi:10.1681/ASN.2014111139 (2016).

120 Haase, V. H. Regulation of erythropoiesis by hypoxia-inducible factors. *Blood Rev* **27**, 41-53, doi:10.1016/j.blre.2012.12.003 (2013).

121 Rosenberger, C., Mandriota, S., Jurgensen, J. S., Wiesener, M. S., Horstrup, J. H., Frei, U. *et al.* Expression of hypoxia-inducible factor-1alpha and -2alpha in hypoxic and ischemic rat kidneys. *J Am Soc Nephrol* **13**, 1721-1732 (2002).

122 Willam, C., Maxwell, P. H., Nichols, L., Lygate, C., Tian, Y. M., Bernhardt, W. *et al.* HIF prolyl hydroxylases in the rat; organ distribution and changes in expression following hypoxia and coronary artery ligation. *J Mol Cell Cardiol* **41**, 68-77, doi:10.1016/j.yjmcc.2006.04.009 (2006).

123 Hyvarinen, J., Hassinen, I. E., Sormunen, R., Maki, J. M., Kivirikko, K. I., Koivunen, P. *et al.* Hearts of hypoxia-inducible factor prolyl 4-hydroxylase-2 hypomorphic mice show protection against acute ischemia-reperfusion injury. *J Biol Chem* **285**, 13646-13657, doi:10.1074/jbc.M109.084855 (2010).

124 Takeda, Y., Costa, S., Delamarre, E., Roncal, C., Leite de Oliveira, R., Squadrito, M. L. *et al.* Macrophage skewing by Phd2 haplodeficiency prevents ischaemia by inducing arteriogenesis. *Nature* **479**, 122-126, doi:10.1038/nature10507 (2011).

125 Aragones, J., Schneider, M., Van Geyte, K., Fraisl, P., Dresselaers, T., Mazzone, M. *et al.* Deficiency or inhibition of oxygen sensor Phd1 induces hypoxia tolerance by reprogramming basal metabolism. *Nat Genet* **40**, 170-180, doi:10.1038/ng.2007.62 (2008).

126 Holscher, M., Silter, M., Krull, S., von Ahlen, M., Hesse, A., Schwartz, P. *et al.* Cardiomyocyte-specific prolyl-4-hydroxylase domain 2 knock out protects from acute myocardial ischemic injury. *J Biol Chem* **286**, 11185-11194, doi:10.1074/jbc.M110.186809 (2011).

127 Takeda, N., O'Dea, E. L., Doedens, A., Kim, J. W., Weidemann, A., Stockmann, C. *et al.* Differential activation and antagonistic function of HIF-{alpha} isoforms in macrophages are essential for NO homeostasis. *Genes Dev* **24**, 491-501, doi:10.1101/gad.1881410 (2010).

128 Deshmane, S. L., Amini, S., Sen, S., Khalili, K. & Sawaya, B. E. Regulation of the HIV-1 promoter by HIF-1alpha and Vpr proteins. *Virol J* **8**, 477, doi:10.1186/1743-422X-8-477 (2011).

129 Robinson, A., Keely, S., Karhausen, J., Gerich, M. E., Furuta, G. T. & Colgan, S. P. Mucosal protection by hypoxia-inducible factor prolyl hydroxylase inhibition. *Gastroenterology* **134**, 145-155, doi:10.1053/j.gastro.2007.09.033 (2008).

130 Gong, H., Rehman, J., Tang, H., Wary, K., Mittal, M., Chaturvedi, P. *et al.* HIF2alpha signaling inhibits adherens junctional disruption in acute lung injury. *J Clin Invest* **125**, 652-664, doi:10.1172/JCI77701 (2015).

131 Ivan, M., Haberberger, T., Gervasi, D. C., Michelson, K. S., Günzler, V., Kondo, K. *et al.* Biochemical purification and pharmacological inhibition of a mammalian prolyl hydroxylase acting on hypoxia-inducible factor. *Proc. Natl. Acad. Sci. U. S. A.* **99**, 13459-13464 (2002).

132 McDonough, M. A., McNeill, L. A., Tilliet, M., Papamicael, C. A., Chen, Q. Y., Banerji, B. *et al.* Selective inhibition of factor inhibiting hypoxia-inducible factor. *J Am Chem Soc* **127**, 7680-7681, doi:10.1021/ja050841b (2005).

133 Chowdhury, R., Candela-Lena, J. I., Chan, M. C., Greenald, D. J., Yeoh, K. K., Tian, Y. M. *et al.* Selective small molecule probes for the hypoxia inducible factor (HIF) prolyl hydroxylases. *ACS Chem Biol* **8**, 1488-1496, doi:10.1021/cb400088q (2013).

134 Chan, M. C., Atasoylu, O., Hodson, E., Tumber, A., Leung, I. K., Chowdhury, R. *et al.* Potent and Selective Triazole-Based Inhibitors of the Hypoxia-Inducible Factor Prolyl-Hydroxylases with Activity in the Murine Brain. *PLoS One* **10**, e0132004, doi:10.1371/journal.pone.0132004 (2015).

135 Yeh, T., Leissing, T. M., Abboud, M. I., Thinnes, C. C., Atasoylu, O., Holt-Martyn, J. P. *et al.* Molecular and Cellular Mechanisms of HIF Prolyl Hydroxylase inhibitors in Clinical Trials. *Chem. Sci* **8**, 7651-7668, doi:10.1039/C7SC02103H (2017).

136 Johnson, B. M., Stier, B. A. & Caltabiano, S. Effect of food and gemfibrozil on the pharmacokinetics of the novel prolyl hydroxylase inhibitor GSK1278863. *Clin Pharmacol Drug Dev* **3**, 109-117, doi:10.1002/cpdd.83 (2014).

137 Thevis, M., Milosovich, S., Licea-Perez, H., Knecht, D., Cavalier, T. & Schanzer, W. Mass spectrometric characterization of a prolyl hydroxylase inhibitor GSK1278863, its bishydroxylated metabolite, and its implementation into routine doping controls. *Drug Test Anal* **8**, 858-863, doi:10.1002/dta.1870 (2016).

138 Maxwell, P. H. & Eckardt, K. U. HIF prolyl hydroxylase inhibitors for the treatment of renal anaemia and beyond. *Nat Rev Nephrol* **12**, 157-168, doi:10.1038/nrneph.2015.193 (2016).

CHAPTER 2 . Identification and Validation of Selective PHD2 Inhibitors

2.1 Criteria For Selective PHD Inhibitors

Successful PHD inhibitors should possess selectivity over other members of the 2OG oxygenase family.[1] 2OG mimetic inhibitors of the PHDs (including the clinical candidates), i.e those that bind to the PHD in a similar fashion to 2OG, may yield off-target inhibition of other 2OG oxygenases due to the structural simplicity of 2OG and the presence of (but not identical) conserved 2OG binding residues in the 2OG oxygenase superfamily enzymes.[1-4] To date, the most popular medicinal chemistry approach for developing PHD inhibitors appears to have been to functional group interconvert (FGI) involving the 1,2-oxo acid 2OG group (**Figure 12**) with the aim of utilising 2OG binding residues, whilst achieving acceptable selectivity.[1,5] At least from the perspective of achieving selectivity against all human 2OG oxygenases, this approach was not successful as summarised in **Table 1**.[5]

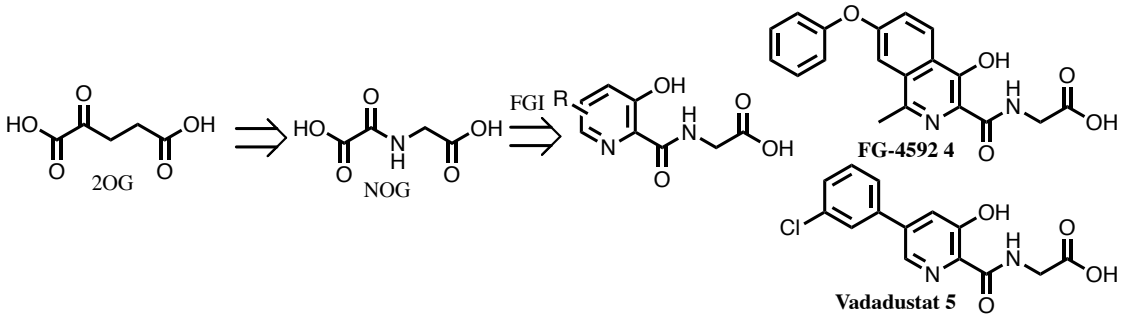

Figure 12: Overview of an example of previous medicinal chemistry efforts on PHD inhibition, showing how the structure of 2OG was 'evolved' to the clinical candidates FG-4592 (**4**) and Vadadustat (**5**).[1]

Crystallographic studies of the 2OG oxygenases PHD2, OGFOD1 and a viral collagen prolyl hydroxylase (CPH) (all prolyl hydroxylases) indicate that key residues of their active

sites are substantially conserved with respect to 2OG binding (**Figure 13**).[6-8] Key residues involved in 2OG binding appear very similar for PHD2 and OGFOD1, i.e Arg-383 (PHD2), Arg-230 (OGFOD1), Tyr-303 (PHD2), Tyr-146 (OGFOD1), Tyr-310 (PHD2) and Tyr-96 (OGFOD1); whilst in CPH, the key residues are Tyr-143, Tyr-150, with Lys-231 in place of Arg-383.[6-8] The active sites of PHD2, OGFOD1 and CPH interact with 2OG in a similar fashion at least in the crystalline state (**Figure 13**). Thus, 2OG mimics including the clinical candidates **4**, **5** and **6**, have potential for off-target inhibition within the 2OG oxygenase family (as indeed observed) (**Table 1**).[5]

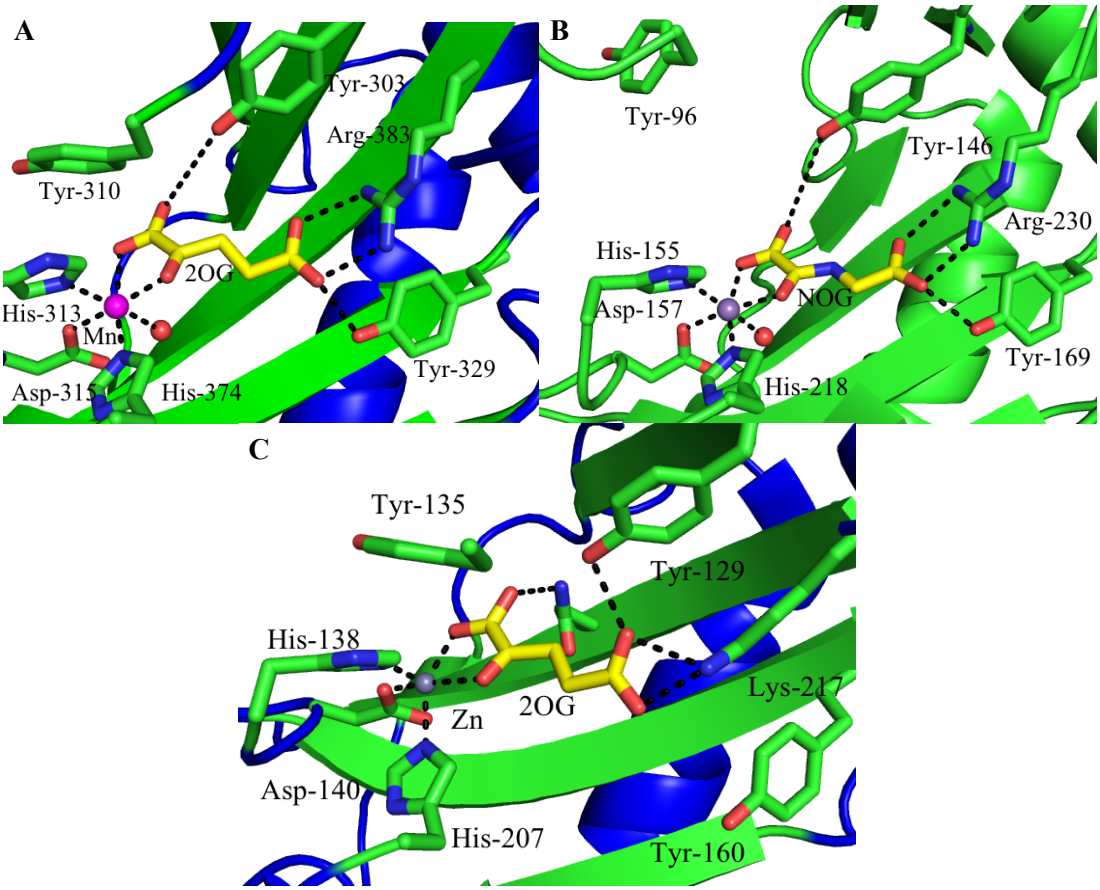

Figure 13: View from crystal structures of 2OG or NOG (yellow sticks) bound to the 2OG oxygenases (green/blue cartoons with the active sites of PHD2 (PDB ID: 519b) **A**), OGFOD1 (PDB ID: 4NHX) **B**) and CPH (PDB ID: 5C5T) **C**).[6-8]

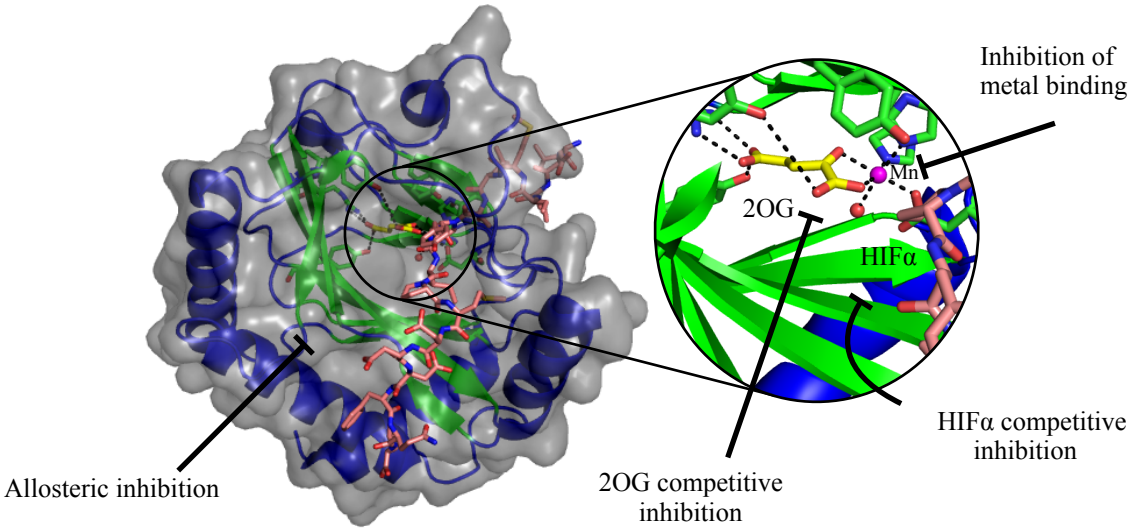

Figure 14: Views from crystal structures a crystal structure of PHD2 with 2OG bound (yellow sticks) (PDB ID: 519b), overlaid with the crystal structure of PHD2 complexed with the HIF-1α CODD substrate (556-574) (PDB ID: 5l9B). Displaying the possible modes of inhibition of PHD2.[6, 29]

It was envisaged that one way to develop selective PHD inhibitors, would be to investigate other potential modes of inhibition including metal chelation, allosteric interactions and mimicking HIF-α binding (**Figure 14**).[1] Inhibition of metal binding (by chelation) was regarded as a challenging approach as it may lead to off-target inhibition (potentially fatal) of human metallo-enzymes.[9] PHD2 inhibition, *via* non-competitive or allosteric binding modes, is an alternative; however, identification of an appropriate allosteric site and ligands

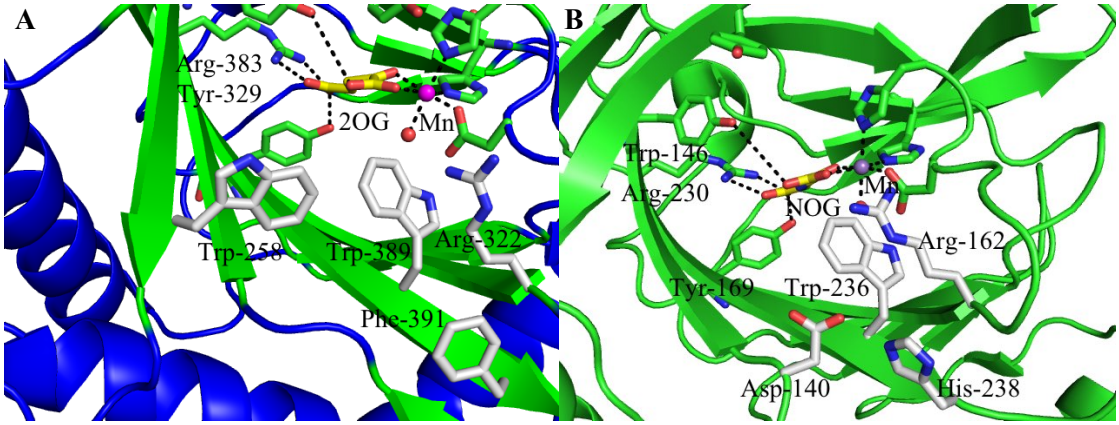

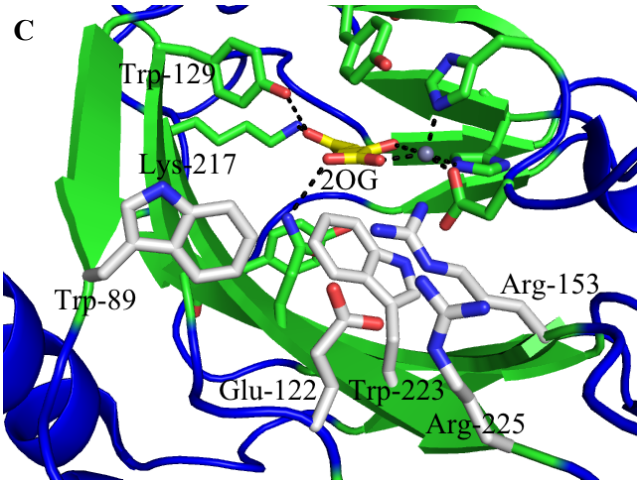

Figure 15: View from crystal structures of 2OG or NOG (yellow sticks) bound to the 2OG oxygenases (white sticks amino acid residues in the aromatic pocket, green/blue cartoons with the active sites of PHD2 (PDB ID: 519b) **A**), OGFOD1 (PDB ID: 4NHX) **B**) and CPH (PDB ID: 5C5T) **C**).[6-8]

is likely challenging.[10] HIF-α substrate mimics, binding to PHD2, in either a competitive or non-competitive fashion were considered to be an attractive option for achieving selective inhibition of the PHDs over the other 2OG oxygenases. It is believed that the PHDs are the only enzyme group that hydroxylates the HIF-α ODD substrates. It has been suggested by some that these substrates are the only substrates that interact with PHD2, through there are reports of other PHD substrates (**Chapter 1.4**). Therefore, HIF-α substrate mimics may lead to reduced off-target effects. Examination of how the CODD substrate binds to PHD2, together with of the OGFOD1 and CPH crystal structures reveals subtle differences in an aromatic pocket just outside the active site. **Figure 15** shows a comparison between the aromatic pocket of the enzymes; the PHD2 aromatic pocket consist of Trp-258, Trp-389 and Phe-391 vs Trp-236 and His-238 in OGFOD1 vs Trp-103, Trp-237 and Glu-136 in vCPH.[6-8] It was envisaged that the differences in the aromatic pockets between the structurally similar enzymes could be exploited to achieve the desired selectivity for PHD2

inhibition. The following set of criteria were used to evaluate potential starting fragments in the development of potentially selective PHD inhibitors :

1. Should not be structurally similar to 2OG;
2. Be able to make interactions with the aromatic pocket of PHD2 that mimic substrate interactions;
3. Possess suitable structural attributes that would enable development of a diverse chemical library for SAR studies.

2.2 Starting Points

The two starting points for developing selective PHD2 inhibitors were the reported 1,3,8-triazaspiro[4.5]decane-2,4-diones and 4-hydroxypyrimidines PHD2 inhibitors (**10** and **11** respectively) (**Figure 16**).[11-14] Both compounds matched the criteria stated above, as neither series are very close structural mimics of 2OG and both possess a bi-phenyl substituent, which it was envisioned could interact with the aromatic pocket of the PHDs.

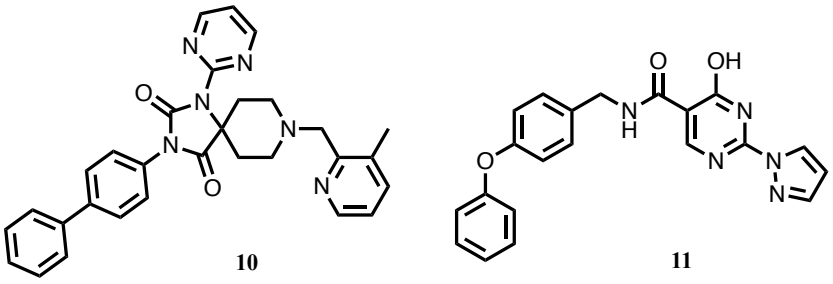

10 PHD IC_{50} 2.1 nM

11 PHD IC_{50} ≤ 10 nM

Figure 16: Starting point inhibitors, 1,3,8-triazaspiro[4.5]decane-2,4-diones (**10**) and 4-hydroxypyrimidines (**11**).[11-14]

A crystal structure of PHD2 with a related compound **12** has been reported.[15] This shows interactions between the bi-phenyl substituent of **12** and the aromatic pocket (**Figure 17**).[15] Compounds **10** and **11** were chosen as starting points for the development of selective PHD2 inhibitors. Both had suitable structural attributes that may interact differently within the active site, thus allowing for diverse SAR studies to be pursued.

Compounds **10** and **11** have molecular weights 504 and 357 Da respectively, satisfying one of Lipinski's rules for optimal physio-chemical properties.[16] Conjugated aromatic systems such as the bi-phenyl group in **10** and **11** can present sub-optimal pharmacokinetic (PK) profiles in *in vivo* stages of drug discovery.[17] It was therefore expected that modification of the bi-phenyl system of **10** and **11** could improve PK profiles. Furthermore, the bi-phenyl substituent (cLogP of 4.0) may increase the risk of off-target inhibition of lipophilic proteins such as the HERG channel, effect cell permeability where the compounds inefficiently being able to pass the cell membrane and result in poor oral bioavailability.

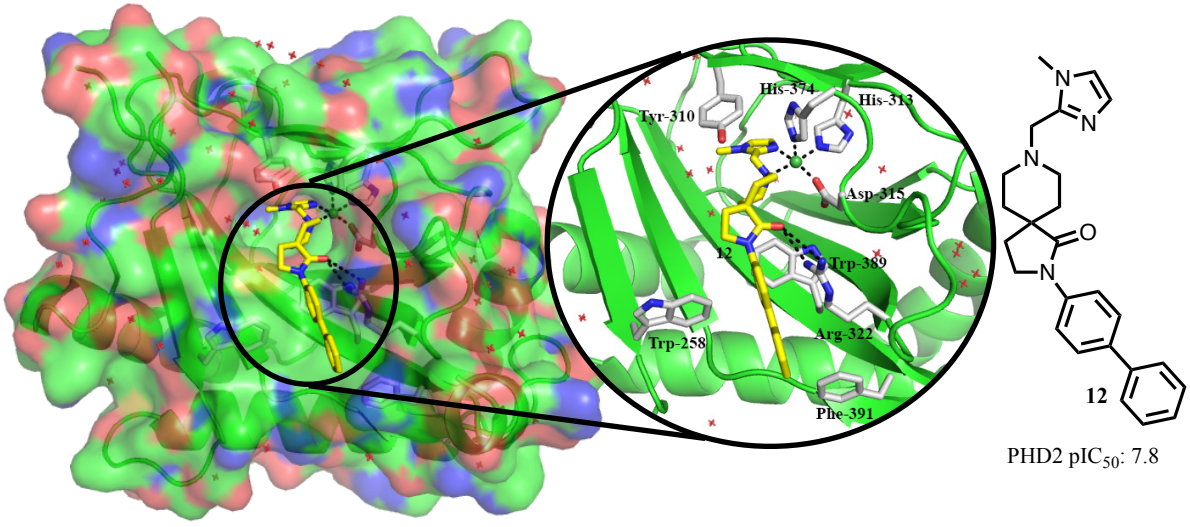

Figure 17: View from a crystal structure of PHD2 with compound **12** bound (PDB ID: 4JRZ), showing the interaction of the biphenyl substituent with the aromatic pocket on PHD2.[15]

However, even with the presence of the biphenyl substituent, both **10** and **11** had reasonable calculated cLogP values (3.96 (**10**) and 2.1 (**11**)) and good calculated total polarity surface area values (tPSA) 82.53 (**10**) and 92.93 (**11**) (using the program DataWarrior [18]). cLogP and tPSA parameters are considered important factors for *in vivo* tolerability.[19]

2.3 *In-Vitro* Screening Methods

Compounds **10** and **11** are reported as potent PHD2 inhibitors, using a fluorescence based binding assay.[11-14] The reported assay utilises a biotinyl-hydroxylated HIF-α CODD substrate that interacts with (His)6-VHL and AF647-labeled streptavidin, producing fluorescence signals at 665 and 620 nm. The ratio of time resolved fluorescence signals are determined, and the percentage inhibition calculated using positive and negative controls.[11-14] It was decided that a number of variables should be changed from the reported assay conditions used to assess **10** and **11**. Reaction time and PHD2 enzyme construct were two such variables to be altered. It was expected these changes may afford different structure-activity relationship (SAR) to that reported. The reported assay employs an unstable full-length FLAG-tagged PHD2 construct, which could produce error due to the instability of FLAG-tagged PHD2.[11-14] Thus the catalytic domain construct $PHD2_{181-426}$ was chosen due to its improved stability and similar level of turnover of HIF-α substrate with respect to naturally occurring PHD2. The total reaction time of 150 minutes was regarded as non-optimal and was shortened.[11-14]

The preferred method was a direct-detection activity assay due to the low chance for interference and reduced the likelihood of false-positive or false-negative results. Mass spectrometry-based methods were chosen as they directly quantify relative amounts of hydroxylated and non-hydoxylated substrate. Initially, in the project a matrix-assisted laser desorption ionisation time-of-flight mass spectrometry (MALDI-TOF) based assay was used.[20] This was subsequently replaced with the RapidFire LC-MS assay due to its increased accuracy and sensitivity.[21] RF-MS is a high throughput mass spectrometry based robotic system that incorporates solid phase extraction (SPE) technology to remove non volatile salts from samples.[22] The RapidFire™ protocol uses an ECHO 550 acoustic dispenser to produce accurate inhibitor concentrations. This method enables direct detection of HIF-α substrate peptide while ensuring high speed and high accuracy. Indeed, the PHD2 enzyme concentration with the RapidFire assay was 6.5 fold lower than the MALDI-TOF based assay. Therefore the RapidFire assay method became the method of choice for PHD2 inhibitor development.

2.4 1,3,8-triazaspiro[4.5]decane-2,4-dione Series

The initial strategy for early SAR generation from **10**, involved retaining the 1,3,8-triazaspiro[4.5]decane-2,4-dione core whilst varying the heterocycle ring that interacts with the Fe^{2+} centre in the active site (**Figure 18**) *via* a reductive amination reaction. The selected heterocycles were designed to explore the role of chelation at the Fe^{2+} centre by varying the following factors: the number of chelation sites on the heterocycle, the

heteroatom that interacts on the heterocycle, the size of the heterocycle, and the substituents on the heterocyclic ring. Vachal *et al.* briefly explored the Fe^{2+} chelation substituent in PHD2 inhibitors but they focused more on the substituents on the bi-phenyl motif.[13]

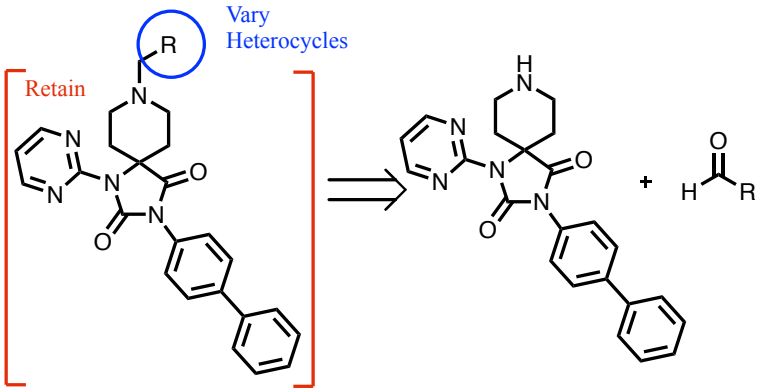

Figure 18: Initial strategy for the 1,3,8-triazaspiro[4.5]decane-2,4-dione series. The 1,3,8-triazaspiro-[4.5]decane-2,4-dione moiety was retained whilst the heterocycle was varied. Disconnection of the tertiary amine bond gives precursors for a reductive amination.

The 1,3,8-triazaspiro[4.5]decane-2,4-dione starting point **10** was synthesized using the route by Vachal *et al.* (**Scheme 6**).[13] The prerequisite piperidone underwent a Burcherer-Bergs reaction to give **13**; consecutive Ullmann couplings gave **14** and **15** respectively. Removal of the Boc protecting group with neat formic acid gave **16**. Reductive amination then gave the targeted compounds **10**, **17 - 21** (**Scheme 6**).

10, **17 - 21** were assayed using the MALDI (**Chapter 8**) and RapidFire assays (**Chapter 8**). Different results were obtained from the different experiments as outlined in **Table 2**; this reflects the different conditions of the assays. According to the MALDI assay, variation of the heterocyclic substituent had a strong impact on inhibition; the starting point **10** showed 98% and 96% PHD2 inhibition at 100 µM and 10 µM respectively. The inactivity of thiophene **17** and precursor **16** indicated the requirement for a second metal chelating group. **18** and **19** showed 70% and 81% inhibition at 100 µM, i.e. neither were as potent as

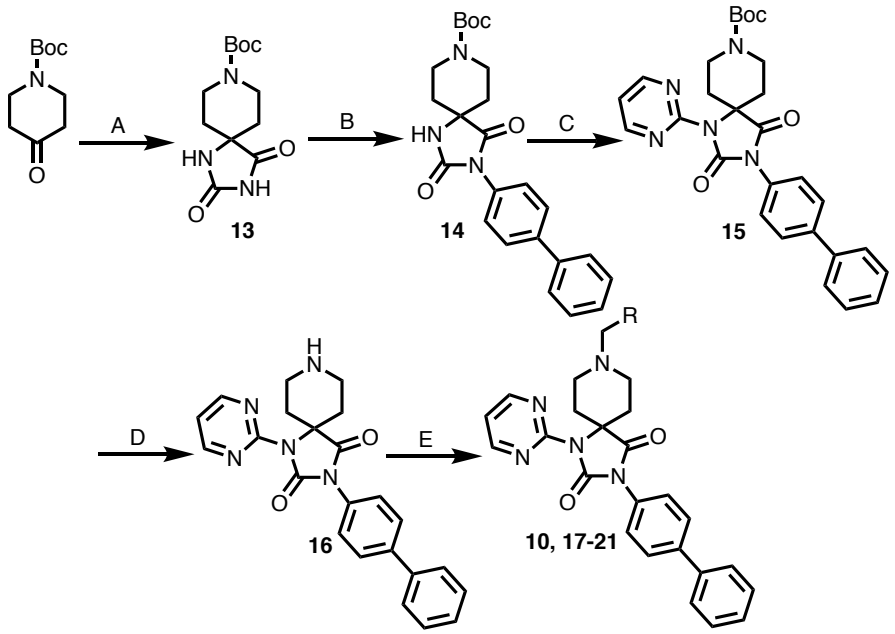

Scheme 6: Synthesis of the 1,3,8-triazaspiro[4.5]decane-2,4-dione series. Reagents and Conditions: **A**) KCN, NH_4CO_3, EtOH:H_2O (1:1), °C (65 %); **B**) **13**, CuI, K_2CO_3, 4-Iodobiphenyl, N,N-dimethyl-ethylenediamine, Na Ascorbate, DMF : ACN (1:1), Reflux (43%); **C**) 2-iodopyrimidine, TMHD, Cs_2CO_3, DMF : ACN (1:1), Reflux (60 %); **D**) Formic Acid (quant); **E**)RCHO, $NaBH(OAc)_3$, CH_2Cl_2 (35 - 84 %).

10. Imidazole **20** and the *O*-methoxy derivative **21** were inactive at 100 μM. The results from the Rapid Fire assay significantly differed compared to the MALDI results and overall they indicated that the Fe^{2+} centre within the active site can accept a wider range of substituents. **18**, **20** and **21** all showing inhibition of PHD2, but were inactive by the MALDI assay. The starting point **10** produced an IC_{50} of 498 nM in the RapidFire assay, whilst the thiophene substituent **17** and precursor **16** were inactive, this supports a requirement for the second chelation site. The 1-methyl-1-H-imidazole **18** had an IC_{50} of 74 nM, an 6.5 fold increase in potency compared to **10**. The phenol **19** had an IC_{50} of 1.27 μM, a loss of 2 fold in potency compared to **10**, indicating a preference for the type of Fe^{2+} chelation. The imidazole **20** produced an IC_{50} of 206 nM suggesting that two possible chelation sites are preferred over one or that the additional nitrogen increased the strength

Table 2 : SAR for PHD2 inhibition as determined by MALDI and RapidFire™ for Fe^{2+} chelating substituents of the 1,3,8-Triazaspiro[4.5]decane-2,4-dione series. MALDI performed by Dr T Yeh and RapidFire performed by Dr A Tumber. Experimental measurements: MALDI n = 3 and RapidFire n=1.

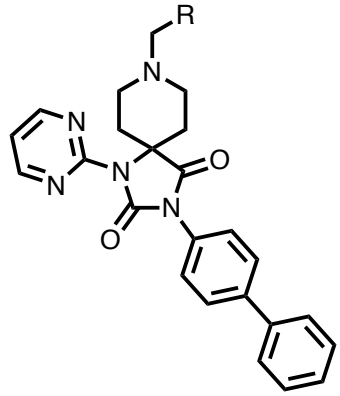

		PHD2 Inhibition		
Cpd	**R**	**% of Inhibition MALDI 100 µM**	**% of Inhibition MALDI 10 µM**	**RapidFire ™ IC_{50} µM**
10	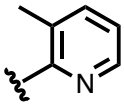	**98.1 ± 8.9**	**96 ± 5.5**	**0.498**
17	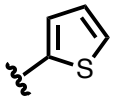	**0±4**	**0±7**	**>25**
16 (precursor)	**-H**	**0±5.5**	**0±4.7**	**>25**
18	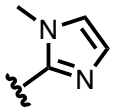	**69.9 ± 6.7**	**47 ± 3.8**	**0.074**
19	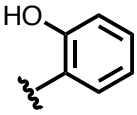	**81.0 ± 1.6**	**52.9 ± 10.5**	**1.27**
20	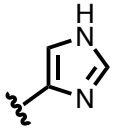	**0±11.9**	**0±8.2**	**0.206**
21	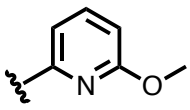	**0±3.4**	**0±10.7**	**1.37**

of the electron donation to the Fe^{2+}. **21** with a methoxy substituent at the 6-position produced an IC_{50} of 1.37 μM, a loss of 2.5 fold in potency compared to **10**, indicating that although a substituent at the 6-position of the pyridine is not preferred, it is still tolerated for inhibition.

2.5 4-hydroxy-2-(1*H*-pyrazol-1-yl)pyrimidine-5-carboxamide Series

The initial strategy used for the 4-hydroxy-2-(1*H*-pyrazol-1-yl)pyrimidine-5-carboxamide series (**11**, **26 - 32**) was similar to that employed for the 1,3,8-triazaspiro[4.5]decane-2,4-dione series (**Chapter 2.4**). The 4-hydroxy-2-(1*H*-pyrazol-1-yl)pyrimidine-5-carboxamide core was retained whilst varying the *C*-5 amide group. The strategy was to efficiently build SAR and investigate a different point of PHD2 inhibition compared to the 1,3,8-triazaspiro-[4.5]decane-2,4-dione series, given the amide group is a structural substituent shared by both starting points (**Figure 19**). The selected amides were chosen to broadly explore the role of the biphenyl substituent. Factors varied such as the length of the substituent, the substituent on the *C*-5 amide methylene linker, the amount of aromaticity and the substituent on the primary phenyl ring.

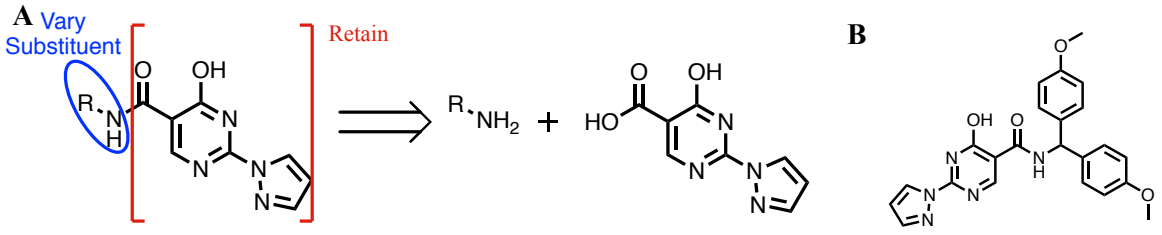

Figure 19: **A**)Initial strategy for the SAR with 4-hydroxy-2-(1*H*-pyrazol-1-yl)pyrimidine-5-carboxamide series. 4-hydroxy-2-(1*H*-pyrazol-1-yl)pyrimidine-5-carboxamide core was retained whilst the amide substituent was varied. Disconnection of amide gives precursors for a amide coupling. **B**) The preferred binding substituent as reported in Debenham *et al*.[23]

Debenham *et al.* have investigated the *C*-5 amide group stated in the published (late 2016) and patent literature, however due to the different assay conditions it was proposed to begin from initial SAR. [11,12,14,23] The final *C*-5 amide group (dimethoxybenzhydryl, **Figure 19B**) chosen by Debenham *et al.* was not chosen in the initial SAR, mainly due to being published late in the project (late 2016) and the concerns that potentially the dimethoxybenzhydryl group may inhibit structurally similar aromatic pockets of 2OG oxygenases OGFOD1 and CPH (**Figure 15B**).[23]

The 4-hydroxy-2-(1*H*-pyrazol-1-yl)pyrimidine-5-carboxamide core (**24**) (**Scheme 7**) was prepared by cyclisation of diethyl-ethoxy methylene malonate **22** and 1H-pyrazole-1-carboximdamide hydrochloride **23** to give the ethyl ester **24**.[23] Ester hydrolysis gave the carboxylic acid **25**. Both reactions proceeded in acceptable yields (64% and 77% respectively). The initial amide coupling was reported with CDI as a coupling agent.[23] However, this protocol gave a poor yield (6 %). Screening of various amide coupling reagents revealed the difficulty of the amide coupling (**Table 3**), with none of the selected amide coupling reagents efficiently producing the desired product.

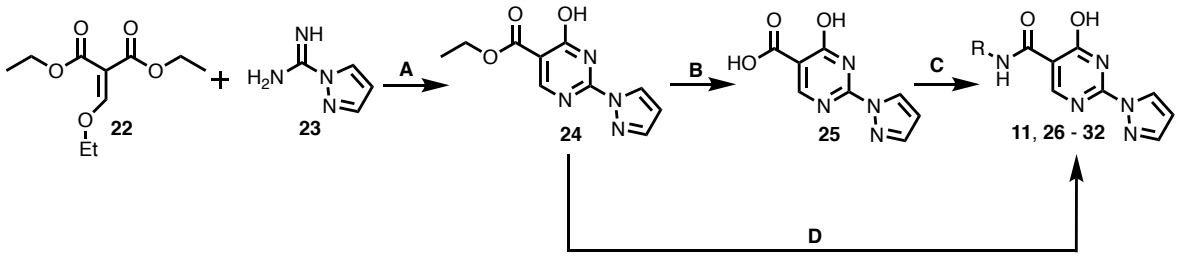

Scheme 7: Synthesis of 4-hydroxy-2-(1*H*-pyrazol-1-yl)pyrimidine-5-carboxamide series : **A**) NaOEt, EtOH, MW 90 °C (64 %); **B**) NaOH, THF : H_2O (10 :1) (77 %); **C**) i) CDI, DMAc, 100 °C ii) R-NH_2, 100 °C (6 %) (D) DABAL-Me_3, R-NH_2, THF, MW 130 °C (11 - 25%).

Table 3 :Reagents and condition for attempted amide bond coupling.

Entry	Reagent	Conditions	Reaction	Yield
1	**CDI**	DIPEA (1.2 Equiv), DMAc, 120°C for 2 hrs.	Yes	6%
2	**T3P**	DIPEA (1.2 Equiv), DMAc, Rt for 24 hrs.	No	-
3	**HATU**	DIPEA (1.2 Equiv), DMAc, Rt for 24 hrs.	No	-
4	**COMU**	DIPEA (1.2 Equiv), DMAc, Rt for 24 hrs.	No	-
5	**Pybop**	DIPEA (1.2 Equiv), DMAc, Rt for 24 hrs.	No	-

It was hypothesised that the failed amide coupling reactions may be due to the presence of the *C*-4 hydroxyl group of the pyrimidine ring interfering with the amide coupling. Use of CDI as a coupling reagent had shown a small amount of product formation, thus consideration was given into how CDI mechanistically differs to the failed coupling reagents was warranted. The reaction mechanism of the failed coupling reagents proceeds by forming an activated ester with the carboxylic acid before the amine attacks the intermediate to form the amide. CDI works in a similar way, however instead of forming an activated ester intermediate, an activated tertiary amide is formed. Therefore, it was envisaged that the desired amide bond could be formed in a similar fashion. Li *et al*. have reported the use of $AlMe_3$ to form a activated aluminium amide intermediate before the addition of the carboxylic acid.[24] Weinreb *et al.* have reported amide coupling from esters and amines, indicating the ester hydrolysis of **24** may not be required.[25] A Lewis acid such as an aluminium compound may also chelate to the free hydroxyl group helping to promote the amide coupling. A possible mechanism is shown in **Scheme 8**. However, the limitations of this method includes the use of a high equivalent of $AlMe_3$, which is pyrophoric in nature and raises safety concerns.

Novak *et al*. have reported an air stable Al adduct $(AlMe_3)_2DABCO$ (DABAL-Me_3).[26] The authors applied DABAL-Me_3 to aminolysis with methyl esters that requires 0.8 equivalence of DABAL-Me_3.[26,27] **24** was reacted with DABAL-Me_3 and the selected amines to yield the targeted compounds (**11**, **26** - **34**). The yields for the amide coupling were acceptable to poor (11% - 25%), albeit an improvement on the initial CDI coupling; further, the ester hydrolysis step is not required in the DABAL-ME_3 method. The poor yields observed were possibly in part due to the conjugation of the 4-hydroxypyrimidine substituent and the free alcohol group. However, formation of aluminum emulsions in the work-up may be largely responsible for the reduced yield.

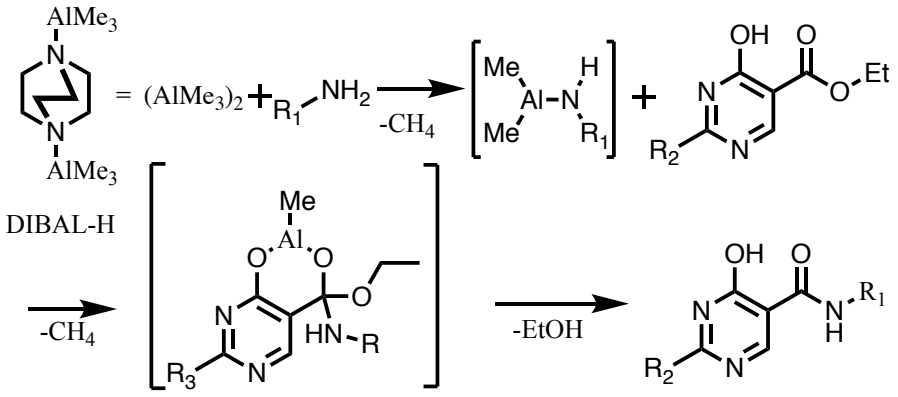

Scheme 8: Proposed mechanism of DABAL-Me_3 aminolysis.

The screening results from the MALDI and RapidFire assays for the 4-hydroxy-2-(1*H*-pyrazol-1-yl)pyrimidine-5-carboxamide series (**11**, **26-34**) are shown in **Table 4**. In general, the results clearly indicated a substituent on the phenyl ring is required for potent PHD2 inhibition, **26** and **27** manifest complete inhibition at 100 μM and 10 μM in MALDI and show strong potency in the Rapid Fire (IC_{50} 0.286 μM and 0.245 μM, respectively). In contrast to **26** and **27**, **24** and **28** were inactive in the MALDI assay suggesting the

importance of the substituent on the phenyl ring. However, **29** was inactive in the MALDI assay but achieved good potency manifested in the RapidFire assay (IC_{50} 0.976 μM), again indicating the differences between the two assays. **30** achieved moderate potency (64 % at 10 μM) suggesting a cyclohexane ring is preferred to the phenyl ring of **29**. The addition of a CF_3 group (**31**) resulted in complete inhibition at 100 μM. The removal of the methylene linker (**32**) resulted in a loss of potency in the MALDI assay (76% inhibition at 100 μM); however, **32** achieved similar levels of potency to **26** in the Rapid Fire assay (IC_{50} 0.258 μM) indicating the methylene linker is not required for PHD2 inhibition. The addition of the CH_2OH group (**33** & **34**) on the methylene linker resulted in improved inhibition in the MALDI assay compared to **28**, with the *R*-Enantiomer (**33**) achieving better inhibition than the *S*-Enantiomer (**34**) (92% and 40% at 10 μM, respectively). A similar result was recorded on the RapidFire for **33** and **34** (IC_{50} 0.329 and 15.68 μM, respectively).

Comparison of the RapidFire and MALDI inhibition data should be taken into account for the different conditions used. However, a similar level of inhibition would normally be expected from both assays, due to the assay similarities in experimental protocol. Having achieved sufficient inhibitor potency, we then assessed the cellular efficacy of a selection of compounds from both series.

Table 4 : SAR for PHD2 inhibition as determined by the observed MALDI and RapidFire™ methods, with various of the amide substituents of the 4-hydroxy-2-(1*H*-pyrazol-1-yl)pyrimidine-5-carboxamide series. MALDI performed by Dr T Yeh and RapidFire performed by Dr A Tumber. Experimental measurements: MALDI n = 3 and RapidFire n=1.

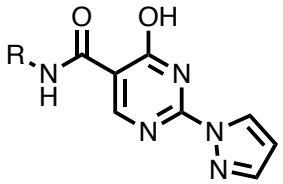

Cpd	R	% of Inhibition MALDI 100 µM	% of Inhibition MALDI 10 µM	RapidFire™ IC_{50} µM
11	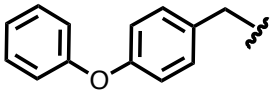	**96 ± 13**	**104 ± 4**	**0.091**
24 (precursor)	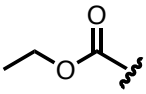	**ND**	**ND**	**>25**
26	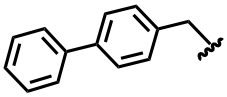	**107 ± 1**	**99 ± 3**	**0.286**
27	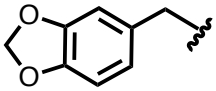	**100 ± 2**	**91 ± 10**	**0.245**
28	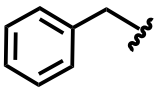	**11 ± 16**	**14 ± 12**	**ND**
29	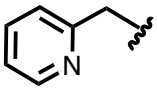	**-2 ± 13**	**-5 ± 1**	**0.976**
30	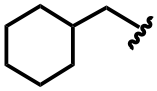	**97 ± 2**	**64 ± 2**	**ND**
31	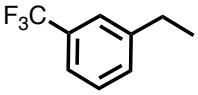	**103 ± 3**	**70 ± 2**	**ND**
32	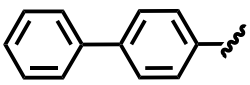	**76 ± 6**	**66 ± 5**	**0.258**
33	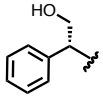	**101 ± 1**	**92 ± 4**	**0.329**
34		**80 ± 0**	**40 ± 2**	**15.68**

2.6 Cellular Characterisation of Initial Hits

The on-target cellular efficacy of the 1,3,8-triazaspiro[4.5]decane-2,4-diones and 4-hydroxy-2-(1*H*-pyrazol-1-yl)pyrimidine-5-carboxamide series was investigated by measuring cellular HIF1-α stabilisation using immunoblotting with a Hep-3B cell line.[5] Successful PHD2 inhibition should lead to a accumulation of HIF-1α and therefore a strong stain on the western blot, the stronger the stain the more HIF-1α stabilised. A selection of compounds were tested for HIF-1α stabilisation, based on inhibition data from the MALDI assays. Most of the compounds screened stabilised HIF1-α at 100 μM, with **10**, **11** and **32** achieving the strongest HIF1-α stabilisation (**Figure 20**). The *S*-Enantiomer **34**, was, however, inactive in cells. **33**; by contrast, the *R*-Enantiomer, showed modest HIF-1α stabilisation, indicating the different levels of PHD2 inhibition observed in the *in-vitro* assays translates to the cellular environment.

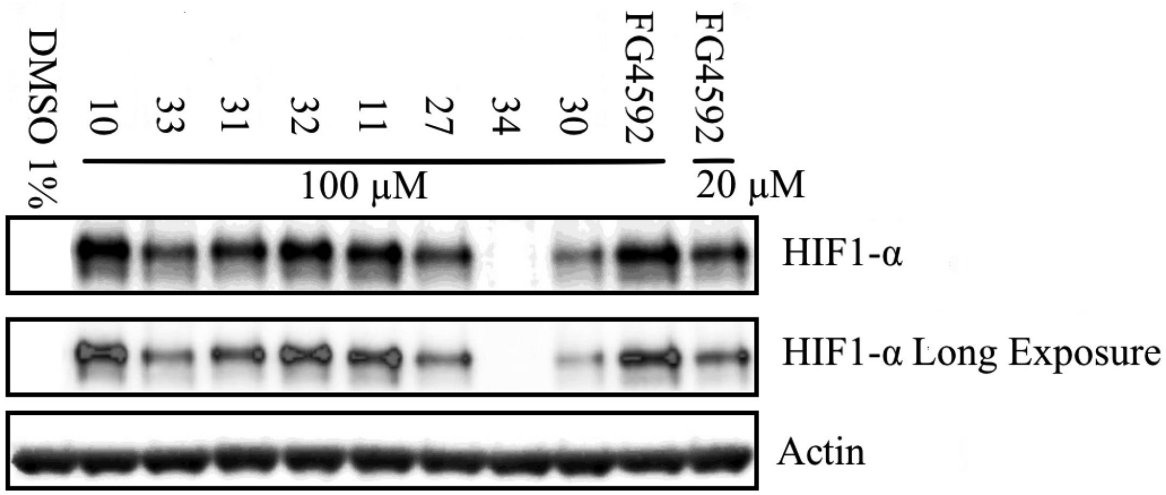

Figure 20: Cellular inhibition studies of the starting point series at 100 μM in the HEP-3B cell line. Immunoblot showing HIF-1α stabilization via inhibition of PHD2. Experiments performed by Dr T. Yeh.

Figure 21 shows the same selection of compounds at 20 μM. **10** and **32** achieved HIF-1α stabilisation indicating the *C*-5 amide group of the 4-hydroxy-2-(1*H*-pyrazol-1-yl)pyrimidine-5-carboxamide series is relatively important, at lower concentrations. **31**, **33** and **34** achieved poor or no HIF-1α stabilisation at 20 μM. The poor cellular potency of **11** and **27** was surprising, given their IC_{50}s. It was envisaged that the poor inhibition of **11** and **27** observed would be due to the metabolism of the *C*-5 amide group of **11** and **27**.

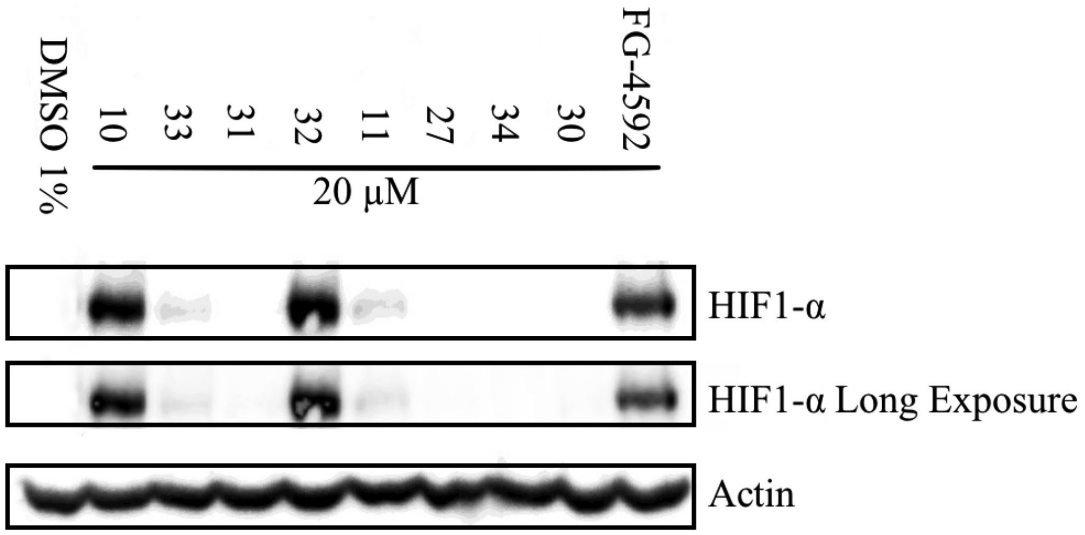

Figure 21: Cellular Inhibition studies of the starting point series at 20 μM in the HEP-3B cell line. Immunoblot showing HIF-1α stabilization via inhibition of PHD2. Experiment performed by Dr T. Yeh.

Compounds **10** and **32** caused strong HIF-1α stabilisation at 100 and 10 μM. They were profiled against a representative set of HIF-α genes (CA9, EPO, BNIP3, GLUT1,VEGFA) at 10 μM in the Hep3B cell line (**Figure 22**).[5] **10** exhibited a similar mRNA upregulation in regards to BNIP3, GLUT1 and VEGFA gene markers to the clinical candidate FG-4592 (**4**). However, **10** resulted in a significant increase in EPO and CA9 gene upregulation in contrast to **4**. A similar level of EPO upregulation was observed for **32** in comparison to **4**.

A similar level of CA9 upregulation was observed for **32** in comparison to **10**. However, **32** achieved a greater increase of VEGFA and GLUT1 upregulation in contrast to **4** and **10**. The differences in gene upregulation between the inhibitors suggest potentially different levels of inhibition of the PHD isoforms and upregulation of different HIF-α isoforms. The significant increase in EPO (a HIF-2α regulated gene) upregulation caused by **10** may suggest HIF-2α selectivity. Indeed, **32** achieved higher levels of HIF-1α regulated genes (CA9, GLUT1 and VEGFA) suggesting HIF-1α selectivity. **10** and **32** were tested against PHD3, as PHD3 regulates HIF-2α more than HIF-1α (PHD2 regulates HIF-1α more than HIF-2α).[28]

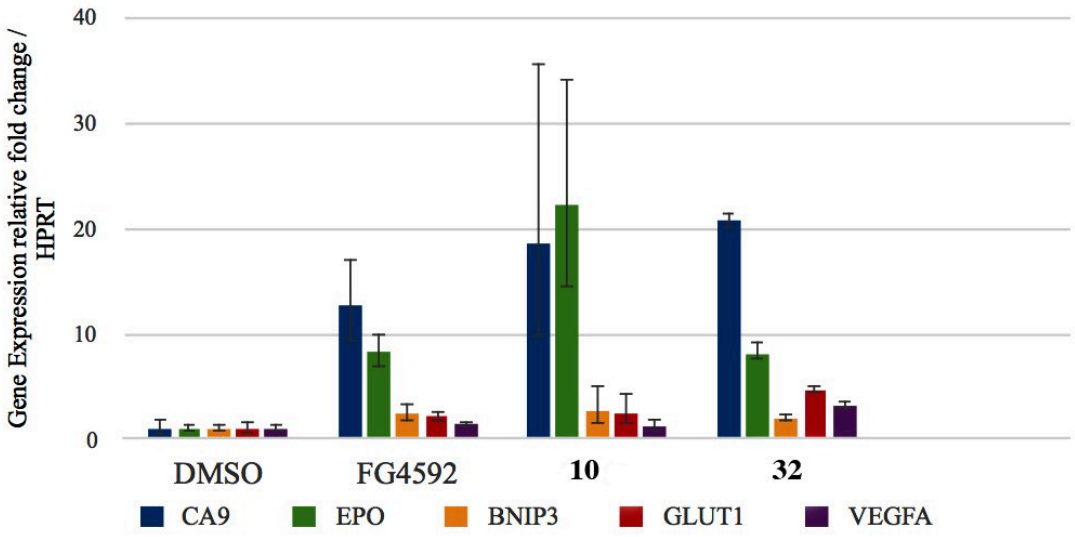

Figure 22: The effects of **10** and **32** on HIF target gene regulation. Regulation of HIF target genes, carbonic anhydrase 9 (CA9), erythipoietin (EPO), BCL2/adenovirus E1B 19 kDa protein-interacting protein 3 (BNIP3), glucose transporter 1 (GLUT1) and vascular endothelial growth factor (VEGFA). Experiment performed by Dr T. Yeh. n = 1.

The IC_{50} values **10** and **32** against PHD2 and PHD3 with the HIF1-α CODD substrate are shown in **Table 5**. **10** achieved 7 fold weaker inhibition on PHD3 compared to PHD2,

however **32** achieved similar levels of inhibition of PHD2 and PHD3. The different levels of potency observed between the two series may rationalise the different levels of gene upregulation observed highlighting the different roles of the PHD isoforms (**Figure 21**). This result was surprising, as EPO is a HIF-2α regulated gene indicating possible PHD3 selectivity for **10**. The different levels of inhibition on the PHD isoforms suggests isoform selective inhibitors are theoretically possible. PHD isoform selective inhibitors may be useful in a clinical setting due to the differences in tissue abundance leading to differences in target gene upregulation (**Chapters 1.2** and **1.4**)

Table 5: The IC_{50} values of PHD2 and PHD3 for **10** and **32** using the RapidFire assay. Experiment performed by Dr A Tumber. Experimental Measurements n = 1.

		RapidFire™	
Cpd	**Structural Formula**	**PHD2 IC_{50} µM**	**PHD3 IC_{50} µM**
10	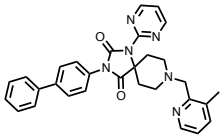	**0.498**	**3.42**
32	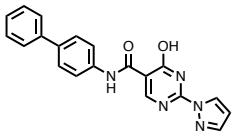	**0.258**	**0.339**

2.7 Crystal Structure of 1,3,8-triazaspiro[4.5]decane-2,4-dione Series

In order to advance the SAR work, X-ray crystallography of compounds from the 1,3,8-triazaspiro[4.5]decane-2,4-dione series was attempted. A crystal structure of PHD2

(residues 181-426) with **10** bound was obtained (**Figure 23**). The structure revealed similar interactions of **12** when bound to PHD2 (**Figure 17**).[15]

The metal atom chelates between the tertiary amine of the piperidine ring and 3-methyl pyridine of **10**, the biphenyl substituent is positioned in the aromatic pocket between Trp-258, Trp-389 and Phe-391, the biphenyl group is positioned to form a hydrophobic and **π**-stacking interactions with the aromatic pocket of PHD2. The primary phenyl ring of the

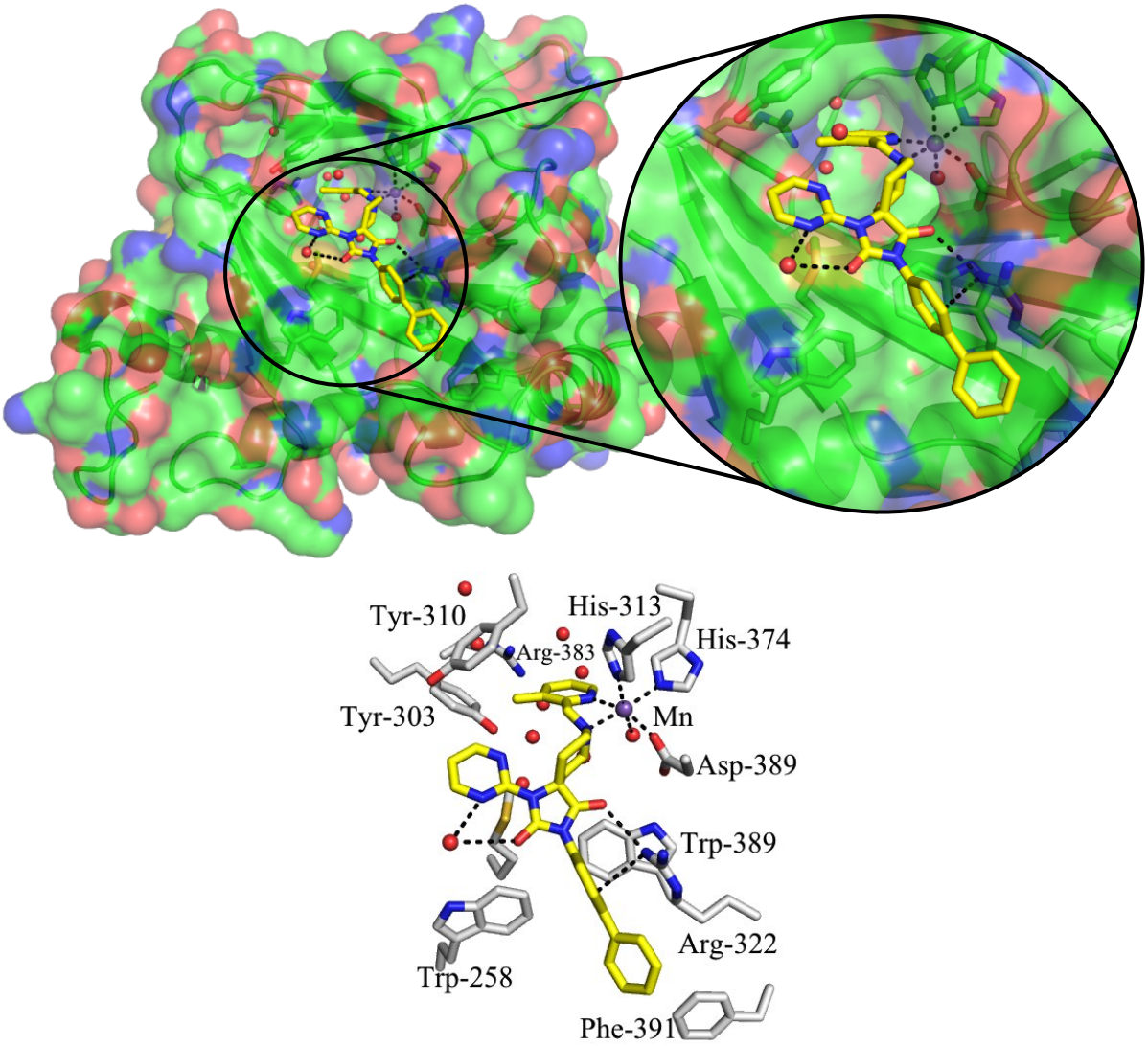

Figure 23 : Views of structure of $PHD2_{181-426}$ complexed with **10**. X-ray crystallography performed by Dr R. Chowdhury.

biphenyl substituent of **10** is positioned to form a cation **π**-interaction with Arg-322 and therefore increasing complex stability. Arg-322 is also positioned to form a hydrogen bond to a carbonyl on the imidazolidine-2,4-dione ring of **10**. The second carbonyl on the imidazolidine-2,4-dione ring of **10** is positioned to form an intramolecular salt bridge with the pyrimidine ring via a water molecule. The pyrimidine ring also is positioned to form a **π**-stacking interaction with Tyr-310.

Comparing X-ray crystal structures of PHD2 with **10** bound and 2OG and CODD bound (**Figure 24**) reveals conformationally a structural clash between **10** and the flexible β2/β3 loop. Catalytically important residues within the active site of PHD2 such as Tyr-303 and Tyr-310 are positioned differently in the PHD2:**10** structure and PHD2:2OG:CODD structure. The position of Tyr-310 in the CODD complex structure (**Figure 24B**) suggest interactions with the CODD substrate; however, in **Figure 24A** Tyr-310 forms a **π**-stacking interaction with the pyrimidine ring of **10**. Tyr-303 is hydrogen bonded to 2OG in **Figure 24B** whereas in **Figure 24A**, Tyr-303 is positioned lower than the metal atom suggesting a steric clash with **10**.

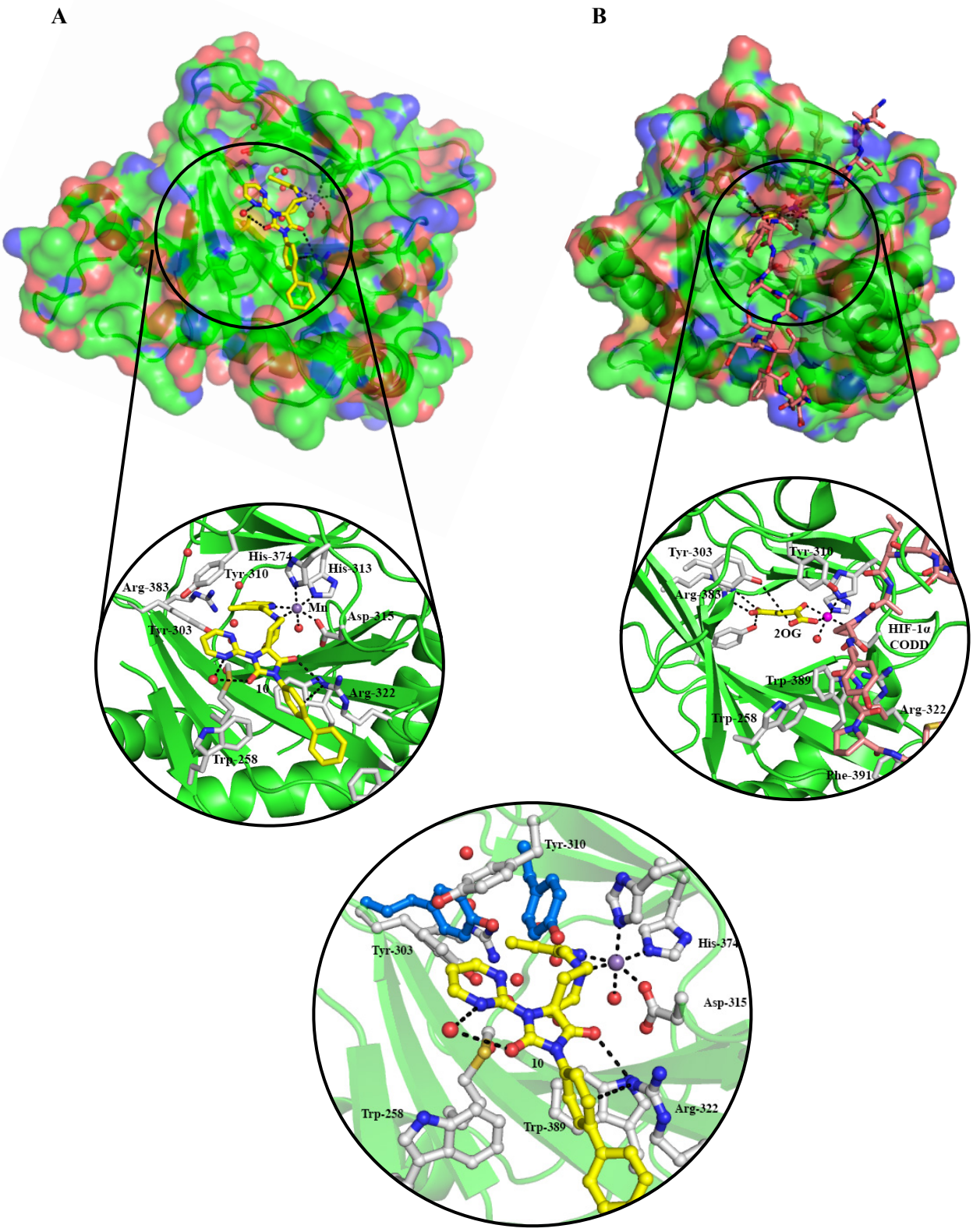

Figure 24 : A comparison of crystal structures of PHD2 with inhibitors (**A**) **10** and (**B**) 2OG (PDB ID: 3OUJ), overlaid with the crystal structure of PHD2 complexed with the HIF-1α CODD substrate (556-574) (PDB ID: 5l9B). (**C**) The active site of crystal structures of PHD2 with **10** and 2OG combined. To highlight the positional differences between the active site amino acid residues Tyr-310 and Tyr-303.[2,29]

2.8 Crystal Structure of 4-hydroxy-2-(1*H*-pyrazol-1-yl)pyrimidine-5-carboxamide Series

X-ray crystallography of compounds from the 4-hydroxy-2-(1*H*-pyrazol-1-yl)pyrimidine-5-carboxamide series was also attempted. A crystal structure of truncated PHD2 (residues 181-426) with compound **33** bound was obtained (**Figure 25**). The structure revealed the metal atom is chelated between the pyrazole and pyrimidine groups of **33**. The pyrimidine ring of **33** is positioned to form a **π**-stacking interaction with Tyr-310 and the hydroxy groups are hydrogen bonded. Identical to the X-ray crystal structure of **10** bound to PHD2, the phenyl ring of **33** is positioned to form a hydrophobic and **π**-stacking interactions with the aromatic pocket. Arg-322 interacts with **33** in an identical fashion to **10**, being positioned to form a cation **π**-interaction with the phenyl ring of **33** and hydrogen bonding to the carbonyl of **33**. From crystal structure analysis, it was difficult to determine how the 2-hydroxy-ethyl substituent interacts with PHD2. The hydroxyl group is 6.6 Å from Tyr-310 and Arg-322, suggesting a direct hydrogen bond is unlikely. No water molecules are observed around the methoxy substituent. This indicates that no intermolecular hydrogen bond interactions via bridging with a water molecule are formed with the methoxy substituent and a PHD2 residue. It was hypothesised that the 2-hydroxy-ethyl substituent of **33** may form one or more intramolecular hydrogen bonds; the amide NH is 2.9 Å and the hydroxyl group on the pyrimidine ring was 3.8 Å from the 2-hydroxy-ethyl substituent. Both interactions are theoretically possible, as hydroxyl groups are known as "flip-flop" hydrogen bond, meaning the hydroxyl can simultaneously be a hydrogen donor

and acceptor. The flexible loop between the β2/β3 strands is not visible in the X-ray crystal structure of **33** bound to PHD2, likely due to the flexible loop being disordered. It is possible the 2-hydroxy-ethyl substituent of **33** is positioned to interact with residues of the flexible loop between the β2/β3 strands.

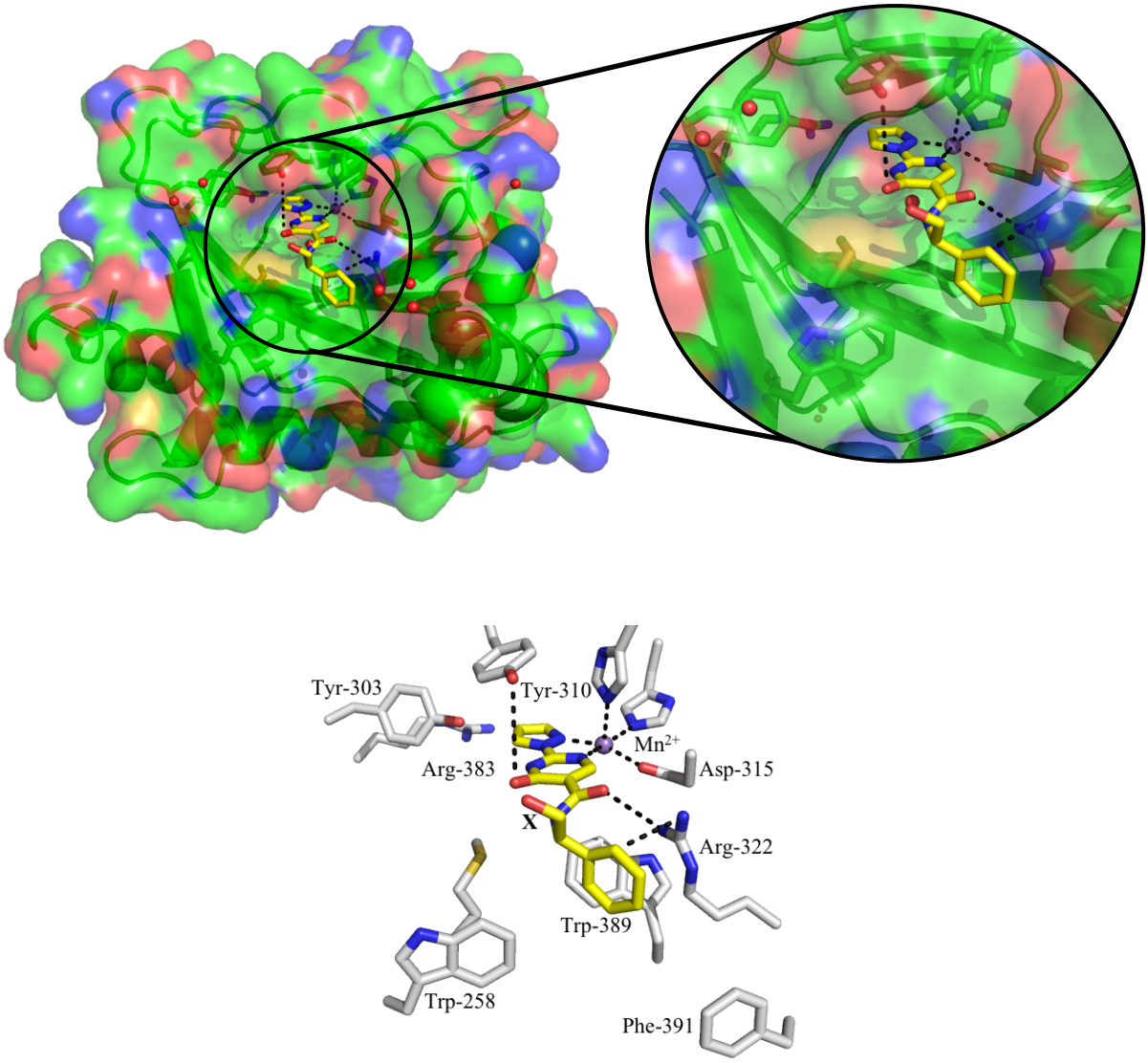

Figure 25 : Views of from the crystal structure of $PHD2_{181-426}$ complexed with **33**. Crystallography was performed by Dr. R. Chowdhury.

2.9 HIF-1α Substrate Displacement and Selectivity

It was observed that compounds from both series bind within the entrance of the active site of PHD2 (**Figure 23** and **25**) and interact with key residues in the active site. The potency observed in cellular experiments may be due to possible substrate displacement. Overlaying X-ray crystal structures of PHD2 with **10** or **32** bound with the CODD or NODD substrate

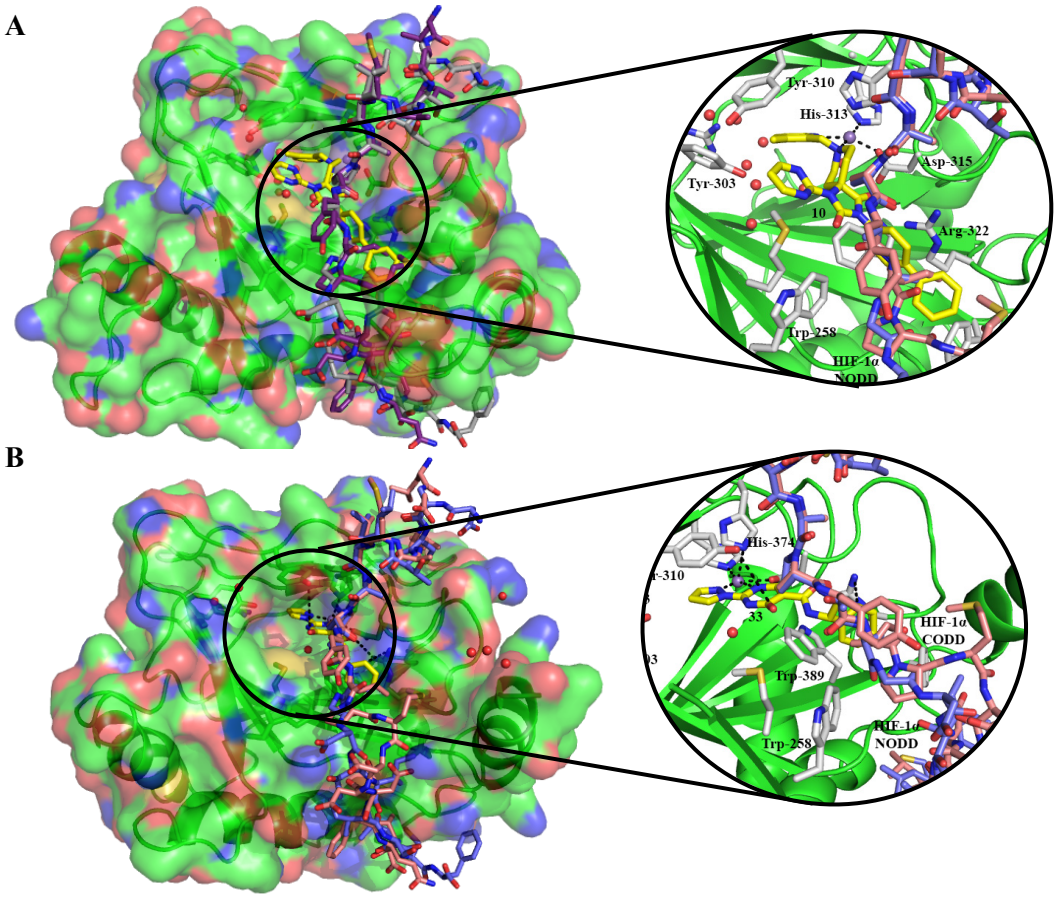

Figure 26: Views from crystal structures of compounds **10** (**A**) and **33** (**B**) complexed with PHD2, overlaid with crystal structures of PHD2 complexed with the NODD and CODD substrates (PDB IDs: 5L9V and 5l9B, respectively).[29]

bound implied steric clashes between the inhibitors and substrate (**Figure 26**), both at the entrance to the active site and in the aromatic pocket of PHD2.[29]

A selection of compounds from both series were tested for substrate displacement *via* an NMR 1D HSQC analyses, using ^{13}C-labelled PHD2 substrates i.e. ^{13}C-NODD and ^{13}C-CODD.[5] If the substrate, was bound no ^{13}C peak would be observed; however, if the substrate was displaced a ^{13}C peak at 24.25 ppm should be observed (**Figure 27**). Both compound series only displaced NODD, similar to most of the clinical candidates (**3**, **4**, **5** and **6**).[5] This was surprising due to both series binding in the aromatic pocket and the

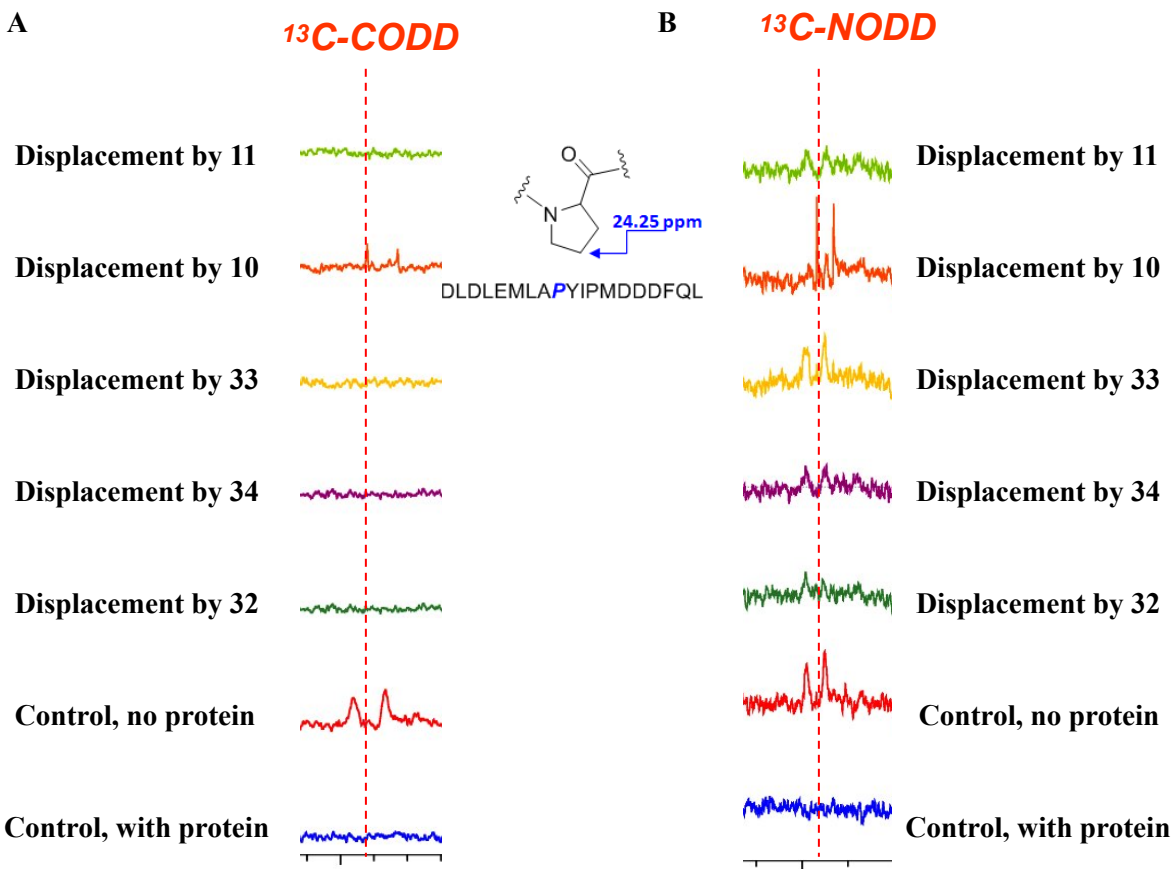

Figure 27 : **A**) Qualitative single concentration screening with various compounds by ^{13}C-CODD displacement as monitored by 1D CLIP HSQC with selective ^{13}C-inversion analyses. **B**) Qualitative single concentration screening with various compounds by ^{13}C-NODD displacement as monitored by 1D CLIP HSQC with selective ^{13}C-inversion analyses. The assay mixture contained 50 µM *apo*-PHD2-181-426, 200 µM Zn(II), 50 µM 2OG, 50 µM ^{13}C-CODD or ^{13}C-NODD, 400 µM compound and 50 mM Tris-D_{11}, pH 7.5 in 10 % D_2O and 90 % H_2O. Experiment performed by Dr. M. Abboud

Table 6 : IC_{50} values of **10** and **32** against PHD2 and CODD and NODD substrates. Experiment performed by Dr A Tumber. Experimental Measurements n = 1.

		PHD2 RapidFire™	
Cpd	**Structural Formula**	**CODD IC_{50} µM**	**NODD IC_{50} µM**
10	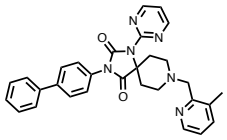	**0.498**	**0.608**
32	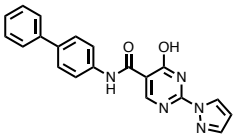	**0.258**	**0.108**

implied steric clashes observed in **Figure 27**. Initially, it was thought that **10** partially displaced CODD; however, the CH_2 within the piperidine ring of **10** resonates at the same chemical shift ^{13}C ppm as the proline CH_2. **Figure 27** suggests that both compound series may be NODD selective for displacing NODD, in order to test this theory, **10** and **32** were screened against NODD using the RapidFire assay. **10** and **32** produced similar IC_{50}s for both HIF-1α substrates on PHD2 suggesting no substrate selectivity (**Table 6**).

2.10 2OG Oxygenase Selectivity

The required criteria stated for successful PHD2 inhibition defined at the start of this chapter was focused on achieving selectivity within the 2OG oxygenase family. **Table 7** shows the selected compounds (**10**, **11**, **32** and **33**) from both series follow screened a range of other 2OG oxygenases: OGFOD1 (enzyme concentration = 1 µM),CPH (enzyme concentration = 1 µM), FIH (enzyme concentration = 0.020 µM).[5] The two main

compounds (**10** and **32**), showed weak inhibition for the selected 2OG oxygenases in comparison to inhibition of PHD2 (enzyme concentration = 0.150 μM), suggesting PHD selectivity for structurally similar 2OG oxygenases is possible. The clinical candidates (**3**, **4** & **5**. **Table 1**) showed similar (or stronger) levels of inhibition of OGFOD1.[5] **4** and **5** showed stronger levels of inhibition of CPH than of PHD2 (**Table 1**). The two main compounds of the chapter (**10** and **32**) may be able to achieve a better safety profile in comparison to the clinical candidates. However, the potency of **11** and **33** against CPH suggest the chosen binding substituent must be selected carefully in order to maintain selectivity over structurally similar 2OG oxygenases.

Table 7 : A selection of PHD inhibitors. OGFOD1: 2OG and iron-dependent oxygenase domain containing 1 (Experiment performed by Dr C Lohans), vCPH: viral Collagen Prolyl Hydroxylase (Experiment performed by Mr. Gareth Langley), FIH: Factor Inhibiting HIF (Experiment performed by Dr A Tumber), PHD2: HIF-prolyl hydroxylase-2. Experimental Measurements n = 1 for Rapid Fire.

Cpd	Structural Formula	OGFOD1 % of Inhibition at 100 μM	vCPH IC_{50} μM	FIH RapidFire™ IC_{50} μM	PHD2 RapidFire™ IC_{50} μM
10	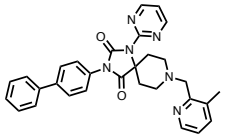	**45%**	**>100**	**14.5**	**0.498**
32	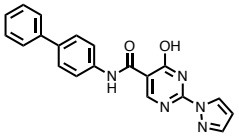	**50%**	**28**	**22.76**	**0.258**
11	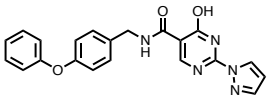	**65%**	**2.0**	**Nd**	**0.091**
33	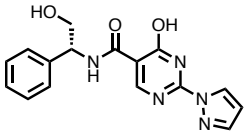	**60%**	**1.1**	**Nd**	**0.329**

2.11 Summary

Figure 28 shows a summary of the identification and characterisation of the inhibitors developed from the two starting points (**10**, **17-21**(**Chapter 2.4**) and **11**, **26-34** (**Chapter 2.5**). A required criteria was set out at the start of the chapter, with the main objective to achieve strong selectivity within the 2OG oxygenase superfamily. Investigation of X-ray crystal structures of PHD2 and other structurally similar 2OG oxygenases identified an aromatic pocket unique to PHD2. This aromatic pocket, which has significant interaction with HIF-α substrates, was targeted to achieve this objective. The two chosen starting points, both shared the desired qualities in regards to potential interaction with the aromatic pocket, but also had structural differences meaning broad structure-activity relationship (SAR) could be explored. Initial SAR *via* final synthetic step modification was explored for both starting points and tested in two different *in-vitro* assays using the same PHD2 construct and CODD substrate. Generally both series showed strong potency towards PHD2 (**10** IC_{50} 0.498 μM and **32** IC_{50} 0.258 μM), 10 fold greater than the most clinically advanced clinical candidate FG-4592 (**4**). For the 1,3,8-triazaspiro[4.5]decane-2,4-dione series (**10**, **17-21**), the RapidFire data indicated the need to have two metal chelation sites for potent inhibition. For the 4-hydroxy-2-(1*H*-pyrazole-1-yl)pyrimidine-5-carboxamide series (**11**, **26-34**), the RapidFire data indicated that changing or altering the biphenyl substituent lead to significant changes in inhibition; with IC_{50} values ranging from 246 nM to 15.68 μM. Only **10** and **32** achieved HIF-1α stabilisation at 20 μM; it was hypothesized

that other factors apart from potency including penetration and metabolism of the binding substituent were responsible for the poor efficacy. **10** and **32** were profiled against a set of HIF-α genes and achieved different levels of upregulation of HIF-α genes indicating different levels of interaction either between the PHD isoforms or the HIF-α isoforms. To further investigate, **10** and **32** were tested against PHD3. **32** achieved similar levels of inhibition of PHD3, whilst **10** was 7-fold weaker inhibition of PHD3, suggesting a reason why the two starting points differed in gene upregulation.

Two crystal structures were obtained for **10** and **33 (Figures 22 and 24**). Analysis of the crystal structures confirmed the interaction with the aromatic pocket for both series and different interactions with key residues within the PHD2 active site. Substrate displacement via an NMR 1D HSQC analyses were tested for both series. Both series displaced NODD but not CODD. Both **10** or **32** achieved similar IC_{50}s for both NODD and CODD (RapidFire) suggesting no substrate selectivity. Both **10** and **32** showed strong selectivity over structurally similar 2OG oxygenases, confirming selective PHD inhibitors are possible. However, **11** and **33** showed strong potency against CPH indicating the binding substituent needs to be chosen carefully (**Table 7**).

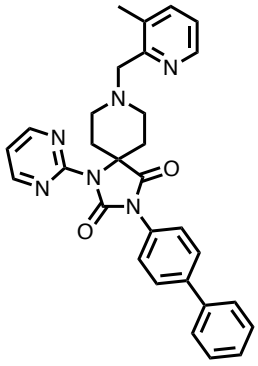

10

PHD2 IC_{50} 0.498 µM
OGFOD1 50% inhibition at 10 µM
Inhibition at 100 µM
CPH IC_{50} >100 µM
FIH IC_{50} 14.5 µM

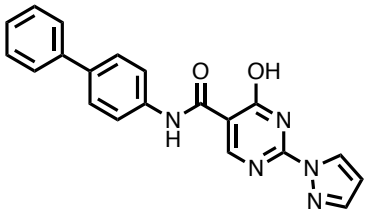

32

PHD2 IC_{50} 0.258 µM
OGFOD1 40% inhibition at 10 µM
Inhibition at 100 µM
CPH IC_{50} 28.0 µM
FIH IC_{50} 22.76 µM

Figure 28 : Summary of the two lead compounds and their selectivity profile against selected 2OG oxygenases.

2.12 Compound Characterisation

General Procedure A :

Reductive Amination: 16 (1 equiv) and the relevant aldehyde (1.2 equivs) were dissolved in either CH_2Cl_2 (4 ml). Sodium triacetoxyborohydride (5 equiv) and AcOH (a few drops) was then added to the solution; the resultant reaction mixture was stirred at room temperature overnight. MeOH (5 ml) was then added and the resultant mixture was stirred for 5 mins. CH_2Cl_2 (15 ml) was added to the reaction mixture; the reaction mixture was then washed with water, brine and then dried over Na_2SO_4. The solvent was removed in *vacuo* and was purified by flash column chromatography using (0% - 5% MeOH, CH_2Cl_2, 1 % NH_3) over 20 column volumes to give the desired compound.

General Procedure B:

Ethyl ester amide coupling: 24 (1 equivs), the relevant amine (1 equivs) and DABACO-$(AlMe_3)_2$ (0.8 equivs) were added; the microwave vial was flushed with N_2 and removed in *vacuo* (3 times) before the addition of anhydrous THF (2 ml). The reaction mixture was then heated at 130°C for 8 minutes under microwave radiation. The reaction mixture was diluted with CH_2Cl_2 (15 ml), followed by the addition of $KNaC_4H_4O_6{\cdot}4H_2O_{aq}$ (50 ml). The resultant mixture was stirred overnight. The phases were then separated and the organic phase was washed with water, brine and dried over Na_2SO_4. The solvent was removed in *vacuo*. The crude compound was

purified by flash column chromatography using (0% - 10 % MeOH, CH_2Cl_2, 1 % NH_3) over 20 column volumes to give the desired compound.

Tert-butyl 2,4-dioxo-1,3,8-triazaspiro[4.5]decane-8-carboxylate 13

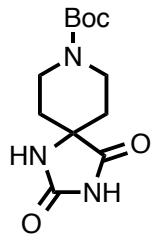

1-Boc-4-piperidone (4g, 0.02 mol), potassium cyanide (1.95g, 0.03 mol) and ammonium carbonate (5.78 g, 0.06 mol) were suspended in water and EtOH (40 ml (1:1)) and the resulting mixture was stirred at room temperature for 4 hr. The reaction mixture was then cooled, to allow precipitation to occur. The precipitate was filtered off and washed with ethanol to give **13** (3.55 g, 0.013 mol, 65.4 %) as a white crystalline solid.

m.p. >250°C. **^{1}H NMR** (400 MHz, DMSO-d_6) δ 10.72 (s, 1H, NH), 8.52 (s, 1H, NH), 3.86 – 3.74 (m, 2H, Piperidine (Pip)), 3.22 – 3.01 (m, 2H, Pip), 1.73 – 1.62 (m, 2H, Pip), 1.56 – 1.47 (m, 2H, Pip), 1.40 (s, 9H, ^{t}Boc). **^{13}C NMR** (101 MHz, DMSO-d_6) δ 177.96, 156.67, 154.29, 79.42, 60.60, 33.23, 28.49. **FT-IR** ν_{max} (film) 3427, 3342, 3050, 2910, 1729, 1713 cm^{-1}. **HRMS** (ESI-TOF) calcd for $C_{12}H_{19}O_4N_3{}^{23}Na_1$ $[M+Na]^+$: 292.1267, found : 292.1264.

Tert-butyl 3-([1,1'-biphenyl]-4-yl)-2,4-dioxo-1,3,8-triazaspiro[4.5]decane-8-carboxylate 14

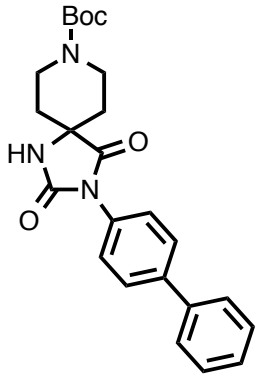

A solution **13** (500mg, 1.85 mmol) and 4-iodobiphenyl (518 mg, 1.85 mmol) was suspended in a mixture of ACN and DMF (20 ml (1:1)) and degassed with a stream of nitrogen for 15 min. *N,N'*-dimethylethylenediamine (36.7 µl, 0.55 mmol), copper (I) iodide (104 mg, 0.55 mmol) and potassium carbonate (895 mg, 6.475 mmol) were added sequentially. The resultant mixture was heated at 85°C for 16 hr, cooled to room temperature and combined with EtOAc (40 ml) and water (40 ml). The organic layer was separated, washed with water (2 x 40 ml) and dried over Na_2SO_4. The volatiles were evaporated in *vacuo* and purified with flash column chromatography (Cyclohexane 100 % - 50%, EtOAc 0 %- 50 %) over 10 column volumes to give **39** (340 mg, 0.805 mmol, 43 %) as a white solid.

m.p. 224-226°C. **^{1}H NMR** (400 MHz, DMSO-d_6) δ 9.15 (s, 1H, NH), 7.82 – 7.68 (m, 4H, Ar), 7.57 – 7.37 (m, 5H, Ar), 3.90 (m, 2H, Pip), 3.39 – 3.34 (m, 2H, Pip), 1.92 – 1.80 (m, 2H, Pip), 1.82 – 1.67 (m, 2H, Pip), 1.44 (s, 9H, ^{t}Boc). **^{13}C NMR** (101 MHz, DMSO-d_6) δ

175.27, 154.98, 154.32, 140.05, 139.80, 131.76, 129.48, 128.21, 127.66, 127.39, 127.26, 79.51, 59.56, 33.30, 28.52. **FT-IR** ν_{max} (film) 3342, 3050, 2910, 1719, 1702 cm^{-1}. **HRMS** (ESI-TOF) calcd for $C_{24}H_{27}O_4N_3{}^{23}Na_1$ $[M+Na]^+$: 444.1893, found : 444.1891.

Tert-butyl 3-([1,1'-biphenyl]-4-yl)-2,4-dioxo-1-(pyrimidin-2-yl)-1,3,8-triazaspiro[4.5]decane-8-carboxylate 15

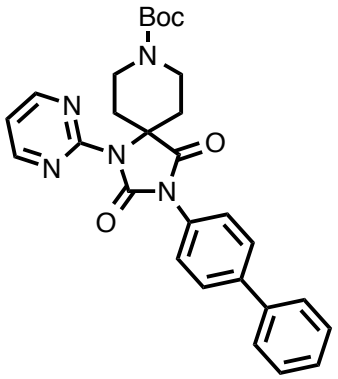

A solution **14** (400 mg, 0.94 mmol). 2-iodo-pyrimidine (585 mg, 2.84 mmol) was suspended in a mixture of ACN and DMF (20 ml (1:1)) and degassed with a stream of nitrogen for 15 min. 2,2,6,6-Tetramethyl-3,5-heptadion (196 µl, 0.94 mmol), copper (I) iodide (179 mg, 0.94 mmol) and Cs_2CO_3 (1.5 g, 4.475 mmol) were added sequentially, The resultant mixture was heated at 85°C for 16 hr, cooled to room temperature and combined with EtOAc (40 ml) and water (40 ml). The organic layer was separated, washed with water (2 x 40ml) and dried over Na_2SO_4. The volatiles were evaporated in *vacuo* and purified

with flash column chromatography (Cyclohexane 100% - 75%, EtOAc 0% - 25%) over 10 column volumes gave **15** (280 mg, 0.56 mmol, 60 %) as a white solid.

m.p. 220-223°C. **^{1}H NMR** (400 MHz, DMSO-d_6) δ 8.82 (d, J = 5.0 Hz, 2H, Pyrimidine (Pym), 7.86 – 7.38 (m, 10H, Ar), 4.04 – 3.88 (m, 2H, Pip), 3.57 – 3.37 (m, 2H, Pip), 2.71 – 2.57 (m, 2H, Pip), 2.18 – 2.11 (m, 2H, Pip), 1.43 (s, 9H, ^{t}Boc). **^{13}C NMR** (101 MHz, DMSO-d_6) δ 172.98, 158.62, 155.79, 154.22, 151.58, 140.30, 139.26, 130.63, 129.03, 128.00, 127.11, 126.88, 118.86, 78.99, 63.12, 39.52, 28.06. **FT-IR** ν_{max} (film) 2936, 1766, 1675, 1517 cm^{-1}. **HRMS** (ESI-TOF) calcd for $C_{28}H_{30}O_4N_5$ $[M+H]^+$: 500.2292, found : 500.2291.

3-([1,1'-biphenyl]-4-yl)-1-(pyrimidin-2-yl)-1,3,8-triazaspiro[4.5]decane-2,4-dione 16

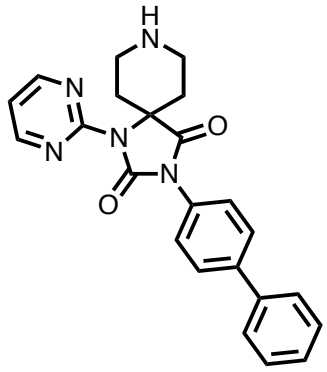

15 (250 mg, 0.501 mmol) was dissolved in neat formic acid (10ml) and stirred at room temperature for 3hr. The volatiles were evaporated in *vacuo* to give a **16** (199 mg, quant) as a orange solid.

m.p. 181-183°C. **^{1}H NMR** (400 MHz, DMSO-d_6) δ 8.88 (d, J = 5.0 Hz, 2H, Pym), 8.02 – 7.23 (m, 10H, Ar), 3.47 – 3.28 (m, 4H, Pip), 2.83 (m, 2H, Pip), 2.39 – 2.20 (m, 2H, Pip). **^{13}C NMR** (101 MHz, DMSO-d_6) δ 173.08, 164.87, 159.30, 155.98, 152.12, 140.81, 139.69, 130.99, 129.50, 128.42, 128.34, 127.56, 127.33, 119.77, 62.11, 40.38, 38.14, 28.28. **FT-IR** ν_{max} (film) 3347, 2932, 1683, 1541 cm^{-1}. **HRMS** (ESI-TOF) calcd for $C_{23}H_{22}O_2N_5$ $[M+H]^+$: 400.1768, found : 400.1763.

3-([1,1'-biphenyl]-4-yl)-8-((3-methylpyridin-2-yl)methyl)-1-(pyrimidin-2-yl)-1,3,8-triazaspiro[4.5]decane-2,4-dione 10

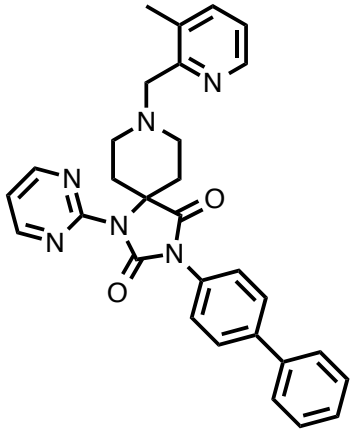

Following general procedure A: **16** (30 mg, 0.075 mmol), 3-methylpyridine-2-carboxaldehyde (10.12 µl, 0.090 mmol) and sodium triacetoxyborohydride (72 mg, 0.350 mmol) gave **10** (13 mg, 0.025 mmol, 35 %) as a white solid.

m.p. 223-226°C. **^{1}H NMR** (400 MHz, DMSO-d_6) δ 8.87 (d, J = 5.0 Hz, 2H, Pym), 8.30 (m, 1H), 7.88 – 7.36 (m, 11H, Ar), 7.19 (m, 1H), 3.66 (s, 2H, Ar-CH_2), 3.00 – 2.57 (m, 6H, Pip), 2.38 (s, 3H, CH_3), 2.15 – 2.00 (m, 2H, , Pip). **^{13}C NMR** (101 MHz, DMSO-d_6) δ 173.57, 172.46, 159.26, 156.31, 152.48, 146.20, 140.66, 139.74, 138.29, 133.33, 131.21, 129.49, 128.37, 127.56, 127.32, 122.90, 119.72, 63.90, 48.89, 30.67, 21.53, 18.48. **FT-IR** ν_{max} (film) 2980, 1671, 1545 cm^{-1}. **HRMS** (ESI-TOF) calcd for $C_{30}H_{29}O_2N_6$ $[M+H]^+$: 505.2346, found : 505.2342.

3-([1,1'-biphenyl]-4-yl)-1-(pyrimidin-2-yl)-8-(thiophen-2-ylmethyl)-1,3,8-triazaspiro[4.5]decane-2,4-dione 17

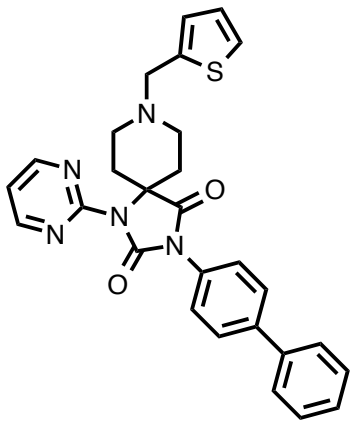

Following general procedure B: **16** (15 mg, 0.037 mmol), 2-thiophene carboxaldehyde (8.4 mg, 0.0751 mmol) and sodium triacetoxyborohydride (39 mg, 0.185 mmol) gave **17** (16 mg, 0.032 mmol, 84 %) as cream solid.

m.p. 207-209°C. **^{1}H NMR** (400 MHz, DMSO-d_6) δ 8.90 (d, J = 5.00 Hz, 2H, Pym), 7.92 – 7.31 (m, 10H, Ar), 6.99 – 6.94 (m, 2H, S-Ar), 3.77 (s, 2H, Ar-CH_2), 2.83 – 2.64 (m, 6H, Pip), 2.10 (m, 2H, Pip). **^{13}C NMR** (101 MHz, DMSO-d_6) δ 173.07, 158.82, 155.85, 152.00, 141.69, 140.19, 139.26, 130.73, 129.03, 127.93, 127.09, 126.86, 126.54, 126.18, 125.41, 119.24, 63.39, 55.74, 47.83, 39.52, 30.26, 21.08. **FT-IR** ν_{max} (film) 2982, 1699, 1644 1554 cm^{-1}. **HRMS** (ESI-TOF) calcd for $C_{28}H_{26}O_2N_5{}^{32}S$ $[M+H]^+$: 496.1801, found : 496.1799.

3-([1,1'-biphenyl]-4-yl)-8-((1-methyl-1H-imidazol-2-yl)methyl)-1-(pyrimidin-2-yl)-1,3,8-triazaspiro[4.5]decane-2,4-dione 18

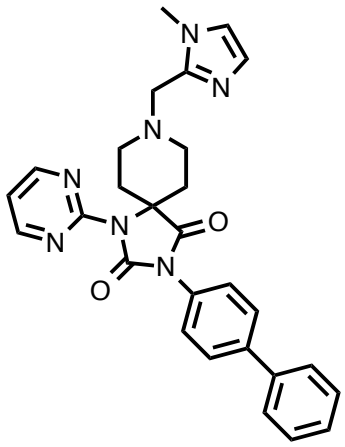

Following general procedure B : **16** (30 mg, 0.075 mmol), 1-methyl-2-imidazole carboxaldehyde (9.9 mg, 0.090 mmol) and sodium triacetoxyborohydride (72 mg, 0.350 mmol) gave **18** (18 mg, 0.036 mmol, 53 %) as cream solid.

m.p. 228-230°C. **^{1}H NMR** (400 MHz, DMSO-d_6) δ 8.88 (d, J = 5.0 Hz, 2H, Pym), 8.11 – 7.29 (m, 10H, Ar), 7.07 (s, 1H), 6.75 (s, 1H), 3.65 (s, 3H, CH_3), 3.59 (s, 2H, Ar-CH_2), 2.86 – 2.61 (m, 6H, Pip), 2.10 – 2.05 (m, 2H, Pip). **^{13}C NMR** (101 MHz, DMSO-d_6) δ 178.31,

164.05, 161.07, 157.18, 145.42, 144.49, 135.96, 134.24, 133.14, 133.05, 132.31, 132.08, 131.36, 127.09, 124.41, 68.56, 58.15, 53.36, 37.71, 35.27. **FT-IR** ν_{max} (film) 2870, 1716, 1560 cm^{-1}. **HRMS** (ESI-TOF) calcd for $C_{28}H_{28}O_2N_7$ $[M+H]^+$: 494.2299, found : 494.2289.

3-([1,1'-biphenyl]-4-yl)-8-(2-hydroxybenzyl)-1-(pyrimidin-2-yl)-1,3,8-triazaspiro[4.5]decane-2,4-dione 19

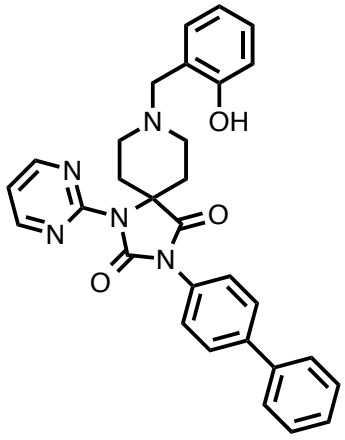

Following general procedure B: **16** (30 mg, 0.075 mmol), salicaldehyde (9.5 µl, 0.090 mmol) and sodium sriacetoxyborohydride (72 mg, 0.350 mmol) gave **19** (15 mg, 0.030 mmol, 40 %) as a cream solid.

m.p. 225-229°C. **^{1}H NMR** (400 MHz, DMSO-d_6) δ 8.90 (d, J = 5.0 Hz, 2H, Pym), 7.86 – 6.71 (m, 15H, Ar), 3.72 (s, 2H, Ar-CH_2), 2.89 – 2.82 (m, 4H, Pip), 2.84 – 2.70 (m, 2H, Pip), 2.21 – 2.13 (m, 2H, Pip). **^{13}C NMR** (101 MHz, DMSO-d_6) δ 173.50, 159.23, 157.36, 156.28, 152.31, 140.70, 139.72, 131.17, 129.79, 129.49, 128.61, 128.42, 128.30, 127.56,

127.33, 122.87, 119.59, 119.24, 115.77, 63.52, 58.62, 48.47, 30.49. **FT-IR** ν_{max} (film) 3387, 2980, 1717 cm^{-1}. **HRMS** (ESI-TOF) calcd for $C_{30}H_{26}O_3N_5$ $[M-H]^-$: 504.2041, found : 504.2049.

8-((1H-imidazol-4-yl)methyl)-3-([1,1'-biphenyl]-4-yl)-1-(pyrimidin-2-yl)-1,3,8-triazaspiro[4.5]decane-2,4-dione 20

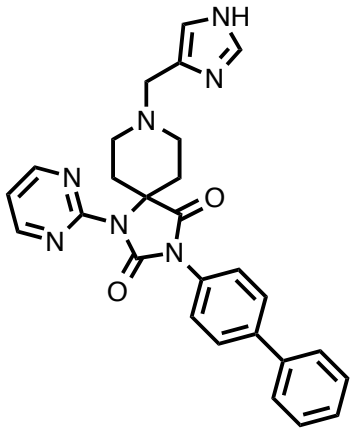

Following general procedure B: **16** (30 mg, 0.075 mmol), 4-imidazolecarboxaldehyde (10.7 mg, 0.090 mmol) and sodium triacetoxyborohydride (72 mg, 0.350 mmol) gave **20** (17 mg, 0.035 mmol, 48 %) as brown solid.

m.p. 138-143°C. **^{1}H NMR** (400 MHz, DMSO-d_6) δ 8.88 (d, J = 5.00 Hz, 2H, Pym), 7.90 – 7.33 (m, 12H, Ar), 3.47 (s, 2H, Ar-CH_2), 2.82 – 2.61 (m, 6H, Pip), 2.14 – 2.02 (m, 2H, Pip). **^{13}C NMR** (101 MHz, DMSO-d_6) δ 173.07, 158.82, 155.85, 152.00, 141.69, 140.19, 139.26, 130.73, 129.03, 127.93, 127.09, 126.86, 126.54, 126.18, 125.41, 119.24, 63.39, 55.74,

47.83, 39.52, 30.26, 21.08. **FT-IR** ν_{max} (film) 3480, 2906, 1776, 1713, 1563 cm^{-1}. **HRMS** (ESI-TOF) calcd for $C_{27}H_{26}O_2N_7$ $[M+H]^+$: 480.2142, found : 480.2140.

3-([1,1'-biphenyl]-4-yl)-8-((6-methoxypyridin-2-yl)methyl)-1-(pyrimidin-2-yl)-1,3,8-triazaspiro[4.5]decane-2,4-dione 21

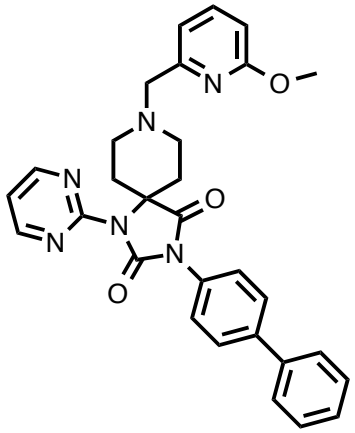

Following general procedure B: **16** (30 mg, 0.075 mmol), 1-methyl-2-imidazole carboxaldehyde (13.47 µl, 0.112 mmol) and sodium triacetoxyborohydride (72 mg, 0.350 mmol) gave **21** (14 mg, 0.027 mmol, 35 %) as a white solid.

m.p. 210-212°C. **^{1}H NMR** (400 MHz, DMSO-d_6) δ 8.91 (d, J = 5.0 Hz, 2H, Pym), 7.85 – 7.37 (m, 11H, Ar), 7.02 (d, J = 7.0 Hz, 1H), 6.68 (d, J = 8.0 Hz, 1H), 3.83 (s, 3H, O-CH_3), 3.61 (s, 2H, Ar-CH_2), 2.93 – 1.66 (m, 8H, Pip). **^{13}C NMR** (MHz, DMSO-d_6) δ 173.57, 163.42, 159.28, 156.75, 156.34, 152.48, 140.66, 139.80, 139.73, 131.22, 129.49, 128.39, 127.56, 127.32, 119.71, 115.91, 108.87, 63.84, 63.35, 53.34, 48.76, 30.90. **FT-IR** ν_{max}

(film) 2902, 1751, 1636, 1457 cm^{-1}. **HRMS** (ESI-TOF) calcd for $C_{30}H_{29}O_3N_6$ $[M+H]^+$: 521.2295, found : 521.2293.

Ethyl 4-hydroxy-2-(1H-pyrazol-1-yl)pyrimidine-5-carboxylate 24

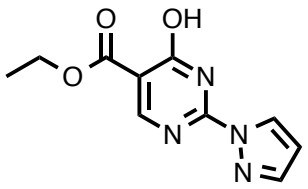

1H-Pyrazole-1-carboximide.HCl **23** (996 mg, 6.8 mmol), diethyl ethyoxymethylmalonate **22** (1.36 ml, 6.8 mmol) and sodium ethoxide (693 mg, 10.2 mol) was dissolved in anhydrous EtOH (10 ml). The reaction mixture was then heated under microwave radiation at 120°C for 90 mins. The precipitate was removed by filtration, then washed with hot EtOH and Et_2O to give **24** (960 mg, 4.10 mmol, 64%) as a cream solid.

m.p. 157-158°C. **^{1}H NMR** (400 MHz, DMSO-d_6) δ 8.46 (s, 1H, Pym), 8.05 – 7.99 (m, 1H, Pyrazole (Pyzl)), 7.73 – 7.68 (m, 1H, Pyzl), 6.72 (m, 1H, Pyzl), 4.12 (q, J = 7 Hz, 2H, $OC\underline{H_2}CH_3$), 1.20 (t, J = 7 Hz, 3H, $OCH_2C\underline{H_3}$). **^{13}C NMR** (101 MHz, DMSO-d_6) δ 170.93, 160.80, 157.49, 152.46, 145.69, 142.79, 131.58, 129.56, 108.27, 59.77, 14.81. **FT-IR** ν_{max} (film) 3251, 3150, 1683, 1513 cm^{-1}. **HRMS** (ESI-TOF) calcd for $C_{10}H_{10}O_3N_4{}^{23}Na_1$ $[M+Na]^+$: 257.0645, found : 257.0646.

4-hydroxy-2-(1H-pyrazol-1-yl)pyrimidine-5-carboxylic acid 25

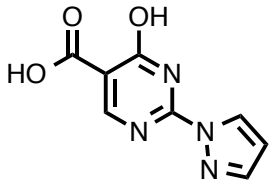

Sodium hydroxide (184 mg, 4.61 mmol) was added to a solution of **24** (500 mg, 1.53 mmol) in THF and H_2O (30ml (1:1)) and the resulting suspension stirred at room temperature for 16hr. The THF was removed in *vacuo* before the resulting mixture was washed with EtOAc (10ml), acidified to PH 2 with HCl_{aq} (1M) and extracted with EtOAc (3 x 10ml). The organic layers combined, dried over Na_2SO_4 and concentrated in *vacuo* to give **25** (391 mg, 0.189 mmol, 77 %) as white solid.

m.p. >250°C. **^{1}H NMR** (400 MHz, DMSO-d_6) δ 8.61 – 8.55 (m, 1H, Pyzl), 8.43 (s, 1H, Pym), 8.00 (s, 1H, Pyzl), 6.69 – 6.59 (m, 1H, Pyzl). **^{13}C NMR** (101 MHz, DMSO-d_6) δ 170.92, 165.14, 158.51, 151.07, 145.62, 130.56, 122.75, 111.25. **FT-IR** ν_{max} (film) 3310, 2770, 1730, 1570 cm^{-1}. **HRMS (ESI-TOF)** calcd for $C_8H_5O_3N_4$ $[M-H]^-$: 205.0367, found 205.0363.

4-Hydroxy-*N*-(4-phenoxybenzyl)-2-(1H-pyrazol-1-yl)pyrimidine-5-carboxamide 11

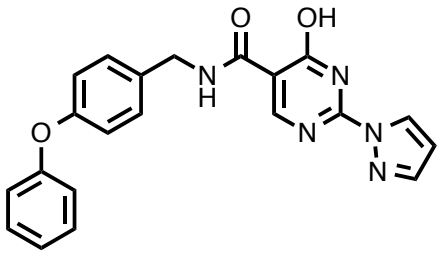

Following general procedure B: **24** (100 mg, 0.425 mmol), 4-phenyoxybenzylamine (75.9 µl, 0.425 mmol) and DABCO-$(AlMe_3)_2$ (87 mg, 0.34 mmol) gave **11** (16 mg, 0.041 mmol, 10 %) as a clear oil.

^{1}H NMR (400 MHz, DMSO-d_6) δ 13.55 (s, 1H, OH), 8.63 (t, J=6.0 Hz, 1H, NH), 8.48 (s, 1H, Pym), 8.08 – 8.04 (m, 1H, Pyzl), 7.41 – 6.90 (m, 10H, Ar), 6.74 – 6.69 (m, 1H, Pyzl), 4.51 (d, J = 6.0 Hz, 2H,$\underline{CH_2}$). **^{13}C NMR** (101 MHz, DMSO-d_6) δ 172.38, 162.82, 157.29, 155.98, 145.33, 134.79, 130.47, 130.26, 129.68, 123.77, 119.22, 118.87, 111.13, 42.11. **FT-IR** ν_{max} (film) 3280, 2876, 1670, 1593 cm^{-1}. **HRMS** (ESI-TOF) calcd for $C_{21}H_{18}O_3N_5$ $[M+H]^+$: 388.1404, found: 388.1401.

N-([1,1'-biphenyl]-4-ylmethyl)-4-hydroxy-2-(1H-pyrazol-1-yl)pyrimidine-5-carboxamide 26

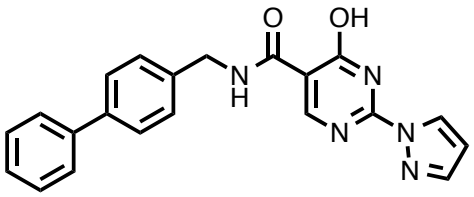

Following general procedure B: **24** (30 mg, 0.127 mmol), 4-phenylbenzylamine (23 mg , 0.120 mmol) and DABCO-$(AlMe_3)_2$ (37 mg, 0.120 mmol) gave **26** (4 mg, 0.0107 mmol, 8.5 %) as a white amorphous solid.

m.p. >250°C. **^{1}H NMR** (400 MHz, DMSO-d_6) δ 10.48 (s, 1H, OH), 8.61 – 8.48 (m, 1H, Pym), 7.85 (s, 1H, Pyzl), 7.77 – 7.26 (m, 10H, Ar), 6.56 (s, 1H, Pyzl), 4.55 (d, J = 6.0 Hz, 2H,$\underline{CH_2}$). **^{13}C NMR** (101 MHz, DMSO-d_6) δ 178.05, 165.07, 158.91, 145.55, 143.76,

142.94, 140.00, 138.77, 137.77, 134.99, 128.91, 128.91, 127.97, 127.32, 126.74, 126.61, 122.52, 103.20, 45.34. **FT-IR** ν_{max} (film) 3269, 3115, 2917, 1656, 1548 cm^{-1}. **HRMS** (ESI-TOF) calcd for $C_{21}H_{18}O_2N_5$ $[M+H]^+$: 372.1453, found: 372.1454.

N-(benzo[d][1,3]dioxol-5-ylmethyl)-4-hydroxy-2-(1H-pyrazol-1-yl)pyrimidine-5-carboxamide

27

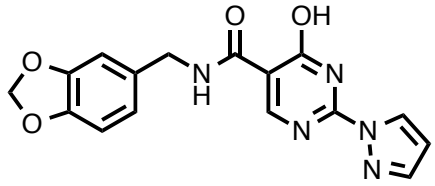

Following general procedure B: **24** (100 mg, 0.425 mmol), 3,4(methylenedioxy)-benzylamine (52 µl, 0.425 mmol) and DABCO-$(AlMe_3)_2$ (87 mg, 0.34 mmol) gave **27** (7 mg, 0.0205 mmol, 5 %) as white solid.

m.p. >250°C. **^{1}H NMR** (400 MHz, DMSO-d_6) δ 9.66 (s, 1H, OH), 8.63 (d, J = 6.0 Hz, 1H, NH), 8.46 (s, 1H, Pym), 8.06 (m, 1H, Pyzl), 6.94 – 6.68 (m, 4H, Ar), 5.98 (s, 2H, O-$\underline{CH_2}$-O), 4.42 (d, J = 6.0 Hz, 2H, $\underline{CH_2}$-NH). **^{13}C NMR** (101 MHz, DMSO-d_6) δ 176.74, 162.70, 155.36, 147.77, 146.69, 145.34, 133.42, 130.26, 121.22, 111.14, 108.60, 101.33, 42.50, 40.62, 40.41. **FT-IR** ν_{max} (film) 3200, 3121, 1668, 1559 cm^{-1}. **HRMS** (ESI-TOF) calcd for $C_{16}H_{13}O_4N_5{}^{23}Na_1$ $[M+Na]^+$: 362.0859, found : 362.0861.

N-Benzyl-4-Hydroxy-2-(1H-pyrazol-1-yl)pyrimidine-5-carboxamide 28

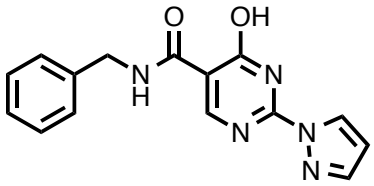

Following general procedure B: **24** (100 mg, 0.485 mmol), Benzylamine (105 µl, 0.97 mmol) and DABCO-$(AlMe_3)_2$ (87 mg, 0.34 mmol) gave **28** (8 mg, 0.0271 mmol, 5.5%) as a clear oil.

^{1}H NMR (400 MHz, DMSO-d_6) δ 8.46 (s, 1H, Pym), 7.83 (m, 1H, Pyzl), 7.43 (m, 1H, Pyzl), 7.38 – 7.17 (m, 5H, Ph), 6.56 (m, 1H, Pyzl), 4.47 (m, 2H, $\underline{CH_2}$-NH). **^{13}C NMR** (101 MHz, DMSO-d_6) δ 174.01, 166.30, 156.65, 143.69, 140.07, 130.16, 128.91, 127.74, 127.58, 127.45, 127.28, 109.01, 44.12. **FT-IR** ν_{max} (film) 3304, 2947, 1670, 1584 cm^{-1}. **HRMS** (ESI-TOF) calcd for $C_{15}H_{14}O_2N_5$ $[M+H]^+$: 296.1142, found : 296.1140.

4-hydroxy-2-(1H-pyrazol-1-yl)-N-(pyridin-2-ylmethyl)pyrimidine-5-carboxamide 29

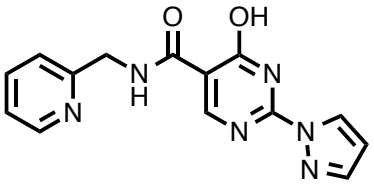

Following general procedure B: **24** (100 mg, 0.425 mmol), 2-picolylamine (43 µl, 0.425 mmol) and DABCO-$(AlMe_3)_2$ (87 mg, 0.34 mmol) gave **29** (7 mg, 0.0236 mmol, 5.5%) as a clear oil.

^{1}H NMR (400 MHz, DMSO-d_6) δ 11.10 (t, J = 6 Hz, 1H, NH), 8.54 (s, 1H, Pym), 8.53 – 8.48 (m, 2H), 7.79 – 7.73 (m, 1H), 7.69 – 7.66 (m, 1H), 7.34 – 7.23 (m, 2H), 6.45 – 6.41 (m, 1H,PyrH), 4.58 (d, J = 6 Hz, 2H, CH_2). **^{13}C NMR** (101 MHz, DMSO-d_6) δ 172.88, 166.63, 159.54, 158.34, 149.38, 141.91, 137.20, 129.29, 122.45, 121.52, 107.52, 44.39. **FT-IR** ν_{max} (film) 3296, 2932, 1643, 1554 cm^{-1}. **HRMS** (ESI-TOF) calcd for $C_{14}H_{13}O_2N_6$ $[M+H]^+$: 297.1094, found: 297.1092.

N-(cyclohexylmethyl)-4-hydroxy-2-(1H-pyrazol-1-yl)pyrimidine-5-carboxamide 30

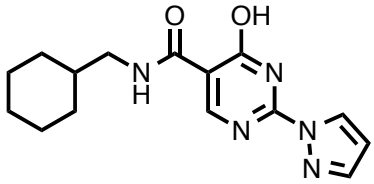

Following general procedure B: **24** (100 mg, 0.425 mmol), cyclohexane methylamine (53 µl, 0.425 mmol) and DABCO-$(AlMe_3)_2$ (87 mg, 0.34 mmol) gave **30** (22 mg, 0.073 mmol, 17.3 %) as a clear oil.

^{1}H NMR (400 MHz, DMSO-d_6) δ 9.68 – 9.55 (m, 1H, NH), 8.60 (s, 1H, Pym), 8.46 (m, 1H, PyzlH), 7.99 (m, 1H, Pyzl), 6.67 (m, 1H, Pyzl), 3.16 (d, J = 7.4 Hz, 2H, $NHCH_2$), 1.73 – 0.85 (m, 11H). **^{13}C NMR** (101 MHz, DMSO-d_6) δ 175.63, 169.27, 151.12, 144.73,

130.03, 121.26, 107.17, 45.05, 38.04, 30.87, 26.47, 25.86. **FT-IR** ν_{max} (film) 3310, 2905, 1532. **HRMS** (ESI-TOF) calcd for $C_{15}H_{20}O_2N_5$ $[M+H]^+$: 302.1612, found : 302.1615.

4-Hydroxy-2-(1H-pyrazol-1-yl)-N-(3-(trifluoromethyl)benzyl)pyrimidine-5-carboxamide 31

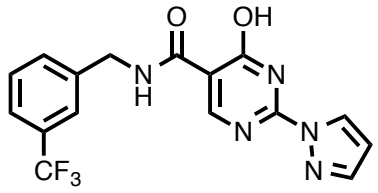

Following general procedure B: **24** (100 mg, 0.425 mmol), 3-(trifluoromethyl)benzylamine (61 µl, 0.425 mmol) and DABCO-$(AlMe_3)_2$ (87 mg, 0.34 mmol) gave **31** (34 mg, 0.093 mmol, 22%) as a white solid.

m.p. 227-232°C. **^{1}H NMR** (400 MHz, DMSO-d_6) δ 13.58 (s, 1H, OH), 9.82 (t, J = 6.0 Hz, 1H, NH), 8.48 (s, 1H, Pym), 8.10 – 8.01 (m, 1H, Pyzl), 7.74 – 7.49 (m, 5H, Ar), 6.76 – 6.68 (m, 1H,Pyr<u>H</u>), 4.61 (d, J = 6.0 Hz, 2H, <u>CH_2</u>). **^{13}C NMR** (101 MHz, DMSO-d_6) δ 177.56, 169.33, 162.64, 150.40, 148.40, 148.24, 144.88, 140.89, 131.57, 129.78, 129.44, 128.91, 125.59, 123.90, 123.61, 122.89, 110.67, 41.82. **FT-IR** ν_{max} (film) 3282, 3119, 1668. **HRMS** (ESI-TOF) calcd for $C_{16}H_{12}O_2N_5F_3{}^{23}Na_1$ $[M+Na]^+$: 386.0835, found: 386.0836.

N-([1,1'-biphenyl]-4-yl)-4-hydroxy-2-(1H-pyrazol-1-yl)pyrimidine-5-carboxamide 32

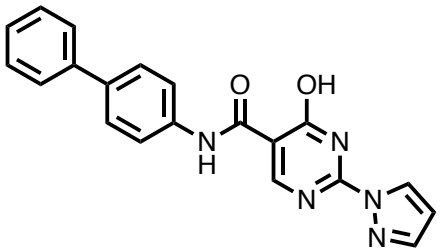

Following general procedure B: **24** (100 mg, 0.425 mmol), 4-aminobiphenyl (77 mg, 0.425 mmol) and DABCO-$(AlMe_3)_2$ (87 mg, 0.34 mmol) gave **32** (6 mg, 0.016 mmol, 4 %) as a white solid.

m.p. >250°C. **^{1}H NMR** (400 MHz, DMSO-d_6) δ 13.20 (s, 1H, OH), 8.70 (s, 1H, NH), 8.54 (s, 1H, Pym), 7.84 – 7.28 (m, 11H, Ar), 6.50 (m, 1H, Pyzl). **^{13}C NMR** (101 MHz, DMSO-d_6) δ 176.79, 164.62, 158.73, 157.19, 146.81, 142.49, 140.26, 139.31, 134.89, 129.51, 129.36, 127.56, 127.38, 126.64, 120.17, 108.10. **FT-IR** ν_{max} (film) 3283, 3087, 1670, 1543 cm^{-1}. **HRMS** (ESI-TOF) calcd for $C_{20}H_{14}O_2N_5$ [M-H]$^-$: 356.1153, found : 356.1155.

(R)-4-hydroxy-N-(2-hydroxy-1-phenylethyl)-2-(1H-pyrazol-1-yl)pyrimidine-5-carboxamide 33

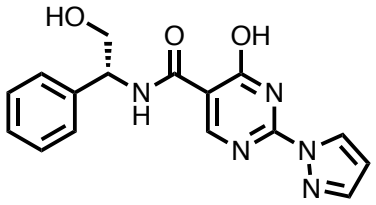

Following general procedure B: **24** (60 mg, 0.291 mmol), (*R*)-(-)-2-Phenylglycinol (119 mg, 0.873 mmol) and DABCO-$(AlMe_3)_2$ (60 mg, 0.232 mmol) gave **33** (11 mg, 0.033 mmol, 11 %) as a clear oil.

^{1}H NMR (400 MHz, DMSO-d_6) δ 11.03 (s, 1H, OH-Pym), 8.73 – 8.27 (m, 2H), 7.72 (s, 1H, Pyzl), 7.55 – 7.03 (m, 6H, Ar), 6.52 – 6.41 (m, 1H, Pyzl), 5.05 (dd, J = 8.0, 5.5 Hz, 1H,

CH), 3.83 – 3.26 (m, 2H, CH_2). **^{13}C NMR** (101 MHz, DMSO-d_6) δ 173.73, 167.24, 157.90, 146.10, 142.28, 139.31, 129.39, 128.55, 127.40, 127.09, 120.81, 107.92, 65.55, 54.84. **FT-IR** ν_{max} (film) 3383, 1638, 1397 cm^{-1}. **HRMS** (ESI-TOF) calcd for $C_{16}H_{16}O_3N_5$ $[M+H]^+$: 326.1247, found : 326.1248. $[\alpha]^D_{25}$ = -32.7° (c = 0.1 in MeOH).

(S)-4-hydroxy-N-(2-hydroxy-1-phenylethyl)-2-(1H-pyrazol-1-yl)pyrimidine-5-carboxamide 34

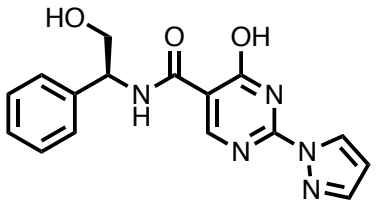

Following general procedure B: **24** (100 mg, 0.425 mmol), (*S*)-(-)-2-phenylglycinol (58 mg, 0.425 mmol) and DABCO-$(AlMe_3)_2$ (87 mg, 0.34 mmol) gave **34** (14 mg, 0.043 mmol, 10 %) as a clear oil.

^{1}H NMR (400 MHz, DMSO-d_6) δ 11.09 (t, J = 8.2 Hz, 1H, OH), 8.56 – 8.49 (s, 1H, Pym), 7.74 – 7.66 (m, 1H, Pyzl), 7.40 – 7.20 (m, 6H, Ar), 6.46 (s, 1H, Pyzl), 5.05 (dd, J = 8.0, 5.5 Hz, 1H, CH-NH), 3.98 – 3.45 (m, 2H, CH_2-OH). **^{13}C NMR** (101 MHz, DMSO-d_6) δ 177.49, 166.42, 155.61, 143.19, 143.17, 139.06, 130.29, 129.95, 128.48, 127.46, 121.14, 106.16, 67.59, 57.62. **FT-IR** ν_{max} (film) 3412, 1643, 1547 cm^{-1}. **HRMS** (ESI-TOF) calcd or $C_{16}H_{14}O_3N_5$ $[M-H]^-$: 324.1102, found : 324. 1102. $[\alpha]^D_{25}$ = +34.4° (c = 0.1 in MeOH).

2.13 References

1 Chan, M. C., Holt-Martyn, J. P., Schofield, C. J. & Ratcliffe, P. J. Pharmacological targeting of the HIF hydroxylases - A new field in medicine development. *Mol Aspects Med* **47-48**, 54-75, doi:10.1016/j.mam.2016.01.001 (2016).

2 Chowdhury, R., McDonough, M. A., Mecinovic, J., Loenarz, C., Flashman, E., Hewitson, K. S. *et al.* Structural basis for binding of hypoxia-inducible factor to the oxygen-sensing prolyl hydroxylases. *Structure* **17**, 981-989 (2009).

3 Rose, N. R., McDonough, M. A., King, O. N. F., Kawamura, A. & Schofield, C. J. Inhibition of 2-oxoglutarate dependent oxygenases. *Chem Soc Rev* **40**, 4364-4397 (2011).

4 Aik, W. S., Chowdhury, R., Clifton, I. J., Hopkinson, R. J., Leissing, T., McDonough, M. A. *et al.* in *2-Oxoglutarate-Dependent Oxygenases* 59-94 (The Royal Society of Chemistry, 2015).

5 T. Yeh, T. M. L., M. I. Abboud, C. C. Thinnes, O. Atasoylu, J. P. Holt-Martyn, D. Zhang, A. Tumber, K. Lippl, C. T. Lohans, I. K. H. Leung, H. Morcrette, A. Kawamura, E. Flashman, X. Lu, P. J. Ratcliffe, R. Chowdhury, C. W. Pugh and C. J. Schofield. Molecular and Cellular Mechanisms of HIF Prolyl Hydroxylase inhibitors in Clinical Trials. *Chem. Sci* **8**, 7651-7668, doi:10.1039/C7SC02103H (2017).

6 Rosen, M. D., Venkatesan, H., Peltier, H. M., Bembenek, S. D., Kanelakis, K. C., Zhao, L. X. *et al.* Benzimidazole-2-pyrazole HIF Prolyl 4-Hydroxylase Inhibitors as Oral Erythropoietin Secretagogues. *ACS Med. Chem. Lett.* **1**, 526 (2010).

7 Horita, S., Scotti, J. S., Thinnes, C., Mottaghi-Taromsari, Y. S., Thalhammer, A., Ge, W. *et al.* Structure of the Ribosomal Oxygenase OGFOD1 Provides Insights into the Regio-and Stereoselectivity of Prolyl Hydroxylases. *Structure* **23**, 639-652, doi:DOI 10.1016/j.str.2015.01.014 (2015).

8 Longbotham, J. E., Levy, C., Johannissen, L. O., Tarhonskaya, H., Jiang, S., Loenarz, C. *et al.* Structure and Mechanism of a Viral Collagen Prolyl Hydroxylase. *Biochemistry* **54**, 6093-6105, doi:10.1021/acs.biochem.5b00789 (2015).

9 Flora, S. J. & Pachauri, V. Chelation in metal intoxication. *Int J Environ Res Public Health* **7**, 2745-2788, doi:10.3390/ijerph7072745 (2010).

10 Abdel-Magid, A. F. Allosteric modulators: an emerging concept in drug discovery. *ACS Med Chem Lett* **6**, 104-107, doi:10.1021/ml5005365 (2015).

11 WO 2009/117269 A1. (2009).

12 WO 2011/130908 A1. (2011).

13 Vachal, P., Miao, S., Pierce, J. M., Guiadeen, D., Colandrea, V. J., Wyvratt, M. J. *et al.* 1,3,8-Triazaspiro[4.5]decane-2,4-diones as Efficacious Pan-Inhibitors of Hypoxia-Inducible Factor Prolyl Hydroxylase 1–3 (HIF PHD1–3) for the Treatment of Anemia. *J. Med. Chem.* **55**, 2945 (2012).

14 WO 2016/057762 A1. (2016).

15 Deng, G., Zhao, B., Ma, Y., Xu, Q., Wang, H., Yang, L. *et al.* Novel complex crystal structure of prolyl hydroxylase domain-containing protein 2 (PHD2): 2,8-Diazaspiro[4.5]decan-1-ones as potent, orally bioavailable PHD2 inhibitors. *Bioorg Med Chem* **21**, 6349-6358, doi:10.1016/j.bmc.2013.08.046 (2013).

16 Lipinski, C. A., Lombardo, F., Dominy, B. W. & Feeney, P. J. Experimental and computational approaches to estimate solubility and permeability in drug discovery and development settings. *Adv Drug Deliv Rev* **46**, 3-26 (2001).

17 Hann, M. M. Molecular obesity, potency and other addictions in drug discovery. *MedChemComm* **2**, 349-355, doi:10.1039/C1MD00017A (2011).

18 Sander, T., Freyss, J., von Korff, M. & Rufener, C. DataWarrior: An Open-Source Program For Chemistry Aware Data Visualization And Analysis. *Journal of Chemical Information and Modeling* **55**, 460-473, doi:10.1021/ci500588j (2015).

19 Lowe, J. in *Resmed* (New York, 2016).

20 Chowdhury, R., Yeoh, K. K., Tian, Y. M., Hillringhaus, L., Bagg, E. A., Rose, N. R. *et al.* The oncometabolite 2-hydroxyglutarate inhibits histone lysine demethylases. *EMBO Rep* **12**, 463-469, doi:10.1038/embor.2011.43 (2011).

21 Chowdhury, R., Candela-Lena, J. I., Chan, M. C., Greenald, D. J., Yeoh, K. K., Tian, Y. M. *et al.* Selective small molecule probes for the hypoxia inducible factor (HIF) prolyl hydroxylases. *ACS Chem Biol* **8**, 1488-1496, doi:10.1021/cb400088q (2013).

22 Hutchinson, S. E., Leveridge, M. V., Heathcote, M. L., Francis, P., Williams, L., Gee, M. *et al.* Enabling lead discovery for histone lysine demethylases by high-throughput RapidFire mass spectrometry. *J Biomol Screen* **17**, 39-48, doi:10.1177/1087057111416660 (2012).

23 Debenham, J. S., Madsen-Duggan, C., Clements, M. J., Walsh, T. F., Kuethe, J. T., Reibarkh, M. *et al.* Discovery of N-[Bis(4-methoxyphenyl)methyl]-4-hydroxy-2-(pyridazin-3-yl)pyrimidine-5-carboxamide (MK-8617), an Orally Active Pan-Inhibitor of Hypoxia-Inducible Factor Prolyl Hydroxylase 1–3 (HIF PHD1–3) for the Treatment of Anemia. *Journal of Medicinal Chemistry* **59**, 11039-11049, doi:10.1021/acs.jmedchem.6b01242 (2016).

24 Li, J., Subramaniam, K., Smith, D., Qiao, J. X., Li, J. J., Qian-Cutrone, J. *et al.* AlMe3-Promoted Formation of Amides from Acids and Amines. *Organic Letters* **14**, 214-217, doi:10.1021/ol203007s (2012).

25 Basha, A., Lipton, M. & Weinreb, S. M. A mild, general method for conversion of esters to amides. *Tetrahedron Letters* **18**, 4171-4172, doi:https://doi.org/10.1016/S0040-4039(01)83457-2 (1977).

26 Novak, A., Humphreys, L. D., Walker, M. D. & Woodward, S. *Tetrahedron Lett.* **47**, 5767 (2006).

27 Dubois, N., Glynn, D., McInally, T., Rhodes, B., Woodward, S., Irvine, D. J. *et al.* On DABAL-Me3 promoted formation of amides. *Tetrahedron* **69**, 9890-9897, doi:https://doi.org/10.1016/j.tet.2013.08.062 (2013).

28 Appelhoff, R. J., Tian, Y. M., Raval, R. R., Turley, H., Harris, A. L., Pugh, C. W. *et al.* Differential function of the prolyl hydroxylases, PHD1, 2 and 3 in the regulation of Hypoxia inducible factor (HIF). *J Biol Chem* (2004).

29 Chowdhury, R., Leung, I. K., Tian, Y. M., Abboud, M. I., Ge, W., Domene, C. *et al.* Structural basis for oxygen degradation domain selectivity of the HIF prolyl hydroxylases. *Nat Commun* **7**, 12673, doi:10.1038/ncomms12673 (2016).

CHAPTER 3 . Structure Activity Relationship of the 1,3,8-triazaspiro[4.5]decane-2,4-dione and 4-hydroxy-2-(1*H*-pyrazol-1-yl)pyrimidine-5-carboxamide series

3.1 Medicinal Chemistry Evaluation

Initial structure activity relationship (SAR) of the 1,3,8-triazaspiro[4.5]decane-2,4-dione series (**10**, **17**-**21**) (**Chapter 2.4**) revealed the requirement of the metal chelating substituent within the active site of PHD2. Conversion to a non-chelating substituent, or removal of the heterocycle ring that interacts with the Fe^{2+} centre, resulted in no inhibition (**Table 2**). SAR of the 4-hydroxy-2-(1*H*-pyrazol-1-yl)pyrimidine-5-carboxamide series (**11**, **26**-**34**) (**Chapter 2.5**) revealed the importance of the *C*-5 amide biphenyl group for inhibition of PHD2. It was decided that a more complete SAR of both series could better define the criteria required for PHD inhibition. The initial 'hit' compounds **10** and **32** showed different levels of inhibition for PHD2 and PHD3 (**Chapter 2.8**), it was therefore envisaged that understanding the role of each substituent of the 'hit' compounds may lead to PHD isoform selective inhibitors. The approach undertaken was to fix the amide biphenyl group whilst exploring the chemical space around the initial 'hits' **10** and **32** through modification/ addition of various substituents around the rest of the structure. The reasons for this were :

1) The biphenyl substituent apparently helped enable strong binding to PHD2 for both series, suggesting that modifying other areas of the structure the binding to aromatic pocket of PHD2 would still be possible.

2) The biphenyl substituent apparently, resulted in selectivity for PHD2 within the 2OG oxygenase superfamily likely due to interaction within the unique aromatic pocket of PHD2; therefore any novel pharmacophore developed may have a good selectivity profile.
3) From a synthetic perspective, the presence of the biphenyl substituent would significantly improve the ease of purification.

As discussed in **Chapter 2.2**, the biphenyl substituent can have poor *in-vivo* parameters.[1] It was thus proposed that following SAR development of novel pharmacophores, modification of the biphenyl substituent may be required.[2]

3.2 1,3,8-triazaspiro[4.5]decane-2,4-dione Series : The Role of The Pyrimidine Ring

A crystal structure of PHD2 bound **10** (**Figure 23**), revealed that the presence of pyrimidine ring apparently distorts catalytically important residues in the active site including Tyr-303, (**Figure 23**). It was unclear whether the pyrimidine ring was required for PHD2 inhibition. **12** was revealed by Deng *et al.* (**Figure 17**); however, the authors used a homogeneous time resolved fluorescence (HTRF) binding assay and therefore may achieve a different result compared to the RapidFire™ assay used in this work.[3] A series of analogues of **10** were designed (**Figure 29**), where the pyrimidine ring was modified or removed; various substituents were introduced based on potential interactions observed in structure of PHD2, with **10** (**Figure 23**). **40**-**44**, were synthesised using the same general route as the previous 1,3,8-triazaspiro[4.5]decane-2,4-dione series (**Scheme 9**).[4] **42** and **44**

were synthesised using the same route; although a longer reaction time was required (**Scheme 9C**). **40** and **41** were synthesised in a similar fashion; however, the second Ullmann coupling step was omitted. **40 - 44** were obtained in similar yields compared to the previous series (initial 'hits' **10**, **17 - 21**). The conversion of the methoxy group of **42** to a hydroxyl group was attempted multiple times; however, the reported procedure resulted in starting material degradation.[5]

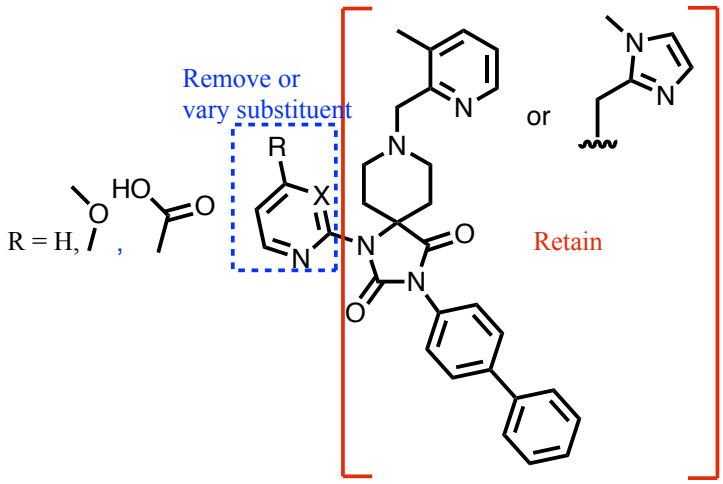

Figure 29: Strategy for the analogues investigating for the role of the pyrimidine ring for PHD inhibition. The pyrimidine was either removed or additional substituents were added to the 4-position of the ring in an attempt to form additional interactions with the PHDs.

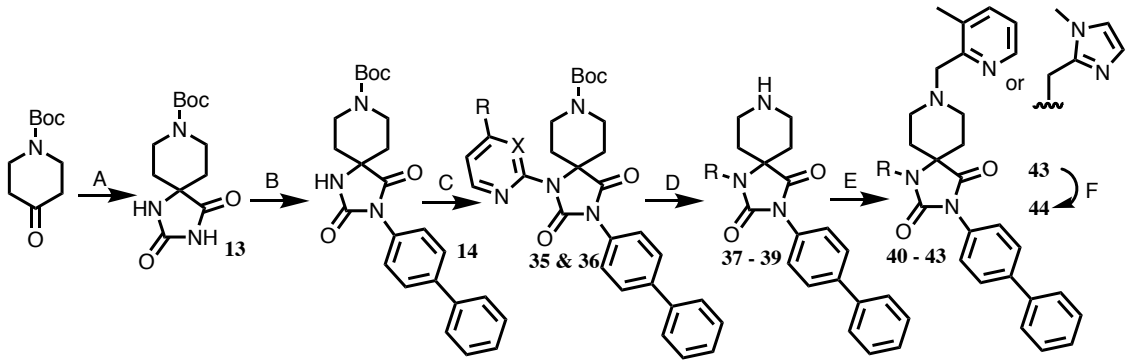

Scheme 9 : Synthesis of 1,3,8-triazaspiro[4.5]decane-2,4-dione compounds **40-44**. Reagents and Conditions: **A**) KCN, NH_4CO_3, EtOH:H_2O (1:1), 60°C, 16hrs (65%); **B**) **13**, CuI, K_2CO_3, 4-iodobiphenyl, N,N-dimethyl-ethylenediamine, Na Ascorbate, DMF : ACN (1:1), reflux 16hrs (43%); **C**) 2-iodo-aryl, TMHD, Cs_2CO_3, DMF : ACN (1:1), Reflux, 48hrs (60 %); **D**) formic Acid, 3hrs (quant); **E**) RCHO, $NaBH(OAc)_3$, CH_2Cl_2, 16hrs (35 - 84 %). **F**) LiOH, THF:H_2O (1:1), RT, 16hrs (46 %).

The screening results for the pyrimidine analogues are shown in **Table 8**. The results indicate that removal of the pyrimidine ring has little impact on PHD2 inhibition. However, the pyrimidine ring was important for selective PHD2 inhibition. **40** lost 2 fold of potency

Table 8 : SAR for the analogues investigating the role of the pyrimidine ring. Screened against PHD2 and PHD3 using the HIF-1α CODD substrate. Experiment performed by Dr A Tumber. Experimental measurement n =1.

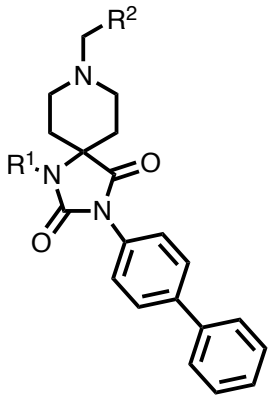

Cpd	R¹	R²	RapidFire™ PHD2 IC_{50} µM	RapidFire™ PHD3 IC_{50} µM
10	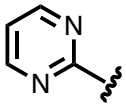	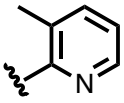	**0.496**	**3.46**
40	**H**	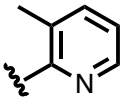	**0.500**	**1.02**
41	**H**	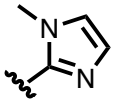	**0.171**	**0.201**
44	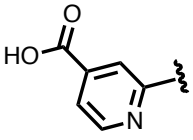	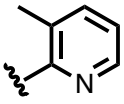	**0.333**	**ND**
42	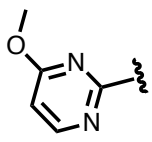	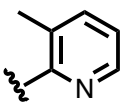	**0.282**	**ND**

on PHD3 (IC_{50} = 1.02 μM) in comparison to PHD2 inhibition (IC_{50} = 0.500 μM); **10** lost 7 fold in potency on PHD3 (IC_{50} 3.46 μM) compared to PHD2 (IC_{50} 0.496 μM) (**Table 8**). The addition of the 4-carboxylic acid (**44**) and the methoxy group (**42**) resulted in an improved potency on PHD2 inhibition (IC_{50} 0.333 μM and 0.282 μM respectively) in comparison to **10**, indicating additional interactions are formed with PHD2 in contrast to **10**. Crystallographic analysis of PHD2 complexed with **10** (**Figure 23**) suggested the additional substituents (**42** and **44**) may interact with the flexible β2/β3 loop of PHD2.

3.3 1,3,8-triazaspiro[4.5]decane-2,4-dione Series : The Role of The Core

Chapter 3.2 revealed that similar levels of inhibition could be achieved without the presence of the pyrimidine ring (**40** and **41**) and highlighted the importance of the core of **10** for potent PHD2 inhibition. For **10**, it is unknown which factors, including the rigidity and the overall structural curve of the core of **10**, are important for PHD2 inhibition (**Figure 30**). The biphenyl substituent is conserved across both the 1,3,8-triazaspiro-[4.5]decane-2,4-dione (**10**, **17-21**) and 4-hydroxy-2-(1H-pyrazol-1-yl)pyrimid-ine-5-carboxamide series (**11**, **26-34**). For **11**, **26-34** the connection between the biphenyl and the 4-hydroxy-pyrimidine substituent is a single amide bond. This lead to the question as to whether replacing the imidazolidine-2,4-dione ring (blue circle, **Figure 30**) with an amide at either the 3 or 4 position of the piperidine substituent would be able to maintain PHD2 inhibition (**Figure 30**). Replacement of the imidazolidine-2,4-dione ring to an amide group would indicate the role of the parameters of the core of **10**, such as the rigidity and the conformational bend of the overall molecule (red curve, **Figure 30**). A selection of

compounds (**51-59**) were designed and synthesised. The substituents for the 4-position of the piperidine amide were either 4-biphenyl or the 4-phenylbenzyl groups; as both substituents maintained potency on the 4-hydroxy-2-(1H-pyrazol-1-yl)pyrimidine-5-carboxamide series (**26** and **32**). As the 3-position (**57-59**) had not been investigated on the 4-hydroxy-2-(1H-pyrazol-1-yl)pyrimidine-5-carboxamide series (**11**, **26-34**), only the 4-biphenyl substituent was used as this was the only group used for 1,3,8-triazaspiro-[4.5]decane-2,4-dione series (**10**, **17-21**).

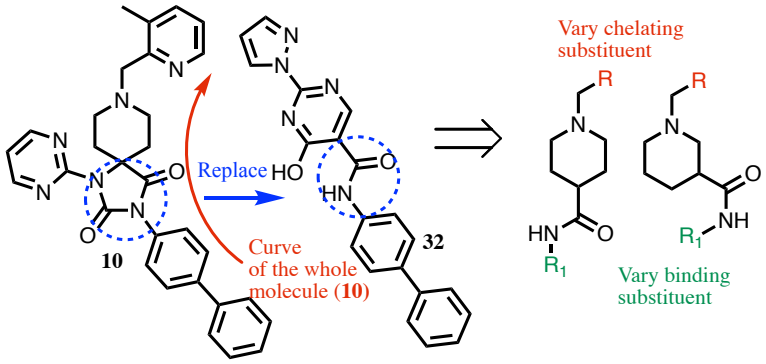

Figure 30 : Strategy for the analogues investigating the imidazolidine-2,4-dione core.

The metal binding substituent was also varied. The 3-methylpyridine and phenol substituents were chosen as they maintained strong inhibition of PHD2 in both the MALDI and RapidFire assays (**Table 2**). The 3-hydroxypyridine group was also chosen. Analysis of the crystal structure of **10** complexed with PHD2 (**Figure 23**) suggested that replacing the methyl group with a hydroxy may mimic interactions of the 4-hydroxy-2-(1H-pyrazol-1-yl)pyrimidine-5-carboxamide series (**11**, **26-34**).

Scheme 10 shows the synthetic route used for **51-59**. The requisite carboxylic acids were coupled with the relevant amine to give **45-47**. **45-47** then underwent a Pd catalysed hydrogenation to remove the Cbz protecting group to give the free secondary amines **48-50**.

The reductive amination conditions developed for the 1,3,8-triazaspiro[4.5]decane-2,4-dione series gave the targeted compounds **51-59**.

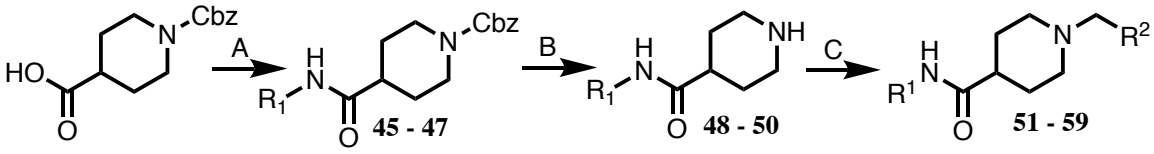

Scheme 10: Synthesis of the analogues investigating the imidazolidine-2,4-dione core. *Note the same conditions were used for the piperidine-3-carboxamide series. Reagents and conditions: **A**) T3P, R-NH_2, DIPEA, DMAc,RT,.16hrs (56 - 83%). **B**) Pd/C, H_2, MeOH, RT,.16hrs (75 - 94%). **C**) RCHO, $NaBH(OAc)_3$, CH_2Cl_2, RT,. (14 - 64 %).

Table 9 shows the screening results of the analogues investigating the role of the imidazolidine-2,4-dione core on PHD2 inhibition. The results indicated that the imidazolidine-2,4-dione core is important for PHD2 inhibition since no compounds (**51-59**) maintained any inhibition. The poor inhibition of **51-59** indicates the importance of the rigidity of the core of **10** between the aromatic pocket and the active site of PHD2.

Table 9 : SAR of analogues investigating the role of the imidazolidine-2,4-dione determined by RapidFire™. Experiment performed by Dr A Tumber. Experimental measurement n =1.

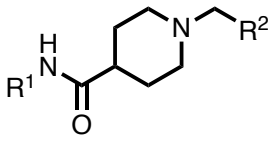

51-56

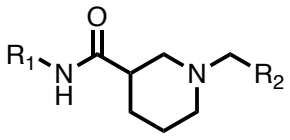

57-59

Cpd	R^1	R^2	PHD2 RapidFire™ IC_{50} µM
51	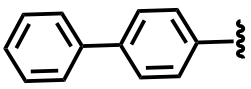	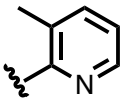	>25
52	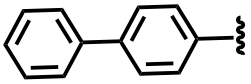	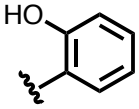	>25

Cpd	R¹	R²	PHD2 RapidFire™ IC_{50} µM
53	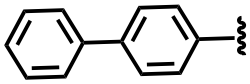	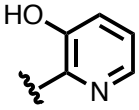	**>25**
54	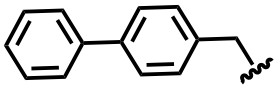	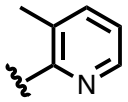	**>25**
55	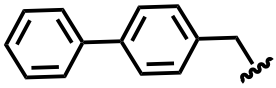	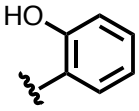	**>25**
56	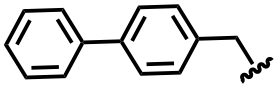	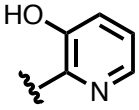	**>25**
57	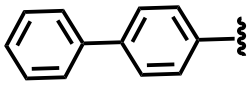	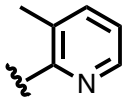	**>25**
58	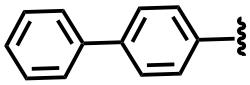	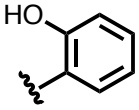	**>25**
59	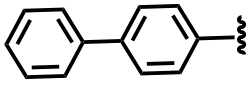	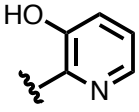	**>25**

3.4 4-hydroxy-2-(1H-pyrazole-1-yl)pyrimidine-5-carboxamide Series : The Role Of The Metal Chelating Groups

The first series of the 1,3,8-triazaspiro[4.5]decane-2,4-dione (**10**, **17-21**) revealed the necessity for a bidentate substituent for inhibition (**Chapter 2.4**). However, this series only interacts with the metal ion within the active site (**Figure 23**). A crystal structure of PHD2 with **33** bound (**Figure 25**) revealed additional interactions within the active site. Tyr-310 is positioned to form a hydrogen bond with the hydroxyl group of 4-hydroxypyrimidine group of **33** and a **π**-stacking interaction with the pyrimidine ring of **33** (**Figure 25**). This led to the question as to whether both metal chelating groups of the 4-hydroxy-2-(1H-pyrazole-1-yl)pyrimidine-5-carboxamide series were required for PHD2 inhibition. A selection of compounds were designed and synthesised to explore the role of the metal chelating groups (**Figure 31**). Due to the additional interactions with Tyr-310, the pryazole group was replaced, first by fusing the two rings together (**61** and **62**) before replacing the pyrazole group with a proton (**63** and **64**) to observe whether these modifications were able to maintain inhibition of PHD2. It was proposed that the metal chelation site furtherest into the active site (the pyrazole group for **11**, **26-34**) may only be required, acting as an anchor, maintaining molecular interactions with the active site of PHD2. The pyrimidine ring was replaced with a phenyl ring **67** to explore this theory.

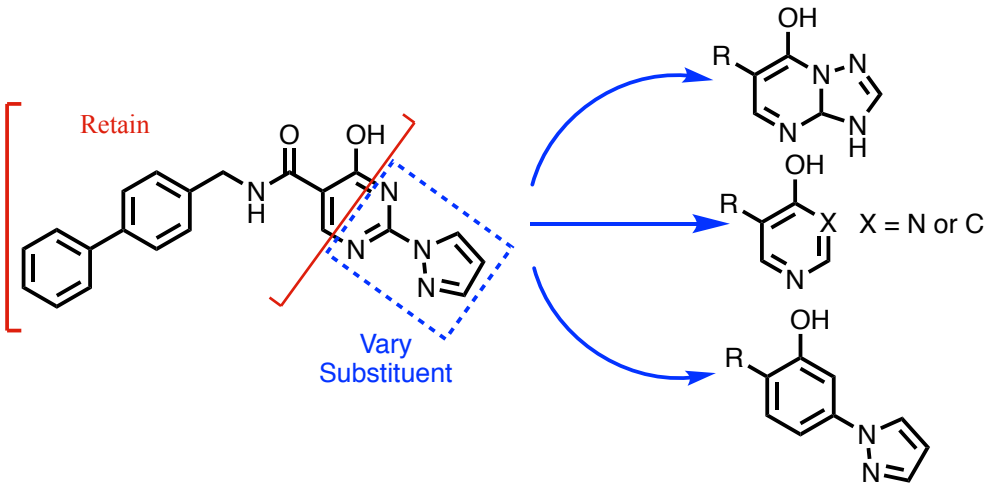

Figure 31: Strategy for the analogues investigating the role of the bidentate moiety.

61 and **62** were obtained in a two steps. The 3,3a-dihydro-[1,2,4]triazolo[1,5-*a*]pyrimidin-7-ol core **60** was first synthesised via acid catalysed cyclisation and following an amide coupling (DABAL-Me_3) gave the target compounds **61** and **62** (**Scheme 11a**).[6] **63** and **64** were synthesised via an amide coupling using either propylphosphonic anhydride (T3P) or DABAL-Me_3 (**Scheme 11b**). **67** was synthesised in three steps. **65** was

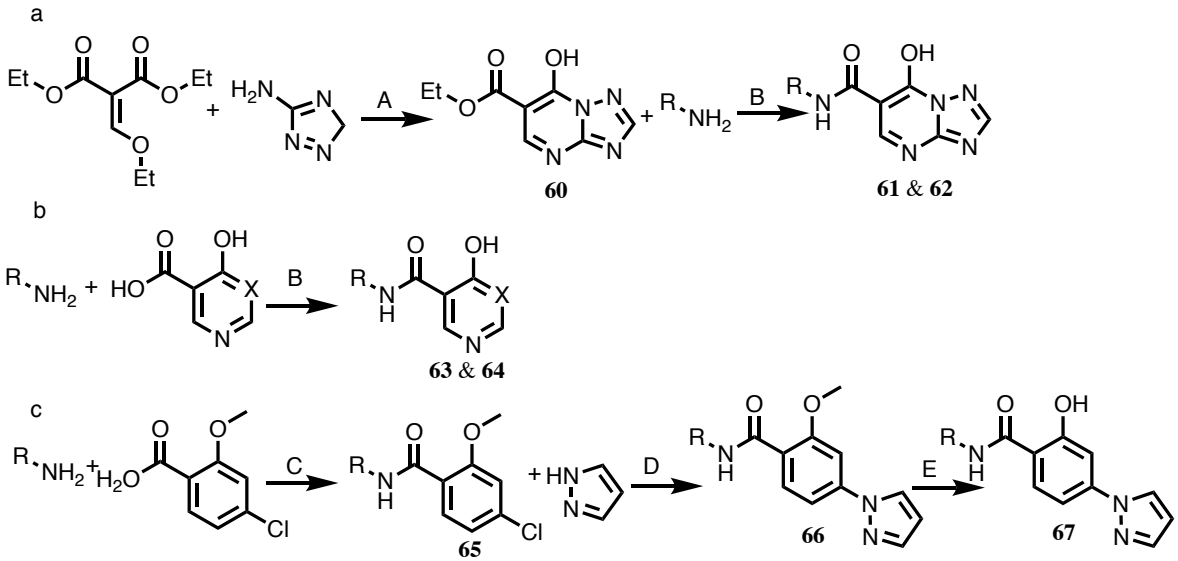

Scheme 11: Synthesis of the analogues investigating the role of the metal chelating substituents Reagents and conditions: **A**)AcOH, reflux, 16hrs (74%) **B**) DABAL-Me_3, R-NH_2, THF, MW 130 °C, 10 min (21 - 31%). **C**) T3P, R-NH_2, DIPEA, DMAc, RT,.16hrs (95%) **D**)Pd^{t}BuXPhos, Cs_2CO_3, DMA:THF, 80 °C, 16hrs (26%) **E**) TMS-I, CH_2Cl_2, 60°C, 8hrs (35%).

synthesised via an amide coupling using T3P, followed by a Buchwald coupling to give **66**. Demethylation with TMS-I gave the targeted compound **67** (**Scheme 11c**).

The screening results for the investigation of the bidentate substituent are shown in **Table 10**. The results indicated the importance of both metal chelating groups. Neither the fused compounds **61** or **62**, or the compounds without the pyrazole moiety **63** and **64** maintained inhibition of PHD2. **67** showed a 100 fold loss of potency (IC_{50} 23.0 μM) compared to **26**. This indicates the pyrazole substituent of **11**, **26-34** (the deepest Fe^{2+} chelation site in the

Table 10: SAR of analogues investigating the role of the bidentate moiety as determined by the RapidFire™ assay. Experiment performed by Dr A Tumber. Experimental measurement n =1

		PHD2 Inhibition
Cpd	**Structural Formula**	**RapidFire™ IC_{50} μM**
61	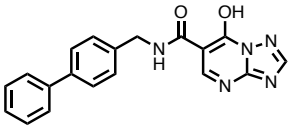	**>25**
62	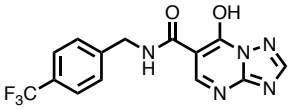	**>25**
63	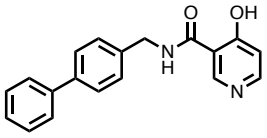	**>25**
64	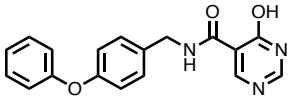	**>25**
67	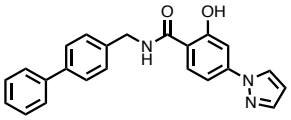	**23**
26	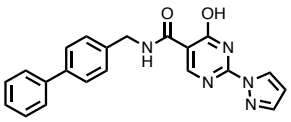	**0.286**

active site) is more important than the pyrimidine substituent of **11**, **26-34** for PHD2 inhibition; however, both chelation sites are required to achieve strong potency of PHD2.

3.5 4-hydroxy-2-(1H-pyrazole-1-yl)pyrimidine-5-carboxamide Series : The Removal or Blocking The Hydroxyl Group

Previous SAR revealed the importance of both the *C*-5 amide biphenyl and the bidentate group for potent PHD2 inhibition (**Chapter 2.5** and **3.4**). **40** and **41** (**Chapter 3.2**) revealed that PHD2 inhibition can be achieved by interacting within the aromatic pocket and chelating to the metal atom within the active site. It was questioned as to whether the *C*-4 hydroxyl group of (**11**, **26-34**) was required for inhibition. Indeed, instead of hydrogen bonding with Tyr-310 residue, the hydroxyl group may improve solubility of the molecule via forming an intramolecular hydrogen bonding interaction with the *C*-5 carbonyl group. An initial series of compounds was designed and synthesised to investigate the role of the hydroxyl group (**Figure 32**). The hydroxyl group was either removed (**71** - **73**) or converted into a benzyloxy substituent (**76** and **77**). The benzyloxy substituent was chosen because

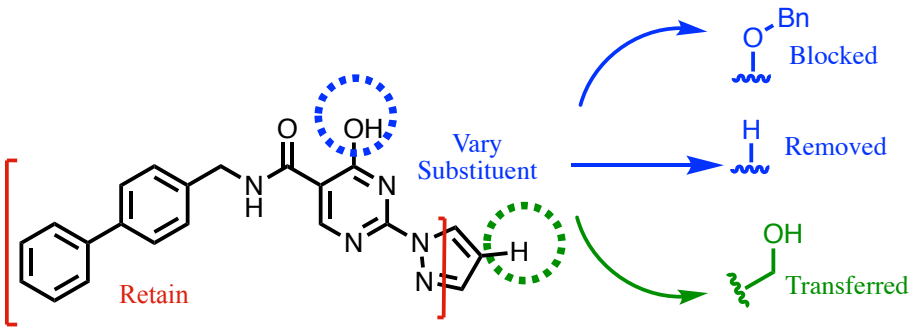

Figure 32: Strategy for the analogues investigating the role of the 4-hydroxyl substituent. The SAR work in blue is discussed in **Chapter 3.5** and the transferring of the hydroxyl group to the *C*-4 position of the pyrazole group in **Chapter 3.6**.

the crystal structure of PHD2 with **33** bound revealed a pocket that may lead to a favourable **π** stacking interaction with Tyr-303 (**Figure 25**).

The pyrimidine group was also replaced with a pyridine group (**73**), to investigate whether the second nitrogen of the pyrimidine group has a role in inhibition. **71** - **73** (**Scheme 12a**) were obtained in two steps. The first step was coupling using either T3P (the carboxylic acid (COOH)) or DABAL-Me_3 (the ester) to give **68** - **70**, in good yields (47 - 91%).[6] **68** - **70** underwent a Pd-catalysed amination via modified conditions to obtain the targeted compounds **71** - **73** (**Scheme 12a**). Issues with the solubility of **71** and **72** were solved by the use of DMAc as a solvent.

The synthesis of the benzyloxy analogues (**76** & **77**) was initially an alternative route to synthesise the first 4-hydroxy-2-(1*H*-pyrazole-1-yl)pyrimidine-5-carboxamide series (**Chapter 2.5**) (**76** for **26** and **77** for **32**); however, the route failed on the deprotection step to obtain the desired compounds (**26** and **32**). Various hydrogenation conditions were attempted including Pearlman's catalyst, acetic acid as the solvent and increasing temperature; all resulted in fragmentation of **76** and **77**.

76 and **77** were synthesised *via* a benzyl protection on **24** to give **74** (**Scheme 12b**). It was found that DMSO was the optimum solvent for **24**. Base catalysed ester hydrolysis gave **75**. Amide coupling of **75** using 1-[Bis(dimethylamino)methylene]-1H-1,2,3-triazolo[4,5-b]pyridinium 3-oxid hexafluorophosphate (HATU) yielded targeted compounds **76** and **77**. The success of this synthetic route supports the proposal that the free hydroxyl group was the reason for the poor amide couplings for the initial series (**Chapter 2.5**).

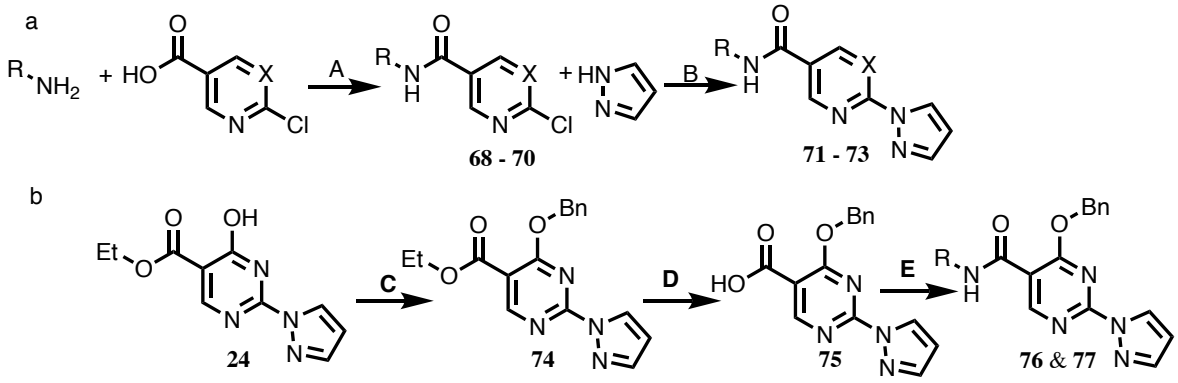

Scheme 12: The synthesis of the analogues investigating the role of the *C*-4 hydroxyl group. Reagents and conditions: **A**) T3P, R-NH_2, DIPEA, DMAc, RT,.16hrs (47-91%). **B**) Pd^{t}BuXPhos, Cs_2CO_3, DMAc:THF(1:1), MW 100°C, 1hr (16 - 58%). **C**) BnBr, Cs_2CO_3, 60°C, 16hrs (42%). **D**) LiOH, THF:H_2O (1:1), RT, 16hrs (77 %). **E**) HATU, amine, DIPEA, DMAc, RT,.16hrs (25 - 40 %).

Table 11 : SAR of analogues investigating the role of the C-4 hydroxyl group determined by RapidFire™. assay. Experiment performed by Dr A Tumber. Experimental measurement n =1

		PHD2 Inhibition
Cpd	**Structural Formula**	**RapidFire™ IC_{50} µM**
71	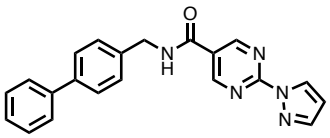	**>25**
72	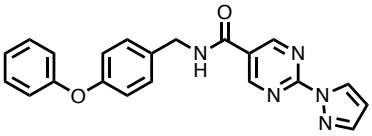	**>25**
73	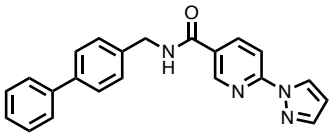	**>25**
76	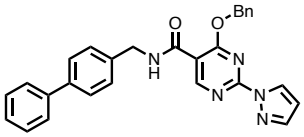	**>25**
77	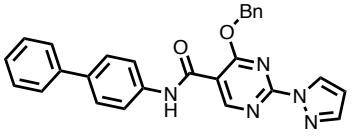	**>25**

The results (**Table 11**) reveal that when the hydroxyl is either removed (**71-73**) or converted into a benzyloxy group (**76** and **77**) PHD2 inhibition is not maintained. This indicates for the 4-hydroxy-2-(1*H*-pyrazole-1-yl)pyrimidine-5-carboxamide series (**11**, **26-34**), all areas of the molecule are required for PHD2 inhibition. Due to previous synthetic challenges and little difference between pyrimidine and pyridine substituents, the pyridine substituent in upcoming series were chosen to replace the pyrimidine substituent.

3.6 4-hydroxy-2-(1H-pyrazole-1-yl)pyrimidine-5-carboxamide Series : Transferring or Replacing The Hydroxyl Group

Clinical candidates such as **4** and **5** possess a 3-hydroxypyridine substituent.[7] Indeed, the PHD2 crystal structure complexed with **3** shows the *C*-3 hydroxyl group is positioned to form a hydrogen bond with Tyr-303 (**Figure 33A**).[8] It was hypothesised that transferring the hydrogen bond interaction from Tyr-310 to Tyr-303 may result in maintained inhibition

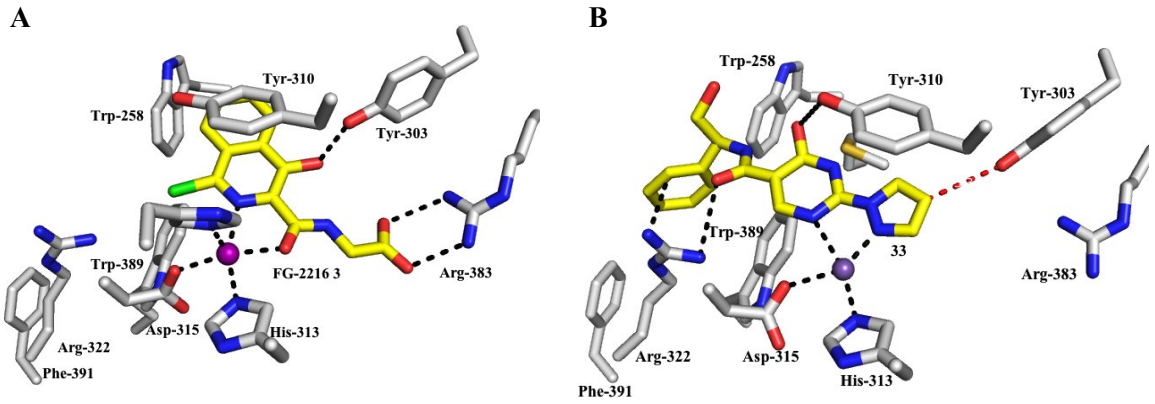

Figure 33: (**A**) View from an X-ray crystal structure of **3** bound to $PHD2_{181-426}$, showing a hydrogen bond between the quinolin-3-ol and Tyr-303 (PDB ID: 2y34).[8] **B**) View from X-ray crystal structure of **33** bound to $PHD2_{181-426}$ (carbon = yellow) , showing a hydrogen-bond between the 4-hydroxypyrimidine and Tyr-310 and the potential hydrogen bond (red line) between Tyr-303 and the 4-position of the pyrazole ring.

of PHD2 (**Figure 33**). **Figure 33** shows a comparison between PHD2 crystal structures with **3** (**A)** and **33** (**B**) bound. For the pyridinyl-pyrazole motif (**73**), to interact with Tyr-303 residue, the 4-position of the pyrazole group of (**73, Figure 32**) was chosen for its optimal distance to Tyr-303 (3.3 Å) (**Figure 33B**). The methoxy group was chosen instead of the direct hydroxyl group on the pyrazole ring for synthetic reason of efficiency.

70 and **78** underwent nucleophilic aromatic substitution (S_NAr) to couple the (1*H*-pyrazol-4-yl)methanol group to give **79** and **80**. The poor yields obtained were believed to the presence of the alcohol, reducing the nucleophilicity of the pyrazole nitrogen. Attempts to couple the (1*H*-pyrazol-4-yl)methanol group to the 2-chloro pyrimidine fragments **68** and **69** via SNAr and Pd-catalysed amination failed to yield product.

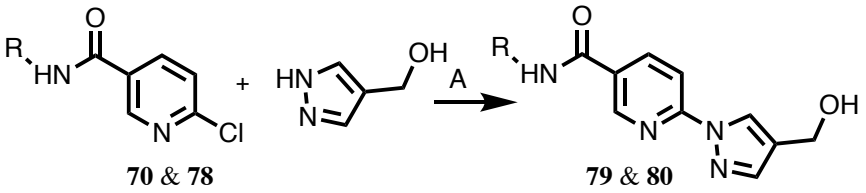

70 & **78** **79** & **80**

Scheme 13: The synthesis of the *C*-4 methoxy group pyrazole analogues. Reagents and conditions: **A**) Cs_2CO_3, DMF (, 120 °C, 3hr (9 - 16 %).

Table 12 shows the attempts to recover potency against PHD2. In general, the RapidFire data indicated the importance of the hydrogen bonding interaction for **11**, **26-34** between the *C*-4 hydroxyl group on the pyrimidine ring and residue Tyr-310 (**Figure 25**). The transfer of the hydroxyl from the pyrimidine ring to the pyrazole resulted in a lack of inhibition of PHD2. However, the poor inhibition may be due to the CH_2 bridge between the pyrazole and the hydroxyl group, increasing the disorder between the hydrogen bond donor and acceptor; therefore resulting in a weaker interaction.

The 1-(4-aminoquinazolin-2-yl)-1*H*-pyrazole-4-carboxylic acid pharmacophore (**Figure 34**) was reported in the patent literature and shares similarities to the 4-hydroxy-2-(1*H*-pyrazole-1-yl)pyrimidine-5-carboxamide pharmacophore, including the Fe^{2+} chelating substituent.[9] Instead of a hydroxy moiety, a secondary or tertiary amine is at the 4-position of the pyrimidine ring.[9] The 1-(4-aminoquinazolin-2-yl)-1*H*-pyrazole-4-carboxylic acid pharmacophore (**Figure 34**) demonstrated pIC_{50} of 7.7 according to the patent literature; however a [^{14}C] succinate capture assay was used to measure PHD2 activity.[9] The main issue with the [^{14}C] succinate capture assay is that the hydroxylation of the substrate is not directly monitored. This is a problem given the possibility for uncoupled 2OG turnover.[7] It was envisaged that replacing the *C*-4 hydroxyl group with a tertiary amine on **11**, **26-34**, may maintain inhibition on PHD2 (**Figure 34**).

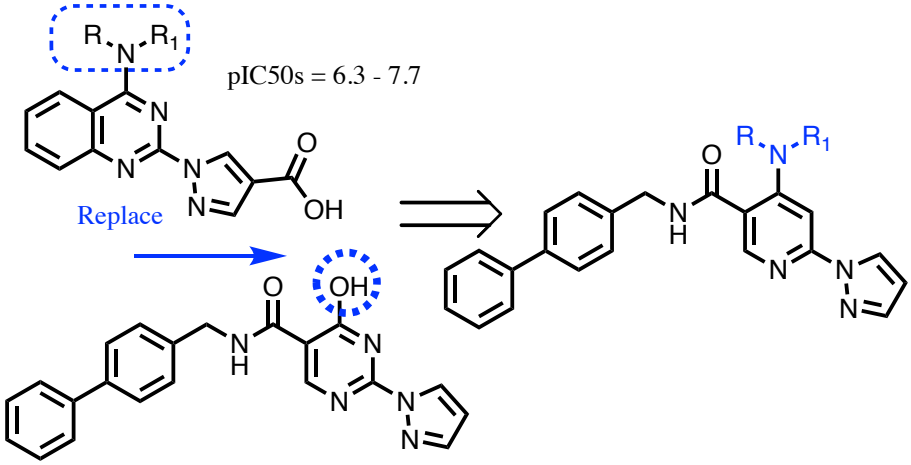

Figure 34 : Comparison of 1-(4-aminoquinazolin-2-yl)-1*H*-pyrazole-4-carboxylic acid pharmacophore and **26,** leading to a combination to investigate 4-aminopyridine analogues for PHD2 inhibition.

83 and **84** were designed and synthesised, the dimethylamine and benzylamine groups were used as the *C*-4 amine substituents. The dimethyl group was chosen as it was heavily featured in the patent literature, whilst the benzylamine was chosen as it differed

structurally and may form additional interactions within the active site such as **π**-stacking interaction.[9] **83** and **84** were synthesised in three steps (**Scheme 14**). Initially, the amide coupling used HATU to give **81**. An SNAr reaction was then used to react pyrazole to the pyridine 2-position to give **82**. **83** was obtained via a Buchwald coupling. **84** was obtained by an additional SNAr with dimethylamine.

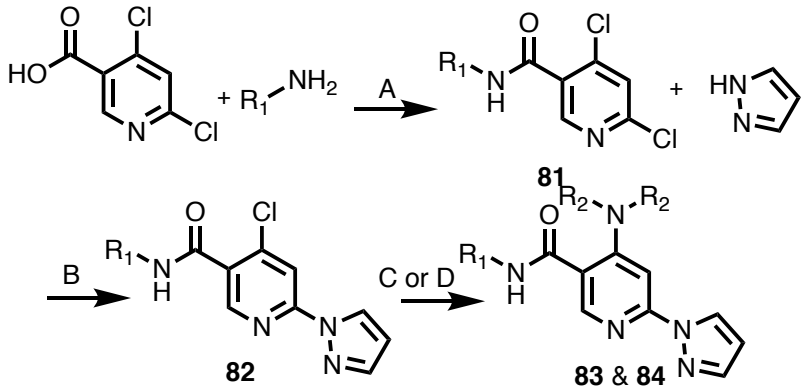

Scheme 14: The synthesis of the C-4 amino analogues. Reagents and conditions: **A**) T3P, R-NH_2, DIPEA, DMAc, RT,.16hrs (47%). **B**) Cs_2CO_3, DMAc, MW 80°C, 30 min (72 %). **C**) $(CH_3)_2NH$, DMAc, MW 120°C, 2 hrs (61 %). **D**) $BnNH_2$, PdBrettPhos, Cs_2CO_3, THF, MW 80°C, 2hrs (14 %).

83 achieved weak inhibition of PHD2 (IC_{50} 14 μM) (**Table 12**). Comparing to benzyloxy derivatives (**76** and **77**), the available proton or electrons from the *C*-4 benzylamine of **83** may form an hydrogen bond with Tyr-310 along with additional **π**-stacking interaction. **84** resulted in an increase in CODD hydroxylation, (61% increase in CODD hydroxylation compared to the DMSO control on the RapidFire assay) indicating the tertiary amine plays a minor role in PHD2 inhibition for the 1-(4-aminoquinazolin-2-yl)-1*H*-pyrazole-4-carboxylic acid pharmacophore (**Figure 34**). The increase in hydroxylation had not been seen before using the rapid-fire assay and was investigated further in order to explore the possibility of small molecule enzymatic activation (**Chapter 5**).

Table 12 : SAR of analogues of 4-methoxy pyrazole derivatives and 4-amino-pyridine determined as by the RapidFire assay. Experiment performed by Dr A Tumber. Experimental measurement n =1.

Cpd	Structural Formula	PHD2 Inhibition RapidFire™ IC_{50} µM
79	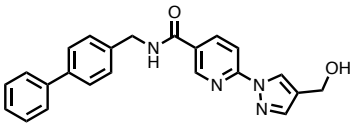	**>25**
80	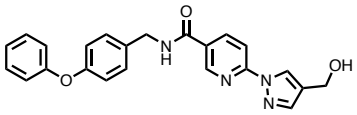	**>25**
83	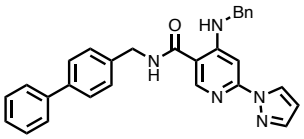	**14.0**
84	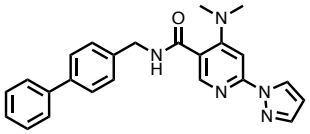	**61 % increase in substrate hydroxylation at 25 µM**

3.7 Summary

This chapter decribes thorough SAR on the 1,3,8-triazaspiro[4.5]decane-2,4-dione and 4-hydroxy-2-(1*H*-pyrazol-1-yl)pyrimidine-5-carboxamide series. Notably, for the 1,3,8-triazaspiro[4.5]decane-2,4-dione series the importance of the imidazolidine-2,4-dione core was identified (**Chapter 3.3**). Replacing the imidazolidine-2,4-dione core with an amide bond resulted in complete loss of activity, indicating that rigidity between the aromatic pocket and the active site is important for PHD2 inhibition (**Table 9**). The reduction of rigidity *via* replacing the *C*-5 amide link of the 4-hydroxy-2-(1H-pyrazole-1-yl)pyrimidine-5-carboxamide series was not attempted due to the poor inhibition of **51** - **59**. The removal of the pyrimidine ring **40** and **41** maintained PHD2 inhibition and improved PHD3 inhibition in comparison to **10**, indicating the pyrimidine substituent may have a role in achieving PHD isoform selectivity (**Table 8**). Additional substituents to the pyrimidine ring of the 1,3,8-triazaspiro[4.5]decane-2,4-dione series (**42** and **43**) improved PHD2 inhibition, suggesting additional interactions can occur at the entrance of the active site (**Table 8**).

For the 4-hydroxy-2-(1H-pyrazole-1-yl)pyrimidine-5-carboxamide series, the broad SAR revealed that all substituents of the initial 'hits' (**11**, **26-34**) were important for PHD2 inhibition. Individually, none of the areas that were investigated (**Chapters 3.4-3.6**) were able to maintain PHD2 inhibition in contrast to the initial 'hits' (**11**, **26-34**). This indicates a synergistic effect between functional groups of the molecules: the *C*-5 amide substituent interacting with the aromatic pocket, the C-4 hydroxyl and the Fe^{2+} bidentate chelating

groups. Replacing the hydroxyl group with an amine substituent resulted in weak inhibition (**76**) and surprisingly an increased turnover in CODD hydroxylation (**77**). Overall, the broad SAR of both initial hits indicate the sensitivity of PHD2 inhibition.

3.8 Compound Characterisation

General Procedure C:

T3P amide coupling: The carboxylic acid (1equiv) and DIPEA (2.5 equiv) was dissolved in DMF (5ml), followed by the addition of T3P (1.5 equiv, 50% in DMF). The resulting reaction mixture was stirred at room temperature for 30 mins before the addition of the amine (1.2 equiv). The resulting mixture was stirred overnight at room temperature. EtOAc (15ml) was added to the reaction mixture before washing with water, brine and drying with anhydrous Na_2SO_4. The crude compound was then purified using flash column chromatography using (Cyclohexane 100 % - 50%, EtOAc 0 %- 50 %) over 10 column volumes to give the desired compound .

General Procedure D:

Pd-catalysed Amination : The microwave vial was dried in a hot oven. Flushed with N_2 and removed in vacuo, repeated 3 times. The aryl halide (1 equiv), amine (1.2 equiv), Cs_2CO_3 (2 equiv), Pd-ligand conjugate (0.1 equiv) were dissolved in a 1:1 mixture of DMA and THF (4 ml) (unless stated). The resulting mixture was heated under microwave radiation for 1 hr at 120°C, allowed to cool to room temperature and filtered through a celite pad. EtOAc (20ml) was added and the resulting mixture was washed with water (2 times), brine and dried with anhydrous Na_2SO_4. The crude compound was then purified using flash column chromatography using (0% - 5% MeOH, CH_2Cl_2, 1 % NH_3) over 20 column volumes to give the desired compound.

Tert-butyl 3-([1,1'-biphenyl]-4-yl)-1-(4-(methoxycarbonyl)pyridin-2-yl)-2,4-dioxo-1,3,8-triazaspiro[4.5]decane-8-carboxylate 35

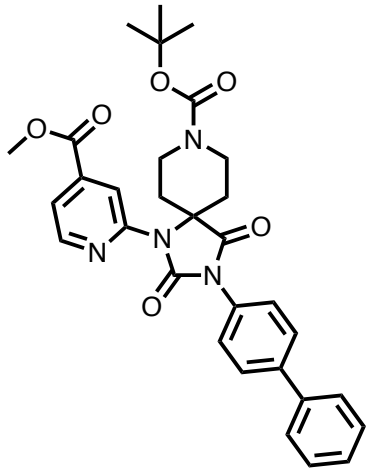

A solution **14** (50mg, 0.118 mmol) and methyl 2-iodoisonicotinate (93 mg, 0.356 mmol) was suspended in a mixture of Acetonitrile and DMF (5 ml (1:1)) and degassed with a stream of nitrogen for 15 min. 2,2,6,6-Tetramethyl-3,5-heptadion (25 µl, 0.118 mmol), Copper (I) iodide (22 mg, 0.118 mmol) and Cs_2CO_3 (192 mg, 0.59 mmol) were added sequentially, The resultant mixture was heated at 85°C for 48 hrs, cooled to room temperature and combined with EtOAc (15 ml) and Water (15 ml). The organic layer was separated, washed with water (2 x 40 ml) and dried with anhydrous Na_2SO_4. The volatiles were evaporated in *vacuo* and purified with flash column chromatography using (Cyclohexane 100 % - 50%, EtOAc 0 %- 50 %) over 10 column volumes to give **35** (29 mg, 0.052 mmol, 45 %) as a clear oil.

^{1}H NMR (400 MHz, Chloroform-*d*) δ 8.66 (d, J = 1.0 Hz, 1H, Pyr), 8.50 (dd, J = 5.0, 1.0 Hz, 1H, Pyr), 7.79 – 7.35 (m, 10H, Ar), 4.33 – 4.03 (m, 2H, Pip), 3.94 (s, 3H, CH_3), 3.59

(m, 2H, Pip), 3.18 (m, 2H, Pip), 1.88 (m, 2H, Pip), 1.52 (s, 9H, ^{t}Boc). **^{13}C NMR** (101 MHz, Chloroform-*d*) δ 173.56, 165.22, 155.13, 153.36, 151.00, 148.27, 141.80, 140.22, 139.75, 130.03, 129.00, 128.04, 127.88, 127.36, 126.78, 119.69, 117.67, 79.91, 77.16, 64.36, 52.95, 39.49, 28.58, 27.02. **FT-IR** ν_{max} (film) 2921, 1742, 1730, 1662, 1517 cm^{-1}. **HRMS** (ESI-TOF) calcd for $C_{31}H_{32}O_6N_4$ $[M+H]^+$: 557.2395, found : 557.2289.

Tert-butyl 3-([1,1'-biphenyl]-4-yl)-1-(4-methoxypyrimidin-2-yl)-2,4-dioxo-1,3,8-triazaspiro[4.5]decane-8-carboxylate 36

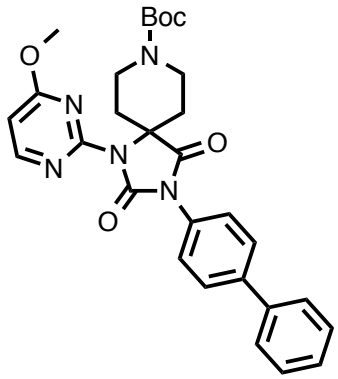

A solution **14** (400 mg, 0.94 mmol). 2-iodo-4-methoxypyrimidine (670 mg, 2.84 mmol) was suspended in a mixture of ACN and DMF (20 ml (1:1)) and degassed with a stream of nitrogen for 15 min. 2,2,6,6-Tetramethyl-3,5-heptadion (196 µl, 0.94 mmol), copper (I) iodide (179 mg, 0.94 mmol) and Cs_2CO_3 (1.5 g, 4.475 mmol) were added sequentially, The resultant mixture was heated at 85°C for 48 hrs, cooled to room temperature and combined with EtOAc (40 ml) and water (40 ml). The organic layer was separated, washed with water

(2 x 40ml) and dried over Na_2SO_4. The volatiles were evaporated in *vacuo* and purified with flash column chromatography using (Cyclohexane 100 % - 75%, EtOAc 0 %- 25 %) over 10 column volumes to give **36** (342 mg, 0.64 mmol, 68.8 %) as clear oil.

^{1}H NMR (400 MHz, Chloroform-*d*) δ 8.32 (d, J = 5.5 Hz, 1H, Pym), 7.66 – 7.26 (m, 9H, Ar), 6.50 (d, J = 5.5 Hz, 1H, Pym), 4.21 – 4.16 (m, 2H, Pip), 4.10 – 4.00 (m, 2H, Pip), 3.90 (s, 3H, O-CH_3), 3.61 – 3.40 (m, 2H, Pip), 3.15 – 2.92 (m, 2H, Pip), 1.42 (s, 3H, ^{t}Boc), 1.36 (s, 6H, ^{t}Boc). **^{13}C NMR** (101 MHz, Chloroform-*d*) δ 173.32, 169.94, 157.88, 155.66, 154.64, 151.84, 141.63, 140.20, 130.02, 128.88, 127.90, 127.27, 126.81, 104.99, 79.82, 63.71, 54.47, 28.46, 26.94. **FT-IR** ν_{max} (film) 2921, 1730, 1662, 1517 cm^{-1}. **HRMS** (ESI-TOF) calcd for $C_{29}H_{32}O_5N_5$ $[M+H]^+$: 530.2398, found : 530.2397.

3-([1,1'-biphenyl]-4-yl)-1,3,8-triazaspiro[4.5]decane-2,4-dione 37

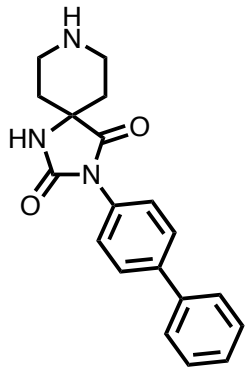

14 (330 mg, 0.652 mmol) was dissolved in CH_2Cl_2 (5 ml) and HCl ((2M) in ether (3 ml)) was added to the solution. The resultant mixture was put under vacuo and flushed with N_2, this was repeated 3 times. The resultant mixture was stirred at room temperature for 16 hrs. The volatiles were evaporated in *vacuo* to give **37** (330 mg, quant) with the appearance of a clear oil.

^{1}H NMR (400 MHz, DMSO-d_6) δ 9.26 (s, 1H, Amide NH), 7.82 – 7.35 (m, 9H, Ar), 3.48 – 3.29 (m, 2H, Pip), 3.26 – 3.04 (m, 2H, Pip), 2.30 – 2.11 (m, 2H, Pip), 2.11 – 1.95 (m, 2H, Pip). **^{13}C NMR** (101 MHz, DMSO-d_6) δ 174.44, 164.71, 154.61, 139.86, 139.41, 131.26, 129.18, 127.93, 127.40, 127.07, 126.92, 57.55, 39.52, 39.10, 30.16. **FT-IR** ν_{max} (film) 3532, 3385, 2901, 1729, 1631, 1504 cm^{-1}. **HRMS** (ESI-TOF) calcd for $C_{19}H_{20}O_2N_3$ $[M+H]^+$: 322.1550, found : 322.1544.

Methyl 2-(3-([1,1'-biphenyl]-4-yl)-2,4-dioxo-1,3,8-triazaspiro[4.5]decan-1-yl)isonicotinate 38

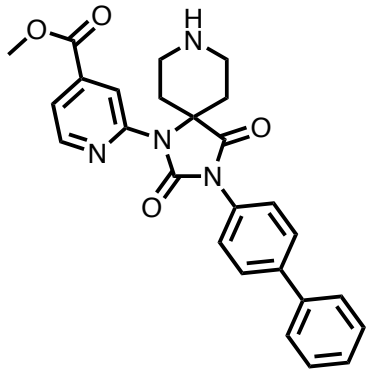

35 (29 mg, 0.0521 mmol) was dissolved in CH_2Cl_2 (5 ml) and HCl (2M) in ether (3 ml) was added to the solution. The resultant mixture was put under *vacuo* and flushed with N_2, this was repeated 3 times. The resultant mixture was stirred at room temperature for 16 hrs. The volatiles were evaporated in *vacuo* to give **38** (20 mg, quant) with the appearance of orange oil.

^{1}H NMR (400 MHz, DMSO-d_6) δ 9.06 – 8.94 (m, 1H, NH), 8.70 (d, J = 5.0 Hz, 1H, Pyr), 8.43 (d, J = 1.0 Hz, 1H, Pyr), 7.93 – 7.37 (m, 10H, Ar), 3.91 (s, 3H, CH_3), 3.49 – 3.33 (m,

4H, Pip), 3.10 – 2.99 (m, 2H, Pip), 2.47 – 2.38 (m, 2H, Pip). **^{13}C NMR** (101 MHz, DMSO-d_6) δ 173.03, 165.03, 153.43, 150.75, 149.51, 140.68, 139.52, 139.36, 130.76, 129.40, 128.23, 127.37, 127.20, 120.20, 118.60, 61.85, 53.36, 39.52, 27.40. **FT-IR** ν_{max} (film) 3360, 2921, 1746, 1662, 1517 cm^{-1}. **HRMS** (ESI-TOF) calcd for $C_{26}H_{25}O_4N_4$ $[M+H]^+$: 457.1870, found : 457.1862.

3-([1,1'-biphenyl]-4-yl)-1-(4-methoxypyrimidin-2-yl)-1,3,8-triazaspiro[4.5]decane-2,4-dione 39

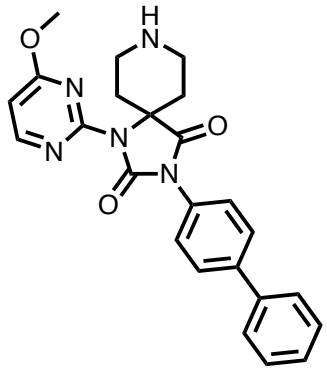

36 (345 mg, 0.652mmol) was dissolved in neat formic acid (10 ml) and stirred at room temperature for 3 hrs. The volatiles were evaporated in *vacuo* to give **39** (240 mg, 0.55 mmol, 86 %) as a yellow oil.

^{1}H NMR (400 MHz, DMSO-d_6) δ 8.54 (d, J = 6.00 Hz, 1H, Pym), 7.78 – 7.37 (m, 9H), 6.89 (d, J = 6.00 Hz, 1H, Pym), 4.00 (s, 3H, O-CH_3), 3.39 (m, 2H, Pip), 3.28 (m, 2H, Pip), 2.89 (m, 2H, Pip), 2.33 (m, 2H, Pip). **^{13}C NMR** (101 MHz, DMSO-d_6) δ 173.08, 170.31, 158.92, 151.92, 140.80, 139.72, 131.03, 129.78, 129.50, 128.43, 128.33, 127.66, 127.54,

127.33, 105.87, 62.39, 54.88, 28.77. **FT-IR** ν_{max} (film) 3342 ,2929, 1720, 1675,1550 cm^{-1}.

HRMS (ESI-TOF) calcd for $C_{24}H_{24}O_3N_5$ $[M+H]^+$: 430.1873, found : 430.1867.

3-([1,1'-biphenyl]-4-yl)-8-((3-methylpyridin-2-yl)methyl)-1,3,8-triazaspiro[4.5]decane-2,4-dione 40

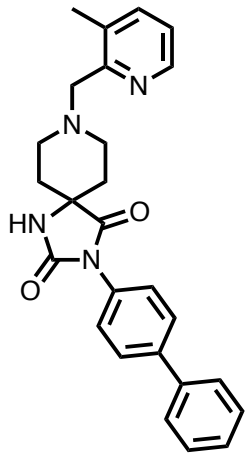

Following general procedure A: **37** (280 mg, 0.87 mmol), 3-methylpyridine-2carboxaldehyde (113 µl, 1.74 mmol) and sodium triacetoxyborohydride (985 mg, 4.65 mmol) gave **40** (180 mg, 0.422 mmol, 49 %) as a orange oil.

^{1}H NMR (400 MHz, DMSO-d_6) δ 9.10 (s, 1H, NH), 8.30 (dd, J = 4.5, 1.5 Hz, 1H, Pyr), 7.81 – 7.16 (m, 11H, Ar), 3.64 (s, 2H, CH_2), 2.80 – 2.70 (m, 2H, Pip), 2.48 – 2.42 (m, 2H, Pip), 2.40 (s, 3H, CH_3), 2.03 – 1.80 (m, 2H, Pip), 1.78 – 1.62 (m, 2H, Pip). **^{13}C NMR** (126 MHz, DMSO-d_6) δ 175.48, 156.35, 154.56, 145.70, 139.56, 139.37, 137.93, 133.12,

131.43, 129.06, 127.77, 127.23, 126.81, 122.59, 62.63, 59.23, 48.62, 48.31, 39.52, 33.32, 29.05, 17.95. **FT-IR** ν_{max} (film) 3556, 1720, 1644, 1504 cm^{-1}. **HRMS** (ESI-TOF) calcd for $C_{26}H_{27}O_2N_4$ $[M+H]^+$: 427.2128, found 427.2127.

3-([1,1'-biphenyl]-4-yl)-8-((1-methyl-1*H*-imidazol-2-yl)methyl)-1,3,8-triazaspiro[4.5]decane-2,4-dione 41

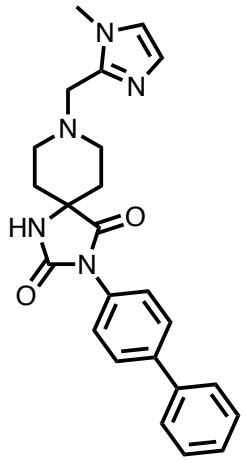

Following general procedure A: **37** (280 mg, 0.87 mmol), 1-methyl–2-imidazole-carboxaldehyde (113 µl, 1.74 mmol) and sodium triacetoxyborohydride (985 mg, 4.65 mmol) gave **41** (321 mg, 0.77 mmol, 89 %) as a white solid.

m.p. >250°C. **^{1}H NMR** (400 MHz, DMSO-d_6) δ 9.06 (s, 1H, NH), 7.80 – 7.67 (m, 4H, Ph), 7.54 – 7.43 (m, 4H, Ph), 7.45 – 7.35 (m, 1H, Ph), 7.10 (d, J = 1.0 Hz, 1H, Imidazole (Im)), 6.77 (d, J = 1.0 Hz, 1H, Im), 3.67 (s, 3H, CH_3), 3.58 (s, 2H, $\underline{CH_2}$Im), 2.79 – 2.69 (m, 2H, Pip), 2.45 – 2.34 (m, 2H, Pip), 1.99 – 1.87 (m, 2H, Pip), 1.78 – 1.70 (m, 2H, Pip). **^{13}C NMR** (101 MHz, DMSO) δ 175.86, 154.99, 144.72, 139.99, 139.81, 131.87, 129.47,

128.18, 127.64, 127.37, 127.24, 126.60, 122.52, 59.62, 54.38, 48.47, 33.69, 32.94. **FT-IR** ν_{max} (film) 3556, 1724, 1641, 1504 cm^{-1}. **HRMS** (ESI-TOF) calcd for $C_{26}H_{27}O_2N_4$ $[M+H]^+$: 416.2081, found : 416.2079.

3-([1,1'-biphenyl]-4-yl)-1-(4-methoxypyrimidin-2-yl)-8-((3-methylpyridin-2-yl)methyl)-1,3,8-triazaspiro[4.5]decane-2,4-dione 42

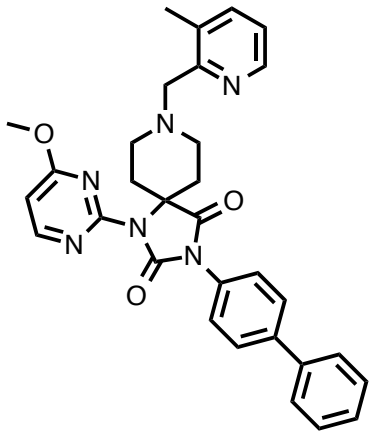

Following general procedure A: **39** (46 mg, 0.107 mmol), 3-methylpyridine-2carboxaldehyde (14.35 µl, 0.128 mmol) and sodium triacetoxyborohydride (113 mg, 0.535 mmol) gave **42** (18 mg, 0.033 mmol, 32 %) as cream solid.

m.p. 173-177°C. **^{1}H NMR** (400 MHz, DMSO-d_6) δ 8.44 (d, J = 6.00 Hz, 1H, Pym), 8.22 (dd, J = 5.00, 2.00 Hz, 1H), 7.85 – 7.06 (m, 11H, Ar), 6.74 (d, J = 6.00 Hz, 1H, Pym), 3.86 (m, 2H, CH_2), 3.59 (s, 3H, O-CH_3), 2.90 – 2.62 (m, 4H, Pip), 2.45 – 2.40 (m, 2H, Pip), 2.32 (s, 3H, Pyridine-CH_3), 1.96 (m, 2H, Pip). **^{13}C NMR** (101 MHz, DMSO-d_6) δ 173.49,

169.93, 158.98, 156.95, 155.80, 151.94, 146.15, 140.68, 139.75, 138.25, 133.40, 131.20, 129.49, 128.43, 128.29, 127.54, 127.32, 122.94, 105.36, 63.88, 62.53, 54.60, 49.11, 30.21, 18.25. **FT-IR** ν_{max} (film) 2980, 1740, 1653, 1572 cm^{-1}. **HRMS** (ESI-TOF) calcd for $C_{31}H_{31}O_3N_6$ $[M+H]^+$: 535.2452, found : 535.2449.

Methyl 2-(3-([1,1'-biphenyl]-4-yl)-8-((3-methylpyridin-2-yl)methyl)-2,4-dioxo-1,3,8-triazaspiro[4.5]decan-1-yl)isonicotinate 43

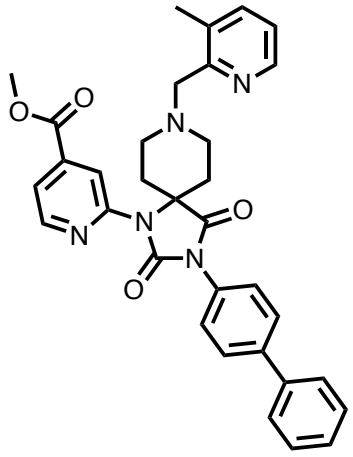

Following general procedure A: **38** (20 mg, 0.0438 mmol), 3-methylpyridine-2carboxaldehyde (6 µl,, 0.0625 mmol) and sodium triacetoxyborohydride (46 mg, 0.219 mmol) gave **43** (14 mg, 0.0249 mmol, 57 %) as a clear oil.

^{1}H NMR (400 MHz, THF-d_8) δ 8.61 (t, J = 1.0 Hz, 1H, Pyr), 8.57 (dd, J = 5.0, 1.0 Hz, 1H, Pyr), 8.26 (dd, J = 5.0, 1.0 Hz, 1H, Pyr), 7.79 – 7.30 (m, 12H, Ar), 3.90 (s, 3H, CH_3), 3.77

(s, 2H, CH_2-Pyr), 3.26 – 3.01 (m, 4H, Pip), 2.87 – 2.74 (m, 2H, Pip), 2.48 (s, 3H, O-CH_3), 1.94 – 1.81 (m, 2H). **^{13}C NMR** (101 MHz, THF-d_8) δ 174.16, 165.78, 158.36, 154.17, 152.85, 149.26, 146.87, 146.24, 140.48, 138.41, 134.32, 132.37, 129.77, 128.48, 128.00, 127.83, 123.09, 119.99, 119.20, 67.57, 65.21, 63.67, 53.02, 49.82, 31.18, 18.74. **FT-IR** ν_{max} (film) 2921, 1744, 1662, 1517 cm^{-1}. **HRMS** (ESI-TOF) calcd for $C_{33}H_{32}O_4N_5$ $[M+H]^+$: 562.2448, found : 562.2437.

2-(3-([1,1'-biphenyl]-4-yl)-8-((3-methylpyridin-2-yl)methyl)-2,4-dioxo-1,3,8-triazaspiro[4.5]decan-1-yl)isonicotinic acid 44

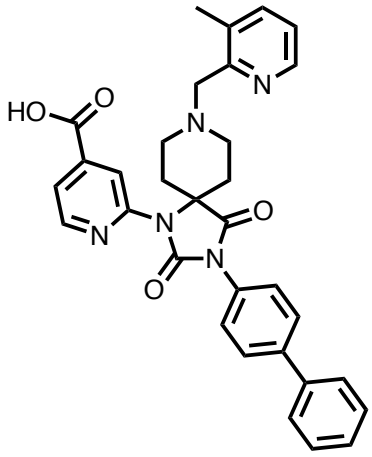

43 (12 mg, 0.024 mmol) was dissolved in a mixture of THF and water (10 :1(3 ml)) before the addition of LiOH-H_2O (2 mg, 0.048 mmol). The reaction mixture was allowed to stir for 16 hr before neutralized with HCl_{aq} (1M). The THF was removed in *vacuo* and the resulting aqueous solution was purified using prep HPLC. The fractions were combined

and the solvent removed under *vacuo* to give **44** (6 mg, 0.0109 mmol, 46 %) as a white solid.

^{1}H NMR (400 MHz, DMSO-d_6) δ 8.84 – 8.33 (m, 2H, Ar), 8.07 – 7.31 (m, 13H, Ar), 4.69 (s, 2H, CH_2), 3.22 (m, 4H, Pip), 2.55 (m, 4H, Pip), 2.35 (s, 3H, CH_3). ^{13}C NMR (126 MHz, DMSO-d_6) δ 172.70, 165.66, 158.33, 158.07, 157.80, 157.54, 153.07, 150.58, 150.31, 149.13, 148.96, 146.18, 140.63, 140.28, 139.17, 138.79, 135.99, 132.02, 130.48, 129.06, 127.91, 127.78, 127.01, 126.86, 123.56, 120.36, 119.83, 115.40, 60.86, 60.18, 48.73, 39.52, 24.26, 18.53, 17.20. **FT-IR** ν_{max} (film) 2921, 2705, 1763, 1662, 1517 cm^{-1}. **HRMS** (ESI-TOF) calcd for $C_{32}H_{30}O_4N_5$ $[M+H]^+$: 548.2286, found : 548.2286.

Benzyl 4-([1,1'-biphenyl]-4-ylcarbamoyl)piperidine-1-carboxylate 45

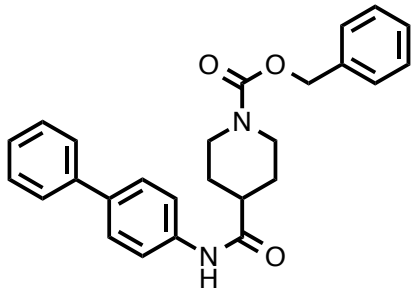

Following general procedure C : 1-Benzyloxycarbonylpiperidine-4-carboxylic acid (1.43 g, 5.46 mmol) and 4-amino-biphenyl (500mg, 2.73 mmol) gave **45** (905 mg, 2.18 mmol, 83%) as a white solid.

m.p. 179 - 181 °C. **^{1}H NMR** (400 MHz, DMSO-d_6) δ 10.03 (s, 1H, NH), 7.76 – 7.58 (m, 6H, Ar), 7.52 – 7.26 (m, 8H, Ar), 5.09 (s, 2H, O-$\underline{CH_2}$), 2.89 (m, 2H, Pip), 2.57 (m, 1H, Pip),

1.89 – 1.46 (m, 6H, Pip). **^{13}C NMR** (101 MHz, DMSO-d_6) δ 172.96, 154.40, 139.70, 138.75, 137.01, 134.71, 128.88, 128.43, 127.83, 127.54, 126.97, 126.84, 126.20, 119.47, 66.17, 43.05, 42.51, 28.20. **FT-IR** ν_{max} (film) 3280, 1699, 1651. cm^{-1}. **HRMS** (ESI-TOF) calcd for $C_{26}H_{25}N_2O_3$ [M-H]$^-$: 413.1943, found 413.1872.

Benzyl 4-(([1,1'-biphenyl]-4-ylmethyl)carbamoyl)piperidine-1-carboxylate 46

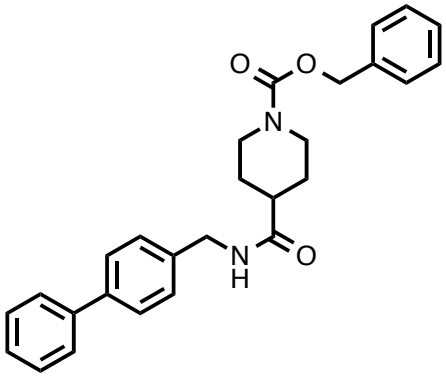

Following general procedure C: 1-Benzyloxycarbonylpiperidine-4-carboxylic acid (431mg, 1.63 mmol) and 4-phenylbenzylamine (250mg, 1.36 mmol) gave **46** (392 mg, 0.915 mmol, 56 %) as a white solid.

m.p. 144 -145 °C. **^{1}H NMR** (400 MHz, Chloroform-*d*) δ 7.72 – 7.14 (m, 14H, Ar), 5.12 (s, 2H, O-CH_2), 4.47 (d, J = 5.5 Hz, 2H, CH_2-NH), 4.23 (m, 2H, Pip), 2.83 (m, 2H, Pip), 2.45 – 2.17 (m, 1H, Pip), 1.94 – 1.63 (m, 4H, Pip). **^{13}C NMR** (101 MHz, Chloroform-*d*) δ 174.11, 155.28, 140.71, 137.29, 136.82, 128.94, 128.62, 128.32, 128.14, 128.01, 127.61,

127.53, 127.16, 77.16, 67.28, 43.57, 43.36, 43.30, 28.72. **FT-IR** ν_{max} (film) 3060, 1696, 1630 cm^{-1}. **HRMS** (ESI-TOF) calcd for $C_{27}H_{28}N_2O_3$ $[M+H]^+$: 429.2100, found 429.2183.

Benzyl 3-([1,1'-biphenyl]-4-ylcarbamoyl)piperidine-1-carboxylate 47

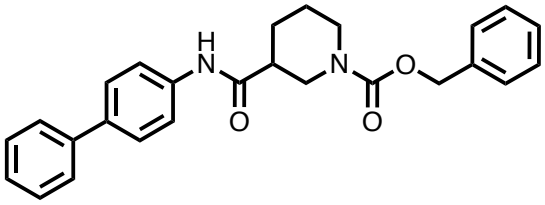

Following general procedure C: 1-Benzyloxycarbonylpiperidine-4-carboxylic acid (300 mg, 1.14 mmol) and 4-amino-biphenyl (229 mg, 1.36 mmol) gave **47** (116 mg, 0.279 mmol, 25 %) as a white solid.

m.p. 144-148°C. **^{1}H NMR** (400 MHz, Chloroform-*d*) δ 7.66 – 7.28 (m, 14H, Ar), 5.25 – 5.08 (s, 2H, CH2), 4.39 – 3.80 (m, 2H, Pip), 3.51 – 2.84 (m, 2H, Pip), 2.58 – 2.37 (m, 1H, Pip), 2.19 – 1.93 (m, 1H, Pip), 1.84 – 1.43 (m, 3H, Pip). **^{13}C NMR** (101 MHz, Chloroform-*d*) δ 178.72, 155.69, 137.06, 129.21, 129.01, 128.94, 128.62, 128.47, 128.33, 127.99, 127.53, 127.28, 120.61, 77.16, 67.72, 46.83, 45.93, 44.61, 41.43, 27.54, 24.53. **FT-IR** ν_{max} (film) 3034, 1696, 1653 cm^{-1} **HRMS** (ESI-TOF) calcd for $C_{26}H_{27}O_3N_2$ $[M+H]^+$: 415.2020, found : 415.2020.

N-([1,1'-biphenyl]-4-yl)piperidine-4-carboxamide 48

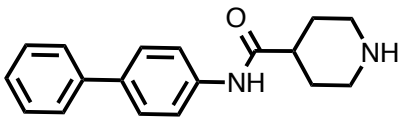

45 (960mg, 2.31 mmol) and palladium on carbon (24 mg, 0.23 mmol) were dissolved in MeOH (10 ml). The resultant reaction mixture was flushed with N_2 and removed in vacuo (repeated 3 times) before the addition of H_2 ballon. The resultant mixture was stirred for 16 hrs, before filtered through a celite pad. The organic fraction was removed under *vacuo* to give **48** (490 mg, 1.75 mmol, 75 %) as a white solid.

m.p. 206 -208 °C. **^{1}H NMR** (400 MHz, DMSO-d_6) δ 9.92 (s, 1H, Amide NH), 8.02 – 6.97 (m, 9H, Ph), 2.98 (m, 3H), 2.48 – 2.33 (m, 1H), 1.74 - 1.52 (m, 6H). **^{13}C NMR** (101 MHz, DMSO-d_6) δ 173.85, 139.74, 138.97, 134.52, 128.88, 126.94, 126.81, 126.19, 119.39, 45.62, 43.76, 39.52, 29.47. **FT-IR** ν_{max} (film) 3277, 2938, 1655 cm^{-1} . **HRMS** (ESI-TOF) calcd for $C_{18}H_{21}N_2O$ $[M+H]^+$: 281.1576, found 281.1684.

N-([1,1'-biphenyl]-4-ylmethyl)piperidine-4-carboxamide 49

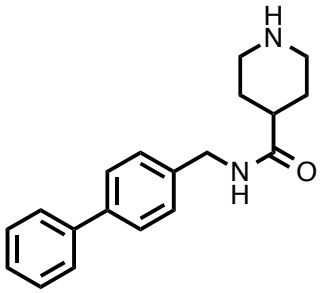

46 (376 mg, 0.87 mmol) and palladium on carbon (9.3 mg, 0.087 mmol) were dissolved in MeOH (10 ml). The resultant reaction mixture was flushed with N_2 and removed in vacuo (repeated 3 times) before the addition of H_2 ballon. The resultant mixture was stirred for 16 hrs, before filtered through a celite pad. The organic fraction was removed under *vacuo* gave **64** (224 mg, 0.80 mmol, 87%) as a white solid.

mp 140 - 141 °C. **^{1}H NMR** (400 MHz, Chloroform-*d*) δ 7.61 – 7.30 (m, 9H, Ar), 4.47 (d, J = 5.5 Hz, 2H, CH2), 3.14 (m, 2H, Pip), 2.62 (m, 2H, Pip), 2.27 (m, 1H, Pip), 1.93 – 1.81 (m, 2H, Pip), 1.74 – 1.56 (m, 2H, Pip). **^{13}C NMR** (101 MHz, Chloroform-*d*) δ 174.90, 140.77, 140.62, 137.51, 128.92, 128.62, 128.33, 128.29, 127.57, 127.49, 127.16, 46.09, 43.89, 43.27, 29.98. **FT-IR** ν_{max} (film) 3287, 2358, 1637 cm^{-1}. **HRMS** (ESI-TOF) calcd for $C_{18}H_{20}N_2O$ $[M+H]^+$: 281.1576, found 281.1648.

N-([1,1'-biphenyl]-4-yl)piperidine-3-carboxamide 50

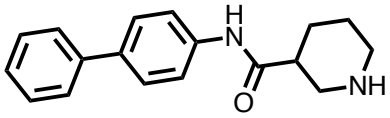

47 (611mg, 1.376 mmol) and palladium on carbon (14.58 mg, 0.137 mmol) were dissolved in MeOH (10 ml). The resultant reaction mixture was flushed with N_2 and removed in vacuo (repeated 3 times) before the addition of H_2 ballon. The resultant mixture was stirred for 16 hrs, before filtered through a celite pad. The organic fraction was removed under *vacuo* gave **50** (362 mg, 1.29 mmol, 94 %) as a white solid.

m.p. >250°C. **^{1}H NMR** (400 MHz, DMSO-d_6) δ 10.44 (s, 1H, NH), 7.82 – 7.57 (m, 6H, Ar), 7.54 – 7.31 (m, 3H, Ar), 3.38 – 2.69 (m, 6H, Pip), 2.11 – 1.50 (m, 3H, Pip). **^{13}C NMR** (101 MHz, DMSO-d_6) δ 170.86, 139.64, 138.42, 135.04, 128.94, 127.09, 126.92, 126.26, 119.62, 44.07, 43.90, 42.87, 39.52, 26.39, 21.17. **FT-IR** ν_{max} (film) 3332, 2361, 1652 cm^{-1} **HRMS** (ESI-TOF) calcd for $C_{18}H_{21}ON_2$ $[M+H]^+$: 281.1644, found : 281.1644.

N-([1,1'-biphenyl]-4-yl)-1-((3-methylpyridin-2-yl)methyl)piperidine-4-carboxamide 51

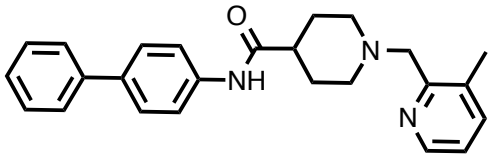

Following general procedure A: **48** (100 mg, 0.357 mmol), 3-methylpyridine-2carboxaldehyde (80 µl, 0.714 mmol) and sodium triacetoxyborohydride (226 mg, 1.07 mmol) gave **51** (70 mg, 0.181 mmol, 51 %) as brown oil.

^{1}H NMR (400 MHz, DMSO-d_6) δ 9.97 (s, 1H, NH), 8.36 – 8.24 (m, 1H, Pyr), 7.77 – 7.07 (m, 11H, Ar), 3.58 (s, 2H, Pyr-$\underline{CH_2}$), 2.39 (s, 3H, CH_3), 2.36 – 2.00 (m, 4H, Pip), 1.81 – 1.52 (m, 5H, Pip). **^{13}C NMR** (101 MHz, DMSO-d_6) δ 174.08, 146.06, 140.19, 139.33, 138.28, 135.05, 133.47, 129.33, 127.27, 126.65, 122.93, 119.88, 63.49, 53.40, 43.43, 29.03, 18.38. **FT-IR** ν_{max} (film) 2912, 1655 cm^{-1}. **HRMS** (ESI-TOF) calcd for $C_{25}H_{27}N_3O$ $[M+H]^+$: 386.2154, found 386.2226.

N-([1,1'-biphenyl]-4-yl)-1-(2-hydroxybenzyl)piperidine-4-carboxamide 52

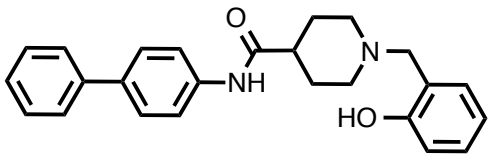

Following general procedure A: **48** (100 mg, 0.357 mmol), Salicylicaldehyde (80 µl, 0.714 mmol) and Sodium Triacetoxyborohydride (226 mg, 1.07 mmol) gave **52** (63 mg, 0.163 mmol, 46 %) as a white solid.

m.p. 161-162 °C. **^{1}H NMR** (400 MHz, DMSO-d_6) δ 10.00 (s, 1H, NH), 7.70 - 7.10 (m, 11H, Ar), 6.81 – 6.69 (m, 2H, Phenol), 3.66 (s, 2H, CH_2), 2.97 (m, 2H, Pip), 2.42 (m, 1H, Pip), 2.10 (m, 2H, Pip), 1.89 – 1.62 (m, 5H, Pip). **^{13}C NMR** (101 MHz, DMSO-d_6) δ 173.77, 157.51, 140.17, 139.27, 135.12, 129.52, 129.35, 128.59, 127.30, 126.66, 122.72, 119.91, 119.19, 115.81, 59.79, 52.54, 43.03, 28.91. **FT-IR** ν_{max} (film) 3233, 1668, 1505 cm^{-1}. **HRMS** (ESI-TOF) calcd for $C_{25}H_{26}N_2O_2$, [M-H]$^-$: 385.1994, found 385.2253.

N-([1,1'-biphenyl]-4-yl)-1-((3-hydroxypyridin-2-yl)methyl)piperidine-4-carboxamide 53

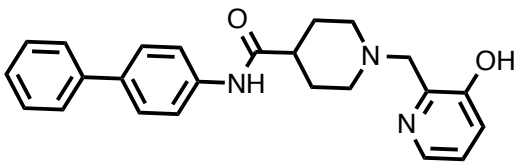

Following general procedure B: **48** (100 mg, 0.357 mmol), 3-hydroxypyridine-2carboxaldehyde (81 mg, 0.714 mmol) and sodium triacetoxyborohydride (226 mg, 1.07 mmol) gave **53** (80 mg, 0.206 mmol, 57%) as a brown solid.

m.p. 197 - 198 °C. **^{1}H NMR** (400 MHz, DMSO-d_6) δ 10.02 (s, 1H, NH), 7.95 – 7.07 (m, 12 H, Ar), 3.85 (s, 2H, CH_2), 2.98 (m, 2H, Pip), 2.43 (m, 1H, Pip), 2.21 (m, 2H, Pip), 1.86 (m, 2H, Pip), 1.69 (m, 2H, Pip). **^{13}C NMR** (101 MHz, DMSO-d_6) δ 173.67, 154.10, 143.57, 140.16, 139.82, 139.24, 135.15, 129.35, 127.44, 127.31, 126.66, 123.87, 122.65, 119.92, 62.64, 52.64, 42.73, 39.34, 28.83. **FT-IR** ν_{max} (film) 3421, 2917, 1686 cm^{-1}. **HRMS** (ESI-TOF) calcd for $C_{24}H_{24}N_3O_2$ $[M-H]^-$: 386.1874, found 386.1947.

N-([1,1'-biphenyl]-4-ylmethyl)-1-((3-methylpyridin-2-yl)methyl)piperidine-4-carboxamide 54

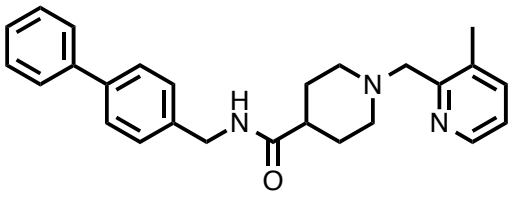

Following general procedure A: **49** (98 mg, 0.33 mmol), 3-methylpyridine-2carboxaldehyde 37µl, 0.33 mmol) and sodium triacetoxyborohydride (280 mg, 1.33 mmol) gave **54** (85 mg, 0.213 mmol, 64 %) as a yellow oil.

^{1}H NMR (400 MHz, DMSO-d_6) δ 8.34 (t, J = 6.0 Hz, 1H, NH), 8.28 (m, 1H, Pyr), 7.68 – 7.18 (m, 11 H, Ar), 4.29 (d, J = 6.0 Hz, 2H, CH_2NH), 3.54 (s, 2H, CH_2Pyr), 2.78 (m, 2H, Pip), 2.37 (s, 3H, CH_3), 2.23 – 1.94 (m, 3H, Pip), 1.70 – 1.50 (m, 4H, Pip). **^{13}C NMR** (101 MHz, DMSO-d_6) δ 174.62, 171.67, 156.56, 145.62, 140.03, 139.06, 138.67, 137.85, 133.07,

128.97, 128.77, 127.99, 127.70, 127.35, 126.63, 126.60, 122.49, 118.74, 118.35, 103.13, 66.32, 66.10, 63.20, 53.06, 42.15, 38.89, 31.93, 28.79, 27.29, 23.22, 22.55, 17.96. **FT-IR** ν_{max} (film) 3195, 2254, 1664 cm^{-1} **HRMS** (ESI-TOF) calcd for $C_{26}H_{29}N_3O$ $[M+H]^+$: 399.2311, found 399.2384.

N-([1,1'-biphenyl]-4-ylmethyl)-1-(2-hydroxybenzyl)piperidine-4-carboxamide 55

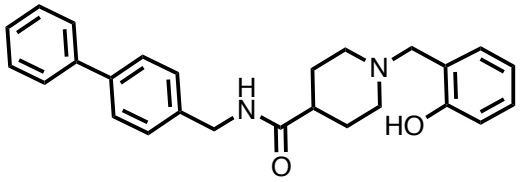

Following general procedure A : **49** (98 mg, 0.333 mmol), salicylicaldehyde (35 µl, 0.333 mmol) and sodium triacetoxyborohydride (278 mg, 1.32 mmol) gave **55** (58 mg, 0.145 mmol, 43 %) as a colourless oil.

^{1}H NMR (400 MHz, DMSO-d_6) δ 8.38 (t, J = 6.0 Hz, 1H, NH), 7.66 – 6.74 (m, 12H), 4.31 (d, J = 6.0 Hz, 2H, CH_2NH), 3.63 (s, 2H, CH_2Phenol), 2.92 (m, 2H, Pip), 2.26 (m, 1H, Pip), 2.06 (m, 2H, Pip), 1.88 – 1.52 (m, 4H, Pip). **^{13}C NMR** (101 MHz, DMSO-d_6) δ 174.15, 157.12, 139.96, 138.96, 138.63, 129.00, 128.91, 128.42, 128.13, 127.66, 127.50, 127.30, 126.59, 126.55, 122.15, 118.70, 115.34, 66.13, 59.43, 52.11, 43.12, 41.61, 28.55. **FT-IR** ν_{max} (film) 3280, 1643 cm^{-1}.**HRMS** (ESI-TOF) calcd for $C_{26}H_{28}N_2O_2$ $[M+H]^+$: 401.2151, found 401.2223.

N-([1,1'-biphenyl]-4-ylmethyl)-1-((3-hydroxypyridin-2-yl)methyl)piperidine-4-carboxamide 56

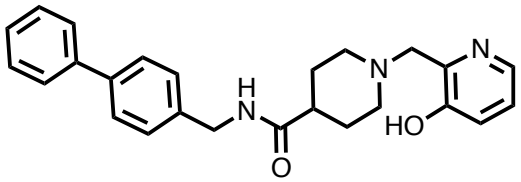

Following general procedure A: **49** (98 mg, 0.33 mmol), 3-hydroxypyridine-2-carboxaldehyde (81 mg, 0.66 mmol) and sodium triacetoxyborohydride (280 mg, 1.33 mmol) gave **56** (60 mg, 0.15 mmol, 45 %) as a white solid.

m.p. 211 - 212 °C. **^{1}H NMR** (400 MHz, DMSO-d_6) δ 8.40 (t, J = 6.0 Hz, 1H, NH), 7.94 (m, 1H, Pyr), 7.72 – 7.04 (m, 11H, Ar), 4.31 (d, J = 6.0 Hz, 2H, $\underline{CH_2}$NH), 3.83 (s, 2H, CH_2Pyr), 2.34 – 2.06 (m, 4H, Pip), 1.86 – 1.56 (m, 5H, Pip). **^{13}C NMR** (101 MHz, DMSO-d_6) δ 174.53, 154.16, 143.52, 140.42, 139.79, 139.40, 139.10, 129.38, 128.13, 127.77, 127.06, 127.02, 123.84, 122.63, 62.75, 52.69, 42.08, 41.78, 28.94. **FT-IR** ν_{max} (film) 3261, 1668 cm^{-1}. **HRMS** (ESI-TOF) calcd for $C_{25}H_{27}N_3O_2$ $[M-H]^-$: 400.2103, found 400.2077.

N-([1,1'-biphenyl]-4-yl)-1-((3-methylpyridin-2-yl)methyl)piperidine-3-carboxamide 57

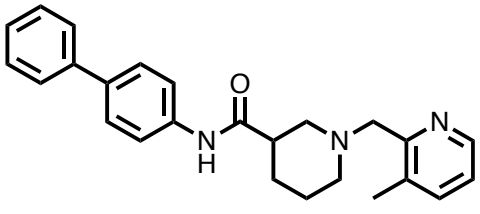

Following general procedure A : **50** (38 mg, 0.137 mmol), 3-methyl pyridine-2 -carboxaldehyde (33 mg, 0.275 mmol) and sodium triacetoxyborohydride (87 mg, 0.41 mmol) gave **57** (7 mg, 0.0181 mmol, 14 %) as a colourless viscous oil.

^{1}H NMR (400 MHz, DMSO-d_6) δ 10.18 (s, 1H, NH), 8.33 – 8.28 (s 1H, Pyr), 7.89 – 6.95 (m, 11H, Ar), 3.61 (s, 2H, CH_2), 2.85 – 2.65 (m, 3H, Pip), 2.38 (s, 3H, CH_3), 2.36 – 2.11 (m, 1H, Pip), 1.88 – 1.36 (m, 5H, Pip). **^{13}C NMR** (101 MHz, DMSO-d_6) δ 172.57, 145.76, 139.72, 138.69, 137.87, 134.69, 132.80, 128.89, 126.98, 126.83, 126.21, 122.46, 119.53, 62.68, 55.70, 53.60, 43.41, 39.52, 27.21, 24.15, 17.97. **FT-IR** ν_{max} (film) 3562, 1664 cm^{-1} .

HRMS (ESI-TOF) calcd for $C_{25}H_{28}ON_3$ $[M+H]^+$: 386.2226, found : 386.2222.

N-([1,1'-biphenyl]-4-yl)-1-(2-hydroxybenzyl)piperidine-3-carboxamide 58

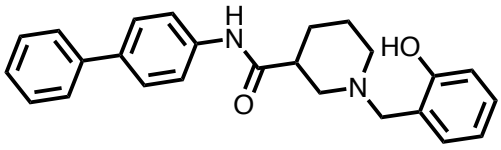

Following general procedure A: **50** (38 mg, 0.137 mmol), salicaldehyde (33 mg, 0.275 mmol) and sodium triacetoxyborohydride (87 mg, 0.41 mmol) gave **58** (10 mg, 0.026 mmol, 19 %) as a colourless oil.

^{1}H NMR (400 MHz, DMSO-d_6) δ 10.09 (s, 1H, NH), 7.73 – 7.56 (m, 6H, Ar), 7.49 – 7.39 (m, 2H, Ar), 7.36 – 7.28 (m, 1H, Ar), 7.10 (m, 2H, Ar), 6.81 – 6.70 (m, 2H, Ar), 3.65 (s,

2H, CH_2), 2.97 (m, 1H, Pip), 2.87 – 2.76 (m, 1H, Pip), 2.69 – 2.60 (m, 1H, Pip), 2.37 – 2.24 (m, 1H, Pip), 2.13 – 2.05 (m, 1H, Pip), 1.89 – 1.84 (m, 1H, Pip), 1.78 – 1.67 (m, 1H, Pip), 1.57 – 1.46 (m, 2H, Pip). **^{13}C NMR** (101 MHz, DMSO-d_6) δ 172.13, 156.93, 139.70, 138.61, 134.78, 129.34, 128.87, 128.21, 127.28, 126.97, 126.82, 126.20, 122.26, 119.54, 118.75, 114.50, 59.23, 55.17, 52.49, 43.43, 39.52, 27.10, 24.20, 21.07. **FT-IR** ν_{max} (film) 3562, 1664 cm^{-1}. **HRMS** (ESI-TOF) calcd for $C_{25}H_{27}O_2N_2$ $[M+H]^+$: 387.2067, found : 387.2068

N-([1,1'-biphenyl]-4-yl)-1-((3-hydroxypyridin-2-yl)methyl)piperidine-3-carboxamide 59

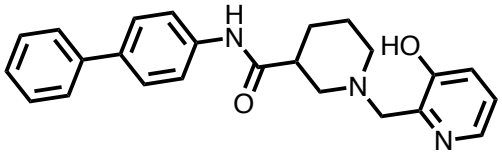

Following general procedure A: **50** (38 mg, 0.137 mmol), 3-hydroxypyridine-2-carboxaldehyde (33 mg, 0.275 mmol) and sodium triacetoxyborohydride (87 mg, 0.41 mmol) gave **59** (7.5 mg, 0.019 mmol, 14%) as a colourless oil.

^{1}H NMR (400 MHz, DMSO-d_6) δ 10.20 (s, 1H, NH), 7.96 (m, 1H, Ar), 7.73 – 7.58 (m, 6H, Ar), 7.47 – 7.39 (m, 2H, Ar), 7.35 – 7.28 (m, 1H, Ar), 7.18 – 7.08 (m, 2H, Ar), 3.96 – 3.71 (s, 2H, CH_2), 3.00 – 2.91 (m, 1H, Pip), 2.77 (m, 1H, Pip), 2.65 (m, 1H, Pip), 2.45 (m, 1H, Pip), 2.29 (m, 1H, Pip), 1.85 (m, 1H, Pip), 1.80 – 1.70 (m, 1H, Pip), 1.55 (m, 2H, Pip). **^{13}C**

NMR (101 MHz, DMSO-d_6) δ 172.09, 153.34, 143.38, 139.72, 139.42, 138.61, 134.82, 128.89, 126.99, 126.85, 126.22, 123.43, 122.19, 119.61, 61.53, 55.07, 52.76, 43.14, 39.52, 26.91, 23.95, 21.09. **FT-IR** ν_{max} (film) 3562, 1664 cm^{-1}. **HRMS** (ESI-TOF) calcd for $C_{24}H_{26}O_2N_3$ $[M+H]^+$: 388.2019, found : 388.2023.

Ethyl 7-hydroxy-[1,2,4]triazolo[1,5-a]pyrimidine-6-carboxylate 60

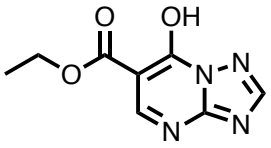

3-amino-1,2,4-triazole (2 g, 23.80 mmol) was dissolved in neat acetic acid (25 ml) before the addition of diethyl ethoxymethylene malonate (3.06 ml, 25.3 mmol). The resultant mixture was refluxed for 16 hrs and then was allowed to cool to room temperature. The precipitate was filtered off and washed with EtOH (3 x 50 ml) and Et_2O (3 x 100 ml) to give **60** (3.55 g, 17.06 mmol, 74 %) as a cream solid.

m.p. 176-179°C. **^{1}H NMR** (400 MHz, DMSO-d_6) δ 8.63 (s, 1H, Ar), 8.34 (s, 1H, Ar), 4.24 (q, J = 7.0 Hz, 2H, CH_2), 1.27 (t, J = 7.0 Hz, 3H, CH_3). **^{13}C NMR** (101 MHz, DMSO-d_6) δ 163.13, 151.50, 150.31, 147.92, 102.66, 60.35, 39.52, 14.22. **FT-IR** ν_{max} (film) 3649, 2981, 2361, 1653, 1383 cm^{-1}. **HRMS** (ESI-TOF) calcd for $C_8H_9O_3N_4$ $[M+H]^+$: 209.0669, found: 209.0669.

N-([1,1'-biphenyl]-4-ylmethyl)-7-hydroxy-[1,2,4]triazolo[1,5-a]pyrimidine-6-carboxamide 61

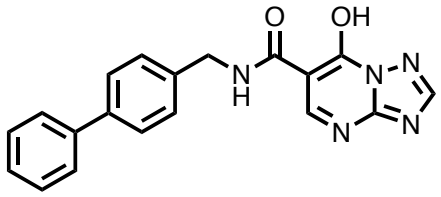

Following general procedure B: **60** (59 mg, 0.28 mmol), 4-phenylbenzylamine (35 mg, 0.191 mmol) and DABCO-$(AlMe_3)_2$ (39 mg, 0.152 mmol) gave **61** (16 mg, 0.047 mmol, 17%) as a colourless oil.

^{1}H NMR (400 MHz, DMSO-d_6) δ 9.49 (t, J = 6.0 Hz, 1H, NH), 8.72 (s, 1H), 8.22 (s, 1H), 7.69 – 7.59 (m, 4H, Ar), 7.53 – 7.40 (m, 4H, Ar), 7.39 – 7.31 (m, 1H, Ar), 4.58 (d, J = 6.0 Hz, 2H. CH_2). **^{13}C NMR** (101 MHz, DMSO-d_6) δ 171.01, 157.49, 154.92, 139.98, 139.70, 138.95, 138.75, 127.90, 127.28, 126.58, 102.21, 41.80, 39.52. **FT-IR** ν_{max} (film) 3660, 2981, 2361, 1651 cm^{-1}. **HRMS** (ESI-TOF) calcd for $C_{19}H_{16}O_2N_5$ $[M+H]^+$: 346.1298, found : 346.1297.

7-hydroxy-*N*-(4-(trifluoromethyl)benzyl)-[1,2,4]triazolo[1,5-*a*]pyrimidine-6-carboxamide 62

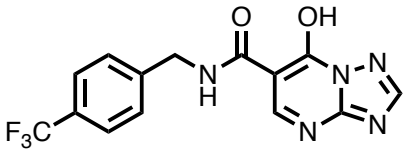

Following general procedure B: **60** (100 mg, 0.48 mmol), 4-trifluoromethylbenzylamine (101 mg, 0.58 mmol) and DABCO-$(AlMe_3)_2$ (98 mg, 0.384 mmol) gave **62** (22 mg, 0.065 mmol, 14%) as clear oil.

^{1}H NMR (400 MHz, DMSO-d_6) δ 9.75 (t, J = 6.0 Hz, 1H, NH), 8.71 (s, 1H, Ar), 8.07 (s, 1H, Ar), 7.69 (d, J = 8.0 Hz, 2H, Ph), 7.53 (d, J = 8.0 Hz, 2H, Ph), 4.67 (d, J = 6.0 Hz, 2H, CH_2). **^{13}C NMR** (101 MHz, DMSO-d_6) δ 166.07, 158.35, 155.68, 152.95, 145.22, 128.96, 127.87, 127.54, 125.30, 125.26, 125.22, 125.19, 100.00, 41.54, 39.52. **FT-IR** ν_{max} (film) 3521, 1621 cm^{-1}. **HRMS** (ESI-TOF) calcd for $C_{14}H_9O_2N_5F_3$ [M-H]$^-$: 336.0713, found : 336.0714.

N-([1,1'-biphenyl]-4-ylmethyl)-4-hydroxynicotinamide 63

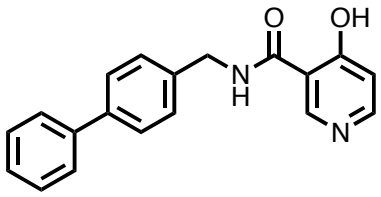

Following general procedure C: 4-hydroxy nicotinic acid (100 mg, 0.719 mmol), 4-phenylbenzylamine (157 mg, 0.863 mmol), T3P (668 mg, 2.157 mmol) and DIPEA (220 mg, 1.7 mmol) gave **63** (63 mg, 0.207 mmol, 29 %) as a white solid.

m.p. 234-238°C. **^{1}H NMR** (400 MHz, DMSO-d_6) δ 12.16 (s, 1H, OH), 10.77 (t, J = 6.0 Hz, 1H, NH), 8.50 (d, J = 1.5 Hz, 1H, Pyr), 7.81 (dd, J = 7.0, 1.5 Hz, 1H, Pyr), 7.69 – 7.30 (m, 9H, Ar), 6.43 (d, J = 7.0 Hz, 1H, Pyr), 4.57 (d, J = 6.0 Hz, 2H, CH_2NH). **^{13}C NMR** (101

MHz, DMSO-d_6) δ 177.58, 164.26, 141.52, 139.96, 138.84, 138.69, 138.03, 128.92, 127.93, 127.35, 126.77, 126.61, 119.40, 118.19, 41.68, 39.52. **FT-IR** ν_{max} (film) 3451, 1694 cm^{-1}. **HRMS** (ESI-TOF) calcd for $C_{19}H_{17}O_2N_2$ $[M+H]^+$: 305.1284, found : 305.1280.

4-hydroxy-N-(4-phenoxybenzyl)pyrimidine-5-carboxamide 64

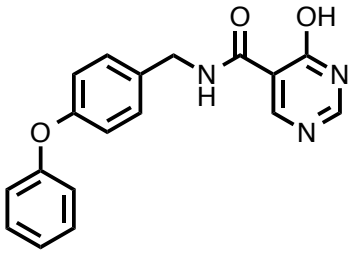

Following general procedure B: Ethyl-4-hydroxy pyrimidine-5-carboxylate (150 mg, 0.89 mmol), 4-phenyoxybenzylamine (144 µl, 0.89 mmol) and DABCO-$(AlMe_3)_2$ (159 mg, 0.9 mmol) gave **64** (85 mg, 0.264 mmol, 30 %) as a colourless solid.

m.p. 262 - 264 °C. **^{1}H NMR** (400 MHz, DMSO-d_6) δ 9.60 (t, J = 6.0 Hz, 1H, NH), 8.68 (s, 1H, Pym), 8.45 (s, 1H, Pym), 7.39 – 6.93 (m, 9H, Ar), 4.50 (d, J = 6.0 Hz, 2H, CH_2). **^{13}C NMR** (101 MHz, DMSO-d_6) δ 163.08, 162.85, 157.27, 156.40, 155.97, 153.13, 134.71, 130.45, 129.64, 123.75, 119.21, 118.85, 117.46, 42.13. **FT-IR** ν_{max} (film) 3255, 1705 cm^{-1}.

HRMS (ESI-TOF) calcd for $C_{18}H_{15}N_3O_3$, $[M-H]^-$: 320.1113; found 320.1040.

N-([1,1'-biphenyl]-4-ylmethyl)-4-chloro-2-methoxybenzamide 65

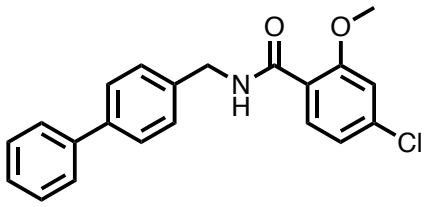

Following general procedure C: 4-Chloro-2-methoxybenzoic acid (250 mg, 1.34 mmol), 4-phenylbenzylamine (294 mg, 1.6 mmol), T3P (1.06 g, 3.36 mmol), DIPEA (412 mg, 3.36 mmol) gave **65** (451 mg, 1.24 mmol, 95 %) as a white solid.

m.p. 139-142°C. **^{1}H NMR** (400 MHz, Chloroform-*d*) δ 8.21 (d, *J* = 8.5 Hz, 1H, Ar-Cl), 8.12 (t, *J* = 6.0 Hz, 1H, NH), 7.60 – 7.56 (m, 4H, Ar), 7.46 – 7.41 (m, 4H, Ar), 7.37 – 7.30 (m, 1H, Ar), 7.08 (dd, *J* = 8.5, 2.0 Hz, 1H, Ar-Cl), 6.97 (d, *J* = 2.0 Hz, 1H, Ar-Cl), 4.71 (d, *J* = 6.0 Hz, 2H, CH_2), 3.93 (s, 3H, CH_3). **^{13}C NMR** (101 MHz, Chloroform-*d*) δ 164.24, 157.62, 140.50, 140.08, 138.29, 137.40, 133.39, 128.57, 127.74, 127.19, 127.10, 126.82, 121.45, 119.74, 111.82, 77.16, 56.13, 43.30. **FT-IR** ν_{max} (film) 1651 cm^{-1}. **HRMS** (ESI-TOF) calcd for $C_{21}H_{19}O_2N^{35}Cl$ $[M+H]^+$: 352.1098, found : 352.1098.

N-([1,1'-biphenyl]-4-ylmethyl)-2-methoxy-4-(1H-pyrazol-1-yl)benzamide 66

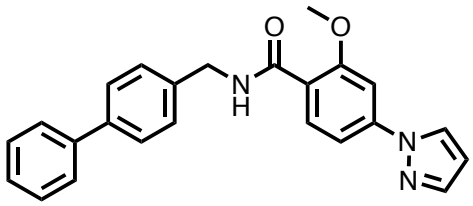

Following general procedure D: **65** (100 mg, 0.284 mmol), Pd^{t}BuXPhos G3 (20 mg, 0.028 mmol), Cs_2CO_3 (185 mg, 0.568 mmol), pyrazole (23 mg, 0.34 mmol) gave **66** (28 mg, 0.073 mmol, 26 %) as a white solid.

m.p. 149-152°C. **^{1}H NMR** (400 MHz, DMSO-d_6) δ 8.77 (t, J = 6.0 Hz, 1H, NH), 8.66 (d, J = 2.5 Hz, 1H, Pyzl), 7.80 (d, J = 1.5 Hz, 1H, Pyzl), 7.69 – 7.32 (m, 12H, Ar), 6.60 (dd, J = 2.5, 1.5 Hz, 1H, Pyzl), 4.56 (d, J = 6.0 Hz, 2H, CH_2), 4.01 (s, 3H, CH_3). **^{13}C NMR** (101 MHz, DMSO-d_6) δ 164.39, 158.07, 142.52, 141.56, 140.02, 139.04, 138.60, 131.98, 128.92, 128.37, 127.71, 127.30, 126.61, 126.58, 120.28, 109.90, 108.38, 101.98, 56.32, 42.37, 39.52. **FT-IR** ν_{max} (film) 1649 cm^{-1}. **HRMS** (ESI-TOF) calcd for $C_{24}H_{22}O_2N_3$ [M+H]$^{+}$: 384.1704, found : 384.1704.

N-([1,1'-biphenyl]-4-ylmethyl)-2-hydroxy-4-(1H-pyrazol-1-yl)benzamide 67

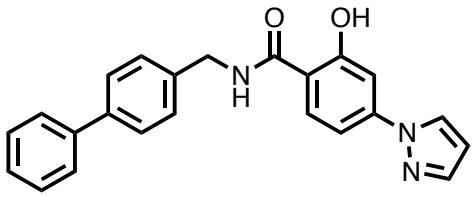

TMS-I (39 mg, 0.195 mmol) was added to a solution of **66** (25 mg, 0.0652 mmol) and CH_2Cl_2 (2.5 ml). The resultant mixture was heated for 8 hrs, then cooled to rt, HCl_{aq} (1.5 ml, 1M) was added before being extracted with CH_2Cl_2 (3 x 10 ml). The organic fractions were combined, dried with anhydrous Na_2SO_4 concentrated in *vacuo* and the crude compound was then purified using flash column chromatography using (0% - 5% MeOH,

CH_2Cl_2, 1 % NH_3) over 20 column volumes gave **67** (7.5 mg, 0.020 mmol, 31%**)** as a white solid.

m.p. 175-179°C. **^{1}H NMR** (400 MHz, DMSO-d_6) δ 12.96 (s, 1H, OH), 9.43 (t, J = 6.0 Hz, 1H, NH), 8.61 (dd, J = 2.5, 1.0 Hz, 1H, Pyzl), 8.05 (d, J = 8.0 Hz, 1H,), 7.79 (d, J = 1.5 Hz, 1H, Pyzl), 7.70 – 7.31 (m, 11H, Ar), 6.58 (dd, J = 2.5, 1.5 Hz, 1H, Pyzl), 4.57 (d, J = 6.0 Hz, 2H, CH_2). **^{13}C NMR** (101 MHz, DMSO-d_6) δ 168.55, 161.39, 143.39, 141.73, 139.93, 138.94, 138.15, 129.29, 128.93, 128.27, 127.99, 127.37, 126.74, 126.60, 112.64, 108.51, 108.41, 106.11, 42.15, 39.52. **FT-IR** ν_{max} (film) 3342, 1653 cm^{-1}. **HRMS** (ESI-TOF) calcd for $C_{23}H_{20}O_2N_3$ $[M+H]^+$: 370.1548, found : 370.1548.

N-([1,1'-biphenyl]-4-ylmethyl)-2-chloropyrimidine-5-carboxamide 68

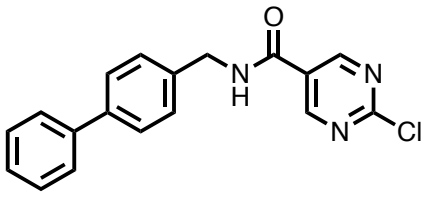

Following general procedure C: 2-chloro-5-carboxypyrimidine (300 mg, 1.89 mmol), 4-phenylbenzylamine (370 mg, 2.26 mmol), T3P (819 mg, 2.83 mmol) and DIPEA (365 mg, 2.83 mmol) gave **68** (285 mg, 0.88 mmol, 47 %) as a colourless oil.

^{1}H NMR (400 MHz, DMSO-d_6) δ 9.46 (t, J = 6.0 Hz, 1H, NH), 9.18 (s, 2H, Pym), 7.87 – 6.86 (m, 9H, Ar), 4.56 (d, J = 6.0 Hz, 2H, CH_2). **^{13}C NMR** (101 MHz, DMSO-d_6) δ 162.54, 162.23, 159.87, 140.37, 139.47, 138.36, 129.39, 128.58, 127.84, 127.17, 127.06, 42.98. **FT-IR** ν_{max} (film) 3033, 1668 cm^{-1}. **HRMS** (ESI-TOF) calcd for $C_{17}H_{29}O_3N_2$ $[M+H]^+$: 429.2166, found : 429.2166.

2-chloro-N-(4-phenoxybenzyl)pyrimidine-5-carboxamide 69

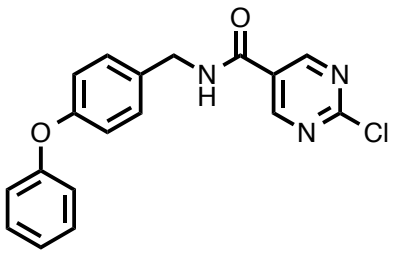

Following general procedure C: 2-chloro-5-carboxypyrimidine (300 mg, 1.89 mmol), 4-phenoxybenzyamine (410 µl, 2.26 mmol) and T3P (1.5 g, 4.72 mmol) gave **69** (336 mg, 0.99 mmol, 52%) as a white solid.

m.p. 149 - 150 °C. **^{1}H NMR** (400 MHz, DMSO-d_6) δ 9.41 (t, J = 6.0 Hz, 1H, NH), 9.16 (s, 2H, Pym), 7.53 – 7.27 (m, 4H, Ar), 7.19 – 6.78 (m, 5H, Ar), 4.50 (d, J = 6.0 Hz, 2H, CH_2). **^{13}C NMR** (101 MHz, DMSO-d_6) δ 162.48, 162.21, 159.86, 157.27, 156.07, 134.26, 130.48, 129.73, 127.22, 123.81, 119.17, 118.86, 42.68. **FT-IR** ν_{max} (film) 3277, 3033, 1668 cm^{-1}. **HRMS** (ESI-TOF) calcd for $C_{18}H_{14}ClN_3O_2$ $[M+H]^+$: 340.0847, found 340.1327.

N-([1,1'-biphenyl]-4-ylmethyl)-6-chloronicotinamide 70

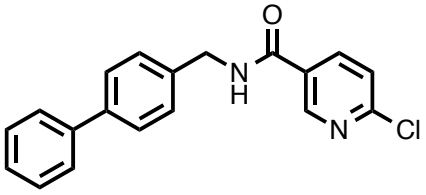

Following general procedure B: 2-chloroethylnicotinate (83 µl, 0.53 mmol), 4-phenyl-benzylamine (97 mg, 0.53 mmol) and DABCO-$(AlMe_3)_2$ (108 mg, 0.424 mmol) gave **70** (154 mg, 0.48 mmol, 91%) as a white solid.

m.p. : 203 - 205 °C. **^{1}H NMR** (400 MHz, DMSO-d_6) δ 9.34 (t, J = 6.0 Hz, 1H, NH), 8.90 (d, J = 2.5 Hz, 1H, Pyr), 8.30 (dd, J = 8.5, 2.5 Hz, 1H, Pyr), 7.87 – 7.19 (m, 10H, Ar), 4.54 (d, J = 6.0 Hz, 2H, CH_2). **^{13}C NMR** (101 MHz, DMSO-d_6) δ 164.19, 153.07, 149.48, 140.40, 139.35, 139.12, 138.77, 129.66, 129.39, 128.46, 127.82, 127.15, 127.05, 124.64, 42.94. **FT-IR** ν_{max} (film) 3032, 2384, 1631, 1543 cm^{-1}. **HRMS** (ESI-TOF) calcd for $C_{19}H_{15}ClN_2O$ $[M+H]^+$: 322.0873, found 322.0821.

N-([1,1'-biphenyl]-4-ylmethyl)-2-(1H-pyrazol-1-yl)pyrimidine-5-carboxamide 71

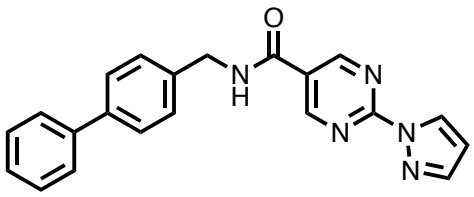

Following general procedure D: **68** (57 mg, 0.176 mmol), Pd^{t}BuXPhos G3 (15 mg, 0.0176 mmol), Cs_2CO_3 (201 mg, 0.619 mmol), pyrazole (42 mg, 0.619 mmol) gave **71** (10 mg, 0.0281 mmol, 16 %) as a orange oil.

^{1}H NMR (400 MHz,DMSO-d_6) δ 9.44 (t, J = 6.0 Hz, 1H, NH), 9.27 (s, 2H, Pym), 8.73 (d, J = 3.0 Hz, 1H, Pyzl), 7.93 (d, J = 1.5 Hz, 1H, Pyzl), 7.74 – 7.60 (m, 4H, Ar), 7.51 – 7.40 (m, 4H, Ar), 7.39 – 7.31 (m, 1H, Ar), 6.65 (dd, J = 3.0, 1.5 Hz, 1H, Pyzl), 4.58 (d, J = 5.8 Hz, 2H, CH_2). **^{13}C NMR** (101 MHz, DMSO-d_6) δ 162.49, 158.57, 156.06, 144.15, 139.93, 138.96, 138.15, 130.07, 128.93, 128.11, 127.37, 126.72, 126.60, 125.14, 109.45, 42.44. **FT-IR** ν_{max} (film) 1665 cm^{-1}. **HRMS** (ESI-TOF) calcd for $C_{21}H_{18}ON_5$ $[M+H]^+$: 356.1505, found : 356.1504.

N-(4-phenoxybenzyl)-2-(1H-pyrazol-1-yl)pyrimidine-5-carboxamide 72

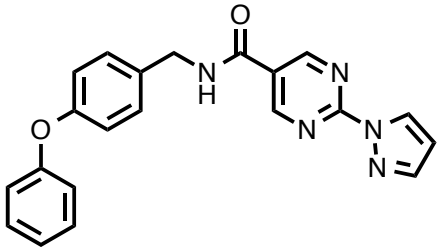

Following general procedure D: **69** (100mg, 0.294 mmol), pyrazole (40mg, 0589 mmol), Pd^{t}BuXPhos G3 (23 mg, 0.0294 mmol), Cs_2CO_3 (238 mg, 0.735 mmol) gave **72** (64 mg, 0.172 mmol, 58%) as a orange solid.

m.p. 194 - 196 °C. **^{1}H NMR** (400 MHz, DMSO-d_6) δ 8.96 (d, J = 3.0 Hz, 1H), 8.68 (d, J = 3.0 Hz, 1H), 8.51 – 8.37 (m, 1H), 8.03 – 7.98 (m, 1H), 7.48 – 6.90 (m, 10H), 6.62 – 6.61

(m, 1H), 4.51 (d, J = 6.0 Hz, 2H, CH_2). **^{13}C NMR** (101 MHz, DMSO-d_6) δ 164.45, 157.34, 155.91, 152.69, 149.48, 148.30, 143.44, 139.09, 134.92, 134.69, 130.46, 129.59, 128.17, 128.04, 123.74, 119.20, 118.80, 109.29, 42.60. **FT-IR** ν_{max} (film) 3336, 3122, 1668, 1427 cm^{-1}. **HRMS** (ESI-TOF) calcd for $C_{21}H_{17}N_5O_2$ $[M-H]^-$: 370.1382, found 370.1309.

N-([1,1'-biphenyl]-4-ylmethyl)-6-(1H-pyrazol-1-yl)nicotinamide 73

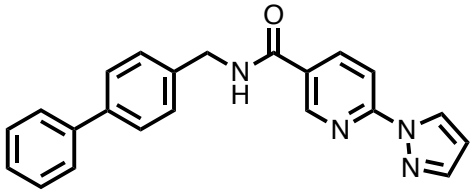

Following procedure D: **70** (100 mg, 0.31 mmol), pyrazole (40 mg, 0589 mmol), Pd^{t}BuXPhos G3 (25 mg, 0.031 mmol), Cs_2CO_3 (238 mg, 0.735 mmol) gave **73** (53 mg, 0.028 mmol, 48 %) as a colourless oil.

^{1}H NMR (400 MHz, DMSO-d_6) δ 9.32 (t, J = 6.0 Hz, 1H, NH), 8.97 (d, J = 2.0 Hz, 1H, Pyr), 8.69 (d, J = 2.5 Hz, 1H, Pyzl), 8.47 (dd, J = 9.0, 2.0 Hz, 1H, Pyr), 8.30 (dd, J = 9.0, 2.0 Hz, 1H, Pyr), 7.90 (d, J = 1.5 Hz, 1H, Pyzl), 7.74 – 7.22 (m, 10H, Ar), 6.63 (dd, J = 2.5, 1.5 Hz, 1H, Pyzl), 4.57 (d, J = 6.0 Hz, 2H, CH_2). **^{13}C NMR** (101 MHz, DMSO-d_6) δ 167.73, 164.19, 152.71, 149.48, 148.30, 143.47, 140.39, 139.35, 138.99, 138.77, 138.19, 129.39, 128.45, 128.18, 128.07, 127.81, 127.15, 127.05, 124.64, 111.86, 109.32, 42.89. **FT-IR** ν_{max} (film) 3032, 2384, 1635, 1543 cm^{-1}.**HRMS** (ESI-TOF) calcd for $C_{22}H_{19}ON_4$ $[M+H]^+$: 355.1553, found : 355.1551.

Ethyl 4-(benzyloxy)-2-(1H-pyrazol-1-yl)pyrimidine-5-carboxylate 74

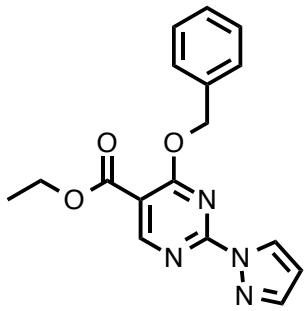

24 (1.9g, 0.008 mol) and Cs_2CO_3 (2.89g, 0.032 mol) were dissolved in DMSO (50 ml) before the addition of benzyl bromide (5ml, 0.032 mol). The resulting mixture stirred at 60°C was left for 15 hrs. The reaction mixture was diluted with EtOAc (50 ml) and was washed with water (8 x 100 ml), dried over anhydrous Na_2SO_4, concentrated in *vacuo* and purified by flash column chromatography using (Cyclohexane 100 % - 75%, EtOAc 0 %-25 %) over 10 column volumes to give **74** (1.1g, 0.003 mol, 44%) as a cream solid.

m.p. 86-88°C. **^{1}H NMR** (400 MHz, DMSO-d_6) δ 9.01 (s, 1H, Pym), 8.78 – 8.75 (m, 1H, Pyzl), 7.99 – 7.92 (m, 1H, Pyzl), 7.61 – 7.01 (m, 5H, Ph), 6.69 – 6.63 (m, 1H, Pyzl), 5.66 (s, 2H, $\underline{CH_2}$Ph), 4.27 (q, J = 7.0 Hz, 2H, $\underline{CH_2}CH_3$), 1.31 – 1.27 (t, J = 7.0 Hz, 3H, $CH_2\underline{CH_3}$). **^{13}C NMR** (101 MHz, DMSO-d_6) δ 168.29, 162.84, 157.42, 144.94, 144.76, 136.27, 130.99, 128.89, 128.81, 128.55, 128.26, 127.67, 127.10, 110.09, 109.54, 61.25, 48.18, 14.57. **FT-IR** ν_{max} (film) 1746 cm^{-1}. **HRMS** (ESI-TOF) calcd for $C_{17}H_{17}O_3N_4$ $[M+H]^+$: 325.1295, found : 325.1289.

4-(benzyloxy)-2-(1H-pyrazol-1-yl)pyrimidine-5-carboxylic acid 75

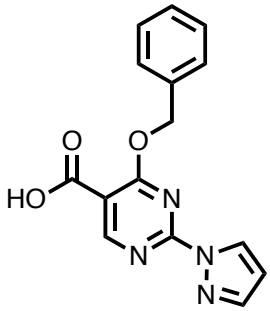

LiOH-H_2O (184 mg, 4.61 mmol) was added to a solution of **74** (500 mg, 1.53 mmol) in a solution of THF and H_2O (30 ml (1:1)). The resultant suspension was stirred at room temperature for 16 hrs. The THF was removed in *vacuo* before the resulting mixture was washed with EtOAc (10ml), acidified to PH2 with HCl (1M aq solution) and extracted with EtOAc (3 x 10ml). The organic layers combined and concentrated in *vacuo* to give **75** (391 mg, 1.32 mmol, 77%) as a orange oil.

^{1}H NMR (400 MHz, DMSO-d_6) δ 8.98 (s, 1H, Pym), 8.74 (d, J = 2.5 Hz, 1H, Pyzl), 7.93 (d, J = 1.5 Hz, 1H, Pyzl), 7.48 – 7.22 (m, 5H, Ph), 6.65 (dd, J = 2.5, 1.5 Hz, 1H, Pyzl), 5.66 (s, 2H, CH_2). **^{13}C NMR** (101 MHz, DMSO-d_6) δ 167.99, 163.83, 162.46, 155.76, 144.36, 135.96, 130.43, 128.46, 127.95, 110.15, 109.53, 68.64, 39.73, 39.52. **FT-IR** ν_{max} (film) 2824, 1768 cm^{-1}. **HRMS (**ESI-TOF) calcd for $C_{15}H_{13}O_3N_4$ $[M+H]^+$: 297.0982, found : 297.0981.

N-([1,1'-biphenyl]-4-ylmethyl)-4-(benzyloxy)-2-(1H-pyrazol-1-yl)pyrimidine-5-carboxamide

76

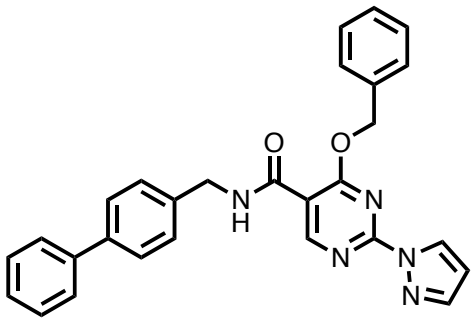

Following general procedure C: **75** (100 mg, 0.337 mmol), HATU (320 mg, 0.842 mmol), DIPEA (144 ul, 0.842 mmol) and 4-phenylbenzylamine (67 mg, 0.37 mmol) gave **76** (37 mg, 0.08 mmol, 24%) as a colourless oil.

^{1}H NMR (400 MHz, DMSO-d_6) δ 8.89 (s, 1H, Pym), 8.78 (t, J = 6.0 Hz, 1H, NH), 8.75 (dd, J = 2.5, 1.0 Hz, 1H, Pyzl), 7.92 (dd, J = 1.5, 1.0 Hz, 1H, Pyzl), 7.60 – 7.28 (m, 14H, Ar), 6.65 (dd, J = 2.5, 1.5 Hz, 1H, Pyzl), 5.68 (s, 2H, OCH_2Ph), 4.54 (d, J = 6.0 Hz, 2H, CH_2NH). **^{13}C NMR** (101 MHz, DMSO-d_6) δ 166.58, 161.97, 160.41, 155.05, 144.12, 139.95, 138.81, 138.09, 135.66, 130.25, 128.97, 128.50, 128.28, 127.83, 127.38, 126.57, 113.60, 109.37, 69.06, 42.39, 39.52. **FT-IR** ν_{max} (film) 1642 cm^{-1}. **HRMS (**ESI-TOF) calcd for $C_{81}H_{24}O_2N_5$ $[M+H]^+$: 462.1924, found : 462.1922.

N-([1,1'-biphenyl]-4-yl)-4-(benzyloxy)-2-(1H-pyrazol-1-yl)pyrimidine-5-carboxamide 77

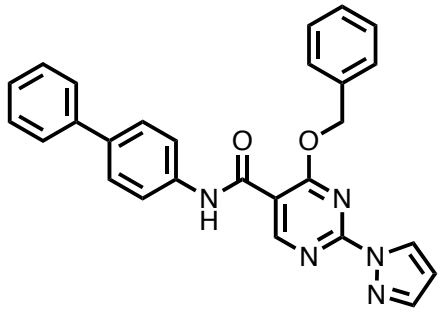

Following general procedure C: **75** (100 mg, 0.337 mmol), HATU (320 mg, 0.842 mmol), DIPEA (144 ul, 0.842 mmol) and 4-aminobiphenyl (112 mg, 0.674 mmol) gave **77** (41 mg, 0.091 mmol, 28 %) as a colourless oil.

^{1}H NMR (400 MHz, Chloroform-*d*) δ 9.45 (s, 1H, Pym), 9.42 (s, 1H, NH), 8.65 – 8.64 (m, 1H, Pyzl), 7.91 (dd, *J* = 1.5, 1.0 Hz, 1H, Pyzl), 7.77 – 7.20 (m, 14H, Ar), 6.56 (dd, *J* = 2.5, 1.5 Hz, 1H, Pyzl), 5.76 (s, 2H, CH_2). **^{13}C NMR** (101 MHz, Chloroform-*d*) δ 170.97, 166.38, 163.53, 159.38, 144.63, 140.12, 137.22, 136.75, 134.07, 129.81, 129.34, 129.05, 128.78, 128.58, 127.43, 126.99, 126.60, 119.89, 110.96, 109.29, 77.16, 70.89. **FT-IR** ν_{max} (film) 1672 cm^{-1}. **HRMS** (ESI-TOF) calcd for $C_{27}H_{22}O_2N_5$ $[M+H]^+$: 448.1768, found : 448.1767.

6-chloro-*N*-(4-phenoxybenzyl)nicotinamide 78

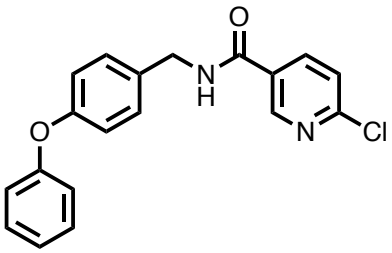

Following general procedure B: 2-chloroethylnicotinate (250 µl, 1.62 mmol), 4-phenylbenzylamine (291 µl, 1.62 mmol) and DABACO-$(AlMe_3)_2$ (337 mg, 1.29 mmol) gave **78** (99 mg, 0.29 mmol, 18%) as a colourless oil.

^{1}H NMR (400 MHz, DMSO-d_6) δ 9.29 (t, J = 6.0 Hz, 1H, NH), 8.88 (d, J = 2.5 Hz, 1H, Pyr), 8.28 (dd, J = 8.5, 2.5 Hz, 1H, Pyr), 7.62 (d, J = 8.5 Hz, 1H, Pyr), 7.42 – 7.19 (m, 4H, Ar), 7.19 – 6.86 (m, 5H, Ar), 4.48 (d, J = 6.0 Hz, 2H, CH_2). **^{13}C NMR** (101 MHz, DMSO-d_6) δ 164.13, 157.31, 155.95, 153.06, 149.48, 139.11, 134.69, 130.48, 129.61, 124.61, 123.77, 119.18, 118.83, 42.64. **FT-IR** ν_{max} (film) 3243, 3033, 1672 cm^{-1}. **HRMS** (ESI-TOF) calcd for $C_{19}H_{15}ClO_2N_2$ $[M+H]^+$: 339.0895, found : 339.0897.

N-([1,1'-biphenyl]-4-ylmethyl)-6-(4-(hydroxymethyl)-1H-pyrazol-1-yl)nicotinamide 79

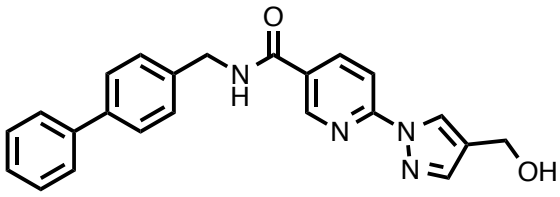

70 (20 mg, 0.062 mmol), pyrazole-4-methanol (9 mg, 0.092 mmol) and Cs_2CO_3 (29 mg, 0.092 mmol) were suspended in DMF (1ml) and heated under microwave radiation at 120°C for 3 hrs. The resultant mixture was diluted with water (5ml) and extracted with EtOAc (3 x 10ml). The organic phases combined and washed with water, brine and dried with anhydrous Na_2SO_4. The volatiles were then evaporated in *vacuo* and purified by flash column chromatography using (0% - 5% MeOH, CH_2Cl_2, 1 % NH_3) over 10 column volumes to give **79** (2 mg, 0.005 mmol, 8.5%) as an brown oil.

^{1}H NMR (400 MHz, DMSO-d_6) δ 9.30 (t, J = 6.0 Hz, 1H, NH), 8.99 – 8.89 (m, 1H), 8.60 – 8.52 (m, 1H), 8.48 – 8.40 (m, 1H), 8.07 – 7.92 (m, 1H), 7.86 – 7.78 (m, 1H), 7.72 – 7.29 (m, 9H, Ar), 5.07 (t, J = 5.5 Hz, 1H, $CH_2\underline{OH}$), 4.56 (d, J = 6.0 Hz, 2H, CH_2NH), 4.46 (d, J = 5.5 Hz, 2H, $\underline{CH_2}OH$). **^{13}C NMR** (101 MHz, DMSO-d_6) δ 169.79, 152.72, 148.31, 146.87, 142.81, 140.42, 139.30, 139.04, 129.39, 129.39, 128.44, 127.15, 127.05, 126.31, 125.79, 111.53, 54.58, 42.89. **FT-IR** ν_{max} (film) 3326, 2359, 1683, 1542, 1401 cm^{-1}. **HRMS** (ESI-TOF) calcd for $C_{23}H_{20}N_4O_2$ $[M-H]^-$: 383.1586, found : 383.1513.

6-(4-(hydroxymethyl)-1*H*-pyrazol-1-yl)-*N*-(4-phenoxybenzyl)nicotinamide 80

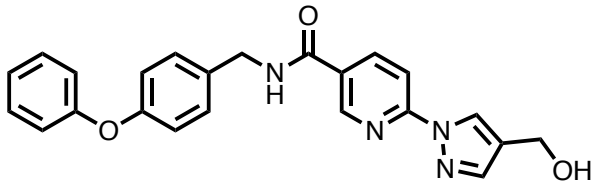

78 (50 mg, 0.202 mmol), pyrazole-4-methanol (29 mg, 0.303 mmol) and Cs_2CO_3 (98 mg, 0.303 mmol) were suspended in DMF (1 ml) and heated under microwave radiation at 120°C for 3 hrs. The resultant mixture was diluted with water (5 ml) and extracted with EtOAc (3 x 10 ml). The organic phases combined and washed with water, brine and dried with anhydrous Na_2SO_4. The volatiles were then evaporated in *vacuo* and purified by flash column chromatography using (0% - 5% MeOH, CH_2Cl_2, 1 % NH_3) over 10 column volumes gave **80** (13 mg, 0.032 mmol, 16%) as a orange solid.

m.p. 215-217°C. **^{1}H NMR** (400 MHz, DMSO-d_6) δ 9.26 (t, J = 6.0 Hz, 1H, NH), 8.96 – 8.93 (m, 1H), 8.60 – 8.53 (m, 1H), 8.42 (dd, J = 8.5, 2.5 Hz, 1H, Pyzl), 8.02 – 7.95 (m, 1H), 7.82 (s, 1H), 7.41 – 7.34 (m, 4H, Ar), 7.20 – 7.08 (m, 1H), 7.04 – 6.96 (m, 4H, Ar), 5.10 (t, J = 5.5 Hz, 1H, $CH_2\underline{OH}$), 4.50 (d, J = 6.0 Hz, 2H, $\underline{CH_2}NH$), 4.47 (d, J = 5.5 Hz, 2H, $\underline{CH_2}OH$). **^{13}C NMR** (101 MHz, DMSO-d_6) δ 164.01, 156.88, 155.43, 152.25, 147.85, 142.34, 138.56, 134.48, 130.01, 129.12, 127.47, 125.84, 125.32, 123.29, 118.75, 118.34, 111.04, 54.13, 42.12. **FT-IR** ν_{max} (film) 3623, 3367, 1688 cm^{-1}. **HRMS** (ESI-TOF) calcd for $C_{23}H_{20}N_4O_3$, $[M+H]^+$: 401.1535, found 401.1619.

N-([1,1'-biphenyl]-4-ylmethyl)-4,6-dichloronicotinamide 81

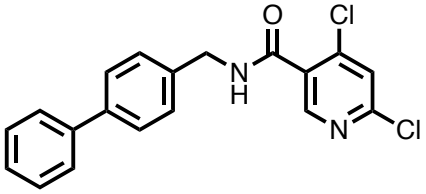

Following general procedure C: 4,6-dichloronicotinic acid (300 mg, 1.56 mmol), 4-phenylbenzylamine (228 mg, 1.24 mmol), T3P (1.48 g, 4.68 mmol) and DIPEA (483 mg, 3.9 mmol) gave **81** (210 mg, 0.58 mmol, 47 %) as a white solid.

m.p. 175-177°C. **^{1}H NMR** (400 MHz, DMSO-d_6) δ 9.26 (t, J = 6.0 Hz, 1H, NH), 8.56 (s, 1H, Pyr), 7.93 (s, 1H, Pyr), 7.73 – 7.31 (m, 9H, Ar), 4.61 (d, J = 6.0 Hz, 2H, CH_2). **^{13}C NMR** (101 MHz, DMSO-d_6) δ 163.33, 151.24, 149.05, 142.60, 139.87, 138.93, 137.78,

131.85, 128.94, 127.96, 127.39, 126.71, 126.59, 124.83, 42.39. **FT-IR**ν_{max} (film) 1673 cm^{-1}.

HRMS (ESI-TOF) calcd for $C_{19}H_{13}ON_2{}^{35}Cl_2$ $[M-H]^-$: 355.0413, found : 355.0413.

N-([1,1'-biphenyl]-4-ylmethyl)-4-chloro-6-(1H-pyrazol-1-yl)nicotinamide 82

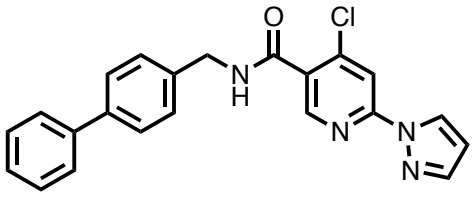

81 (250 mg, 0.702 mmol), pyrazole (12 mg, 0.17 mmol) and Cs_2CO_3 (456 mg, 1.40 mmol) were suspended in DMF (5 ml) and heated at 80°C for 30 min. An additional equivalent of pyrazole was added to the reaction mixture and the resulting mixture was heated again at 80°C for 30 mins, this was repeated 2 more times. The resultant mixture was diluted with water (15 ml) and extracted with EtOAc (3 x 20 ml). The organic phases combined and washed with water, brine and dried with anhydrous Na_2SO_4. The volatiles were then evaporated in *vacuo* and purified by flash column chromatography using (Cyclohexane 100 % - 75%, EtOAc 0 %- 25 %) over 10 column volumes gave **82** (196 mg, 0.51 mmol, 72 %) as a white solid.

m.p. 174-177°C. **^{1}H NMR** (400 MHz, DMSO-d_6) δ 9.17 (t, J = 6.0 Hz, 1H, NH), 8.52 (s, 1H, Pyr), 8.36 (d, J = 2.5 Hz, 1H, Pyzl), 7.96 (s, 1H, Pyr), 7.86 (d, J = 2.5 Hz, 1H, Pyzl), 7.74 – 7.28 (m, 9H, Ar), 6.59 – 6.58 (m, 1H, Pyzl), 4.51 (d, J = 6.0 Hz, 2H, CH_2). **^{13}C NMR** (101 MHz, DMSO-d_6) δ 164.97, 151.50, 150.04, 145.12, 142.86, 139.99, 138.88, 137.92, 130.35, 128.95, 128.25, 127.36, 126.62, 126.58, 124.67, 115.78, 109.21, 42.51,

39.52. **FT-IR** ν_{max} (film) 1653 cm^{-1}. **HRMS** (ESI-TOF) calcd for $C_{22}H_{16}ON_4{}^{35}Cl$ $[M-H]^-$: 387.1020, found : 387.1021.

N-([1,1'-biphenyl]-4-ylmethyl)-4-(benzylamino)-6-(1H-pyrazol-1-yl)nicotinamide 83

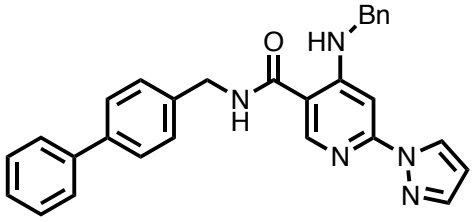

Following general procedure D: **82** (100 mg, 0.257 mmol), BrettPhos Pd G3 (20 mg, 0.028 mmol), Cs_2CO_3 (185 mg, 0.568 mmol) and Benzylamine (27 mg, 0.257 mmol) gave 83 (15 mg, 0.032 mmol, 14 %) as a orange oil.

^{1}H NMR (400 MHz, DMSO-d_6) δ 8.88 (t, J = 6.0 Hz, 1H, NH), 8.14 (s, 1H, Pyr), 7.93 (d, J = 2.5 Hz, 1H), 7.75 – 7.59 (m, 5H, Ar), 7.50 – 7.28 (m, 10H, Ar), 6.76 (s, 1H, Pyr), 6.45 – 6.43 (m, 1H, Pyzl), 4.57 (d, J = 6.0 Hz, 2H, CH_2), 4.39 (d, J = 6.0 Hz, 2H, CH_2). **^{13}C NMR** (101 MHz, DMSO-d_6) δ 166.57, 160.44, 149.39, 145.38, 141.72, 140.51, 139.11, 139.05, 130.65, 129.38, 128.74, 128.40, 127.77, 127.56, 127.11, 127.04, 126.98, 115.57, 108.11, 59.19, 42.72, 27.94. **FT-IR** ν_{max} (film) 3362, 1651 cm^{-1} . **HRMS** (ESI-TOF) calcd for $C_{29}H_{26}ON_5$ $[M+H]^+$: 460.2125, found : 460.2125.

N-([1,1'-biphenyl]-4-ylmethyl)-4-(dimethylamino)-6-(1H-pyrazol-1-yl)nicotinamide 84

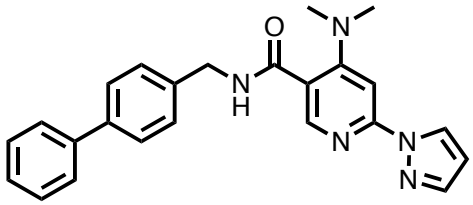

82 (29 mg, 0.0747 mmol) was dissolved in DMAc (2 ml) before the addition of Dimethylamine (2M in THF) (11 mg, 0.234 mmol). The resultant mixture was heated under microwave radiation at 120°C for 2 hrs. The resulting mixture was diluted with water (15 ml) and extracted with EtOAc (3 x 20 ml). The organic phases combined and washed with water, brine and dried over Na_2SO_4. The volatiles were then evaporated in *vacuo* and purified by flash column chromatography using (Cyclohexane 100 % - 75%, EtOAc 0 %-25 %) over 10 column volumes gave **84** (18 mg, 0.045 mmol, 61%) as a white solid.

m.p. 160-162°C. **^{1}H NMR** (400 MHz, DMSO-d_6) δ 8.83 (t, J = 6.0 Hz, 1H, NH), 8.24 (s, 1H, Pyr), 8.10 (d, J = 2.5 Hz, 1H, Pyzl), 7.74 (d, J = 2.0 Hz, 1H, Pyzl), 7.70 – 7.31 (m, 9H, Ar), 6.76 (s, 1H, Pyr), 6.48 (t, J = 2.5, 2.0 Hz, 1H, Pyzl), 4.41 (d, J = 6.0 Hz, 2H, CH_2), 3.10 (s, 6H, $(CH_3)_2$). **^{13}C NMR** (101 MHz, DMSO-d_6) δ 166.17, 159.98, 148.75, 145.38, 141.26, 140.03, 138.67, 138.63, 130.38, 128.92, 127.96, 127.30, 126.59, 126.50, 114.56, 107.59, 98.20, 42.28, 39.52, 37.71. **FT-IR** ν_{max} (film) 1645 cm^{-1} **HRMS** (ESI-TOF) calcd for $C_{24}H_{24}ON_5$ $[M+H]^+$: 398.1975, found : 398.1970.

3.9 References

1 Lowe, J. in *Resmed* (New York, 2016).

2 Hann, M. M. Molecular obesity, potency and other addictions in drug discovery. *MedChemComm* **2**, 349-355, doi:10.1039/C1MD00017A (2011).

3 Deng, G., Zhao, B., Ma, Y., Xu, Q., Wang, H., Yang, L. *et al.* Novel complex crystal structure of prolyl hydroxylase domain-containing protein 2 (PHD2): 2,8-Diazaspiro[4.5]decan-1-ones as potent, orally bioavailable PHD2 inhibitors. *Bioorganic & medicinal chemistry* **21**, 6349-6358, doi:10.1016/j.bmc.2013.08.046 (2013).

4 Vachal, P., Miao, S., Pierce, J. M., Guiadeen, D., Colandrea, V. J., Wyvratt, M. J. *et al.* 1,3,8-Triazaspiro[4.5]decane-2,4-diones as efficacious pan-inhibitors of hypoxia-inducible factor prolyl hydroxylase 1-3 (HIF PHD1-3) for the treatment of anemia. *J Med Chem* **55**, 2945-2959, doi: 10.1021/jm201542d (2012).

5 Vachal, P., Miao, S., Pierce, J. M., Guiadeen, D., Colandrea, V. J., Wyvratt, M. J. *et al.* 1,3,8-Triazaspiro[4.5]decane-2,4-diones as Efficacious Pan-Inhibitors of Hypoxia-Inducible Factor Prolyl Hydroxylase 1–3 (HIF PHD1–3) for the Treatment of Anemia. *J. Med. Chem.* **55**, 2945 (2012).

6 Dubois, N., Glynn, D., McInally, T., Rhodes, B., Woodward, S., Irvine, D. J. *et al.* On DABAL-Me3 promoted formation of amides. *Tetrahedron* **69**, 9890-9897, doi:https://doi.org/ 10.1016/j.tet.2013.08.062 (2013).

7 Chan, M. C., Holt-Martyn, J. P., Schofield, C. J. & Ratcliffe, P. J. Pharmacological targeting of the HIF hydroxylases - A new field in medicine development. *Mol Aspects Med* **47-48**, 54-75, doi:10.1016/j.mam.2016.01.001 (2016).

8 Chowdhury, R., McDonough, M. A., Mecinovic, J., Loenarz, C., Flashman, E., Hewitson, K. S. *et al.* Structural basis for binding of hypoxia-inducible factor to the oxygen-sensing prolyl hydroxylases. *Structure* **17**, 981-989, doi:10.1016/j.str.2009.06.002 (2009).

9 WO 2012/021830 A1. (2012).

CHAPTER 4. Novel PHD Inhibitors

4.1 Synthetic Investigation of The 4-hydroxy Pyridine Series

In **Chapter 3**, the 4-hydroxy-2-(1H-pyrazol-1-yl)pyrimidine-5-carboxamide scaffold (**11, 26 - 34**) had undergone broad SAR (**Chapter 3**). The results indicated that all substituents of compound **11** were required for PHD2 inhibition. Removal of just one of the substituents, resulted in no inhibition was observed. The molecular requirements to achieve potent PHD2 inhibition are:

1) Bidentate chelation to the metal ion;

2) Hydrogen bond interaction with Tyr-310;

3) Interaction with the aromatic pocket at the entrance of the PHD2 active site.

Investigation of the patents first describing the 4-hydroxy-2-(1H-pyrazol-1-yl)pyrimidine-5-carboxamide series (**11, 26 - 34**) identified the 4-hydroxy pyrimidine as the core pharmacophore.[1-3] However, modification to a 4-hydroxy pyridine (**94**) and the broad SAR was not claimed.[1-3] It was proposed that the 4-hydroxy pyridine core would maintain all the necessary features required for PHD2 inhibition (**Figure 35**).

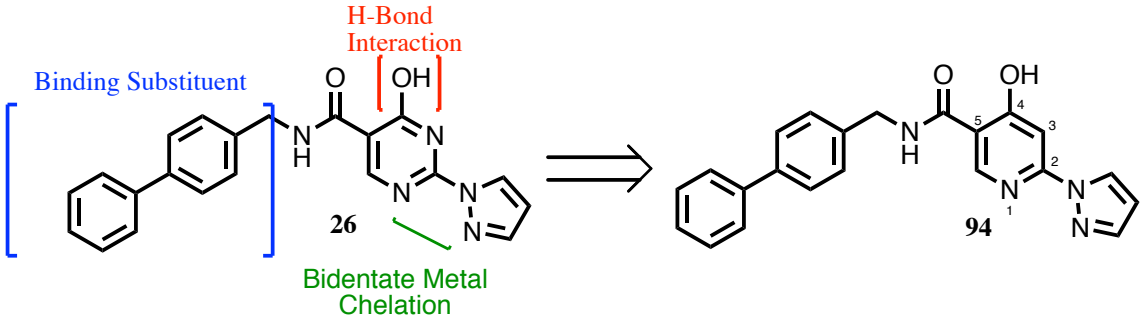

Figure 35: The substituents required for potent PHD2 inhibition and the modification to maintain inhibition.

A selection of analogues (**94 - 97**) were synthesised using the 4-hydroxy pyridine group instead of the 4-hydroxy pyrimidine group whilst varying the biphenyl substituent (**Figure 35**) (**Table 4**). It was envisaged **82** (**Chapter 3.5**) would undergo a S_NAr reaction with a deprotonated methoxy fragment to give the 4-methoxy pyridine precursor (**90)**. However, attempts at the reaction involving variation in temperature, base and solvent resulted in either no reaction or starting material degradation. **85** was found to be commercially available and therefore an alternative synthesis of **94** was envisaged. An amide coupling to give **86**, before an S_NAr or coupling of the pyrazole substituent to give **90**, followed by a demethylation to give **94** was proposed (**Scheme 15a**). The amide coupling gave **86-89** (**Scheme15A**). The S_NAr reaction of **86-89** failed to yield **90-93** (**Scheme 15B).** A Buchwald coupling was next attempted, initially using the same conditions as described in **Chapter 3.5**. This yielded **90-93** in acceptable yields (18-57%) (**Scheme 15B**). Demethylation of **90-93** using TMS-I with a high temperature yielded **94 - 97** (**Scheme 15C**).

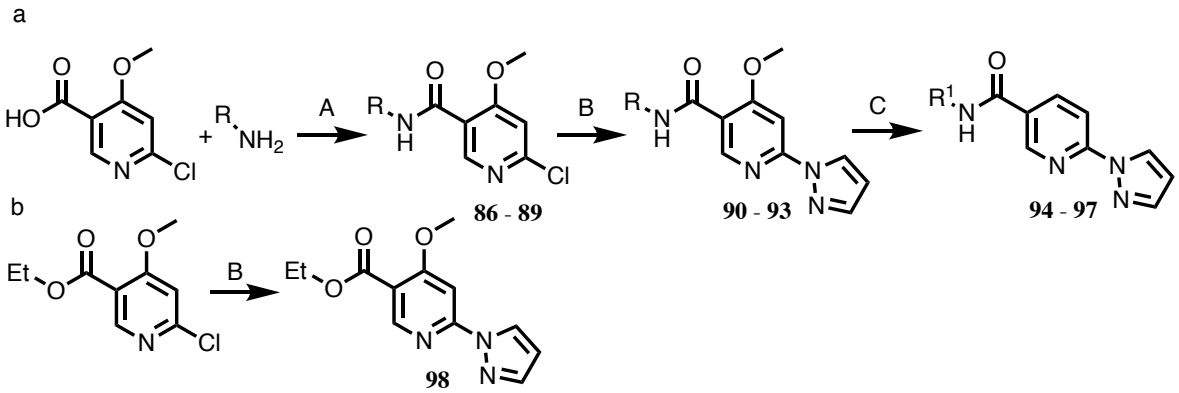

Scheme 15: The synthesis of the initial C-4 hydroxy pyridine analoges. Reagents and conditions: **A**) T3P, amine, DIPEA, DMAc, RT, 16hrs (34-76%). Initial **B**) Pd^{t}BuXPhos, Cs_2CO_3, THF:DMAc (1:1), MW 120°C, 1hr (40-55%). Initial **C**) TMS-I, CH_2Cl_2, 60°C, 90 min (18-57%). Optimised **B**) Pd^{t}BuXPhos, Cs_2CO_3, ^{t}BuOH, sandbath 80°C, 16 hr (24-74%). Optimised **C**) LiCl, DMAc, MW, 100°C, 2 hrs (9-64%).

The screening results for the initial 4-hydroxy pyridine series are shown in **Table 13**. Comparison of **26** and **32** to **94** and **95** (IC_{50} 286, 258, 145 and 317 nM, respectively), indicated replacing the 4-hydroxy pyrimidine core of **26** and **32** with the 4-hydroxy pyridine core of **94** and **95** maintains inhibition of PHD2. The 4-hydroxy pyridine pharmacophore is significantly synthetically easier to prepare compared to the 4-hydroxy-2-(1H-pyrazol-1-yl)pyrimidine-5-carboxamide pharmacophore (**11, 26-34**).

Table 13 : Initial SAR of the 4-hydroxy-pyridine analogues screened against $PHD2_{181-426}$ and the HIF-1α CODD substrate. The cLogPs of **94-97** were calculated using DataWarrior [10]. Experiment performed by Dr A Tumber. Experimental measurement n =1.

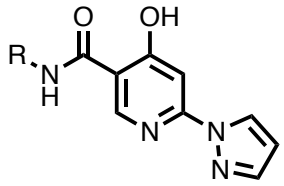

Cpd	R	RapidFire™ PHD2 IC_{50}	cLogP
94	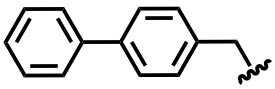	**0.145**	**3.43**
95	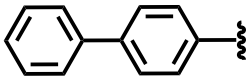	**0.317**	**3.72**
96	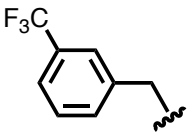	**6.12**	**2.62**
97	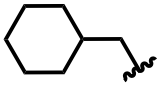	**10.75**	**2.11**

Allowing for broad and in-depth SAR to be undertaken on the 4-hydroxy pyridine analogues (**94-97**).

In late 2016, Merck filed a patent on a similar structure to the 4-hydroxy pyridine pharmacophore, but a *C*-5 di-phenyl amide was used (**Figure 36**).[4] As stated in **Chapter 2.5**, the di-phenyl analogue (**Figure 19B**) was not synthesised because it was disclosed late into the PHD2 project and it was envisaged that the di-phenyl substituent may cause strong inhibition of structurally similar 2OG oxygenases such as OGFOD1 and vCPH (**Figure 15, 19 & 36**).

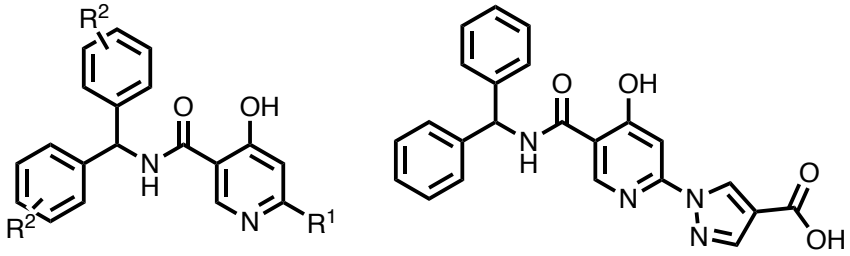

Figure 36: **A**) The patented pharmacophore structure by Merck. **B**) The structurally similar inhibitor on the patent, IC_{50} : 0.875 nM.[4]

An alternative route was attempted to synthesise the pyrazol-nicotinate core of **98** (**Scheme 15b**). A Buchwald coupling of **98**, before an ester hydrolysis and then an amide coupling was envisaged to minimise the synthetic steps required for in-depth investigation of **94**. However, the Buchwald coupling of **98** resulted in very poor yields (3%) and the route was not viable (**Scheme 15b**).

The synthetic steps (**Scheme 15B** and **C**) **(**Pd-catalysed amination and methoxy demethylation, respectively) for the synthesis of **94-97** had many synthetic complications. For the Buchwald coupling, when the amide substituent was varied (**90-93**) poor yields

were recorded due to increased side reactions. Although, the Buchwald coupling was successful, multiple side reactions occurred including the demethylation of the methoxy group of **86,** (likely) resulting in catalyst poisoning and pyrazole group coupling at the *C*-4 position of **86,** with replacement of the methoxy substituent yielding **189**. In order to circumvent unwanted coupling of the pyrazole to the 4-position and demethylation of **86**; a number of different reaction conditions were screened, the results of which are presented in **Table 14**. Variables such as solvent, base and temperature were investigated beginning with the reported protocols.[5] It was hypothesised that the demethylation side reaction was a result of the use of the Cs_2CO_3. **Entries 1-3** present reactions attempted using bases typically used in Pd-catalysed amination (**Table 14**).[5] Unfortunately, weaker bases such as K_3PO_4 resulted in no product formation; whereas stronger bases such as LHMDS resulted in an increase in side products and poor yields of **90**. This indicates Cs_2CO_3 was the best base for this Pd-catalysed amination.

Demethylation of methoxy groups often requires a high temperature. It was envisaged that the use of microwave radiation and DMAc (high amount of absorption) may promote side reactions. DMAc had been previously used due to solubility issues of the 2-chloro-pyrimidine analogues (**69** and **70**). Common solvents used for Pd-catalysed reactions were tested (**Entries 4-8**).[5] Use of dioxane resulted in a reduction of demethylation but a significant increase in production of **189**. An increase in the di-pyrazole coupling also occurred when THF and toluene were used as solvents. ^{t}BuOH achieved a reduction in the side-product **189** produced and no *C*-4 methoxy demethylation of **90** was observed. It was envisaged that the pyrazole coupling at the *C*-4 position of **90** had a higher energy barrier

compared to coupling with the 2-chloro substituent due to the preference of the Pd catalyst for aryl-halides.[6] The high absorption of DMAc with microwave radiation, likely resulted in energy transmission that was above the required energy for both aryl-chloride and aryl-methoxy couplings. Therefore, in combination with ^{t}BuOH as a solvent, microwave radiation was replaced with a sand bath to give an improved yield (30% improvement in yield) of **90** without side products. An Ullmann reaction was used in the reported patent.[4] However, the reaction was poorly yielding (15%), lower in contrast to the Pd-catalysed amination of **90** (85%), demonstrating the superiority of the Pd-catalysed amination.

Table 14 : Conditions attempted for the Buchwald amination to synthesise **90**.

Entry	Base	Solvent	Temperature °C	Method of Heating	Yield (%) for 90	Demethylation	4-Pyrazole Coupling
1	Cs_2CO_3	DMA:THF (1:1)	100	MW	55	Yes	Yes (minor)
2	K_3PO_4	DMA:THF (1:1)	100	MW	-	Yes	No
3	LHMDS	DMA:THF (1:1)	100	MW	22	Yes (major) and other side reactions	Yes
4	Cs_2CO_3	Dioxane	100	MW	18	minor	yes (major product)
5	Cs_2CO_3	THF	100	MW	16	minor	yes (major product)
6	Cs_2CO_3	Toluene	100	MW	15	minor	yes (major product)
7	Cs_2CO_3	^{t}BuOH	100	MW	60	No	Yes (minor)
8	Cs_2CO_3	^{t}BuOH	80	Sand Bath	85	No	No

90 was initially demethylated using TMS-I, although high temperatures were required often resulting in substantial reductions in yields due to starting material degradation (**Scheme 15C**). In order to achieve acceptable yields in demethylation of the methoxy group of **90**, a number of different reaction conditions were screened (**Table 15**). BBr_3 was attempted using typical conditions, but gave no product. Increasing the reaction temperature only promoted starting material degradation. According to the reported patent, 4M HCl in dioxane for 3 hours was sufficient for complete demethylation of **90**.[4] However, only the starting material was present even after 2 days under the patent conditions (in addition to a increase in reaction temperature). Methoxy demethylation was an initial side reaction for the Pd amination. It was postulated that the caesium or palladium metal atom chelates between to the methoxy moiety and the carbonyl of the *C*-5 amide, following a similar mechanism to TMS-I demethylation. Cs_2CO_3 in DMAc was attempted at 100°C on **90** to give **94**. Partial demethylation of **90** did occur (yield = 3%), the reaction proceeded at slow rate indicating in prior conditions possible chelation by the Pd catalyst accelerated demethylation. An increase in reaction temperatures, using the Cs_2CO_3 in DMAc resulted starting material degradation. It was envisaged that starting material degradation in TMS-I and Cs_2CO_3 reactions was due to the acidic and basic conditions respectively; a neutral Lewis acid with a stronger nucleophilic anion than I^- may lead to an improved yield of **94**. Fang *et al.* reported a method using LiCl-DMF system using microwave radiation and proposed a mechanism for demethylation similar to the proposed TMS-I demethylation mechanism (**Scheme 16**).[7] It was proposed that replacing DMF for DMAc would improve reaction yields due of DMAc improved stability at a higher temperature. This resulted in

improved yields of **94** (57% increase in contrast to TMS-I conditions) and no starting material degradation was observed (**Table 15**).

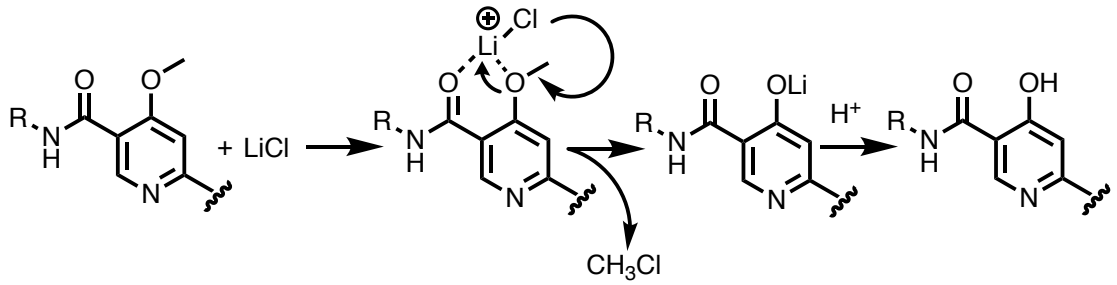

Scheme 16: Proposed mechanism of LiCl.[7]

Table 15 : Conditions attempted for the methoxy demethylation

Entry	Reagent	Conditions	Reaction	Yield	Side Reactions
1	TMS-I	CH_2Cl_2, 80 °C, MW, 10 hrs	Yes	20%	Yes Fragmentation
2	4M HCl	1) CH_2Cl_2, 48 hrs. 2) CH_2Cl_2, 100 °C, 16 hrs	No	-	-
3	BBr_3	1) CH_2Cl_2, 48 hrs. 2) CH_2Cl_2, 100 °C, 16 hrs	No	-	-
4	Cs_2CO_3	DMAc, 100 °C, 4 hrs	Yes	3%	Yes Fragmentation
5	LiCl	DMAc, 100 °C, 2 hrs	Yes	77%	No

With the synthetic route now optimised (**Scheme 15**), in-depth SAR was undertaken to explore and improve on PHD2 inhibition and investigate possibilities of PHD isoform and substrate selectivity. Three areas were investigated (**Figure 37**) :

1) Further exploration of the sensitivity of the aromatic binding pocket to other substituents;
2) Moving the hydroxyl group to the *C*-3 position on the pyridine ring;

3) Pyrazole modifications to improve binding with PHD2 via Tyr303 and Arg383 interactions.

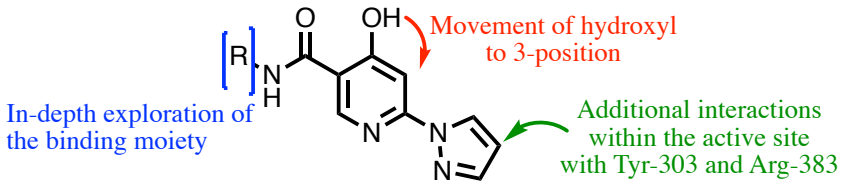

Figure 37: Strategy for in-depth SAR for the 4-hydroxy pyridine pharmacophore.

4.2 In-depth Structure Activity Relationship of The Amide Substituent of The 4-hydroxy Pyridine Pharmacophore

The bi-phenyl amide group had been briefly investigated in the first 4-hydroxy-2-(1H-pyrazol-1-yl)pyrimidine-5-carboxamide series (**Chapter 2.5**, **Table 4**). The results for the more in-depth SAR are shown in **Table 16**.

117 - **119** were designed to investigate the preference for a 3- or 4-position of the first phenyl ring in the bi-phenyl system. Transferring the trifluoromethyl group (CF_3) to the 4-position (**117**) resulted in a substantial improvement of inhibition in comparison to **96** (IC_{50} 63 nM and 6.12 µM respectively). Transferring the phenyl substituent to the 3 position (**118** and **119**) of the primary phenyl ring of **94** and **95**, resulted in an increase of 3-fold of inhibition of PHD2 (**118** and **119**, IC_{50} = 0.055 & 0.106 µM respectively).

The strong potency of **117** warranted further investigation of the CF_3 substituent. It was suggested that the potency of the biphenyl compounds (**94** and **95**) may be related to the length of the biphenyl amide group of **94** and **95**. It was proposed that increasing the length of the CF_3 group in **117** by converting it to a trifluoromethyoxy group (**120**) may result in a

improvement. **120** resulted in similar levels of inhibition to **117** (IC_{50} = 103 nM), although both compounds may have stronger inhibition but the RapidFire assay limited by the enzyme concentration used (150 nM).

A potential drawback of compounds such as **94** and **95**, is their high level of hydrophobicity (cLogP of **94** = 3.43 and **95** = 3.72, respectively), which may promote off target effects in a *in-vivo* environment.[8] However, replacing the secondary phenyl substituent of **94** with a CF_3 substituent (**117**) improved potency whilst reducing cLogP (**117** = 2.62) to an acceptable figure (2.5).[8,9] One potential solution considered was to reduce the amount of sp^2 character in the compounds.[8,9] **97** showed poor inhibition of PHD2; however, SAR has revealed the importance of the second substituent on the first phenyl ring of the *C*-5 amide substituent (**Figure 35**). It was hypothesised, the addition of a *C*-4 CF_3 group to **97** may lead to a substantial improvement of PHD2 inhibition whilst reducing cLogP (2.86). The addition of the CF_3 group to the *C*-4 cyclohexyl amide (**121**) resulted in a 104 fold increase in PHD2 inhibition (IC_{50} = 119 nM). Similar levels of inhibition were observed with **117** and **120**, indicating that the **π**-stacking interaction is not essential for interaction within the aromatic pocket.

Another solution to reduce cLogP is to add heteroatoms into the area where hydrophobicity is strongest within the molecule.[8,9] It was proposed that replacing the primary phenyl ring of **94** with a pyridine ring, may maintain interactions while reducing the cLogP by 1 log unit (cLogP for **94** = 3.43, **121** = 2.52). The 6-phenylpyridine amino group (**105**) was synthesised from 6-chloropyridin-3-yl)methamine via a Boc protection (**103**) of the primary amine before a Suzuki coupling of the phenyl moiety gave **104**. A

deprotection gave **105** (**Scheme 17**). The primary amine underwent the same synthetic route described in **Chapter 4.1** to give targeted compound **122**. Replacing the phenyl ring with a pyridine ring maintained strong PHD2 inhibition (**122**, IC_{50} 335 nM) but lost potency by 1 fold in comparison to **94**.

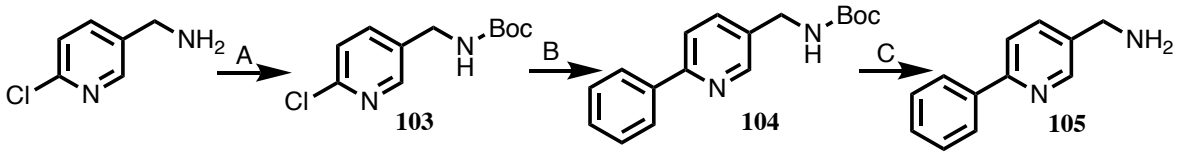

Scheme 17: The synthesis of 6-chloropyridin-3-yl)methamine. Reagents and Conditions: **A**) Di tert-butyl dicarbonate, DIPEA, CH_2Cl_2, rt, 16 hrs (89%) **B**) Pd Tetrakis, Cs_2CO_3, dioxane, 120°C MW, 30 mins, (89%) **C**) HCl (2M) in Et_2O, CH_2Cl_2, rt, 16 hrs, (96%).

As discussed in **Chapter 2**, the potency of **33** in comparison to **28** indicates that additional substituents on the methylene linker of the *C*-5 amide can lead to improved potency. Debenham *et al.* also revealed improvements of PHD2 inhibition on the methylene linker of the *C*-5 amide with chiral methyl moieties and the dimethyl substituents, although this may improve inhibition by increasing the overall hydrophobicity, thereby improving binding with the aromatic pocket.[10] **33** (IC_{50} 329 nM) showed strong inhibition with PHD2 due to the methoxy substituent on *C*-5 amide of **33**. The crystal structure of **33** complexed with PHD2 (**Chapter 2.8**) was unclear on how the hydroxy group interacted with PHD2 (**Figure 25**). The flexible loop between β2 and β3 strands (not observed in the crystal structure of PHD2 complexed with **33** due to disorder) of PHD2 folds over the HIF-α substrate.[11,12] The hydroxyl group of the methoxy substituent of **33** may interact with a residue on the loop, such as Ser-242. Due to differences between the PHD isoforms on the flexible loop (**Chapter 1.4**), substituents such as the 4-methoxy group may exhibit selectivity for the PHD isoforms. It was envisaged that a COOH group on the *C*-5 amide methylene bridge

(**123** and **124**) may potentially identify new interactions with the flexible loop between β2 and β3 strands of PHD2. It was proposed that the *S*-Enantiomer (**124**) may improve PHD2 inhibition via possible ionic interaction with Arg322 (**Figure 25**), whereas the *R*-Enantiomer (**123**) may follow the trend of **33** by forming additional interactions. The *R*-Enantiomer (**123**) caused a 3-fold increase in potency compared to the *S*-Enantiomer (**124**) (IC_{50} 182 nM and 589 nM, respectively), indicating additional interaction with PHD2 may occur with the *S*-enantiomer (**Figure 25**).

The screening results and the cLogPs (calculated used the program DataWarrior [13]) for the additional SAR work of the *C*-5 amide group are shown in **Table 16**. The results indicate that interaction with the hydrophobic pocket of PHD2 can be achieved in using a combination of different parameters. Not one parameter is essential for interaction with the aromatic pocket of PHD2. Potency of PHD2 can be achieved using a range of parameters for interacting with the aromatic pocket including aromaticity, hydrophobicity, the *C*-5 amide group and additional hydrogen bonding interactions on the methylene linker. Strong potency has been achieved with a wide range of cLogP values, ranging from 0.125-3.728, indicating overall molecular hydrophobicity is not an essential factor for interacting with the aromatic pocket as compounds **117** and **123** achieved strong inhibition of PHD2 and have low cLogPs (2.62 and 0.618, respectively). The cation **π** interactions made via the phenyl ring observed in crystal structures with **10** and **32** (**Figures 23** and **25**) can be replaced with other interactions whilst maintaining PHD2 inhibition (**121**, IC_{50} 117 nM).

Table 16: SAR of analogues investigating the binding substituent for the 4-hydroxy pyridine pharmacophore against $PHD2_{181-426}$ using the HIF-1α CODD and the cLogP calculated using the data-warrior program.[10] Experiment performed by Dr A Tumber. Experimental measurement n =1.

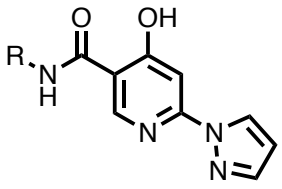

Cpd	R	RapidFire™ PHD2 IC_{50} µM	cLogP
117	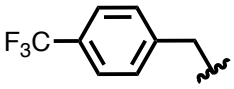	**0.063**	**2.62**
118	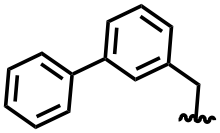	**0.055**	**3.43**
119	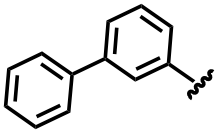	**0.106**	**3.72**
120	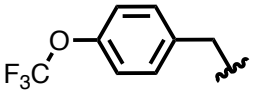	**0.103**	**2.87**
121	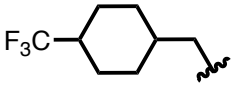	**0.119**	**2.86**
122	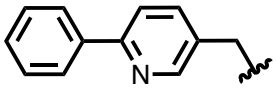	**0.335**	**2.52**
123	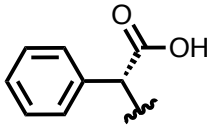	**0.182**	**0.61**
124	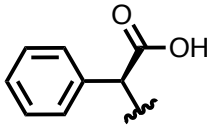	**0.589**	**0.61**

4.3 3-Hydroxypyridine Series

Initial SAR studies revealed the importance of the C-4 hydroxyl group for PHD2 inhibition for the 4-hydroxy-2-(1H-pyrazol-1-yl)pyrimidine-5-carboxamide series (**Chapter 3.5**). Clinical candidates such as FG-2216 (**3**) and Vadadustat (**5**) inhibit PHD2 by forming hydrogen bonds with residues Arg-383 and Tyr-303 of PHD2.[14,15] As demonstrated by the crystal structure of **3** complexed with $PHD2_{181-426}$, the Tyr-303 is positioned to form a hydrogen bond with a 1-chloroisoquinolin-4-ol moiety of **3** (**Figure 38A**).[14] It was hypothesised that replacing the 4-hydroxypyridine with the 3-hydroxy pyridine would maintain or improve PHD2 inhibition (**Figure 38B**).

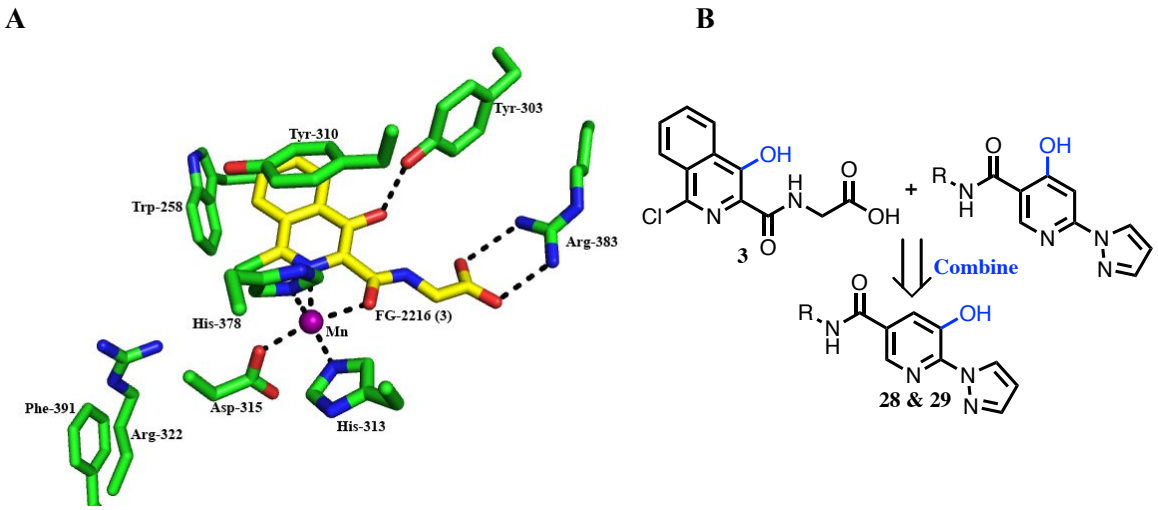

Figure 38: **A**) View of crystal structure of the amino acid residues of the active site of $PHD2_{181-426}$ complexed with FG-2216 **3**. (PDB ID: 2y34).[14] **B**) The strategy combining the interactions of the 1-chloroisoquinolin-4-ol with the 4-hydroxypyridine pharmacophore.

The 4-phenylbenzyl and 3-phenylbenzyl groups were chosen for the *C*-5 amide group as it was unclear whether the linear binding mode would be optimal for the 3-hydroxypyrdine

pharmacophore. **128** and **129** were synthesised using the route described in **Chapter 4.1**, with similar yields obtained for 4-hydroxypyridine analogues (**117-124**).

Table 17 directly compares the 3-hydroxypyridine and 4-hydroxypyridine series. The results indicate the moving the *C*-4 hydroxy group to the 3-position results in substantial loss of potency. **128** (IC_{50} 2.88 μM) had a 20 fold loss of potency in contrast to **94** (**Table 17**). The conversion to a 3-phenylbenzyl *C*-5 amide group (**129)** (IC_{50} 4.20 μM) resulted in an even greater loss, a 77-fold difference in potency compared to **118**, confirming the importance of the 4-position hydroxyl group, regardless of the 5-position amide group.

Table 17: SAR of the 3-hydroxy pyridine analogues in comparison with the 4-hydroxy pyridine analogues. Experiment performed by Dr A Tumber. Experimental measurement n =1.

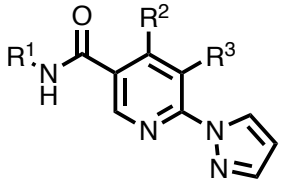

Cpd	R1	R2	R3	RapidFire™ PHD2 IC_{50} μM
128	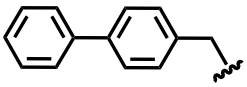	**H**	**OH**	**2.88**
129	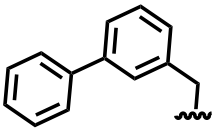	**H**	**OH**	**4.20**
94	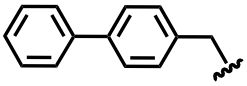	**OH**	**H**	**0.145**
118	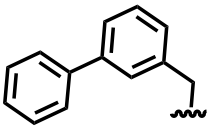	**OH**	**H**	**0.055**

4.4 Additional Interactions Within The Active Site On The *C*-4 position of The Pyrazole Group

All clinical candidates, to date interact with PHD2 as 2OG mimics; binding within the active site occurs via formation of two hydrogen bonds with Tyr-303 and Arg-383 as shown by the crystal structures of PHD2 bound with compound **3** and **5** (**Chapter 1.8**) (**Figure 38A**).[14-17] The initial 'hits' (**11**, **26-34**) revealed the hydrogen bond formed by the clinical candidates with Arg-383 in the active site of PHD2 can be 'replaced' or compensated for by binding to the aromatic pocket resulting in improved inhibition of PHD2. Furthermore, a better selectivity profile against other 2OG oxygenases, in comparison to the clinical candidates was observed (**Table 1** and **7**). Forming additional interactions with PHD2 may therefore lead to tighter binding to PHD2, leading to stronger inhibition, although at the cost of selectivity within the 2OG oxygenase family. **Chapters 3.5** and **4.3** revealed the importance of the hydrogen bond between the *C*-4 hydroxyl group and the residue Tyr-310, which proved to be difficult to replace. However comparing the crystal structures of PHD2 with **33** (**Figure 39A**) and **RJ8** (**Figure 39B** and **Chapter 1.8**) complexed, suggested the possibility of additional interaction with Tyr-303 (**Figure 39A**).[16]

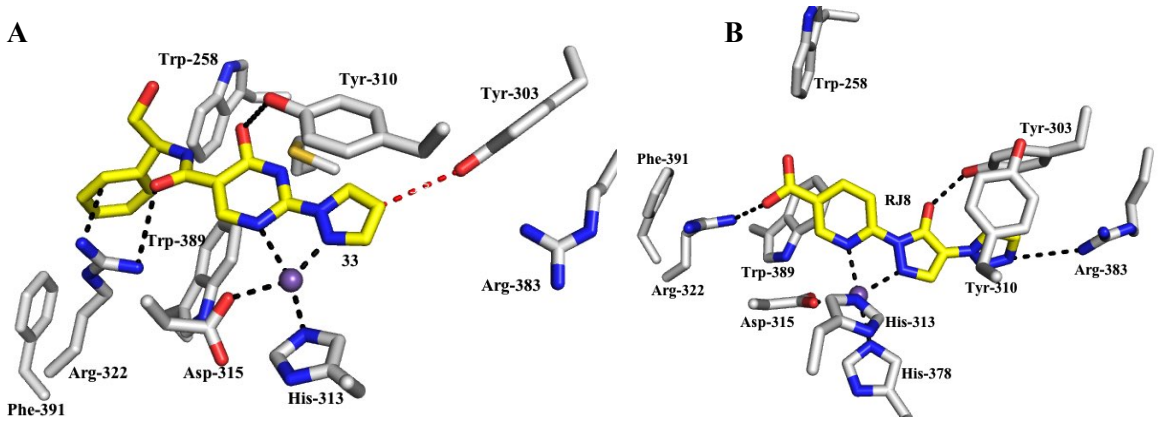

Figure 39: **A**) View of crystal structure of the amino acid residues of the active site of $PHD2_{181-426}$ complexed with **33**. **B**) View of crystal structure of the amino acid residues of the active site of $PHD2_{181-426}$ complexed with **RJ8**. (PDB ID: 5A3U).[16]

The 2,4-dihydro-3*H*-pyrazol-3-one core of **RJ8** forms a hydrogen bond with Tyr-303 and a **π**-stacking interaction with Tyr-310, whilst the triazole group hydrogen bonds with Arg383 (**Figure 38B**).[16] The 4-position of the pyrazole of the 4-hydoxy pyridine pharmacophore was chosen to explore additional interactions within the PHD2 active site (**Figure 39A** and **40**). Previously, it was proposed that the reason for **79** and **80** (**Chapter 3.5**) apparent inactivity was due to the rotational flexibility of the methoxy substituent. Substituents on the pyrazole group were introduced directly to the pyrazole ring to reduce flexibility. Nitrile (CN) and carboxylic acid (COOH) substituents were chosen as both have a high degree of rigidity and can form either hydrogen bond acceptor or donor roles (**Figure 40**). The 3-hydroxy-pyridine pharmacophore described in **Chapter 4.3** achieved weaker PHD2 inhibition. Therefore, it was envisaged that an additional interaction within the active-site of PHD2 may improve potency (**Figure 40**). The 4-phenylbenzyl, the 4-trifluorobenzyl and the 6-phenylpyridyl groups were chosen (**Figure 40**) as the *C*-5 amide group and the same

synthetic route developed in **Chapter 4.1** was used apart from a final step ester hydrolysis to give the free acids (**138**, **142-144**).

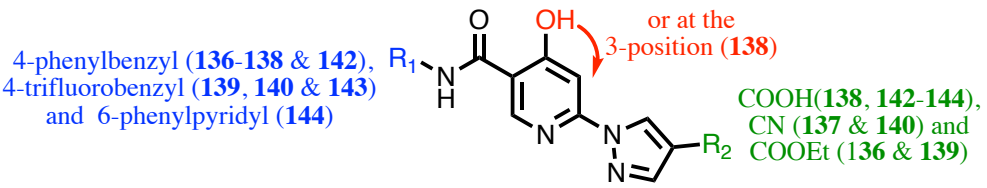

Figure 40: Summary of the analogues investigating the additional substituents to the 4-position of the pyrazole group.

Table 18 outlines the screening results for **136-144**. Compounds with the 4-phenylbenzyl amide group (**137**, **138** and **142**) improved in potency compared to **94** and **128**. Both **137** and **142** (IC_{50} 89 nM and 87 nM, respectively) were two-fold more potent than **94**. However, the potency is at the limits of detection of the RapidFire assay and therefore **137** and **142** may be more potent. For the 3-hydroxy pyridine analogue (**128**) (IC_{50} 2.88 μM) the addition of the COOH group to the pyrazole group (**138**) (IC_{50} 169 nM) resulted in an 25-fold increase in potency. This indicates that the hydrogen bond interaction with Tyr-310 can be replaced whilst maintaining strong inhibition of PHD2. The 4-trifluorobenzyl containing analogues **140** and **143**, resulted in loss of potency (IC_{50} 129 nM and 486 nM, respectively) in contrast to **117**. A similar effect was observed with **144** (IC_{50} 649 nM), which resulted in a 2 fold loss in potency in comparison to **122**. The ethyl ester precursors **136** and **139** also resulted in a loss of potency (IC_{50} 410 nM and 571 nM respectively), losing 4-fold and 9-fold in potency respectively in comparison to **94** and **117**. **136**, **139-142** & **144** may experience a loss in potency due to competing interactions between the active site and the aromatic pocket. The additional interaction (on the pyrazole group) within the active site may alter other interactions formed by the analogues with PHD2, resulting in different

Table 18 : SAR of the analogues investigating additional interactions within the PHD2 active for the 4-hydroxy and 3-hydroxy pyridine pharmacophores. Experiment performed by Dr A Tumber. Experimental measurement n =1.

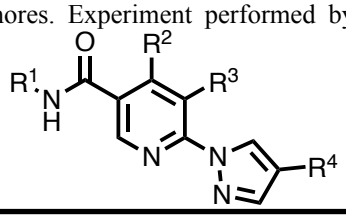

Cpd	R^1	R^2	R^3	R^4	PHD2 RapidFire™ IC_{50} µM
136	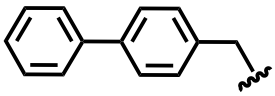	**OH**	**H**	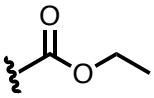	**0.4108**
142	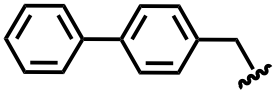	**OH**	**H**	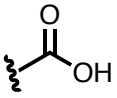	**0.087**
137	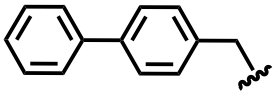	**OH**	**H**	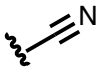	**0.089**
138	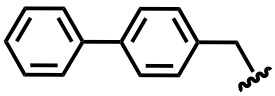	**H**	**OH**	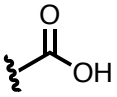	**0.163**
139	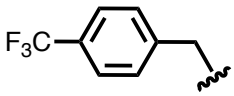	**OH**	**H**	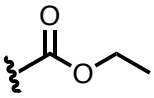	**0.571**
143	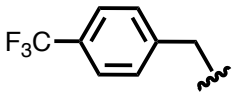	**OH**	**H**	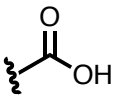	**0.129**
140	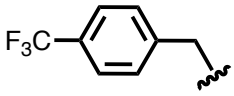	**OH**	**H**	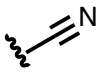	**0.486**
144	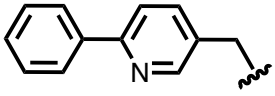	**OH**	**H**	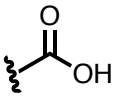	**0.649**

interactions of the 4-trifluorobenzyl amide group with the aromatic pocket that are not observed with other substituents, such as the shape or electronegativity of the CF_3 group.

It was proposed that the improved inhibition via the addition of the COOH substituent to the pyrazole group (**138** and **142**), may not require the presence of the *C*-4 hydroxyl group. Without the presence of a *C*-5 amide group (**24**) the 4-hydroxy-2-(1H-pyrazol-1-yl)pyrimidine-5-carboxamide pharmacophore was inactive towards PHD2 (**Chapter 2.5**, **Table 3**). However, interaction with the additional residue in **138 and 142** (in combination with interaction with the aromatic pocket of PHD2) may be sufficient for strong PHD2 inhibition. **148** was designed to test this hypothesis by using the 4-phenylbenzyl amide group. To directly compare the binding strength of the COOH and hydroxyl substituents, **149** was designed with the benzyl substituent as a 5-position amide. **148** and **149** were synthesised in a similar fashion to the compound series in **Chapter 3.5** (**Scheme 18**). 2-chloro-ethylnicotinate underwent an amide coupling with the relevant amine to give **145**. **70** and **145** were coupled to pyrazole-4-carboxylate ethyl ester via a Buchwald amination, using the optimized conditions described in **Chapter 4.1**, yielded **146** and **147**. **146** and **147** underwent a base-catalysed ester hydrolysis to give **148** and **149**.

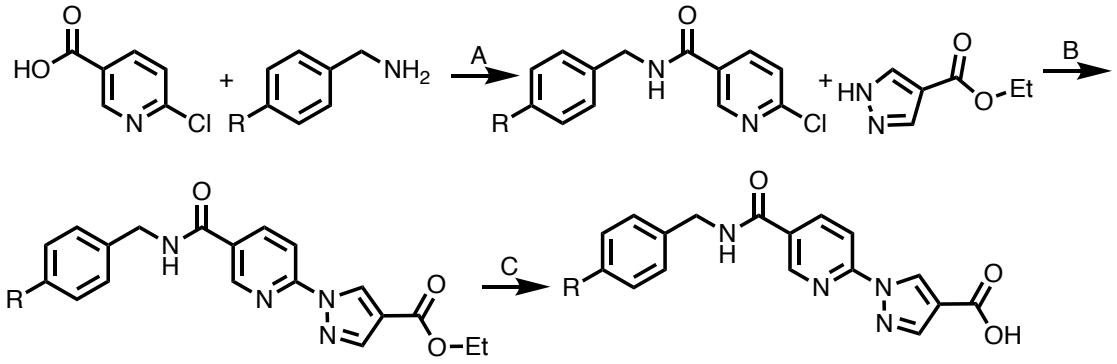

Scheme 18: Synthesis of 1-(5-carbamoylpyridin-2-yl)-1*H*-pyrazole-4-carboxylic acid series. Reagents and Conditions : **A**) T3P, DIPEA, DMAc, rt, 16hrs (85%). **B**) PdtBuXPhos, Cs_2CO_3, ^{t}BuOH, 100 °C, 90 mins (36-59 %). **C**) LiOH, THF:H_2O (1:1), RT, 16hrs (26-94 %).

The screening results of the COOH analogues (**Table 19**), indicated that strong potency can be achieved with the COOH substituent. In comparison to the 4-hydroxy pyridine analogue (**94**), **148** was 4.5 fold weaker than **94 (**IC_{50} 704 nM and 145 nM, respectively)**.** The results in **Table 19** demonstrate, in addition from the 3-hydroxy pyridine series (**Chapter 4.3**), that the hydrogen bond with the Tyr-310 residue is the dominant interaction in comparison to Tyr-303 and Arg-383 for PHD2 inhibition. Replacing the 4-phenylbenzyl (**148**) group for the benzyl group (**149**) resulted in a loss of inhibition (IC_{50} 1.18 μM). However, **149** achieved good inhibition of PHD2, (a similar level of PHD2 inhibition to the clinical candidates (**3** - **6**)) indicating that by partially removing the biphenyl interaction with the aromatic pocket of PHD2, the binding affinity can be replaced by interacting within the active site of PHD2.

Table 19: SAR of the COOH analogues without the *C*-4 hydroxy group. Experiment performed by Dr A Tumber. Experimental measurement n =1.

Cpd	Structural Formula	PHD2 Inhibition Rapid Fire IC_{50} μM
148	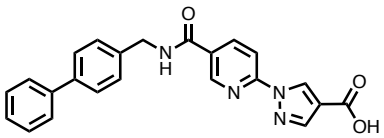	**0.704**
149	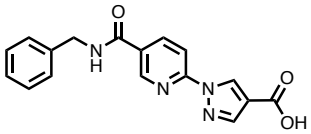	**1.18**

4.5 Cellular Characterisation of The 4-hydroxy Pyridine Pharmacophore

To confirm the on-target efficacy, **94** and **95** were then tested in the Hep3B cell line to measure HIF1-α stabilisation (**Figure 41**), the same protocol as described in **Chapter 2.6**. **95** showed HIF-1α stabilisation at 100 and 20 μM. **94** showed weak HIF-1α stabilisation at 20 μM but not at 100 μM. In comparison to the initial hit (**32**), **32** showed significantly stronger HIF-1α stabilisation at both concentrations. The poor efficacy observed with **94** and **95** may be due to the higher cLogP or the free hydroxyl groups pKa that may need to tautomerise into the amide form to pass through the cell membrane.

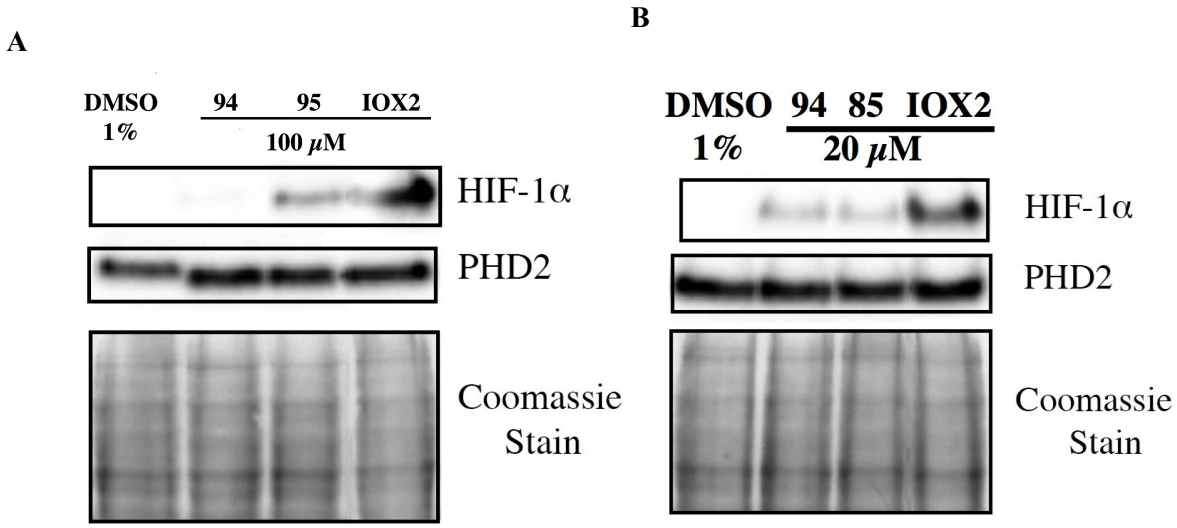

Figure 41: Cellular Inhibition studies of the initial 4-hydroxypyridine series (**94** and **95**) at 100 μM in the HEP-3B cell line. Immunoblot showing HIF-1α stabilization via inhibition of PHD2. Experiment performed by Dr T.Yeh

Figure 42 shows the cellular efficacy of the analogues investigating the SAR of the binding substituent (**Chapter 4.2**). Replacing or modifying the bi-phenyl substituent resulted in an significant improvement in HIF-1α stabilisation (in contrast to **94** and **95**)

indicating the bi-phenyl substituent does readily impact cell permeability. The replacement of the 'first' phenyl group of **94** with a pyridine (**122**), resulted in significant increase in HIF-1α stabilisation indicating that the cLogP may have a role in cellular permeability. **122** achieved moderate HIF-1α stabilisation at 20 μM. Replacing the terminal phenyl ring of **94** with either a CF_3 (**117**) or a OCF_3 (**120**) group, resulted in significant increase in HIF-1α stabilisation and showed moderate HIF-1α stabilisation at 20 μM (**Figure 42**). Replacing the 4-biphenyl substituent with a 4-trifluoromethyl-cyclohexane group (**121**) achieved strong HIF-1α stabilisation at both concentrations. However, the additional COOH group to the methylene linker (**123** and **124**) resulted in no HIF-1α stabilisation at either concentration. It was possible that the carboxylic acid and hydroxyl groups prevented **123** and **124** from passing through the cell membrane.

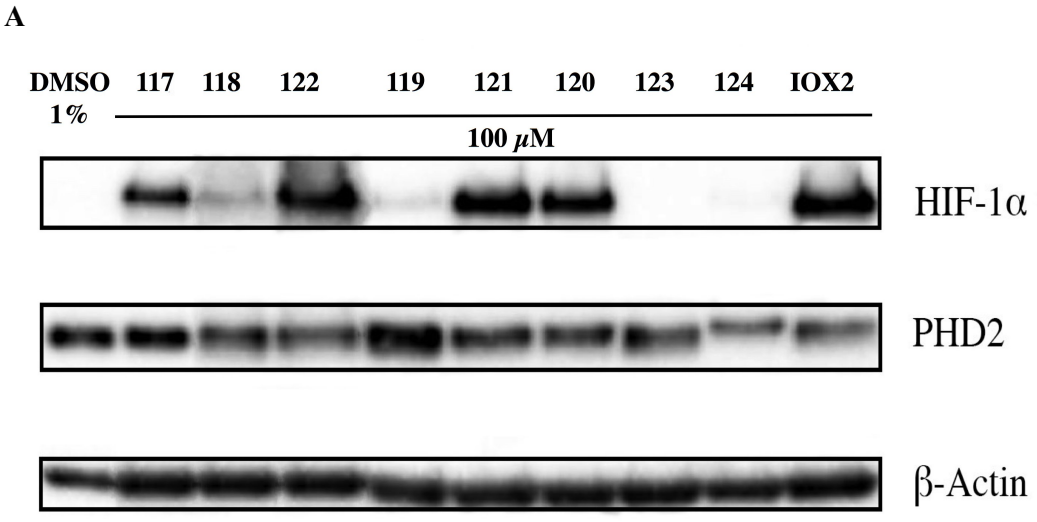

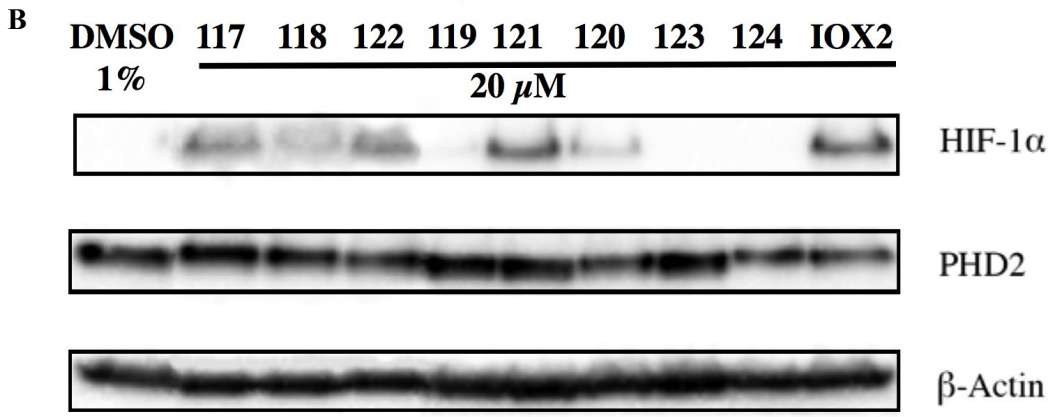

Figure 42: Cellular Inhibition studies of analogues investigating the binding substituent (**117**-**124**) at 100 μM in the HEP-3B cell line. Immunoblot showing HIF-1α stabilization via inhibition of PHD2. Experiment performed by Dr T.Yeh

Figure 43 shows the cellular efficacy of **139**-**144** investigating the additional interactions for the 4-hydroxy pyridine pharmacophore. The addition of a COOH moiety to **94** to give **142**, resulted in significant increase in HIF-1α stabilisation in contrast to **94**. However, the addition of a COOH moiety to **117** or **122** did not result in an improvement in HIF-1α stabilisation. At 20 μM **143** and **144**, resulted in weaker HIF-1α stabilisation in contrast to **117** and **122**, suggesting an increased difficulty in getting through the cell membrane as observed with **123** and **124**. The ethyl ester derivative (**139**) showed no HIF-1α stabilisation at either concentration. This may be due to incubation time (4 hours) and HIF-1α stabilisation may occur if the experiment was conducted for a longer period. The addition of a nitrile substituent (**140**) resulted in no HIF-1α stabilisation at either concentration indicating the nitrile substituent apparently had a significant impact in cell permeability.

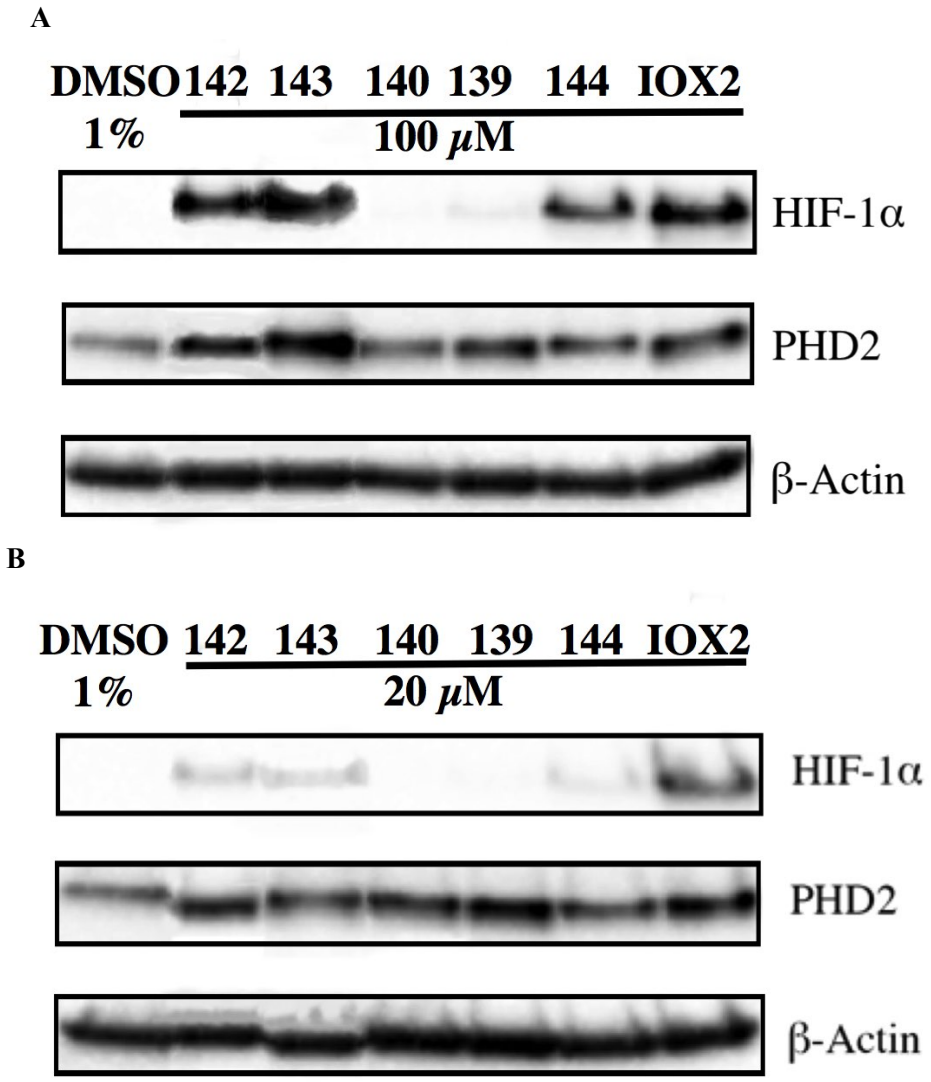

Figure 43: Cellular inhibition studies of the analogues investigating additional interactions at 100 **A**) and 20 μM **B**) in the HEP-3B cell line. Immunoblot showing HIF-1α stabilization via inhibition of PHD2. Experiment performed by Dr T.Yeh

Comparing the 4-hydroxy pyridine analogue's cellular efficacy with the clinical candidates (**3**-**8**)(**Figure 44**) indicates that certain analogues (**117**, **120** and **121**) can stabilise HIF-1α at similar concentrations to the clinical candidates (**3**-**8**). However, most analogues caused weaker HIF-1α compared to the clinical candidates (**3**-**8**). Analysis of cLogP values of both the 4-hydroxy pyridine analogues (**94**-**144**) and the clinical candidates (**3**-**8**) that cLogP values alone may not be the reason for the difference in cell permeability. As described in

Chapter 2.6, **32** showed strong HIF-1α stabilisation at 20 μM. It was suggested that difference in cellular efficacy between **32** and **95** may either be due to cLogP or that the free hydroxyl substituent may need to tautomerise to pass through the cell membrane. The hydroxyl group of the 4-hydroxy pyridine core may not tautomerise into the carbonyl form as easily as the pyrimidin-4-ol core. Modification to the amide or pyrazole substituent may effect the tautomerisation and therefore possibly improve cell-penetration. To overcome the possible absorption issue, pro-drugging the hydroxyl form may lead to strong HIF-1α stabilisation.

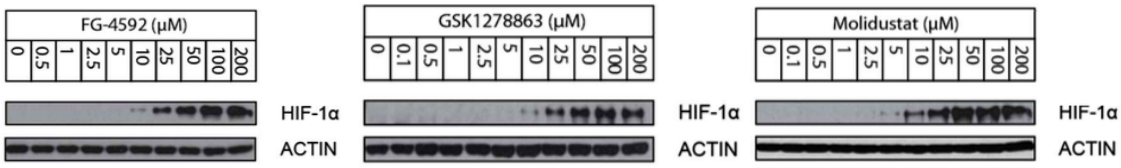

Figure 44: Cellular Inhibition studies of the clinical candidates FG-4592, GSK1278863, Molidustat in HEP-3B cell line. Immunoblot showing HIF-1α stabilization via inhibition of PHD2.Adapted from Yeh *et al*.[15]

4.6 The Reverse 4-hydroxypyridine Pharmacophore

Structure activity relationship (SAR) of the 4-hydroxy-2-(1H-pyrazol-1-yl)pyrimidine-5-carboxamide starting point (**32**) was described in **Chapters 2-4.4**. The SAR revealed a criteria on what is required for strong PHD2 inhibition whilst maintaining a high degree of 2OG oxygenase selectivity.

137 and **142** represent molecules containing the required binding substituents for strong inhibition of PHD2, namely the *C*-5 amide group, hydroxyl group, Fe^{2+} chelation moiety and an additional hydrogen bond interaction within the active site (**Figure 43**). It was

envisaged that switching the position of *C*-5 amide group and additional substituent on the *C*-4 pyrazole group of **137** and **142** could develop a novel PHD pharmacophore (**153** and **154**) (**Figure 45**). Such molecules would technically have all the above listed requirements for potent PHD2 inhibition, but may interact differently with PHD2 due to the differences in the angle of the interactions formed between the molecules and PHD2. **153** and **154** were designed, in order to investigate this proposal.

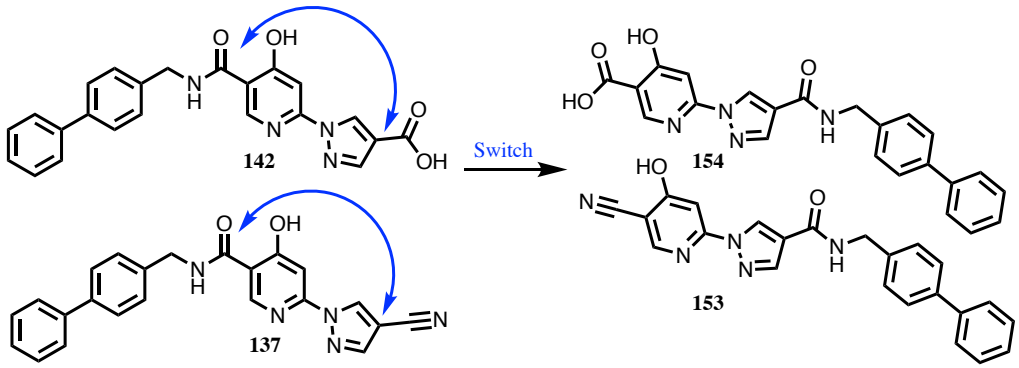

Figure 45: Logical approach for the reverse 4-hydroxy pyridine pharmacophore.

153 and **154** were synthesised in a similar approach to the 4-hydroxy pyridine compounds (**94 -144**, **Scheme 19**). As the 4-hydroxy pyridine moiety was being varied. It was decided that the best approach was to leave the Pd-catalysed amination as late as possible in the route, in order to reduce the required number of steps (**Scheme 19**). The first step, an amide coupling on the requisite carboxylic acid, gave **150** and resulted in a poor yield (19%), likely due to issues with the work-up. **150** was then coupled with the relevant protected 4-hydroxy-2-chloro-pyridine group via a Buchwald coupling to give precursors **151** and **152** (yields = 12 and 28%, respectively). **151** and **152** were demethylated using LiCl-DMAc to give **153** and **154**.

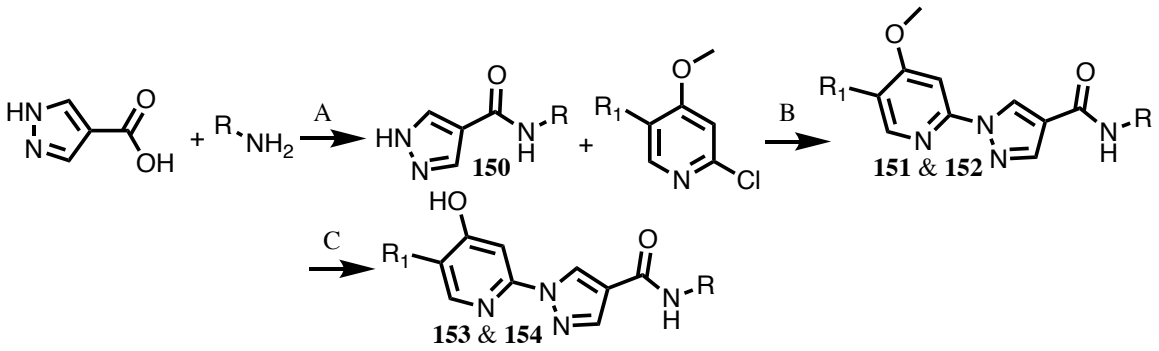

Scheme 19: The synthetic route of initial reverse 4-hydroxy pyridine pharmacophore. Reagents and Condiditons: **A**) T3P, R-NH_2, DIPEA, DMAc,RT,.16hrs (19%). **B**) Pd^{t}BuXPhos, Cs_2CO_3, ^{t}BuOH, sandbath 80°C, 16 hr (12 - 28%). **C**) LiCl, DMAc, MW, 100°C, 2 hrs (35-43%).

Both compounds (**153** and **154)** achieved PHD2 inhibition (**Table 20**), although a drop in inhibition was observed in comparison with the original structurally similar compounds (**153** IC_{50} 388 nM to **137** 87 nM) and (**154** IC_{50} 2.88 µM and **142** 0.089 µM); again displaying the sensitivity within the active site for PHD2 inhibition.

Table 20 : Initial analogues for the reverse 4-hydroxy pyridine pharmacophore, using the RapidFire™ assay. Experiment performed by Dr A Tumber. Experimental measurement n =1.

Cpd	Structural Formula	RapidFire™ PHD2 IC_{50} µM
153	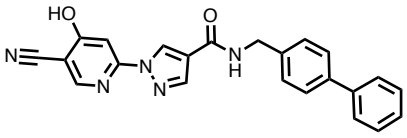	**0.388**
154	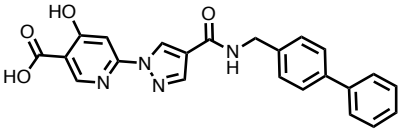	**2.23**

Attention turned to synthesising pyridine analogues **155-164**, aimed to investigate interactions within the active site that were important for PHD2 inhibition for the reverse 4-hydroxypyridine pharmacophore (**Figure 46**). The differences in PHD2 inhibition between **142** and **154** suggested that the reverse pharmacophore may interact differently with the

active site of PHD2. Therefore, a selection of compounds with substituents such as the hydroxyl and COOH group at different positions were targeted (**Figure 46**).

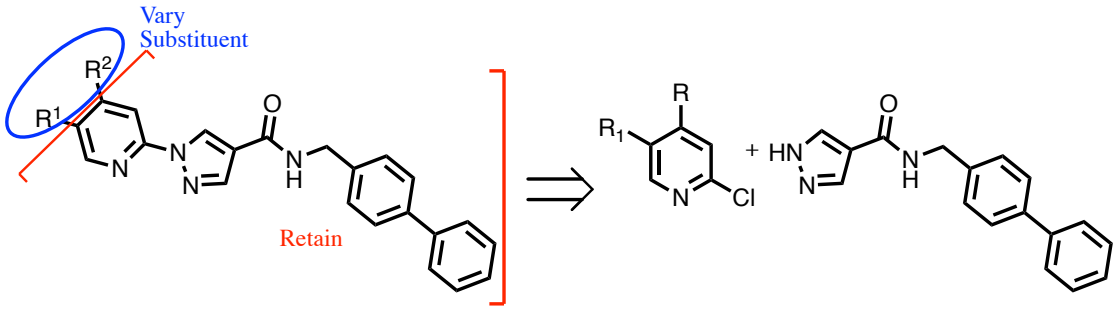

Figure 46: The strategy for investigating active site PHD2 interactions for the reverse pharmacophore.

The synthetic route to obtain **151-164** was identical to that used for **153** and **154** (i.e. **Scheme 19**). However, variation of 2-chloro pyridine groups in the Pd-catalysed amination resulted in similar low yields or no reaction (**Scheme 19**). It was hypothesised that the poor yields were linked to the weak nucleophilicity of the *N*-1 atom of the pyrazole group (**150**). As all conditions of Pd-catalysed amination apart from the catalyst ligand had been optimised (**Chapter 4.1**) for the 4-hydroxy pyridine and pyrazole coupling, optimisation of the ligand was therefore attempted.

It was envisaged that the mechanistic issue for this Pd-catalysed amination was either the pyrazole binding to the metal or the reductive elimination step of the catalytic reaction cycle.[5] Promoting reductive elimination was attempted; Buchwald *et al.* reported that the ligands used for Pd amination are sensitive to the type of amine that is used in the reaction.[5] For aromatic amines, ^{t}BuXPhos is the preferred ligand of Pd-catalysed amination.[18] To accelerate reductive elimination, electron rich substituents can be added to the primary phenyl ring of the catalyst.[5] Various ligands (RockPhos, Me$_4$^{t}BuXPhos and ^{t}BuBrettPhos)

gave improved yields (22% increase in yields), RockPhos was chosen as the ligand for the Buchwald coupling for the reverse 4-hydroxyl pyridine series.

The screening results of analogues used in order to investigate the active interactions for the reverse 4-hydroxy pyridine pharmacophore (**151**-**164**) (**Table 21**) demonstrate how sensitive the active site of PHD2 is towards modifications of PHD2-inhibitor active site interactions. The methoxy precursor of **153** (**151**) resulted in no inhibition of PHD2. Removal of the hydroxyl substituent of **153** (**155**) also resulted in no inhibition of PHD2, indicating an essential requirement of the hydroxyl group for PHD2 inhibition for **153**. Removal of the nitrile group of **153** (**157**) (**157** IC_{50} 1.0 μM) resulted in a loss of 3-fold of inhibition in contrast to **153** (IC_{50} 388 nM). However, **157** was 2 fold more potent in comparison to **154** (IC_{50} 2.23 μM). This suggests strained or competing interactions between the hydroxyl and COOH groups of **154** exist when interacting with the active site of PHD2. The removal of the hydroxyl group of **154** (**159**) (IC_{50} 4.7 μM) resulted in a 2-fold loss of inhibition in contrast to **154** (IC_{50} 2.23 μM). In comparison to the *C*-4 COOH pyrazole analogues **148** and **149** (IC_{50} 0.704 and 1.07 μM, respectively), **159** is 4-fold weaker in potency. The differences in IC_{50} values of **148**, **149** and **159** indicate differences in PHD2 interaction between the pharmacophores. The COOH analogue at the *C*-4 position of the pyridine ring (**161**) (IC_{50} 14.43 μM) further lost potency, revealing the preference of the *C*-5 position of the pyridine ring. Comparison of **155** and **159** reveal that the COOH group is the better substituent than the nitrile group at the *C*-5 position of the pyridine ring for PHD2 inhibition (IC_{50} >25 and 4.70 μM, respectively). The presence of the hydroxyl and the nitrile groups of **153** apparently produces a synergistic effect with an improved IC_{50}

of PHD2 in comparison to **157** (IC_{50} 0.388 and 1.00 μM, respectively). In contrast, the hydroxyl and COOH groups of **154** seem to change other interactions within the active site, potentially resulting in multiple binding modes explaining the loss in potency in

Table 21: Analogues investigating the active site PHD2 interactions for the reverse pyridine pharmacophore. Experiment performed by Dr A Tumber. Experimental measurement n =1.

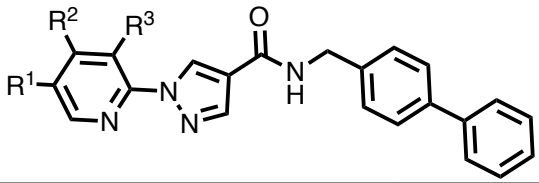

Cpd	R^1	R^2	R^3	RapidFire™ PHD2 IC_{50} μM
151	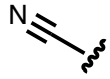		**H**	**>25**
155	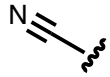	**H**	**H**	**>25**
157	**H**	**OH**	**H**	**1.00**
159	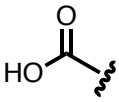	**H**	**H**	**4.70**
161	**H**	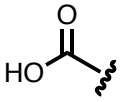	**H**	**14.43**
162	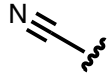	**H**		**>25**
164	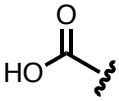	**H**		**11.94**

comparison to **157** (IC_{50} 2.23 and 1.00 μM, respectively). The hydroxyl group was transferred to the 3-position of the pyridine ring (**162** and **164**). The demethylation of the *C*-4 methoxy group failed and due to time constraints, this was not solved. **162** and **164** demonstrated that the importance of the 4-hydroxyl substituent and the active site interaction clash between the COOH and other substituents, as **164** showed a 3-fold loss in potency in comparison to **159** (IC_{50} 11.94 and 4.70 μM, respectively).

Initial investigation of the PHD2 active site interactions, suggest that the reverse pharmacophores may interact differently with the aromatic pocket in comparison to the 4-hydroxy pyridine pharmacophore. To further investigate this, the 3-biphenyl and 3-phenylbenzyl *C*-4 amide groups were chosen as they partially differ in interaction with the aromatic pocket in binding compared to the 4-phenylbenzyl substituent. To reduce the steps required to obtain **169** and **170**, a different synthetic route was chosen and to overcome the Pd-catalysis issue (**Scheme 20**). The 4-hydroxy pyridine group was chosen as it maintains the essential interactions within the active and a better yield was achieved on the demethylation step in comparison to the 4-hydroxy-nicotinonitrile group (yields = 35 and 45%, respectively). **165** was synthesised *via* the optimised Buchwald coupling described for previous analogues (**151-164**), then base-promoted ester hydrolysis yielded **166**. An amide coupling with the relevant amine gave the methyl protected precursor **167** and **168**. Demethylation using the LiCl-DMAc gave targeted compounds **169** and **170**.

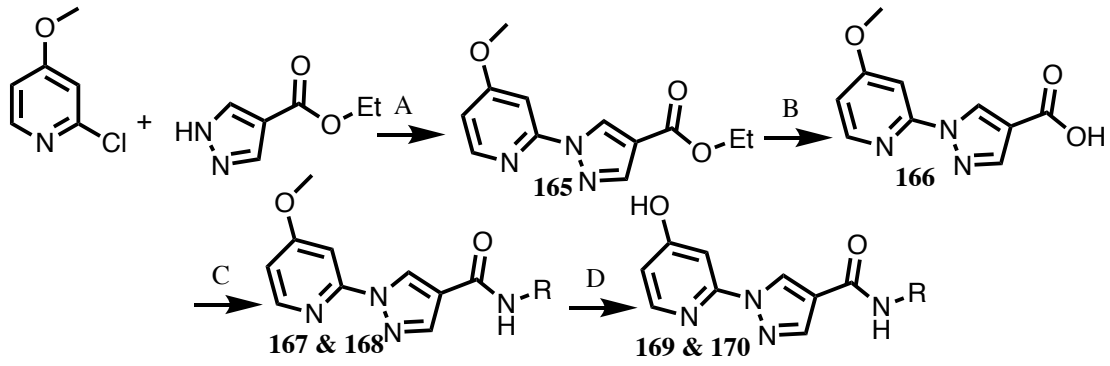

Scheme 20: The synthetic route of the analogues investigating the active site interactions on the reverse 4-hydroxy pyridine pharmacophore. Reagents and Conditions: **A**) RockPhos Pd G3, Cs_2CO_3, ^tBuOH, sandbath 80°C, 16 hr (22 %). **B**) LiOH, THF:H_2O (1:1), RT, 16hrs (44%) **C**) T3P, R-NH_2, DIPEA, DMAc, RT, 16hrs (54 - 61%). **D**) LiCl, DMAc, MW, 100°C, 2 hrs (36 - 57%).

Table 22 summarises, the analogues investigating whether the reverse pharmacophore interacts with the aromatic pocket of PHD2 in a similar fashion to the 4-hydroxy pyridine pharmacophore (**169** and **170**). Removal of the CH_2 group (**169**) lost 2.5 fold in potency in contrast to **157** (IC_{50} 3.62 and 1.00 μM, respectively), a similar difference of potency was observed with the 4-hydroxy pyridine pharmacophore (between **94** and **95**). The 3-phenylbenzyl analogue (**170**) resulted in substantial drop in potency (15 fold loss in potency) in contrast to **157** (IC_{50} 15.42 and 1.00 μM, respectively). In comparison to the 4-hydroxy pyridine pharmacophore, the 3-phenylbenzyl analogue (**118**) improved PHD2 inhibition by 3 fold in contrast to **94** (**Table 22**). The results indicated that the reverse 4-hydroxy pyridine pharmacophore interacts with PHD2 differently to the 4-hydroxy pyridine series.

Table 22: Analogues investigating the binding substituents for the reverse 4-hydroxy pyridine pharmacophore in comparison with related compounds from the 4-hydroxy pyridine series. Experiment performed by Dr A Tumber. Experimental measurement n =1.

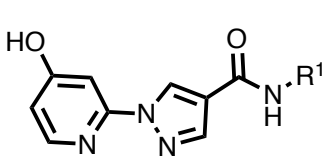

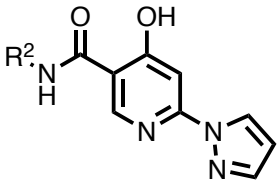

Cpd	R^1	R^2	RapidFire™ PHD2 IC_{50} µM
169	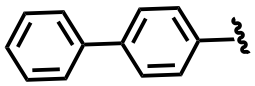	-	**3.62**
170	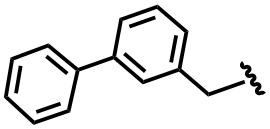	-	**15.42**
157	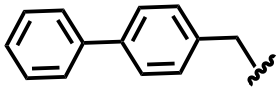	-	**1.00**
95	-	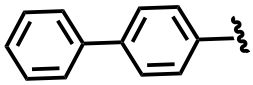	**0.317**
118	-	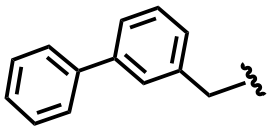	**0.055**
94	-	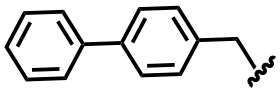	**0.145**

The results disclosed above highlight that for the reverse pharmacophore, the methylene linker and the linearity of the *C*-4 amide group are important for PHD2 inhibition. Combining all acquired SAR whilst improving the cLogP further inhibitor development

was attempted (**Figure 47**). The 4-trifluorobenzyl and the 6-phenylpyridyl substituents showed strong PHD2 inhibition for the 4-hydroxy pyridine series (**117** and **122**) whilst reducing the overall hydrophobicity of the compounds. This was used in combination with the 4-hydroxynicotinonitrile group, as this substituent achieved the strongest potency against PHD2 for the reverse pyridine series (**153**, IC_{50} 388 nM) (**Figure 47**).

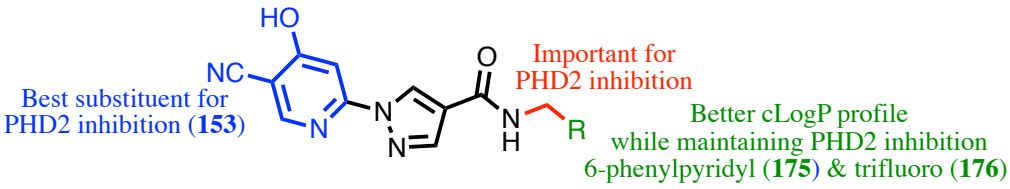

Figure 47: The strategy for combining the SAR work of the reverse 4-hydroxy pyridine series and attempts to improve cLogP using optimised amide groups.

175 and **176** were synthesised in a similar fashion to **169** and **170** (**Scheme 20**). **175** and **176** demonstrated the differences between the two pharmacophores and the importance of the substituent on the phenyl ring of the *C*-4 amide group. **175** showed a similar drop (2 fold loss) in potency in comparison to **153** (IC_{50} 388 and 834 nM, respectively), as observed for the 4-hydroxy pyridine pharmacophore (**122** to **94**). Replacing the terminal

Table 23: Analogues combining the SAR of each motif in combination with attempts to reduce cLogP of overall molecule. Experiment performed by Dr A Tumber. Experimental measurement n =1.

Cpd	Structural Formula	RapidFire™ PHD2 IC_{50} µM
175	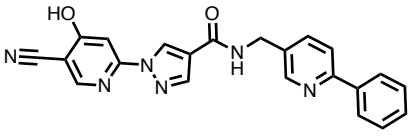	**0.834**
176	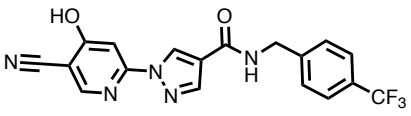	**11.56**

phenyl substituent with a CF_3 moiety, **176** (IC_{50} 11.56 μM) resulted in a significant loss in PHD2 inhibition. This indicates the differences in binding between the two pharmacophores.

4.7 Cellular Characterisation of Reverse 4-hydroxy Pyridine Pharmacophore

The reverse pyridine analogues (**153**, **154**, **157**, **175** and **176**) achieved strong PHD2 inhibition. To confirm the on-target efficacy, the reverse pyridine analogues were tested in the Hep3B cell line to measure HIF1-α stabilisation. **Figure 45** shows **153**, **154**, **157**, **175** and **176** tested at 100 μM and 20 μM in the Hep3B cell line. None of the compounds tested showed HIF-1α stabilisation at either concentration.

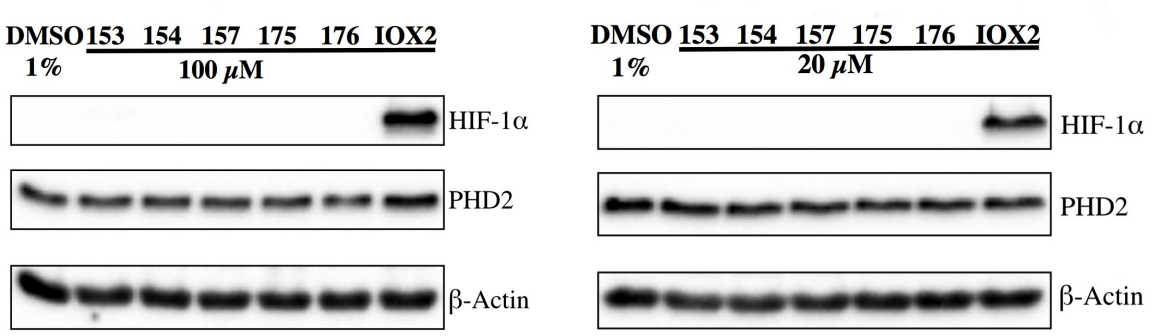

Figure 48: Cellular Inhibition studies of the reverse 4-hydroxy pyridine series at 100 μM and 20 μM in the HEP-3B cell line. Immunoblot showing HIF-1α stabilisation via inhibition of PHD2. Experiment performed by Dr T.Yeh

The lack of cellular efficacy in contrast to the strong potency in the in-vitro assay suggests similar issues with cell permeability exist as observed with the 4-hydroxy pyridine analogue **137**.

4.8 Tricyclic Pharmacophore

Structural rigidity of all the novel PHD2 inhibitors disclosed in this work was a variable that has not yet been addressed. It was envisaged that increasing the rigidity between the two Fe^{2+} chelation group may improve PHD2 inhibition (**Figure 49**). As in **Chapter 3.3**, the removal of the 5-membered ring from the initial 1,3,8-triazaspiro[4.5]decane-2,4-dione series (**10**) resulted in complete loss of PHD2 inhibition (**51-59**). The investigation of the bidentate substituent discussed in **Chapter 3.4**, whereby the bidentate substituent was highlighted as essential for strong PHD2 inhibition.

FG-0041 (**177**) (IC_{50} 10.70 µM) was an early PHD2 inhibitor. **177** is a tri-cyclic molecule possessing a bidentate group with the required 4-hydroxyl substituent (**Figure 49**). The concept for the tricyclic pharmacophore was to combine the 4-hydroxy pyridine pharmacophore (**94**) with the rigidity of **177**, whilst at the same time maintaining or improving the hydrophilicity of the molecule. It was proposed that the additional link joining the pyrazole and 4-hydroxy pyridine substituents must include a nitrogen to achieve an acceptable cLogP (**Figure 49**).

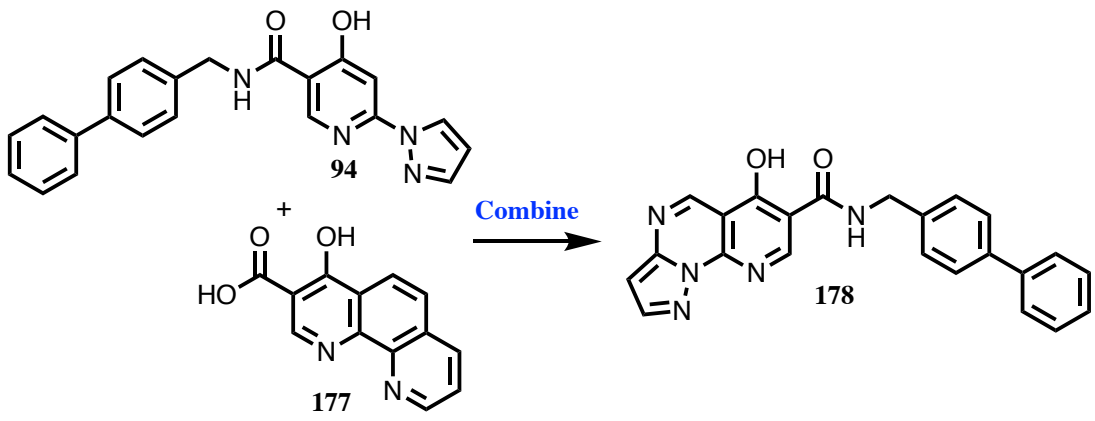

Figure 49 : The logic used for the approach to develop the novel tricyclic pharmacophore.

Retrosynthesis of **179** involved disconnecting the carbonyl bond, to enable an amide coupling using the aforementioned DABCO-$(AlMe_3)_2$ reagent (**Chapter 2.5**) (**Figure 50a**). It was envisaged the ethyl 6-hydroxy-pyrazolo[1,5-*a*]pyrido[3,2-*e*]pyrimidine-7-carboxylate fragment **178** could be synthesised via conjugate addition and an intramolecular cyclisation using diethyl ethyoxymethylmalonate and pyrazolo[1,5-*a*]pyrimidin-7-amine (**Figure 50A**) reported in the patent literature.[19]

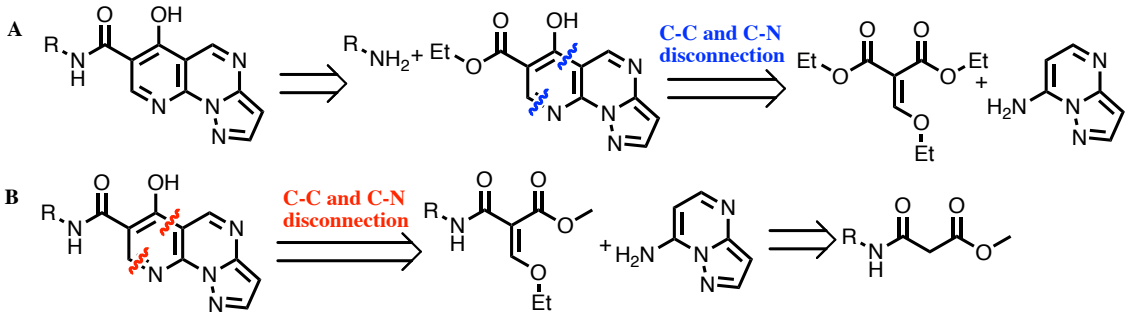

Figure 50 :Strategies for synthesis of the tricyclic compounds

Reacting diethyl ethyoxymethylmalonate and pyrazolo[1,5-*a*]pyrimidin-7-amine via Michael addition and subsequent intramolecular cyclisation gave **178** in good yield (43%). **178** was then reacted with 4-phenylbenzylamine in the presence of DABCO-$(AlMe_3)_2$ to give the targeted compound **179** with a poor yield of 3% (**Scheme 21**).[20]

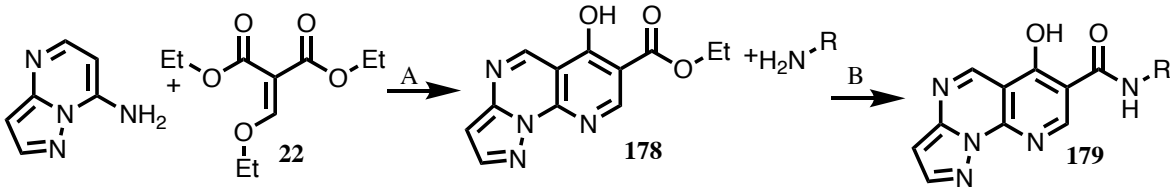

Scheme 21: Initial synthetic route for the tricyclic pharmacophore **A**) i) NaOEt, EtOH, 100°C, 2hrs. ii) Diphenylether, 240°C, 30 mins (43%). **B**) DABCO-$(AlMe_3)_2$, R-NH_2, THF, MW 130 °C (3%).

Table 24 summaries the SAR of the tricyclic pharmacophore. **179** (IC_{50} 0.306 µM) was a potent inhibitor. Comparison of **179** to compound **94** (IC_{50} 306 and 145 nM, respectively)

indicates fusing the two Fe^{2+} chelation moieties resulted in a 2-fold drop in PHD2 inhibition. However, it was envisaged that the reduction in cLogP (**179** = 2.33 and **94** = 3.43) may improve cellular potency.

Synthetic efforts were then focused on confirming whether the tricyclic pharmacophore binding mode is analagous to the 4-hydroxy pyridine pharmacophore (**94**), or differently as observed with the reverse pyridine pharmacophore (**153**). Thus, **181** was targeted as a means to address this hypothesis. However, poor yields of the amide coupling led to attempts to discover an alternative synthetic route. Due to synthetic similarities with synthesis of the 4-hydroxy-2-(1H-pyrazol-1-yl)pyrimidine-5-carboxamide analogues (**11**, **26 - 34**), protection and deprotection of the hydroxy substituent was not attempted (**Chapter 3.5**). Additional retrosynthetic analysis suggested that if one of the ethyl esters of diethyl ethyoxymethylmalonate (**22**) was replaced with the appropriate amide, the intramolecular cyclisation may lead to targeted compound **181** (**Figure 50b**). The 3-methoxy-3-oxopropanoic acid underwent an amide coupling to give **180**, which was reacted with ethyl orthoformate to give the Michael acceptor before the addition of pyrazolo[1,5-*a*]pyrimidin-7-amine to yield the targeted compound **181** (**Scheme 22**).[21]

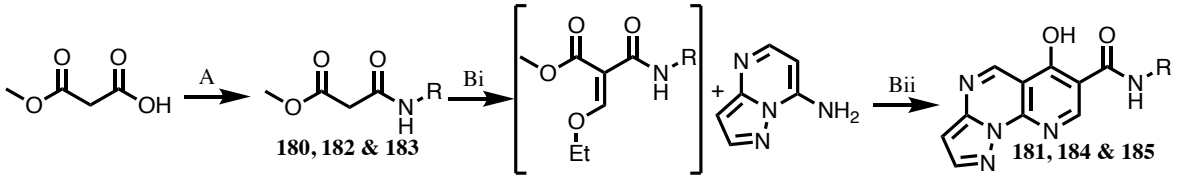

Scheme 22: Alternative synthetic route for the tricyclic pharmacophore: **A**) T3P, R-NH_2, DIPEA, DMAc, RT, 16hrs (22 - 60%). **B**) i) Ethyl orthoformate, MW, 120°C, 3hrs. ii) Diphenylether, 240°C, 30 mins (3 - 4%).

181 was 2 fold more potent than **179** (IC_{50} 181 and 306 nM, respectively), the opposite trend was observed with the 4-hydroxy pyridine series (**Table 24**), highlighting the potential differences in PHD2 interactions with the previously developed pharmacophores.

Although the formation of Michael acceptor is still not synthetically robust, the yield was sufficient for our purposes and the tricyclic pharmacophore was briefly investigated. A series of analogues of **179** were designed (**Figure 51**) whereby the tricyclic ring was varied by means of including a hydroxyl group instead of the pyrazole group and incorporating methyl groups to increase electron density. As observed with the 1,3,8-triazaspiro[4.5]-decane-2,4-dione series might be replicated (**Chapter 2.4** and **Figure 51**), it was envisaged that incorporation of methyl groups may improve the strength of the active site interactions.

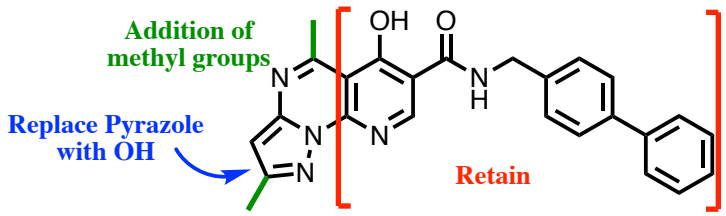

Figure 51 :Strategy for investigation of SAR of the tricyclic pharmacophore.

Unfortunately, synthesis of the tricyclic motif failed for all but one tricyclic core (**184** & **185**), indicating the need to improve the synthetic procedure in the future. Nevertheless, the addition of the two methyl substituents (**184**) to the tricyclic core **179**, (IC_{50} 216 and 306 nM, respectively) improved potency of PHD2. The 4-trifluoromethylbenzyl susbstituent-containing compounds (**117**, **120** and **121**) were previously identified as potent PHD2 inhibitors (**Chapter 4.2**). Therefore, **185** was designed in order improve PHD2 potency whilst improving physiological properties by the inclusion of a 4-trifluoromethylbenzyl susbstituent. **185** was synthesised using the improved synthetic route described above

(**Scheme 21**). **184** achieved near identical level of potency compared to **185** (IC_{50} 216 and 207 nM, respectively). Comparing **184** and **185** with analogues of the 4-hydroxy-pyridine pharmacophore suggests slight differences between the two pharmacophores in relation to their interaction with PHD2.

Table 24 : SAR for the tricyclic analogues for PHD2 inhibition using the RapidFire assay. Experiment performed by Dr A Tumber. Experimental measurement n =1.

Cpd	Structural Formula	RapidFire™ PHD2 IC_{50} µM
177	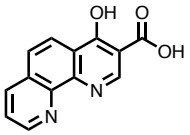	**10.70**
178	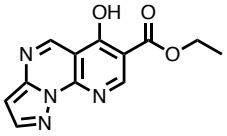	**>25**
179	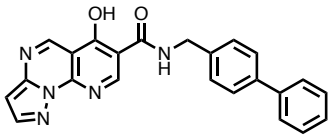	**0.306**
181	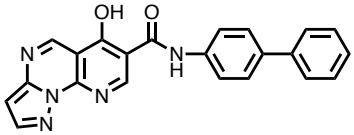	**0.181**
184	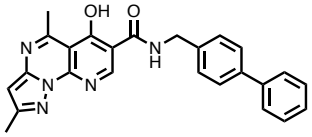	**0.216**
185	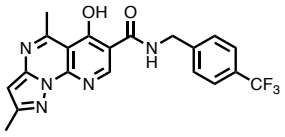	**0.207**

4.9 Cellular Characterisation of Tricyclic Pharmacophore

To confirm the on-target efficacy, the tricyclic analogues were tested in the Hep3B cell line to measure HIF-1α stabilisation. **Figure 52** shows **179**, **181**, **184** & **185** tested at 100 μM in the Hep3B cell line. In general, all compounds showed strong HIF-1α stabilisation with **179** achieving the weakest stabilisation of HIF-1α. However, **179** achieved more HIF-1α stabilisation than **94**, demonstrating the impact of the addition of the nitrogen (of the central ring of the tricyclic substituent and the reduction in cLogP (similar to **122**).

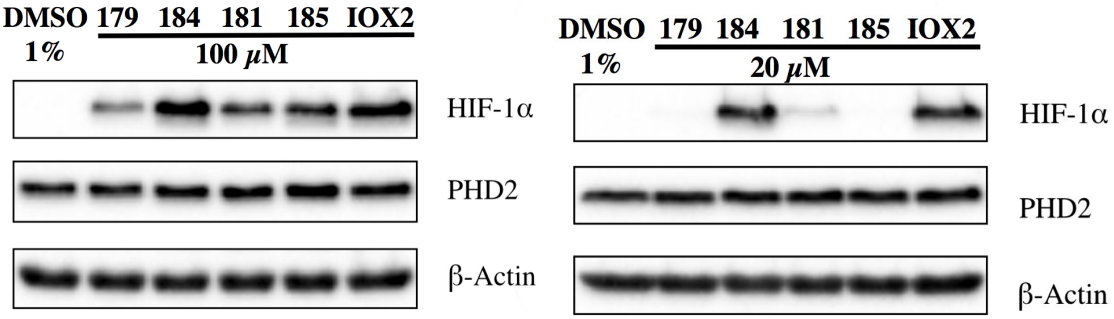

Figure 52: Cellular Inhibition studies of the tricyclic series at 100 and 20μM in the HEP-3B cell line. Immunoblot showing HIF-1α stabilization via inhibition of PHD2. Experiment performed by Dr T.Yeh

The analogues were then tested at 20 μM, only **184** showed strong stabilisation of HIF-1α (**Figure 52**). The differences in cellular efficacy of **179** and **184** likely indicate the importance of the two methyl groups on **178**. Additionally, the differences in cellular efficacy between **179**, **181**, **184** & **185** indicate the role of the 5-position amide substituent for the cell permeability.

4.10 2OG Oxygenases Selectivity

In **Chapter 2**, the work focused on achieving selectivity within the 2OG oxygenase super family. Both starting points (**10** and **32**) achieved strong selectivity over structurally similar 2OG oxygenases. To investigate whether the novel pharmacophores divulged in this chapter maintain a strong selectivity profile, a selection of compounds from all pharmacophores were tested against the 2OG oxygenases FIH, vCPH and OGFOD1. All compounds showed very weak inhibition on FIH and thus maintaining selectivity for the HIF prolyl hydroxylases (**Table 25**). Only **94** and **142** were tested against vCPH due to MALDI instrument issues. Both **94** and **142** showed poor inhibition of vCPH, with **94** achieving an IC_{50} greater than 100 μM. **142** achieved an IC_{50} of 16.5 μM suggesting the additional hydrogen bonding interaction with the active site of PHD2 does reduce selectivity within the 2OG oxygenase super-family. The tricyclic pharmacophore (**Chapter 4.8**) and the 4-hydroxy-pyridine pharmacophore (**94**, **117**, **118**, **142**, **179** and **181**) displayed weak inhibition of OGFOD1 (**117** and **179** achieving only 37 and 20% inhibition at 10 μM, respectively). However, the compounds from the reverse 4-hydroxy-pyridine pharmacophore displayed stronger inhibition of OGFOD1 achieving 50% inhibition at 10 μM. The reverse 4-hydroxy pyridine analogue **176** showed stronger levels of OGFOD1 inhibition in comparison to PHD2. However, in general (not including **176**), all novel pharmacophores achieved a strong selectivity profile over structurally similar 2OG oxygenases.

Table 25:A selection of analogues from the novel pharmacophores screened against FIH (performed by Dr.A Tumber), vCPH (performed by Mr. G Langley) and OGFOD1 (Performed by Dr C Lohans). Experiment performed by Dr A Tumber. Experimental measurement n =1.

		μM			
Cpd	**Structural Formula**	**PHD2 RapidFire™ IC_{50}**	**FIH RapidFire™ IC_{50}**	**vCPH MALDI IC_{50}**	**OGFOD1 MALDI % Inhibition at 10 μM**
94	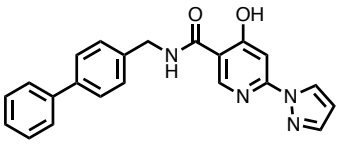	**0.145**	**>100**	**>100**	**ND**
117	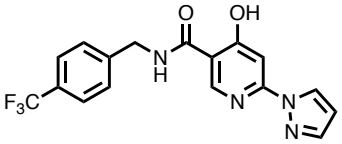	**0.063**	**33.8**	**ND**	**37%**
118	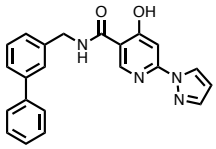	**0.055**	**32.57**	**ND**	**33%**
142	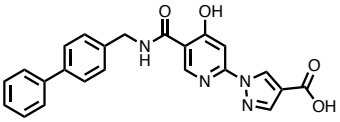	**0.087**	**26.3**	**16.5**	**ND**
153	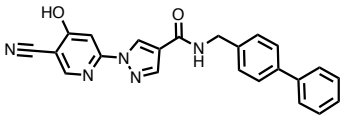	**0.388**	**26.62**	**ND**	**46%**
176	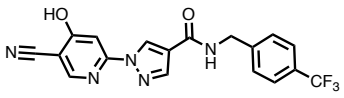	**11.56**	**ND**	**ND**	**68%**
179	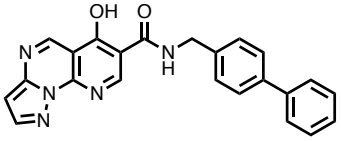	**0.306**	**27.2**	**ND**	**20%**
181	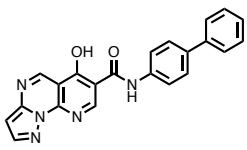	**0.181**	**>100**	**ND**	**25%**

4.11 PHD Isoform and Substrate Selectivity

The novel PHD inhibitors described in this chapter, likely bind to the PHD enzymes through interacting with the aromatic pocket at the entrance of the active site. In **Chapter 4.2**, it was discovered that PHD2 inhibition can be achieved by varying parameters such as hydrophobicity, aromaticity, length of various substituents and additional substituents on the methylene linker between the active site and aromatic pocket. In **Chapter 1.4**, the differences between PHD isoforms and substrate binding were discussed. Differences between PHD isoforms are present at the entrance of the active site.[12] It was envisaged that the different pharmacophores and different 5-position amide substituents may either demonstrate PHD isoform or HIF substrate selectivity. A selection of compounds were chosen from the novel pharmacophores identified in this work were screened against $PHD2_{181-426}$ with HIF-1α NODD, PHD3 with HIF-1-3α CODD (**Table 26**).

Table 26: A selection of compounds from the novel pharmacophores screened against PHD2 with HIF-1α CODD and NODD, PHD3 with HIF1-3α CODD (performed by Ms Kerstin Lippl and Dr A.Tumber). Experiment performed by Dr A Tumber. Experimental measurement n =1.

		RapidFire™ µM				
Cpd	**Structural Formula**	**PHD2 & HIF-1 CODD**	**PHD2 & HIF-1 NODD**	**PHD3 & HIF-1 CODD**	**PHD3 & HIF-2 CODD**	**PHD3 & HIF-3 CODD**
117	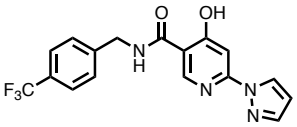	**0.063**	**0.117**	**0.138**	**0.069**	**0.053**

		RapidFire™ µM				
Cpd	**Structural Formula**	**PHD2 & HIF-1 CODD**	**PHD2 & HIF-1 NODD**	**PHD3 & HIF-1 CODD**	**PHD3 & HIF-2 CODD**	**PHD3 & HIF-3 CODD**
118	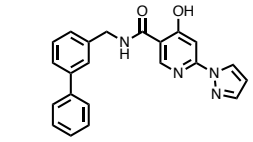	**0.055**	**0.097**	**0.192**	**0.088**	**0.068**
121	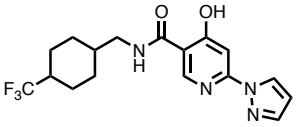	**0.119**	**ND**	**0.065**	**0.070**	**0.056**
123	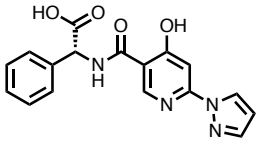	**0.182**	**ND**	**0.295**	**0.338**	**0.242**
124	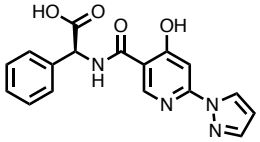	**0.589**	**ND**	**0.108**	**0.133**	**0.102**
142	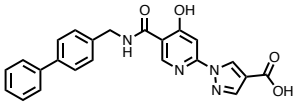	**0.087**	**0.040**	**0.150**	**ND**	**ND**
154	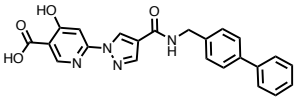	**2.23**	**ND**	**0.057**	**0.078**	**0.049**
153	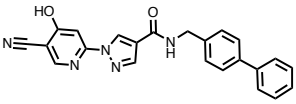	**0.388**	**0.090**	**0.314**	**ND**	**ND**
179	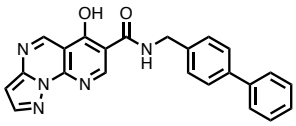	**0.306**	**0.195**	**0.189**	**0.280**	**0.189**
181	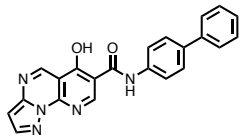	**0.181**	**ND**	**0.512**	**0.618**	**0.405**

Compounds possessing the methylene linker (**117**, **118** and **121)** resulted in minimal differences in PHD isoform and substrate selectivity and displayed strong potency in all screens. All compounds achieved similar levels of competitive inhibition of all HIF-α CODD substrates on PHD3. The analogues with a COOH group on the CH linker (**123** and **124**) achieved potent inhibition of PHD3. The *S*-Enantiomer **124** achieved a 5-fold stronger potency for PHD3 over PHD2, whilst the *R*-Enantiomer **123** achieved a similar level of inhibition to PHD3. The reverse 4-hydroxy-pyridine pharmacophore analogues **153** and **154**, demonstrated isoform and substrate selectivity. **154** showed clear selectivity for PHD3 over PHD2, achieving 40-fold stronger potency for PHD3 over PHD2; whereas **153** demonstrated similar levels of inhibition for the PHD2 and PHD3. **153** showed a 4-fold selectivity for the NODD over the CODD substrate with PHD2. **153** and **154** possess a 5-nitrile and 5-carboxyl moiety respectively; which may explain the difference in data obtained for the two compounds. The differences between **153** and **154** demonstrate how relatively minor changes to the pharmacophore can impact PHD isoform selectivity. In a cellular environment, this may have a knock-on effect to the overall therapeutic effect of PHD inhibitors. The tricyclic analogue (**179**) demonstrated similar levels of inhibition against the screened isoforms and substrates. (**181**) achieved apparent 3-fold selectivity for PHD2 over PHD3.

4.12 Summary & Future Work

In this chapter, the novel 4-hydroxy-pyridine PHD pharmacophore was designed from SAR work discussed in **chapters 2 and 3**. A synthetic route was optimised in order for in-depth SAR investigation (**Chapter 4.1**). **Figure 53** shows a summary of the SAR explored on the 4-hydroxy-pyridine pharmacophore. It was discovered that strong PHD inhibition can be achieved by varying parameters including hydrophobicity, aromaticity, length of amide substituents and additional substituents on the methylene linker between the active site and aromatic pocket (**Chapter 4.2**). **123** and **124** have highlighted that alongside targeting active site interactions, interacting with the flexible loop between the β2/β3 strands may be possible. Replacing the 4-hydroxy-pyridine core with a 3-hydroxy-pyridine core resulted in 20-fold loss in potency in comparison to 4-hydroxy-pyridine core, demonstrating the importance of the hydrogen bonding interaction with Tyr-310 (**Chapter 4.3**). However, additional interactions within the active site by adding a substituent to the 4-position of the pyrazole group demonstrated that any important interaction within the 4-hydroxy-pyridine pharmacophore can be replaced and strong PHD inhibition can be maintained (**Chapter 4.4**).

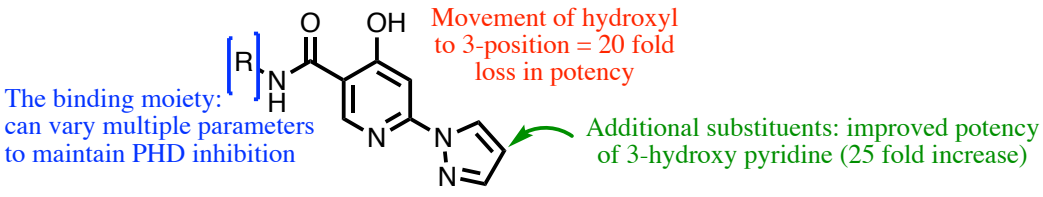

Figure 53: Summary of the SAR for the 4-hydroxy pyridine pharmacophore.

All novel PHD2 inhibitors of the 4-hydroxy pyridine series were tested in a cellular environment. **94** and **95**, demonstrated poor HIF-1α stabilisation at 100 and 20 μM. This was surprising due to the structural similarities to **32**. It was proposed that **94** and **95** poor HIF-1α stabilisation was due to poor cell permeability (possibly because of their high cLogP or tautomerisation of the free hydroxyl group). Analogues with varied 5-position amide substituents series achieved strong HIF-1α stabilisation at 100 μM indicating the biphenyl substituent and the high cLogP was partially responsible for the poor cellular efficacy of **94** and **95** (**Figure 41**). **117**, **120** and **121** showed moderate HIF-1α stabilisation at 20 μM suggesting acceptable cellular efficacy could be achieved at lower concentrations. Although, the additional active site interactions (**142** in contrast **94**) did improve cellular efficacy (**142** in contrast **94**), cellular efficacy was not improved in relation to **117**, **120** and **121**.

Having confirmed molecular requirements for successful PHD inhibition, it was hoped that the identified compounds could be further tailored to identify novel even more efficacious pharmacophores (**Figure 54**). The reverse 4-hydroxy-pyridine pharmacophore was designed on the assumption that substituents required for PHD inhibition could be reorganised (**Chapter 4.6**). **153** achieved strong PHD inhibition but the reverse pharmacophore demonstrated the sensitivity of interacting with the PHD2 active site. Unfortunately no analogues of this series achieved HIF-1α stabilisation in a cellular setting. It was envisaged that the poor cellular efficacy was attributed to the free hydroxyl and nitrile substituents.

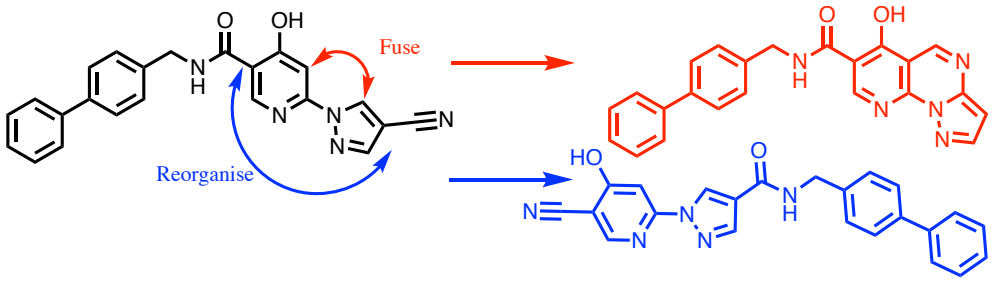

Figure 54: Summary of the logical approach applied in designing the novel pharmacophores.

Tricyclic pharmacophore (**Chapter 4.8**) provided additional rigidity in comparison to the 4-hydroxy pyridine pharmacophore, identified as a recurring problem during this PHD2 inhibitor discovery project. It was envisaged that improving the rigidity between the metal chelation sites may lead to improved PHD2 inhibition. **179** - **185** achieved strong PHD2 inhibition and showed strong HIF-1α stabilisation at 100 μM. **184** achieved strong HIF-1α stabilisation at 20 μM, indicating the additional methyl groups may improve cell-penetration. This important modification highlights an addition that may help the 4-hydroxy-pyridine and reverse 4-hydroxy-pyridine pharmacophores.

Importantly, all novel PHD pharmacophores described, achieved strong selectivity over structurally similar 2OG oxygenases (**Table 25**), a feat that no clinical candidate achieved (**Table 1**).[15] Most analogues screened against other PHD isoforms and HIF-α achieved minimum selectivity. However, **154** achieved 40-fold selectivity for PHD3 over PHD2 demonstrating that significant PHD isoform selectivity is possible (**Table 26**).

A number of novel PHD inhibitors synthesised disclosed in this chapter, resulted in a 20-fold increase in PHD2 inhibition on isolated enzyme, in contrast to the clinical candidates (**3**-**5**) and maintained a strong selectivity over structurally similar 2OG oxygenases. A number of novel inhibitors matched the cellular efficacy of the clinical candidates (**3**-**8**)

(**Figure 42**). Indeed, for one person to outperform the pharmaceutical companies (usually have large teams of experienced scientists and vast amounts project funds) is an achievement.

Future work will be aimed at improving cellular efficacy and isoform selectivity. To improve cellular efficacy, it has been envisaged that pro-drugging the *C*-4 hydroxyl group may lead to better cellular efficacy. The addition of a methyl group to the 3-position of the pyrazole substituent observed with **184** may also lead to greater cellular efficacy. **174** produced a 40-fold selectivity for PHD3 and indicates PHD isoform selectivity is possible.

4.13 Compound Characterisation

General Procedure G: *C*-4 Methoxy Demethylation.

The methoxy protected compound (1 equiv) was dissolved in DMAc (X ml) before the addition of the $LiCl.H_2O$ (10 equivs). The resultant mixture was heated under microwave radiation at 100°C for 2 hrs. The resultant mixture was diluted with water (15 ml) and extracted with EtOAc (3 x 20 ml). The organic phases were combined and washed with water, brine and dried with anhydrous Na_2SO_4. The volatiles were then evaporated in *vacuo* and purified by flash column chromatography using (100 % - 95% CH_2CL_2, 0% - 20% MeOH) over 15 column volumes to give the desired compound.

N-([1,1'-biphenyl]-4-ylmethyl)-6-chloro-4-methoxynicotinamide 86

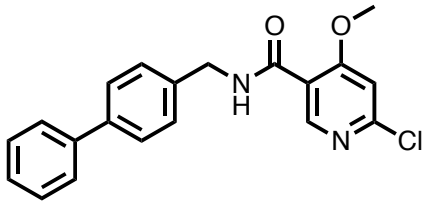

Following general procedure C: 6-chloro-4-methoxy-nicotinic acid **85** (300 mg, 1.60 mmol), 4-phenylbenzyl amine (439 mg, 2.4 mmol), T3P (1.27 g, 4 mmol) and DIPEA (595 mg, 4.8 mmol) gave **86** (432 mg, 1.22 mmol, 76%) as a white solid.

m.p. 160-163°C. **^{1}H NMR** (400 MHz, DMSO-d_6) δ 8.82 (t, J = 6.0 Hz, 1H, NH), 8.51 (s, 1H, Pyr), 7.68 – 7.60 (m, 4H, Ar), 7.57 – 7.27 (m, 6H, Ar), 4.53 (d, J = 6.0 Hz, 2H, CH_2),

3.99 (s, 3H, CH_3). **^{13}C NMR** (101 MHz, DMSO-d_6) δ 164.51, 162.91, 153.34, 150.43, 139.95, 138.47, 128.90, 127.74, 127.31, 126.61, 126.56, 119.77, 107.89, 56.92, 42.32. **FT-IR** ν_{max} (film) 3360, 1636, 1574 cm^{-1}. **HRMS (**ESI-TOF) calcd for $C_{20}H_{18}O_2N_2{}^{35}Cl$ [M+H]$^+$: 353.1051, found : 353.1048.

([1,1'-biphenyl]-4-yl)-6-chloro-4-methoxynicotinamide 87

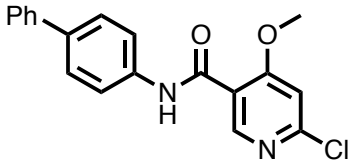

Following general procedure C: 6-chloro-4-methoxy-nicotinic acid (500 mg, 2.67 mmol), 4-aminobiphenyl (540 mg, 3.2 mmol), T3P (2.12 g, 6.68 mmol) and DIPEA (846 ul, 6.68 mmol) gave **87** (311 mg, 0.92 mmol, 34%) as a orange oil.

^{1}H NMR (400 MHz, DMSO-d_6) δ 10.36 (s, 1H, NH), 8.46 (s, 1H, Pyr), 7.87 – 7.77 (m, 2H, Ar), 7.71 – 7.62 (m, 4H, Ar), 7.52 – 7.30 (m, 4H, Ar), 3.99 (s, 3H, CH_3). **^{13}C NMR** (101 MHz, DMSO-d_6) δ 164.29, 161.98, 153.16, 149.46, 139.59, 138.17, 135.55, 128.94, 127.16, 126.98, 126.32, 121.74, 120.05, 107.98, 56.94. **FT-IR** ν_{max} (film) 3132, 1670, 1585 cm^{-1}. **HRMS (**ESI-TOF) calcd for $C_{19}H_{16}O_2N_2{}^{35}Cl$ [M+H]$^+$: 339.0894, found : 339.0893.

6-chloro-4-methoxy-N-(3-(trifluoromethyl)benzyl)nicotinamide 88

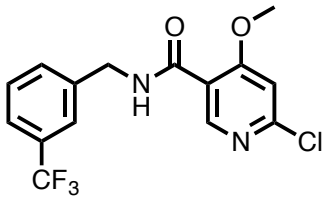

Following general procedure C: 6-chloro-4-methoxy-nicotinic acid (500mg, 2.67 mmol), 3-trifluoromethylbenzyl amine (566 mg, 3.2 mmol), T3P (2.12 g, 6.68 mmol) and DIPEA (846 ul, 6.68 mmol) gave **88** (518 mg, 1.505 mmol, 56 %) as a white solid.

m.p. 101-103°C. **^{1}H NMR** (400 MHz, DMSO-d6) δ 8.91 (t, J = 6.0 Hz, 1H, NH), 8.48 (s, 1H, Pyr), 7.75 – 7.53 (m, 4H, Ar), 7.35 (s, 1H, Pyr), 4.57 (d, J = 6.0 Hz, 2H, CH_2), 3.98 (s, 3H, CH_3). **^{13}C NMR** (101 MHz, DMSO-d_6) δ 164.47, 163.16, 153.39, 150.31, 140.83, 131.27, 129.39, 129.18, 128.87, 125.66, 123.51, 119.82, 107.94, 56.88, 42.16 **FT-IR** ν_{max} (film) 3390, 1641, 1555 cm^{-1}. **HRMS (**ESI-TOF) calcd for $C_{15}H_{13}O_2N_2{}^{35}ClF_3$ $[M+H]^+$: 345.0612, found : 345.0613.

6-chloro-N-(cyclohexylmethyl)-4-methoxynicotinamide 89

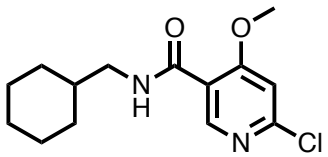

Following general procedure C: 6-chloro-4-methoxy-nicotinic acid (500mg, 2.67 mmol), cyclohexane-methylamine (361 mg, 3.2 mmol), T3P (2.12 g, 6.68 mmol) and DIPEA (846 ul, 6.68 mmol) gave **89** (438 mg, 1.55 mmol, 58%) as a white solid.

m.p. 107-108°C. **^{1}H NMR** (400 MHz, DMSO-d_6) δ 8.40 (s, 1H, Pyr), 8.17 (t, J = 6.0 Hz, 1H, NH), 7.30 (s, 1H, Pyr), 3.95 (s, 3H, CH_3), 3.12 – 3.06 (m, 2H, CH_2), 1.87 – 0.75 (m, 11H, Cyclohexane ring). **^{13}C NMR** (101 MHz, DMSO-d_6) δ 164.34, 162.74, 152.98, 150.08, 120.41, 107.80, 56.85, 45.26, 37.41, 30.40, 26.07, 25.44. **FT-IR** ν_{max} (film) 3412, 1637, 1592 cm^{-1}. **HRMS (**ESI-TOF) calcd for $C_{14}H_{20}O_2N_2{}^{35}Cl$ $[M+H]^+$: 283.1207, found : 283.1208.

([1,1'-biphenyl]-4-ylmethyl)-4-methoxy-6-(1H-pyrazol-1-yl)nicotinamide 90

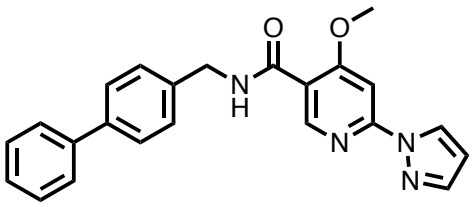

Following general procedure D: **86** (50 mg, 0.142 mmol), Pd^{t}BuXPhos G3 (11.2 mg, 0.0142 mmol), Cs_2CO_3 (138 mg, 0.426 mmol), pyrazole (24mg, 0.355 mmol) gave **90** (30 mg, 0.078 mmol, 55%) as colourless oil.

^{1}H NMR (400 MHz, DMSO-d_6) δ 8.79 (t, J = 6.0 Hz, 1H, NH), 8.68 – 8.65 (m, 2H, Ar), 7.88 (dd, J = 1.5, 1.0 Hz, 1H, Pyzl), 7.67 – 7.46 (m, 9H, Ar), 7.39 – 7.33 (m, 1H, Ar), 6.61 (dd, J = 2.5, 1.5 Hz, 1H, Pyzl), 4.55 (d, J = 6.0 Hz, 2H, CH_2), 4.08 (s, 3H, CH_3). **^{13}C NMR** (126 MHz, DMSO-d_6) δ 165.22, 163.20, 153.77, 150.48, 142.84, 140.03, 138.75, 128.98, 127.83, 127.38, 126.68, 126.63, 117.85, 108.85, 104.27, 94.93, 56.60, 42.40. **FT-IR** ν_{max}

(film) 3388, 1651, 1583 cm^{-1}. **HRMS** (ESI-TOF) calcd for $C_{23}H_{21}O_2N_4[M+H]^+$: 385.1659, found : 385.1658.

([1,1'-biphenyl]-4-yl)-4-methoxy-6-(1H-pyrazol-1-yl)nicotinamide 91

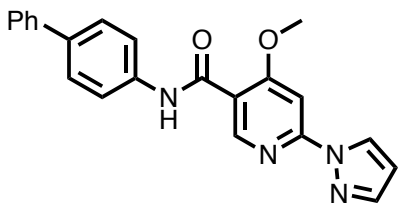

Following general procedure D: **87** (150 mg, 0.43 mmol), Pd^{t}BuXPhos G3 (34 mg, 0.043 mmol), Cs_2CO_3 (354 mg, 1.09 mmol), pyrazole (74 mg, 1.09 mmol) gave **91** (67 mg, 0.181 mmol, 40%) as a colourless oil.

^{1}H NMR (400 MHz, DMSO-d_6) δ 8.68 (d, J = 2.5 Hz, 1H, Pyzl), 8.59 (s, 1H, NH), 7.90 (d, J = 1.5 Hz, 1H, Pyzl), 7.70 – 7.63 (m, 6H, Ar), 7.52 – 7.42 (m, 4H, Ar), 6.63 (dd, J = 2.5, 1.5 Hz, 1H, Pyzl), 4.08 (s, 3H, CH_3). **^{13}C NMR** (101 MHz, DMSO-d_6) δ 164.85, 162.17, 153.60, 149.38, 142.75, 139.61, 138.24, 135.44, 128.91, 127.71, 126.93, 126.29, 120.13, 108.79, 94.94, 56.56. **FT-IR** ν_{max} (film) 3403, 1636, 1583 cm^{-1}. **HRMS (**ESI-TOF) calcd for $C_{22}H_{19}O_2N_4$ $[M+H]^+$: 371.1502, found : 371.1501.

6-chloro-4-methoxy-N-(3-(trifluoromethyl)benzyl)nicotinamide 92

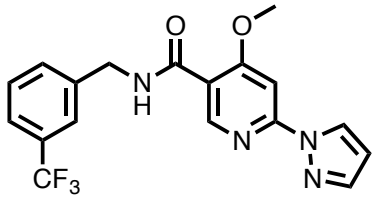

Following general procedure D: **88** (150 mg, 0.43 mmol), Pd^{t}BuXPhos G3 (34 mg, 0.043 mmol), Cs_2CO_3 (354 mg, 1.09 mmol), Pyrazole (74 mg, 1.09 mmol) gave **92** (72 mg, 0.191 mmol, 44%) as a colourless oil.

^{1}H NMR (400 MHz, DMSO-d_6) δ 9.26 (t, J = 6.0 Hz, 1H, NH), 8.66 (dd, J = 2.5, 1.0 Hz, 1H, Pyzl), 8.62 (s, 1H), 8.33 (d, J = 2.5 Hz, 1H, Pyr), 7.88 (dd, J = 1.5, 1.0 Hz, 1H, Pyzl), 7.68 – 7.57 (m, 6H, Ar), 6.61 (dd, J = 2.5, 1.5 Hz, 1H, Pyzl), 4.59 (d, J = 6.0 Hz, 2H CH_2), 4.07 (s, 3H, CH_3). **^{13}C NMR** (101 MHz, DMSO-d_6) δ 165.09, 163.33, 153.72, 150.24, 142.75, 141.03, 131.79, 131.30, 130.33, 129.36, 127.71, 123.57, 117.88, 108.75, 94.88, 56.47, 42.19. **FT-IR**ν_{max} (film) 3369 1641, 1555 cm^{-1}. **HRMS (**ESI-TOF) calcd for $C_{18}H_{16}O_2N_4F_3$ $[M+H]^+$: 377.1219, found : 377.1220.

(cyclohexylmethyl)-4-methoxy-6-(1H-pyrazol-1-yl)nicotinamide 93

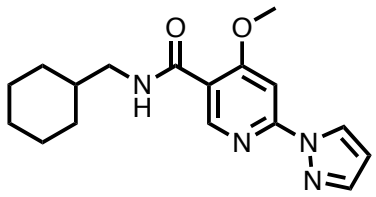

Following general procedure D: **89** (150 mg, 0.43 mmol), Pd^{t}BuXPhos G3 (34 mg, 0.043 mmol), Cs_2CO_3 (354 mg, 1.09 mmol), pyrazole (74 mg, 1.09 mmol) gave **93** (67 mg, 0.21 mmol, 40%) as a colourless oil.

^{1}H NMR (400 MHz, DMSO-d_6) δ 8.68 (dd, J = 2.5, 1.0 Hz, 1H, Pyzl), 8.56 (s, 1H, Pyr), 7.90 (dd, J = 1.5, 1.0 Hz, 1H, Pyzl), 7.57 (s, 1H, Pyr), 6.64 (dd, J = 2.5, 1.5 Hz, 1H, Pyzl), 3.95 (s, 3H, CH_3), 3.06 – 3.03 (m, 2H, $\underline{CH_2}$NH), 1.79 – 1.58 (m, 5H, Cyclohexane), 1.28 – 1.09 (m, 4H, Cyclohexane), 1.00 – 0.83 (m, 2H, Cyclohexane). **^{13}C NMR** (101 MHz, DMSO-d_6) δ 165.04, 162.90, 153.47, 150.03, 142.46, 127.62, 123.59, 107.78, 94.81, 56.46, 45.24, 38.89, 30.43, 26.07, 25.42. **FT-IR**ν_{max} (film) 3330, 1639, 1574 cm^{-1}. **HRMS (**ESI-TOF) calcd for $C_{17}H_{23}O_2N_4$ $[M+H]^+$: 315.1815, found : 315.1816.

([1,1'-biphenyl]-4-ylmethyl)-4-hydroxy-6-(1H-pyrazol-1-yl)nicotinamide 94

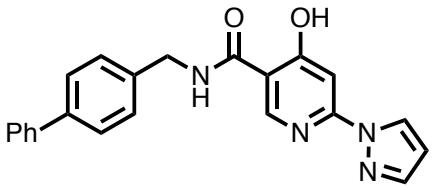

TMS-I (17 mg ,0.0858 mmol) was added to the mixture of **90** (11 mg, 0.0286 mmol) and CH_2Cl_2 (1 ml). The resultant mixture was heated at 90°C for 90 minutes, then cooled to rt, HCl_{aq} (1.5 ml, 1M) was added before being extracted with CH_2Cl_2 (3 x 10 ml). The organic fractions were combined, dried with anhydrous Na_2SO_4 concentrated in *vacuo* and the crude compound was then purified using flash column chromatography using (0% - 5%

MeOH, CH_2Cl_2, 1 % NH_3) over 20 column volumes gave **94** (2 mg, 0.0054 mmol, 20%) as a colourless oil.

^{1}H NMR (400 MHz, DMSO-d_6) δ 8.76 (s, 1H, NH), 8.64 (d, J = 2.5 Hz, 1H, Pyzl), 7.86 (d, J = 1.5 Hz, 1H, Pyzl), 7.70 – 7.60 (m, 5H, Ar), 7.52 – 7.29 (m, 6H, Ar), 6.60 (dd, J = 2.5, 1.5 Hz, 1H, Pyzl), 4.59 (d, J = 6.0 Hz, 2H, CH_2). **^{13}C NMR** (126 MHz, DMSO-d_6) δ 166.06, 165.77, 142.84, 139.96, 138.93, 138.28, 128.96, 128.00, 127.40, 126.77, 126.63, 108.82, 104.24, 42.09. **FT-IR** ν_{max} (film) 3697, 3479, 1641, 1556 cm^{-1}. **HRMS** (ESI-TOF) calcd for $C_{22}H_{19}O_2N_4[M+H]^+$: 371.1502, found : 371.1502.

([1,1'-biphenyl]-4-yl)-4-hydroxy-6-(1H-pyrazol-1-yl)nicotinamide 95

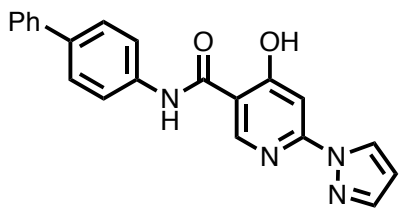

TMS-I (66 mg ,0.33 mmol) was added to the reaction mixture of **91** (41 mg, 0.11 mmol) and CH_2Cl_2 (2.5 ml). The resultant mixture was heated at 90°C for 90 minutes, then cooled to rt, HCl_{aq} (1.5 ml, 1M) was added before being extracted with CH_2Cl_2 (3 x 10 ml). The organic fractions were combined, dried with anhydrous Na_2SO_4 concentrated in *vacuo* and the crude compound was then purified using flash column chromatography using (0% - 5% MeOH, CH_2Cl_2, 1 % NH_3) over 20 column volumes gave **95** (7 mg, 0.0196 mmol, 18 %) as a colourless oil.

^{1}H NMR (400 MHz, DMSO-d_6) δ 8.70 (d, J = 2.0 Hz, 1H, Pyzl), 8.64 (s, 1H, NH), 7.92 (d, J = 2.0 Hz, 1H, Pyzl), 7.72 – 7.62 (m, 5H, Ar), 7.55 – 7.27 (m, 6H, Ar), 6.65 (dd, J = 2.0 Hz, 1H, Pyzl). **^{13}C NMR** (126 MHz, DMSO-d_6) δ 163.04, 162.16, 142.94, 139.62, 137.92, 135.49, 129.19, 128.95, 128.36, 127.10, 126.27, 120.45, 120.17, 120.07, 116.12, 109.17, 100.83. **FT-IR** ν_{max} (film) 3592, 3421, 1630, 1592 cm^{-1}. **HRMS (**ESI-TOF) calcd for $C_{21}H_{17}O_2N_4$ $[M+H]^+$: 357.1346, found : 357.1343.

4-hydroxy-6-(1H-pyrazol-1-yl)-N-(3-(trifluoromethyl)benzyl)nicotinamide 96

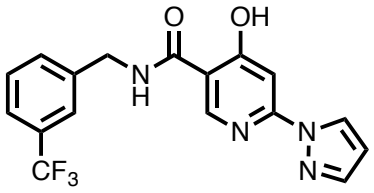

TMS-I (59 mg, 0.295 mmol) was added to the reaction mixture of **92** (37 mg, 0.0986 mmol) and CH_2Cl_2 (2.5 ml). The resultant mixture was heated for 90 minutes, then cooled to rt, HCl_{aq} (1.5 ml, 1M) was added before being extracted with CH_2Cl_2 (3 x 10 ml). The organic fractions were combined, dried with anhydrous Na_2SO_4 concentrated in *vacuo* and the crude compound was then purified using flash column chromatography using (0% - 5% MeOH, CH_2Cl_2, 1 % NH_3) over 20 column volumes gave **96** (20 mg, 0.055 mmol, 57%) as a white solid.

m.p. 191-196°C. **^{1}H NMR** (400 MHz, DMSO-d_6) δ 8.66 (s, 1H, Pyr), 8.59 (dd, J = 2.5, 1.0 Hz, 1H, Pyzl), 7.82 (dd, J = 1.5, 1.0 Hz, 1H, Pyzl), 7.71 – 7.49 (m, 4H, Ar), 7.26 (s, 1H, Pyr), 6.55 (dd, J = 2.5, 1.5 Hz, 1H, Pyzl), 4.59 (d, J = 6.0 Hz, 2H, CH_2). **^{13}C NMR** (126

MHz, DMSO-d_6) δ 168.82, 165.68, 149.11, 142.72, 140.78, 131.49, 129.47, 129.18, 128.93, 128.68, 127.87, 127.51, 126.41, 125.35, 123.89, 123.86, 123.66, 123.19, 121.02, 108.68, 99.77, 41.92. **FT-IR** ν_{max} (film) 3657, 3312, 1639, 1571 cm^{-1}. **HRMS (**ESI-TOF) calcd for $C_{17}H_{14}O_2N_4F_3$ $[M+H]^+$: 363.1063, found : 363.1067.

(cyclohexylmethyl)-4-hydroxy-6-(1H-pyrazol-1-yl)nicotinamide 97

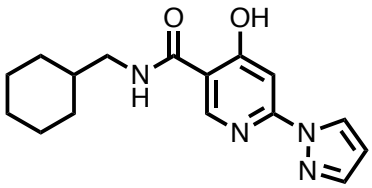

TMS-I (128 mg ,0.64 mmol) was added to the reaction mixture of **93** (67 mg, 0.214 mmol) and CH_2Cl_2 (2.5 ml). The resultant mixture was heated for 90 minutes, then cooled to rt, HCl_{aq} (1.5 ml, 1M) was added before being extracted with CH_2Cl_2 (3 x 10 ml). The organic fractions were combined, dried with anhydrous Na_2SO_4 concentrated in *vacuo* and the crude compound was then purified using flash column chromatography using (0% - 5% MeOH, CH_2Cl_2, 1 % NH_3) over 20 column volumes gave **97** (17 mg, 0.056 mmol, 26%) as a colourless oil.

^{1}H NMR (400 MHz, DMSO-d_6) δ 8.63 (d, J = 2.5 Hz, 1H, Pyzl), 8.47 (s, 1H, Pyr), 8.29 (d, J = 2.5 Hz, 1H, Pyzl), 8.21 (s, 1H, Pyr), 6.65 – 6.63 (m, 1H, Pyzl), 3.05 (t, J = 6.0 Hz, 2H, $\underline{CH_2}$NH), 1.75 – 1.44 (m, 5H, Cyclohexane), 1.27 – 1.10 (m, 3H, Cyclohexane), 1.05 – 0.80

(m, 2H, Cyclohexane). **^{13}C NMR** (101 MHz, DMSO-d_6) δ 165.10, 151.93, 148.98, 143.02, 142.53, 130.39, 127.67, 123.63, 109.01, 103.96, 45.56, 37.01, 30.47, 26.05, 25.42. **FT-IR** ν_{max} (film) 3697, 3339, 1639, 1584 cm^{-1}. **HRMS (**ESI-TOF) calcd for $C_{16}H_{21}O_2N_4$ $[M+H]^+$: 301.1659, found : 301.1656.

6-chloro-4-methoxy-N-(4-(trifluoromethyl)benzyl)nicotinamide 98

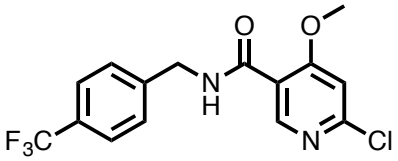

Following general procedure C: 6-chloro-5-methoxy-nicotinic acid (350 mg, 1.87 mmol), 4-trifluoromethylbenzylamine (448 mg, 2.56 mmol), T3P (1.48 g, 4.67 mmol) and DIPEA (600 mg, 467 mmol) gave **98** (437 mg, 1.27 mmol, 66 %) as a white solid.

m.p. 152-154°C. **^{1}H NMR** (400 MHz, Chloroform-*d*) δ 9.02 (s, 1H, Pyr), 7.81 (t, *J* = 6.0 Hz, 1H, NH), 7.58 (d, *J* = 8.0 Hz, 2H, Ar), 7.43 (d, *J* = 8.0 Hz, 2H, Ar), 6.93 (s, 1H, Pyr), 4.69 (d, *J* = 6.0 Hz, 2H, CH_2), 4.01 (s, 3H, CH_3). **^{13}C NMR** (101 MHz, Chloroform-*d*) δ 164.13, 162.87, 155.51, 153.61, 142.05, 129.63, 129.31, 127.53, 125.48, 125.44, 125.40, 125.36, 125.19, 122.49, 116.18, 106.70, 77.16, 56.54, 43.03. **FT-IR** ν_{max} (film 3390, 1674, 1585 cm^{-1}. **HRMS (**ESI-TOF) calcd for $C_{15}H_{13}O_2N_2{}^{35}ClF_3$ $[M+H]^+$: 345.0612, found : 345.0608.

N-([1,1'-biphenyl]-3-ylmethyl)-6-chloro-4-methoxynicotinamide 99

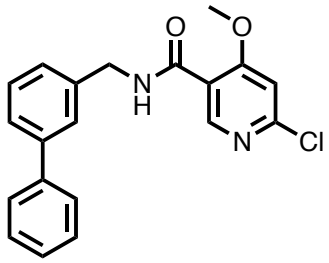

Following general procedure C: 6-chloro-5-methoxy-nicotinic acid (400 mg, 2.13 mmol), 3-phenylbenzyl amine (469 mg, 2.56 mmol), T3P (1.62 g, 5.12 mmol) and DIPEA (634 mg, 5.12 mmol) gave **98** as a white solid (570 mg, 1.61 mmol, 76 %).

^{1}H NMR (400 MHz, DMSO-d_6) δ 8.85 (t, J = 6.0 Hz, 1H, NH), 8.48 (s, 1H, Pyr), 7.70 – 7.30 (m, 10H, Ar), 4.56 (d, J = 6.0 Hz, 2H, CH_2), 3.96 (s, 3H, CH_3). **^{13}C NMR** (101 MHz, DMSO-d_6) δ 164.48, 163.05, 153.27, 150.27, 140.23, 139.90, 128.98, 127.51, 126.68, 126.25, 125.57, 125.20, 120.07, 107.93, 56.91, 42.61. **FT-IR** ν_{max} (film) 3364, 1632, 1586 cm^{-1}. **HRMS (**ESI-TOF) calcd for $C_{20}H_{18}O_2N_2{}^{35}Cl$ $[M+H]^+$: 353.1051, found : 353.1053.

N-([1,1'-biphenyl]-3-yl)-6-chloro-4-methoxynicotinamide 100

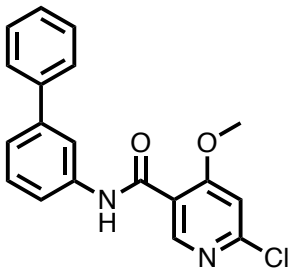

Following general procedure C: 6-chloro-5-methoxy-nicotinic acid (350 mg, 1.87 mmol), 3-aminobiphenyl (411 mg, 2.43 mmol), T3P (1.48 g, 4.67 mmol) and DIPEA (600 mg, 467 mmol) gave **100** (421 mg, 1.24 mmol, 66 %) as a white solid.

m.p. 105-107°C. **^{1}H NMR** (400 MHz, Chloroform-*d*) δ 9.24 (s, 1H, Pyr), 9.05 (s, 1H, NH), 7.90 – 7.87 (m, 1H, Ar), 7.66 – 7.30 (m, 8H, Ar), 6.91 (s, 1H, Pyr), 4.06 (s, 3H, CH_3). **^{13}C NMR** (101 MHz, Chloroform-*d*) δ 164.02, 160.95, 155.85, 153.82, 142.16, 140.52, 138.02, 129.46, 128.83, 127.64, 127.18, 119.43, 117.10, 107.05, 77.16, 57.01. **FT-IR** ν_{max} (film) 3332, 1641, 1572 cm^{-1}. **HRMS (**ESI-TOF) calcd for $C_{19}H_{16}O_2N_2{}^{35}Cl$ $[M+H]^+$: 339.0894, found : 339.0894.

6-chloro-4-methoxy-N-(4-(trifluoromethoxy)benzyl)nicotinamide 101

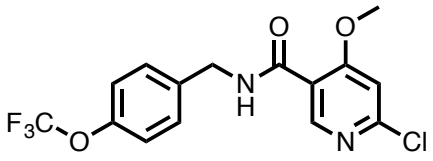

Following general procedure C: 6-chloro-5-methoxy-nicotinic acid (300 mg, 1.60 mmol), 4-trifluoromethoxybenzylamine (367 mg, 1.92 mmol), T3P (1.01 g, 3.2 mmol) and DIPEA (600 mg, 467 mmol) gave **101** (434 mg, 1.20 mmol, 75 %) as a white solid.

m.p. 191-121°C. **^{1}H NMR** (400 MHz, Chloroform-*d*) δ 8.97 (s, 1H, Pyr), 7.78 (t, *J* = 6.0 Hz, 1H, NH), 7.37 – 7.29 (m, 2H, Ar), 7.17 – 7.11 (m, 2H, Ar), 6.90 (s, 1H, Pyr), 4.61 (d, *J* = 6.0 Hz, 2H, CH_2), 3.98 (s, 3H, CH_3). **^{13}C NMR** (101 MHz, Chloroform-*d*) δ 164.10, 162.74, 155.34, 153.40, 148.16, 136.73, 128.67, 121.42, 120.92, 118.87, 116.28, 106.66,

77.16, 56.48, 42.68. **FT-IR** ν_{max} (film) 3369, 1641, 1577 cm^{-1}. **HRMS (**ESI-TOF) calcd for $C_{15}H_{13}O_3N_2{}^{35}ClF_3$ $[M+H]+$: 361.0561, found : 361.0563.

6-chloro-4-methoxy-N-((4-(trifluoromethyl)cyclohexyl)methyl)nicotinamide 102

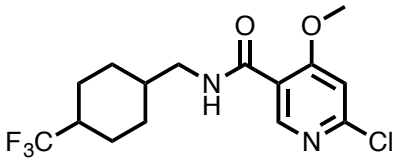

Following general procedure C: 6-chloro-5-methoxy-nicotinic acid (250 mg, 1.33 mmol), C-(4-trifluoromethyl-cyclohexylamine (255 mg, 1.59 mmol), T3P (827 mg, 2.6 mmol) and DIPEA (600 mg, 467 mmol) gave **102** (402 mg, 1.14 mmol, 86 %) as a white solid.

m.p. 67-70°C. **^{1}H NMR** (400 MHz, Chloroform-*d*) δ 9.00 (s, 1H), 6.92 (d, *J* = 1.3 Hz, 1H), 4.03 (s, 2H), 2.79 (s, 3H), 2.20 – 1.85 (m, 3H), 1.78 – 1.49 (m, 5H), 1.47 – 0.91 (m, 1H). **^{13}C NMR** (101 MHz, Chloroform-*d*) δ 164.37, 163.08, 155.51, 153.88, 116.96, 106.94, 77.16, 56.81, 45.58, 42.32, 40.58, 40.32, 40.06, 39.84, 38.74, 37.46, 33.83, 29.33, 26.30, 24.59, 21.08. **FT-IR** ν_{max} (film) 3411, 1652 cm^{-1}. **HRMS (**ESI-TOF) calcd for $C_{15}H_{19}O_2N_2{}^{35}ClF_3$ $[M+H]^+$: 351.1081, found : 351.1078.

Tert-butyl ((6-chloropyridin-3-yl)methyl)carbamate 103

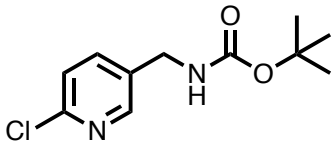

6-chloropyridin-3-yl)methamine (4 g, 0.0281 mmol) was dissolved in CH_2Cl_2 (50 ml) before the addition of DIPEA (6.35 g, 0.049 mmol). Di tert-butyl dicarbonate (7.6 g, 0.035 mmol) was added slowly to the reaction mixture and the resultant mixture was allowed to stir for 16 hrs at room temperature. The reaction mixture was then washed with water (3 x 50 ml), brine (50 ml) and dried over Na_2SO_4. The organic phase was reduced in *vacuo* before being purified by flash column chromatography using (Cyclohexane 100 % - 50%, EtOAc 0% - 50%) over 10 column volumes gave **103** (6.08 g, 0.0251 mmol, 89 %) with the appearance of a colourless solid.

m.p. 59-60°C. **^{1}H NMR** (400 MHz, Chloroform-*d*) δ 8.25 (dd, J = 2.5, 1.0 Hz, 1H, Pyr), 7.58 (dd, J = 8.5, 2.5 Hz, 1H, Pyr), 7.24 (d, J = 1.0 Hz, 1H, Pyr), 5.08 (s, 1H, NH), 4.26 (d, J = 6.0 Hz, 2H, CH_2), 1.41 (s, 9H, ^{t}Boc). **^{13}C NMR** (101 MHz, Chloroform-d_3) δ 155.96, 150.47, 148.80, 138.29, 133.83, 124.27, 80.15, 77.16, 41.51, 28.44. **FT-IR** ν_{max} (film) 3423, 1695, 1585 cm^{-1}. **HRMS (**ESI-TOF) calcd for $C_{11}H_{16}O_2N_2{}^{35}Cl$ $[M+H]^+$: 243.0894, found : 243.0895.

tert-butyl ((6-phenylpyridin-3-yl)methyl)carbamate 104

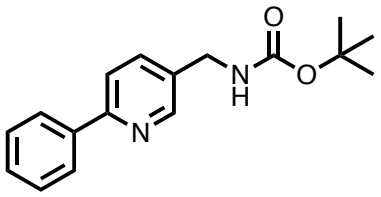

103 (500 mg, 2.06 mmol), Phenyl boronic acid (249 mg, 2.06 mmol), Pd Tetrakis (118 mg, 0.103 mmol) and Cs_2CO_3 (1.33 g, 4.12 mmol) were dissolved in dioxane (5 ml). The resultant mixture was heated under microwave radiation at 100°C for 30 mins. The reaction mixture was filtered through a celite pad, water (15 ml) was added to the reaction mixture and was extracted with CH_2Cl_2 (3 x 25 ml). The organic fractions were combined, washed with water (3 x 50 ml), brine (50 ml) and dried over Na_2SO_4. The organic phase was removed in *vacuo* before being purified by flash column chromatography using (Cyclohexane 100 % - 50%, EtOAc 0% - 50%) over 10 column volumes gave **104** (520 mg, 1.83 mmol, 89 %) as a colourless oil.

^{1}H NMR (400 MHz, Chloroform-*d*) δ 8.58 (t, *J* = 1.5 Hz, 1H, Pyr), 7.98 – 7.93 (m, 2H, Ar), 7.67 (d, *J* = 1.5 Hz, 2H, Ar), 7.48 – 7.38 (m, 3H, Ar), 5.08 (s, 1H, NH), 4.34 (d, *J* = 6.0 Hz, 2H), 1.46 (s, 9H, ^{t}Boc). **^{13}C NMR** (101 MHz, Chloroform-*d*) δ 157.01, 156.35, 149.24, 139.49, 136.52, 133.37, 129.35, 129.16, 127.26, 120.78, 80.24, 77.16, 42.38, 28.81. **FT-IR** ν_{max} (film) 3415, 1692, 1577 cm^{-1}. **HRMS (**ESI-TOF) calcd for $C_{17}H_{21}O_2N_2$ $[M+H]^+$: 285.1597, found : 285.1594.

(6-phenylpyridin-3-yl)methanamine 105

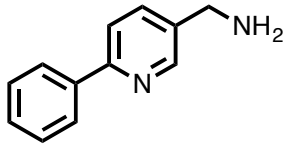

104 (500 mg, 1.76 mmol) was dissolved in CH_2Cl_2 (5 ml) and HCl ((2M) in ether (3 ml)) was added to the solution. The resultant mixture was put under vacuo and flushed with N_2, this was repeated 3 times. The resultant mixture was stirred at room temperature for 16 hrs. The volatiles were evaporated in *vacuo* to give **105** (312 mg, 1.69 mmol, 96%) as a white solid.

m.p. >250°C. **^{1}H NMR** (400 MHz, DMSO-d_6) δ 8.85 (s, 2H, NH_2), 8.79 (dd, J = 2.5, 1.0 Hz, 1H, Pyr), 8.15 – 8.07 (m, 3H, Ar), 8.02 (dd, J = 8.0, 1.0 Hz, 1H, Pyr), 7.55 – 7.41 (m, 3H, Ar), 4.08 (s, 2H, CH_2). **^{13}C NMR** (101 MHz, DMSO-d_6) δ 155.83, 150.25, 138.15, 129.28, 128.83, 128.69, 126.58, 119.73, 39.52, 39.42. **FT-IR** ν_{max} (film) 3390, 3341, 1556 cm^{-1}. **HRMS (**ESI-TOF) calcd for $C_{12}H_{13}N_2$ $[M+H]^+$: 185.1073, found : 185.1073.

6-chloro-4-methoxy-N-((6-phenylpyridin-3-yl)methyl)nicotinamide 106

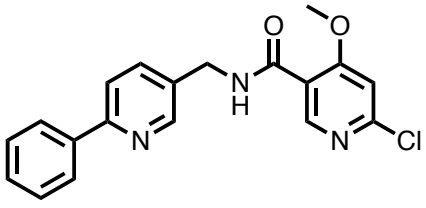

Following general procedure C: **105** (100 mg, 0.54 mmol), 6-chloro-4-methoxy-nicotinic acid (85 mg, 0.45 mmol) and T3P (358 mg, 1.125 mmol) gave **106** (144 mg, 0.41 mmol, 90%) as a thick orange oil.

^{1}H NMR (400 MHz, DMSO-d_6) δ 8.91 (t, J = 6.0 Hz, 1H, NH), 8.51 (s, 1H, Pyr), 8.13 – 7.79 (m, 5H, Ar), 7.63 – 7.37 (m, 4H, Ar), 7.32 (s, 1H, Pyr), 4.54 (d, J = 6.0 Hz, 2H, CH_2), 3.98 (s, 3H, CH_3). **^{13}C NMR** (101 MHz, DMSO-d_6) δ 169.96, 164.70, 163.27, 154.87, 153.69, 150.71, 148.82, 138.62, 136.37, 133.68, 129.08, 128.91, 126.56, 120.06, 119.53, 108.03, 57.09, 40.37, 39.52. **FT-IR** ν_{max} (film) 3132, 1662, 1577 cm^{-1}. **HRMS (**ESI-TOF) calcd for $C_{19}H_{17}O_2N_3{}^{35}Cl$ $[M+H]^+$: 354.1003, found 354.1002.

Methyl (R)-2-(6-chloro-4-methoxynicotinamido)-2-phenylacetate 107

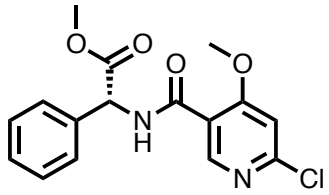

Following general procedure C: (*R*)-methyl-2-amino-2-phenylacetate (400 mg, 1.99 mmol), 6-chloro-4-methoxy-nicotinic acid (250 mg, 1.33 mmol), T3P (1.05 g, 3.32 mmol) gave **107** (163 mg, 0.48 mmol, 25%) as a white solid.

m.p. 156-158°C. **^{1}H NMR** (400 MHz, Chloroform-*d*) δ 8.96 (s, 1H, Pyr), 8.59 (d, J = 6.5 Hz, 1H, NH), 7.47 – 7.28 (m, 5H, Ar), 6.93 (s, 1H, Pyr), 5.72 (d, J = 6.5 Hz, 1H, CH), 4.07 (s, 3H, OCO$\underline{CH_3}$), 3.74 (s, 3H, PyrO$\underline{CH_3}$). **^{13}C NMR** (101 MHz, Chloroform-*d*) δ 171.39,

164.68, 162.11, 155.89, 153.86, 136.55, 129.10, 128.69, 127.30, 116.20, 106.99, 77.16, 57.10, 56.91, 53.03. **FT-IR** ν_{max} (film) 3390, 1622, 1571 cm^{-1}. **HRMS (**ESI-TOF) calcd for $C_{16}H_{16}O_4N_2{}^{35}Cl$ $[M+H]^+$: 335.0793, found : 335:0796.

Methyl (S)-2-(6-chloro-4-methoxynicotinamido)-2-phenylacetate 108

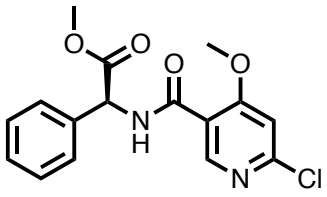

Following general procedure C: (*S*)-methyl (400 mg, 1.99 mmol), 6-chloro-4-methoxy-nicotinic acid (250 mg, 1.33 mmol) and T3P (1.05 g, 3.32 mmol) gave **108** (215 mg, 0.64 mmol, 32%) as a white solid.

m.p. 155-157°C. **^{1}H NMR** (400 MHz, Chloroform-*d*) δ 8.96 (s, 1H, Pyr), 8.59 (d, *J* = 6.5 Hz, 1H, NH), 7.46 – 7.29 (m, 5H, Ar), 6.93 (s, 1H, Pyr), 5.72 (d, *J* = 6.5 Hz, 1H, CH), 4.07 (s, 3H, OCO$\underline{CH_3}$), 3.74 (s, 3H, PyrO$\underline{CH_3}$). **^{13}C NMR** (101 MHz, Chloroform-*d*) δ 171.40, 164.70, 162.13, 155.89, 153.84, 136.53, 129.10, 128.70, 127.30, 116.20, 107.01, 77.16, 57.11, 56.92, 53.05. **FT-IR** ν_{max} (film) 3302, 1743, 1644, 1577 cm^{-1}. **HRMS (**ESI-TOF) calcd for $C_{16}H_{16}O_4N_2{}^{35}Cl$ $[M+H]^+$: 335.0793, found : 335.0789.

4-methoxy-6-(1H-pyrazol-1-yl)-N-(4-(trifluoromethyl)benzyl)nicotinamide 109

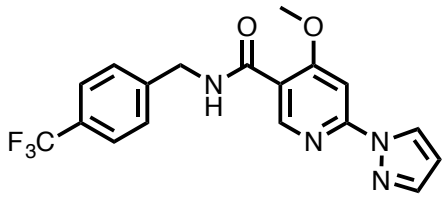

Following general procedure D: **98** (200 mg, 0.58 mmol), Pd^{t}BuXPhos G3 (46 mg, 0.058 mmol), Cs_2CO_3 (377 mg, 1.16 mmol), pyrazole (42 mg, 0.63 mmol) and ^{t}BuOH (2 ml) gave **109** (69 mg, 0.185 mmol, 32%) as a clear oil.

^{1}H NMR (400 MHz, DMSO-d_6) δ 8.88 (t, J = 6.0 Hz, 1H, NH), 8.66 (dd, J = 2.5, 1.0 Hz, 1H, Pyzl), 8.64 (s, 1H, Pyr), 7.89 (t, J = 1.5, 1.0 Hz, 1H, Pyzl), 7.72 (d, J = 7.0 Hz, 2H, Ar), 7.60 (s, 1H, Pyr), 7.56 (d, J = 7.0 Hz, 2H, Ar), 6.62 (dd, J = 2.5, 1.5 Hz, 1H, Pyzl), 4.59 (d, J = 6.0 Hz, 2H, CH_2), 4.08 (s, 3H, CH_3). **^{13}C NMR** (126 MHz, DMSO-d_6) δ 165.68, 163.78, 154.28, 150.96, 144.94, 143.30, 128.27, 128.13, 128.03, 127.78, 127.53, 125.97, 125.71, 125.66, 123.81, 118.12, 109.31, 95.38, 57.06, 42.84, 39.52. **FT-IR** ν_{max} (film) 3301, 1641, 1552 cm^{-1}. **HRMS (**ESI-TOF) calcd for $C_{18}H_{16}O_2N_4F_3$ $[M+H]^+$: 377.1221, found : 377.1221.

N-([1,1'-biphenyl]-3-ylmethyl)-4-methoxy-6-(1H-pyrazol-1-yl)nicotinamide 110

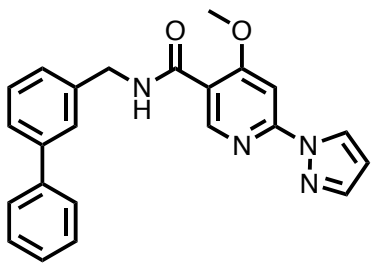

Following general procedure D: **99** (150 mg, 0.42 mmol), Pd^{t}BuXPhos G3 (33 mg, 0.0426 mmol), Cs_2CO_3 (341 mg, 1.05 mmol), pyrazole (42 mg, 0.63 mmol) and ^{t}BuOH (2 ml) gave **110** (78 mg, 0.203 mmol, 48 %) with the appearance of a clear oil.

^{1}H NMR (400 MHz, Chloroform-*d*) δ 9.03 (d, J = 2.0 Hz, 1H, Pyzl), 8.53 (d, J = 2.5 Hz, 1H, Pyzl), 7.85 – 7.76 (m, 1H, Ar), 7.70 – 7.63 (m, 1H, Ar), 7.56 – 7.20 (m, 9H, Ar), 7.20 – 7.15 (m, 1H, Ar), 6.40 (dd, J = 2.5, 2.0 Hz, 1H, Pyzl), 4.66 (d, J = 6.0 Hz, 2H, CH_2), 3.97 (s, 3H, CH_3). **^{13}C NMR** (101 MHz, Chloroform-*d*) δ 165.03, 163.36, 154.65, 153.09, 142.58, 138.70, 129.01, 128.62, 127.76, 127.28, 126.97, 126.68, 126.27, 126.14, 108.26, 94.37, 77.16, 56.42, 43.57. **FT-IR** ν_{max} (film) 3391, 1640, 1576 cm^{-1}. **HRMS (**ESI-TOF) calcd for $C_{23}H_{21}O_2N_4$ $[M+H]^+$: 385.1659, found : 385.1656.

N-([1,1'-biphenyl]-3-yl)-4-methoxy-6-(1H-pyrazol-1-yl)nicotinamide 111

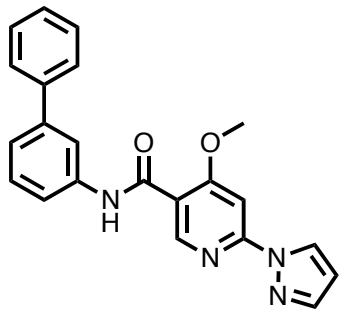

Following general procedure D: **100** (100 mg, 0.295 mmol), Pd^{t}BuXPhos G3 (20 mg, 0.028 mmol), Cs_2CO_3 (185 mg, 0.568 mmol), pyrazole (23 mg, 0.34 mmol) and ^{t}BuOH (2 ml) gave **111** (50 mg, 0.13 mmol, 46%) with the appearance of a white soild.

m.p. 172-176°C. **^{1}H NMR** (400 MHz, Chloroform-*d*) δ 9.42 (s, 1H, NH), 9.18 (s, 1H, Pyr), 8.64 (dd, *J* = 2.5, 1.0 Hz, 1H, Pyzl), 7.91 (m, 1H, Ar), 7.78 (dd, *J* = 1.5, 1.0 Hz, 1H, Pyzl), 7.69 – 7.33 (m, 9H, Ar), 6.51 (dd, *J* = 2.5, 1.5 Hz, 1H, Pyzl), 4.23 (s, 3H, CH_3). **^{13}C NMR** (101 MHz, Chloroform-*d*) δ 164.74, 161.37, 154.90, 153.38, 142.75, 142.08, 140.54, 138.09, 129.25, 128.58, 127.84, 127.36, 127.08, 123.28, 119.28, 115.44, 108.41, 94.47, 77.16, 56.74. **FT-IR** ν_{max} (film) 3361, 1641, 1577 cm^{-1}. **HRMS (**ESI-TOF) calcd for $C_{22}H_{19}O_2N_4$ $[M+H]^+$: 371.1502, found : 371.1497.

4-methoxy-6-(1H-pyrazol-1-yl)-N-(4-(trifluoromethoxy)benzyl)nicotinamide 112

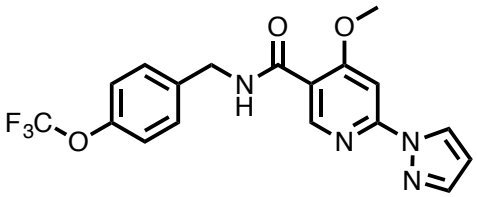

Following general procedure D: **101** (100 mg, 0.277 mmol), Pd^{t}BuXPhos G3 (19 mg, 0.027 mmol), Cs_2CO_3 (180 mg, 0.554 mmol), pyrazole (23 mg, 0.33 mmol) and ^{t}BuOH (2 ml) gave **112** (79 mg, 0.201 mmol, 73%) as a white solid.

m.p. 144-148°C. **^{1}H NMR** (400 MHz, Chloroform-*d*) δ 9.12 (s, 1H, Pyr), 8.63 (dd, *J* = 2.5, 1.0 Hz, 1H, Pyzl), 7.76 (t, *J* = 1.5, 1.0 Hz, 1H, Pyzl), 7.61 (s, 1H, Pyr), 7.40 (d, *J* = 7.5 Hz, 2H, Ar), 7.20 (d, *J* = 7.5 Hz, 2H, Ar), 6.50 (dd, *J* = 2.5, 1.5 Hz, 1H, Pyzl), 4.68 (d, *J* = 6.0 Hz, 2H, CH_2), 4.10 (s, 3H, CH_3). **^{13}C NMR** (101 MHz, Chloroform-*d*) δ 165.68, 164.08, 155.40, 153.81, 137.69, 129.43, 128.44, 121.72, 115.50, 108.96, 95.03, 77.16, 57.13, 43.39.

FT-IR ν_{max} (film) 3287, 1642, 1574 cm^{-1}. **HRMS (**ESI-TOF) calcd for $C_{18}H_{16}O_3N_4F_3$ $[M+H]^+$: 393.1169, found : 393.1163.

4-methoxy-6-(1H-pyrazol-1-yl)-N-((4-(trifluoromethyl)cyclohexyl)methyl)nicotinamide 113

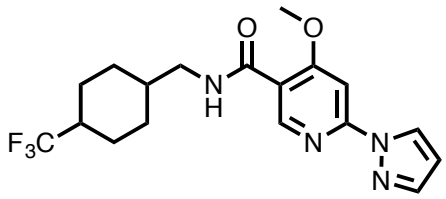

Following general procedure D: **102** (100 mg, 0.277 mmol), Pd^{t}BuXPhos G3 (19 mg, 0.027 mmol), Cs_2CO_3 (180 mg, 0.554 mmol), pyrazole (23 mg, 0.33 mmol) and ^{t}BuOH (2 ml) gave **113** (49 mg, 0.127 mmol, 46 %) as a colourless oil.

^{1}H NMR (400 MHz, Chloroform-*d*) δ 9.06 (s, 1H, Pyr), 8.61 (dd, *J* = 2.5, 1.0 Hz, 1H, Pyzl), 7.75 (dd, *J* = 1.5, 1.0 Hz, 1H, Pyzl), 6.92 (s, 1H, Pyr), 6.49 (dd, *J* = 2.5, 1.5 Hz, 1H, Pyzl), 6.35 (t, *J* = 2.1 Hz, 1H), 4.04 (d, *J* = 3.6 Hz, 3H), 3.51 – 3.41 (m, 3H), 2.20 – 1.21 (m, 9H). **^{13}C NMR** (101 MHz, Chloroform-*d*) δ 164.93, 163.40, 153.58, 152.95, 142.56, 127.75, 108.25, 106.61, 104.92, 94.37, 77.16, 56.48, 45.21, 42.01, 41.91, 33.55, 29.02, 28.88, 26.05, 24.30, 20.77. **FT-IR** ν_{max} (film) 3132, 1640, 1550 cm^{-1}. **HRMS (**ESI-TOF) calcd for $C_{18}H_{22}O_2N_4F_3$ $[M+H]^+$: 383.1689, found : 383.1689.

4-methoxy-N-((6-phenylpyridin-3-yl)methyl)-6-(1H-pyrazol-1-yl)nicotinamide 114

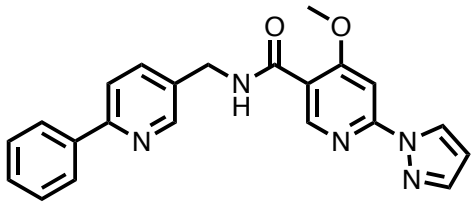

Following general procedure D: **106** (80 mg, 0.226 mmol), Pd^{t}BuXPhos G1 (14 mg, 0.0226 mmol), Cs_2CO_3 (145 mg, 0.452 mmol), pyrazole (15 mg, 0.226 mmol) and ^{t}BuOH (2 ml) gave **114** (16 mg, 0.043 mmol, 19 %) with the appearance of a clear oil.

^{1}H NMR (400 MHz, Chloroform-*d*) δ 9.11 (s, 1H, Pyr), 8.69 (dd, *J* = 2.5, 1.0 Hz, 1H, Pyzl), 8.62 (dd, *J* = 2.5, 1.0 Hz, 1H, Pyzl), 8.01 – 7.68 (m, 7H, Ar), 7.52 – 7.38 (m, 3H, Ar), 6.48 (dd, *J* = 2.5, 1.5 Hz, 1H, Pyzl), 4.73 (d, *J* = 6.0 Hz, 2H, CH_2), 4.10 (s, 3H, CH_3). **^{13}C NMR** (101 MHz, Chloroform-*d*) δ 165.04, 163.57, 153.11, 148.66, 142.65, 136.39, 132.27, 128.86, 128.60, 127.79, 126.69, 120.41, 108.33, 94.40, 77.16, 56.51, 40.82. **FT-IR** ν_{max} (film) 3392, 1641, 1574 cm^{-1}. **HRMS** (ESI-TOF) calcd for $C_{22}H_{20}O_2N_4[M+H]^+$: 386.1611, found : 386.1604.

(R)-2-(4-methoxy-6-(1H-pyrazol-1-yl)nicotinamido)-2-phenylacetic acid 115

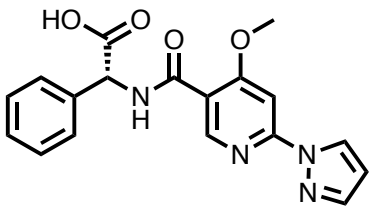

Following general procedure D: **107** (100 mg, 0.299 mmol), Pd^{t}BuXPhos G1 (20 mg, 0.0299 mmol), Cs_2CO_3 (194 mg, 0.598 mmol), pyrazole (15 mg, 0.226 mmol), ^{t}BuOH (2 ml) gave **115** (25 mg, 0.071 mmol, 24 %) as a colourless oil.

^{1}H NMR (400 MHz, THF-d_8) δ 8.77 (s, 1H), 8.66 (s, 1H), 8.63 (d, J = 7.0 Hz, 1H), 8.56 (d, J = 7.0 Hz, 1H), 8.50 (dd, J = 2.5, 1.0 Hz, 1H), 7.83 (s, 2H), 7.62 – 7.56 (m, 2H), 7.42 – 7.30 (m, 4H), 7.24 – 7.09 (m, 7H), 7.08 (s, 1H), 6.36 (t, J = 2.5, 1.5 Hz, 1H), 5.58 (dd, J = 11.2, 6.8 Hz, 2H), 4.04 (s, 3H), 3.96 (s, 3H). **^{13}C NMR** (101 MHz, THF-d_8) δ 172.82, 172.72, 166.79, 166.04, 162.76, 162.53, 162.38, 156.13, 155.96, 153.91, 153.64, 143.38, 139.53, 139.34, 129.40, 128.75, 128.70, 128.33, 118.15, 116.62, 109.02, 108.29, 95.53, 67.57, 57.80, 57.54, 57.25. **FT-IR** ν_{max} (film) 3383, 3201, 1712, 1641, 1574 cm^{-1}. **HRMS** **(**ESI-TOF) calcd for $C_{18}H_{17}O_4N_4$ $[M+H]^+$: 353.1244, found : 353.1242.

(S)-2-(4-methoxy-6-(1H-pyrazol-1-yl)nicotinamido)-2-phenylacetic acid 116

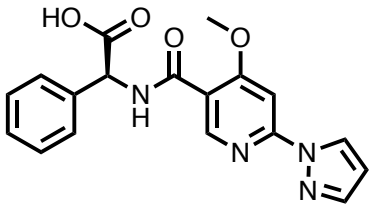

Following general procedure D: **108** (100 mg, 0.299 mmol), Pd^{t}BuXPhos G1 (20 mg, 0.0299 mmol), Cs_2CO_3 (194 mg, 0.598 mmol), pyrazole (15 mg, 0.226 mmol), ^{t}BuOH (2 ml) gave **116** (61 mg, 0.173 mmol, 58 %) as a colourless oil.

^{1}H NMR (400 MHz, THF-d_8) δ 8.89 (s, 1H, Pyr), 8.62 (dd, J = 2.5, 1.5 Hz, 1H, Pyzl), 7.93 (s, 1H,Pyr), 7.53 – 7.42 (m, 3H, Ar), 7.36 – 7.23 (m, 3H, Ar), 6.48 (dd, J = 2.5, 1.5 Hz, 1H, Pyzl), 5.71 (d, J = 7.0 Hz, 1H, CH), 4.17 (s, 3H, CH_3). **^{13}C NMR** (101 MHz, THF-d_8) δ 172.70, 165.93, 162.20, 156.02, 153.84, 143.24, 139.29, 129.28, 128.61, 128.56, 128.22, 116.55, 108.15, 95.41, 57.67, 57.12, 25.37. **FT-IR** ν_{max} (film) 3419, 3183, 1706, 1639, 1585 cm^{-1}. **HRMS (**ESI-TOF) calcd for $C_{18}H_{17}O_4N_4$ $[M+H]^+$: 353.1244, found : 353.121.

4-hydroxy-6-(1H-pyrazol-1-yl)-N-(4-(trifluoromethyl)benzyl)nicotinamide 117

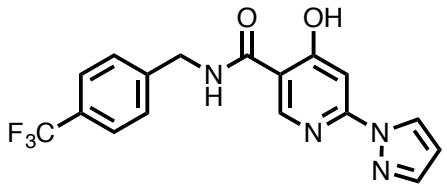

Following general procedure G: **109** (12 mg, 0.0319 mmol) and LiCl (19 mg, 0.319 mmol) in DMAc (2 ml) gave **117** (6 mg, 0.016 mmol, 52%) with the appearance as a yellow solid. **m.p.** 220°C (decomp). **^{1}H NMR** (400 MHz, DMSO-d_6) δ 10.12 (s, 1H, OH), 8.68 (s, 1H, Pyr), 8.64 – 8.58 (m, 1H, Pyzl), 7.81 (s, 1H, Pyr), 7.71 (d, J = 8.0 Hz, 2H, Ar), 7.56 (d, J = 8.0 Hz, 2H, Ar), 7.20 (m, 1H, Pyr), 6.60 – 6.53 (m, 1H, Pyzl), 4.61 (d, J = 6.0 Hz, 2H, CH_2). **^{13}C NMR** (126 MHz, DMSO-d_6) δ 176.82, 166.59, 150.00, 149.79, 144.94, 142.85, 128.74, 128.43, 128.17, 128.11, 127.86, 125.77, 123.80, 114.76, 108.80, 100.95, 42.36,

39.52. **FT-IR** ν_{max} (film) 3732, 3392, 1630, 1555 cm^{-1}. **HRMS (**ESI-TOF) calcd for $C_{17}H_{12}O_2N_4F_3$ $[M+H]^+$: 361.0917, found : 361.0917.

N-([1,1'-biphenyl]-3-ylmethyl)-4-hydroxy-6-(1H-pyrazol-1-yl)nicotinamide 118

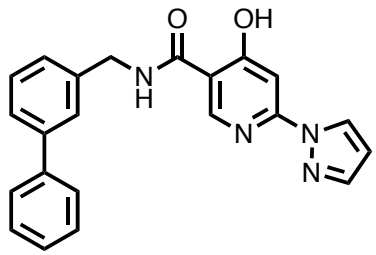

Following general procedure G: **110** (50 mg, 0.129 mmol) and LiCl (78 mg, 1.29 mmol) in DMAc (5 ml) gave **118** (30 mg, 0.081 mmol, 63 %) as a colourless oil.

^{1}H NMR (400 MHz, DMSO-d_6) δ 13.21 (s, 1H, OH), 9.26 (t, J = 6.0 Hz, 1H, NH), 8.69 (dd, J = 2.5, 1.0 Hz, 1H, Pyzl), 8.64 (d, J = 2.5 Hz, 1H, Pyr), 8.28 (d, J = 2.5 Hz, 1H, Pyr), 7.91 (dd, J = 1.5, 1.0 Hz, 1H, Pyzl), 7.59 – 7.29 (m, 9H, Ar), 6.64 (dd, J = 2.5, 1.5 Hz, 1H, Pyzl), 4.63 (d, J = 6.0 Hz, 2H, CH_2). **^{13}C NMR** (101 MHz, DMSO-d_6) δ 165.21, 152.07, 149.08, 145.65, 142.89, 140.34, 140.11, 139.64, 130.39, 129.08, 128.97, 127.51, 126.70, 126.49, 125.86, 125.41, 108.94, 103.93, 42.46, 39.52. **FT-IR** ν_{max} (film) 3692, 3287, 1636, 1542 cm^{-1}. **HRMS (**ESI-TOF) calcd for $C_{22}H_{19}O_2N_4$ $[M+H]^+$: 371.1502, found : 371.1507

N-([1,1'-biphenyl]-3-yl)-4-hydroxy-6-(1H-pyrazol-1-yl)nicotinamide 119

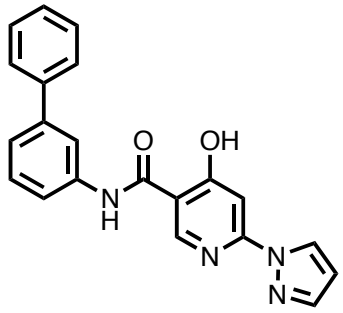

Following general procedure G: **111** (40 mg, 0.107 mmol) and LiCl (45 mg, 1.07 mmol) in DMAc (2 ml) gave **119** (19 mg, 0.053 mmol, 50 %) as a white solid.

m.p. >-250°C. **^{1}H NMR** (400 MHz, DMSO-d_6) δ 8.74 – 8.64 (m, 2H, Ar), 8.04 (s, 1H, Ar), 7.93 (s, 1H, Ar), 7.76 – 7.63 (m, 3H, Ar), 7.56 – 7.29 (m, 7H, Ar), 6.68 – 6.63 (m, 1H, Pyzl). **^{13}C NMR** (101 MHz, DMSO-d_6) δ 178.13, 173.16, 163.04, 147.77, 143.02, 140.94, 140.00, 138.93, 129.53, 129.00, 127.66, 126.72, 122.37, 119.22, 118.44, 99.54, 39.52. **FT-IR** ν_{max} (film) 3634, 3237, 1641, 1586 cm^{-1}. **HRMS (**ESI-TOF) calcd for $C_{21}H_{17}O_2N_4$ $[M+H]^+$: 357.1346, found: 357.1345.

4-hydroxy-6-(1H-pyrazol-1-yl)-N-(4-(trifluoromethyoxy)benzyl)nicotinamide 120

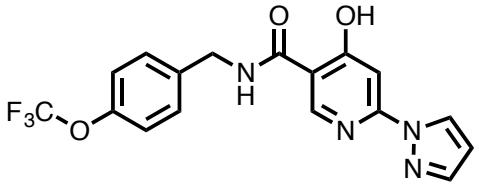

Following general procedure G: **112** (70 mg, 0.178 mmol) and LiCl (74 mg, 1.78 mmol) in DMAc (2 ml) gave **120** (43 mg, 0.114 mmol, 64 %) as a white solid.

m.p. 209-213°C. **^{1}H NMR** (400 MHz, DMSO-d_6) δ 13.16 (s, 1H, OH), 9.41 (s, 1H), 8.76 (s, 1H), 8.67 – 8.61 (m, 1H, Ar), 7.89 – 7.84 (m, 1H, Ar), 7.51 – 7.45 (m, 2H, Ar), 7.35 – 7.31 (m, 3H, Ar), 6.61 – 6.58 (m, 1H, Pyzl), 4.57 (d, J = 6.0 Hz, 2H, CH_2). **^{13}C NMR** (101 MHz, DMSO-d_6) δ 165.71, 147.28, 142.89, 138.59, 129.18, 128.04, 127.94, 121.38, 121.05, 118.84, 108.79, 99.54, 41.71, 39.52. **FT-IR** ν_{max}(film) 3697, 3365, 1653, 1552 cm^{-1}. **HRMS (**ESI-TOF) calcd for $C_{17}H_{12}O_3N_4F_3$ $[M+H]^+$: 377.0867, found : 377.865.

4-hydroxy-6-(1H-pyrazol-1-yl)-N-((4-(trifluoromethyl)cyclohexyl)methyl)nicotinamide 121

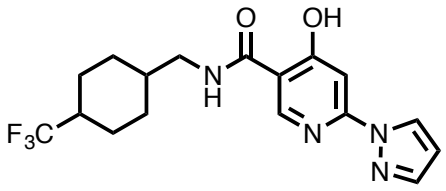

Following general procedure G: **113** (30 mg, 0.078 mmol) and LiCl (33 mg, 0.78 mmol) in DMAc (2 ml) gave **121** (8.5 mg, 0.023 mmol, 30 %) as a white solid.

m.p. 176-181°C. **^{1}H NMR** (400 MHz, DMSO-d_6) δ 9.00 (s, 1H), 8.72 (s, 1H, Pyr), 8.63 (d, J = 2.5 Hz, 1H, Pyzl), 7.86 (s, 1H, Pyr), 7.30 (d, J = 3.0 Hz, 1H, Pyzl), 6.60 (dd, J = 3.0, 2.5 Hz, 1H, Pyzl), 3.23 – 3.17 (m, 1H), 2.37 – 2.11 (m, 1H), 1.95 – 1.78 (m, 2H), 1.67 – 1.49 (m, 6H), 1.32 – 1.16 (m, 1H), 1.14 – 0.94 (m, 1H). **^{13}C NMR** (101 MHz, DMSO-d_6) δ 169.61, 169.57, 147.29, 147.17, 142.86, 130.39, 129.69, 128.99, 127.91, 126.72, 119.57,

108.80, 42.67, 40.47, 39.52, 37.45, 34.49, 32.48, 28.48, 28.42, 25.50, 25.47, 24.11, 21.42, 20.04. **FT-IR** ν_{max} (film) 3649, 3442, 1641, 1574 cm^{-1}. **HRMS (**ESI-TOF) calcd for $C_{17}H_{20}O_2N_4F_3$ $[M+H]^+$: 369.1532, found : 369.1533.

4-hydroxy-N-((6-phenylpyridin-3-yl)methyl)-6-(1H-pyrazol-1-yl)nicotinamide 122

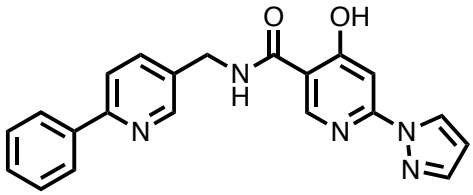

Following general procedure G: **114** (16 mg, 0.041 mmol) and LiCl (17 mg, 0.41 mmol) in DMAc (2 ml) gave **122** (6 mg, 0.0161 mmol, 40 %) as a white solid.

m.p. 213-215°C. **^{1}H NMR** (400 MHz, DMSO-d_6) δ 8.80 – 8.62 (m, 3H, Ar), 8.15 – 7.86 (m, 6H, Ar), 7.56 – 7.43 (m, 4H, Ar), 6.62 – 6.59 (m, 1H, Pyzl), 4.62 (d, J = 6.0 Hz, 2H, CH_2). **^{13}C NMR** (126 MHz, DMSO-d_6) δ 165.58, 163.06, 154.25, 147.90, 142.94, 137.56, 133.92, 129.35, 128.86, 128.00, 126.69, 120.68, 108.91, 40.11, 39.52. **FT-IR** ν_{max} (film) 3657, 3301, 1639, 1584 cm^{-1}. **HRMS** (ESI-TOF) calcd for $C_{21}H_{18}O_2N_5[M+H]^+$: 372.1455, found : 372.1447.

(*R*)-2-(4-hydroxy-6-(1H-pyrazol-1-yl)nicotinamido)-2-phenylacetic acid 123

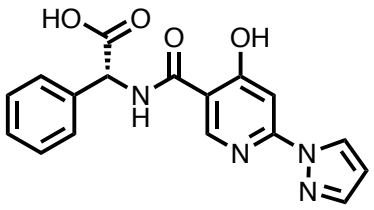

Following general procedure G: **115** (20 mg, 0.056 mmol) and LiCl (24 mg, 0.56 mmol) in DMAc (2 ml) using HPLC purification gave **123** (2 mg, 0.0052 mmol, 9 %) as a white TFA salt.

^{1}H NMR (500 MHz, DMSO-d_6) δ 8.65 (s, 1H, Pyr), 8.02 – 7.95 (m, 1H, Ar), 7.89 (s, 1H), 7.62 – 7.56 (m, 1H, Ar), 7.47 – 7.31 (m, 6H, Ar), 6.62 (s, 1H, Pyr), 5.54 (d, J = 7.0 Hz, 1H, CH). **^{13}C NMR** (126 MHz, DMSO-d_6) δ 171.60, 163.22, 142.98, 137.44, 133.34, 133.04, 133.02, 129.02, 128.74, 128.10, 127.65, 127.27, 56.52, 39.52. **FT-IR** ν_{max} (film) 3732, 3392, 3183, 1717, 1639, 1555 cm^{-1}. **HRMS (**ESI-TOF) calcd for $C_{17}H_{13}O_4N_4$ $[M+H]^+$: 337.0942, found : 337.0941.

(*S*)-2-(4-hydroxy-6-(1H-pyrazol-1-yl)nicotinamido)-2-phenylacetic acid 124

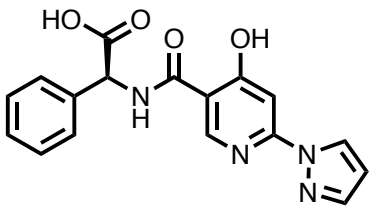

Following general procedure G: **116** (20 mg, 0.056 mmol) and LiCl (24 mg, 0.56 mmol) in DMAc (2 ml) using HPLC purification gave **124** (2 mg, 0.0059 mmol, 11%) as a yellow oil.

^{1}H NMR (500 MHz, DMSO-d_6) δ 13.20 (s, 2H, OH & COOH), 8.66 (s, 1H, Pyr), 7.98 (dd, J = 2.5, 1.5 Hz, 1H, Pyzl), 7.90 (s, 1H, Pyr), 7.63 – 7.58 (m, 1H, Ar), 7.48 – 7.32 (m, 5H, Ar), 6.65 – 6.60 (m, 1H, Pyzl), 5.55 (d, J = 7.0 Hz, 1H, CH). **^{13}C NMR** (126 MHz, DMSO-d_6) δ 172.07, 163.69, 143.45, 137.90, 133.91, 133.48, 129.47, 129.21, 128.56, 128.18, 128.12, 127.74, 56.98, 39.99. **FT-IR** ν_{max} (film) 3692, 3206, 1714, 1639, 1580 cm^{-1}.

HRMS (ESI-TOF) calcd for $C_{17}H_{13}O_4N_4$ $[M+H]^+$: 337.0942, found : 337.0941.

([1,1'-biphenyl]-4-ylmethyl)-6-chloro-5-methoxynicotinamide 125

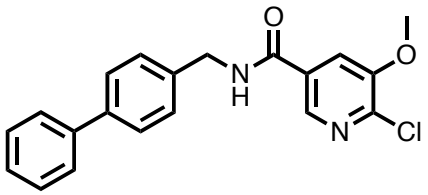

Following general procedure C: 6-chloro-5-methoxy-nicotinic acid (850 mg, 4.55 mmol), 4-phenylbenzyl amine (1g, 5.46 mmol), T3P (4.32 g, 13.6 mmol) and DIPEA (2.2 ml, 6.68 mmol) gave **125** (502 mg, 1.42 mmol, 31 %) as a colourless oil.

^{1}H NMR (400 MHz, DMSO-d_6) δ 9.32 (t, J = 6.0 Hz, 1H, NH), 8.50 (d, J = 2.0 Hz, 1H, Pyr), 7.96 (d, J = 2.0 Hz, 1H, Pyr), 7.74 – 7.31 (m, 9H, Ar), 4.56 (d, J = 6.0 Hz, 2H, CH_2), 3.96 (s, 3H, CH_3). **^{13}C NMR** (101 MHz, DMSO-d_6) δ 165.55, 150.90, 140.95, 139.92,

139.17, 138.92, 138.31, 130.38, 128.90, 128.04, 127.33, 126.68, 120.10, 118.90, 56.51, 42.54. **FT-IR** ν_{max} (film) 3359, 1639, 1574 cm^{-1}. **HRMS (**ESI-TOF) calcd for $C_{20}H_{18}O_2N_2{}^{35}Cl$ $[M+H]^+$: 353.1051, found : 353.1049.

([1,1'-biphenyl]-4-ylmethyl)-5-methoxy-6-(1H-pyrazol-1-yl)nicotinamide 126

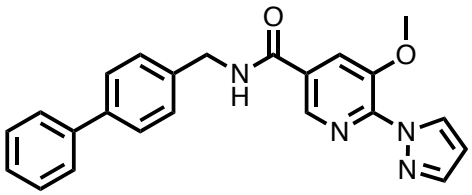

Following general procedure D: **125** (100 mg, 0.284 mmol), Pd^{t}BuXPhos G3 (22 mg, 0.0284 mmol), Cs_2CO_3 (279 mg, 0.852 mmol), pyrazole (38 mg, 0.568 mmol) and ^{t}BuOH (2 ml) gave **126** (23 mg, 0.0598 mmol, 20%) as a colourless oil.

^{1}H NMR (400 MHz, Chloroform-*d*) δ 8.46 (d, J = 2.0 Hz, 1H, Pyr), 8.30 (dd, J = 2.5, 1.0 Hz, 1H, Pyzl), 7.97 (d, J = 2.0 Hz, 1H, Pyr), 7.76 (dd, J = 1.5, 1.0 Hz, 1H, Pyzl), 7.64 – 7.32 (m, 9H, Ar), 6.46 (dd, J = 2.5, 1.5 Hz, 1H, Pyzl), 4.67 (d, J = 6.0 Hz, 2H, CH_2), 3.93 (s, 3H, CH_3). **^{13}C NMR** (101 MHz, Chloroform-*d*) δ 164.84, 146.84, 142.83, 142.02, 140.69, 137.62, 136.95, 131.54, 129.67, 128.94, 128.55, 127.57, 127.53, 127.17, 120.60, 107.51, 77.16, 56.51, 44.07. **FT-IR** ν_{max} (film) 3339, 1641, 1582 cm^{-1}. **HRMS (**ESI-TOF) calcd for $C_{23}H_{21}O_2N_4$ $[M+H]^+$: 385.1659, found : 385.1661.

N-([1,1'-biphenyl]-3-ylmethyl)-5-methoxy-6-(1H-pyrazol-1-yl)nicotinamide 127

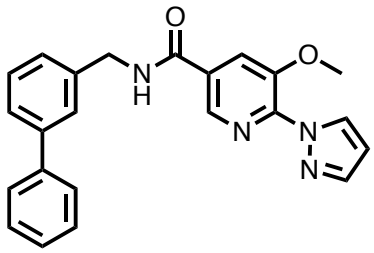

Following general procedure C: 6-chloro-5-methoxy-nicotinic acid (250 mg, 1.33 mmol), 3-phenylbenzyl amine (285 mg, 1.56 mmol), T3P (1.08 g, 3.4 mmol) and DIPEA (414 mg, 3,34 mmol) gave [*N*-([1,1'-biphenyl]-3-ylmethyl)-6-chloro-5-methoxynicotinamide. Reacted on without purification and following general procedure D: *N*-([1,1'-biphenyl]-3-ylmethyl)-6-chloro-5-methoxynicotinamide (100 mg, 0.284 mmol), Pd^{t}BuXPhos G3 (20 mg, 0.028 mmol), Cs_2CO_3 (185 mg, 0.568 mmol), pyrazole (23 mg, 0.34 mmol) gave **127** (54 mg, 0.14 mmol, 49 %) with the appearance of a clear oil.

^{1}H NMR (400 MHz, DMSO-d_6) δ 9.37 (t, J = 6.0 Hz, 1H, NH), 8.62 (d, J = 2.0 Hz, 1H, Pyr), 8.28 (dd, J = 2.5, 1.0 Hz, 1H, Pyzl), 8.10 (d, J = 2.0 Hz, 1H, Pyr), 7.77 (t, J = 1.5, 1.0 Hz, 1H, Pyzl), 7.69 – 7.32 (m, 9H, Ar), 6.53 (dd, J = 2.5, 1.5 Hz, 1H, Pyzl), 4.62 (d, J = 6.0 Hz, 2H, CH_2), 3.94 (s, 3H, CH_3). **^{13}C NMR** (126 MHz, DMSO-d_6) δ 169.15, 146.80, 141.93, 140.58, 139.84, 139.65, 137.97, 130.99, 129.55, 128.60, 128.51, 127.05, 126.22, 126.07, 125.45, 124.91, 119.98, 106.43, 55.96, 42.40, 39.52. **FT-IR** ν_{max} (film) 3363, 1641, 1579 cm^{-1}. **HRMS (**ESI-TOF) calcd for $C_{23}H_{21}O_2N_4[M+H]^+$: 385.1659, found: 385.1661.

N-([1,1'-biphenyl]-4-ylmethyl)-5-hydroxy-6-(1H-pyrazol-1-yl)nicotinamide 128

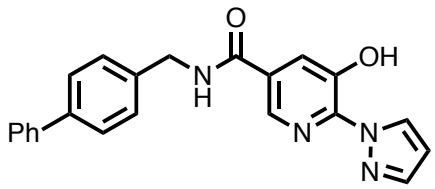

Following general procedure G: **126** (12 mg, 0.031 mmol) and LiCl (19 mg, 0.31 mmol) in DMAc (2 ml) gave **128** (4 mg, 0.01 mmol, 35%) as a colourless oil.

^{1}H NMR (500 MHz, DMSO-d_6) δ 11.68 (s, 1H, OH), 9.28 (t, J = 6.0 Hz, 1H, NH), 8.76 (d, J = 2.5 Hz, 1H, Pyzl), 8.52 (d, J = 2.0 Hz, 1H, Pyr), 7.96 (d, J = 2.0 Hz, 1H, Pyr), 7.72 – 7.60 (m, 4H, Ar), 7.48 – 7.41 (m, 4H, Ar), 7.39 – 7.30 (m, 1H, Ar), 6.74 – 6.72 (m, 1H, Pyzl), 4.55 (d, J = 6.0 Hz, 2H, CH_2). **^{13}C NMR** (126 MHz, DMSO-d_6) δ 163.75, 143.55, 140.88, 139.95, 138.48, 137.81, 129.45, 128.93, 128.70, 127.97, 127.35, 126.68, 126.59, 124.96, 107.83, 42.43. **FT-IR** ν_{max} (film) 3569, 3176, 1641, 1585 cm^{-1}. **HRMS** (ESI-TOF) calcd for $C_{22}H_{19}O_2N_4$ $[M+H]^+$: 371.1502, found : 371.1503.

N-([1,1'-biphenyl]-3-ylmethyl)-5-hydroxy-6-(1H-pyrazol-1-yl)nicotinamide 129

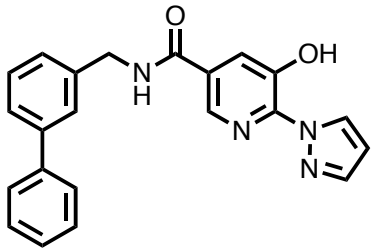

Following general procedure G: **127** (45 mg, 0.117 mmol) and LiCl (71 mg, 1.17 mmol) in DMAc (3.5 ml) gave **129** (14 mg, 0.037 mmol, 32%) as a colourless oil.

^{1}H NMR (400 MHz,DMSO-d_6) δ 11.68 (s, 1H, OH), 9.28 (t, J = 6.0 Hz, 1H, NH), 8.76 (d, J = 2.5 Hz, 1H, Pyzl), 8.52 (d, J = 2.0 Hz, 1H, Pyr), 7.97 (d, J = 2.0 Hz, 1H, Pyr), 7.71 – 7.32 (m, 10H, Ar), 6.75 – 6.71 (m, 1H, Pyzl), 4.59 (d, J = 6.0 Hz, 2H, CH_2). **^{13}C NMR** (101 MHz, DMSO-d_6) δ 163.79, 143.55, 140.27, 140.14, 139.91, 137.82, 128.97, 128.69, 127.50, 126.69, 126.50, 125.94, 125.88, 125.38, 125.33, 124.98, 120.44, 107.83, 42.80, 39.52. **FT-IR** ν_{max} (film) 3553, 3192, 1641, 1577 cm^{-1}. **HRMS (**ESI-TOF) calcd for $C_{22}H_{19}O_2N_4$ $[M+H]^+$: 371.1502, found : 371.1502.

Ethyl 1-(5-(([1,1'-biphenyl]-4-ylmethyl)carbamoyl)-4-methoxypyridin-2-yl)-1H-pyrazole-4-carboxylate 130

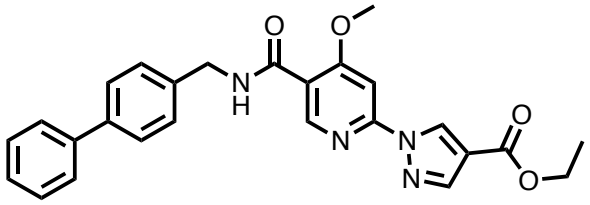

Following general procedure D: **86** (150 mg, 0.43 mmol), Pd^{t}BuXPhos G3 (34 mg, 0.043 mmol), Cs_2CO_3 (354 mg, 1.09 mmol), pyrazole-4-carboxylate ethyl ester (89 mg, 0.649 mmol) and ^{t}BuOH (2 ml) gave **130** (93 mg, 0.20 mmol, 48 %) as a colourless oil.

^{1}H NMR (400 MHz, DMSO-d_6) δ 9.37 (s, 1H, Pyr), 8.24 (s, 1H, Pyr), 7.69 – 7.62 (m, 4H, Ar), 7.54 – 7.29 (m, 6H, Ar), 4.59 (d, J = 6.0 Hz, 2H, $\underline{CH_2}$NH), 4.28 (q, J = 7.0 Hz, 2H, $\underline{CH_2}CH_3$), 4.09 (s, 3H, O$\underline{CH_3}$), 1.31 (t, J = 7.0 Hz, 3H, $\underline{CH_3}$). **^{13}C NMR** (126 MHz, DMSO-d_6) δ 165.64, 163.29, 163.03, 162.07, 150.71, 143.38, 140.25, 139.27, 138.42,

129.27, 128.31, 128.11, 127.71, 126.94, 96.18, 60.61, 57.06, 42.52, 14.55. **FT-IR** ν_{max} (film) 3421, 1738, 1641, 1557 cm^{-1}. **HRMS (**ESI-TOF) calcd for $C_{26}H_{25}O_4N_4$ $[M+H]^+$: 457.1870, found : 457.1876.

N-([1,1'-biphenyl]-4-ylmethyl)-6-(4-cyano-1H-pyrazol-1-yl)-4-methoxynicotinamide 131

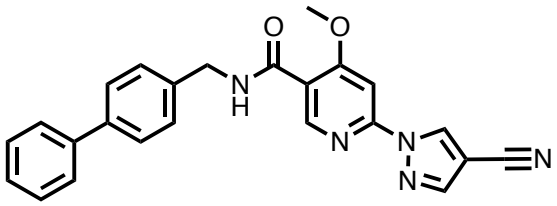

Following general procedure D: **86** (150 mg, 0.426 mmol), Pd^{t}BuXPhos G3 (16 mg, 0.0213 mmol), Cs_2CO_3 (276 mg, 0.852 mmol), pyrazole-4-nitrile (47 mg, 0.511 mmol) and ^{t}BuOH (4 ml) gave **131** (9 mg, 0.022 mmol, 5%) as a orange solid.

m.p. 236-240°C. **^{1}H NMR** (400 MHz, DMSO-d_6) δ 9.47 (d, J =.0 1 Hz, 1H, Pyr), 8.87 (t, J = 6.0 Hz, 1H, NH), 8.66 (s, 1H, Pyzl), 8.48 (d, J = 1.0 Hz, 1H, Pyr), 7.70 – 7.31 (m, 10H, Ar), 4.55 (d, J = 6.0 Hz, 2H, CH_2), 4.09 (s, 3H, CH_3). **^{13}C NMR** (126 MHz, DMSO-d_6) δ 165.36, 162.89, 152.35, 150.21, 144.65, 139.97, 138.57, 134.29, 128.93, 127.78, 127.33, 126.58, 119.50, 113.29, 96.30, 94.28, 56.78, 42.37, 39.52. **FT-IR** ν_{max} (film) 3421, 2360, 1653, 1592 cm^{-1}. **HRMS (**ESI-TOF) calcd for $C_{24}H_{18}O_2N_5$ $[M-H]^-$: 408.1466, found : 408.1467.

Ethyl 1-(5-(([1,1'-biphenyl]-4-ylmethyl)carbamoyl)-3-methoxypyridin-2-yl)-1H-pyrazole-4-carboxylate 132

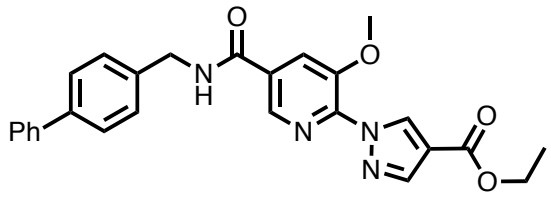

Following general procedure D: **125** (150 mg, 0.43 mmol), Pd^{t}BuXPhos G3 (34 mg, 0.043 mmol), Cs_2CO_3 (354 mg, 1.09 mmol), pyrazole-4-carboxylate ethyl ester (89 mg, 0.649 mmol) and ^{t}BuOH (4 ml) gave **132** (44 mg, 0.096 mmol, 23 %) as a colourless oil.

^{1}H NMR (400 MHz, DMSO-d_6) δ 9.41 (d, J = 6.0 Hz, 1H, NH), 8.78 – 8.75 (m, 1H, Pyzl), 8.64 (d, J = 2.5 Hz, 1H, Pyr), 8.15 (d, J = 2.5 Hz, 2H, Pyr), 7.67 – 7.61 (m, 5H, Ar), 7.53 – 7.42 (m, 4H, Ar), 7.39 – 7.34 (m, 1H, Pyzl), 4.59 (d, J = 6.0 Hz, 2H, $\underline{CH_2}$NH), 4.27 (q, J = 7.0 Hz, 2H, $\underline{CH_2}CH_3$), 4.00 – 3.94 (s, 3H, O$\underline{CH_3}$), 1.30 (t, J = 7.0 Hz, 3H, $CH_2\underline{CH_3}$). **^{13}C NMR** (126 MHz, DMSO-d_6) δ 163.73, 162.04, 147.86, 141.50, 139.93, 138.92, 138.52, 138.34, 135.02, 131.20, 128.94, 128.03, 127.37, 126.72, 126.60, 120.69, 115.35, 60.06, 56.61, 42.55, 14.30. **FT-IR** ν_{max} (film) 3416, 1741, 1639, 1576 cm^{-1}. **HRMS (**ESI-TOF) calcd for $C_{26}H_{25}O_4N_4$ $[M+H]^+$: 457.1870, found : 457.1874.

Ethyl 1-(4-methoxy-5-((4-(trifluoromethyl)benzyl)carbamoyl)pyridin-2-yl)-1H-pyrazole-4-carboxylate 133

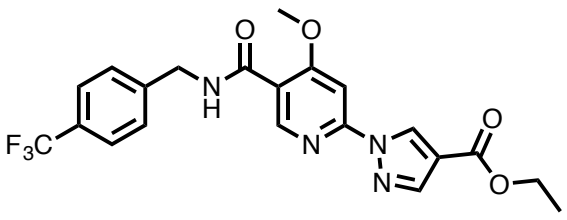

Following general procedure D: **98** (100 mg, 0.29 mmol), RockPhos Pd G3 (20 mg, 0.029 mmol), Cs_2CO_3 (188 mg, 0.58 mmol), 4-ethyl ester pyrazole (24 mg, 0.63 mmol) and ^{t}BuOH (4 ml) gave **133** (86 mg, 0.192 mmol, 66 %) as a colourless oil.

^{1}H NMR (400 MHz, Chloroform-*d*) δ 9.12 (s, 1H, Pyzl), 9.07 (d, *J* = 1.0 Hz, 1H, Pyr), 8.11 (d, *J* = 1.0 Hz, 1H, Pyr), 7.89 (t, *J* = 6.0 Hz, 1H, NH), 7.63 (s, 1H, Pyzl), 7.62 – 7.58 (m, 2H, Ar), 7.50 – 7.45 (m, 2H, Ar), 4.73 (d, *J* = 6.0 Hz, 2H, CH_2NH), 4.35 (q, *J* = 7.0 Hz, 2H, $\underline{CH_2}CH_3$), 4.11 (s, 3H, O$\underline{CH_3}$), 1.37 (t, *J* = 7.0 Hz, 3H, $CH_2\underline{CH_3}$). **^{13}C NMR** (101 MHz, Chloroform-*d*) δ 165.47, 163.56, 162.65, 154.33, 153.58, 143.54, 142.54, 131.04, 127.90, 125.79, 117.70, 115.98, 95.41, 77.16, 60.77, 56.95, 43.40, 14.48. **FT-IR** ν_{max} (film) 3402, 1736, 1641, 1582 cm^{-1}. **HRMS (**ESI-TOF) calcd for $C_{21}H_{18}O_4N_4F_3$ $[M+H]^+$: 447.1285, found : 447.1281.

6-(4-cyano-1H-pyrazol-1-yl)-4-methoxy-N-(4-(trifluoromethyl)benzyl)nicotinamide 134

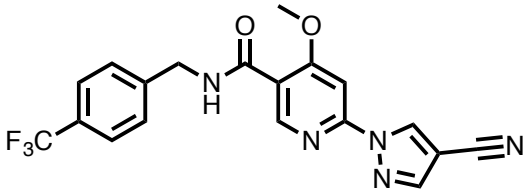

Following general procedure D: **98** (100 mg, 0.29 mmol), RockPhos Pd G3 (24 mg, 0.029 mmol), Cs_2CO_3 (180 mg, 0.554 mmol), pyrazole-4-nitrile (24 mg, 0.35 mmol) and ^{t}BuOH (4 ml) gave X (23 mg, 0.057 mmol, 20 %) as a white solid.

m.p. 189-197°C. **^{1}H NMR** (400 MHz, Chloroform-*d*) δ 9.13 (s, 1H), 9.04 (d, *J* = 1.0 Hz, 1H), 7.99 (d, *J* = 1.0 Hz, 1H), 7.88 (t, *J* = 6.0 Hz, 1H, NH), 7.67 – 7.56 (m, 3H, Ar), 7.51 – 7.42 (m, 2H, Ar), 4.74 (d, *J* = 6.0 Hz, 2H, $\underline{CH_2}$NH), 4.03 (s, 3H, $\underline{CH_3}$). **^{13}C NMR** (101 MHz, Chloroform-*d*) δ 165.29, 164.15, 162.98, 153.80, 153.37, 153.22, 143.84, 132.80, 127.60, 125.50, 116.29, 106.71, 95.39, 95.10, 77.16, 56.57, 43.10. **FT-IR** ν_{max} (film) 3405, 2360, 1651, 1592 cm^{-1}. **HRMS (**ESI-TOF) calcd for $C_{18}H_{12}O_4N_4F_3$ $[M+H]^+$: 402.1172, found : 402.1172.

ethyl 1-(4-methoxy-5-(((6-phenylpyridin-3-yl)methyl)carbamoyl)pyridin-2-yl)-1H-pyrazole-4-carboxylate 135

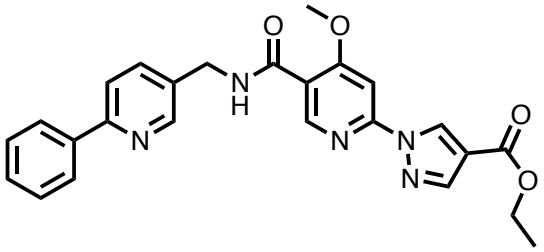

Following general procedure D: **106** (80 mg, 0.226 mmol), RockPhosPd G3 (19 mg, 0.0226 mmol), Cs_2CO_3 (145 mg, 0.452 mmol), 4-ethyl ester pyrazole (31 mg, 0.226 mmol) and ^{t}BuOH (2.5 ml) gave **135** (11 mg, 0.024 mmol, 11 %) as a colourless oil.

^{1}H NMR (400 MHz, Chloroform-*d*) δ 9.13 (s, 1H), 9.08 (s, 1H), 8.70 – 8.68 (m, 1H), 8.12 (s, 1H), 8.01 – 7.94 (m, 2H, Ar), 7.90 (t, *J* = 6.0 Hz, 1H, NH), 7.84 – 7.37 (m, 6H, Are), 4.73 (d, *J* = 6.0 Hz, 2H, $\underline{CH_2}NH$), 4.32 (q, *J* = 7.0 Hz, 2H, $\underline{CH_2}CH_3$), 4.11 (s, 3H, OCH_3), 1.37 (t, *J* = 7.0 Hz, 3H, $CH_2\underline{CH_3}$). **^{13}C NMR** (101 MHz, Chloroform-*d*) δ 165.78, 163.89, 162.99, 157.26, 154.62, 153.87, 149.37, 143.85, 139.37, 136.98, 132.77, 131.37, 129.50, 129.24, 127.30, 120.97, 117.98, 116.30, 95.73, 77.16, 61.09, 57.29, 41.52, 14.81. **FT-IR** ν_{max} (film) 3421, 1738, 1641, 1557 cm^{-1}. **HRMS** (ESI-TOF) calcd for $C_{25}H_{24}O_4N_5[M+H]^+$: 458.1822, found : 458.1816.

Ethyl 1-(5-(([1,1'-biphenyl]-4-ylmethyl)carbamoyl)-4-hydroxypyridin-2-yl)-1H-pyrazole-4-carboxylate 136

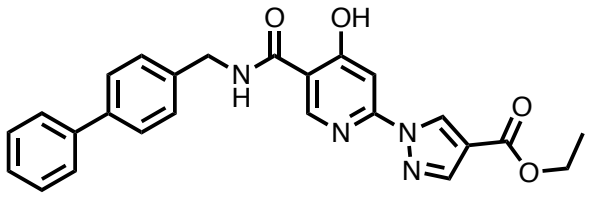

Following general procedure G: **130** (82 mg, 0.179 mmol) and LiCl (mg, 1.79 mmol) in DMAc (35 ml) gave **136** (70 mg, 0.158 mmol, 90 %) as a colourless oil.

^{1}H NMR (400 MHz, DMSO-d_6) δ 9.42 (s, 1H), 9.00 (s, 1H), 8.85 (s, 1H), 8.24 (s, 1H), 7.72 – 7.58 (m, 4H, Ar), 7.54 – 7.39 (m, 5H, Ar), 7.38 – 7.29 (m, 1H, Ar), 4.59 (d, J = 6.0 Hz, 2H, $\underline{CH_2}NH$), 4.27 (q, J = 7.0 Hz, 2H, $\underline{CH_2}CH_3$), 1.30 (t, J = 7.0 Hz, 3H, $CH_2\underline{CH_3}$). **^{13}C NMR** (101 MHz, DMSO-d_6) δ 165.61, 161.70, 143.02, 139.90, 138.93, 138.04, 130.43,

128.90, 127.96, 127.35, 126.72, 126.58, 116.75, 60.25, 42.18, 14.19. **FT-IR** ν_{max} (film) , 3693, 3372, 1743, 1639, 1590 cm^{-1}. **HRMS** (ESI-TOF) calcd for $C_{25}H_{23}O_4N_4[M+H]^+$: 443.1713, found : 443.1713.

N-([1,1'-biphenyl]-4-ylmethyl)-6-(4-cyano-1H-pyrazol-1-yl)-4-hydroxynicotinamide 137

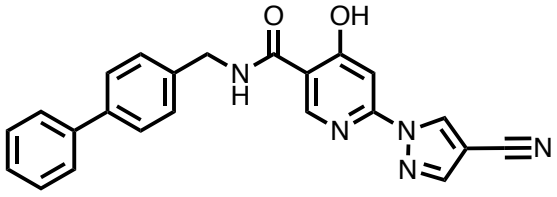

131 (6 mg, 0.0146 mmol) was dissolved in DMAc (1.5 ml) in a microwave vial, before the addition of Cs_2CO_3 (14.3 mg, 0.044 mmol). The resultant reaction mixture was heated under microwave radiation at 130°C for 1hr. Water (5 ml) was added and the resultant mixture was extracted with EtOAc (3 x 15 ml). The combined organic fractions were washed with brine, dried over Na_2SO_4 and the solvents were removed in *vacuo*. The crude compound was then purified using flash column chromatography using (CH_2Cl_2: MeOH 0 - 10%) over 10 column volumes to give **137** (2.5 mg, 0.006 mmol, 44 %) as a white solid. **m.p.** 220°C (decomp). **^{1}H NMR** (400 MHz, DMSO-d_6) δ 9.45 (s, 1H, Pyr), 8.87 (d, J = 2.0 Hz, 1H, Pyzl), 8.44 (s, 1H, Pyr), 7.73 – 7.42 (m, 11H, Ar), 4.60 (d, J = 6.0 Hz, 2H, CH_2). **^{13}C NMR** (126 MHz, DMSO-d_6) δ 165.15, 149.16, 144.40, 139.58, 138.61, 137.72, 133.98,

128.60, 127.93, 127.64, 127.05, 126.67, 126.27, 114.19, 112.96, 99.81, 93.84, 41.89, 39.52. **FT-IR** ν_{max} (film) 3634, 3405, 2360, 1642, 1562 cm^{-1}. **HRMS (**ESI-TOF) calcd for $C_{23}H_{16}O_2N_5$ $[M-H]^-$: 394.1309, found : 394.1309.

1-(5-(([1,1'-biphenyl]-4-ylmethyl)carbamoyl)-3-hydroxypyridin-2-yl)-1H-pyrazole-4-carboxylic acid 138

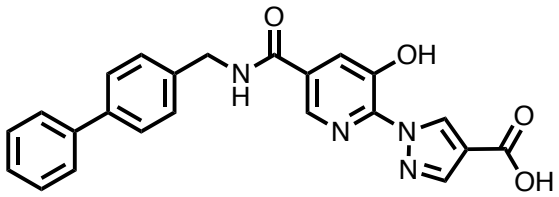

132 (20 mg, 0.043 mmol) was dissolved in THF (2 ml), MeOH (2 ml) and water (0.5 ml) was added to the reaction mixture before the addition of LiOH-monohydrate (16 mg, 0.40 mmol). The resultant mixture was stirred overnight at room temperature. The reaction mixture was acidified to PH3 with HCl_{aq} (1M) solution and extracted with EtOAc (3 x 25 ml), washed with brine dried with anhydrous Na_2SO_4. The crude compound was then purified using flash column chromatography using (CH_2Cl_2: MeOH 0 - 20%: Formic acid 1%) over 20 column volumes to gave **138** (8 mg, 0.019 mmol, 45%) with the appearance of a white solid.

m.p. 230(decomp)°C. **^{1}H NMR** (400 MHz, DMSO-d_6) δ 9.09 (s, 1H), 8.90 (d, J = 6.0 Hz, 1H, NH), 7.92 – 7.09 (m, 12H, Ar), 4.47 (d, J = 6.0 Hz, 2H, CH_2). **^{13}C NMR** (126 MHz,

DMSO-d_6) δ 174.38, 167.31, 166.89, 165.81, 142.33, 140.27, 139.75, 138.90, 138.31, 131.40, 129.26, 128.63, 127.53, 126.99, 126.35, 126.29, 124.91, 123.36, 123.24, 41.88, 39.52. **FT-IR** ν_{max} (film) 3624, 3273, 1710, 1651, 1592 cm^{-1}. **HRMS (**ESI-TOF) calcd for $C_{23}H_{17}O_4N_4$ [M-H]$^-$: 413.1255, found : 413.1252.

Ethyl 1-(4-hydroxy-5-((4-(trifluoromethyl)benzyl)carbamoyl)pyridin-2-yl)-1H-pyrazole-4-carboxylate 139

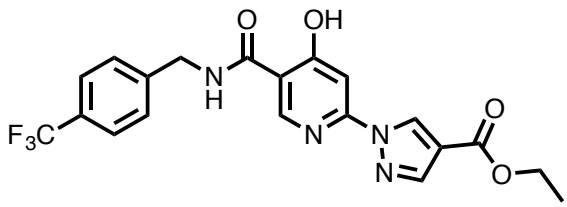

Following general procedure G: **133** (68 mg, 0.151 mmol) and LiCl (91 mg, 1.51 mmol) in DMAc (3.5 ml) gave **139** (48 mg, 0.110 mmol, 73 %) as a white solid.

m.p. >250°C. **^{1}H NMR** (400 MHz, THF-d_8) δ 13.46 (s, 1H, OH), 8.99 (d, J = 1.0 Hz, 1H, Pyzl), 8.93 – 8.85 (m, 1H), 8.74 (s, 1H, Pyr), 8.07 (d, J = 1.0 Hz, 1H, Pyzl), 7.65 (d, J = 7.0 Hz, 2H, Ar), 7.58 (d, J = 7.0 Hz, 2H, Ar), 7.48 (s, 1H, Pyr), 4.71 (d, J = 6.0 Hz, 2H, $\underline{CH_2}$NH), 4.29 (q, J = 7.0 Hz, 2H, $\underline{CH_2}CH_3$), 1.33 (t, J = 7.0 Hz, 3H, $CH_2\underline{CH_3}$). **^{13}C NMR** (101 MHz, THF-d_8) δ 170.78, 169.67, 162.59, 149.25, 143.86, 131.08, 129.16, 126.34, 126.30, 126.26, 126.23, 101.23, 60.89, 43.48, 25.37, 14.72. **FT-IR** ν_{max} (film) 3600, 3321, 1743, 1641, 1576 cm^{-1}. **HRMS (**ESI-TOF) calcd for $C_{20}H_{16}O_4N_4F_3$ [M+H]$^+$: 433.1129, found : 433.1125.

6-(4-cyano-1H-pyrazol-1-yl)-4-hydroxy-N-(4-(trifluoromethyl)benzyl)nicotinamide 140

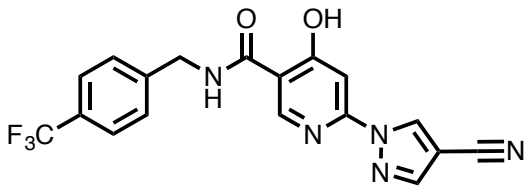

Following general procedure G: **134** (20 mg, 0.049 mmol) and LiCl (30 mg, 0.50 mmol) in DMAc (2 ml) gave **140** (5 mg, 0.012 mmol, 26%) as a white solid.

m.p. 220-225°C. **^{1}H NMR** (400 MHz, DMSO-d_6) δ 9.43 (d, J = 1.0 Hz, 1H, Pyzl), 8.81 (s, 1H, Pyr), 8.43 (d, J = 1.0 Hz, 1H, Pyzl), 7.71 (d, J = 8.0 Hz, 2H, Ar), 7.57 (d, J = 8.0 Hz, 2H, Ar), 7.42 (s, 1H, Pyr), 4.63 (d, J = 6.0 Hz, 2H, $\underline{CH_2}$NH). **^{13}C NMR (**126 MHz, DMSO-d_6) δ 169.07, 164.93, 149.73, 144.18, 143.43, 133.75, 127.43, 126.94, 124.71, 122.75, 99.97, 93.59, 41.64, 39.52. **FT-IR** ν_{max} (film) 3649, 2360, 1650, 1586 cm^{-1}. **HRMS (**ESI-TOF) calcd for $C_{18}H_{12}O_4N_4F_3$ $[M-H]^-$: 386.0870, found : 386.0867.

Ethyl 1-(4-hydroxy-5-(((6-phenylpyridin-3-yl)methyl)carbamoyl)pyridin-2-yl)-1H-pyrazole-4-carboxylate 141

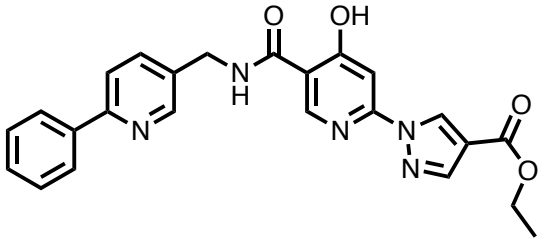

Following general procedure G :**135** (7 mg, 0.015 mmol) and LiCl (9 mg, 0.15 mmol) in DMAc (2 ml) gave **141** (3.5 mg, 0.0079 mmol, 53 %) as a colourless oil..

^{1}H NMR (400 MHz, DMSO-d_6) δ 9.00 (s, 1H, PyrOH), 8.80 (s, 1H), 8.67 (d, J = 2.0 Hz, 1H), 8.24 (s, 1H, PyrOH), 8.07 (dd, J = 8.0, 2.0 Hz, 2H, Pyr), 7.95 (d, J = 8.0 Hz, 1H, Pyr), 7.85 (dd, J = 8.0, 2.0 Hz, 1H, Pyr), 7.54 – 7.39 (m, 5H, Ar), 4.61 (d, J = 6.0 Hz, 2H, $\underline{CH_2}NH$), 4.26 (q, J = 7.0 Hz, 2H, $\underline{CH_2}CH_3$), 1.30 (t, J = 7.0 Hz, 3H, $CH_2\underline{CH_3}$). **^{13}C NMR** (126 MHz, DMSO-d_6) δ 167.64, 165.57, 161.77, 154.86, 148.87, 143.02, 138.49, 136.43, 133.33, 130.45, 128.98, 128.78, 126.46, 119.97, 116.73, 114.48, 100.27, 60.29, 40.11, 39.52, 14.23. **FT-IR** ν_{max} (film) 3649, 3330, 1741, 1639, 1556 cm^{-1}. **HRMS** (ESI-TOF) calcd for $C_{24}H_{22}O_4N_5[M+H]^+$: 444.1666, found : 444.1659.

1-(5-(([1,1'-biphenyl]-4-ylmethyl)carbamoyl)-4-hydroxypyridin-2-yl)-1H-pyrazole-4-carboxylic acid 142

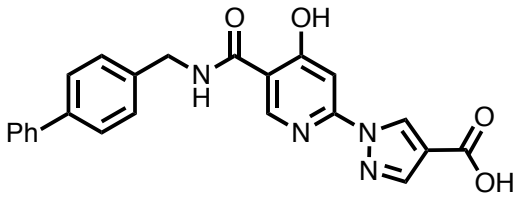

136 (65 mg, 0.147 mmol) was dissolved in THF (5 ml) and water (0.5 ml) was added to the reaction mixture before the addition of LiOH-monohydrate (16 mg, 0.40 mmol). The resultant mixture was stirred overnight at room temperature. The reaction mixture was acidified to PH 3 with HCL_{aq} (1M) and extracted with EtOAc (3 x 25 ml), washed with brine dried with anhydrous Na_2SO_4. The crude compound was then purified using flash

column chromatography using (CH_2Cl_2 : MeOH 0 - 20%: Formic Acid 1%) over 20 columns volumes gave **143** (52 mg, 0.125 mmol, 85 %) as an off-white solid.

m.p. 200(decomp)°C. **^{1}H NMR** (400 MHz, DMSO-d_6) δ 13.34 (s, 1H, OH), 8.96 (s, 1H, Pyr), 8.19 (s, 1H, Pyr), 7.71 – 7.31 (m, 11H, Ar), 4.59 (d, J = 6.0 Hz, 2H, $\underline{CH_2}$NH). **^{13}C NMR** (101 MHz, DMSO-d_6) δ 163.19, 143.35, 139.91, 138.93, 138.08, 128.91, 127.95, 127.35, 126.73, 126.59, 88.95, 42.16. **FT-IR** ν_{max} (film) 3600, 3390, 1714, 1650, 1571 cm^{-1}.

HRMS (ESI-TOF) calcd for $C_{23}H_{19}O_4N_4[M+H]^+$: 415.1400, found : 415.1401.

1-(4-hydroxy-5-((4-(trifluoromethyl)benzyl)carbamoyl)pyridin-2-yl)-1H-pyrazole-4-carboxylic acid 143

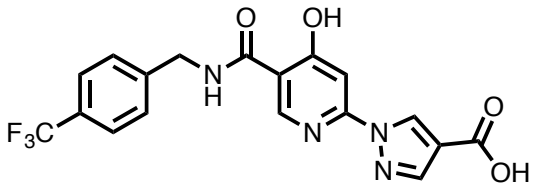

139 (40 mg, 0.092 mmol) was dissolved in THF (2 ml), MeOH (2 ml) and water (0.5 ml) was added to the reaction mixture before the addition of LiOH-monohydrate (19 mg, 0.46 mmol). The resultant mixture was stirred overnight at room temperature. The reaction mixture was acidified to PH 3 with HCL_{aq} (1M) and extracted with EtOAc (3 x 25 ml), washed with brine, dried with anhydrous Na_2SO_4. The crude compound was then purified using flash column chromatography using (CH_2Cl_2: MeOH 0 - 20%: Formic acid 1%) over 20 column volumes gave **143** (17 mg, 0.042 mmol, 46 %) as a yellow oil.

^{1}H NMR (400 MHz, DMSO-d_6) δ 9.56 (s, 1H, OH), 8.94 (s, 1H, Pyr), 8.78 (s, 1H), 8.17 (s, 1H, Pyr), 7.70 (d, *J* = 8.0 Hz, 2H, Ar), 7.56 (d, *J* = 8.0 Hz, 2H, Ar), 7.38 (s, 1H), 4.63 (d, *J* = 6.0 Hz, 2H, $\underline{CH_2}$NH). **^{13}C NMR** (101 MHz, DMSO-d_6) δ 165.62, 163.30, 144.04, 143.34, 130.41, 127.97, 127.45, 125.32, 125.28, 117.72, 99.58, 42.12, 39.52. **FT-IR** ν_{max} (film) 3736, 3339, 1712, 1640, 1550 cm^{-1}. **HRMS (**ESI-TOF) calcd for $C_{18}H_{12}O_4N_4F_3$ $[M+H]^+$: 405.0816, found : 405.0815.

1-(4-hydroxy-5-(((6-phenylpyridin-3-yl)methyl)carbamoyl)pyridin-2-yl)-1H-pyrazole-4-carboxylic acid 144

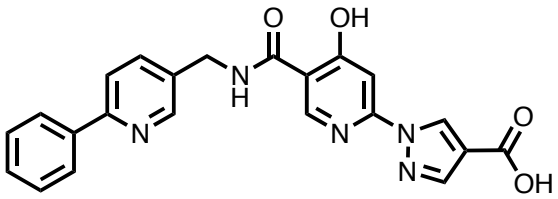

141 (3 mg, 0.0072 mmol) was dissolved in THF (0.8 ml), MeOH (0.15 ml) and water (0.05 ml) was added to the reaction mixture before the addition of LiOH-monohydrate (1 mg, 0.023 mmol). The resultant mixture was stirred overnight at room temperature. The reaction mixture was acidified to PH3 with HCL_{aq} (1M) and was using preparative HPLC to give **144** (1 mg, 0.0024 mmol, 33%) as a TFA salt.

^{1}H NMR (500 MHz, DMSO-d_6) δ 8.94 (s, 1H, Pyr), 8.68 (s, 1H), 8.19 (s, 1H, Pyr), 8.13 – 8.05 (m, 2H), 7.96 (d, *J* = 8.5 Hz, 1H), 7.87 (d, *J* = 8.5 Hz, 1H), 7.55 – 7.39 (m, 6H, Ar), 4.62 (d, *J* = 6.0 Hz, 2H, $\underline{CH_2}$NH). Not enough for **^{13}C**. **FT-IR** ν_{max} (film) 3600, 3390, 1714,

1650, 1571 cm^{-1}. **HRMS** (ESI-TOF) calcd for $C_{22}H_{18}O_4N_5[M+H]^+$: 416.1353, found : 416.1352.

N-benzyl-6-chloronicotinamide 145

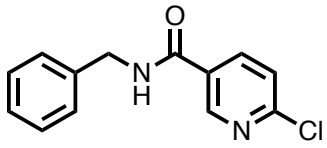

Following general procedure B: 2-chloro-ethylnicotinate (200 mg, 1.081 mmol), benzylamine (116 mg, 1.08 mmol) and DABACO-$AlMe_3$ (221 mg, 0.864 mmol) gave **145** (220 mg, 0.897 mmol, 83 %) as a colourless oil.

^{1}H NMR (400 MHz, DMSO-d_6) δ 9.32 (t, J = 6.0 Hz, 1H, NH), 8.89 (dd, J = 2.5, 1.0 Hz, 1H, Pyr), 8.29 (dd, J = 8.5, 2.5 Hz, 1H, Pyr), 7.87 – 7.57 (m, 1H, Pyr), 7.50 – 6.86 (m, 5H, Ar), 4.51 (d, J = 6.0 Hz, 2H, $\underline{CH_2}$NH). **^{13}C NMR** (101 MHz, DMSO-d_6) δ 164.17, 153.06, 149.48, 139.52, 139.10, 129.65, 128.81, 127.79, 127.37, 124.60, 43.19. **FT-IR** ν_{max} (film) 3032, 2384, 1631, 1543 cm^{-1}. **HRMS (**ESI-TOF) calcd for $C_{13}H_{10}ON_2{}^{35}Cl$ $[M+H]^+$: 245.0487, found : 245.0482.

Ethyl 1-(5-(([1,1'-biphenyl]-4-ylmethyl)carbamoyl)pyridin-2-yl)-1H-pyrazole-4-carboxylate 146

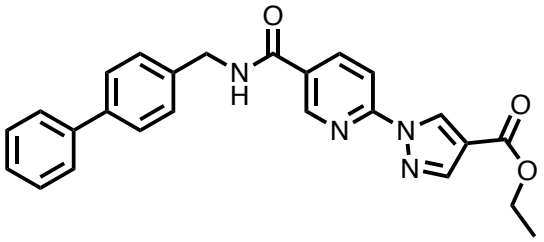

Following general procedure D: **70** (125 mg, 0.388 mmol), pyrazole-4-carboxylate ethyl ester (65 mg, 0.465 mmol), PdtBuXPhos G3 (31 mg, 0.0388 mmol), Cs_2CO_3 (252 mg, 0.776 mmol) and ^{t}BuOH (3 ml) gave **146** (97 mg, 0.227 mmol, 59 %) as a colourless oil. **^{1}H NMR** (400 MHz, DMSO-d_6) δ 9.38 (t, J = 6.0 Hz, 1H, NH), 9.04 (s, 1H, Pyr), 9.02 (d, J = 2.5 Hz, 1H), 8.51 (dd, J = 8.5, 2.5 Hz, 1H), 8.27 (s, 1H, Pyr), 8.07 (d, J = 8.5 Hz, 1H), 7.69 – 7.30 (m, 9H, Ar), 4.54 (d, J = 6.0 Hz, 2H, $\underline{CH_2}$NH), 4.21 (q, J = 7.0 Hz, 2H, $\underline{CH_2}CH_3$), 1.31 (t, J = 7.0 Hz, 3H, $CH_2\underline{CH_3}$). **^{13}C NMR** (101 MHz, DMSO-d_6) δ 164.28, 162.22, 151.82, 148.45, 143.61, 140.55, 140.41, 139.48, 139.33, 138.90, 132.61, 130.68, 129.38, 128.46, 127.81, 127.15, 127.05, 117.32, 112.57, 59.96, 42.93, 14.80. **FT-IR** ν_{max} (film) 1743, 1685, 1542, cm^{-1}. **HRMS** (ESI-TOF) calcd for $C_{25}H_{21}O_3N_4$ $[M-H]^-$: 425.1619, found : 425.1622.

Ethyl 1-(5-(benzylcarbamoyl)pyridin-2-yl)-1H-pyrazole-4-carboxylate 147

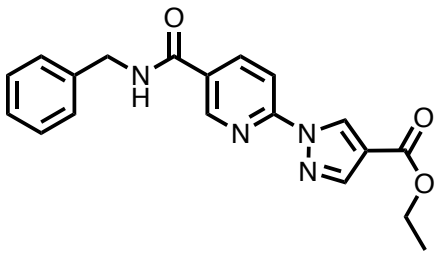

Following general procedure D: **145** (80 mg, 0.325 mmol), Pd^{t}BuXPhos G3 (25 mg, 0.0325 mmol), Cs_2CO_3 (317 mg, 0.97 mmol), pyrazole-4-carboxylate ethyl ester (67 mg, 0.48 mmol) and ^{t}BuOH (3 ml) gave **147** (41 mg, 0.117 mmol, 36 %) as a white solid.

m.p. 163-164°C. **^{1}H NMR** (400 MHz, DMSO-d_6) δ 9.33 (t, J = 6.0 Hz, 1H, NH), 9.04 (d, J = 1.0 Hz, 1H, Pyzl), 8.99 (dd, J = 2.5, 1.0 Hz, 1H, Pyr), 8.49 (dd, J = 8.5, 2.5 Hz, 1H, Pyr), 8.27 (d, J = 1.0 Hz, 1H, Pyzl), 8.06 (dd, J = 8.5, 1.0 Hz, 1H, Pyr), 7.38 – 7.32 (m, 5H, Ar), 4.53 (d, J = 6.0 Hz, 2H, $\underline{CH_2}$NH), 4.28 (q, J = 7.0 Hz, 2H, $\underline{CH_2}CH_3$), 1.31 (t, J = 7.0 Hz, 3H, $CH_2\underline{CH_3}$). **^{13}C NMR** (101 MHz, DMSO-d_6) δ 164.26, 162.22, 151.81, 148.44, 143.61, 139.49, 130.69, 128.82, 127.80, 127.36, 117.32, 112.56, 60.75, 43.18, 14.68. **FT-IR** ν_{max} (film) 1741, 1673, 1553 cm^{-1}. **HRMS (**ESI-TOF) calcd for $C_{19}H_{17}O_3N_4$ $[M+H]^+$: 349.1306, found : 349.1302.

1-(5-(([1,1'-biphenyl]-4-ylmethyl)carbamoyl)pyridin-2-yl)-1H-pyrazole-4-carboxylic acid 148

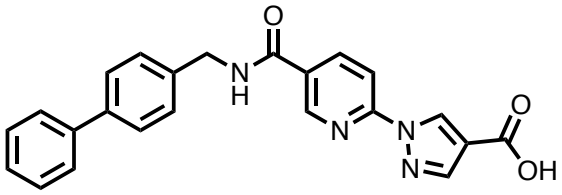

146 (63 mg, 0.147 mmol) was dissolved in a mixture of THF and water (10 ml (10:1)) before the addition of LiOH-monohydrate (19 mg, 0.45 mmol). The resultant mixture was allowed to stir for 16 hr and confirmed to have gone to completion by TLC. HCL_{aq} (10 ml, 1 M) was added the reaction mixture and the resulting mixture was extracted with EtOAc

(3 x 20 ml). The organic fractions were combined and washed with brine, dried with Na_2SO_4 and purified by flash column chromatography using (CH_2Cl_2, MeOH 0 - 5 %, formic acid 1 %) over 10 column volumes gave **148** (15 mg, 0.037 mmol, 26%) as a as a colourless oil.

^{1}H NMR (400 MHz, DMSO-d_6) δ 9.37 – 9.34 (m, 1H), 9.01 (d, J = 2.5 Hz, 1H), 8.92 (d, J = 2.5 Hz, 1H), 8.53 – 8.47 (m, 1H), 8.09 – 8.01 (m, 1H), 7.70 – 7.62 (m, 4H, Ar), 7.46 (t, J = 7.8 Hz, 4H), 7.39 – 7.30 (m, 2H), 4.56 (d, J = 6.0 Hz, 2H, $\underline{CH_2}$NH).**^{13}C NMR** (126 MHz, DMSO) δ 173.50, 163.58, 151.28, 147.66, 143.24, 139.63, 138.62, 138.13, 129.54, 128.61, 128.30, 128.04, 127.67, 127.00, 126.57, 126.37, 126.27, 111.66, 42.14, 39.52.. **FT-IR** ν_{max} (film) 2764 ,1721, 1682, 1542 cm^{-1}. **HRMS** (ESI-TOF) calcd for $C_{23}H_{17}O_3N_4$ [M-H]$^-$: 397.1306, found 397.1310.

1-(5-(benzylcarbamoyl)pyridin-2-yl)-1H-pyrazole-4-carboxylic acid 149

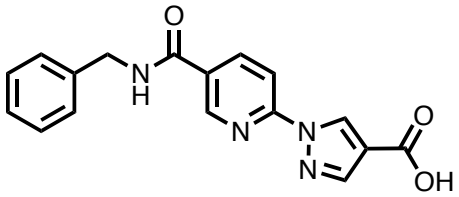

147 (20 mg, 0.043 mmol) was dissolved in THF (2 ml), MeOH (2 ml) and water (0.5 ml) was added to the reaction mixture before the addition of LiOH-monohydrate (16 mg, 0.40 mmol). The resultant mixture was stirred overnight at room temperature. The reaction mixture was acidified to PH3 with HCl (1M) solution and extracted with EtOAc (3 x 25

ml), washed with brine dried with anhydrous Na_2SO_4. The crude compound was then purified using flash column chromatography using (CH_2Cl_2, MeOH 0 - 5 %, formic acid 1 %) over 10 column volumes gave **149** (13 mg, 0.040 mmol, 94%**)** as a colourless oil.

^{1}H NMR (400 MHz, DMSO-d_6) δ 9.34 (t, J = 6.0 Hz, 1H, NH), 8.99 (dd, J = 2.5, 1.0 Hz, 1H, Pyr), 8.96 (s, 1H, Pyzl), 8.48 (dd, J = 8.5, 2.5 Hz, 1H, Pyr), 8.19 (s, 1H, Pyzl), 8.08 – 8.02 (m, 1H, Pyr), 7.48 – 7.21 (m, 5H, Ar), 4.54 (d, J = 6.0 Hz, 2H,$\underline{CH_2}$NH). **^{13}C NMR** (101 MHz, DMSO-d_6) δ 169.55, 163.87, 147.96, 143.51, 139.18, 138.93, 129.97, 128.35, 127.32, 126.88, 111.99, 99.51, 42.71, 39.52. **FT-IR** ν_{max} (film) 2764 ,1721, 1682, 1552 cm^{-1}. **HRMS** (ESI-TOF) calcd for $C_{17}H_{13}O_3N_4[M+H]^+$: 321.0993, found : 321.0994.

N-([1,1'-biphenyl]-4-ylmethyl)-1H-pyrazole-4-carboxamide 150

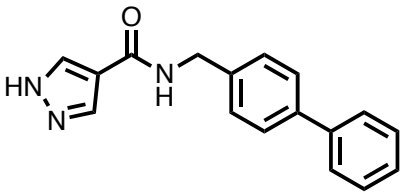

Following general procedure C: 1H-pyrazole-4-carboxylic acid (1g, 8.9 mmol), 4-phenylbenzylamine (2.44 g, 13.35 mmol), T3P (7.05 g, 22.2 mmol) and DIPEA (4.6 g, 35.7 mmol) gave **150** (462 mg, 1.66 mmol, 19%) as a white amorphous solid.

m.p. 240°C(decomp). **^{1}H NMR** (400 MHz, DMSO-d_6) δ 8.66 (t, J = 6.0 Hz, 1H, NH), 8.09 (s, 2H), 7.70 – 7.58 (m, 4H, Ph), 7.50 – 7.30 (m, 5H, Ph), 4.47 (d, J = 6.0 Hz, 2H, CH_2). **^{13}C NMR** (101 MHz, DMSO-d_6) δ 162.17, 140.00, 139.19, 138.67, 138.53, 128.90, 127.99, 127.86, 127.26, 126.59, 126.54, 126.47, 117.78, 41.64, 39.52. **FT-IR** ν_{max} (film) 3301, 1626, 1578 cm^{-1}. **HRMS** (ESI-TOF) calcd for $C_{17}H_{16}ON_3$ $[M+H]^+$: 278.1287, found : 278.1290.

N-([1,1'-biphenyl]-4-ylmethyl)-1-(5-cyano-4-methoxypyridin-2-yl)-1H-pyrazole-4-carboxamide 151

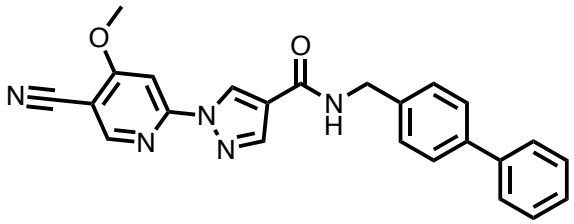

General Procedure D: 6-chloro-4-methoxynicotinonitrile (40 mg, 0.238 mmol), **150** (65 mg, 0.238 mmol), Pd^{t}BuXPhos Pd G3(19 mg, 0.023 mmol) and Cs_2CO_3 (232 mg, 0.714 mmol) in gave **151** (14 mg, 0.034 mmol, 12%) as a clear oil.

^{1}H NMR (400 MHz, DMSO-d_6) δ 9.03 (t, J = 6.0 Hz, 1H, NH), 8.82 (s, 1H), 8.30 – 8.29 (m, 1H, Ar), 7.70 – 7.59 (m, 5H, Ar), 7.50 – 7.31 (m, 6H, Ar), 4.50 (d, J = 6.0 Hz, 2H, CH_2NH), 4.12 (s, 3H, CH_3). **^{13}C NMR** (101 MHz, DMSO-d_6) δ 168.61, 160.84, 154.18, 153.93, 143.05, 139.99, 138.87, 138.66, 128.97, 128.72, 128.09, 127.39, 126.71, 126.62,

121.29, 114.37, 95.70, 57.39, 41.94, 39.52. **FT-IR** ν_{max} (film) 3321, 2230, 1636, 1575 cm^{-1}. **HRMS** (ESI-TOF) calcd for $C_{24}H_{20}O_2N_5$ $[M+H]^+$: 410.1622, found : 410. 1611.

Ethyl 6-(4-(([1,1'-biphenyl]-4-ylmethyl)carbamoyl)-1H-pyrazol-1-yl)-4-methoxynicotinate 152

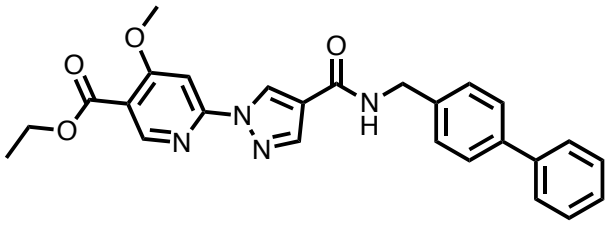

Following general procedure D: Ethyl 6-chloro-4-methoxynicotinate (39 mg, 0.18 mmol), **150** (50 mg, 0.18 mmol), Pd^{t}BuXPhos Pd G3 (25mg, 0.009 mmol) and dioxane (3ml) gave **152** as a clear oil (23 mg, 0.05 mmol, 28%).

^{1}H NMR (400 MHz, THF-d_8) δ 9.08 (d, J = 1.0 Hz, 1H, Pyr), 8.68 (s, 1H, Pyzl), 8.13 (d, J = 1.0 Hz, 1H, Pyzl), 8.05 (t, J = 6.0 Hz, 1H, NH), 7.69 (s, 1H, Pyr), 7.64 – 7.23 (m, 9H, Ph), 4.59 (d, J = 6.0 Hz, 2H, $\underline{CH_2}NH$), 4.30 (q, J = 7.0 Hz, 2H, $\underline{CH_2}CH_3$), 4.03 (s, 3H, OCH_3), 1.34 (t, J = 7.0 Hz, 3H, $CH_2\underline{CH_3}$). **^{13}C NMR** (101 MHz, THF-d_8) δ 168.32, 164.31, 162.05, 155.67, 152.82, 143.12, 141.85, 140.85, 139.88, 129.55, 129.13, 128.64, 127.96, 127.74, 127.66, 122.39, 116.37, 96.28, 61.47, 56.68, 43.43, 25.37, 14.66. **FT-IR** ν_{max} (film) 3403, 1739, 1641, 1587 cm^{-1}. **HRMS** (ESI-TOF) calcd for $C_{26}H_{25}O_4N_4$ $[M+H]^+$: 457.1870, found : 457.1868.

N-([1,1'-biphenyl]-4-ylmethyl)-1-(5-cyano-4-hydroxypyridin-2-yl)-1H-pyrazole-4-carboxamide 153

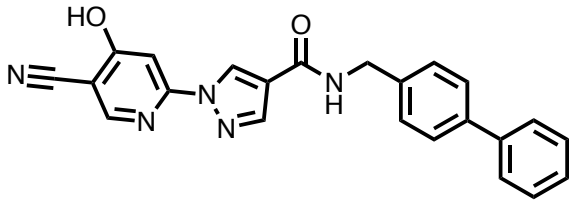

Following general procedure G: **151** (6 mg, 0.014 mmol) and LiCl (8.5 mg, 0.14 mmol) in DMAc (1 ml) gave **153** (1.9 mg, 0.0048 mmol, 35 %) as a yellow oil.

^{1}H NMR (400 MHz, DMSO-d_6) δ 9.14 (s, 1H, Pyr), 8.95 (t, J = 6.0 Hz, 1H, NH), 8.45 (s, 1H, Pyzl), 8.16 (s, 1H, Pyzl), 7.70 – 7.59 (m, 4H, Ar), 7.53 – 7.29 (m, 5H, Ar), 7.16 (s, 1H, Pyr), 4.48 (d, J = 6.0 Hz, 2H, CH_2). **^{13}C NMR** (126 MHz, DMSO-d_6) δ 172.03, 161.45, 154.23, 153.58, 142.42, 140.32, 139.10, 129.25, 128.52, 128.31, 127.66, 126.98, 126.92, 120.63, 117.32, 100.45, 98.30, 42.16, 39.52. **FT-IR** ν_{max} (film) 3649, 3312, 2242, 1634, 1596 cm^{-1}. **HRMS** (ESI-TOF) calcd for $C_{23}H_{18}O_2N_5$ $[M+H]^+$: 396.1466, found: 396.1456.

6-(4-(([1,1'-biphenyl]-4-ylmethyl)carbamoyl)-1H-pyrazol-1-yl)-4-hydroxynicotinic acid 154

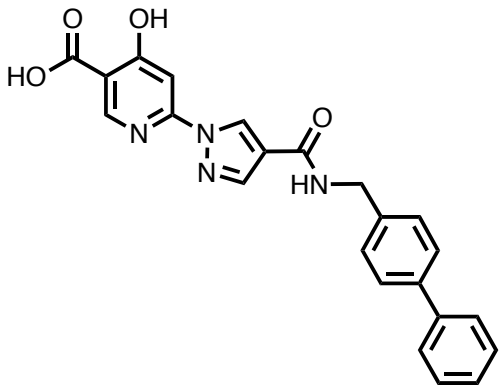

Following general procedure G: **152** (23 mg, 0.0504 mmol) and LiCl (30 mg, 0.504 mmol) in DMAc (3 ml) gave **154** as a yellow oil (9 mg, 0.0216 mmol, 43%).

^{1}H NMR (600 MHz, DMSO-d_6) δ 9.21 (s, 1H, Pyr), 8.96 (t, J = 6.0 Hz, 1H, NH), 8.71 (s, 1H), 8.22 (s, 1H), 7.64 (m, 5H, Ar), 7.51 – 7.32 (m, 5H, Ar), 4.49 (d, J = 6.0 Hz, 2H, CH_2). **^{13}C NMR** (151 MHz, DMSO-d_6) δ 168.65, 160.59, 142.02, 139.57, 138.39, 138.29, 128.51, 127.97, 127.58, 126.92, 126.24, 126.17, 120.32, 111.43, 99.30, 41.46, 39.52. **FT-IR** ν_{max} (film) 3753, 3649, 2981, 1717, 1699 cm^{-1}. **HRMS** (ESI-TOF) calcd for $C_{23}H_{19}O_4N_4$ $[M+H]^+$: 415.1400, found : 415.1401.

N-([1,1'-biphenyl]-4-ylmethyl)-1-(5-cyanopyridin-2-yl)-1H-pyrazole-4-carboxamide 155

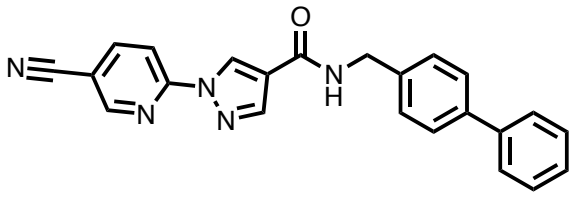

Following general procedure D: 6-chloro-nicotinonitrile (30 mg, 0.216 mmol), **150** (30 mg, 0.108 mmol), PdtBuXPhos G3 (17 mg, 0.0216 mmol), Cs_2CO_3 (175 mg, 0.432 mmol) gave **155** (6 mg, 0.015 mmol, 16 %) as a white solid.

m.p. 173-179°C. **^{1}H NMR** (400 MHz, DMSO-d_6) δ 9.27 (d, J = 1.0 Hz, 1H), 9.10 – 8.96 (m, 2H), 8.51 (dd, J = 8.5, 2.0 Hz, 1H, Pyr), 8.29 (d, J = 1.0 Hz, 1H, Pyr), 8.10 (dd, J = 8.5, 1.0 Hz, 1H, Pyr), 7.67 – 7.59 (m, 4H, Ph), 7.51 – 7.31 (m, 5H, Ph), 4.50 (d, J = 6.0 Hz, 2H, CH_2). **^{13}C NMR** (126 MHz, DMSO-d_6) δ 161.84, 152.15, 151.60, 143.06, 142.75, 139.47, 138.35, 138.14, 136.87, 128.44, 127.97, 127.73, 127.54, 126.86, 126.19, 126.10, 124.84, 120.85, 116.21, 111.98, 106.70, 41.41, 39.52. **FT-IR** ν_{max} (film) 3070, 2242, 1634, 1541 cm^{-1}. **HRMS (**ESI-TOF) calcd for $C_{23}H_{16}ON_5$ $[M+H]^+$: 378.1360, found : 378.1354.

N-([1,1'-biphenyl]-4-ylmethyl)-1-(4-methoxypyridin-2-yl)-1H-pyrazole-4-carboxamide 156

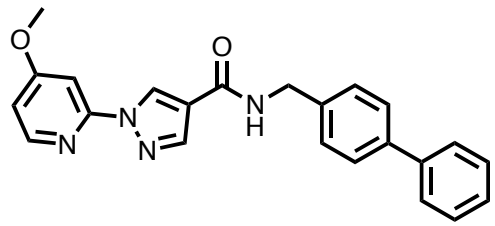

Following general procedure D: 2-chloro-4-methoxypyridine (16 mg, 0.114 mmol), **150** (31 mg, 0.114 mmol), RockPhos Pd G3 (9.5 mg, 0.0114 mmol) and Cs_2CO_3 (92 mg, 0.285 mmol) gave **156** (28 mg, 0.072 mmol, 63%) as a white solid.

m.p. 194-200°C. **^{1}H NMR** (400 MHz, DMSO-d_6) δ 9.18 (d, J = 1.0 Hz, 1H, Pyzl), 8.95 (t, J = 6.0 Hz, 1H, NH), 8.32 (d, J =6.0 Hz, 1H, Pyr), 8.19 (d, J = 1.0 Hz, 1H, Pyzl), 7.69 – 7.31 (m, 10H, Ar), 7.00 (dd, J = 6.0, 2.5 Hz, 1H, Pyr), 4.49 (d, J = 6.0 Hz, 2H, CH_2), 3.93 (s, 3H, CH_3). **^{13}C NMR** (101 MHz, DMSO-d_6) δ 167.66, 161.17, 149.69, 142.43, 141.72, 138.79, 128.93, 128.01, 127.76, 127.35, 126.59, 126.46, 120.34, 99.54, 97.44, 55.92, 41.85, 39.52. **FT-IR** ν_{max} (film) 3302, 1631 cm^{-1}. **HRMS (**ESI-TOF) calcd for $C_{23}H_{21}O_2N_4$ [M+H]+ : 385.1690, found : 385.1659.

N-([1,1'-biphenyl]-4-ylmethyl)-1-(4-hydroxypyridin-2-yl)-1H-pyrazole-4-carboxamide 157

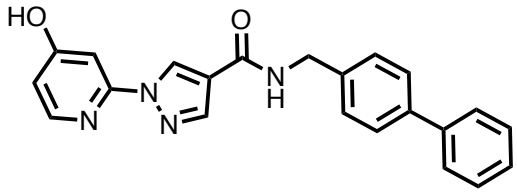

Following general procedure G: **156** (7 mg, 0.018 mmol) and LiCl (11 mg, 0.18 mmol) dissolved in DMAc (1 ml) gave **157** (3 mg, 0.008 mmol, 45%) as a clear oil.

^{1}H NMR (400 MHz, DMSO-d_6) δ 9.14 (d, J = 1.0 Hz, 1H), 8.89 (t, J = 6.0 Hz, 1H, NH), 8.73 – 8.66 (m, 1H), 8.33 – 8.29 (m, 1H), 7.91 – 7.89 (m, 1H), 7.50 – 7.28 (m, 9H, Ph), 6.77 (dd, J =6.0, 2.5 Hz, 1H), 4.48 (d, J = 6.0 Hz, 2H, CH_2). **^{13}C NMR** (126 MHz, DMSO-d_6) δ 166.40, 161.03, 151.32, 149.67, 145.06, 141.58, 141.41, 140.00, 138.80, 138.70, 129.90, 128.96, 128.02, 127.61, 127.38, 126.70, 126.68, 126.61, 121.50, 120.12, 112.57,

99.10, 41.89, 39.52. **FT-IR** ν_{max} (film) 3657, 3302, 1631 cm^{-1}. **HRMS** (ESI-TOF) calcd for $C_{22}H_{19}O_2N_4$ $[M+H]^+$: 371.1506, found : 371.1506.

Ethyl 6-(4-(([1,1'-biphenyl]-4-ylmethyl)carbamoyl)-1H-pyrazol-1-yl)nicotinate 158

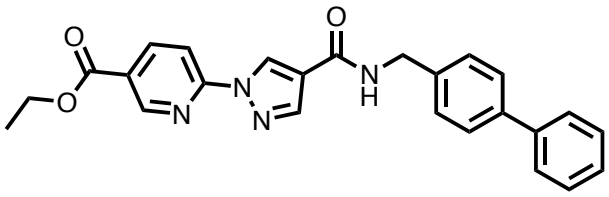

Following general procedure D: Ethyl 6-chloronicotinate (42 mg, 0.23 mmol), **150** (30 mg, 0.108 mmol), PdtBuXPhos G3 (18 mg, 0.023 mmol), Cs_2CO_3 (149 mg, 0.46 mmol) in dioxane (5 ml) gave **158** as a (10 mg, 0.023 mmol, 21 %) as a white solid.

m.p. 185-191°C. **^{1}H NMR** (400 MHz, THF-d_8) δ 9.09 (d, J = 1.0 Hz, 1H), 9.00 (dd, J = 2.0, 1.0 Hz, 1H), 8.70 – 8.60 (m, 1H), 8.14 – 8.10 (m, 1H), 7.96 (t, J = 6.0 Hz, 1H, NH), 7.67 – 7.35 (m, 10H, Ar), 4.59 (d, J = 6.0 Hz, 2H, $\underline{CH_2}$NH), 4.40 (q, J = 7.0 Hz, 2H, $\underline{CH_2}CH_3$), 1.38 (t, J = 7.0 Hz, 3H, $CH_2\underline{CH_3}$). **^{13}C NMR** (126 MHz, THF-d_8) δ 164.89, 161.83, 150.90, 143.41, 142.62, 140.93, 139.96, 129.55, 129.35, 129.14, 128.59, 127.67, 122.70, 112.74, 61.99, 43.42, 25.37, 14.61. **FT-IR** ν_{max} (film) 1743, 1636, 1542, cm^{-1}. **HRMS** (ESI-TOF) calcd for $C_{25}H_{23}O_3N_4$ $[M+H]^+$: 427.1766, found : 427.1766.

6-(4-(([1,1'-biphenyl]-4-ylmethyl)carbamoyl)-1H-pyrazol-1-yl)nicotinic acid 159

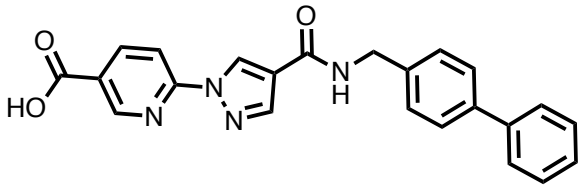

158 (8 mg, 0.0187 mmol) was dissolved in a mixture of THF and water (3ml (10:1). Lithium Hydroxide monohydrate (1.5 mg, 0.0374 mmol) was added to the reaction mixture and the resulting mixture was allowed to stir at room temperature for 16 hrs. The reaction was confirmed to have gone to completion by TLC and HCl_{aq} (5 ml, 1M) was added to the reaction mixture. The resulting mixture was extracted with EtOAc (3 x 10ml), then washed with brine, then dried with anhydrous Na_2SO_4 and purified using flash column chromatography using (CH_2Cl_2, MeOH 0-5%, 1% formic acid) gave **159** (2 mg, 0.005 mmol, 27 %) as a colourless oil.

^{1}H NMR (400 MHz, DMSO-d_6) δ 9.26 (d, J = 1.0 Hz, 1H, Pyr), 8.97 (t, J = 6.0 Hz, 1H, NH), 8.87 (s, 1H), 8.35 (d, J = 2.0 Hz, 1H), 8.19 (d, J = 7.0 Hz, 1H, Pyr), 7.89 (d, J = 7.0 Hz, 1H, Pyzl), 7.68 – 7.55 (m, 4H, Ph), 7.52 – 7.29 (m, 5H, Ph), 4.49 (d, J = 6.0 Hz, 2H, CH_2NH). **^{13}C NMR** (126 MHz, DMSO-d_6) δ 164.88, 161.24, 150.35, 149.52, 141.93, 140.01, 138.82, 128.94, 128.00, 127.64, 127.33, 126.67, 126.60, 120.32, 110.95, 41.87, 39.52. **FT-IR** ν_{max} (film) 3201, 1721, 1628, 1541 cm^{-1}. **HRMS** (ESI-TOF) calcd for $C_{23}H_{17}O_3N_4$ $[M-H]^-$: 397.1304, found : 397.1304.

Methyl 2-(4-(([1,1'-biphenyl]-4-ylmethyl)carbamoyl)-1H-pyrazol-1-yl)isonicotinate 160

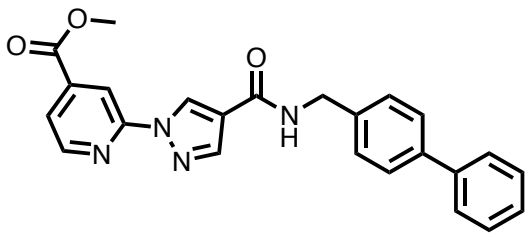

Following general procedure D: Methyl 2-chloroisonictinate (37 mg, 0.216 mmol), **160** (30 mg, 0.108 mmol), PdtBuXPhos Pd G3 (17 mg, 0.0216 mmol) and Cs_2CO_3 (175 mg, 0.54 mmol) in dioxane (3 ml) gave **160** (6 mg, 0.014 mmol, 13 %) as a clear oil.

^{1}H NMR (400 MHz, DMSO-d_6) δ 9.24 (d, J = 1.0 Hz, 1H, Pyzl), 8.99 (t, J = 6.0 Hz, 1H, NH), 8.73 (dd, J = 5.0, 1.0 Hz, 1H, Pyr), 8.34 (dd, J = 1.5, 1.0 Hz, 1H, Pyr), 8.26 (d, J = 1.0 Hz, 1H, Pyzl), 7.85 (dd, J = 5.0, 1.5 Hz, 1H. Pyr), 7.66 – 7.61 (m, 4H, Ar), 7.51 – 7.29 (m, 5H, Ar), 4.50 (d, J = 6.0 Hz, 2H, CH_2NH), 3.95 (s, 3H, CH_3). **^{13}C NMR** (126 MHz, DMSO-d_6) δ 164.36, 161.02, 151.19, 150.03, 142.37, 140.26, 139.98, 138.82, 128.94, 128.01, 127.84, 127.35, 126.68, 126.60, 121.37, 120.82, 111.30, 53.12, 41.88, 39.52. **FT-IR** ν_{max} (film) 1736, 1629, 1577 cm^{-1}. **HRMS** (ESI-TOF) calcd for $C_{24}H_{21}O_3N_4$ $[M+H]^+$: 413.1608, found : 413.1608.

2-(4-(([1,1'-biphenyl]-4-ylmethyl)carbamoyl)-1H-pyrazol-1-yl)isonicotinic acid 161

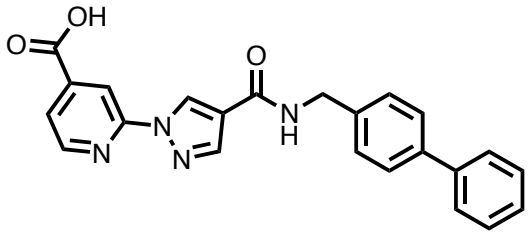

161 (4 mg, 0.0097 mmol) was dissolved in a mixture of THF and water (3ml (10:1). Lithium hydroxide monohydrate (1 mg, 0.0194 mmol) was added to the reaction mixture and the resulting mixture was allowed to stir at room temperature for 16hrs. The reaction was confirmed to have gone to completion by LCMS and HCl_{aq} (5 ml, 1M) was added to the reaction mixture. The resultant mixture was extracted with EtOAc (3x10 ml), then washed with brine, dried with anhydrous Na_2SO_4 and purified using flash column chromatography using (CH_2Cl_2, MeOH 0 - 5%, formic acid 1%) over 15 column volumes gave **161** (3 mg, 0.0075 mmol, 78 %) as a white solid.

^{1}H NMR (400 MHz, DMSO-d_6) δ 9.24 (s, 1H, Pyr), 8.98 (t, J = 6.0 Hz, 1H, NH), 8.68 (d, J = 5.0 Hz, 1H), 8.33 (t, J = 1.5 Hz, 1H), 8.24 (s, 1H), 7.81 (dd, J = 5.0, 1.5 Hz, 1H), 7.69 – 7.61 (m, 4H, Ph), 7.50 – 7.37 (m, 5H, Ph), 4.50 (d, J = 6.0 Hz, 2H, CH_2). **^{13}C NMR (**101 MHz, DMSO-d_6) δ 164.88, 162.79, 150.02, 142.62, 136.37, 128.21, 128.97, 127.86, 127.07, 122.08, 111.88, 42.37. **FT-IR** ν_{max} (film) 3143, 1730, 1631, 1577 cm^{-1}. **HRMS** (ESI-TOF) calcd for $C_{23}H_{17}O_3N_4$ $[M-H]^-$: 397.1304, found : 397.1304.

N-([1,1'-biphenyl]-4-ylmethyl)-1-(5-cyano-3-methoxypyridin-2-yl)-1H-pyrazole-4-carboxamide 162

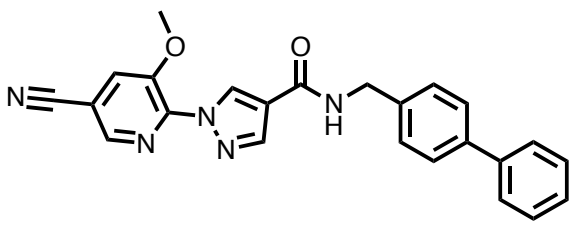

Following general procedure D: 6-chloro-5-methoxynicotinonitrile (37 mg, 0.216 mmol), **150** (30 mg, 0.108 mmol), RockPhos Pd G3 (17 mg, 0.0216 mmol), Cs_2CO_3 (175 mg, 0.432 mmol) gave **162** (9 mg, 0.022 mmol, 20 %) as a clear oil.

^{1}H NMR (400 MHz, DMSO-d_6) δ 8.93 (t, J = 6.0 Hz, 1H, NH), 8.87 (d, J = 1.0 Hz, 1H), 8.62 (d, J = 1.5 Hz, 1H), 8.34 (d, J = 1.5 Hz, 1H), 8.23 (d, J = 1.0 Hz, 1H), 7.67 – 7.62 (m, 4H, Ph), 7.50 – 7.32 (m, 5H, Ph), 4.50 (d, J = 6.0 Hz, 2H, CH_2), 3.98 (s, 3H, CH_3). **^{13}C NMR** (126 MHz, DMSO-d_6) δ 160.66, 146.74, 142.38, 142.05, 140.64, 139.49, 138.33, 132.33, 128.46, 127.48, 126.87, 126.19, 126.11, 124.86, 119.47, 115.92, 108.44, 56.67, 41.34, 39.52. **FT-IR** ν_{max} (film) 3321, 2230, 1636, 1575 cm^{-1}. **HRMS (**ESI-TOF) calcd for $C_{24}H_{20}O_2N_5$ $[M+H]^+$: 410.1615, found : 410.1612.

Ethyl 6-(4-(([1,1'-biphenyl]-4-ylmethyl)carbamoyl)-1H-pyrazol-1-yl)-5-methoxynicotinate 163

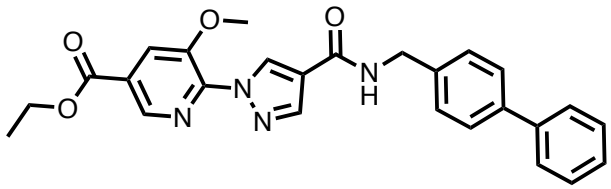

Following general procedure D: Ethyl 6-chloro-5-methoxynicotinate (30 mg, 0.14 mmol), **150** (30 mg, 0.108 mmol), RockPhos G3 (10 mg, 0.014 mmol), Cs_2CO_3 (77 mg, 0.238 mmol) in dioxane (5 ml) for 7 days gave **163** (5 mg, 0.01 mmol, 9 %) as a clear oil.

^{1}H NMR (400 MHz, THF-d_8) δ 8.71 (s, 1H,), 8.65 (d, J = 1.0 Hz, 1H, Pyzl), 8.07 – 8.05 (m, 1H), 7.91 (t, J = 6.0 Hz, 1H, NH), 7.75 (d, J = 1.0 Hz, 1H, Pyzl), 7.46 – 7.24 (m, 10H, Ar), 4.58 (d, J = 6.0 Hz, 2H, CH_2NH), 4.40 (q, J = 7.0 Hz, 2H, $\underline{CH_2}CH_3$), 3.98 (s, 3H, OCH_3), 1.42 (t, J = 7.0 Hz, 3H, $CH_2\underline{CH_3}$). **^{13}C NMR** (126 MHz, THF-d_8) δ 165.10, 162.87, 148.92, 144.92, 142.07, 142.03, 141.51, 140.91, 140.58, 138.83, 132.80, 131.05, 129.65, 129.20, 129.12, 127.82, 127.77, 127.65, 122.82, 120.06, 67.57, 62.30, 57.02, 43.28, 14.72. **FT-IR** ν_{max} (film) 1739, 1639, 1548 cm^{-1}. **HRMS (**ESI-TOF) calcd for $C_{26}H_{25}O_4N_4$ [M+H]$^+$: 457.1870, found : 457.1867.

6-(4-(([1,1'-biphenyl]-4-ylmethyl)carbamoyl)-1H-pyrazol-1-yl)-5-methoxynicotinic acid 164

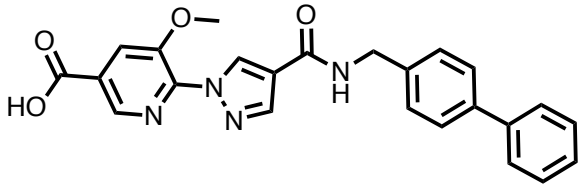

163 (5 mg, 0.0109 mmol) was dissolved in a mixture of THF and water (1.5 ml (10:1). Lithium hydroxide monohydrate (1.0 mg, 0.021 mmol) was added to the reaction mixture and the resulting mixture was allowed to stir at room temperature for 16 hrs. The reaction was confirmed to have gone to completion by TLC and HCL_{aq} (5 ml, 1M) was added to the reaction mixture. The resultant mixture was extracted with EtOAc (3 x 10 ml), then washed

with brine, then dried with anhydrous Na_2SO_4 and purified using flash column chromatography using (CH_2Cl_2, MeOH 0 - 5%, 1% formic acid) over 20 column volumes gave **164** (3.5 mg, 0.0082 mmol, 76%) as a clear oil.

^{1}H NMR (400 MHz, DMSO-d_6) δ 8.69 (s, 1H), 8.47 (s, 1H), 8.12 (s, 1H), 7.99 (s, 1H), 7.70 – 7.61 (m, 4H, Ph), 7.50 – 7.32 (m, 5H, Ph), 4.50 (d, J = 6.0 Hz, 2H, CH_2), 3.89 (s, 3H, CH_3). **^{13}C NMR** (126 MHz, DMSO-d_6) δ 169.98, 169.37, 151.86, 151.06, 140.01, 138.98, 138.74, 137.61, 137.39, 135.30, 132.22, 127.93, 127.32, 126.59, 122.26, 119.06, 56.00, 43.20, 39.52. **FT-IR** ν_{max} (film) 3143, 1730, 1577 cm^{-1}. **HRMS (**ESI-TOF) calcd for $C_{24}H_{21}O_4N_4$ $[M+H]^+$: 429.1557, found : 429.1557.

Ethyl 1-(4-methoxypyridin-2-yl)-1H-pyrazole-4-carboxylate 165

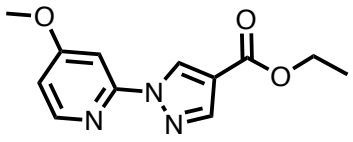

Following general procedure D: 4-methoxy-2-chloropyridine (500 mg, 3.49 mmol), 4-ethyl ester pyrazole (725 mg, 5.2 mmol), RockPhos Pd G3 (244 mg, 0.349 mmol), Cs_2CO_3 (2.8 g, 8.7 mmol) and ^{t}BuOH (10 ml) gave **165** (190 mg, 0.769 mmol, 22%) as a clear oil**.**

^{1}H NMR (400 MHz, THF-d_8) δ 8.23 (d, J = 5.5 Hz, 1H, Pyr), 8.13 (d, J = 5.5 Hz, 1H, Pyr), 7.57 (d, J = 2.0 Hz, 1H, Ar), 6.94 (d, J = 2.0 Hz, 2H, Ar), 4.29 (q, J = 7.0 Hz, 2H, $\underline{CH_2}CH_3$), 3.94 (s, 3H, O$\underline{CH_3}$), 1.33 (t, J = 7.0 Hz, 3H, $CH_2\underline{CH_3}$). **^{13}C NMR** (101 MHz, THF-d_8) δ 168.58, 162.85, 153.56, 151.24, 143.27, 130.77, 120.48, 110.81, 110.18, 67.57, 60.88,

56.26, 23.32. **FT-IR** ν_{max} (film) 1730, 1577 cm^{-1}. **HRMS** (ESI-TOF) calcd for $C_{12}H_{14}O_3N_3$ $[M+H]^+$: 248.1029, found : 248.1033.

1-(4-methoxypyridin-2-yl)-1H-pyrazole-4-carboxylic acid 166

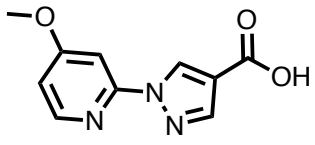

165 (190 mg, 0.769 mmol) was dissolved in a mixture of THF and water (11 ml (10:1)). Lithium hydroxide monohydrate (78 mg, 2.19 mmol) was added to the reaction mixture and the resultant mixture was allowed to stir at room temperature for 16 hrs. The reaction was confirmed to have gone to completion by LCMS and HCl (1M, 5 ml) was added to the reaction mixture. The resultant mixture was extracted with EtOAc (3 x 10ml), then washed with brine, then dried over Na_2SO_4. The solvents was removed in vacuo to give **166** (73 mg, 0.33 mmol, 44%) as a white solid.

m.p. 214-220°C. **^{1}H NMR** (400 MHz, DMSO-d_6) δ 8.90 (s, 1H, Pyzl), 8.34 (d, J = 6.0 Hz, 1H, Pyr), 8.15 (s, 1H, Pyzl), 7.45 (d, J = 2.5 Hz, 1H, Pyr), 7.03 (dd, J = 6.0, 2.5 Hz, 1H, Pyr), 3.93 (s, 3H, CH_3). **^{13}C NMR** (101 MHz, DMSO-d_6) δ 167.69, 149.79, 142.81, 129.82, 110.01, 97.80, 55.97, 39.52. **FT-IR** ν_{max} (film) 3174, 1730, 1577 cm^{-1}. **HRMS** (ESI-TOF) calcd for $C_{10}H_8O_3N_3$ $[M+H]^+$: 218.0569, found : 218.0571.

N-([1,1'-biphenyl]-4-yl)-1-(4-methoxypyridin-2-yl)-1H-pyrazole-4-carboxamide 167

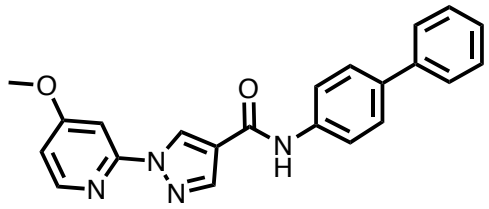

Following general procedure C: **166** (30 mg, 0.136 mmol), 4-aminobiphenyl (35 mg, 0.204 mmol), T3P (108 mg, 0.34 mmol) and DIPEA (116 ul, 0.68 mmol) gave **167** (27 mg, 0.072 mmol, 54%) as a clear oil**.**

^{1}H NMR (400 MHz, THF-d_8) δ 9.29 (s, 1H, NH), 9.18 (d, J = 1.0 Hz, 1H, Pyzl), 8.24 (d, J = 6.0 Hz, 1H, Pyr), 8.17 (d, J = 1.0 Hz, 1H, Pyzl), 7.91 – 7.84 (m, 2H, Ar), 7.68 – 7.21 (m, 8H, Ar), 6.87 (d, J = 6.0 Hz, 1H, Pyr), 3.95 (s, 3H, CH_3). **^{13}C NMR** (101 MHz, THF-d_8) δ 169.14, 160.67, 153.84, 150.18, 142.54, 141.73, 140.07, 136.83, 129.52, 128.38, 127.84, 127.58, 127.34, 122.10, 120.69, 110.29, 98.34, 56.14, 25.37. **FT-IR** ν_{max} (film) 3302, 1631 cm^{-1}. **HRMS (**ESI-TOF) calcd for $C_{22}H_{19}O_2N_4$ $[M+H]^+$: 371.1502, found 371.1396.

N-([1,1'-biphenyl]-3-ylmethyl)-1-(4-methoxypyridin-2-yl)-1H-pyrazole-4-carboxamide 168

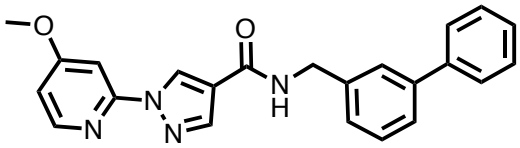

Following general procedure C: **166** (30 mg, 0.136 mmol), 3-aminomethylbiphenyl (36 mg, 0.204 mmol), T3P (108 mg, 0.34 mmol) and DIPEA (88 mg, 0.68 mmol) gave **168** (32 mg, 0.083 mmol, 61%) as a orange oil.

^{1}H NMR (400 MHz, Chloroform-*d*) δ 8.97 (d, J = 1.0 Hz, 1H, Pyzl), 8.15 (d, J = 6.0 Hz, 1H, Pyr), 8.07 (d, J = 1.0 Hz, 1H, Pyzl), 7.58 – 7.28 (m, 10H, Ar), 6.73 (d, J = 6.0 Hz, 1H, Pyr), 6.59 (t, J = 6.0 Hz, 1H, NH), 4.64 (d, J = 6.0 Hz, 2H, CH_2), 3.90 (s, 3H, CH_3). **^{13}C NMR** (101 MHz, Chloroform-*d*) δ 167.65, 162.00, 152.25, 148.81, 141.48, 140.90, 140.51, 138.43, 128.97, 128.55, 127.42, 127.20, 126.92, 126.60, 126.52, 126.18, 119.67, 109.76, 97.28, 77.16, 55.43, 43.46. **FT-IR** ν_{max} (film) 3302, 1631 cm^{-1}. **HRMS (**ESI-TOF) calcd for $C_{23}H_{21}O_2N_4$ $[M+H]^+$: 385.1659, found : 385.1656.

N-([1,1'-biphenyl]-4-yl)-1-(4-hydroxypyridin-2-yl)-1H-pyrazole-4-carboxamide 169

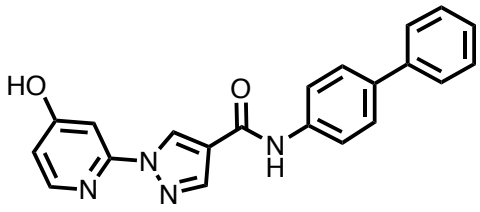

Following general procedure G: **167** (27 mg, 0.073 mmol) and LiCl (29 mg, 0.73 mmol) in DMAc (2 ml) for 8 hrs gave **169** (15 mg, 0.0421 mmol, 57%) as a orange oil.

^{1}H NMR (400 MHz, DMSO-d_6) δ 10.18 (s, 1H, OH), 9.39 (s, 1H, NH), 8.32 – 8.18 (m, 2H, Ar), 7.91 – 7.82 (m, 2H, Ar), 7.70 – 7.63 (m, 4H, Ar), 7.50 – 7.31 (m, 4H, Ar), 6.82 (dd, *J* = 5.5, 2.5 Hz, 1H, Pyr). **^{13}C NMR** (126 MHz, DMSO-d_6) δ 166.96, 160.46, 158.82, 158.53,

152.39, 150.16, 142.65, 140.21, 139.08, 135.56, 129.42, 128.49, 127.56, 127.39, 126.77, 120.70, 111.58, 99.67. FT-IR ν_{max} (film) 3657, 3302, 1631 cm^{-1}. **HRMS (**ESI-TOF) calcd for $C_{21}H_{17}O_2N_4$ $[M+H]^+$: 357.1346, found : 357.1348.

N-([1,1'-biphenyl]-3-ylmethyl)-1-(4-hydroxypyridin-2-yl)-1H-pyrazole-4-carboxamide 170

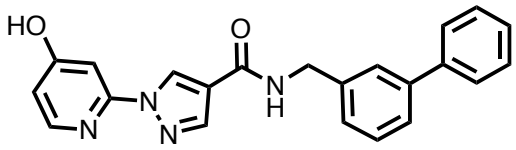

Following general procedure G: **168** (32 mg, 0.083 mmol) and LiCl (35 mg, 0.83 mmol) in DMAc (2 ml) at for 8 hrs gave **170** (11 mg, 0.029 mmol, 36 %) as a orange oil.

^{1}H NMR (400 MHz, DMSO-d_6) δ 11.23 (s, 1H, OH), 9.14 (d, J = 1.0 Hz, 1H, Pyzl), 8.93 (t, J = 6.0 Hz, 1H, NH), 8.19 (d, J = 5.5 Hz, 1H, Pyr), 8.15 (d, J = 1.0 Hz, 1H, Pyzl), 7.70 – 7.27 (m, 10H, Ar), 6.78 (dd, J = 5.5, 2.5 Hz, 1H, Pyr), 4.52 (d, J = 6.0 Hz, 2H, CH_2).**^{13}C NMR** (101 MHz, DMSO-d_6) δ 165.96, 165.68, 160.83, 151.51, 149.21, 141.18, 139.84, 128.57, 128.56, 127.18, 127.07, 126.27, 126.11, 125.48, 124.84, 110.52, 41.77, 39.52. **FT-IR** ν_{max} (film) 3657, 3302, 1631 cm^{-1}. **HRMS (**ESI-TOF) calcd for $C_{22}H_{19}O_2N_4$ $[M+H]^+$: 371.1502, found : 371.1497.

Ethyl 1-(5-cyano-4-methoxypyridin-2-yl)-1H-pyrazole-4-carboxylate 171

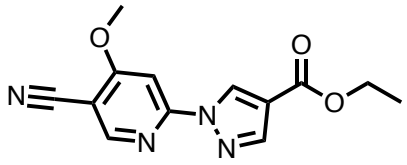

Following general procedure D: 6-chloro-4-methoxynicotinonitrile (400mg, 2.38 mmol), pyrazole-4-carboxylate ethyl ester (500mg, 3.57 mmol), PdtBuxPhos G3 (188mg, 0.238 mmol) and Cs_2CO_3 (2.3g, 7.14 mmol) in dioxane (10ml) gave **171** (110 mg, 0.40 mmol, 17%) as a white solid.

m.p. 245(decomp)°C. **^{1}H NMR** (400 MHz, DMSO-d_6) δ 9.02 (s, 1H), 8.83 (s, 1H), 8.32 (s, 1H), 7.69 (s, 1H), 4.28 (q, J = 7.0 Hz, 2H, $\underline{CH_2}CH_3$), 4.13 (s, 3H, OCH_3), 1.30 (t, J = 7.0 Hz, 3H, $CH_2\underline{CH_3}$). **^{13}C NMR** (101 MHz, DMSO-d_6) δ 168.56, 163.05, 161.43, 153.22, 143.38, 139.92, 132.02, 130.80, 126.14, 120.23, 112.22, 95.95, 60.26, 57.29, 39.52, 14.02. **FT-IR** ν_{max} (film) 2342, 1709 cm^{-1}. **HRMS** (ESI-TOF) calcd for $C_{13}H_{13}O_3N_4$ [M+H]+ : 273.0978, found : 273.0978.

1-(5-cyano-4-methoxypyridin-2-yl)-1H-pyrazole-4-carboxylic acid 172

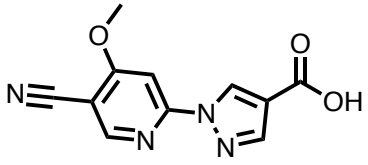

172 (95mg, 0.399 mmol) was dissolved in a mixture of THF and water (11 ml (10:1)). Lithium hydroxide monohydrate (14mg, 0.399 mmol) was added to the reaction mixture and the resulting mixture was allowed to stir at room temperature for 16hrs. The reaction

was confirmed to have gone to completion by TLC and HCl (10ml, 1M) was added to the reaction mixture. The resultant mixture was extracted with EtOAc (3 x 10ml), then washed with brine, then dried with anhydrous Na_2SO_4 and concentrated under *vacuo* gave **172** (90 mg, 0.368 mmol, 93%) as a white solid.

m.p. 210°C(decomp). **^{1}H NMR** (400 MHz, DMSO-d_6) δ 8.89 (d, J = 1.0 Hz, 1H, Pyzl), 8.76 (s, 1H), 8.20 (d, J = 1.0 Hz, 1H, Pyzl), 7.63 (s, 1H), 4.08 (s, 3H, CH_3). **^{13}C NMR** (101 MHz, DMSO-d_6) δ 168.63, 163.06, 153.91, 153.85, 143.87, 130.80, 118.36, 114.23, 97.79, 96.00, 57.41, 39.52. **FT-IR** ν_{max} (film) 3070, 2342, 1709 cm^{-1}. **HRMS** (ESI-TOF) calcd for $C_{11}H_7O_3N_4$ $[M+H]^+$: 243.0523, found : 243.0520.

1-(5-cyano-4-methoxypyridin-2-yl)-N-((6-phenylpyridin-3-yl)methyl)-1H-pyrazole-4-carboxamide 173

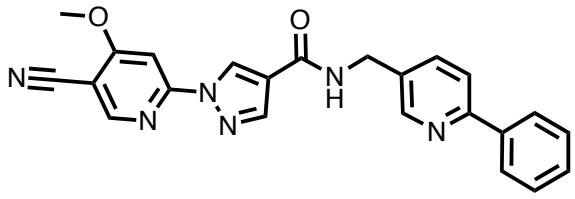

Following general procedure C: **172** (40 mg, 0.164 mmol), **105** (56 mg, 0.306 mmol), T3P (130 mg, 0.409 mmol) and DIPEA (79 mg, 0.68 mmol) gave **173** (28 mg, 0.068 mmol, 35 %) as a orange solid.

m.p. 101-110°C. **^{1}H NMR** (400 MHz, THF-d_8) δ 9.06 (d, *J* = 1.0 Hz, 1H), 8.57 (s, 1H), 8.34 (dd, *J* = 8.5, 1.5 Hz, 1H), 8.18 (t, *J* = 6.0 Hz, 1H, NH), 8.12 – 8.04 (m, 2H), 7.81 (d, *J*

= 1.5 Hz, 2H), 7.73 (s, 1H), 7.44 – 7.31 (m, 4H), 4.59 (d, *J* = 6.0 Hz, 2H, CH_2), 4.12 (s, 3H, CH_3). **^{13}C NMR** (101 MHz, THF-d_8) δ 169.76, 162.02, 156.65, 154.44, 150.13, 143.54, 140.07, 137.25, 134.65, 129.52, 129.30, 127.45, 122.61, 120.76, 120.33, 114.29, 99.47, 96.19, 57.47, 41.13, 25.37. **FT-IR** ν_{max} (film) 3406, 2230, 1636, 1575 cm^{-1}. **HRMS (**ESI-TOF) calcd for $C_{23}H_{19}O_2N_6$ $[M+H]^+$: 411.1564, found : 411.1555.

1-(5-cyano-4-methoxypyridin-2-yl)-N-(4-(trifluoromethyl)benzyl)-1H-pyrazole-4-carboxamide 174

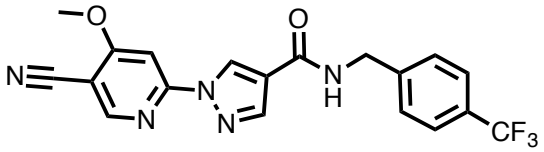

Following general procedure C: **172** (40 mg, 0.164 mmol), 4-trifluoromethyl benzylamine (54 mg, 0.306 mmol), T3P (130 mg, 0.409 mmol) and DIPEA (79 mg, 0.68 mmol) gave **174** (38 mg, 0.0947 mmol, 47 %) as a colourless oil.

^{1}H NMR (400 MHz, THF-d_8) δ 8.82 (s, 1H, Pyzl), 8.41 (dd, *J* = 4.5, 1.5 Hz, 1H), 8.11 (dd, *J* = 8.5, 1.5 Hz, 1H), 7.50 (s, 1H), 7.39 – 7.29 (m, 4H, Ph), 7.23 (t, *J* = 6.0 Hz, 1H), 4.39 (d, *J* = 6.0 Hz, 2H, CH_2), 3.89 (s, 3H, CH_3). **^{13}C NMR** (101 MHz, THF-d_8) δ 169.90, 162.93, 162.12, 155.84, 154.56, 151.52, 143.61, 143.04, 141.30, 129.44, 129.42, 129.23, 126.67, 126.25, 126.17, 126.13, 120.96, 96.31, 68.01, 67.57, 57.60, 40.29. **FT-IR** ν_{max} (film) 3321, 2230, 1636, 1575 cm^{-1}. **HRMS (**ESI-TOF) calcd for $C_{19}H_{13}O_2N_5F_3$$[M+H]^+$: 400.1026, found : 400.1022.

1-(5-cyano-4-hydroxypyridin-2-yl)-N-((6-phenylpyridin-3-yl)methyl)-1H-pyrazole-4-carboxamide 175

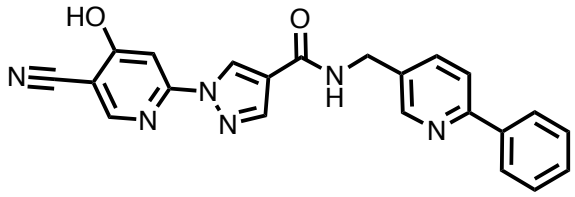

Following general procedure G :**173** (20 mg, 0.0487 mmol) and LiCl (20.5 mg, 0.487 mmol) in DMAc (2 ml) gave **175** (8 mg, 0.020 mmol, 42 %) as a colourless oil.

^{1}H NMR (400 MHz, DMSO-d_6) δ 9.11 (d, J = 1.0 Hz, 1H), 9.10 – 9.04 (m, 1H), 8.64 – 8.61 (m, 1H), 8.37 (s, 1H), 8.16 (s, 1H), 8.09 – 8.03 (m, 2H), 7.93 (dd, J = 8.0, 1.0 Hz, 1H), 7.81 (dd, J = 8.0, 2.5 Hz, 1H), 7.53 – 7.38 (m, 3H), 7.15 (s, 1H), 4.49 (d, J = 6.0 Hz, 2H, CH_2). **^{13}C NMR** (101 MHz, DMSO-d_6) δ 162.62, 161.34, 154.74, 153.76, 153.14, 148.87, 148.15, 141.88, 138.54, 136.44, 133.81, 128.92, 128.76, 128.21, 126.43, 119.92, 104.50, 100.63, 39.73, 39.52. **FT-IR** ν_{max} (film) 3657, 3312, 2230, 1639, 1593 cm^{-1}. **HRMS (**ESI-TOF) calcd for $C_{22}H_{17}O_2N_6$ $[M+H]^+$: 397.1407, found : 397.1407.

1-(5-cyano-4-hydroxypyridin-2-yl)-N-(4-(trifluoromethyl)benzyl)-1H-pyrazole-4-carboxamide 176

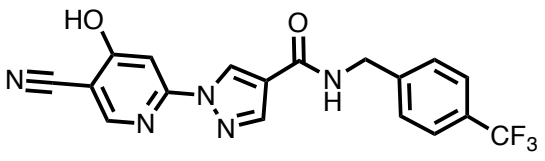

Following general procedure G: **174** (25 mg, 0.062 mmol) and LiCl (26 mg, 0.62 mmol) in DMAc (2 ml) gave **176** (5 mg, 0.0129 mmol, 21 %) as a colourless oil.

^{1}H NMR (400 MHz, DMSO-d_6) δ 9.06 (s, 1H), 8.96 (t, J = 6.0 Hz, 1H, NH), 8.13 (s, 1H), 8.08 (s, 1H), 7.70 (d, J = 8.0 Hz, 2H, Ph), 7.53 (d, J = 8.0 Hz, 2H, Ph), 6.78 (s, 1H), 4.51 (d, J = 6.0 Hz, 2H, CH_2). **^{13}C NMR** (126 MHz, DMSO-d_6) δ 171.51, 170.43, 161.00, 160.47, 152.99, 152.41, 149.83, 144.09, 140.80, 139.00, 131.12, 127.95, 127.42, 127.38, 126.81, 124.71, 124.68, 122.79, 118.92, 101.63, 98.73, 41.21, 39.52. **FT-IR** ν_{max} (film) 3657, 3301, 2230, 1634, 1596 cm^{-1}. **HRMS (**ESI-TOF) calcd for $C_{18}H_{11}O_2N_5F_3$ $[M-H]^-$: 386.0864, found : 386.0867.

Ethyl 6-hydroxypyrazolo[1,5-a]pyrido[3,2-e]pyrimidine-7-carboxylate 178

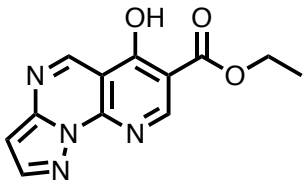

Pyrazolo[1,5-a]pyrimidin-7-amine (250 mg, 1.86 mmol), diethyl ethoxymethylenemalonate (402 mg, 1.86 mmol) were added to a microwave vial and dissolved in anhydrous EtOH (5 ml) before the addition of NaOEt (189 mg, 2.79 mmol). The reaction mixture was heated under microwave radiation at 100°C for 2 hrs before allowing to cool back to room temperature. The reaction mixture was then filtered, dried and before the addition of diphenyl ether (2 ml). The resultant mixture was then heated to 240°C for 30 minutes and

then allowed to cool to room temperature. The reaction mixture was then filtered, washed with Et_2O (4 x 50 ml) and dried gave **178** (210 mg, 0.81 mmol, 43 %) as a white solid.

m.p. >250°C. **^{1}H NMR** (400 MHz, DMSO-d_6) δ 8.97 (s, 1H, Ar), 8.62 (s, 1H, Ar), 8.15 (d, J = 2.0 Hz, 1H, Pyzl), 6.68 (d, J = 2.0 Hz, 1H, Pyzl), 4.20 (q, J = 7.0 Hz, 2H, $\underline{CH_2}CH_3$), 1.28 (t, J = 7.0 Hz, 3H, $CH_2\underline{CH_3}$). **^{13}C NMR** (101 MHz, DMSO-d_6) δ 173.16, 165.75, 154.57, 148.96, 143.96, 130.05, 118.61, 114.48, 109.30, 97.64, 59.27, 39.52, 14.37. **FT-IR** ν_{max} (film) 3649, 2981, 2361,1653, 1383 cm^{-1}. **HRMS (**ESI-TOF) calcd for $C_{12}H_{11}O_3N_4$ $[M+H]^+$: 259.0825, found : 259.0826.

N-([1,1'-biphenyl]-4-ylmethyl)-6-hydroxypyrazolo[1,5-a]pyrido[3,2-e]pyrimidine-7-carboxamide 179

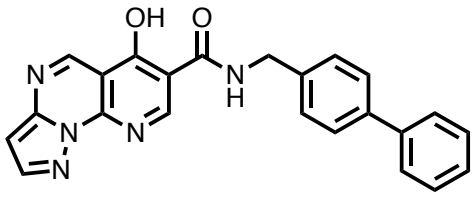

General Procedure B: **178** (100 mg, 0.38 mmol), [1,1'-biphenyl]-4-ylmethanamine (70 mg, 0.38 mmol), DABCO-$(AlMe_3)_2$ (100 mg, 0.38 mmol) gave **179** (4 mg, 0.01 mmol, 3 %) as a brown oil.

^{1}H NMR (400 MHz, DMSO-d_6) δ 9.04 (s, 1H, Ar), 8.72 (s, 1H, Ar), 8.26 (d, J = 2.0 Hz, 1H, Pyzl), 7.74 – 7.59 (m, 4H, Ph), 7.54 – 7.25 (m, 5H, Ph), 6.78 (d, J = 2.0 Hz, 1H, Pyzl), 4.60 (d, J = 6.0 Hz, 2H, $\underline{CH_2}NH$). **^{13}C NMR** (126 MHz, DMSO-d_6) δ 175.37, 163.54,

149.16, 140.51, 139.29, 129.41, 128.47, 127.81, 127.27, 116.18, 108.85, 98.72, 42.24. **FT-IR** ν_{max} (film) 3660, 2981, 2361, 1651 cm^{-1}. **HRMS (**ESI-TOF) calcd for $C_{23}H_{16}O_2N_5$ [M-H-]$^-$: 394.1309, found 394.1303.

Methyl 3-([1,1'-biphenyl]-4-ylamino)-3-oxopropanoate 180

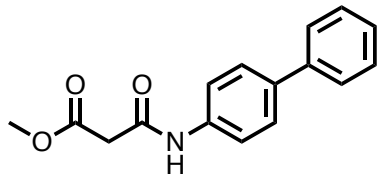

Following General Procedure C: Methyl hydrogen malonate (585 mg, 4.97 mmol), 4-aminobiphenyl (600 mg, 3.55 mmol), T3P (3.16 g, 9.94 mmol) and DIPEA (1.8 g, 14.2 mmol) gave **180** (230 mg, 0.855 mmol, 24 %) as a cream solid.

m.p. 120-124°C. **^{1}H NMR** (400 MHz, Chloroform-*d*) δ 9.27 (s, 1H, NH), 7.68 – 7.30 (m, 9H, Ph), 3.82 (s, 3H, CH_3), 3.52 (s, 2H, CH_2). **^{13}C NMR** (101 MHz, Chloroform-*d*) δ 170.58, 162.89, 140.56, 137.59, 136.80, 128.91, 127.74, 127.27, 126.98, 120.54, 77.16, 52.86, 41.42. **FT-IR** ν_{max} (film) 2361, 1734, 1638 cm^{-1}. **HRMS (**ESI-TOF) calcd for $C_{16}H_{16}O_3N$ $[M+H]^+$: 270.1124, found : 270.1122.

N-([1,1'-biphenyl]-4-yl)-6-hydroxypyrazolo[1,5-a]pyrido[3,2-e]pyrimidine-7-carboxamide 181

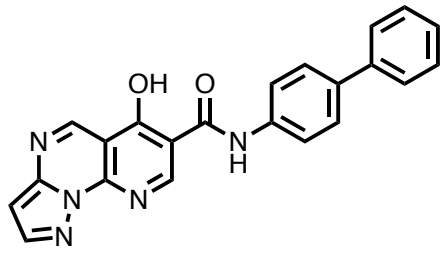

Pyrazolo[1,5-a]pyrimidin-7-amine (75 mg, 0.55 mmol) and **180** (100 mg, 0.37 mmol) were added to a microwave vial and flushed with N_2 and removed in *vacuo* (3 times) before the addition of anhydrous ethyl orthoformate (3 ml). The reaction mixture was heated at 120°C for 3 hrs. The excess ethyl orthoformate was removed in *vacuo* and the resultant mixture was taken up in diphenyl ether (5 ml) and heated to 240°C for 30 minutes, allowed to cool to room temperature and directly purified by by flash column chromatography using (CH_2Cl_2, MeOH 0-10%, 1% HCOOH) 20 column volumes gave **181** (5.5 mg, 0.015 mmol, 4 %) as a brown solid.

m.p. >250°C. **^{1}H NMR** (400 MHz, DMSO-d_6) δ 13.31 (s, 1H, OH), 9.11 (s, 1H, Ar), 8.95 (s, 1H, Ar), 8.11 (d, J = 2.0 Hz, 1H, Pyzl), 7.85 – 7.27 (m, 9H, Ph), 6.68 (d, J = 2.0 Hz, 1H, Pyzl). **^{13}C NMR** (126 MHz, DMSO-d_6) δ 174.26, 164.37, 155.53, 148.78, 148.48, 143.00, 139.52, 138.80, 133.97, 128.58, 126.79, 126.56, 125.86, 119.42, 114.19, 108.31, 97.37, 39.52. **FT-IR** ν_{max} (film) 3699, 3654, 1653 cm^{-1}. **HRMS (**ESI-TOF) calcd for $C_{22}H_{14}O_2N_5$ [M-H-]$^-$: 380.1153, found : 380.1150.

Methyl 3-(([1,1'-biphenyl]-4-ylmethyl)amino)-3-oxopropanoate 182

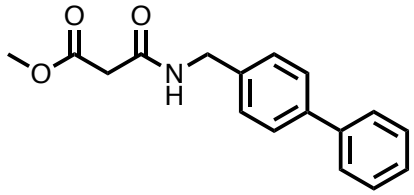

Following General Procedure C: Methyl hydrogen malonate (1.00 g, 8.9 mmol), 4-aminomethyl biphenyl (1.83 g, 10.0 mmol), T3P (6.7 g, 21.1 mmol) and DIPEA (2.7 g, 21.1 mmol) gave **182** (1.5 g, 5.3 mmol, 60.0 %) as a white solid.

m.p.77-83°C. **^{1}H NMR** (400 MHz, THF-d_8) δ 7.71 (s, 1H, NH), 7.41 – 7.03 (m, 9H, Ph), 4.23 (d, J = 6.0 Hz, 2H, CH_2NH), 3.46 (s, 3H, CH_3), 3.10 (s, 2H, $CO\underline{CH_2}CO$). **^{13}C NMR** (101 MHz, THF-d_8) δ 169.66, 166.20, 141.80, 140.88, 139.26, 129.57, 128.96, 127.99, 127.74, 127.65, 52.28, 43.69, 42.52, 25.37. **FT-IR** ν_{max} (film) 2361, 1734, 1642 cm^{-1}. **HRMS (**ESI-TOF) calcd for $C_{17}H_{18}O_3N$ $[M+H]^+$: 284.1281, found : 284.1281.

Methyl 3-oxo-3-((4-(trifluoromethyl)benzyl)amino)propanoate 183

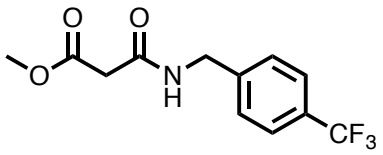

Following General Procedure C: Methyl hydrogen malonate (1.00 g, 8.9 mmol), 4-trifluorobenzyl amine (1.75 g, 10.0 mmol), T3P (6.7 g, 21.1 mmol) and DIPEA (2.7 g, 21.1 mmol) gave **183** (736 mg, 2.67 mmol, 30 %) as a white solid.

m.p. 88-92°C. **^{1}H NMR** (400 MHz, Chloroform-*d*) δ 7.86 (s, 1H, NH), 7.52 (d, J = 8.0 Hz, 2H, Ph), 7.35 (d, J = 8.0 Hz, 2H, Ph), 4.46 (d, J = 6.0 Hz, 2H, $\underline{CH_2}NH$), 3.68 (s, 3H, CH_3), 3.33 (s, 2H, $CO\underline{CH_2}CO$). **^{13}C NMR** (101 MHz, Chloroform-*d*) δ 169.31, 165.21, 141.91, 129.74, 129.42,

129.10, 128.78, 127.47, 125.23, 122.44, 77.16, 52.14, 42.66, 40.80. **FT-IR** ν_{max} (film) 2361, 1740, 1642 cm^{-1}. **HRMS (**ESI-TOF) calcd for $C_{12}H_{13}O_3NF_3$ $[M+H]^+$: 276.0842, found : 276.0843.

N-([1,1'-biphenyl]-4-ylmethyl)-6-hydroxy-2,5-dimethylpyrazolo[1,5-a]pyrido[3,2-e]pyrimidine-7-carboxamide 184

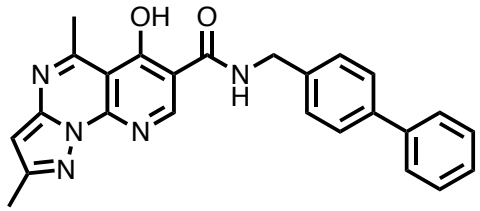

2,5-dimethylpyrazolo[1,5-a]pyrimidin-7-amine (114 mg, 0.70 mmol) and **182** (200 mg, 0.70 mmol) were added to a microwave vial and flushed with N_2 and removed in *vacuo* (3 times) before the addition of anhydrous ethyl orthoformate (5 ml). The reaction mixture was heated under microwave radiation at 120°C for 3 hrs. The excess ethyl orthoformate was removed in vacuo and the resultant mixture was taken up in diphenyl ether (5 ml) and heated to 240°C for 30 minutes, allowed to cool to room temperature and directly purified by by flash column chromatography using (CH_2Cl_2:MeOH 0-10%, 1% formic acid) over 20 column volumes to gave **184** (10 mg, 0.024 mmol, 3 %) as a brown solid.

m.p. >250°C. **^{1}H NMR** (400 MHz, DMSO-d_6) δ 10.54 (s, 1H, OH), 8.59 (s, 1H, Ar), 7.69 – 7.30 (m, 9H, Ar), 6.44 (s, 1H, Pyzl), 4.59 (d, J = 6.0 Hz, 2H, CH_2), 2.88 (s, 3H, CH_3), 2.45 (s, 3H, CH_3).**^{13}C NMR** (126 MHz, DMSO-d_6) δ 179.08, 176.21, 163.77, 159.84, 154.55, 146.99, 139.65, 138.50, 138.47, 128.58, 127.76, 127.00, 126.44, 126.28, 116.25, 106.35,

96.44, 41.51, 39.52, 27.03, 14.02. **FT-IR** ν_{max} (film) 3670, 3549, 1699 cm^{-1}. **HRMS (**ESI-TOF) calcd for $C_{25}H_{22}O_2N_5$ $[M+H]^+$: 424.1768, found : 424.1768.

6-Hydroxy-2,5-Dimethyl-N-(4-(trifluoromethyl)benzyl)pyrazolo[1,5-a]pyrido[3,2-e]pyrimidine-7-carboxamide 185

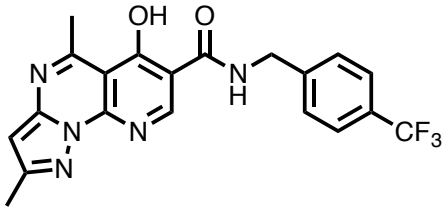

2,5-dimethylpyrazolo[1,5-a]pyrimidin-7-amine (114 mg, 0.70 mmol) and **183** (200 mg, 0.70 mmol) were added to a microwave vial and flushed with N_2 and removed in vacuo 3 times before the addition of anhydrous ethyl orthoformate (5 ml). The reaction mixture was heated under microwave radiation at 120°C for 3 hrs. The excess ethyl orthformate was removed in vacuo and the resultant mixture was taken up in diphenyl ether (5 ml) and heated to 240°C for 30 minutes, allowed to cool to room temperature and directly purified by by flash column chromatography using (CH_2Cl_2:MeOH 0-10%, 1% formic acid) over 20 column volumes to gave **185** (8 mg, 0.020 mmol, 3%) as a white solid.

m.p. >250°C. **^{1}H NMR** (400 MHz, DMSO-d_6) δ 8.52 (s, 1H, Ar), 7.71 (d, J = 8.1 Hz, 2H, Ph), 7.55 (d, J = 8.0 Hz, 2H, Ph), 6.50 (s, 1H, Pyrzl), 4.64 (d, J = 6.0 Hz, 2H, CH_2), 2.89 (s, 3H, CH_3), 2.47 (s, 3H, CH_3). **^{13}C NMR** (126 MHz, DMSO-d_6) δ 177.06, 164.47, 163.55, 160.59, 155.86, 147.79, 145.06, 128.55, 128.10, 127.85, 125.94, 125.82, 125.79, 125.73,

123.78, 117.20, 107.05, 97.52, 42.31, 39.52, 27.78, 14.85. **FT-IR** ν_{max} (film) 3521, 1621 cm^{-1}. **HRMS (**ESI-TOF) calcd for $C_{23}H_{16}O_2N_5$ [M-H-]$^-$: 394.1309, found : 394.1311.

4.14 References

1 WO 2009/117269 A1. (2009).

2 WO 2011/130908 A1. (2011).

3 WO 2016/057762 A1. (2016).

4 WO 2016/054806 A1. (2016).

5 Surry, D. S. & Buchwald, S. L. Dialkylbiaryl Phosphines in Pd-Catalyzed Amination: A User's Guide. *Chem Sci* **2**, 27-50, doi:10.1039/C0SC00331J (2011).

6 Fors, B. P. & Buchwald, S. L. Pd-catalyzed conversion of aryl chlorides, triflates, and nonaflates to nitroaromatics. *J Am Chem Soc* **131**, 12898-12899, doi:10.1021/ja905768k (2009).

7 Fang, Z., Zhou, G.-C., Zheng, S.-L., He, G.-L., Li, J.-L., He, L. *et al.* Lithium chloride-catalyzed selective demethylation of aryl methyl ethers under microwave irradiation. *Journal of Molecular Catalysis A: Chemical* **274**, 16-23, doi:https://doi.org/10.1016/j.molcata.2007.04.013 (2007).

8 Hann, M. M. Molecular obesity, potency and other addictions in drug discovery. *MedChemComm* **2**, 349-355, doi:10.1039/C1MD00017A (2011).

9 Lowe, J. in *Resmed* (New York, 2016).

10 Debenham, J. S., Madsen-Duggan, C., Clements, M. J., Walsh, T. F., Kuethe, J. T., Reibarkh, M. *et al.* Discovery of N-[Bis(4-methoxyphenyl)methyl]-4-hydroxy-2-(pyridazin-3-yl)pyrimidine-5-carboxamide (MK-8617), an Orally Active Pan-Inhibitor of Hypoxia-Inducible Factor Prolyl Hydroxylase 1–3 (HIF PHD1–3) for the Treatment of Anemia. *Journal of Medicinal Chemistry* **59**, 11039-11049, doi:10.1021/acs.jmedchem.6b01242 (2016).

11 Aik, W., McDonough, M. A., Thalhammer, A., Chowdhury, R. & Schofield, C. J. Role of the jelly-roll fold in substrate binding by 2-oxoglutarate oxygenases. *Curr Opin Struct Biol* **22**, 691-700, doi:10.1016/j.sbi.2012.10.001 (2012).

12 Chowdhury, R., Leung, I. K., Tian, Y. M., Abboud, M. I., Ge, W., Domene, C. *et al.* Structural basis for oxygen degradation domain selectivity of the HIF prolyl hydroxylases. *Nat Commun* **7**, 12673, doi:10.1038/ncomms12673 (2016).

13 Sander, T., Freyss, J., von Korff, M. & Rufener, C. DataWarrior: An Open-Source Program For Chemistry Aware Data Visualization And Analysis. *Journal of Chemical Information and Modeling* **55**, 460-473, doi:10.1021/ci500588j (2015).

14 Chowdhury, R., Flashman, E., Mecinovic, J., Kramer, H. B., Kessler, B. M., Frapart, Y. M. *et al.* Studies on the reaction of nitric oxide with the hypoxia-inducible factor prolyl hydroxylase domain 2 (EGLN1). *J Mol Biol* **410**, 268-279, doi:10.1016/j.jmb.2011.04.075 (2011).

15 T. Yeh, T. M. L., M. I. Abboud, C. C. Thinnes, O. Atasoylu, J. P. Holt-Martyn, D. Zhang, A. Tumber, K. Lippl, C. T. Lohans, I. K. H. Leung, H. Morcrette, A. Kawamura, E. Flashman, X. Lu, P. J. Ratcliffe, R. Chowdhury, C. W. Pugh and C. J. Schofield. Molecular and Cellular Mechanisms of HIF Prolyl Hydroxylase inhibitors in Clinical Trials. *Chem. Sci* **8**, 7651-7668, doi:10.1039/C7SC02103H (2017).

16 Chan, M. C., Atasoylu, O., Hodson, E., Tumber, A., Leung, I. K., Chowdhury, R. *et al.* Potent and Selective Triazole-Based Inhibitors of the Hypoxia-Inducible Factor Prolyl-Hydroxylases with Activity in the Murine Brain. *PLoS One* **10**, e0132004, doi:10.1371/journal.pone.0132004 (2015).

17 Chan, M. C., Holt-Martyn, J. P., Schofield, C. J. & Ratcliffe, P. J. Pharmacological targeting of the HIF hydroxylases - A new field in medicine development. *Mol Aspects Med* **47-48**, 54-75, doi:10.1016/j.mam.2016.01.001 (2016).

18 Anderson, K. W., Tundel, R. E., Ikawa, T., Altman, R. A. & Buchwald, S. L. Monodentate phosphines provide highly active catalysts for Pd-catalyzed C-N bond-forming reactions of heteroaromatic halides/amines and (H)N-heterocycles. *Angew Chem Int Ed Engl* **45**, 6523-6527, doi:10.1002/anie.200601612 (2006).

19 US4066643A. (1978).

20 Dubois, N., Glynn, D., McInally, T., Rhodes, B., Woodward, S., Irvine, D. J. *et al.* On DABAL-Me3 promoted formation of amides. *Tetrahedron* **69**, 9890-9897, doi:https://doi.org/10.1016/j.tet.2013.08.062 (2013).

21 Mikhalev, A. I., Ukhov, S. V. & Konshin, M. E. Synthesis and properties of amides of 2-substituted 3-aryl- and 3-pyridylaminoacrylic acids. *Chemistry of Heterocyclic Compounds* **30**, 551-555, doi:10.1007/BF01169832 (1994).

22 (2016).

CHAPTER 5: Investigation of Small Molecules for Increased Substrate Hydroxylation on PHD2

5.1 Potential Activation

In receptor pharmacology, an agonist is a small molecule that when bound to a receptor activates the receptor and produces a biological response.[1] In relation to enzymology, the concept of small molecule "enzymatic activators" (defined here as a small molecule that by interaction with the target protein increases the target proteins activity) are rare and only twelve examples of well characterised small molecule activators have been published in recent years.[2] These small molecules interact with a range of enzymes including deacetylayses, kinases, nucleases and proteases.[2] To date, these small molecules have induced enzymatic activation via four mechanisms, usually binding to an allosteric site near or directly on the catalytic domain to promote the active conformation:

1) Interacting with the enzyme through an allosteric site to stabilize the active conformation. This can occur cooperatively with the substrate.[3,4]
2) Binding to an allosteric site irreversibly, leading to an activating post-translational modification.[2]
3) Interaction with a regulatory sub unit to promote enzymatic activation.[5,6]
4) Activation via oligomerisation induced interaction with a regulatory subunit.[7]

84 resulted in an increase of CODD hydroxylation compared to the DMSO control in the presence of PHD2 (**Chapter 3.6**, **Table 12** and **Figure 55**). Initially, it was thought that this result could well be a false positive (using the RapidFire assay), due to an assay artifact.

However, **84** repeatedly showed increased CODD hydroxylation with different batches of PHD2 and substrate. Similar levels of increased turnover were recorded using the RapidFire™ protocol (57 % and 62%).

Some previous claims of increased substrate turnover via small molecule interactions have been discovered to be false. For example: the small molecule Resveratrol was claimed to be an enzymatic activator, activating the SIRT1 enzyme (which catalyses NAD+-dependent deacetylation of acetyl lysine residues).[8,9] Initially the work involved in a fluorescence-based assay, where the deacetylation of a residue occurred on a fluorophore labelled substrate.[10] However, it was later reported that the observation was due to an assay artifact. Thus, SIRT1 "activators" did not promote deacetylation of substrates lacking the fluorophore.[11,12]

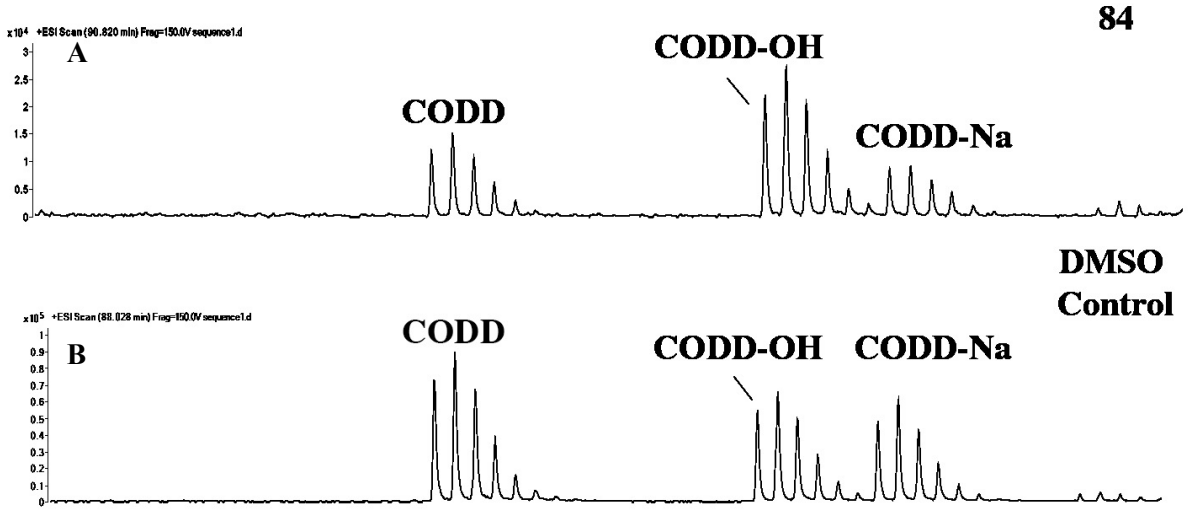

Figure 55: **A**) The profile spectra of the CODD peptide and hydroxylated CODD peptide in the presence of compound **84**. The amount of CODD is 1.5 x 10^4, whereas the CODD-OH is 2.5 x 10^4 **B**) The chromatograph of the DMSO control for the CODD peptide and hydroxylated CODD peptide. The amount of CODD is 0.7 x 10^5, whereas the CODD-OH is 0.6 x 10^5 * Note: The peak next to CODD-OH is the sodium adduct of CODD and was not taken into the calculation of any substrate hydroxylation ratio.

Figure 55 shows the profile spectra of the CODD substrate hydroxylated and non-hydroxylated in the presence of either **84** or the DMSO control, from the RapidFire assay. The profile spectra with **84**, showed a greater proportion of CODD hydroxylation (**Figure 51A**) (as evidenced by a +16 Da shift) compared to the DMSO control (**Figure 55B**). It is clear that the ratio of hydroxylated CODD to non-hydroxylated CODD is increased in the presence of **84**.

The work described in this chapter aimed to investigate:

- How this effect occurs through initial SAR work of **84**. The *C*-4 amino (**Chapters 5.2**), *C*-5 amide (**Chapters 5.3**), and the *C*-2 pyrazole groups (**Chapters 5.4**) were investigated (**Figure 56**).
- Investigations of the activity of **84** in a cellular environment are developed (**Chapter 5.5**).
- A selection of small molecules that showed an increase in CODD hydroxylation were tested against varied biochemical factors including substrates, enzyme construct and temperature, in order to hypothesise how this effect may occur (**Chapters 5.6**).

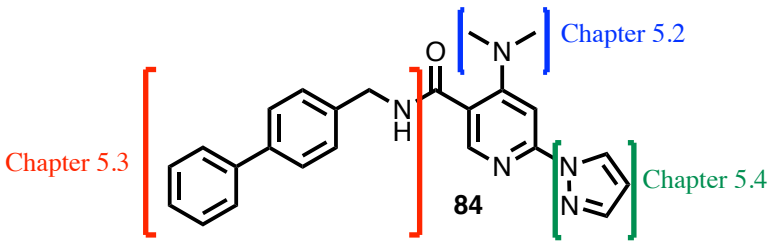

Figure 56: Summary of the proposed SAR work of **84**, investigating the increase in CODD hydroxylation by PHD2 in the presence of **84** in comparison to the DMSO control.

5.2 Investigation of the Amine Substituent

Due to the differences in interactions with PHD2 between **83** and **84** as described in **Chapter 3.5**. Further series of analogues were designed, to further investigate the role of the amino group of **83** and **84**. The compounds aimed to vary the length, rigidity and three-dimensional shape of the amino group, using either acyclic and cyclic systems (**185-190** & **192**). **185-190** were synthesised in one step (**Scheme 23**), identical to the final step to obtain **84** (**Scheme 14**). **82** underwent an S_NAr reaction with the corresponding amine to give **185-190** (**Scheme 23a**). **192** was synthesised in two steps. An amide coupling of the requisite carboxylic acid (COOH) gave **191**. Buchwald amination yielded the targeted compound **192** (**Scheme 22b**).

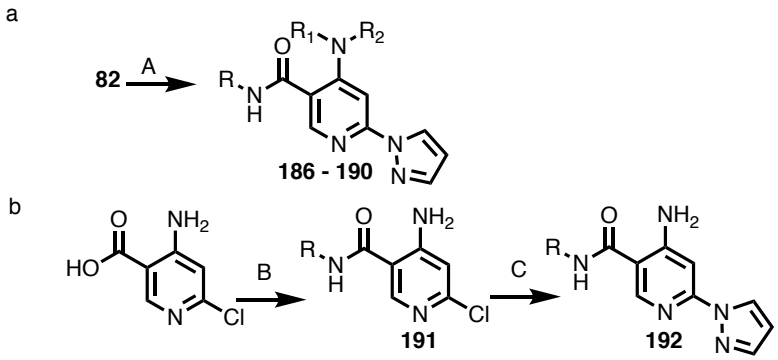

Scheme 23: Synthesis of 4-amino-6-(1*H*-pyrazol-1-yl)nicotinamide series. Reagents and conditions : **A**) NHR_1R_2,Cs_2CO_3, DMAc, MW 100 °C, 3 hrs (38-76%). **B**) T3P, DIPEA, DMAc, rt, 16hrs (85%). **C**) Pd^{t}BuXPhos, Cs_2CO_3, DMAc:THF(1:1), 100 °C, 90 mins (21 %).

The results indicated that the amino substituent has a significant impact on the rate of increased hydroxylation as observed by PHD2 RapidFire assay (**Table 27**). **186** and **188**, resulted in a high increase in substrate hydroxylation in relation to the DMSO control. Removal of the methyl groups by converting a tertiary amine (**84**), to a secondary amine

(**186**) and to a primary amine (**192**), resulted in a drop in the increase CODD hydroxylation as the methyl groups were subsequently removed (61%, 41% and 15% increase in CODD hydroxylation respectively relative to DMSO control). The di-ethyl analogue (**187**) resulted in a substantial drop in the increase of CODD hydroxylation in comparison to **84** (16% and 61%, respectively). However, the pyrrolidine analogue (**188**) resulted in 25% increase in substrate hydroxylation in comparison to **187** (41% and 16%, respectively). The di-pyrazole analogue (**189**) showed no increase in substrate hydroxylation by PHD2 with respect to the DMSO control with PHD2. The morpholine analogue (**190**) achieved a weak increase in CODD hydroxylation in relation to the DMSO control (14 %) (**Table 27**).

The SAR on **84** indicates the sensitivity of the amino group in relation to the increase in CODD hydroxylation. The differences (in activation rates) between the tertiary (**84**), secondary (**186**) and primary amines (**192**) suggest that the 3-dimensional shape of the amine substituent is important for the effect observed. As the size of the amino substituent increases (**84**, **188**, **187**), a weaker increase in CODD hydroxylation was observed until weak inhibition (**83**) was observed (61%, 41% and 16% increase in CODD hydroxylation and IC_{50} 14 μM respectively). The difference between **84**, **188** and **189** indicate that small aliphatic amino groups improve CODD hydroxylation rates.

Table 27: SAR of 4-amino-6-(1*H*-pyrazol-1-yl)nicotinamide analogues using the RapidFire assay. Experiment performed by Dr A Tumber. Experimental measurement n =1.

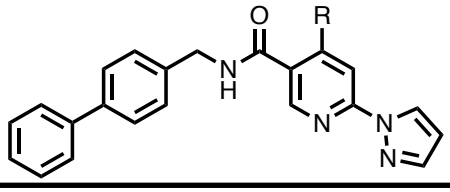

		PHD2 Interaction at 25 µM of Compound
Cpd	**R¹**	**RapidFire™ Increase In CODD**
84		**61%**
186		**41%**
192		**15%**
187	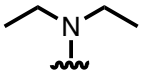	**16%**
188	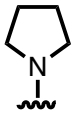	**41%**
189	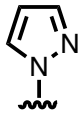	**Inactive**
190	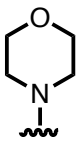	**14%**
83		**IC_{50} = 14 µM**

5.3 Investigation of The Role of The 4-phenylbenzyl Substituent

It was envisaged that the 4-phenylbenzyl substituent may have many potential roles in the increased CODD hydroxylation induced by **84** in relation to the DMSO control. Firstly, it was proposed that the 4-phenylbenzyl group improved the solubility of PHD2. It is known that a small amount of enzyme can stick to the side of the well under assay conditions. Binding of the 4-phenylbenzyl group of **84**, may detach the enzyme from the well and thereby increase the amount of active enzyme within the well, leading to an increased turnover of CODD. Secondly, the 4-phenylbenzyl group may have an important role in the activation by interaction with the aromatic pocket of PHD2. To maintain interaction with the aromatic pocket of PHD2, the 4-phenylbenzyl substituent was used in the SAR for both initial series (interactions confirmed by structures of **10** and **33, Figure 23** and **25**) whilst varying other substituents of the series (**Chapter 3**). A crystal structure of PHD2 with two FG-2216 (**3**) molecules bound to the same PHD2 monomer (**Figure 52**) was reported.[13] This indicates two binding sites may be possible, with the 1-chloroisoquinolin-4-ol group of **3** bound to the aromatic pocket of PHD2. Comparison of the crystal structure of **3** with structures of **10** and **33** bound to PHD2, confirms the biphenyl/phenyl substituent interacts with the same aromatic pocket of PHD2 (**Figures 23 and 25**). It was envisaged that the increase in CODD hydroxylation may have resulted from binding of the 4-phenylbenzyl substituent of **84**, in a similar fashion as **3**, in the aromatic pocket (orange, **Figure 57**).

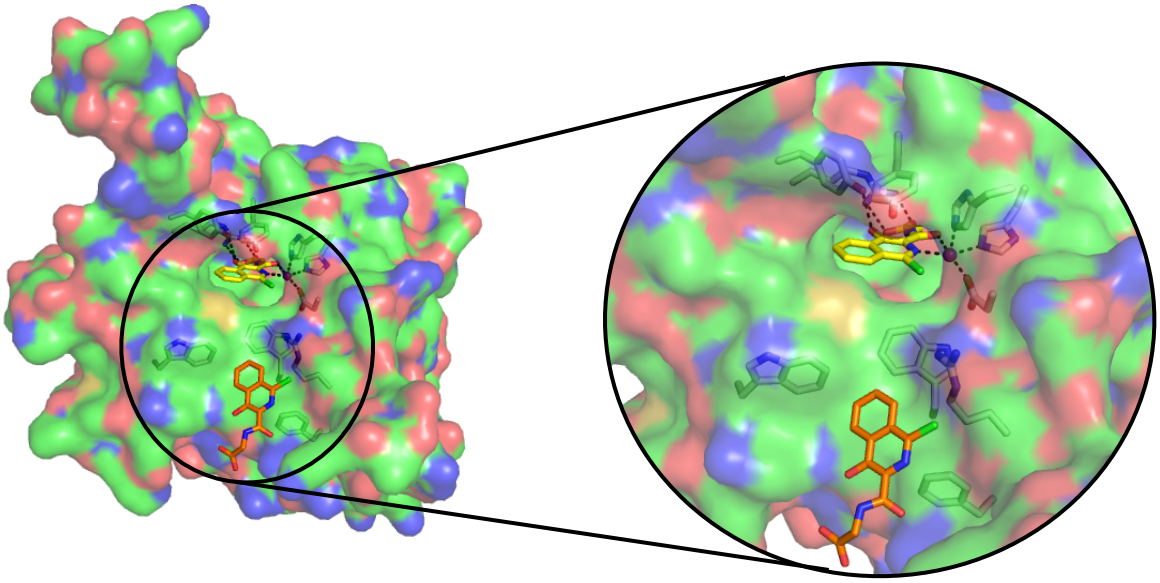

Figure 57: Views of crystal structure of **3** complexed with $PHD2_{181-426}$. **3** (yellow sticks) is bound within the active site of PHD2 whilst in orange **3** is bound to the aromatic pocket of PHD2. (PDB ID: 2y34).[13]

For **84**, it is unclear what the role of the 4-phenylbenzyl group is in relation to the increase in CODD hydroxylation with PHD2. A selection of binding substituents were taken from the novel 4-hydroxypyridine pharmacophore (**94-124**). It was envisaged that the variation in *C*-5 amide substituents would inform on factors including the amide methylene linker, the cLogP, length of the substituent, the preference of 3- or 4-position of the 'first' phenyl ring, and the aromaticity of the *C*-5 amide group for the activation of PHD2 for CODD hydroxylation. **197-201** were synthesised in an identical fashion to **84** (**Scheme 24**). Amide coupling with the chosen amine gave **193 - 196**. An S_NAr reaction to place the pyrazole moiety at the *C*-2 position and the dimethylamine at the *C*-4 position of the pyridine ring gave the desired compounds **197 - 201** (**Scheme 24**).

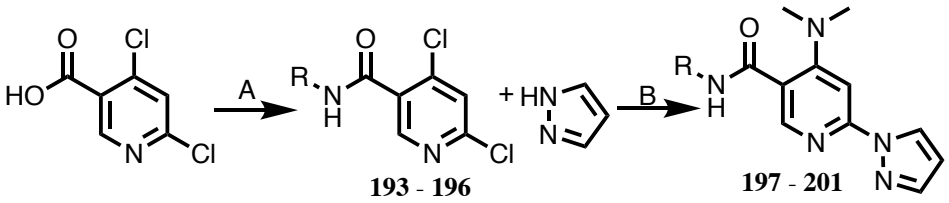

Scheme 24: Synthesis of analogues investigating the role of the binding substituent. Reagents and conditions: **A**) T3P, R-NH_2, DIPEA, DMAc, rt, 16hrs (14 - 75%). **B**)i: ,Cs_2CO_3, DMAc, MW 70 °C, 3 hrs ii: $NHMe_2$, Cs_2CO_3, DMAc, MW 100 °C, 3 hrs (12 - 31%).

The results (**Table 28**) indicated the importance of the 4-biphenyl group for the increase in CODD hydroxylation by PHD2 in relation to the DMSO control. Removal of the methylene linker between the amide bond and the 4-biphenyl moiety (**197**) resulted in a similar increase in CODD hydroxylation in contrast to **84** (65% and 60%, respectively). The 3-phenylbenzyl analogue (**201**) was half as potent as **84** (30% increase). This indicates the importance of the linearity of amide substituent and suggests that the hydrophobicity (cLogP) of the amide group is not important for the increase in CODD hydroxylation. The requirement of the substituent at the 4-position on the phenyl ring was further confirmed with the triflouromethylbenzyl analogues (**199** and **200)**. **200** achieved 25% increase in CODD hydroxylation, whereas **199** had no impact on the rate of hydroxylation in comparison to the DMSO control. The 3-trifluoromethylbenzyl substituent achieved poor inhibition with the 4-hydroxypyridine pharmacophore (**96**) suggesting the increased CODD hydroxylation observed with **84** is a result from a direct molecular interaction with PHD2. **198** also showed no increase in CODD hydroxylation.

Comparing the results for **197-201** indicates the importance of the length of the amide substituent and the size of the substituent on the primary phenyl ring. The length of the amide group provides information on how the analogues interact with PHD2. In order to

cause increased substrate hydroxylation rates, the analogues may have to reach from the active site towards the *C*-terminal region of PHD2. This proposal may explain the difference in increased hydroxylation between **84** and **200**. The phenyl substituent of **84** and **197** is larger than the CF_3 group (**200**). This difference in size may explain why **84** and **197** achieved a higher increase in CODD hydroxylation in comparison to **200**.

Table 28 : SAR for the analogues investigating the role of the binding substituent for the increase hydroxylation of substrate. Experiment performed by Dr A Tumber. Experimental measurement n =1.

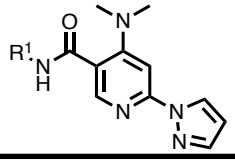

		PHD2 Interaction at 25 µM
Cpd	**R¹**	**RapidFire™ Increase In CODD Hydroxylation**
84	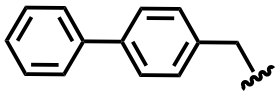	**61%**
197	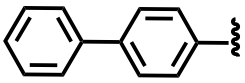	**65%**
198	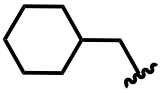	**0%**
199	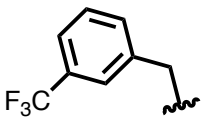	**0%**
200	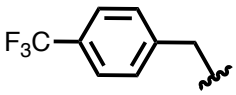	**26%**
201	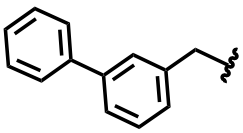	**30%**

5.4 Investigation of the Metal Chelating Substituent

The SAR of both starting points **10** and **32** revealed the requirement of the bidentate metal chelating substituent for PHD2 inhibition (**Chapters 2.4** and **3.4** respectively). For the increased turnover of substrate hydroxylation to occur, chelation of the Fe^{2+} atom by **84** must not occur as it would result in inhibition. The role of the pyrazole group of **84** was evaluated. It was envisaged that the pyrazole group of **84** may help increase PHD2-catalysed HIF-1α CODD turnover as it contributes to the three-dimensional (3D) shape of **84**. Analogues of **84** investigating the role of the pyrazole substituent were synthesised in an identical fashion to previous analogues **197** - **201** (**Scheme 25**). The results with the analogues (**203** and **204**) are shown in **Table 29**.

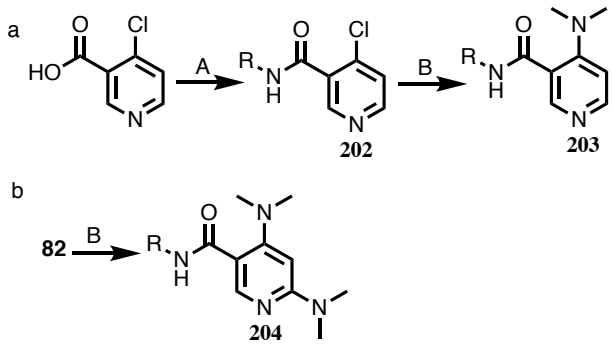

Scheme 25: Synthesis of analogues investigating the role of the bidentate substituent. Reagents and conditions: **A**) T3P, R-NH_2, DIPEA, DMAc, rt, 16hrs (47 -50 %). **B**) $NHMe_2$, Cs_2CO_3, DMAc, MW 100 °C, 3 hrs (19 - 55%).

Removal of the pyrazole ring (**203)** resulted in no increase in CODD hydroxylation compared to the DMSO control. This result indicates the importance of the pyrazole for the observed increase in hydroxylation; however, the reason for this was unclear. Conversion of the *C*-2 pyrazole group to a dimethylamine (**204**) resulted in an 50% increase in substrate

hydroxylation, i.e. similar level to those observed for **84**. The result of **204** suggests that the metal chelating motif of **84** is not necessary for the increased activity. However, the contribution of the pyrazole group towards the 3D shape of **84** is important for the increase in CODD hydroxylation. The importance of the 3D shape of **84**, suggests that additional interactions with PHD2, other than interaction with the aromatic pocket, are important for the increased activity.

Table 29 : SAR of the analogues investigating the role of the bidentate substituent. Experiment performed by Dr A Tumber. Experimental measurement n =1.

		PHD2 Interaction at 25 µM
Cpd	**Structural Formula**	**RapidFire™ Increase In CODD Hydroxylation**
84	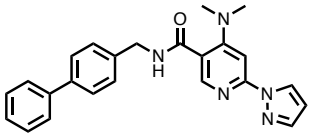	**61%**
203	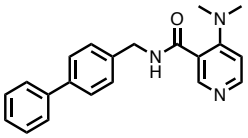	**0%**
204	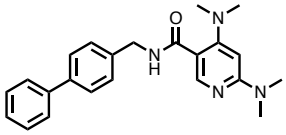	**50%**

5.5 Cellular Investigation of **84**

The SAR of **84** indicated that the increase of PHD2-catalysed CODD hydroxylation in the presence of **84** may not be due to an assay artifact. Therefore, **84** was further tested in a cellular environment (Hep3B cell line). The experiment could not be done in normoxic conditions due to HIF-1α degradation, meaning the effect would not be possible to measure

the impact of **84** on HIF-1α stability. It was decided the experiment would be carried out at mild hypoxia (3% O_2), so that HIF-1α is partially stabilised and if the addition of **84** led to degradation of the HIF-1α could be measured under the chosen conditions (no stain with the immunoblot).

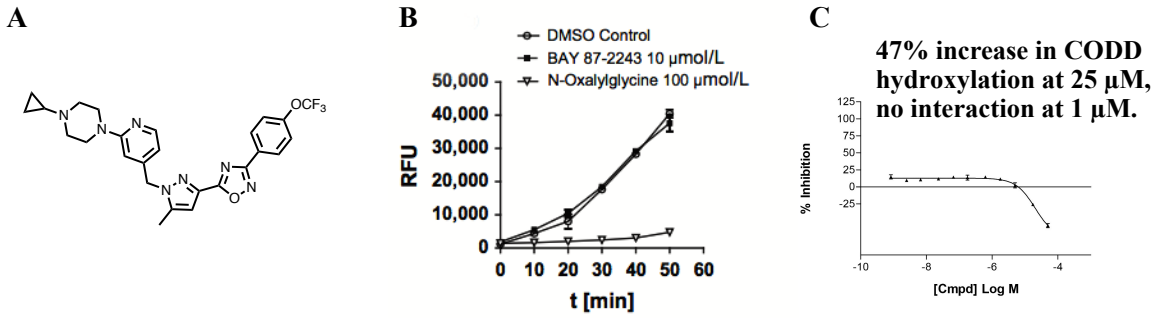

Figure 58: Summary of BAY 87-2243, **205**. **A**) The chemical structure of **205**. **B**) BAY 87-2243 **205** against PHD2 mediated hydroxylation of HIF-1a peptide over time. Hydroxylated peptide was measured after incubation with purified VBC complex labeled with europium using fluorescence intensity readout by P. Ellinghaus *et al*. [14] **C**) BAY 87-2243 **205** IC_{50} against $PHD2_{181-426}$ with the CODD substrate using the RapidFire™ protocol.

BAY 87-2243 (**205**) is a mitochondrial complex 1 inhibitor (**Figure 58A**) and inhibits stabilisation of HIF-1α under hypoxic conditions (1% O_2) by increasing the cellular O_2 concentration (thus activating the PHDs).[14] The authors reported that the activity of **205** depends on intact VHL and PHD activity; however, the authors reported that **205** had no effect on PHD2 activity at 10 µM (**Figure 58B**) (the concentration of PHD2 used in the assay was not disclosed).[14] Using the previously disclosed RapidFire assay (**Chapter 2.3**), **205** achieved a 47 % increase in CODD hydroxylation at 25 µM (150 nM PHD2) (**Figure 58C**). This observation suggests that the efficacy of **205** may involve direct interaction with PHD2, in addition to mitochondrial inhibition. **205** was only tested at 1 µM in a cellular environment and **205** showed no inhibition of PHD2 under those conditions (**Figure 58C**).

Figure 59A shows **84** and **205** treated in cells for 22 hours at 3% O_2, both compounds achieved degradation of HIF-1α. **84** apparently caused complete HIF-1α degradation at 100, 50 μM and partial HIF-1α degradation at 10 μM. The same experiment was repeated at extreme hypoxia (0.5% O_2), only **84** caused apparent HIF-1α degradation at 100 μM whereas **205** resulted in similar levels of stabilised HIF-1α as the DMSO control. These observations suggest, that at higher O_2 concentrations, **84** and **205** may have different mechanism of action (possibly overlapping) (**Figure 59B**).

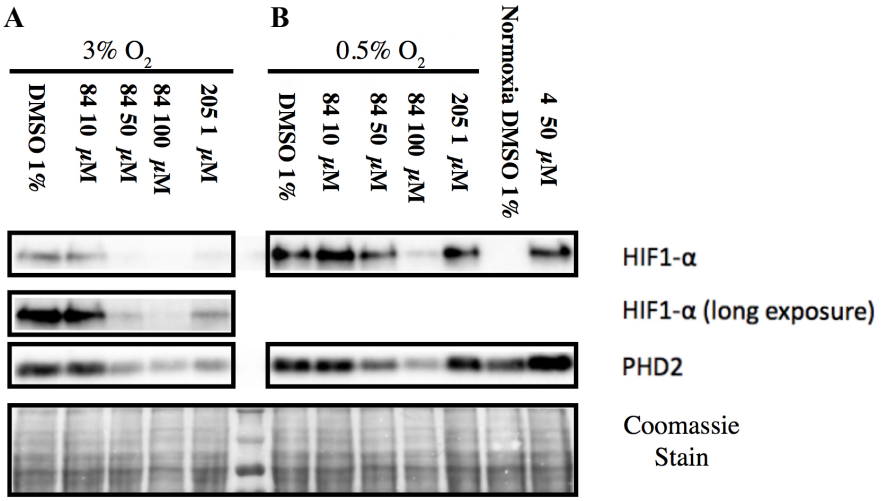

Figure 59: **A**) Immunoblot from Hep3B cells treated with **84** and **205** under 3% O_2 atmosphere **B**) Immunoblot from Hep3B cells treated with **84** and **205** under 0.5% O_2 atmosphere. Performed by Dr,T.Yeh.

An issue with the initial cellular experiments is that the exact concentrations of O_2 in cells are unknown and may be higher than the initial 3% at the start of the experiment. Therefore the same experiment was repeated but the cells were incubated in hypoxic conditions for 3 hours prior to compound treatment (3% O_2) (**Figure 60**). Under the conditions, **84** and **205** resulted in HIF-1α destabilisation. **84** achieved complete HIF-1α degradation at 100 μM and no impact on HIF-1α degradation at 10 μM.

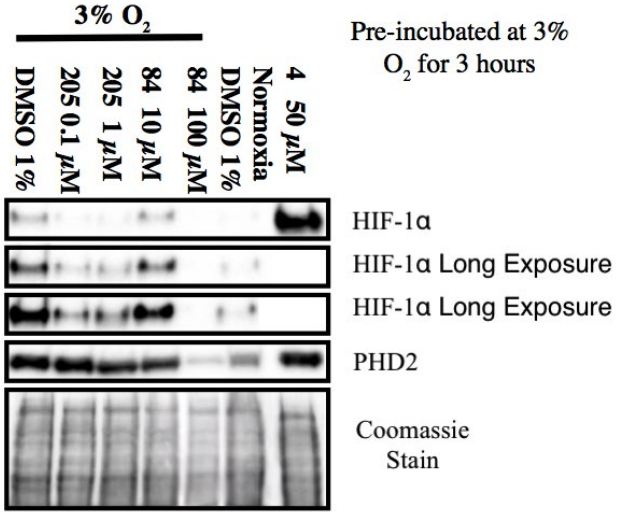

Figure 60: Immunoblot from Hep3B cells treated with **84** and **205** under 3% O_2 atmosphere and pre-incubated for 3hrs at 3% O_2 . Experiment performed by Dr. T. Yeh.

84 may be achieving HIF-1α degradation through mitochondrial inhibition, a similar mechanism as **205**. The oxygen consumption rate (OCR) of the Hep3B cell line was measured, using a Seahorse assay (as described in **chapter 6.1**), after 24 hours incubation with selected compounds (**83**, **84**, **10** and **32**) (**Figure 61**).[15,16] **83** was selected due to the structural similarities of **84**, but caused weak inhibition on PHD2 (IC_{50} 14 μM). Here, if

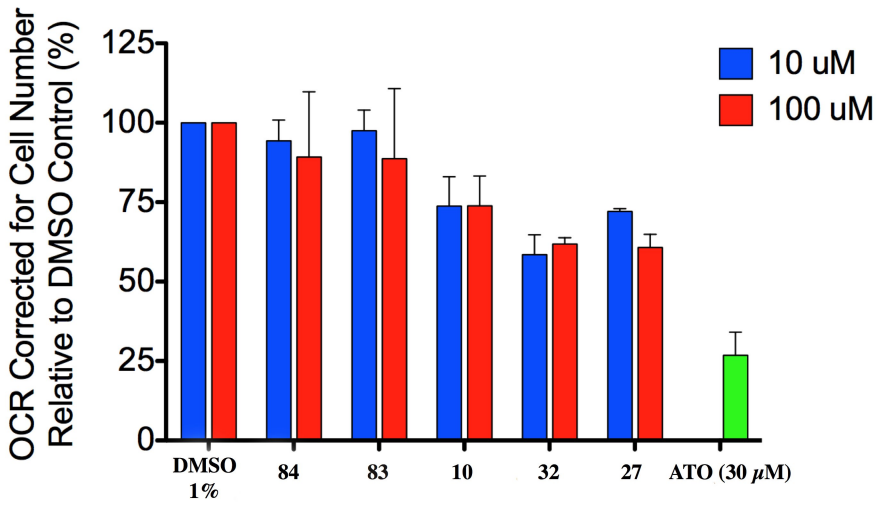

Figure 61: Oxygen Consumption Rate (OCR) of Hep3B cells measuring using Seahorse equipment after 24 hours incubation with **10**, **32**, **83** and **84.** Performed by Mr. James Coates. ATO = Atovaquone. An OCR inhibitor (a mitochondrial inhibitor)

there was any mitochondrial inhibition it would be observed for both **83** and **84**. Compounds from the initial pharmacophores (**Chapter 2**) were also tested due to structural similarities such as the biphenyl substituent. **10** and **32** caused strong HIF1-α stabilisation in the Hep3B cell line. **Figure 61** shows the results of the OCR. The initial 'hits' (**10** and **32**) showed a reduced consumption of oxygen possibly due to the inhibition of PHD2 and the upregulation of HIF dependent genes. **83** and **84** caused a weak reduction in the OCR. This suggests minimal interaction with the mitochondrial complexes.

It was further investigated whether the **84**-mediated HIF-1α destabilisation is not *via* mitochondrial interaction and, due to interaction with the PHDs. **84** was tested in a mitochondrial deficient cell line (206p0). **Figure 62A** shows the results, where **84** and **205** were tested in the mitochondrial deficient cell line 206p0 at 3% and 0.5% O_2. HIF-1α stabilisation occurred when treated with **205**, whereas treatment of **84** at 100 μM resulted in HIF-1α degradation. This suggests that **84** and **205** may act via different mechanisms. **84** and **205** were tested in the 206p0 parent cell line 143B, to provide further evidence that the HIF-1α destabilisation does not involved mitochondrial interaction (**Figure 62B**). **84** (100 μM) resulted in HIF-1α degradation but only at 3% O_2. This indicates the need for a certain level of O_2 concentration for the degradation to occur. It also shows that HIF-1α degradation by **84** is likely occurring rather than an interruption of HIF-1α production. The destabilisation of HIF-1α in the mitochondrial deficient cell lines indicates mitochondrial inhibition is not involved in the mechanism of action for HIF-1α degradation.

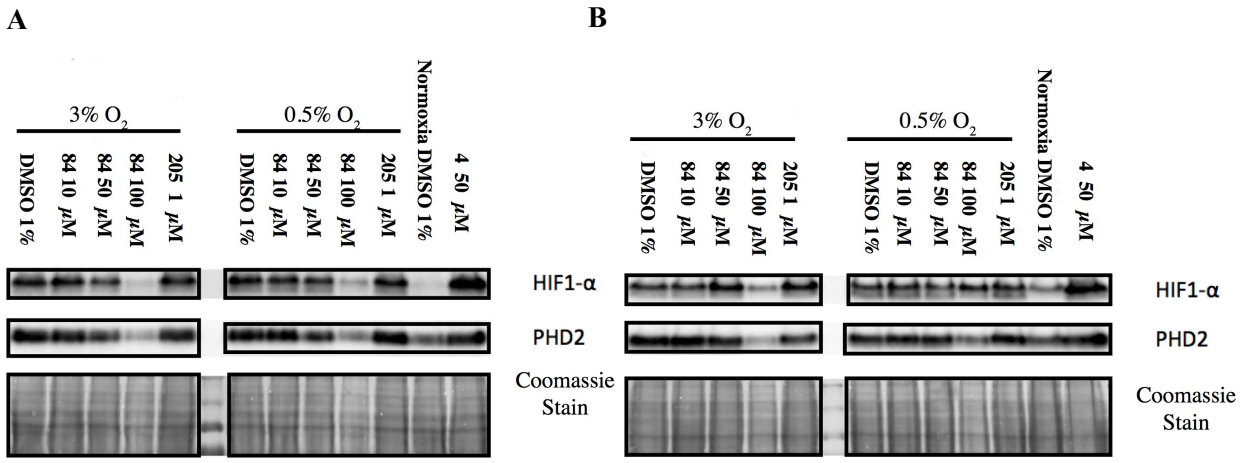

Figure 62: **A**) Immunoblot from 206p0 cells treated with **84** and **205** under atmosphere of 3% O_2 and 0.5% O_2 **B**) Immunoblot from 143B cells treated with **84** and **205** under atmosphere of 3% O_2 and 0.5% O_2 . Experiment performed by Dr.T.Yeh

Analogues of **84** bind differently to PHD2 compared to the clinical candidates (**3**-**8**) (**Figure 25**). **84** may interact with PHD2 via an alternative binding mode (**Chapter 5.3**) resulting in the increased turnover of substrate hydroxylation; as binding in the active site would interfere with the interactions of 2OG with PHD2. It was postulated that the combination of a clinical candidate FG-4592 (**4**) with **84**, would either lead to HIF-α stabilisation or destabilisation in a cellular environment. **Figure 63** shows a combination of FG-4592 (**4**) with **84**, **205** and fenofibrate* **206** at extreme hypoxia (0.5% O_2) for 15 hours. The mitochondrial inhibitors **205** and **206** in combination with FG-4592 (**4**) resulted in HIF-1α stabilisation, suggesting **4** inhibited the destabilisation of HIF-1α caused by **205** and **206**. However, for **84** and in the presence of **4,** resulted in HIF-1α destabilisation and therefore confirming a different mechanism of action compared to **205**.

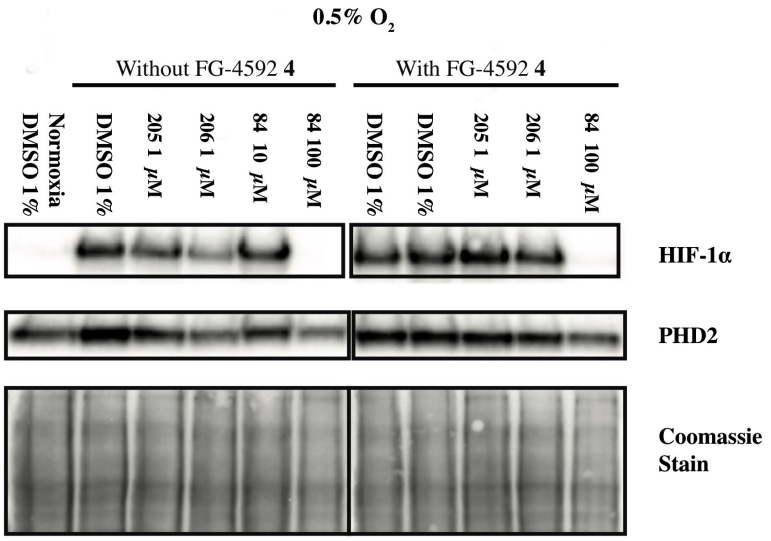

Figure 63: Immunoblot from Hep3B cells treated with compounds **205**, **206** and **84** without **A**) and in the presence **B**) of PHD inhibitor **4** under 0.5 % O_2 atmosphere. Experiment were performed by Dr. T. Yeh.

***Note**: Fenofibrate **206** was the starting point for the novel inhibitor for reduction oxygen consumption rate (OCR) project via mitochondrial complex 1 inhibition **(See Chapter 6)**.

It was envisaged that the design of compound **200**, could further investigate if the HIF-α degradation observed in the cellular environment was a result of molecular interaction with PHD2. **200** was designed because the 4-trifluoromethylbenzyl amide substituent resulted in a potent PHD2 inhibitor **117** (IC_{50} = 65 nM), which stabilises HIF-1α in the Hep3B cell line (**Figure 42**), indicating that interactions between **117** and PHD2 occurs within a cellular environment (**Chapter 4.5**). If **200** destabilised HIF-1α in the Hep3B cell line, it would suggest that the effect observed was due to interaction with PHD2. **200** achieved HIF-1α destabilisation at 100 μM at both 3% and 0.5% O_2 (**Figure 64**) suggesting the HIF-1α destabilisation is due to interaction with PHD2.

It was proposed that **204** would improve cell permeability of the series by replacing the pyrazole group with a dimethylamine group. As **204** maintained potency in contrast to **84**

(**Table 29**), the improved cell-penetration may reduce the dose required to destabilise HIF-1α. **204** achieved HIF-1α destabilisation at 100 μM at both 3% and 0.5% O_2 (**Figure 64**); however it did not destabilise HIF-1α at 10 μM.

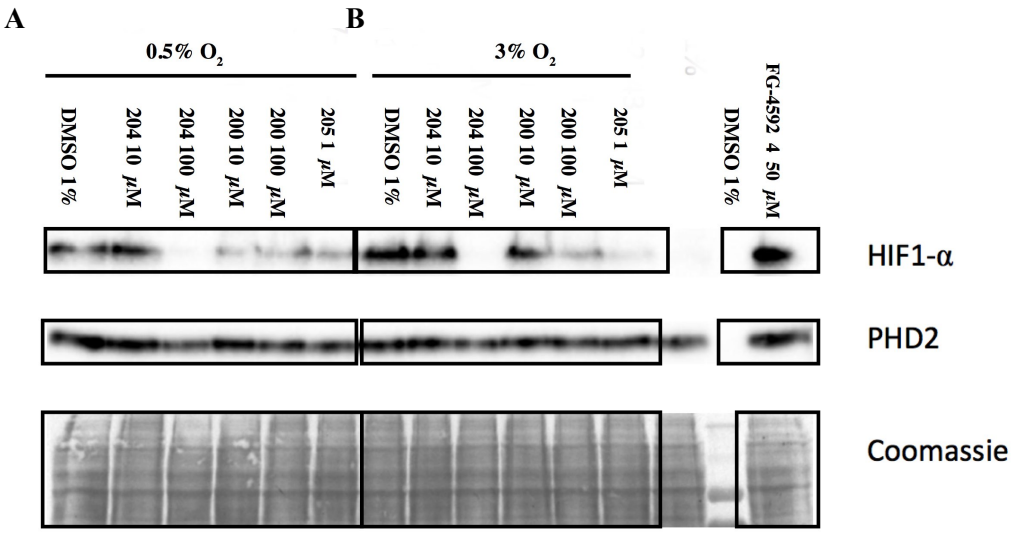

Figure 64: **A**) Immunoblot from Hep3B cells treated with **204, 200** and **205** under 0.5 % O_2 atmosphere **B**) Immunoblot from Hep3B cells treated with **204, 200** and **205** under 3 % O_2 atmosphere. Performed by Dr. T Yeh.

5.6 'Inverted' Medicinal Chemistry

Following the results observed *in-vitro* with the PHD2-CODD system, further *in-vitro* investigations were undertaken with the strongest small molecule activators from the SAR work, in order to assess their potential to regulate NODD hydroxylation. **84**, **188**, **197** and **201** had shown a strong increase in CODD hydroxylation with PHD2 and were used for assessment. **Table 30** shows the increase of hydroxylation with NODD and CODD substrates in comparison with the DMSO control. All the tested compounds led to an

Table 30: SAR of selected compounds **84**, **188**, **197** and **201** on different HIF-1α substrates (Rate of hydroxylation at 25μM). Experiment performed by Dr A Tumber. Experimental measurement n =1.

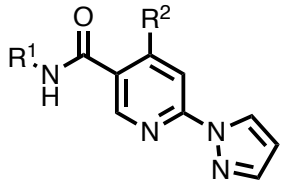

			PHD2 Interaction at 25 μM	
Cpd	**R¹**	**R²**	**Rapid Fire Increase In CODD Hydroxylation**	**Rapid Fire Increase In NODD Hydroxylation**
84	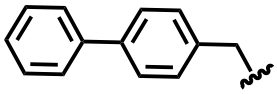		**61%**	**36%**
188	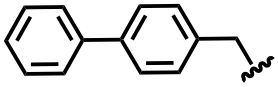	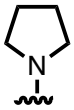	**41%**	**59%**
197	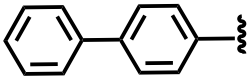		**65%**	**46%**
201	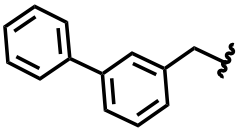		**30%**	**25%**

increase in substrate turnover using the RapidFire protocol. However, **84**, **188** and **197** resulted in an apparently different rate of hydroxylation between the two substrates. The di-methylamino analogues (**84** and **197**) were less effective against the NODD substrate. **84** and **197**, recorded a substantial drop in substrate hydroxylation of NODD compared to CODD (40% and 30% decrease respectively). The 3-phenylbenzyl analogue (**201**) achieved a similar level of substrate hydroxylation on both CODD and NODD, indicating a role for the binding substituent in substrate selectivity with respect to increased substrate turnover. The pyrrolidine analogue (**188**) resulted in an increase in substrate hydroxylation indicating a role in substrate selectivity for the amino substituents.

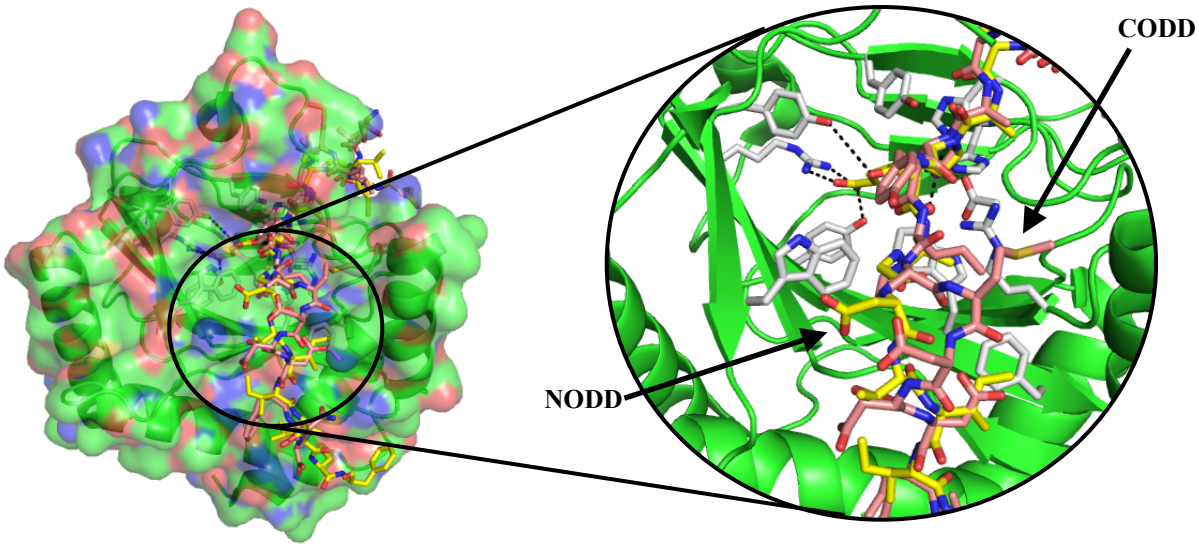

Figure 65: Views from a crystal structure of 2OG complexed with $PHD2_{181-426}$, with the NODD substrate (yellow) and $PHD2_{181-426}$ with the CODD substrate (light red). (PDB IDs: 5L9V and 5l9B, respectively).[17]

As discussed in **Chapter 1**, the NODD and CODD substrates interact differently with PHD2. Crystallographic evidence shows differences in how the substrates bind to PHD2 (**Figure 65**) [17]. One difference between how the HIF-α substrates bind, can be seen close to the aromatic pocket of PHD2. The CODD substrate is positioned closer to Trp-258 by 2 Å and the NODD substrate to Phe-391 by 2 Å (**Figure 65**).[17] These differences may (partially) explain how the amino substituents of **84**, **188**, **197** and **201** interact the with PHD2-substrate complex. **188**, has a bulkier amino group, caused a 50% increase of substrate hydroxylation of the NODD peptide compared to CODD. **84** and **197**, with a smaller amino group, showed a 50% increase in substrate hydroxylation of the CODD peptide over the NODD peptide. The substrate binding differences close to the aromatic pocket indicate the importance of the specific type of amino group. The 4-phenybenzyl substituent (**84** and **188**) showed apparent CODD selectivity, whereas the 3-phenybenzyl

substituted analogue (**201**) showed a similar level of increase in hydroxylation of both HIF-1α substrates, suggesting a role for the *C*-5 amide substituent in substrate selectivity.

Due to the difference observed in the presence of **84**, **188**, **197** and **201** between CODD and NODD with PHD2, attention was turned to the PHD2 construct. The PHD2 construct used for standard testing includes residues 181 - 426 (the catalytic domain of PHD2), with 426 being the end of the *C*-terminus of the full length protein. This construct is used because its activity is enzymatically similar to the full length PHD2. However, the *N*-terminus of full-length PHD2 has not been fully characterised in relation to function and structural impact on the protein.[18,19] It was decided to test **84**, **188**, **197** and **201** on full-length PHD2 to identify any differences in activity. Unfortunately both screening attempts using full-length PHD2 failed because both batches were inactive. As discussed in **Chapter 1**, the *C*-terminal region of PHD2 has a role in substrate recruitment and turnover. Indeed, it was envisaged that these small molecules may bind and interact with PHD2 via an alternative binding mode near the *C*-terminus of PHD2.

It was proposed that the *C*-terminus of full length PHD2 may play a significant in the role observed for the increase in substrate hydroxylation. Biophysical analyses indicate the last 15 residues of the *C*-terminus are disordered and are known to be important for substrate interaction.[20,21] A selection of small molecules (**84**, **188**, **197** and **201**) were tested against a *C*-terminally truncated construct that can still hydroxylate the CODD substrate to similar amount as the $PHD2_{181-426}$ construct. The $PHD2_{177-404}$ construct was chosen, as it hydroxylated a similar amount of CODD (~40% over 20 minutes) to the $PHD2_{181-426}$ construct using the RapidFire protocol. The results (**Table 31**) indicated that the length of

the *C*-terminus had an substantial impact on the increase in substrate hydroxylation in the presence of **84**, **188**, **197** and **201**. All the screened compounds were at least 40% weaker (in terms of activation) on the $PHD2_{177-404}$ construct in contrast to the $PHD2_{181-426}$ construct, with **188** causing an 8% increase in CODD hydroxylation on the $PHD2_{177-404}$ construct in comparison to 41% increase on the $PHD2_{181-426}$ construct.

PHD3 preferably hydroxylates the CODD substrate suggesting that PHD3 may form a different quaternary complex with the HIF-α substrate in contrast to PHD2.[18,22,23] PHD2 and PHD3 differ in the flexible loop between β2/β3 strands that folds over the highly conserved LXXLAP motif of the HIF-α substrates (**Chapter 1**.**4**).[17,20,21] The same selection of compounds were tested against PHD3 with the CODD substrate (**Table 31**). All compounds failed to increase the amount of the hydroxylation of CODD on PHD3 in comparison to the DMSO control. This suggests **84**, **188**, **197** and **201** may display an certain amount of PHD isoform selectivity. The lack of effect observed on PHD3 suggests the possible importance the enzyme construct-substrate complex rather than the substrate for the increased hydroxylation. The stability of the enzyme construct-substrate complex would depend on factors such as temperature. It was envisaged that if the temperature was increased to 37°C, the complex would fragment at a faster rate reducing the efficacy of the analogues and therefore reducing the difference between the DMSO control. **84**, **188**, **197** and **201** were tested at 37°C with $PHD2_{181-426}$ and CODD substrate (**Table 31**). Only **84** and **197** resulted in an increase in enzyme turnover. In general, there was a 40% loss in the increase in turnover in comparison to the room temperature experiment. **188** and **201** resulted in no difference in substrate turnover. The reduced efficacy of analogues **84** and

197 suggest the effect observed is not due to increasing the rate of reaction but rather a result of an impact on rate limiting steps such as substrate recruitment and ejection.

Table 31: SAR the of selected compounds **84**, **188**, **197** and **201** on different PHD2 constructs and PHD3 using the CODD substrate. PHD3 experiments was performed by Ms Kerstin Lippl and Dr A Tumber. Experiment performed by Dr A Tumber. Experimental measurement n =1.

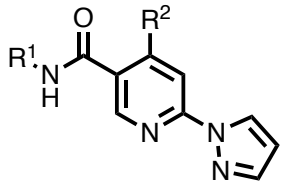

			Increase in CODD hydroxylation in comparison to DMSO Ctrl using 25 µM of compound			
Cpd	**R¹**	**R²**	**PHD2$_{181-426}$**	**PHD2$_{177-404}$**	**PHD3**	**PHD2$_{181-426}$ at 37°C**
84	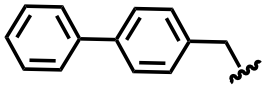		**61%**	**36%**	**0%**	**18%**
188	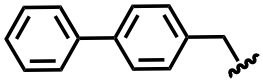	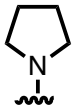	**41%**	**8%**	**0%**	**0%**
197	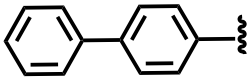		**65%**	**22%**	**0%**	**27%**
201	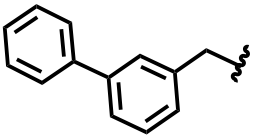		**30%**	**ND**	**ND**	**0%**

5.7 Summary

In this chapter, investigations on small molecules that increased the PHD2-catalysed HIF-α prolyl hydroxylation have been described. **84** was shown to destabilise HIF1-α in multiple cell lines including Hep3B and mitochondrial deficient cell lines 206p0 and 143B under hypoxic conditions (**Figures 54**, **55**, **57** & **58**). **200** also achieved HIF1-α degradation in the hypoxic Hep3B cell line. **200** was designed because the 4-hydroxy analogue (**117**) demonstrated HIF-1α stabilisation in the Hep3B cell line indicating interaction with PHD2 in a cellular environment. Even in the presence of the pan-PHD inhibitor FG-4592 (**4**), HIF1-α was degraded in the presence of **84**.

The SAR suggested that all substituents of **84** were important for the effect observed (**Figure 66**). SAR investigating the role of the *C*-5 amide substituent revealed, hydrophobicity was not an important factor for the increased turnover (**197**-**201**). However, the length and the linearity of the binding substituent were important for the effect observed indicating a preference for the substituents at the *C*-4 of the phenyl ring of **84** (**Table 28**) (**Figure 66**). The bidentate metal chelating group was shown to be required for activation of PHD2. However, this is not for chelation of the active site metal, but due to the three-dimensional shape of the pharmacophore as the compound-mediated increase in CODD turnover by PHD2 was maintained by replacing the pyrazole group of **84** (**Table 29**) (**Figure 66**). SAR of the *C*-4 amino substituent revealed the sensitivity to the observed effect in relation to the size, rigidity and three-dimensional shape of the amino substituent (**Table 27**).

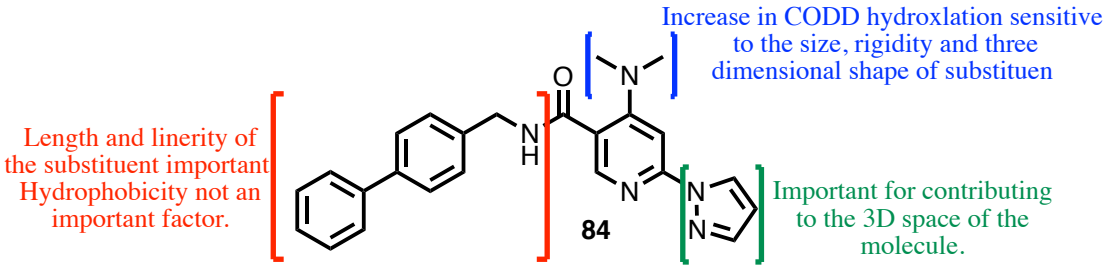

Figure 66: Summary of the SAR work of **84**, investigating the increase in CODD hydroxylation in comparison to the DMSO control.

In preliminary results, **84**, **188**, **197** and **201** resulted in different levels of increased hydroxylation of NODD and CODD (**Table 30**). It was envisaged that the different levels of increased hydroxylation observed could be due to how NODD and CODD substrates bind to PHD2 (**Figure 65**).[17] Selectivity over PHD3 was assessed with the same CODD substrate; no increased activity was observed in this case (**Table 31**), demonstrating the importance of the enzyme-substrate complex for the increased hydroxylation. A $PHD2_{177\text{-}404}$ construct (truncated *C*-terminal region) resulted in substantial reduction in the amount of increase of CODD hydroxylation, indicating an interaction of the *C*-terminus with **84**, **188**, **197** and **201**.

Four mechanisms of enzymatic activation were discussed (**Chapter 5.1**).[2,3,4,5,6,7] The *in-vitro* data collected within this chapter indicated a novel mechanism of action, as the data suggested the analogues affect the enzyme-substrate complex. This novel mechanism of action may provide an explanation for the observed differences between the hydroxylation rates of NODD and CODD, selectivity over the PHD isoforms, temperature effects and PHD2 constructs. One mechanism of action described was enzyme stabilisation; however, if this were true for analogues of **84**, the temperature increase and a difference in CODD/ NODD selectivity and efficacy loss would not occur.

It was shown in **Chapter 2.9**, that neither series displaced the CODD substrate. It was envisaged that the structural similarities between **32** and **84**, may suggest that **84** also does not displace CODD. It was suggested that **84** may bind in an similar fashion observed with FG-2216 (**3**) (**Figure 57**). It was envisaged that the presence of 2OG may compete with analogues of **84** for the active site, thus forcing an alternative binding mode for analogues of **84**. The rate limiting steps of the enzyme catalytic cycle could be either: oxygen delivery displacing the water molecule on the metal, substrate recruitment or the release of the hydroxylated substrate (**Figure 5**). Unpublished data from the Schofield group, (from Abboud *et al*.), have shown that the hydroxylated CODD substrate can still bind to the PHD2 Fe(II) complex, but that the presence of the 2OG displaces the hydroxylated CODD. It has been envisaged that the analogues of **84** may work in a similar fashion to 2OG. **84** may bind allosterically, towards the PHD2 *C*-terminus effectively between the enzyme and substrate, thus weakening the hydroxylated substrate-enzyme complex. This allosteric binding may lead to an increased amount of available catalytically active enzyme and therefore, increasing the amount of hydroxylated HIF-1α substrate. Improving oxygen delivery to the PHD2 may be an important factor and may explain the increased turnover; however, this parameter has not been explored.

5.8 Compound Characterisation

General Procedure E: S_NAr of the pyrazole group to the *C*-2 position of the pyridine ring:

82 (1 equiv) was dissolved in DMAc (2 ml) before the addition of the selected amine (3 equivs). The resultant mixture was heated under microwave radiation at 120°C for 2 hrs. The resultant mixture was diluted with water (15 ml) and extracted with EtOAc (3 x 20 ml). The organic phases combined and washed with water, brine and dried with anhydrous Na_2SO_4. The volatiles were then evaporated in *vacuo* and purified by flash column chromatography using (100 % - 95% CH_2CL_2, 0% - 5% MeOH) over 15 column volumes to give the desired compound.

General Procedure F: S_NAr of the pyrazole group to the *C*-2 position of the di-chloropyridine and dimethylamine group to the *C*-4 position of di-chloropyridine:

The requisite di-chloropyridine (1 equiv), Pyrazole (0.25 equiv) and Cs_2CO_3 (2.5 equiv) was suspended in DMAc (2.5 ml) and heated under microwave radiation at 80°C for 30 min. An additional equivalent of pyrazole was added to the reaction mixture and the resulting mixture was heated again at 80°C for 30 mins, this was repeated 2 more times. Dimethylamine (5 equiv) was then added to the reaction mixture and the resulting mixture was heated under microwave radiation at 120°C for 3 hrs. The resultant mixture was diluted with water (15 ml) and extracted with EtOAc (3 x 20 ml). The organic phases combined and washed with water, brine and dried with anhydrous Na_2SO_4. The volatiles were then evaporated in *vacuo* and purified by flash column

chromatography using (Cyclohexane 100% - 75%, EtOAc 0 - 25%) over 15 column volumes to give the desired compound.

N-([1,1'-biphenyl]-4-ylmethyl)-4-(methylamino)-6-(1H-pyrazol-1-yl)nicotinamide 186

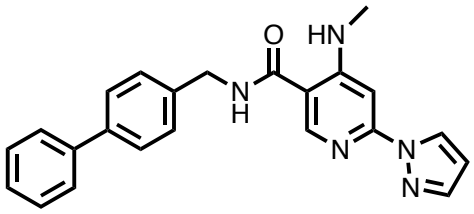

Following general procedure E: **82** (29 mg, 0.0747 mmol), methylamine (2M in THF) (7.5 mg, 0.234 mmol) gave **186** (16 mg ,0.041 mmol, 55%) with the appearance as a clear oil. **^{1}H NMR** (400 MHz, DMSO-d_6) δ 8.85 (t, J = 6.0 Hz, 1H, NH), 8.16 (s, 1H, Pyr), 7.96 (d, J = 2.5 Hz, 1H, Pyzl), 7.78 – 7.31 (m, 10H, Ar), 6.65 (s, 1H, Pyr), 6.45 (dd, J = 2.5, 1.5 Hz, 1H, Pyzl), 4.40 (d, J = 6.0 Hz, 2H, CH_2), 2.82 (d, J = 5.0 Hz, 3H, CH_3). **^{13}C NMR** (101 MHz, DMSO-d_6) δ 166.19, 149.03, 141.20, 138.65, 130.25, 128.93, 127.96, 127.32, 126.74, 126.52, 114.64, 107.59, 99.66, 42.28, 39.52, 28.03. **FT-IR** ν_{max} (film) 3394, 1654 cm^{-1} **HRMS** $C_{23}H_{22}ON_5$ $[M+H]^+$: 384.1818, found : 384.1814.

N-([1,1'-biphenyl]-4-ylmethyl)-4-(diethylamino)-6-(1H-pyrazol-1-yl)nicotinamide 187

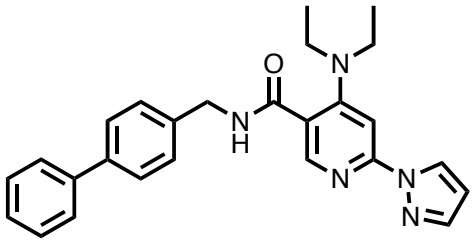

Following General Procedure E: **82** (50 mg, 0.128 mmol), diethylamine (14 mg, 0.192 mmol) in DMAc (3 ml) gave **187** (38 mg, 0.089 mmol, 69 %) as a clear oil.

^{1}H NMR (400 MHz, DMSO-d_6) δ 8.81 (t, J = 6.0 Hz, 1H, NH), 8.22 (s, 1H, Pyr), 8.07 (dd, J = 2.5, 0.5 Hz, 1H, Pyzl), 7.74 (dd, J = 1.5, 0.5 Hz, 1H, Pyzl), 7.70 – 7.60 (m, 5H, Ar), 7.50 – 7.39 (m, 4H, Ar), 6.70 (s, 1H, Pyr), 6.46 (dd, J = 2.5, 1.5 Hz, 1H, Pyzl), 4.40 (d, J = 6.0 Hz, 2H, CH_2NH), 3.56 (q, J = 7.0 Hz, 4H, $\underline{CH_2}CH_3$), 1.13 (t, J = 7.0 Hz, 6H, $CH_2\underline{CH_3}$). **^{13}C NMR** (126 MHz, DMSO-d_6) δ 166.58, 158.55, 149.43, 145.94, 141.62, 140.40, 139.02, 130.81, 129.33, 128.32, 127.70, 126.97, 126.89, 114.62, 107.94, 98.25, 42.65, 42.52, 39.52, 13.13. **FT-IR** ν_{max} (film) 1658 cm^{-1}. **HRMS** (ESI-TOF) calcd for $C_{26}H_{28}ON_5$ $[M+H]^+$: 426.2284, found: 426.2284.

N-([1,1'-biphenyl]-4-ylmethyl)-6-(1H-pyrazol-1-yl)-4-(pyrrolidin-1-yl)nicotinamide 188

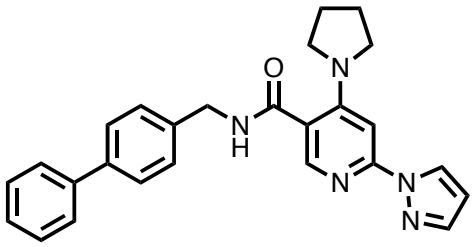

Following General Procedure E: **82** (50 mg, 0.128 mmol), pyrolidine (13.5 mg, 0.192 mmol) in DMAc (3 ml) gave **188** (37 mg, 0.087 mmol, 68%) as a white solid.

m.p. 135-139°C. **^{1}H NMR** (400 MHz, DMSO-d_6) δ 8.82 (t, J = 6.0 Hz, 1H, NH), 8.24 (s, 1H, Pyr), 8.08 (d, J = 2.5 Hz, 1H, Pyzl), 7.75 (d, J = 1.5 Hz, 1H, Pyzl), 7.72 – 7.38 (m, 9H,

Ar), 6.59 (s, 1H, Pyr), 6.47 (dd, J = 2.5, 1.5 Hz, 1H, Pyzl), 4.41 (d, J = 6.0 Hz, 2H, CH_2), 3.51 – 3.42 (m, 4H, pyrrolidine), 1.96 – 1.95 (m, 4H, pyrrolidine). **^{13}C NMR** (101 MHz, DMSO-d_6) δ 169.60, 166.26, 157.88, 149.15, 145.14, 141.25, 140.04, 138.71, 138.65, 130.38, 128.94, 127.98, 127.32, 126.60, 126.52, 114.31, 107.59, 98.76, 46.66, 42.30, 39.52, 24.98. **FT-IR** ν_{max} (film) 1649 cm^{-1}. **HRMS** (ESI-TOF) calcd for $C_{26}H_{26}ON_5$ $[M+H]^+$: 424.2131, found : 424.2126.

_N_-([1,1'-biphenyl]-4-ylmethyl)-4,6-di(1_H_-pyrazol-1-yl)nicotinamide 189

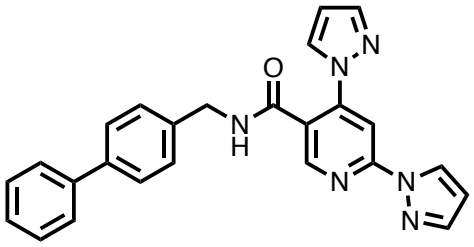

Following general procedure E: **82** (50 mg, 0.128 mmol), pyrazole (17 mg, 0.256 mmol) and Cs_2CO_3 (104 mg, 0.32 mmol) gave **189** (41 mg, 0.097 mmol, 76%) as a clear oil.

^{1}H NMR (400 MHz, DMSO-d_6) δ 9.25 (t, *J* = 6.0 Hz, 1H, NH), 8.70 (d, *J* = 2.5 Hz, 1H, Pyzl), 8.57 (s, 1H, Pyr), 8.31 (d, *J* = 2.5 Hz, 1H, Pyzl), 8.23 (s, 1H, Pyr), 7.91 (d, *J* = 1.5 Hz, 1H, Pyzl), 7.88 (d, *J* = 1.5 Hz, 1H, Pyzl), 7.72 – 7.59 (m, 4H, Ar), 7.51 – 7.43 (m, 4H, Ar), 7.41 – 7.33 (m, 1H, Ar), 6.65 (dd, *J* = 2.5, 1.5 Hz, 1H, Pyzl), 6.57 (dd, *J* = 2.5, 1.5 Hz, 1H, Pyzl), 4.51 (d, *J* = 6.0 Hz, 2H, CH_2). **^{13}C NMR** (101 MHz, DMSO-d_6) δ 165.23, 152.06, 149.08, 145.63, 143.03, 142.61, 139.96, 138.88, 137.94, 130.41, 128.95, 128.23,

127.71, 127.37, 123.26, 109.04, 108.97, 103.87, 42.52, 39.52. **FT-IR** ν_{max} (film) 1658 cm^{-1}. **HRMS** (ESI-TOF) calcd for $C_{25}H_{21}ON_6$ $[M+H]^+$: 421.1771, found : 421.1769.

N-([1,1'-biphenyl]-4-ylmethyl)-4-morpholino-6-(1H-pyrazol-1-yl)nicotinamide 190

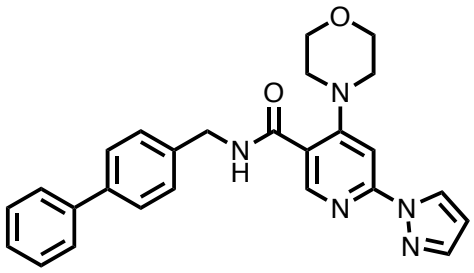

Following General Procedure E: **82** (50 mg, 0.128 mmol), morpholine (17 mg, 0.192 mmol) in DMAc (3 ml) gave **190** (21 mg, 0.047 mmol, 38%) as a clear oil.

^{1}H NMR (400 MHz, DMSO-d_6) δ 8.86 (t, J = 6.0 Hz, 1H, NH), 8.27 (s, 1H, Pyr), 8.16 (d, J = 2.5 Hz, 1H, Pyzl), 7.76 (d, J = 1.5 Hz, 1H, Pyzl), 7.71 – 7.30 (m, 10H, Ar), 6.99 (s, 1H, Pyr), 6.49 (dd, J = 2.5, 1.5 Hz, 1H, Pyzl), 4.42 (d, J = 6.0 Hz, 2H, CH_2), 3.70 (t, J = 6.0, 4.0 Hz, 4H, Morpholine (Mor)), 3.57 (t, J = 6.0, 4.0 Hz, 4H, Mor). **^{13}C NMR** (101 MHz, DMSO-d_6) δ 39.52, 42.29, 44.99, 65.88, 99.23, 107.76, 116.30, 126.50, 126.60, 127.31, 127.98, 128.93, 130.31, 138.65, 140.02, 141.43, 145.60, 148.62, 160.07, 165.99. **FT-IR** ν_{max} (film) 1649 cm^{-1}. **HRMS** (ESI-TOF) calcd for $C_{26}H_{26}O_2N_5$ $[M+H]^+$: 440.2081, found 440.2081.

N-([1,1'-biphenyl]-4-ylmethyl)-4-amino-6-chloronicotinamide 191

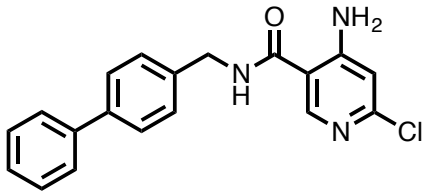

Following general procedure C: 4-amino-6-chloronicotinic acid (450 mg, 2.61 mmol), 4-phenylbenzylamine (1.1 g, 6.54 mmol), T3P (2.4 g, 7.83 mmol) and DIPEA (970 mg, 7.8 mmol) gave **191** (750 mg, 2.22 mmol, 85 %) as a white solid.

m.p. 218-221°C. **^{1}H NMR** (400 MHz, DMSO-d_6) δ 9.10 (t, J = 6.0 Hz, 1H, NH), 8.42 (s, 1H, Pyr), 7.67 – 7.27 (m, 11H), 6.69 (s, 1H), 4.48 (d, J = 6.0 Hz, 2H, CH_2). **^{13}C NMR** (101 MHz, DMSO-d_6) δ 166.68, 156.50, 151.92, 149.44, 139.96, 138.76, 138.61, 128.91, 127.86, 127.32, 126.64, 126.57, 110.68, 108.38, 41.96, 39.52. **FT-IR** ν_{max} (film) 3376, 3362, 1638 cm^{-1}. **HRMS** (ESI-TOF) calcd for $C_{19}H_{17}O_4N_3{}^{35}Cl$ $[M+H]^+$: 338.1054, found : 338.1053.

N-([1,1'-biphenyl]-4-ylmethyl)-4-amino-6-(1H-pyrazol-1-yl)nicotinamide 192

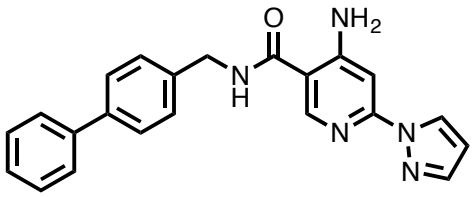

Following general procedure E: **191** (882 mg, 2.6 mmol), Pd^{t}BuXPhos G3 (206 mg, 0.26 mmol), Cs_2CO_3 (2.5 g, 7.82 mmol) and pyrazole (442 mg, 6.5 mmol) gave **192** (204 mg, 0.55 mmol, 21%) as a white solid.

m.p. 209-214°C. **^{1}H NMR** (400 MHz, DMSO-d_6) δ 9.09 (t, J = 6.0 Hz, 1H, NH), 8.57 (s, 1H, Pyr), 8.56 (d, J = 1.0 Hz, 1H, Pyzl), 7.78 (dd, J = 1.5, 1.0 Hz, 1H, Pyzl), 7.70 – 7.59 (m, 4H, Ar), 7.50 – 7.31 (m, 5H, Ar), 7.24 (s, 1H, Pyr), 6.53 (dd, J = 2.5, 1.5 Hz, 1H, Pyzl), 4.51 (d, J = 6.0 Hz, 2H, CH_2).**^{13}C NMR** (101 MHz, DMSO-d_6) δ 167.10, 156.82, 152.05, 148.92, 142.06, 139.99, 138.86, 138.73, 128.93, 127.97, 127.84, 127.32, 127.30, 126.66, 126.58, 109.76, 107.84, 96.20, 41.94, 39.52. **FT-IR** ν_{max} (film) 3372, 3357, 1641 cm^{-1}. **HRMS** (ESI-TOF) calcd for $C_{22}H_{22}ON_5$ $[M+H]^+$: 370.1662, found : 370.1659.

N-([1,1'-biphenyl]-4-yl)-4,6-dichloronicotinamide 193

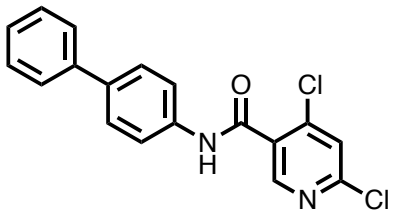

Following general procedure C: 4,6-dichloronicotinic acid (1.36 g, 7.1 mmol), 4-biphenylamine (1.2 g, 7.1 mmol), T3P (6.8 g, 21 mmol) and DIPEA (2.2 g, 17.7 mmol) gave **193** (322 mg, 0.943 mmol, 14 %) as a clear oil.

^{1}H NMR (400 MHz, DMSO-d_6) δ 10.82 (s, 1H, NH), 8.71 (s, 1H, Pyr), 8.00 (s, 1H, Pyr), 7.85 – 7.23 (m, 9H, Ar). **^{13}C NMR** (101 MHz, DMSO-d_6) δ 161.74, 151.78, 151.54, 149.24, 142.69, 139.54, 137.91, 135.96, 127.23, 127.11, 126.36, 126.27, 124.86, 120.03,

39.52. **FT-IR** ν_{max} (film) 1673 cm^{-1}. **HRMS** (ESI-TOF) calcd for $C_{18}H_{11}ON_2{}^{35}Cl_2$ $[M-H]^-$: 341.0253, found : 341.0254.

4,6-dichloro-N-(cyclohexylmethyl)nicotinamide 194

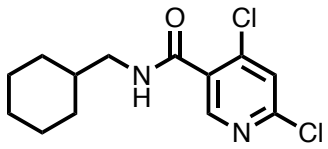

Following general procedure C: 4,6-dichloronicotinic acid (300 mg, 1.56 mmol), cyclohexyl methylamine (211 mg, 1.24 mmol), T3P (1.48 g, 4.68 mmol) and DIPEA (483 mg, 3.9 mmol) gave **194** (326 mg, 1.13 mmol, 72 %) as a white solid.

m.p. 126-127°C. **^{1}H NMR** (400 MHz, DMSO-d_6) δ 8.65 (t, J = 6.0 Hz, 1H, NH), 8.45 (s, 1H, Pyr), 7.90 (s, 1H, Pyr), 3.12 – 3.05 (m, 2H), 1.78 – 0.85 (m, 11H). **^{13}C NMR** (101 MHz, DMSO-d_6) δ 25.42, 26.01, 26.36, 30.39, 37.34, 39.52, 45.38, 124.69, 132.32, 142.42, 148.91, 150.96, 163.15. **FT-IR** ν_{max} (film) 1650 cm^{-1}. **HRMS** (ESI-TOF) calcd for $C_{13}H_{15}ON_2{}^{35}Cl_2$ $[M+H]^+$: 285.05616, found : 285.0566.

4,6-dichloro-N-(3-(trifluoromethyl)benzyl)nicotinamide 194

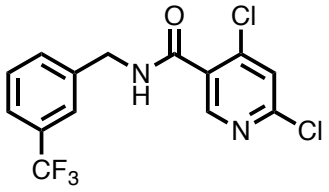

Following general procedure C: 4,6-dichloronicotinic acid (300 mg, 1.56 mmol), 3-trifluoromethyl benzylamine (328 mg, 1.24 mmol), T3P (1.48 g, 4.68 mmol) and DIPEA (483 mg, 3.9 mmol) gave **194** (411 mg, 1.26 mmol, 75%) as a white solid.

m.p. 108-110°C. **^{1}H NMR** (400 MHz, DMSO-d_6) δ 9.33 (t, J = 6.0 Hz, 1H, NH), 8.56 (s, 1H Pyr), 7.94 (s, 1H, Pyr), 7.75 – 7.56 (m, 4H, Ar), 4.58 (d, J = 6.0 Hz, 2H, CH_2). **^{13}C NMR** (101 MHz, DMSO-d_6) δ 39.52, 42.17, 123.76, 124.86, 125.62, 128.94, 129.51, 131.43, 131.70, 140.12, 142.50, 149.02, 151.35, 163.53. **FT-IR** ν_{max} (film) 1633 cm^{-1}. **HRMS** (ESI-TOF) calcd for $C_{14}H_8ON_2{}^{35}Cl_2F_3$ [M-H]$^-$: 346.9968, found : 346.9969.

4,6-dichloro-N-(4-(trifluoromethyl)benzyl)nicotinamide 195

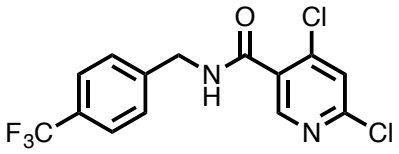

Following general procedure C: 4,6-dichloronicotinic acid (300 mg, 1.56 mmol), 4-trifluorobenzylamine (327 mg, 1.87 mmol), T3P (1.48 g, 4.68 mmol) and DIPEA (483 mg, 3.9 mmol) gave **195** (180 mg, 0.517 mmol, 33%) as a white solid.

m.p. 164-167°C. **^{1}H NMR** (400 MHz, DMSO-d_6) δ 9.33 (t, J = 6.0 Hz, 1H, NH), 8.57 (s, 1H, Pyr), 7.94 (s, 1H, Pyr), 7.76 – 7.71 (m, 2H, Ar), 7.63 – 7.56 (m, 2H, Ar), 4.57 (d, J = 6.0 Hz, 2H, CH_2). **^{13}C NMR** (101 MHz, DMSO-d_6) δ 163.50, 151.35, 149.07, 143.48, 142.59, 131.65, 127.96, 125.35, 125.32, 125.28, 125.24, 124.85, 42.27, 39.52. **FT-IR** ν_{max}

(film) 1632 cm^{-1}. **HRMS** (ESI-TOF) calcd for $C_{14}H_8ON_2{}^{35}Cl_2F_3$ $[M-H]^-$: 346.9969, found : found : 346.9969.

N-([1,1'-biphenyl]-3-ylmethyl)-4,6-dichloronicotinamide 196

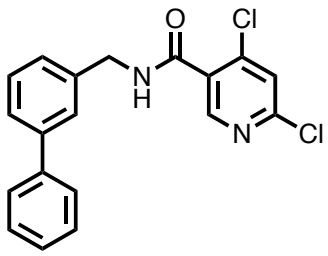

Following general procedure C: 4,6-dichloronicotinic acid (300 mg, 1.56 mmol), 3-phenylbenzylamine (342 mg, 1.87 mmol), T3P (1.48 g, 4.68 mmol) and DIPEA (483 mg, 3.9 mmol) gave **196** (289 mg, 0.79 mmol, 52 %) as a white solid.

m.p. 119-124°C. **^{1}H NMR** (400 MHz, Chloroform-*d*) δ 8.61 (t, J = 5.5 Hz, 1H, NH), 7.59 – 7.14 (m, 10H, Ar), 6.51 (s, 1H), 4.66 (d, J = 5.5 Hz, 2H, CH_2). **^{13}C NMR** (101 MHz, Chloroform-*d*) δ 163.27, 153.64, 150.88, 142.71, 142.10, 140.72, 137.71, 129.51, 129.00, 127.73, 127.26, 126.91, 126.87, 125.19, 77.16, 44.61. **FT-IR** ν_{max} (film) 1654 cm^{-1}. **HRMS** (ESI-TOF) calcd for $C_{19}H_{13}ON_2{}^{35}Cl_2$ $[M+H]^+$: 355.0409, found : 355.0409.

N-([1,1'-biphenyl]-4-yl)-4-(dimethylamino)-6-(1H-pyrazol-1-yl)nicotinamide 197

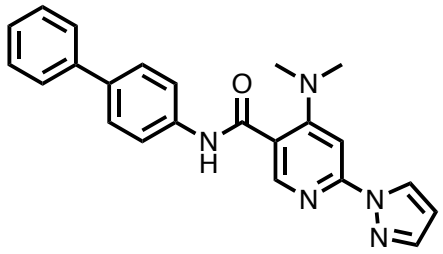

Following general procedure F**: 193** (150 mg, 0.43 mmol), pyrazole (29 mg, 0.43 mmol) and Cs_2CO_3 (279 mg, 0.86 mmol) in DMF (5 ml) gave **197** (20 mg, 0.0522 mmol, 12 %) as a clear oil.

^{1}H NMR (400 MHz, DMSO-d_6) δ 8.33 (s, 1H, NH), 8.26 – 8.24 (m, 1H, Pyr), 7.72 – 7.59 (m, 6H, Ar), 7.49 – 7.41 (m, 2H, Ar), 7.35 – 7.31 (m, 1H, Ar), 6.80 (s, 1H, Pyr), 6.50 (dd, J = 2.5, 1.5 Hz, 1H, Pyzl), 3.14 (s, 6H, $(CH_3)_2$). **^{13}C NMR** (101 MHz, DMSO-d_6) δ 160.13, 149.08, 145.44, 141.41, 139.80, 139.02, 134.90, 130.33, 128.91, 127.01, 126.82, 126.27, 119.75, 114.85, 107.74, 97.92, 39.52, 37.79. **FT-IR** ν_{max} (film) 1642 cm^{-1}. **HRMS** (ESI-TOF) calcd for $C_{23}H_{22}ON_5$ $[M+H]^+$: 384.1816, found : 384.1816.

N-(cyclohexylmethyl)-4-(dimethylamino)-6-(1H-pyrazol-1-yl)nicotinamide 198

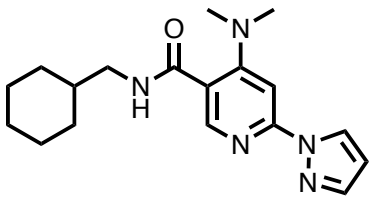

Following general procedure F: **194** (150 mg, 0.52 mmol), pyrazole (31 mg, 0.47 mmol), Cs_2CO_3 (338 mg, 1.04 mmol) and Dimethylamine ((2M in THF) (47 mg, 1.04 mmol)) gave **198** (54 mg, 0.16 mmol, 31 %) as a white solid.

m.p. 138-143°C. **^{1}H NMR** (400 MHz, DMSO-d_6) δ 8.20 (t, J = 6.0 Hz, 1H, NH), 8.14 (d, J = 0.5 Hz, 1H, Pyr), 8.07 (dd, J = 2.5, 1.0 Hz, 1H, Pyzl), 7.70 (dd, J = 1.5, 1.0 Hz, 1H, Pyzl), 6.74 (d, J = 0.5 Hz, 1H, Pyr), 6.49 (dd, J = 2.5, 1.5 Hz, 1H, Pyzl), 3.09 (s, 6H, $(CH_3)_2$), 2.96 (t, J = 6.0 Hz, 2H, CH_2NH), 1.74 – 0.75 (m, 12H, Cyclohexane). **^{13}C NMR** (101 MHz, DMSO-d_6) δ 25.47, 26.09, 30.48, 37.22, 37.74, 39.52, 45.37, 98.20, 107.57, 114.95, 130.41, 148.69, 165.97. **FT-IR** ν_{max} (film) 1662 cm^{-1}. **HRMS** (ESI-TOF) calcd for $C_{18}H_{26}ON_5$ $[M+H]^+$: 328.2127, found : 328.2127.

4-(dimethylamino)-6-(1H-pyrazol-1-yl)-N-(3-(trifluoromethyl)benzyl)nicotinamide 199

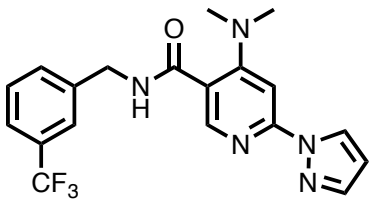

Following general procedure F: **195** (150 mg, 0.429 mmol), pyrazole (25 mg, 0.38 mmol), Cs_2CO_3 (278 mg, 0.858 mmol) and Dimethylamine (2M in THF) 38 mg, 0.858 mmol) gave **199** (26 mg, 0.066 mmol, 16%) as a white solid.

m.p. 85-93°C. **^{1}H NMR** (400 MHz, DMSO-d_6) δ 8.86 (t, J = 6.0 Hz, 1H, NH), 8.23 (s, 1H, Pyr), 8.12 (dd, J = 2.5, 1.0 Hz, 1H, Pyzl), 7.77 – 7.53 (m, 4H, Ar), 6.74 (s, 1H, Pyr), 6.45 (t,

J = 2.5, 1.5 Hz, 1H, Pyzl), 4.46 (d, J = 6.0 Hz, 2H, CH_2), 3.10 (s, 6H, $(CH_3)_2$). **^{13}C NMR** (101 MHz, DMSO-d_6) δ 37.74, 39.52, 42.13, 98.26, 107.55, 114.49, 123.04, 123.45, 123.83, 125.75, 129.25, 130.28, 131.56, 141.13, 145.45, 148.76, 160.05, 166.38. **FT-IR** ν_{max} (film) 1647 cm^{-1}. **HRMS** (ESI-TOF) calcd for $C_{19}H_{19}ON_5F_3$ $[M+H]^+$: 390.1530, found : 390.1530.

4-(dimethylamino)-6-(1H-pyrazol-1-yl)-N-(4-(trifluoromethyl)benzyl)nicotinamide 200

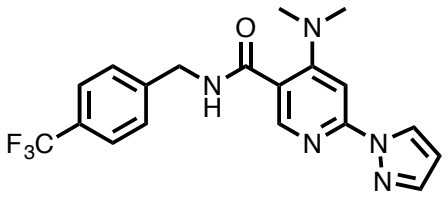

Following general procedure F: **195** (100 mg, 0.286 mmol), pyrazole (20 mg, 0.286 mmol), Cs_2CO_3 (185 mg, 0.572 mmol) and dimethylamine ((2M in THF) (26 mg, 0.57 mmol)) gave **200** (34 mg, 0.087 mmol, 31%) as a clear viscous oil.

^{1}H NMR (400 MHz, DMSO-d_6) δ 8.86 (t, J = 6.0 Hz, 1H, NH), 8.25 (s, 1H, Pyr), 8.13 (dd, J = 2.5, 1.0 Hz, 1H, Pyzl), 7.80 – 7.53 (m, 4H, Ar), 6.75 (s, 1H, Pyr), 6.46 (dd, J = 2.5, 1.5 Hz, 1H, Pyzl), 4.45 (d, J = 6.0 Hz, 2H, CH_2), 3.11 (s, 6H, $(CH_3)_2$). **^{13}C NMR** (101 MHz, DMSO-d_6) δ 37.72, 39.52, 42.20, 98.22, 107.58, 114.51, 125.06, 127.98, 130.32, 141.28, 144.40, 145.42, 148.76, 160.02, 166.37. **FT-IR** ν_{max} (film) 1642 cm^{-1}. **HRMS** (ESI-TOF) calcd for $C_{19}H_{19}ON_5F_3$ $[M+H]^+$: 390.1536, found : 390.1535.

N-([1,1'-biphenyl]-3-ylmethyl)-4-(dimethylamino)-6-(1H-pyrazol-1-yl)nicotinamide 201

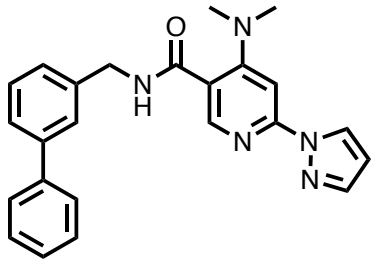

Following general procedure F: **196** (50 mg, 0.14 mmol), pyrazole (9.5 mg, 0.14 mmol), Cs_2CO_3 (91 mg, 0.28 mmol) and dimethylamine ((2M in THF) (13 mg, 0.28 mmol)) gave **201** (15 mg, 0.037 mmol, 27 %) as a clear viscous oil.

^{1}H NMR (400 MHz, DMSO-d_6) δ 8.83 (t, J = 6.0 Hz, 1H, NH), 8.23 (s, 1H, Pyr), 8.08 (dd, J = 2.5, 1.0 Hz, 1H, Pyzl), 7.71 – 7.26 (m, 11H, Ar), 6.38 (dd, J = 2.5, 1.5 Hz, 1H, Pyzl), 4.44 (d, J = 6.0 Hz, 2H, CH_2), 3.10 (s, 6H, $(CH_3)_2$). **^{13}C NMR** (126 MHz, DMSO-d_6) δ 166.51, 160.33, 149.08, 145.74, 141.47, 140.62, 140.38, 130.70, 129.27, 129.19, 127.80, 127.08, 126.87, 126.13, 125.49, 114.88, 107.84, 98.61, 42.97, 39.52, 38.06. **FT-IR** ν_{max} (film) 1664 cm^{-1} **HRMS** (ESI-TOF) calcd for $C_{24}H_{24}ON_5$ $[M+H]^+$: 398.1973, found : 398.1973.

N-([1,1'-biphenyl]-4-ylmethyl)-4,6-dichloronicotinamide 202

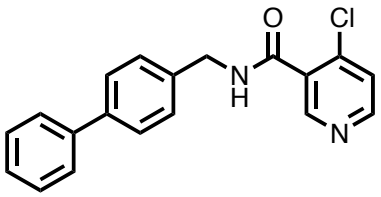

Following general procedure C: 4-chloronicotinic acid (300 mg, 1.91 mmol), 4-phenylbenzylamine (419 mg, 2.29 mmol), T3P (1.5 g, 4.77 mmol) and DIPEA (599 mg, 4.77 mmol) gave **202** (310 mg, 0.955 mmol, 50%) as a orange gum.

^{1}H NMR (400 MHz, Chloroform-*d*) δ 8.90 (s, 1H, Pyr), 8.53 (s, 1H, Pyr), 7.66 – 7.30 (m, 10H, Ar), 6.88 (s, 1H, Pyr), 4.71 (d, J = 5.0 Hz, 2H, Pyzl). **^{13}C NMR** (126 MHz, Chloroform-*d*) δ 174.53, 170.85, 166.19, 142.45, 140.44, 139.94, 136.27, 135.96, 130.17, 128.76, 128.66, 127.20, 126.89, 115.92, 113.74, 77.16, 43.30. **FT-IR** ν_{max} (film) 1656 cm^{-1}.

HRMS (ESI-TOF) calcd for $C_{19}H_5ON_2{}^{35}Cl_2$ $[M+H]^+$: 323.0945, found : 323.0946.

N-([1,1'-biphenyl]-4-ylmethyl)-4-(dimethylamino)nicotinamide 203

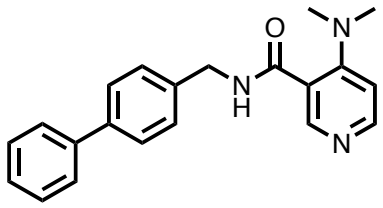

Following General Procedure E: **202** (100 mg, 0.31 mmol), dimethylamine ((2M in THF) (28 mg, 0.621 mmol) in DMAc (3 ml) gave **203** (57 mg, 0.171 mmol, 55 %) as a clear viscous oil.

^{1}H NMR (400 MHz, Chloroform-*d*) δ 10.89 (t, J = 6.0 Hz, 1H, NH), 8.50 – 8.47 (m, 1H, Pyr), 8.18 (d, J = 6.0 Hz, 1H, Pyr), 7.63 – 7.29 (m, 9H, Ar), 6.65 (d, J = 6.0 Hz, 1H, Pyr), 4.64 (d, J = 6.0 Hz, 2H, CH_2), 2.86 (s, 6H, $(CH_3)_2$). **^{13}C NMR** (101 MHz, Chloroform-*d*) δ 41.98, 43.47, 77.16, 119.99, 126.77, 127.08, 127.20, 127.47, 128.24, 128.59, 136.72, 140.30, 141.34, 149.86, 150.34, 154.80, 165.15, 167.61, 178.32. **FT-IR** ν_{max} (film) 1662 cm^{-1}. **HRMS** (ESI-TOF) calcd for $C_{21}H_{22}ON_3$ $[M+H]^+$: 332.1757, found : 332.1756.

N-([1,1'-biphenyl]-4-ylmethyl)-4,6-bis(dimethylamino)nicotinamide 204

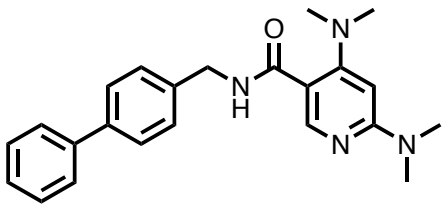

Following General Procedure E: **82** (70 mg, 0.20 mmol), Dimethylamine ((2M in THF) (18 mg, 0.39 mmol) in DMAc (3 ml) gave **204** (10 mg, 0.026 mmol, 13%) as a clear oil.

^{1}H NMR (400 MHz, DMSO-d_6) δ 8.66 (t, J = 6.0 Hz, 1H, NH), 8.02 (s, 1H, Pyr), 7.73 – 7.30 (m, 9H, Ar), 5.80 (s, 1H, Pyr), 4.45 (d, J = 6.0 Hz, 2H, CH_2), 3.02 (s, 6H, $(CH_3)_2$), 2.76 (s, 6H, $(CH_3)_2$). **^{13}C NMR** (101 MHz, DMSO-d_6) δ 37.71, 39.52, 41.79, 42.19, 90.02, 111.20, 126.55, 127.31, 127.99, 128.92, 138.57, 139.18, 139.96, 149.26, 156.70, 160.54,

167.77. **FT-IR** ν_{max} (film) 1645 cm^{-1}. **HRMS** (ESI-TOF) calcd for $C_{23}H_{27}ON_4$ $[M+H]^+$: 375.2179, found : 375.2173.

5.9 References

1 Rang, H. P. The receptor concept: pharmacology's big idea. *Br J Pharmacol* **147 Suppl 1**, S9-16, doi:10.1038/sj.bjp.0706457 (2006).

2 Zorn, J. A. & Wells, J. A. Turning enzymes ON with small molecules. *Nat Chem Biol* **6**, 179-188, doi:10.1038/nchembio.318 (2010).

3 Grimsby, J., Sarabu, R., Corbett, W. L., Haynes, N. E., Bizzarro, F. T., Coffey, J. W. *et al.* Allosteric activators of glucokinase: potential role in diabetes therapy. *Science* **301**, 370-373, doi: 10.1126/science.1084073 (2003).

4 Engel, M., Hindie, V., Lopez-Garcia, L. A., Stroba, A., Schaeffer, F., Adrian, I. *et al.* Allosteric activation of the protein kinase PDK1 with low molecular weight compounds. *EMBO J* **25**, 5469-5480, doi:10.1038/sj.emboj.7601416 (2006).

5 Cool, B., Zinker, B., Chiou, W., Kifle, L., Cao, N., Perham, M. *et al.* Identification and characterization of a small molecule AMPK activator that treats key components of type 2 diabetes and the metabolic syndrome. *Cell Metab* **3**, 403-416, doi:10.1016/j.cmet.2006.05.005 (2006).

6 Wolan, D. W., Zorn, J. A., Gray, D. C. & Wells, J. A. Small-molecule activators of a proenzyme. *Science* **326**, 853-858, doi:10.1126/science.1177585 (2009).

7 Thakur, C. S., Jha, B. K., Dong, B., Das Gupta, J., Silverman, K. M., Mao, H. *et al.* Small-molecule activators of RNase L with broad-spectrum antiviral activity. *Proc Natl Acad Sci U S A* **104**, 9585-9590, doi:10.1073/pnas.0700590104 (2007).

8 Kim, E. J., Kho, J. H., Kang, M. R. & Um, S. J. Active regulator of SIRT1 cooperates with SIRT1 and facilitates suppression of p53 activity. *Mol Cell* **28**, 277-290, doi:10.1016/j.molcel. 2007.08.030 (2007).

9 Zhao, W., Kruse, J. P., Tang, Y., Jung, S. Y., Qin, J. & Gu, W. Negative regulation of the deacetylase SIRT1 by DBC1. *Nature* **451**, 587-590, doi:10.1038/nature06515 (2008).

10 Howitz, K. T., Bitterman, K. J., Cohen, H. Y., Lamming, D. W., Lavu, S., Wood, J. G. *et al.* Small molecule activators of sirtuins extend Saccharomyces cerevisiae lifespan. *Nature* **425**, 191-196, doi:10.1038/nature01960 (2003).

11 Kaeberlein, M., McDonagh, T., Heltweg, B., Hixon, J., Westman, E. A., Caldwell, S. D. *et al.* Substrate-specific activation of sirtuins by resveratrol. *J Biol Chem* **280**, 17038-17045, doi: 10.1074/jbc.M500655200 (2005).

12 Pacholec, M., Bleasdale, J. E., Chrunyk, B., Cunningham, D., Flynn, D., Garofalo, R. S. *et al.* SRT1720, SRT2183, SRT1460, and resveratrol are not direct activators of SIRT1. *J Biol Chem* **285**, 8340-8351, doi:10.1074/jbc.M109.088682 (2010).

13 Chowdhury, R., Flashman, E., Mecinovic, J., Kramer, H. B., Kessler, B. M., Frapart, Y. M. *et al.* Studies on the reaction of nitric oxide with the hypoxia-inducible factor prolyl hydroxylase domain 2 (EGLN1). *J Mol Biol* **410**, 268-279, doi:10.1016/j.jmb.2011.04.075 (2011).

14 Ellinghaus, P., Heisler, I., Unterschemmann, K., Haerter, M., Beck, H., Greschat, S. *et al.* BAY 87-2243, a highly potent and selective inhibitor of hypoxia-induced gene activation has antitumor activities by inhibition of mitochondrial complex I. *Cancer Med* **2**, 611-624, doi:10.1002/ cam4.112 (2013).

15 Beeson, C. C., Beeson, G. C. & Schnellmann, R. G. A high-throughput respirometric assay for mitochondrial biogenesis and toxicity. *Anal Biochem* **404**, 75-81, doi:10.1016/j.ab.2010.04.040 (2010).

16 Wang, R., Novick, S. J., Mangum, J. B., Queen, K., Ferrick, D. A., Rogers, G. W. *et al.* The acute extracellular flux (XF) assay to assess compound effects on mitochondrial function. *J Biomol Screen* **20**, 422-429, doi:10.1177/1087057114557621 (2015).

17 Chowdhury, R., Leung, I. K., Tian, Y. M., Abboud, M. I., Ge, W., Domene, C. *et al.* Structural basis for oxygen degradation domain selectivity of the HIF prolyl hydroxylases. *Nat Commun* **7**, 12673, doi:10.1038/ncomms12673 (2016).

18 Epstein, A. C. R., Gleadle, J. M., McNeill, L. A., Hewitson, K. S., O'Rourke, J., Mole, D. R. *et al.* C. elegans EGL-9 and mammalian homologs define a family of dioxygenases that regulate

HIF by prolyl hydroxylation. *Cell (Cambridge, MA, U. S.)* **107**, 43-54, doi:10.1016/S0092-8674(01)00507-4 (2001).

19 Fong, G. H. & Takeda, K. Role and regulation of prolyl hydroxylase domain proteins. *Cell Death Differ* **15**, 635-641 (2008).

20 McDonough, M. A., Li, V., Flashman, E., Chowdhury, R., Mohr, C., Lienard, B. M. *et al.* Cellular oxygen sensing: Crystal structure of hypoxia-inducible factor prolyl hydroxylase (PHD2). *Proc Natl Acad Sci U S A* **103**, 9814-9819, doi:10.1073/pnas.0601283103 (2006).

21 Chowdhury, R., McDonough, M. A., Mecinovic, J., Loenarz, C., Flashman, E., Hewitson, K. S. *et al.* Structural basis for binding of hypoxia-inducible factor to the oxygen-sensing prolyl hydroxylases. *Structure* **17**, 981-989 (2009).

22 Hirsila, M., Koivunen, P., Gunzler, V., Kivirikko, K. I. & Myllyharju, J. Characterization of the human prolyl 4-hydroxylases that modify the hypoxia-inducible factor. *J Biol Chem* **278**, 30772-30780, doi:10.1074/jbc.M304982200 (2003).

23 Landazuri, M. O., Vara-Vega, A., Viton, M., Cuevas, Y. & del Peso, L. Analysis of HIF-prolyl hydroxylases binding to substrates. *Biochem Biophys Res Commun* **351**, 313-320 (2006).

CHAPTER 6: Novel Inhibitors To Reduce The Oxygen Consumption Rate (OCR) for Hypoxic Tumours in Radiotherapy.

6.1 Introduction

Hypoxic regions are frequent within solid malignancies and represent aggressive and treatment-resistant cancer.[1] Tumour cells can consume a higher level of oxygen compared to many normal tissues and consume more nutrients than their local vasculature network can offer. This creates the net negative effect of high nutrient demand and suboptimal delivery. The sustained high metabolic requirement of tumour cells eventually promotes rapid oncogene-driven growth of inefficient and immature vasculature.[2] Abnormal vasculature leads to the generation of diffusion-based oxygen gradients that forms hypoxia regions.[2] Gray *et al.*, discovered that hypoxic tumour cells are up to three times more resistant to ionizing radiation in contrast to normoxic tumour cells.[3] The resistance to radiation occurs because the radiation-induced cell damage is mediated primarily by indirect free-radical damage (the oxygen enhancement effect).[1,2] Radicals induced through radiolysis of water including stable hydroxides, have been shown to be responsible for up to two-thirds of initial radiation-induced damage.[4] The production of stable organic peroxides interact with broken DNA strands making radiation-induced damage further difficult for the cell to repair.[1,2] Previous attempts to alleviate tumour hypoxia in the clinic include the use of hyperbaric chambers and oxygen supplementation. However, such treatments showed poor efficaciousness or a lack of robustness across patient cohorts.[5]

Compounds that normalise tumour vasculature (remodelling agents) have been shown to act efficaciously in alleviating hypoxia.[6] However, multiple attempts at increasing the delivery or using oxygen mimetics such as, nimorazole have met with very limited success.[6] The use of transduction inhibitors such as, bevacizumab have been used to reduce tumour hypoxia and to increase the effectiveness of radiation.[7] Unfortunately, screening vasculature remodelling agents is difficult *in vitro* and not easily conductible to high-throughput screening.[6]

It was envisaged that an alternative strategy to reduce tumour hypoxia, and so improve the response to radiation therapy, would be to reduce the oxygen consumption rate (OCR). It has been shown that a reduction of the OCR in multicellular tumour spheroids can cause a reduction in the volume of the central region of hypoxia via improving the availability of oxygen.[8,9] Secomb *et al*., have suggested that a 30% decrease in OCR would alleviate severe tumour hypoxia using mathematical modelling and may be a more effective approach to reduce hypoxia than increasing the oxygen levels in blood or elevating blood flow. [10]

The only FDA-approved drug that is reported to reduce tumour hypoxia and the OCR, is the anti-diabetic, metformin via inhibition of mitochondrial complex I.[11] However, metformin only reduces OCR by 10-20% at pharmaceutical concentrations, indicating a need to identify small molecules with a significant OCR reduction, which may reduce the resistance to radiotherapy.[11] Previously, small molecules that inhibit OCR have only been identified using high throughput screening (HTS) to identify inhibitors of the HIF system. BAY 87-2243 (**205**, **Chapter 5**) was developed from this type of screen.[12,13]

Assessing the cellular OCR is possible through HTS techniques. Ashton *et al*. were the first to design a HTS to identify inhibitors of OCR in cancer cells.[6] Classical measurements of OCR are made using electron paramagnetic resonance (EPR) oximetry or a Clark electrode; however, modern approaches exist such as the Seahorse XF Analyzer (Agilent) which is capable of high throughput screening (HTS).[14,15] The Seahorse experiment (assay used and used in **Chapter 5.6** for OCR of **84**) works by using fluorophores that react with O_2 and thus can directly measure the concentration of O_2 from the changes in fluorescence over time from the medium in a transient sealed microchamber at the bottom of the well of cells.[14,15]

6.2 Previous Work: High Throughput Screening To Assess Oxygen Consumption

To identify a suitable starting point for OCR inhibitor the approach, coined by Noble prize Laurette James Black was used i.e. "*the best starting point for a new drug is an old drug*".[16] Ashton *et al*., collaborators used a library of 1,697 FDA-approved drugs was used to identify small molecules that decrease the OCR of cancer cells using the Seahorse XF Analyzer assay. FaDu hypopharyngeal carcinoma cells were incubated with the FDA-approved compounds at either 2 or 10 μM for 24 hours.[6] The mitochondrial specific OCR was determined by taking a basal OCR measurement and subtracting the OCR measure, following injection of 2 μM antimycin A to inhibit mitochondrial respiration.[6] The OCR measurements were then corrected to responding cell number using the relative Hoechst fluorescence of the cells fixed after the assay. The secondary screen was conducted with the

top 130 rank small molecules and used the same protocol as the primary screen, except that the chosen compounds were tested at lower concentrations i.e. 80 nM, 400 nM, 2 or 10 μM. [6] **Table 32** shows the highest ranked small molecules that caused a decrease in the OCR from the HTS using FaDu cells.

Table 32 : The highest ranked compounds that reduce OCR at 10 μM and the reasons for exclusion. Adapted from Ashton *et al*. [6]

Rank	Compound	Exclusion Criteria
1	**Pyrvinium**	Antihelminth and poor bioavailability
2	**Berberine**	Hypoxia modifier and known radiosensitiser
3	**Niclosamide**	Antihelminth and poor bioavailability
4	**Acriflavinium**	Radiosensitiser
5	**Sorafenib**	Radiosensitiser
6	**Emetine**	Poor safety profile
7	**Plicamycin**	Plasma concentration is too low (0.37 μM)
8	**Suloctidil**	Poor safety profile
9	**Pentamidine**	Plasma concentration is too low (1.03 μM)
10	**Amsacrine**	Poor safety profile
11	**Phenformin**	Already studied in reducing OCR in cancer cells
12	**Irinotecan**	Radiosensitiser
13	**Itraconazole**	Plasma concentration is too low (2.8 μM)
14	**Mitomycin**	Radiosensitiser
15	**Atovaquone**	**Taken forward**
16	**Hydoxyprogesterone**	Plasma concentration is too low (0.056 μM)
17	**Cyclosporine**	Known to increase cancer risk
18	**Fenofibrate**	**Taken forward**

Most of the compounds in **Table 32** were subsequently not taken forward for further study (compounds ranked 1-18 in **Table 32**) on the basis of a range of criteria including [6]:

- Known radiosensitisers or in vivo hypoxia modifiers, such as acriflavinium;
- Anti-helminths with poor bioavailability, such as pyrvinium;

- Small molecules that don't achieve the required concentration in plasma to cause the required OCR reduction, such as dactinomycin;
- Small molecules with known unsuitable safety profile, such as emetine.

Atovaquone was taken forward for further evaluation due to its acceptable pharmacokinetic properties and safety profile, described by Ashton *et al*.[6] Fenofibrate (**206**), a widely used treatment for hyperlipidemia in the clinic, was selected for further evaluation due to its brilliant toxicity profile.[17]

6.3 Previous Work: Fenofibrate and its Derivatives to Reduce The OCR

Fenofibrate (**206**) reduces the OCR in isolated rat mitochondria and glioblastoma cells via inhibition of the mitochondrial electron transport chain complex I.[6,18-20] **206** is a pro-drug and is hydrolysed to its active form fenofibric acid (**207**), *via* plasma and tissue esterases.[21] **207** has a minimal impact on OCR, revealing the importance of the isopropyl ester for mitochondrial inhibition or for cell-penetration (**Table 33**).

In previous work, Dr. Cyrille Thinnes designed and synthesised a selection of fenofibrate derivatives (**208-211) (Table 33**). **208** and **209** were designed to further investigate the hydrolysis of fenofibrate, with the amide derivative **208** expected to be less prone to hydrolysis whilst the ethyl ester derivative **209** was expected to be more prone to hydrolysis. The dihydro derivative (**210**) was designed to investigate the redox potential of **206**. **210** was expected to be less redox active than **206** and therefore register a weaker OCR. **211** was designed because the acyl-β-D-glucoronide was expected to have different cellular uptake properties than **206**. To evaluate the effect of these derivatives of **206** (and

in form on future SAR), they were tested on FaDu cells using the Seahorse assay. The OCR was measured after 60 minutes with the desired compound. **Table 33** shows the results of the initial fenofibrate analogues.

Treatment with **206** resulted in a 72% decrease at 100 µM and a 10% decrease in the OCR at 10 µM. The di-hydro derivative (**210)** achieved a similar response to **206**, indicating that the redox potential of fenofibrate is not relevant to the OCR effect. Compounds **207**, **208** and **211** resulted in a 20% decrease in OCR at 100 µM, However, the ethyl ester analogue

Table 33: Initial SAR of fenofibrate analogues.

		OCR relative to DMSO and cell number after treatment [%]	
Cpd	**Structural Formula**	**OCR at 100 µM**	**OCR at 10 µM**
206	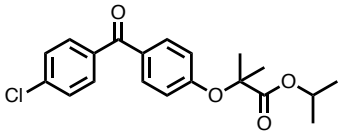	**28**	**90**
207	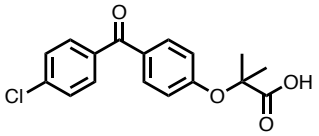	**80**	**100**
208	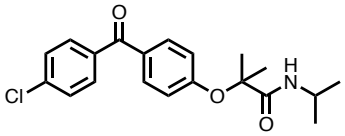	**80**	**100**
209	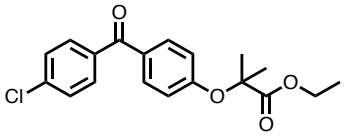	**30**	**90**
210	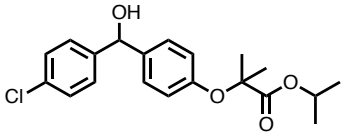	**30**	**90**
211	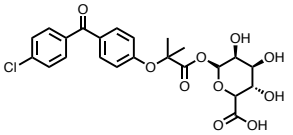	**80**	**100**

(**209**) showed similar levels of potency in comparison to **206** (70% decrease at 100 μM and a 10% decrease at 10 μM). The differences between **206**, **209** & **211** indicates the sensitivity of the ester substituent in relation to the effect in OCR. **207** can reach concentrations of more than 60 μM in blood plasma of patients with hyperlipideia, indicating that the dose of fenofibrate derivatives required to reduce OCR in tumours could be achieved if the toxicity profile is similar to **207**.[22]

6.4 Further Investigation of Fenofibric Esters and Amides

A series of analogues (**212** - **217**) of **206** were designed. The ester was varied with the aim of introducing bulkier substituents to reduce the rate of hydrolysis whilst maintaining the potency of **206**. Additionally two other amide analogues, ethyl and cyclohexane substituents (**216** and **217** respectively), were designed and synthesised to confirm the loss of OCR reduction when the ester is converted into an amide. **212** - **217** were synthesised in 1 step by coupling fenofibric acid to the relevant alcohol or amine using coupling agents COMU and HATU, respectively, to yield the targeted compounds (**Scheme 26**).

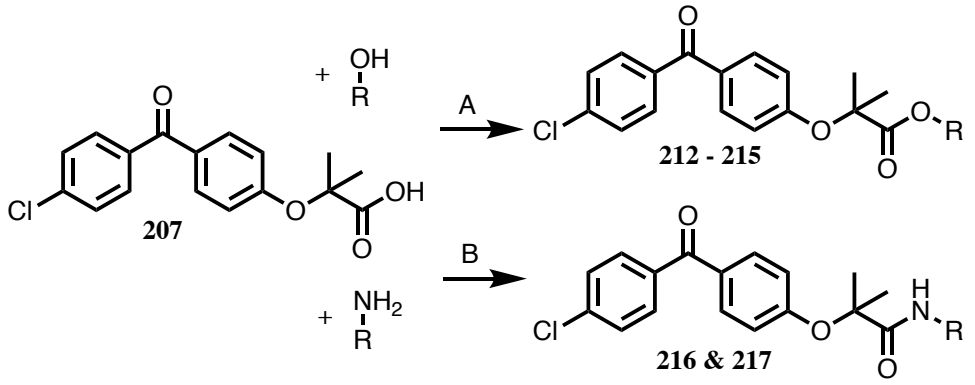

Scheme 26: Synthesis of fenofibric esters and amides series. Reagents and Conditions: **A**) COMU, DIPEA, DMAc, 16hrs, (22 - 63%). **B**) HATU, DIPEA, DMAc, RT, 16 hrs (72 - 84 %).

The screening results for **212** - **217** are shown in **table 34**. The results confirmed the sensitivity of the ester substituent. Converting the isopropyl ester into a aromatic moiety (**212** and **213**) resulted in a complete loss of OCR reduction. Increasing the bulkiness of the isopropyl substituent, replacing it with a cyclohexane (**214**) or a *DL*-menthol (**215**) group, resulted in a reduction in OCR. **214** produced a reduction in the OCR of 85% at 100 µM. Both of the amide analogues (**216** and **217**) showed a strong reduction in the OCR,

Table 34: SAR of deeper investigation of the ester and amide analogues. The OCR of FaDu cells using Seahorse equipment after 24 hours incubation with analogues. Performed by Mr. James Coates.

		OCR relative to DMSO and cell number after treatment [%]	
Cpd	**Structural Formula**	**OCR at 100 µM**	**OCR at 10 µM**
212	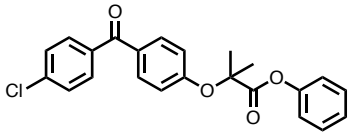	**98**	**98**
213	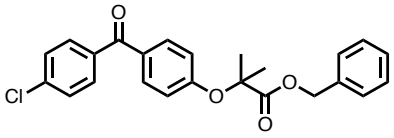	**98**	**98**
214	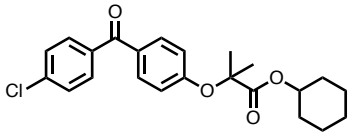	**15**	**82**
215	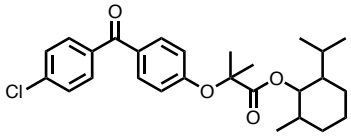	**50**	**90**
216	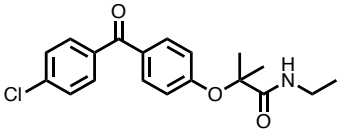	**33**	**99**
217	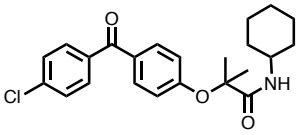	**6**	**22**

indicating that potent reduction in the OCR, can be achieved by replacement of the ester with an amide. **216** resulted in similar levels of OCR reduction as **206**. The cyclohexane analogue (**217**) was more potent in contrast to **206**, at 10 µM **217** reduced the OCR by 78% and near complete reduction of the OCR at 100 µM.

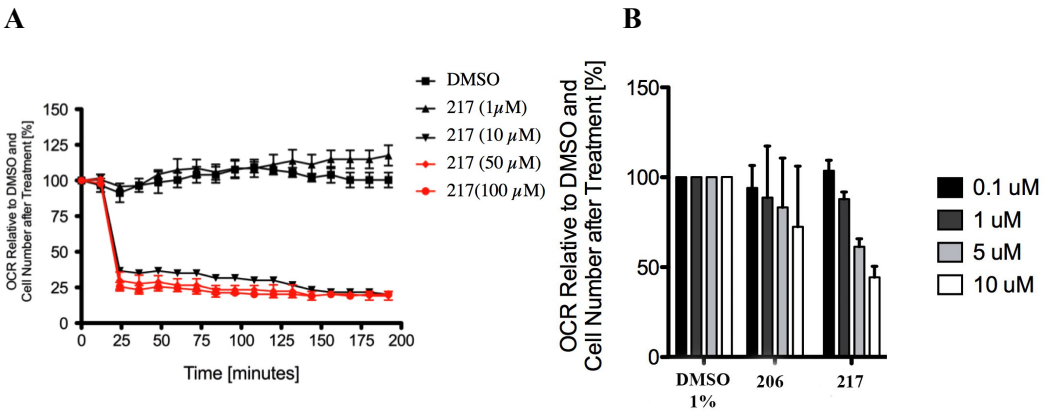

Figure 67: A) The OCR of FaDu cells were measured for 200 minutes after injection of **217**. **B**) The OCR of FaDu cells were measured after 24 hours when treated with **217** at lower concentrations. Performed by Mr. James Coates.

The OCR potency of **217** was further investigated over short term kinetics (up to 200 minutes **Figure 67A**). At 100, 50 and 10 µM at 200 minutes **217** maintained a 75% decrease in OCR. Indeed, at 5 µM **217** reduced the OCR by 45% but at 1 µM, it had little impact on the OCR (**Figure 67B**).

6.5 Investigation of The Quaternary Carbon

It was envisaged that the di-methyl motif next to the isopropyl ester may impact the rate of ester hydrolysis and therefore a role in the OCR of **206**. To investigate the role of the quaternary carbon, a further series of compounds were designed. The methyl (**218**) and methylene (**219**) linked derivatives were synthesised to investigate the impact of the methyl groups in relation to inhibition of the OCR. The ethyl (**220**) and benzyl (**221**) analogues were synthesised as they explore different degrees of bulkiness may sterically hinder ester hydrolysis. The ethyl ester was used instead of the isopropyl ester due improvements in synthetic efficiency and achieved similar levels of reduction in OCR in FaDu cells apart from **219**, where the isopropyl 2-bromoacetate was commercially available. **218 - 221** were synthesised in one step; the (4-chlorophenyl)(4-hydroxy-phenyl)-methanone was reacted with the relevant α-halocarbonyl under mild basic conditions to give the targeted compounds (**Scheme 27**).

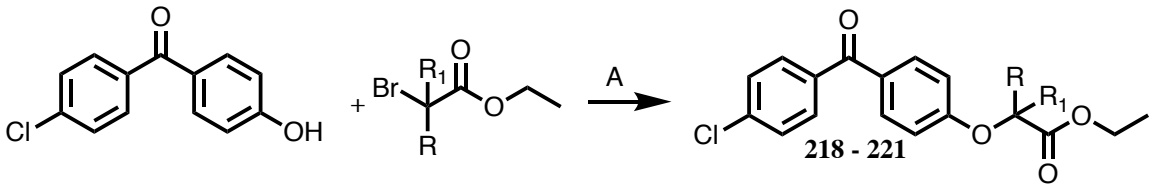

Scheme 27: Synthesis of analogues investigating the quaternary carbon. Reagents and Conditions: **A**).Cs_2CO_3, DMAc, 80°C, 16hrs (46 - 94 %).

The screening results of the analogues investigating the role of the quaternary carbon are shown in **Table 35**. The results indicate that the importance of the di-methyl substituent for reducing the OCR. The methyl analogue (**218**) resulted in a significant reduction in potency

in contrast to **206** (23% reduction in the OCR at 100 μM). The CH_2 derivative (**219**) resulted in no inhibition in the OCR. The ethyl moiety (**220**) resulted in a 48% reduction in the OCR at 100 μM. The benzyl analogue (**221**) achieved similar level in reduction of the OCR in comparison to **206**.

Table 35: SAR of the analogues investigating the di-methyl substituent. The OCR of FaDu cells using Seahorse equipment after 24 hours incubation with analogues. Performed by Mr. James Coates.

		OCR relative to DMSO and cell number after treatment [%]	
Cpd	**Structural Formula**	**OCR at 100 μM**	**OCR at 10 μM**
218	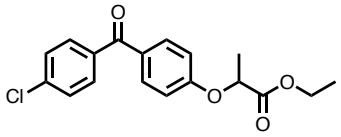	**77**	**100**
219	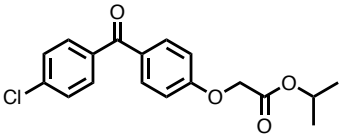	**100**	**100**
220	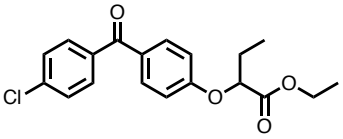	**52**	**84**
221	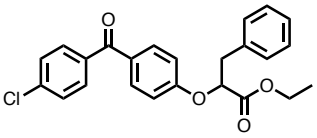	**27**	**89**

The OCR potency of **221** was further investigated over short term kinetics (up to 200 minutes)(**Figure 68A**). **221** achieved a similar profile to Fenofibrate **206**, at 100 and 50 µM resulted in a stable 75% decrease in OCR at 200 minutes. At 10, 5 and 1 µM a 50% reduction in the OCR was maintained. This suggests that at low concentrations, the benzyl substituent (**221**) can either prevent hydrolysis of the ethyl ester to greater extent than the di-methyl substituent or the benzyl substituent improves inhibition of mitochondrial complex I (**Figure 69B**).

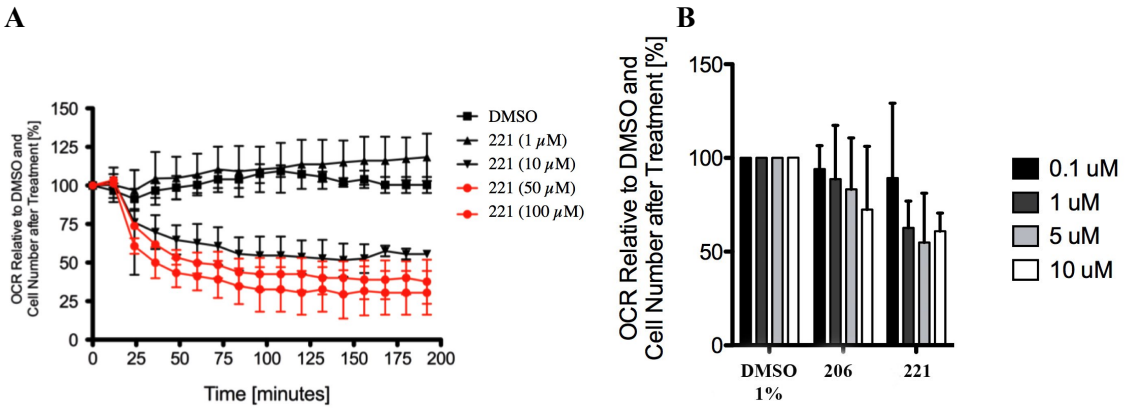

Figure 68: A) The OCR of FaDu cells were measured for 200 minutes after injection of **221**. **B**) The OCR of FaDu cells were measured after 24 hours when treated with **221** at lower concentrations. Performed by Mr. James Coates.

6.6 Investigation of The Role of The Chlorine Substituent

It was envisaged that the role of the *C*-1 chlorine group may be to prevent metabolism of the phenyl ring to maintain concentrations of the active metabolite **207**. However, for inhibition of the OCR, the role of the chlorine group was unknown. To confirm the role of the chlorine group, the fenofibrate derivative without chlorine (**222**) was synthesised. **222**

was synthesised in an identical fashion to the analogues investigating the role of the di-methyl substituent (**Scheme 28a**). An aryl-chloro moiety has access to a whole range of chemistry, in particular Pd-mediated couplings. To maintain or improve the physiochemical properties of **206**, a series of analogues (**223 - 226**) was designed where a broad range amines replaced the chlorine moiety. The amines were chosen varying in length, bulkiness and either secondary or tertiary amines. **223 - 226** were synthesised in one step, **206** underwent a Pd-catalysed amination using the corresponding ligands for the relevant amine (BrettPhos for primary and RuPhos for secondary amines), yielding the targeted compounds (**Scheme 28b**).[23]

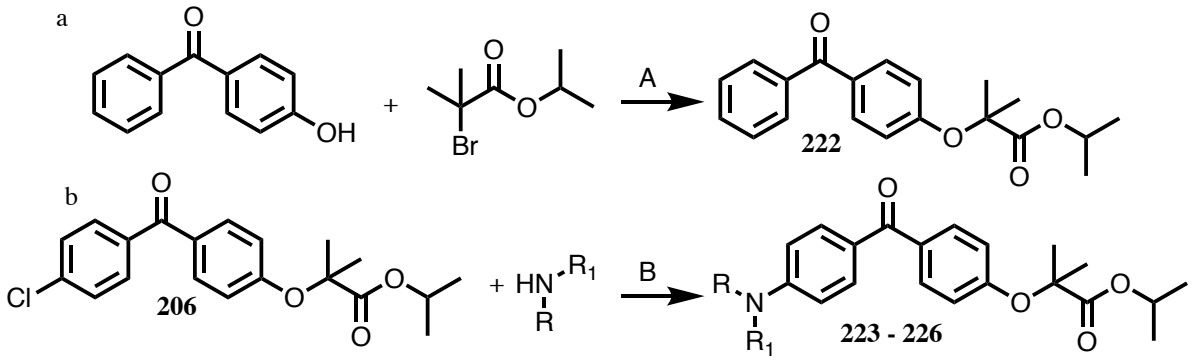

Scheme 28: Synthesis of analogues investigating the role of the chlorine substituent. Reagents and Conditions: **A**) Cs_2CO_3, DMAc, 80°C, 16hrs (46-94%). **B**) BrettPhosPd G3 or RuPhosPd G3, Cs_2CO_3, THF, DMAc, 80°C, 16hrs (17-83%).

The chlorine free analogue (**222**) achieved a similar level of reduction in the OCR in comparison to **206**, suggesting a very minor role for the chlorine substituent for the reduction in OCR (**Table 36**). Replacing the chlorine group with an amine substituent increased the potency in contrast to **206** (**Table 36**). At 100 μM all amine analogues showed an increase in potency in the reduction in the OCR with **223** reducing the OCR by 95% at 100μM, 20% greater than **206**. At 10 μM, **223** showed a similar drop in potency to that for

206, suggesting the dimethylamine substituent improved cell penetration rather than improving inhibition. A similar result was observed for the glycine analogue (**224**). The bulkier substituents achieved a potent reduction in OCR in contrast to **206**. **225** decreased the OCR by 50 % at 10 μM. The benzyl piperazine-1-carboxylate analogue (**226**)

Table 36: SAR for the analogues investigating the role of the chlorine substituent and amine analogues. The OCR of FaDu cells using Seahorse equipment after 24 hours incubation with analogues. Performed by Mr. James Coates.

		OCR relative to DMSO and cell number after treatment [%]	
Cpd	**Structural Formula**	**OCR at 100 μM**	**OCR at 10 μM**
222	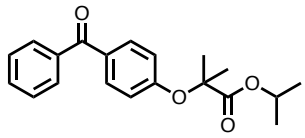	**17**	**85.3**
223	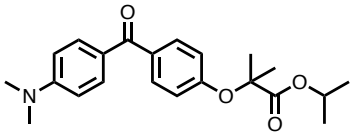	**5**	**86**
224	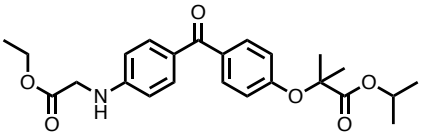	**11**	**100**
225	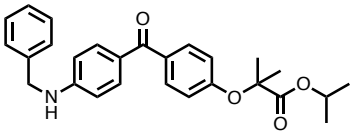	**12**	**54**
226	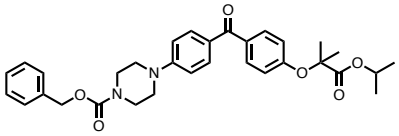	**5**	**19**

maintained a strong reduction in the OCR at 10 μM achieving a 81 % decrease the OCR.

All compounds achieved similar or greater level of reduction in the OCR in contrast to **206**, **222-226** were further investigated at concentrations 10, 5, 1 and 0.1 μM (**Figure 69B**). **222-224** maintained a in similar profile to **206** at low concentrations. **225** produced a

partially better profile in contrast to **206**, achieving a 40% decrease in the OCR at 5 µM. **226** showed strong potency at lower concentrations and resulting in a reduction of 60% in the OCR at 1 µM. This demonstrates that a stronger potency can be achieved than Atovaquone [6].

A

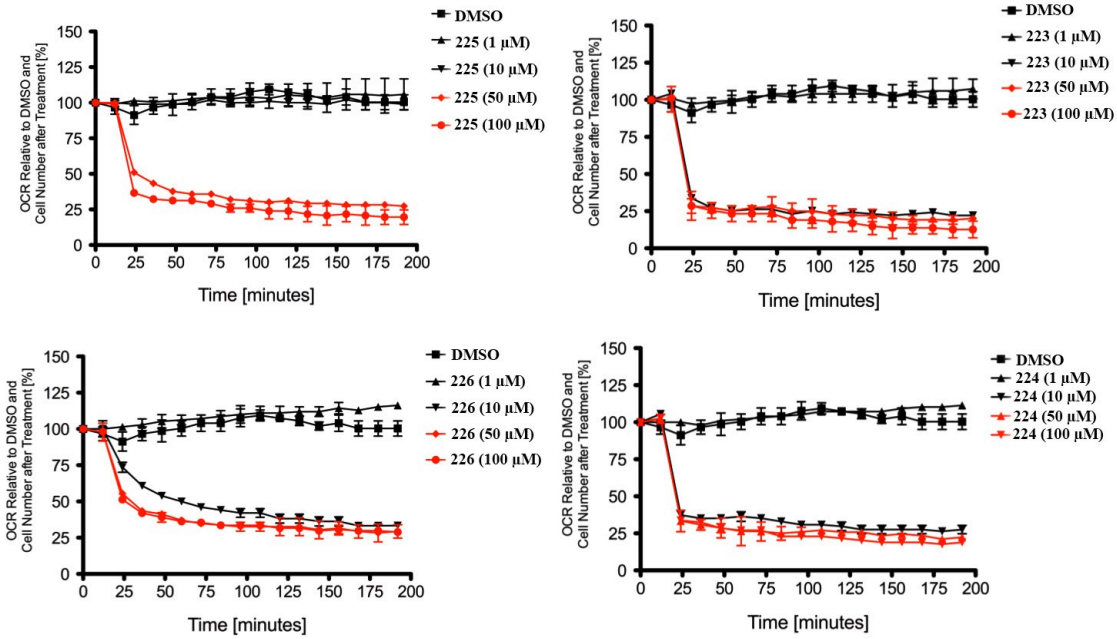

B

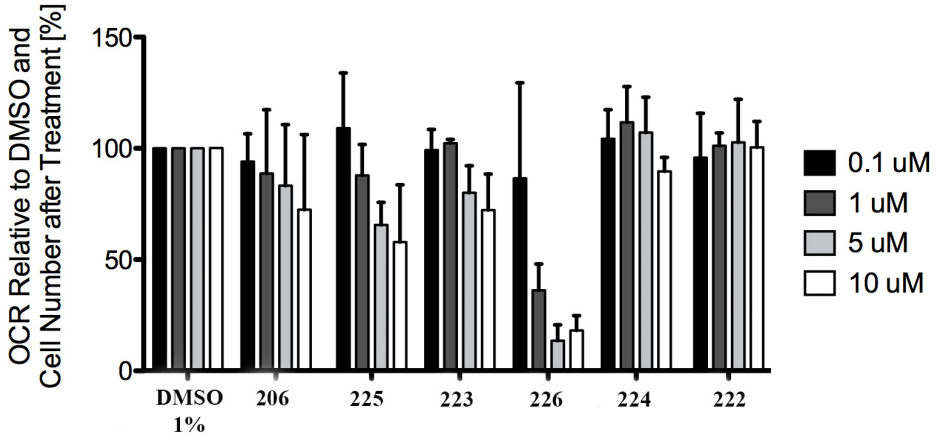

Figure 69: A) The OCR of FaDu cells were measured for 200 minutes after injection of **223 - 226**. **B**) The OCR of FaDu cells were measured after 24 hours when treated with at **222 - 226** lower concentrations. Performed by Mr. James Coates.

6.7 Summary & Future Work

In this section, the development of fenofibrate derivatives for reducing the cellular oxygen consumption rate (OCR) has been described. This work led to inhibitors that reduced OCR by 60% at 1 μM (**226**). **Figure 70** summaries the SAR of the fenofibrate pharmacophore. Further investigation of the ester (**Chapter 6.4**) revealed sensitivity to the ester substituent and suggested that replacing the ester with an amide can maintain OCR inhibition (**216** and **217**). **217** was tested at lower concentrations and reduced the OCR by 40% at 5 μM. Investigation into the di-methyl substituent revealed its importance for inhibition of the OCR (**Chapter 6.5**). Removal of the methyl groups resulted in a complete loss of effect on the OCR and replacing with bulkier substituents such as the benzyl moiety (**221**) achieved similar level of reduction in OCR to **206**. SAR revealed the *para*-chlorine substituent had a minor role in reduction of the OCR (**Chapter 6.6**). Replacing the chlorine group with a bulkier amino substituent (**225** and **226**) resulted in a relatively high reduction in the OCR. Indeed, the amino analogues were tested at lower concentrations (**Figure 70**), with **226** reducing the OCR by 60 % at 1 μM.

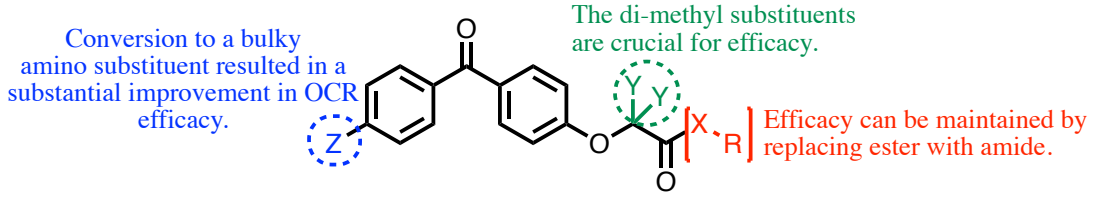

Figure 70: Summary of the SAR of the fenofibrate derivatives.

The initial SAR of the fenofibrate derivatives suggests potency may be improved with additional investigation of the amino moiety or by a combination of the amino group (**225** and **226**) and the amide substituent modifications (**216** and **217**).

6.8 Compound Characterisation

Phenyl 2-(4-(4-chlorobenzoyl)phenoxy)-2-methylpropanoate 212

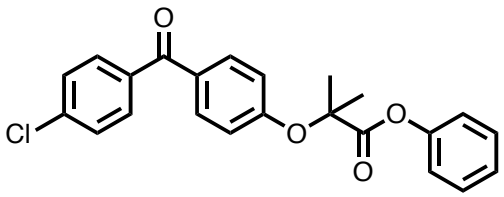

Following general procedure C: Fenofibric Acid (100 mg, 0.314 mmol), COMU (399 mg, 0.943 mmol), DIPEA (116 mg, 0.943 mmol) and phenol (90 mg, 0.943 mmol) gave **212** (48 mg, 0.121 mmol, 39 %) as a colourless oil.

^{1}H NMR (400 MHz, DMSO-d_6) δ 7.86 – 7.55 (m, 6H, Ar), 7.50 – 7.23 (m, 3H, Ar), 7.15 – 7.03 (m, 4H, Ar), 1.79 (s, 6H, $(CH_3)_2$). **^{13}C NMR** (101 MHz, DMSO-d_6) δ 193.25, 171.70, 158.99, 150.07, 137.08, 136.22, 131.19, 129.67, 128.59, 126.34, 121.40, 117.28, 79.09, 39.52, 25.09. **FT-IR** ν_{max} (film) 1728, 1651, 1595 cm^{-1}. **HRMS** (ESI-TOF) calcd for $C_{23}H_{20}O_4{}^{35}Cl$ $[M+H]^+$: 395.1044, found : 395.1042.

Benzyl 2-(4-(4-chlorobenzoyl)phenoxy)-2-methylpropanoate 213

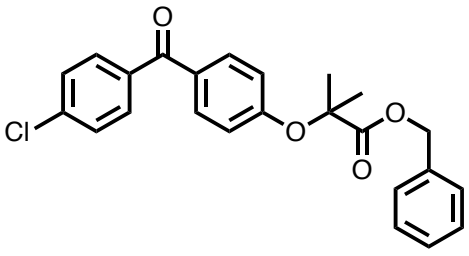

Following general procedure C: Fenofibric Acid (100 mg, 0.314 mmol), COMU (399 mg, 0.943 mmol), DIPEA (116 mg, 0.943 mmol) and benzyl alcohol (101 mg, 0.943 mmol) gave **213** (39 mg, 0.0955 mmol, 31%) as a colourless oil.

^{1}H NMR (400 MHz, Chloroform-*d*) δ 7.74 – 7.48 (m, 4H, Ar), 7.48 – 7.13 (m, 8H, Ar), 6.87 – 6.65 (m, 2H, Ar), 5.16 (s, 2H, CH_2), 1.64 (s, 6H, $(CH_3)_2$). **^{13}C NMR** (101 MHz, Chloroform-*d*) δ 194.38, 173.70, 159.81, 138.62, 136.66, 135.40, 132.27, 131.48, 130.58, 129.47, 129.20, 129.08, 128.84, 128.83, 128.79, 128.76, 117.54, 79.72, 77.16, 67.63, 25.73. **FT-IR** ν_{max} (film) 1730, 1655, 1593 cm^{-1}. **HRMS** (ESI-TOF) calcd for $C_{24}H_{21}O_4{}^{35}Cl^{23}Na$ $[M+H]^+$: 431.1015, found : 431.1015.

Cyclohexyl 2-(4-(4-chlorobenzoyl)phenoxy)-2-methylpropanoate 214

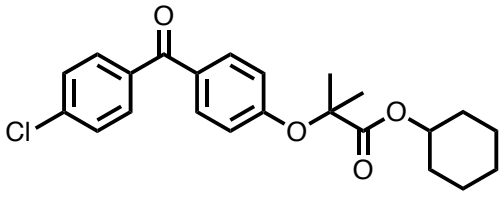

Following general procedure C: Fenofibric Acid (100 mg, 0.314 mmol), COMU (399 mg, 0.943 mmol), DIPEA (116 mg, 0.943 mmol) and cyclohexanol (94 mg, 0.943 mmol) gave **214** (79 mg, 0.197 mmol, 63 %) as a colourless oil.

m.p. 85-92°C. **^{1}H NMR** (400 MHz, DMSO-d_6) δ 7.74 – 7.53 (m, 6H, Ar), 6.86 (d, J = 8.5 Hz, 2H, Ar), 4.48 (tq, J = 7.0, 3.5 Hz, 1H), 2.05 – 1.41 (m, 16H). **^{13}C NMR** (101 MHz, DMSO-d_6) δ 193.21, 171.95, 159.28, 157.67, 137.04, 136.25, 131.85, 131.15, 129.49, 128.59, 117.05, 79.13, 73.07, 39.52, 30.60, 25.10, 22.81. **FT-IR** ν_{max} (film) 1733, 1656,

1597 cm^{-1}. **HRMS** (ESI-TOF) calcd for $C_{25}H_{26}O_4{}^{35}Cl$ $[M+H]^+$: 401.1514, found : 401.1510.

2-isopropyl-6-methylcyclohexyl 2-(4-(4-chlorobenzoyl)phenoxy)-2-methylpropanoate 215

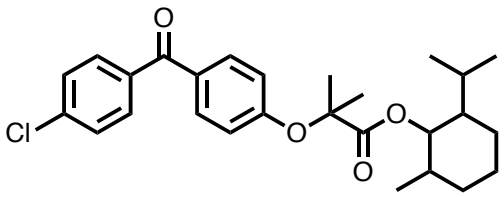

Following general procedure C: Fenofibric Acid (100 mg, 0.314 mmol), COMU (399 mg, 0.943 mmol), DIPEA (116 mg, 0.943 mmol) and DL menthanol (150 mg, 0.943 mmol) gave **215** (31 mg, 0.067 mmol, 22 %) as a white solid.

m.p. 124-128°C. **^{1}H NMR** (400 MHz, Chloroform-*d*) δ 7.76 – 7.67 (m, 4H, Ar), 7.47 – 7.40 (m, 2H, Ar), 6.91 – 6.80 (m, 2H, Ar), 4.72 (td, *J* = 11.0, 4.5 Hz, 1H), 1.96 (dq, *J* = 11.0, 3.5, 2.0 Hz, 1H), 1.73 – 1.61 (m, 9H), 1.49 (dtd, *J* = 11.0, 8.5, 7.0, 3.5 Hz, 1H), 1.38 (tt, *J* = 12.0, 11.0, 3.5 Hz, 1H), 1.09 – 0.76 (m, 9H), 0.67 (d, *J* = 7.0 Hz, 3H, CH_3). **^{13}C NMR** (101 MHz, Chloroform-*d*) δ 194.02, 173.03, 159.57, 138.17, 136.22, 131.75, 130.96, 129.94, 128.34, 116.88, 79.28, 77.16, 75.71, 46.49, 40.05, 33.88, 31.15, 25.57, 25.49, 25.04, 22.73, 21.81, 20.58, 15.59. **FT-IR** ν_{max} (film) 1735, 1657, 1592 cm^{-1}. **HRMS** (ESI-TOF) calcd for $C_{27}H_{34}O_4{}^{35}Cl$ $[M+H]^+$: 457.2140, found : 457.2136.

2-(4-(4-chlorobenzoyl)phenoxy)-N-ethyl-2-methylpropanamide 216

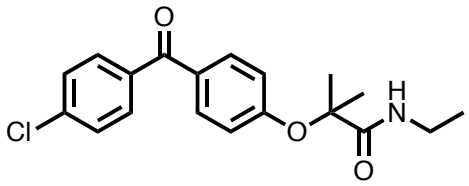

Following general procedure C: Fenofibric Acid (250 mg, 0.78 mmol), T3P (623 mg, 1.96 mmol), DIPEA (290 mg, 2.34 mmol) and ethylamine (2M in THF (67 mg, 1.56 mmol)) gave **216** (219 mg, 0.63 mmol, 81%) as a white solid.

m.p. 137-139°C. **^{1}H NMR** (400 MHz, DMSO-d_6) δ 8.16 (t, J = 6.0 Hz, 1H, NH), 7.76 – 7.56 (m, 6H, Ar), 7.01 – 6.90 (m, 2H, Ar), 3.12 (qd, J = 7.0, 6.0 Hz, 2H, $\underline{CH_2}CH_3$), 1.51 (s, 6H, $(CH_3)_2$), 0.95 (t, J = 7.0 Hz, 3H, $CH_2\underline{CH_3}$). **^{13}C NMR** (101 MHz, DMSO-d_6) δ 193.24, 172.28, 159.21, 137.06, 136.22, 131.63, 131.16, 129.69, 128.58, 118.24, 80.65, 39.52, 33.65, 25.01, 14.49. **FT-IR** ν_{max} (film) 3649, 1679, 1649, 1596 cm^{-1}. **HRMS** (ESI-TOF) calcd for $C_{19}H_{21}O_3N^{35}Cl$ $[M+H]^+$: 346.1207, found : 346.1207.

2-(4-(4-chlorobenzoyl)phenoxy)-N-cyclohexyl-2-methylpropanamide 217

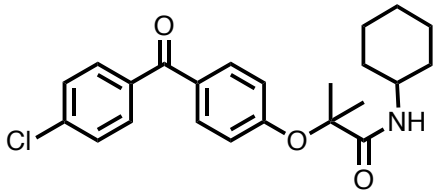

Following general procedure C: Fenofibric Acid (250 mg, 0.78 mmol), T3P (623 mg, 1.96 mmol), DIPEA (290 mg, 2.34 mmol) and cyclohexylamine (154 mg, 1.56 mmol) gave **217** (278 mg, 0.69 mmol, 89%) as a white solid.

m.p. 137-139°C. **^{1}H NMR** (400 MHz, DMSO-d_6) δ 7.85 (d, J = 8.0 Hz, 1H, NH), 7.74 – 7.52 (m, 6H, Ar), 7.00 – 6.90 (m, 2H, Ar), 3.65 – 3.53 (m, 1H), 1.67 – 1.58 (m, 4H), 1.51 (s, 6H, $(CH_3)_2$), 1.29 – 0.95 (m, 6H). **^{13}C NMR** (101 MHz, DMSO-d_6) δ 193.29, 171.49, 159.26, 137.05, 136.27, 131.63, 131.19, 129.59, 128.62, 118.15, 80.62, 47.96, 39.52, 31.96, 25.06, 24.87. **FT-IR** ν_{max} (film) 3643, 1720 ,1650, 1596 cm^{-1}. **HRMS** (ESI-TOF) calcd for $C_{23}H_{27}O_3N^{35}Cl$ $[M+H]^+$: 400.1674, found : 400.1674

Ethyl 2-(4-(4-chlorobenzoyl)phenoxy)propanoate 218

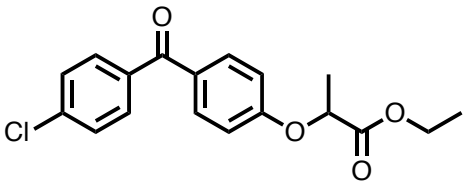

A mixture of (4-chlorophenyl)(4-hydroxyphenyl)methanone (300 mg, 1.29 mmol), Ethyl 2-bromopropanoate (280 mg, 1.55 mmol), Cs_2CO_3 (504 mg, 1.55 mmol) and DMAc (10 ml) was prepared. The resultant mixture was heated at 80°C overnight. Water (30 ml) was then added before extracting with EtOAc (3 x 30 ml). The organic fractions were combined, washed with brine, dried (Na_2SO_4) and the solvent was removed in *vacuo*. The crude mixture was then purified using flash column chromatography using (Cyclohexane 100 % -

75%, EtOAc 0 %- 25%) over 10 column volumes to give **218** (402 mg, 1.21 mmol, 94 %) as a white solid.

m.p. 123-126°C. **^{1}H NMR** (400 MHz, DMSO-d_6) δ 7.79 – 7.56 (m, 6H, Ar), 7.08 – 6.99 (m, 2H, Ar), 5.13 (q, J = 6.5 Hz, 1H, CH), 4.18 – 4.13 (q, J = 7.0 Hz, 2H, $\underline{CH_2}CH_3$), 1.55 (d, J = 6.5 Hz, 3H, $\underline{CH}CH_3$), 1.17 (t, J = 7.0 Hz, 3H, $CH_2\underline{CH_3}$). **^{13}C NMR** (101 MHz, DMSO-d_6) δ 193.21, 170.92, 161.04, 137.04, 136.27, 132.14, 131.17, 129.58, 128.60, 128.60, 114.75, 71.74, 61.01, 39.52, 18.10, 13.98. **FT-IR** ν_{max} (film) 1733, 1653, 1593 cm^{-1}. **HRMS** (ESI-TOF) calcd for $C_{18}H_{18}O_4{}^{35}Cl$ $[M+H]^+$: 333.0885, found : 333.0885.

Isopropyl 2-(4-(4-chlorobenzoyl)phenoxy)acetate 219

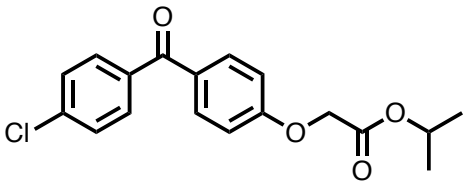

Following general procedure C: Fenofibric Acid (50 mg, 0.172 mmol), COMU (221 mg, 0.517 mmol), DIPEA (64 mg, 0.517 mmol) and isopropanol (31 mg, 0.517 mmol) gave **219** (26 mg, 0.078 mmol, 46%) as a colourless oil.

^{1}H NMR (400 MHz, DMSO-d_6) δ 7.80 – 7.56 (m, 6H, Ar), 7.12 – 7.05 (m, 2H, Ar), 5.01 (hept, J = 6.0 Hz, 1H, $\underline{CH}(CH_3)_2$), 4.88 (s, 2H, CH_2), 1.22 (d, J = 6.0 Hz, 6H, $CH(\underline{CH_3})_2$). **^{13}C NMR** (101 MHz, DMSO-d_6) δ 193.25, 167.75, 161.42, 137.03, 136.30, 132.07, 131.17, 129.64, 128.60, 114.52, 64.85, 62.62, 39.52, 20.13. **FT-IR** ν_{max} (film) 1729, 1654, 1597 cm^{-1}. **HRMS** (ESI-TOF) calcd for $C_{18}H_{18}O_4{}^{35}Cl$ $[M+H]^+$: 333.0888, found : 333.0889.

Ethyl 2-(4-(4-chlorobenzoyl)phenoxy)butanoate 220

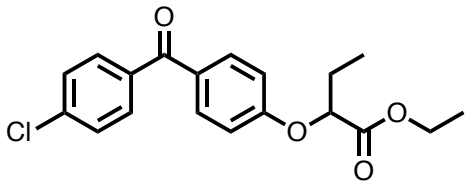

A mixture of (4-chlorophenyl)(4-hydroxyphenyl)methanone (300 mg, 1.29 mmol), Ethyl 2-bromobutanoate (302 mg, 1.55 mmol), Cs_2CO_3 (504 mg, 1.55 mmol) and DMAc (10 ml) was prepared. The resultant mixture was heated at 80°C overnight. Water (30 ml) was then added before extracting with EtOAc (3 x 30 ml). The organic fractions were combined, washed with brine, dried (Na_2SO_4) and the solvent was removed in *vacuo*. The crude mixture was then purified using flash column chromatography using (Cyclohexane 100 % - 75%, EtOAc 0 %- 25%) over 10 column volumes to give **220** (375 mg, 1.08 mmol, 84%) as a white solid.

m.p. 114-116°C. **^{1}H NMR** (400 MHz, DMSO-d_6) δ 7.80 – 7.55 (m, 6H, Ar), 7.07 – 6.99 (m, 2H, Ar), 4.96 (t, J = 7.0, 5.0 Hz, 1H), 4.16 (qt, J = 7.0, 3.5 Hz, 2H), 1.95 (dq, J = 14.5, 7.0 Hz, 2H), 1.18 (t, J = 7.0 Hz, 3H), 1.00 (t, J = 7.0 Hz, 3H). **^{13}C NMR** (101 MHz, DMSO-d_6) δ 193.19, 170.27, 161.35, 137.06, 136.27, 132.15, 131.18, 129.60, 128.58, 114.76, 76.42, 60.93, 39.52, 25.41, 14.03, 9.22. **FT-IR** ν_{max} (film) 1731, 1656, 1597 cm^{-1}.

HRMS (ESI-TOF) calcd for $C_{19}H_{20}O_4{}^{35}Cl$ $[M+H]^+$: 347.1044, found : 347.1043.

Ethyl 2-(4-(4-chlorobenzoyl)phenoxy)-3-phenylpropanoate 221

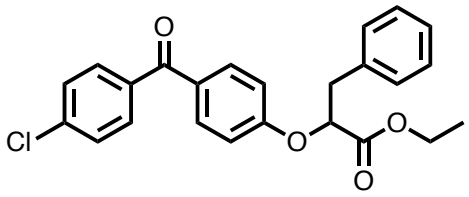

A mixture of (4-chlorophenyl)(4-hydroxyphenyl)methanone (300 mg, 1.29 mmol), Ethyl 2-bromo-3-phenylpropanoate (396 mg, 1.55 mmol), Cs_2CO_3 (504 mg, 1.55 mmol) and DMAc (10 ml) was prepared. The resultant mixture was heated at 80°C overnight. Water (30 ml) was then added before extracting with EtOAc (3 x 30 ml). The organic fractions were combined, washed with brine, dried (Na_2SO_4) and the solvent was removed in *vacuo*. The crude mixture was then purified using flash column chromatography using (Cyclohexane 100 % - 75%, EtOAc 0 %- 25%) over 10 column volumes gave **221** (82 mg, 0.20 mmol, 16%) with the colourless oil.

^{1}H NMR (400 MHz, DMSO-d_6) δ 7.74 – 7.55 (m, 6H, Ar), 7.37 – 7.18 (m, 5H, Ar), 7.07 – 6.98 (m, 2H, Ar), 5.27 (t, J = 7.0, 5.5 Hz, 1H, $\underline{CH}CH_2$), 4.10 (d, J = 7.0 Hz, 2H, $\underline{CH_2}CH_3$), 3.24 (dd, J = 7.0, 2.0 Hz, 2H, $CH\underline{CH_2}$), 1.11 (t, J = 7.1 Hz, 3H, $CH_2\underline{CH_3}$). **^{13}C NMR** (101 MHz, DMSO-d_6) δ 193.24, 169.78, 161.09, 137.08, 136.03, 132.15, 131.21, 128.62, 128.29, 126.81, 114.83, 76.27, 61.05, 39.52, 37.96, 13.94. **FT-IR** ν_{max} (film) 1727, 1652, 1595 cm^{-1}. **HRMS** (ESI-TOF) calcd for $C_{24}H_{22}O_4{}^{35}Cl$ $[M+H]^+$: 409.1201, found : 409.1202.

Isopropyl 2-(4-benzoylphenoxy)-2-methylpropanoate 222

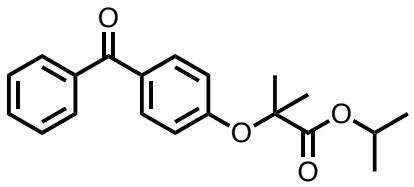

A mixture of (4-hydroxyphenyl)(phenyl)methanone (300 mg, 1.51 mmol), Isopropyl 2-bromo-2-methylpropanoate (380 mg, 1.81 mmol), Cs_2CO_3 (588 mg, 1.81 mmol) and DMAc (10 ml) was prepared. The resultant mixture was heated at 80°C overnight. Water (30 ml) was added to the resultant mixture before extracting with EtOAc (3 x 30 ml). The organic fractions were combined, washed with brine, dried (Na_2SO_4) and the solvent was removed in *vacuo*. The crude mixture was then purified using flash column chromatography using (Cyclohexane 100 % - 75%, EtOAc 0 %- 25%) over 10 column volumes gave **223** (123 mg, 0.377 mmol, 25 %) as a white solid.

m.p. 85-88°C. **^{1}H NMR** (400 MHz, DMSO-d_6) δ 7.76 – 7.50 (m, 7H, Ar), 6.93 – 6.86 (m, 2H, Ar), 4.95 (hept, J = 6.0 Hz, 1H, $\underline{CH}(CH_3)_2$), 1.60 (s, 6H, $C(\underline{CH_3})_2$), 1.14 (d, J = 6.0 Hz, 6H, $CH(\underline{CH_3})_2$). **^{13}C NMR** (101 MHz, DMSO-d_6) δ 194.32, 172.12, 159.07, 137.59, 132.13, 131.82, 129.83, 129.25, 128.44, 117.04, 79.02, 68.90, 39.52, 25.02, 21.20. **FT-IR** ν_{max} (film) 1728, 1672, 1593 cm^{-1}. **HRMS** (ESI-TOF) calcd for $C_{20}H_{23}O_4$ $[M+H]^+$: 327.1590, found : 327.1588.

Isopropyl 2-(4-(4-(dimethylamino)benzoyl)phenoxy)-2-methylpropanoate 223

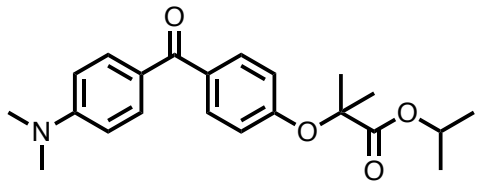

Following general procedure D: Fenofibrate (200 mg, 0.555 mmol), ruPhos Pd G3 (23 mg, 0.0277 mmol), Cs_2CO_3 (541 mg, 1.66 mmol) and Dimethylamine (2M in THF (30 mg, 0.666 mmol)) gave **223** (34 mg, 0.092 mmol, 17%) as a white solid.

m.p. 91-93°C. **^{1}H NMR** (400 MHz, DMSO-d_6) δ 7.79 – 7.47 (m, 4H, Ar), 7.02 – 6.39 (m, 4H, Ar), 4.98 (hept, J = 6.0 Hz, 1H, $\underline{CH}(CH_3)_2$), 3.03 (s, 6H, $N(\underline{CH_3})_2$), 1.59 (s, 6H, $C(\underline{CH_3})_2$), 1.16 (d, J = 6.0 Hz, 6H, $CH(\underline{CH_3})_2$). **^{13}C NMR** (101 MHz, DMSO-d_6) δ 192.39, 172.30, 157.92, 153.02, 131.89, 130.98, 123.99, 116.98, 110.70, 78.90, 68.83, 39.52, 25.07, 21.24. **FT-IR** ν_{max} (film) 1732, 1594 cm^{-1}. **HRMS** (ESI-TOF) calcd for $C_{22}H_{28}O_4N$ $[M+H]^+$: 370.2013, found : 370.2006.

Isopropyl 2-(4-(4-((2-ethoxy-2-oxoethyl)amino)benzoyl)phenoxy)-2-methylpropanoate 224

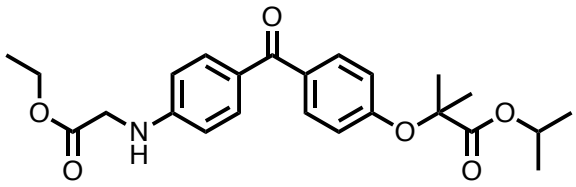

Following general procedure D: Fenofibrate (200 mg, 0.555 mmol), brettPhos Pd G3 (25 mg, 0.0277 mmol), Cs_2CO_3 (541 mg, 1.66 mmol) and glycine ethyl ester (92 mg, 0.666 mmol) gave **224** (212 mg, 0.49 mmol, 89%) as a clear oil.

^{1}H NMR (400 MHz, Chloroform-*d*) δ 7.73 – 7.62 (m, 4H, Ar), 6.86 – 6.81 (m, 2H, Ar), 6.61 – 6.55 (m, 2H, Ar), 5.07 (hept, J = 6.0 Hz, 1H, $\underline{CH}(CH_3)_2$), 4.25 (q, J = 7.0 Hz, 2H, $\underline{CH_2}CH_3$), 3.94 (s, 2H, $NH\underline{CH_2}$), 1.63 (s, 6H, $C(\underline{CH_3})_2$), 1.29 (t, J = 7.0 Hz, 3H, $CH_2\underline{CH_3}$), 1.18 (d, J = 6.0 Hz, 6H, $CH(\underline{CH_3})_2$). **^{13}C NMR** (101 MHz, Chloroform-*d*) δ 193.96, 173.06, 170.11, 158.40, 150.23, 132.39, 131.61, 131.20, 127.08, 118.94, 116.93, 111.36, 78.99, 77.16, 68.99, 61.38, 44.80, 25.11, 21.26, 13.93. **FT-IR** ν_{max} (film) 3352, 1731, 1599 cm^{-1}.

HRMS (ESI-TOF) calcd for $C_{24}H_{30}O_6N$ [M+H$^+$]: 428.2068, found : 428.2066.

Isopropyl 2-(4-(4-(benzylamino)benzoyl)phenoxy)-2-methylpropanoate 225

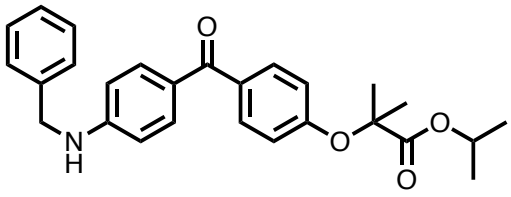

Following general procedure D: Fenofibrate (200 mg, 0.55 mmol), brettPhos Pd G3 (25 mg, 0.0277 mmol), Cs_2CO_3 (541 mg, 1.66 mmol) and benzylamine (71 mg, 0.66 mmol) gave **225** (194 mg, 0.45 mmol, 82%) as a clear oil.

^{1}H NMR (400 MHz, Chloroform-*d*) δ 7.81 – 7.47 (m, 4H, Ar), 7.29 – 7.17 (m, 5H, Ar), 6.78 – 6.74 (m, 2H, Ar), 6.54 – 6.50 (m, 2H, Ar), 5.00 (hept, J = 6.0 Hz, 1H, $\underline{CH}(CH_3)_2$),

4.74 (t, J = 5.5 Hz, 1H, NHCH$_2$), 4.31 (d, J = 5.5 Hz, 2H, NHCH$_2$), 1.56 (s, 6H, C(CH$_3$)$_2$), 1.12 (d, J = 6.0 Hz, 6H, CH(CH$_3$)$_2$). **^{13}C NMR** (101 MHz, Chloroform-*d*) δ 193.89, 173.09, 158.28, 151.42, 138.11, 132.44, 131.80, 131.14, 128.49, 127.05, 116.93, 111.24, 78.97, 77.16, 68.98, 47.27, 25.11, 21.27. **FT-IR** ν_{max} (film) 3339, 1729, 1598 cm^{-1}. **HRMS** (ESI-TOF) calcd for $C_{27}H_{30}O_4N$ $[M+H]^+$: 432.2169, found : 432.2159.

Benzyl 4-(4-(4-((1-isopropoxy-2-methyl-1-oxopropan-2-yl)oxy)benzoyl)phenyl)piperazine-1-carboxylate 226

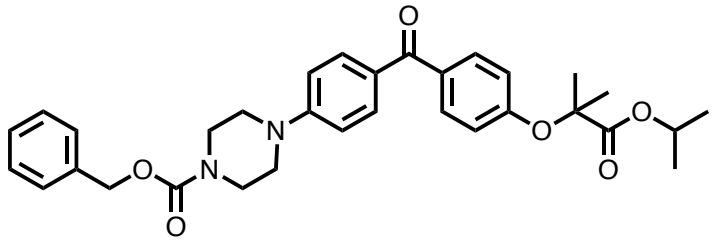

Following general procedure D: Fenofibrate (200 mg, 0.555 mmol), RuPhos Pd G3 (23 mg, 0.0277 mmol), Cs_2CO_3 (541 mg, 1.66 mmol) and Benzyl piperazine-1-carboxylate (145 mg, 0.666 mmol) gave **226** (102 mg, 0.187 mmol, 34%) as a yellow oil.

^{1}H NMR (400 MHz, DMSO-*d*$_6$) δ 7.69 – 7.58 (m, 4H, Ar), 7.43 – 7.28 (m, 5H, Ar), 7.07 – 6.96 (m, 2H, Ar), 6.92 – 6.80 (m, 2H, Ar), 5.11 (s, 2H, CH$_2$), 4.97 (hept, J = 6.0 Hz, 1H, CH(CH$_3$)$_2$), 3.62 – 3.51 (m, 4H, Pip), 3.40 – 3.37 (m, 4H, Pip), 1.59 (s, 6H, C(CH$_3$)$_2$), 1.15 (d, J = 6.0 Hz, 6H, CH(CH$_3$)$_2$). **^{13}C NMR** (101 MHz, DMSO-*d*$_6$) δ 192.58, 172.27, 158.23, 154.45, 153.20, 136.81, 131.73, 131.19, 128.46, 127.91, 127.65, 116.99, 113.38, 78.93,

68.86, 66.38, 46.43, 42.95, 39.52, 25.07, 21.24. **FT-IR** ν_{max} (film) 2981, 1703, 1644, 1599 cm^{-1}. **HRMS** (ESI-TOF) calcd for $C_{32}H_{37}O_6N_2$ [M+H]+: 545.2646, found : 545.2643.

6.9 References

1 Wilson, W. R. & Hay, M. P. Targeting hypoxia in cancer therapy. *Nat Rev Cancer* **11**, 393-410, doi:10.1038/nrc3064 (2011).

2 LaGory, E. L. & Giaccia, A. J. The ever-expanding role of HIF in tumour and stromal biology. *Nat Cell Biol* **18**, 356-365, doi:10.1038/ncb3330 (2016).

3 Thomlinson, R. H. & Gray, L. H. The histological structure of some human lung cancers and the possible implications for radiotherapy. *Br J Cancer* **9**, 539-549 (1955).

4 Ward, J. F. The complexity of DNA damage: relevance to biological consequences. *Int J Radiat Biol* **66**, 427-432 (1994).

5 Daruwalla, J. & Christophi, C. Hyperbaric oxygen therapy for malignancy: a review. *World J Surg* **30**, 2112-2131, doi:10.1007/s00268-006-0190-6 (2006).

6 Ashton, T. M., Fokas, E., Kunz-Schughart, L. A., Folkes, L. K., Anbalagan, S., Huether, M. *et al.* The anti-malarial atovaquone increases radiosensitivity by alleviating tumour hypoxia. *Nat Commun* **7**, 12308, doi:10.1038/ncomms12308 (2016).

7 Masunaga, S., Liu, Y., Tanaka, H., Sakurai, Y., Suzuki, M., Kondo, N. *et al.* Reducing intratumour acute hypoxia through bevacizumab treatment, referring to the response of quiescent tumour cells and metastatic potential. *Br J Radiol* **84**, 1131-1138, doi:10.1259/bjr/38457938 (2011).

8 Grimes, D. R., Kelly, C., Bloch, K. & Partridge, M. A method for estimating the oxygen consumption rate in multicellular tumour spheroids. *J R Soc Interface* **11**, 20131124, doi:10.1098/rsif.2013.1124 (2014).

9 Kelly, C. J., Hussien, K., Fokas, E., Kannan, P., Shipley, R. J., Ashton, T. M. *et al.* Regulation of O2 consumption by the PI3K and mTOR pathways contributes to tumor hypoxia. *Radiother Oncol* **111**, 72-80, doi:10.1016/j.radonc.2014.02.007 (2014).

10 Secomb, T. W., Hsu, R., Ong, E. T., Gross, J. F. & Dewhirst, M. W. Analysis of the effects of oxygen supply and demand on hypoxic fraction in tumors. *Acta Oncol* **34**, 313-316 (1995).

11 Koritzinsky, M. Metformin: A Novel Biological Modifier of Tumor Response to Radiation Therapy. *Int J Radiat Oncol Biol Phys* **93**, 454-464, doi:10.1016/j.ijrobp.2015.06.003 (2015).

12 Lin, X., David, C. A., Donnelly, J. B., Michaelides, M., Chandel, N. S., Huang, X. *et al.* A chemical genomics screen highlights the essential role of mitochondria in HIF-1 regulation. *Proc Natl Acad Sci U S A* **105**, 174-179, doi:10.1073/pnas.0706585104 (2008).

13 Ellinghaus, P., Heisler, I., Unterschemmann, K., Haerter, M., Beck, H., Greschat, S. *et al.* BAY 87-2243, a highly potent and selective inhibitor of hypoxia-induced gene activation has antitumor activities by inhibition of mitochondrial complex I. *Cancer Med* **2**, 611-624, doi:10.1002/cam4.112 (2013).

14 Beeson, C. C., Beeson, G. C. & Schnellmann, R. G. A high-throughput respirometric assay for mitochondrial biogenesis and toxicity. *Anal Biochem* **404**, 75-81, doi:10.1016/j.ab.2010.04.040 (2010).

15 Wang, R., Novick, S. J., Mangum, J. B., Queen, K., Ferrick, D. A., Rogers, G. W. *et al.* The acute extracellular flux (XF) assay to assess compound effects on mitochondrial function. *J Biomol Screen* **20**, 422-429, doi:10.1177/1087057114557621 (2015).

16 Walker, M. J. The major impacts of James Black's drug discoveries on medicine and pharmacology. *Trends Pharmacol Sci* **32**, 183-188, doi:10.1016/j.tips.2011.02.001 (2011).

17 Keating, G. M. Fenofibrate: a review of its lipid-modifying effects in dyslipidemia and its vascular effects in type 2 diabetes mellitus. *Am J Cardiovasc Drugs* **11**, 227-247, doi:10.2165/11207690-000000000-00000 (2011).

18 Brunmair, B., Lest, A., Staniek, K., Gras, F., Scharf, N., Roden, M. *et al.* Fenofibrate impairs rat mitochondrial function by inhibition of respiratory complex I. *J Pharmacol Exp Ther* **311**, 109-114, doi:10.1124/jpet.104.068312 (2004).

19 Zungu, M., Felix, R. & Essop, M. F. Wy-14,643 and fenofibrate inhibit mitochondrial respiration in isolated rat cardiac mitochondria. *Mitochondrion* **6**, 315-322, doi:10.1016/j.mito.2006.09.001 (2006).

20 Wilk, A., Wyczechowska, D., Zapata, A., Dean, M., Mullinax, J., Marrero, L. *et al.* Molecular mechanisms of fenofibrate-induced metabolic catastrophe and glioblastoma cell death. *Mol Cell Biol* **35**, 182-198, doi:10.1128/MCB.00562-14 (2015).

21 Desager, J. P. & Harvengt, C. Clinical pharmacokinetic study of procetofene, a new hypolipidemic drug, in volunteers. *Int J Clin Pharmacol Biopharm* **16**, 570-574 (1978).

22 Keating, G. M. & Ormrod, D. Micronised fenofibrate: an updated review of its clinical efficacy in the management of dyslipidaemia. *Drugs* **62**, 1909-1944 (2002).

23 Surry, D. S. & Buchwald, S. L. Dialkylbiaryl Phosphines in Pd-Catalyzed Amination: A User's Guide. *Chem Sci* **2**, 27-50, doi:10.1039/C0SC00331J (2011).

CHAPTER 7 : Conclusion

7.1 Novel PHD Inhibitors

The insufficient delivery of oxygen (hypoxia) to animal cells and tissues is associated with diseases including anaemia. Anaemia can be caused by the loss of red blood cells (hemorrhage), excessive red blood cell destruction (hemolysis) or deficiencies in erythropoiesis (production of red blood cells from precursors found in the bone marrow). The symptoms of anaemia can include weakness, dizziness, fatigue, pallor, impairment of cognitive function and a general reduction in quality of life. Chronic and/or severe anaemia can lead to the exacerbation of myocardial, cerebral or peripheral ischaemia and to heart failure. Many other diseases are related to ischaemia hypoxia damage relating to limiting oxygen availability. These include stroke, diabetes and wound healing.

In animals chronic cellular responses to chronic hypoxia involve the α,β heterodimeric hypoxia-inducible factor transcription factor (HIFs). HIFs function as master regulators of oxygen homeostasis and have a key role in the physiological responses to hypoxia, which include angiogenesis and erythropoiesis. Under hypoxia, levels of HIF-α subunits rise and they translocate to the nucleus where they hetereodimerise with the HIF-β subunit. The HIF-heterodimer binds to specific DNA sequences known as hypoxia-responsive elements, promoting the initiation of transcription of HIF target genes. There are three human HIF-α isoforms which have different biological functions. HIF target genes are associated with various aspects of erythropoiesis, glycolysis and angiogenesis and includes genes associated with physiological responses to hypoxia.

Under normoxia, oxygen dependent HIF-α degradation is promoted by hydroxylation of either of two proline residues (Pro402 and Pro564) within the oxygen-dependent degradation domains (ODD) in HIFα isoforms, known as NODD (*N*-terminal proline) and CODD (*C*-terminal proline) domains respectively. The interaction of HIF1α prolyl-hydroxylated with the Von Hippel-Lindau protein (pVHL) promotes hydrolytic degradation of HIFα through an E3 ubiquitin ligase proteasomal pathway. HIF prolyl hydroxylation is catalysed by three 2-oxoglutarate (2OG)-dependent oxygenases known as prolyl hydroxylase domain (PHD 1-3) proteins, through an Fe(II) mediated catalytic process using 2OG, and oxygen.

The HIF-α prolyl hydroxylases are part of the family of Fe(II) bound 2OG dependent oxygenases. There are approximately 70 human 2OG oxygenases many of which have biologically important roles, which do not directly involve the HIF mediated hypoxic response.

PHD inhibitors have entered clinical trials for anaemic diseases. All clinical candidates focused on using 2OG as a template and mimicking the majority of the interactions within the active site of the PHDs. Due to the structural simplicity of 2OG, the clinical candidates inhibit other 2OG oxygenases such as OGFOD1 and CPH. Therefore, the therapeutic effect of these PHD inhibitors in a clinical setting, may alter due to off-target inhibition, especially if the treatment is long term.

The aim of this project was to design and synthesise novel potent selective PHD2 inhibitors. The project began by identifying an aromatic pocket at the entrance of PHD2 which differed to structurally similar 2OG oxygenases. A set criteria for initial ‘hits’ was

identified to achieve strong selectivity within the 2OG oxygenases whilst maintaining potent PHD2 inhibition. The criteria included that the compounds: 1) Must be structurally differentiated from 2OG; 2) Be able to make interactions with the hydrophobic pocket of PHD2 *via* mimicking interactions made by substrates; 3) Possess suitable structural features in order to enable development of a diverse chemical library.

The two chosen starting points were the reported PHD2 inhibitors 1,3,8-triazaspiro[4.5]decane-2,4-dione and 4-hydroxy-2-(1*H*-pyrazol-1-yl)pyrimidine-5-carboxamide series. Initial SAR via final synthetic step modification was explored for both starting point derived series. Both series showed strong potency towards PHD2 (**10** IC_{50} = 0.498 μM and **32** IC_{50} = 0.258 μM using the RapidFire assay). The work revealed the importance of a 'second' metal chelation group (from the 1,3,8-triazaspiro[4.5]decane-2,4-dione series) and the biphenyl substituent (from the 4-hydroxy-2-(1*H*-pyrazol-1-yl)pyrimidine-5-carboxamide series) for potent PHD2 inhibition. **10** and **32** achieved strong HIF-1α stabilisation at 20 μM in the Hep3B cell line, matching the potency of the clinical candidates. Two crystal structures were obtained, one for each series. Analysis of the crystal structures confirmed the interaction with the aromatic pocket for both series and different interactions with key residues within the PHD2 active site. Both **10** and **32** displayed strong selectivity over structurally similar 2OG oxygenases, confirming that interaction with the aromatic pocket at the entrance of the active site of PHD2 can lead to potent PHD2 inhibition whilst achieving a strong selectivity profile within the 2OG oxygenases (**Figure 71**).

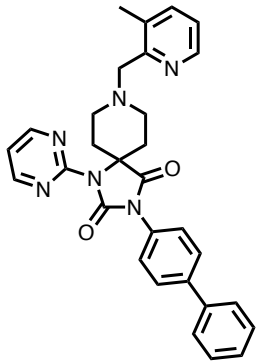

10

PHD2 IC_{50} 0.498 μM
OGFOD1 50%
Inhibition at 100 μM
CPH IC_{50} >100 μM
FIH IC_{50} 14.5 μM

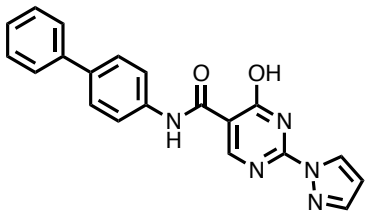

32

PHD2 IC_{50} 0.258 μM
OGFOD1 40%
Inhibition at 100 μM
CPH IC_{50} 28.0 μM
FIH IC_{50} 22.76 μM

Figure 71: Summary of **10** and **32** PHD2 inhibition and selectivity profiles against selected 2OG oxygenases.

With two initial 'hits' confirmed as potent selective PHD2 inhibitors. It was envisaged that a complete SAR of both series could define the criteria required for selective PHD inhibition. The approach undertaken was to fix the amide biphenyl group whilst exploring the chemical space around the initial 'hits' **10** and **32**.

For the 1,3,8-triazaspiro-[4.5]decane-2,4-dione series (**10**), the work reveals the importance of the imidazolidine-2,4-dione core of **10** for PHD2 inhibition. Replacing the imidazolidine-2,4-dione core with an amide bond resulted in no PHD2 inhibition. However, it was shown that the removal of the pyrimidine ring of **10** had little impact on PHD2 inhibition, but did improve inhibition of PHD3, by contrast to **10 (Figure 72A)** (**Chapter 3**).

For the 4-hydroxy-2-(1H-pyrazole-1-yl)pyrimidine-5-carboxamide series, the in-depth SAR revealed that all substituents of **32** were crucial for PHD2 inhibition (**Figure 72B**).

Removal of either the C-4 hydroxyl, pyrazole, pyrimidine groups and C-5 amide groups resulted in loss of PHD2 inhibition (**Chapter 3**). This observation indicates a synergistic effect between the substituents of **32** to achieve potent selective PHD2 inhibition. The complete SAR of both series demonstrated the sensitivity of PHD2 inhibition in relation to

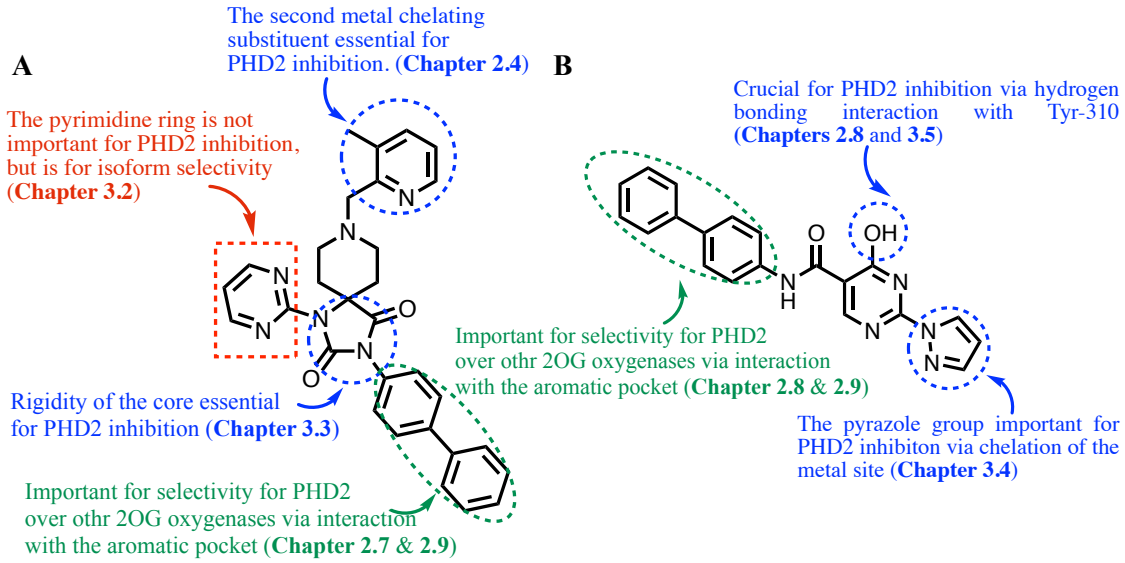

Figure 72: Summary of the SAR work on both initial 'hits' (**Chapter 2** and **3**). The blue boxes show the substituents that are essential for PHD2 inhibition i.e. if the substituent is not present no PHD2 inhibition was recorded. The green boxes show substituents that are important to the pharmacophore but modifications can occur and PHD2 is maintained. The red boxes show substituents that are not important for PHD2 inhibition .

the precise substituents of both series (**Chapter 3**).

The completed SAR of **32** revealed the requirements for potent PHD2 inhibition: bidentate chelation to the metal ion, a hydrogen bond interaction with Tyr-310, and interaction with the hydrophobic pocket at the entrance of the PHD2 active site are all required. It was envisaged that conversion of the 4-hydroxy pyrimidine core of **32** to a 4-hydroxy pyridine core (**94**) would maintain the substituent requirements for PHD2 inhibition. Indeed, **94** maintained similar levels of PHD2 inhibition in comparison to **32**. In-depth SAR was undertaken of **94** through optimised Buchwald and *C*-4 methoxy demethylation reactions.

Investigation into the *C*-5 amide bond resulted in analogues with improved of PHD2 inhibition and cLogP in contrast to **94**. The SAR revealed a combination of different parameters can used to interact with the aromatic pocket of PHD2 including aromaticity, hydrophobicity and additional hydrogen bonding interactions on the methylene linker (**Figure 73**). Moving the C-4 hydroxyl group of **94** to the *C*-3 position of the pyridine ring (**128**), resulted in a substantial drop in PHD2 inhibition in contrast to **94**. An additional substituent on the *C*-4 pyrazole group (COOH or CN) improved the potency of **94** and **128** (by 3-and 25-fold respectively) indicating that replacement of the hydrogen bond interaction with Tyr-310 can still maintain PHD2 inhibition (**Figure 73**). However, changing the *C*-5 amide group resulted in a loss of potency in the presence of COOH or CN on the *C*-4 pyrazole group (**Chapter 4**).

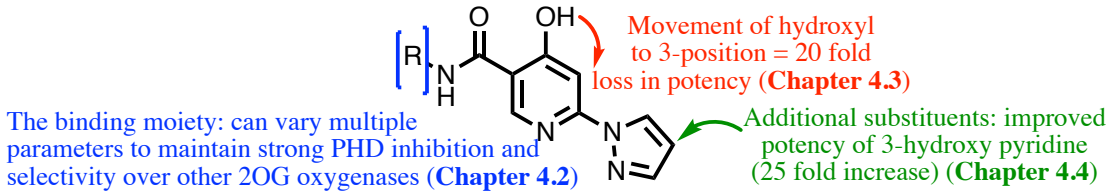

Figure 73: Summaries of the SAR work of the 4-hydroxy pyridine pharmacophore.

The completed SAR for successful PHD inhibition led to the attempt to further develop novel PHD2 pharmacophores. The reverse 4-hydroxy-pyridine pharmacophore was designed on the assumption that substituents required for PHD inhibition could be reorganised and achieve strong PHD2 inhibition. **153** achieved strong PHD inhibition but the reverse pharmacophore SAR demonstrated the sensitivity of interacting with the PHD2 active site. Rigidity was identified as a important parameter during this PHD2 inhibitor discovery project. It was envisaged that improving the rigidity between the metal chelation

sites (the tricyclic pharmacophore) may lead to improved PHD2 inhibition. Indeed, analogues of **184** achieved strong PHD2 inhibition. However, the (likely) additional rigidity of the tricyclic pharmacophore in comparison to **94** showed no improved in PHD2 inhibition (**Chapter 4**).

The novel PHD inhibitors were tested in a cellular environment. Surprisingly **94** demonstrated poor HIF-1α stabilisation in contrast to **32**. It was proposed that the poor HIF-1α stabilisation was due to poor cell permeability possibly because of **94**s high cLogP or tautomerisation of the free hydroxyl group. Analogues with varied C-5 amide group (**117**, **120** and **121**) achieved strong HIF-1α stabilisation at 100 μM indicating the biphenyl substituent and the high cLogP was partially responsible for the poor cellular efficacy of **94**. **117**, **120** and **121** showed moderate HIF-1α stabilisation at 20 μM suggesting acceptable cellular efficacy could be achieved at lower concentrations. Unfortunately, no analogues of the reverse 4-hydroxy pyridine pharmacophore achieved HIF-1α stabilisation in a cellular setting. However, analogues of the tricyclic pharmacophore all (**179 - 185**) achieved strong HIF-1α stabilisation at 100 μM. **184** achieved strong HIF-1α stabilisation at 20 μM and indicated that **184** may be able to stabilise HIF-1α at lower concentrations. None of the novel PHD2 pharmacophores achieved strong inhibition over structurally similar 2OG oxygenases (**Table 25**) (**Chapter 4**), a feat that no clinical candidate achieved (**Table 1**) (**Chapter 1**).

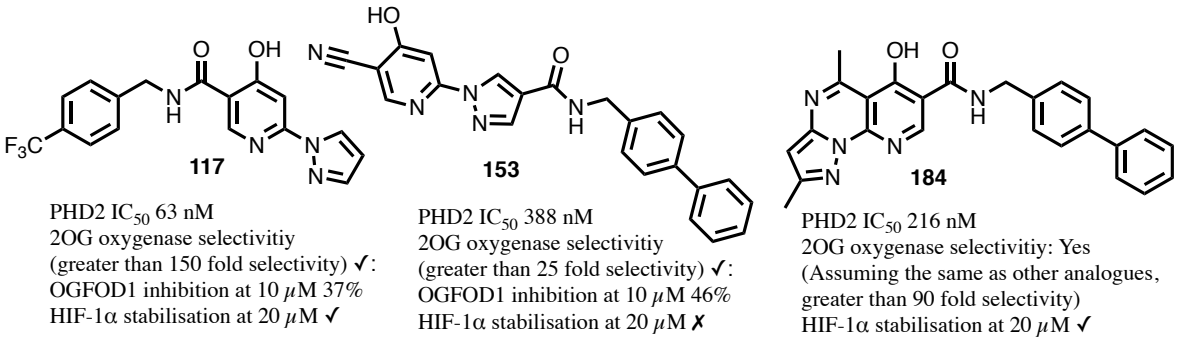

Figure 74: The best analogue from each novel pharmacophore and summary of their potency on isolated enzyme and in a cellular setting. Their selectivity against the structurally similar 2OG oxygenase OGFOD1.

In conclusion, three novel PHD2 pharmacophores have been designed and synthesised through in-depth SAR of initial 'hits' **10** and **32** (**Figure74**). A number of analogues were synthesised leading to the potent and selective PHD inhibitors **117**, **120**, **121**, **153** and **184** which are significantly more potent on PHD2 (on isolated enzyme) and more selective over other 2OG oxygenases than the clinical candidates to date (**3**-**8**, **Chapter 1**) (**Figure74**). **117**, **120**, **121** and **184** achieved the HIF-1α stabilisation at the same concentrations as the clinical candidates. These pharmacophores have the potential to clinically treat patients with anaemic and ischemic diseases. However, further development is required on these novel pharmacophores in order to maximise cellular HIF-α stabilisation and achieve an acceptable pharmacokinetic and pharmacodynamic parameters.

7.2 Small Molecule PHD Activators

Unexpectedly, **84** displayed an increase in CODD hydroxylation with PHD2 (**Chapter 3**). Possible explanation for the observed effect were enzymatic activation by the interactions of **84** or an assay artifact. To explain the observed increase in CODD hydroxylation with PHD2 SAR work of **84** was conducted. The SAR suggested that all groups of **84** (**Figure X**) were important for the effect observed. This indicated that the increase in CODD

hydroxylation with PHD2 was not an assay artifact. Investigation of the *C*-5 amide revealed, hydrophobicity was not an important factor for the increased turnover, but the length and the linearity of the amide group were important for the increase in CODD hydroxylation with PHD2. The pyrazole group was required for the increase in CODD hydroxylation with PHD2. The results imply this is not due chelation of the active site metal, but relates to the three-dimensional shape of **84** (**Figure 75**). The SAR of the *C*-4 amino substituent demonstrated substantial sensitivity to the observed effect in relation to the amino group. **84 w**as shown to destabilise HIF1-α in multiple cell lines including Hep3B and mitochondrial deficient cell lines (206p0 and 143B) under hypoxic conditions. This observation indicates that the effect observed is not an assay artifact and does not involve mitochondrial inhibition. Investigation of the possible mechanism of action for the increase in CODD hydroxylation with PHD2 in the presence of **84** revealed that the effect is PHD2 selective, also occurs with the NODD substrate, and that the *C*-terminal regions is involved in the increase in CODD hydroxylation. It was proposed that one possible mechanism for the increase in CODD hydroxylation with PHD2 in the presence of analogues of **84** occurs by destabilising the hydroxylated substrate-PHD2 complex. Thus, weakening the hydroxylated substrate-PHD2 complex to fragment and leading to an increased amount of available catalytically active enzyme, resulting in an increase in the amount of hydroxylated HIF-1α substrate in comparison to the DMSO control (**Chapter 5**).

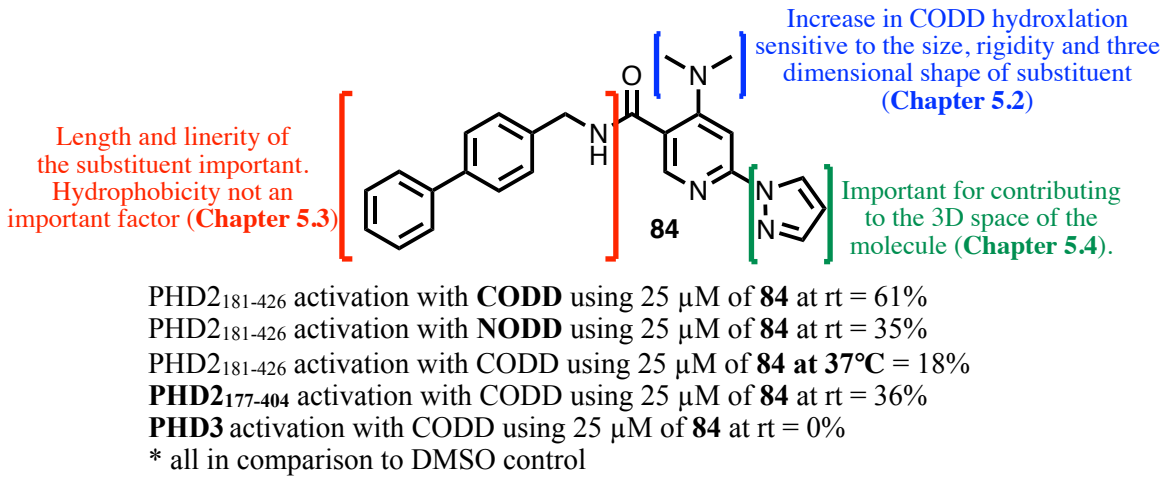

Figure 75 : Summaries of the role of the substituents of **84** in relation to the increase in HIF-1α substrates and biochemical SAR using **84** (In bold are the differences between each SAR point).

Overall, this work represents the discovery of the first PHD2 small molecule activator (**84**). The approach highlights in depth SAR from a molecular, biochemical and cellular perspective. The results conclude that the increase in CODD hydroxylation of PHD2 with **84**, may be true. Clinically PHD2 activators may have an application in negatively regulating over-expressed target genes in the HIF system.

7.3 Novel Oxygen Consumption Rate Inhibitors

Hypoxic regions in cancers are aggressive and treatment-resistant. Hypoxic tumour cells are up to three times more resistant to ionizing radiation in contrast to normoxic tumour cells. It was proposed that reducing tumour hypoxia would improve the response to radiation therapy. A strategy to reduce tumour hypoxia would be to reduce the oxygen consumption rate (OCR). A library of 1,697 FDA-approved drugs to identify small molecules that decrease the OCR of cancer cells Seahorse XF Analyzer assay was used. From the screen, Fenofibrate (**206**) (a widely used treatment for hyperlipidemia in the clinic) was selected

for SAR evaluation. The SAR investigation revealed the importance of the of the dimethyl group. However, the isopropyl ester could be replaced with an amide (**216** and **217**) and maintain or improve inhibition of the OCR. Conversion of the *C*-4 chloro group to a bulky amino group *via* a Buchwald amination resulted in a substainal increase in the inhibition of OCR, **226** resulted in a 60% decrease in OCR at 1 μM.

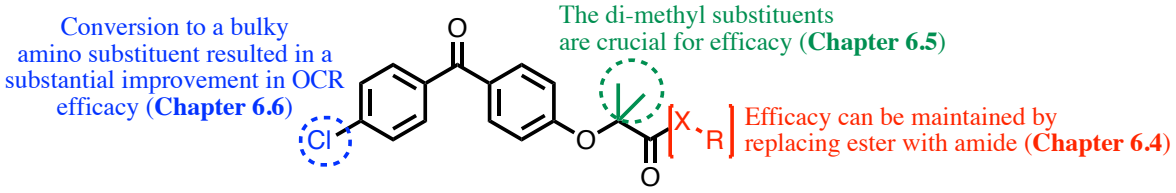

Figure 76: Summary of the SAR work of fenofibrate for novel inhibitors of the OCR.

In conclusion, the SAR of Fenofibrate (**206**) indicated the potential of developing a highly potent inhibitor of the OCR. The initial SAR of the fenofibrate derivatives suggest potency may be improved with additional investigation of the amino moiety or by a combination of the amino group (**226**) and the amide substituent modifications (**216** and **217**)

7.4 General Comments

To compare the novel pharmacophores to the clinical candidates (in which Fibrogen, GSK and Bayer have masses of experienced scientists and have spent £100s of millions on the medicinal chemistry part of the PHD2/HIF project (they are now in phase 3 of clinical trials), for one DPhil student to design and synthesise the most potent (on isolated PHD2) pharmacophores to date, and to have a strong selectivity profile against structurally similar 2OG oxygenases (arguably the most selective 2OG oxygenase inhibitors ever) in which no clinical candidate possesses is an achievement. Indeed, the medicinal chemistry philosophy

attempted throughout this DPhil, of just using mental logic (trial and error, willing to fail) and no *in silico* programs or intense literature searches, demonstrates the dire situation the pharmaceutical industry is in today.

CHAPTER 8. Materials and Methods

8.1 Chemical Synthesis

All reactions involving moisture-sensitive reagents were carried out under a nitrogen atmosphere using standard vacuum line techniques and glassware that was oven dried and cooled under nitrogen before use. Commercial anhydrous solvents used in reactions and HPLC grade solvents were employed for work-up and chromatography. Water was purified using an Elix UV-10 system. Aqueous solutions were made using de-ionized water. Thin layer chromatography (TLC) was carried out using Merck (Darmstadt, Germany) silica gel 60 F254 TLC plates. TLC visualisation was carried out under UV light and stained with one of three stains; ninhydrin, potassium permanganate, or anisaldehyde. Chromatographic purifications were carried out using a Biotage® (Uppsala, Sweden) Isolera One or Biotage® SP4 flash purification system, using Biotage® pre-packed SNAP columns. Reactions were monitored using an Agilent (Cheshire, UK) 1200 series, 6120 quadrupole LC-MS system using a Merck Chromolith® Performance RP-18 HPLC column. Deuterated solvents were obtained from Sigma-Aldrich, and ^{1}H NMR spectra were obtained on a Bruker AVANCE AVIII HD 400 nanobay (400 MHz) or Bruker AV500 (500M Hz) with a ^{13}C cryoprobe . All signals are described in δ ppm with multiplets being denoted as singlet, doublet, triplet, quartet, and multiplet using the abbreviations s, d, t, q, and m, respectively. Chemical shifts in presented NMR spectra were referenced using residual solvent peaks with coupling constants, *J*, reported in hertz (Hz) to an accuracy of 0.5 Hz. For high-resolution mass

spectrometry (HR-MS), a Bruker MicroTOF instrument with an ESI source and Time of Flight (TOF) analyser was used. MS data are represented as a ratio of mass to charge (m/z) in Daltons. A Bruker Tensor 27 instrument was used to obtain Fourier transform infrared spectra (FT-IR). Spectroscopic grade solvents and a Perkin Elmer 241 Polarimeter were used to obtain optical rotations.

All chemicals, reagents, and solvents were obtained from Sigma-Aldrich (Dorset, UK) and used without further purification. HPLC grade solvents were used for reactions, chromatography, and work-ups.

8.2 PHD2/3 RapidFire Assay Protocol

Performed By Dr Anthony Tumber & Ms Kerstin Lippl

The inhibition of PHD2 activity was assessed by using liquid-chromatography mass spectrometry. The tPHD2 (181 - 426 residues) assay monitors turnover of a C-terminal oxygenase dependent domain peptide substrate (CODD) DLDLEMLAPYIPMDDDFQL (with a C-terminal amide) and appearance of the hydroxylated peptide product (hydroxylation of proline 564) with a typical enzyme incubation time of 15 minutes. Assays were performed in 50 mM Tris.Cl pH 7.8, 50 mM NaCl, titrations of compounds for IC_{50} determinations (3-fold and 11-point IC_{50}) were performed using an ECHO 550 acoustic dispenser (Labcyte) and dry dispensed into 384-well polypropylene assay plates. The final assay concentration of DMSO was kept constant at 0.5%. tPHD2 (181 - 426

residues) was used at a concentration of 300 nM in assay buffer and 25 µl dispensed across each 384-well assay plate. tPHD2 (181 - 426 residues) was allowed to equilibrate with compounds for 15 minutes and the enzyme reaction then initiated by dispense of 25 µl of substrate (20 µM Ferrous Iron Sulfate, 200 µM L-Ascrobic Acid, 10 µM CODD peptide and 20 µM 2-Oxoglutarate in assay buffer). Enzyme reactions were allowed to proceed for 15 minutes and the reaction terminated by addition of 10% formic acid (5 µl). Assay plates were then transferred to a RapidFire RF360 sampling robot (Agilent) connected to an Agilent 6530 quadrupole-time-of-flight (Q-TOF) mass spectrometer. Assay samples were aspirated under vacuum and loaded onto a C4 solid phase extraction (SPE) cartridge. After loading the C4 SPE was washed with 0.1 % formic acid in water to remove non-volatile buffer salts. The peptide was then eluted from the SPE with 85% acetonitrile, 15% water containing 0.1% formic acid onto the mass spectrometer. Peptide charge states were monitored in positive mode. Ion chromatogram data were extracted for the +2 charge state and peak area data integrated using RapidFire Integrator software (Agilent). % conversion of the CODD peptide substrate to the +16 hydroxylated peptide was calculated using the equation:

% conversion = 100 x hydroxylated / (hydroxylated + non-hydroxylated peptide)

IC50 data were determined from non-linear regression plots using GraphPad prism 6.0.

8.3 PHD2 MALDI Assay Protocol

Performed By Dr Tzu-lan Yeh

The PHD2 inhibition assay used matrix-assisted laser desorption/ionization time of flight (MALDI-TOF) mass spectrometry to measure the extent of hydroxylation of HIF-1 CODD peptide substrate (HIF-1 residues 556-574) using a Waters® Micromass® MALDI micro MXTM mass spectrometer and MassLynxTM 4.1 as previously described. The optimised hydroxylation assay involved incubation of PHD2 (1 μM) with inhibitor (1 % *v*/*v* in DMSO) in the presence of Fe(II) (10 μM), 2OG (60 μM), ascorbate (100 μM) and HIF-1 CODD 556-574 (50 μM) in HEPES (50 mM, pH 7.5) at 37 °C for 15 min. Reactions were quenched with formic acid (1 % *v*/*v*). Samples were prepared by mixing reaction mixture (1 μL) with α- cyano-4-hydrocinnamic acid (CHCA) solution (water: acetonitrile 1:1) (1 μL). Dose-response was assessed in 8-point triplicates. Data were analysed using GraphPad Prism® 5.04.

8.4 PHD2 NMR Displacement Protocol

Performed By Dr Martine Abboud

Nuclear Magnetic Resonance (NMR) spectra were recorded using either a Bruker AVIII 600 MHz NMR spectrometer equipped with a BB19F/1H Prodigy N2 cryoprobe, or a

Bruker AVIII 700 MHz NMR spectrometer equipped with a 5-mm inverse cryoprobe using 5 mm diameter NMR tubes (Norell) or 3 mm MATCH NMR tubes (Cortectnet). Data were processed using the Bruker 3.1 software. Prior to Fourier transformation, data were processed with a line broadening of 0.3 Hz. The catalytic domain of human PHD2 (residues 181-426) was used in all the protein NMR experiments.

For 13C-CODD and 13N-CODD displacement experiments, 1D Clean In-Phase (CLIP) HSQC with selective 13C-inversion displacement experiments were conducted using a Bruker AV700 instrument. 3 mm MATCH NMR tubes were used (Cortecnet). All experiments were conducted at 298 K. The reporter CODD or NODD molecule was uniformly 13C labelled on its prolyl-ring. 7 The CLIP-HSQC sequence was used for 1D HSQC experiments (without 13C decoupling). 8 Relaxation delay was 2s. The 1 JCH was set to 160 Hz. A 6.8 ms Q3.1000 180 degree pulse was used and selective irradiation was applied at the selected chemical shift

8.5 PHD2 Crystallography Protocol

Performed By Dr Rashed Chowdhury

Crystals of PHD2 (residues 181–426) in complex with Mn(II)/**1** were grown in sitting drops at 293K using vapor diffusion methods at a protein to reservoir ratio of 1:1. PHD2 protein solution contained 32.0 mg/mL protein (in 50 mM Tris·HCl pH 7.5), 2.8 mM $MnCl_2$ and 2.8 mM **1**. The reservoir solution contained 1.6 M sodium citrate/citric acid pH 6.5 (Hampton Research Crystal Screen-II). Mn(II) was used as a replacement for Fe(II) during

crystallisation to prevent metal oxidation and consequent formation of heterogenous sample. The crystals were cryoprotected using well solution that was diluted to 30% v/v glycerol and flash frozen in liquid nitrogen. Data were collected from a single crystal at 100K at the Diamond MX beamline I04-1 (0.9200 Å) equipped with a Pilatus 2M detector. The data were indexed, integrated and scaled using MOSFLM and SCALA. The structure was determined by molecular replacement using PHASER and PDB ID: 4BQY as the search model. Iterative rounds of model building (COOT) and refinement (CNS and PHENIX) were performed until the R and R_{free}converged.

8.6 FIH RapidFire Protocol

Performed by Dr Anthony Tumber

IC_{50} determination for clinically relevant PHD2 inhibitors was determined by a RapidFire mass spectrometry based assay using a synthetic ankyrin peptide (HLEVVKLLLE-AGADVNAQDK) as a substrate for FIH. All assay steps were performed in assay buffer (50 mM Tris.Cl pH 7.5, 50 mM NaCl). Titrations of PHD2 inhibitors (100 – 0.0017 mM) were prepared using an ECHO 550 acoustic dispenser and FIH (100 nM) dispensed across the plate (25 µl/well) using a Multidrop dispenser (Thermo Scientific). Inhibitors were allowed to equilibrate with FIH for 15 minutes at room temperature and the enzyme reaction initiated by 25 µl dispense per well of substrate (200 µM L-AA, 20 µM FAS, 10 µM ankyrin peptide substrate and 20 µM αKG) in assay buffer. After 20 minutes the enzyme reaction was stopped by dispense of 10 % formic acid (5 µl/well) and the plate

transferred to a RapidFire (RF360) high throughput sampler connected to an Agilent 6530 QTOF. Assay samples were aspirated under vacuum and loaded onto a C4 solid phase extraction (SPE) cartridge. After loading the C4 SPE was washed with 0.1 % formic acid in water to remove non-volatile buffer salts and then peptide was eluted from the SPE with 85% acetonitrile, 15% water containing 0.1% formic acid onto the mass spectrometer. Peptide charge states were monitored in positive mode. Ion chromatogram data were extracted for the +3 charge state and peak area data integrated using RapidFire Integrator software (Agilent). % conversion of the ankyrin peptide substrate to the +16 hydroxylated peptide was calculated using the equation:

% conversion = 100 x hydroxylated / (hydroxylated + non-hydroxylated peptide)

IC50 data were determined from non-linear regression plots using GraphPad prism 6.0

8.7 OGFOD1 MALDI Protocol

Performed by Dr Christopher Lohans

The OGFOD1 inhibition assay used matrix-assisted laser desorption/ionization time of flight (MALDI-TOF) mass spectrometry to measure the extent of OGFOD1-catalysed hydroxylation of a peptide substrate in the presence of inhibitors. Assays were carried out

in 50 mM HEPES, pH 7.5, with 1 μM OGFOD1, 25 μM 2-oxoglutarate (disodium salt), 1 mM ascorbate (sodium salt), 50 μM ammonium ferrous sulfate, 25 μM RPS23 20mer peptide (H_2N-VLEKVGVEAKQPNSAIRKCV-$CONH_2$), and the indicated concentrations of inhibitor. Reactions (20 μL) were quenched after 10 min via the addition of 5 μL 5 % formic acid. Samples (1 μL) were mixed 1:1 with α-cyano-4-hydroxycinnamic acid (prepared in 50 % acetonitrile), and applied onto a stainless steel plate. Mass spectra were acquired on a Waters MALDI Micro MX instrument in reflectron mode monitoring positive ions. The extent of inhibition was normalized to control experiments in which no enzyme was added (i.e., no hydroxylation), and in which no inhibitor was added (i.e., no inhibition). The data presented represent the average percentage inhibition of three replicates, and the error bars represent the standard deviation.

8.8 vCPH MALDI Protocol

Performed by Dr Gareth Langley

Component	Final Concentration / μM
$(NH_4)_2Fe(SO_4)_2$	50
vCPH	1
Peptide	10
Sodium-L-Ascorbate	100
2OG (Disodium Salt)	50
Inhibitor	100 for broad screen, varied for IC_{50} determination

Table A - Reaction Composition of vCPH Inhibition Assay. Reactions were conducted in 50 mM HEPES pH 7.5.

Final reaction concentrations are indicated in Table 50. Inhibitor and enzyme were incubated for 5 minutes prior to the addition of a solution of 2OG, Ascorbate, Fe^{II} and peptide. Reactions were conducted in triplicate at room temperature and quenched after 5 minutes *via* the addition of 20 µL MeOH. Reactions were analysed by MALDI-TOF MS; percent hydroxylation was calculated by comparing the ion intensities of peaks corresponding to $[M+H]^+$ and $[M+Na]^+$ to $[M+O+H]^+$ and $[M+O+Na]^+$. Percentage response was then calculated by comparing the reaction mixture to a no inhibitor control. Data was fitted using GraphPad Prism.

8.9 Cell Based Protocols

Performed by Dr Tzu-Lan Yeh

Hep3B, 206 p0 and 143B cells were cultured in Dulbecco's Modified Eagle's Medium (DMEM; Sigma Aldrich D6546-500ML) supplemented with 10% fetal bovine serum (Sigma Aldrich F7524- 500ML), 4 mM L-glutamine (Sigma Aldrich G7513- 100ML), 50 U/mL penicillin, and 50 µg/mL streptomycin (Sigma Aldrich P0781-100ML). Cells were seeded to reach 90-100% confluency prior to compound treatment. Cells were exposed to

the inhibitor at a final concentration of 1% DMSO for 5-6 hours. For Fe(II) titration in the presence of inhibitors, ferric ammonium citrate was added to the cells for further 16 hours after 6 hours of incubation with the inhibitors. Cells were harvested in urea/SDS buffer (6.7 M urea, 10 mM Tris-Cl pH 6.8, 10% glycerol, and1% SDS) supplemented with 1mM dithiothreitol following a phosphate-buffered saline (PBS) rinse. Cell extracts were analyzed with SDS-PAGE, electroblotted to polyvinylidene difluoride (PVDF) membrane (Millipore) and probed with the corresponding primary antibody for 1 hour at room temperature or overnight at 4 °C. The secondary antibody specific to primary antibody species conjugated with HRP were applied at room temperature for 1 hour. The antibodies used for immonoblotting were as follows: pan-anti-HIF-1α (clone 54, BD Transduction Laboratories™), anti-HIF-1α Hyp402 (catalogue number 07-1585, Merck Millipore), anti-HIF-1α Hyp564 (D43B5, Cell Signaling), anti-HIF-1α HyN803, PHD216, PHD316, and HRP-conjugated anti-β-actin (clone AC15, Abcam). Detection of signal was achieved using SuperSignal™ West Dura Extended Duration Substrate kit (Thermo Scientific 34075, unless otherwise stated) either with film or ChemiDocTM MP (BIO-RAD) imaging system. Quantification of the immunobloting signal was performed with Image LabTM software from BIO-RAD.

Details of hypoxic cellular experiments not given.

8.10 Oxygen Consumption Rate Cellular Protocol

Performed by Mr James Coates

The FaDu cells were grown for 24 h in DMEM containing 5 mM glucose and 4 mM L-glutamine, and then measurements of the OCR were taken in XF assay medium (Seahorse Biosciences) containing 5 mM glucose, 5 mM sodium pyruvate and 4 mM L-glutamine using an XF96 Analyzer (Seahorse Biosciences). For the kinetics experiments, measurements were collected every 15 min following injection of atovaquone. The OCR measurements were corrected for cell number using Hoechst staining, as described above. For the experiments using permeabilized FaDu cells, 0.005% digitonin was the permeabilization agent, and the % OCR was measured within 15 min of its addition. Permeabilization of the plasma membrane allows the substrates respired by the mitochondria to be dictated by the added medium, and allows non-membrane permeable substrates to access the mitochondria